Title
Functionalizable poly(2-oxazoline) stabilizers in a perfluorocarbon-in-water nanoemulsion drug delivery system

Author
Estabrook, Daniel A.

Publication Date
2021

Peer reviewed|Thesis/dissertation

UNIVERSITY OF CALIFORNIA,

Los Angeles

Functionalizable poly(2-oxazoline) stabilizers in a perfluorocarbon-in-water nanoemulsion drug delivery system

A dissertation submitted in partial satisfaction of the

requirements for the degree

Doctor of Philosophy in Chemistry

by

Daniel Adam Estabrook

2021

ABSTRACT OF THE DISSERTATION

Functionalizable poly(2-oxazoline) stabilizers in a

perfluorocarbon-in-water nanoemulsion drug delivery system

by

Daniel Adam Estabrook

Doctor of Philosophy in Chemistry

University of California, 2021

Professor Ellen May Sletten, Chair

Effective drug delivery requires exquisite chemical control in the complex environment of the body. To enable a general approach to drug delivery, a modular scaffold that relies on chemistry orthogonal to that found in nature is required. This dissertation focuses on exploiting the unique properties of the perfluorocarbon (PFC) phase to create a versatile drug delivery system, accomplished by developing new polymeric amphiphiles to kinetically stabilize droplets of PFC in water, known as PFC nanoemulsions. PFC nanoemulsions are non-toxic, dynamic nanomaterials that have been previously employed as oxygen carriers and contrast agents. However, their use has been limited by nonfunctional poloxamer surfactants that result in size heterogeneity, instability, and multi-dose toxicity. The development of a biocompatible, functionalizable surfactant would expand the versatility and utility of PFC emulsions, enabling

responsive and targeted nanomaterials. This dissertation reports the use of multifunctional poly(2-oxazoline) (POx) surfactants to control the size, charge, surface chemistry, cellular uptake, and the controlled disassembly of these nanomaterials.

Chapter One is a perspective on the historical development of drug delivery carriers, the challenges that underlie them, and how PFC emulsions can be viewed as a solution to these limitations. Similarly, it discusses previous surfactants employed in PFC emulsion formation and explains the motivation behind the choice of POx as a modular surfactant platform.

Chapter Two outlines our early efforts in developing POx surfactants that can both form and stabilize PFC nanoemulsions (<300 nm) over time and discusses the structure-property relationships that underlie these amphiphiles in the context of nanomedicine.

Chapter Three reports selectively modifying surface properties of PFC nanoemulsions by leveraging functionalizable POx surfactants. Post-emulsion surface charge modifications are shown to affect cytotoxicity and the magnitude of cellular uptake in macrophage and non-macrophage cells.

Chapter Four illustrates the development of redox-cleavable POx block copolymers that allow for the formation of glutathione-responsive PFC nanoemulsions. These nanoemulsions can selectively degrade in response to intracellular triggers. These advances are leveraged alongside a noncovalent fluorous tagging strategy that allows one to solubilize a GFP plasmid within the fluorous phase, whereafter protein expression is achieved selectively when employing stimuli-responsive surfactants. This work contributes a methodology for non-viral gene delivery and represents a general approach to nanoemulsions that respond to endogenous stimuli.

Chapter Five establishes a new intracellular stimulus–macromolecular crowding–as a trigger for responsive nanomaterials. Transition temperatures of thermoresponsive POx are shown

to vary with changes in crowding, and this dependence can be tuned such that the system is stable to low extracellular concentrations of protein but destabilizes at high intracellular concentrations. Ultimately, we demonstrate that the cytosol is an effective stimulus for nanoemulsions, with droplet fusion occurring upon injection into cells of zebrafish embryos. With this report, we set the stage for the wide-ranging class of thermoresponsive materials to respond to macromolecule concentration rather than conventional temperature changes.

Chapter Six is a compilation of collaborative highlights, preliminary work and future directions for this platform. It discusses internal collaborations with Professor Chong Liu and Professor Jeffrey Zink's lab, including manuscripts that are either accepted, in revision, or in preparation. Additionally, it discusses preliminary findings in host-guest mediated emulsion fusion, laying the groundwork for *in situ* prodrug synthesis in living systems using the fluorous phase.

The dissertation of Daniel Adam Estabrook is approved.

Timothy J. Deming

Yi Tang

Jeffrey I. Zink

Ellen May Sletten, Chair

University of California, Los Angeles

2020

Functionalizable poly(2-oxazoline) stabilizers in a perfluorocarbon-in-water nanoemulsion drug delivery system

Table of Contents

Chapter 5. Macromolecular Crowding as an Intracellular Stimulus for Responsive Nanomaterials

Chapter 6. Collaborative Highlights, Preliminary Work, and Future Directions

List of Figures

List of Tables

Acknowledgements

It is an extremely strange sensation to be tasked with summing up my time at UCLA. In a way it seems like my PhD flew by, on the other hand it feels like it was the longest five years of my life. The truth is probably somewhere in the middle. It turns out that you are bound to personally experience nearly every aspect of graduate school that you are told constantly about—there will be highs and lows, and I found it best to try and keep both moderate. There are so many people that I need to thank for making this journey what it was that it actually makes me anxious to think that I will forget any of you. Hopefully you all know who you are.

First and foremost, I need to thank my advisor, Ellen Sletten. I have told the story plenty of times, but I still remember our first meeting back in January 2016. It was the middle of a New Hampshire winter and I was still an undergraduate, having just recently gotten the congratulatory phone call from Ellen that I had been accepted to UCLA's Chemistry PhD program. Also being from NH, Ellen had invited me to meet at a roadside Dunkin' Donuts to talk about the projects she was trying to get off the ground in her new lab. There, my soon-to-be-PhD-advisor spoke to me about "exploiting the orthogonality of the fluorous phase" and "modular scaffolds for nanotherapeutics"—phrases that, at the time, I knew nothing about. Six months later, I rotated in her group, and stayed there for the remainder of my PhD. I like this story because it gets at one of the things that I value most about Ellen as a PI, which is her capability to treat her students almost as junior colleagues. She is great at recognizing and understanding what certain students want or even need in a mentor and is always willing to adjust accordingly. My first year and second years at UCLA in particular were really some of the most formative times in my life, and certainly in my career. Like everyone says, working in the lab of a new professor is not always the most comfortable or easy-going experience, but I like to think that everyone was getting through it

together. It is a whole lot easier to put in the work that we all did when Ellen's office light was almost always on even when you were just leaving a late night in lab. I still do not know how she does it, but I can only hope that during my last five years, even 10% of Ellen's work ethic rubbed off on me. Ellen is also, of course, an incredible scientist, and she taught me a great deal about designing and executing experiments, how to incorporate controls to squeeze the most out of those experiments, and the importance of a thorough SI. Whenever I see graphs without error bars, I will imagine her cringing. Likewise, I would like to thank Ellen for always being supportive of my project directions, and the willingness to let her students expand the scope of their expertise and familiarity into different aspects of science, everywhere from synthesis to cell studies. Finally, I would like to both briefly shout out and simultaneously apologize to Dom for any half-empty kegs that our lab get-togethers left behind. Hopefully Ellen can recruit a couple more beer aficionados in the upcoming draft class.

Over the last five years, the lab has grown at a crazy rate. At this point we have transitioned group meetings and journal clubs from Ellen's office table, to a classroom, to a lecture hall–I believe the LaMonica's Pizza receipts will reflect that. I would like to thank some of the students that were in Ellen's lab when I first joined, including the two above me, Maly Cosco and Wendell Scott. Maly was supportive of me before and throughout my PhD, from her recruitment emails reminding me that I really (definitely) should join Ellen's lab, until the day she left to start her postdoc at Stanford. Her productivity in her PhD is admirable, and she certainly left the SWIR team in a great place. Wendell was a fantastic colleague who remained a good friend even after moving to the Deming Lab, and the get-togethers he hosted in my first few years were a great glue between different cohorts and departments at UCLA.

Of course, my biggest thanks goes out to our cohort in Ellen's lab. If you ran the numbers, you would think that seven coworkers in a high-intensity environment could be recipe for at least an ounce of animosity here and there, but somehow, we defied the odds. The six of you were fantastic to work with, and I am looking forward to seeing you all go on to achieve great things. In retrospect, Ellen tasking us each with our own individual projects made it rewarding to watch those projects grow over the course of five years, and taught me a good deal about the day-to-day effort that doing good science requires. Margeaux's synthetic talents speak for themselves, but I am incredibly grateful for her being a constant source of humor, common interests, and support over the last couple years. Rachael was a great labmate and roommate, from showing me everything I know about cell studies to being the (self-proclaimed) backbone of the apartment. If I had to describe the ideal colleague it would probably be Joe, as his synthetic/polymer knowledge and meme-making abilities are admirable and he either gets along with everyone or hides it very well. Monica has an incredible work ethic driven by an exploratory attitude that is only rivaled by her great taste in music, though I suspect that her future decision to travel back to LA to see a Weeknd concert may age poorly. I need to thank Gina for introducing me to KBBQ and, perhaps more importantly, soju. Though my palate still disappoints you, we'll continue to work on it in Cambridge. Anna, I was always impressed by your seemingly photographic memory and attempts at teaching us the value of having a life outside of lab.

I would also like to thank the many older mentors I had throughout my time at UCLA, including the postdocs that have come into Ellen's lab. First, Wei Cao, who was an efficient researcher and great source of information for a lab that, at the time, was filled with a bunch of 23-year-old graduate students. It was great working with you at the time and watching you continue to succeed at Northwestern. Second, Jon Axtell, who was one of the most intelligent, hard-working

and down-to-earth people that I had the pleasure of meeting here. I always appreciated your chemistry, career and life advice, especially when it was over a Nickel IPA or a Barney's blonde ale, preferably with any and all sports playing in the background–yes, even Jaguars games. I am sorry that Blake Bortles didn't work out. Third, thank you to Heidi van de Wouw for making the choice to jump from one assistant professor in her PhD to another in her postdoc. You taught me a great deal about synthetic chemistry, were always up for an in-lab conversation about reaction troubleshooting and are a great tool to the polymer chemists within the group. I know we both struggled through COVID-cancelled concerts, but I hope for both of our sakes that things open up again soon. Thank you to Shang Jia, who brought his expertise in bioconjugation to the lab, and soon after a new lab baby. I look forward to following your findings with Ellen and your independent career thereafter. Finally, I would like to thank all of the older students outside of Ellen's lab that were nonetheless incredibly helpful to me, particularly Jeong Hoon Ko (JK) for his polymer-centric mentorship in my first few years at UCLA.

As the lab progressed, Ellen did a great job in recruiting a number of wonderful younger students. Irene, you were an invaluable resource for fluorous-soluble fluorophores. As someone who commiserates with the challenges of fluorous solubility but rarely has to actually deal with them, I was always impressed by your synthetic prowess and ingenuity–I am sure that both the Sletten and Campas groups will continue to use many of your molecules for years to come. Cesar and Anthony, I have many stories about the two of you but very few that can be appropriately shared in this format. Thank you to Cesar for introducing me to rock climbing, perhaps the only activity that has motivated me to go to a gym. Anthony, thank you for providing some much-needed humor and music to 4224. To the first- and second-years, I look forward to seeing you all

take these projects forward and hope that things (and occupancy) soon begins to resemble some sense of normal.

To the previous undergraduates in the lab, it has been great to both get to know and mentor some of you. Thank you to Amanda Ennis, a very talented undergraduate that I had the opportunity to work with for a summer, who helped significantly with the publication of emulsion functionalization work described in Chapter 3. It was great to work with and mentor John Chapman, who spent nearly the better half of two years working with me. You were invaluable to work discussed in Chapters 2, 5, and 6, and I really have your control experiments with thermoresponsive polymers to thank for launching our protein-responsive delivery project. Though you unfortunately did not choose to pursue synthetic polymer chemistry, I will chalk up you pursuing your PhD researching glycans as a technical win for team (bio)polymer.

There are several faculty and staff at UCLA that make it the fantastic place it is. Thank you to my committee, including Prof. Tim Deming, Prof. Jeffrey Zink and Prof. Yi Tang for their help along the way. Prof. Deming was kind enough to be my out-of-department collaborative mentor for the NIH Biotechnology Training Grant, headed by Prof. Tang. I am extremely grateful for having been granted this training program during my second and third year at UCLA, particularly the opportunity to do a summer internship at 3M, which solidified my decision to move into an industrial postdoc after my PhD. Prof. Zink and his students, particularly Wei Chen, Chi-An (Annie) Cheng, and Tian Deng, were great collaborators throughout my PhD. Unfortunately, some of these collaborations were not always successful and not for lack of trying, but a ~50% success rate is not so bad. On that note, thank you to Prof. Chong Liu for the scientific discussions and collaborations with his student, Roselyn Rodrigues, a fruitful and ongoing collaboration that worked out even better than we had initially hoped. Thank you to several professors that provided

insights, discussions and even instruments when I needed them most, including Professor Alex Spokoyny, Heather Maynard and Hosea Nelson. Finally, I would like to thank two staff that were incredibly helpful in the day-to-day life of a grad student, Ricky Ruiz and Janette Kropat. I am convinced that the Molecular Sciences Building would cease to exist if it were not for those two.

At the start of my academic career, there were a number of teachers and professors that have since made a lasting impact. At the top of the list, however, is Professor Thai Thayumanavan, my undergraduate advisor at the University of Massachusetts, Amherst. Thai allowed me to come into his lab as a sophomore undergraduate, where I first learned about the concepts of "smart" polymers and drug delivery. I have him to thank for both setting me off on this career trajectory, as well as teaching me valuable lessons about the importance of communication in science, especially how to put together a scientific presentation that tells a story that will be of interest to a large, broad audience. Thai also set me up with a fantastic graduate student, Celia Homyak, who I owe a great deal to. Celia taught me the basics of polymer synthesis and materials formulations; tools that I borrowed heavily from when I began my graduate school career.

Finally, I would like to thank my friends and family. To my mother, father, grandparents and extended family for their advice and support throughout my undergraduate and graduate training, as well as my siblings Brian, Caroline and William for making me the person I am today. I had a number of friends, on both the East and West coasts, that made this journey a lot more fun than it would have been otherwise. That includes my friends back home, as well as new friends I made in Los Angeles. To my roommates, Edris Rivera, Rachael Day and Sydnee Green, you were a great group of people to survive a global pandemic with. It seems fitting to conclude my acknowledgments section with you three. I couldn't have done it without you all.

Chapter One is an unpublished perspective written by Dan Estabrook.

Chapter Two is a version of two published manuscripts, Estabrook, D. A.; Ennis, A.F.; Day, R.A.; Sletten, E. M. "Controlling nanoemulsion surface chemistry with poly(2-oxazoline) amphiphiles." *Chem. Sci.*, **2019**, *10*, 3994., and Day, R.A.; Estabrook, D.A.; Wu, C.; Chapman, J.O.; Togle, A.J.; Sletten, E. M. "Systematic study of perfluorocarbon nanoemulsions stabilized by polymer amphiphiles" *ACS Appl. Mater. Interfaces* **2020**, *12*, 38887. Estabrook, Day, Ennis, Wu, Chapman and Togle contributed to experimental work. Estabrook, Day and Sletten contributed to writing.

Chapter Three is a version of a published manuscript, Estabrook, D. A.; Ennis, A.F.; Day, R.A.; Sletten, E. M. "Controlling nanoemulsion surface chemistry with poly(2-oxazoline) amphiphiles." *Chem. Sci.*, **2019**, *10*, 3994. Estabrook, Ennis, and Day contributed to experimental work. Estabrook and Sletten contributed to writing.

Chapter Four is a version of an accepted manuscript, Estabrook, D.A.; Day, R.A.; Sletten, E. M. "Redox-responsive gene delivery from perfluorocarbon nanoemulsions through cleavable poly(2-oxazoline) surfactants. *Angew. Chem. Int. Ed.,* **2020**, *Accepted.* Estabrook and Day contributed to experimental work. Estabrook and Sletten contributed to writing.

Chapter Five is a version of a submitted manuscript, Estabrook, D.A.; Chapman, J.O.; Yen, S.T.; Campàs, O.; Sletten, E. M. "Macromolecular crowding as an intracellular stimulus for responsive nanomaterials." *In Review*. Estabrook, Chapman, and Yen contributed to experimental work. Estabrook and Sletten contributed to writing.

Chapter Six is a version of accepted manuscripts and those in preparation, as well as unpublished studies. Collaborations include the manuscripts Rodrigues, R.M.; Guan, X.; Iñiguez, J.A.; Estabrook, D.A.; Chapman, J.O.; Huang, S.; Sletten, E.M.; Liu, C. "Perfluorocarbon

nanoemulsion promotes the delivery of reducing equivalents for electricity-driven microbial CO_2 reduction", *Nat. Catal.*, **2019**, *2*, 407., and Lu, S.; Rodrigues, R.M.; Huang, S.; Estabrook, D.A.; Chapman, J.O.; Guan, Xun; Sletten E.M; Chong L. "Perfluorocarbon Nanoemulsions Create a Beneficial O_2 Microenvironment in N_2-fixing Biological | Inorganic Hybrid." *In Revision*., and a manuscript in preparation by Tian Deng. For unpublished studies, Estabrook is responsible for experimental work and writing.

Throughout these studies, Daniel Adam Estabrook was funded by the NIH (T32 training grant to D.A.E., 5T32GM067555-12), UCLA's Dissertation Year Fellowship and the Majeti-Alapati Fellowship. Additional funding sources include UCLA, the NSF MRI (CHE-1048804), University of California Cancer Research Coordinating Committee (CNR-18-524809), American Chemical Society Petroleum Research Fund (57379-DNI4), Alfred P. Sloan Award (FG-2018-10855), and Hellman Fellows Award. We thank the Spokoyny, Maynard, Garcia-Garibay and Deming groups for the use of equipment, as well as the Molecular Instrumentation Center.

BIOGRAPHICAL SKETCH

EDUCATION

University of California, Los Angeles 2018
Master of Science in Organic Chemistry GPA: 3.75 / 4.00

University of Massachusetts, Amherst 2016
B.S. in Chemistry *Cum Laude*, GPA: 3.71 / 4.00
B.A. in Philosophy Honors Thesis: "Stimuli-sensitive lipogels for use in protein delivery"

RESEARCH AND WORK EXPERIENCE

Sletten Research Group, UCLA June 2016 – Current

- Developing nanoemulsions that encapsulate (transiently) fluorous-soluble payloads, including drugs, dyes, and pDNA until release is triggered by intracellular stimuli (*e.g.,* reducing agents, protein concentrations)
- Synthesize custom poly(2-oxazoline) surfactants to address unmet needs in the bench-top stability, surface functionalization, and responsive capabilities of perfluorocarbon-in-water nanoemulsions *in vitro*
- Systematically study property-dependent nanomaterial cellular uptake, localization, and payload release
- Developed a novel methodology through which polymeric materials can respond to protein concentrations
- Collaborated with labs at UCLA and UCSB and have mentored two students now pursuing doctoral degrees

3M, St. Paul, MN 55144: R&D Intern June 2019 – August 2019

- Mid-stream PhD internship working in the Pressure Sensitive Adhesives (PSA) and Release Materials division of the Corporate Research Materials Laboratory, developing latex formulations that enhance adhesive performance by decoupling material properties (*e.g.,* peel/tack strength, shear resistance, *etc.*)
- Learned basic knowledge of polymer solution casting, adhesive properties and characterization techniques

Thayumanavan Research Group, UMass Amherst January 2014 – May 2016

- Integrated a hydrophilic copolymer network into liposomes for use in the encapsulation and release of biomolecules (*e.g.*, proteins and peptides) and small molecule therapeutics for intracellular and oral delivery
- Gained familiarity with controlled radical polymerizations and liposomal/hydrogel formulations

Weck Research Group, New York University May 2015 – August 2015

- Developed "patchy" colloids to induce self-assembly of silica nanoparticles through directional interactions

PCI Synthesis, Newburyport, MA 01950: Laboratory Aide April 2014 – January 2015

- Worked within the Quality Control department of a contract manufacturing organization, routinely performing analytical testing according to FDA and current good manufacturing practices regulations

AWARDS, HONORS AND FELLOWSHIPS:

Majeti-Alapati Dissertation Award (2021)
Dissertation Year Fellowship (2020–2021)
Donald J. Cram Excellence in Research Award (2020)
UCLA Chemistry and Biochemistry Excellence in Research Fellowship (2020)
Majeti-Alapati Fellowship (2020)
Christopher S. Foote Fellowship in Organic Chemistry (2019)
UCLA Excellence in Second Year Academics and Research Award (2019)
NIH UCLA Biotechnology Training in Biomedical Sciences and Engineering Fellowship (2017-2019)
UCLA Alumni Association Fellowship (2016-2018)
UCLA Graduate Dean's Scholar Award (2016)

PUBLICATIONS:

1. **Estabrook, D.A.**; Chapman, J.O.; Yen, S.T.; Campàs, O.; Sletten, E. M. "Macromolecular crowding as an intracellular stimulus for responsive nanomaterials." *In Revision.*
2. **Estabrook, D.A.**; Day, R.A.; Sletten, E. M. "Redox-responsive gene delivery from perfluorocarbon nanoemulsions through cleavable poly(2-oxazoline) surfactants." *Angew. Chem. Int. Ed.*, **2021**, *Accepted*. DOI: https://doi.org/10.1002/ange.202102413.
3. Lu, S.; Rodrigues, R.M.; Huang, S.; **Estabrook, D.A.**; Chapman, J.O.; Guan, Xun; Sletten E.M; Chong L. "Perfluorocarbon Nanoemulsions Create a Beneficial O_2 Microenvironment in N_2-fixing Biological | Inorganic Hybrid." *In Revision.*
4. **Estabrook, D.A.**; Sletten, E.M. "Printing Precise Materials with Visible Light." *ACS Cent. Sci.* **2020**, *6*, 1482. Highlighting article: "Rapid High Resolution Visible Light 3D Printing" *ACS Cent. Sci*. **2020**, *6*, 1555.
5. Day, R.A.; **Estabrook, D.A.**; Wu, C.; Chapman, J.O.; Togle, A.J.; Sletten, E. M. "Systematic study of perfluorocarbon nanoemulsions stabilized by polymer amphiphiles" *ACS Appl. Mater. Interfaces* **2020**, *12*, 38887.
6. Miller, M.A.*; Day, R.D.*; **Estabrook, D.A.***; Sletten, E.M. "A reduction-sensitive fluorous fluorogenic coumarin." *Synlett* **2020**, *31*, 450. *Authors contributed equally.
7. Rodrigues, R.M.; Guan, X.; Iñiguez, J.A.; **Estabrook, D.A.**; Chapman, J.O.; Huang, S.; Sletten, E.M.; Liu, C. "Perfluorocarbon nanoemulsion promotes the delivery of reducing equivalents for electricity-driven microbial CO_2 reduction", *Nat. Catal.*, **2019**, *2*, 407.
8. **Estabrook, D. A.**; Ennis, A.F.; Day, R.A.; Sletten, E. M. "Controlling nanoemulsion surface chemistry with poly(2-oxazoline) amphiphiles." *Chem. Sci.*, **2019**, *10*, 3994.
9. Day, R.A.; **Estabrook. D.A.**; Logan, J.K.; Sletten, E.M. "Fluorous photosensitizers enhance photodynamic therapy with perfluorocarbon nanoemulsions." *Chem. Commun.,* **2017**, *53*, 13043.

CHAPTER ONE

Perfluorocarbon Nanoemulsions as a Bioorthogonal Drug Delivery Platform

1.1 Perspective

The challenges associated with developing new drugs are well-appreciated, having an overall clinical success rate of ~14%.[1] Moreover, these numbers differ dramatically depending on the therapeutic group, with vaccines against infectious disease achieving a ~33% success rate, while oncological drugs are considerably less successful at ~3%. With these hurdles, R&D spending has continued to increase enormously—per the Congressional Budget Office, the pharmaceutical industry spent $83B on R&D, a number ~10x that which the industry spent per year in the 1980s. These investments have been fruitful, as four of the five most productive years in novel FDA approvals since 1993 have occurred from 2017–2020.[2] Additionally, recent years have seen an uprising interest in therapeutic modalities like antibodies and oligonucleotides, which themselves contain new sets of translational challenges.[3–6] At each step in the process, novel therapeutics–whether they be small molecules or biopharmaceuticals–must be screened for efficiency, specificity, biodistribution, and toxicity. An alternative, attractive approach is the concept of "packaging" therapeutics within a vehicle that traffics the therapeutic to its target site, such that the efficiency of the encapsulated (bio)molecule can be decoupled from its biodistribution (Figure 1.1).[7] These delivery vehicles can be found at the intersection of nanomaterials, chemistry, and biomedicine, spawning the field of nanomedicine.[8,9]

Though the goals of delivery vehicles are numerous, the first challenge is in increasing the half-life of the therapeutic agent. It is well-known that the physicochemical properties of vehicles

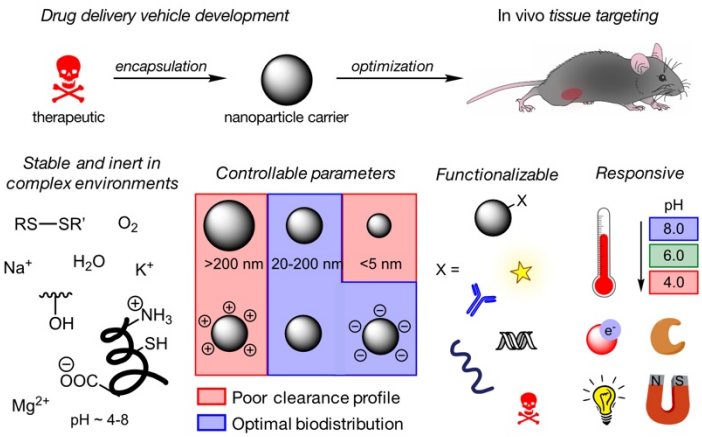

Figure 1.1. Drug delivery vehicles have gained popularity as a means to encapsulate and selectively deliver therapeutics *in vivo*. These carriers, like their encapsulated payload, must be optimized for a variety of parameters. Of these, considerations include stability and inertness in complex environments, reliably controlling size and surface charge, ease and modularity of functionalization, and engineering responsive behavior such that vehicles can respond to exogenous or endogenous stimuli.

influences their half-lives and biodistribution, including size, shape, surface charge, hydrophilicity, surface ligand identity and density (Figure 1.1).[10] Size is an early discriminating factor, and a general rule of thumb is that these nanomaterials must be above 10 nm to avoid renal clearance (*i.e.,* kidneys), but less than 200 nm to avoid activation of the complement system and accumulation in the liver and spleen.[11] This necessitates the formation of materials with a width ~1000 times thinner than a human hair. Fortunately, an explosion of interest within the last few decades in nanomaterials[12] for a variety of applications has better-informed us on ways to precisely control nanoparticle properties via either bottom-up or top-down techniques.[13] This has allowed researchers to systematically vary size and shape[14], though spherical nanomaterials remain dominant in the field due to their comparatively straight-forward methods of fabrication.[15] Surface properties have largely been controlled either *a priori* via an understanding of self-assembly dynamics in the nanoparticle formulations themselves (*e.g.,* within layer-by-layer[16], spherical nucleic acid[17], or lipid nanoparticle formulations[18]), or *a posteriori* via efficient surface functionalization chemistries (*e.g.,* alkyne-azide[19,20], Michael addition[21], carbodiimide[22], thiol-

ene[23], thiol-maleimide[24], ligand exchange[25], *etc.*). These conjugation methods have been employed for a variety of ligand attachments, including tissue-targeting moieties and "stealth" shielding agents to enhance therapeutic specificity and promote longer *in vivo* half-lives, respectively.[26–29] In either case, the density of functionalized ligand on the particle surface plays a significant role in their various applications.[30] Understanding and controlling physicochemical properties is a generic need that extends to all classes of nanocarriers from which one can choose (Figure 1.1).

The timeline of nanomedicine is often drawn to begin in 1965, the seminal report of the liposome. In the five decades since, the classes of nanomaterials with biomedical utility has expanded dramatically to include organic materials such as polymeric nanoparticles, micelles, dendrimers, emulsions and polymer-drug conjugates, along with inorganic materials including carbon nanotubes and nanoparticles with cores made up of silica, gold, iron oxide, or quantum dots (Figure 1.2).[31–35] These materials compose many of the abundant advanced pharmaceutical drug delivery systems to-date, particularly nanoparticles, emulsions, liposomes, and inorganic nanoparticles. With respect to the number of global clinic trials for each class, as of 2018 nanoparticles, liposomes and emulsions were employed in 601, 342 and 269 ongoing trials, respectively.[36] However, nanoparticles suffer from low translational efficiency, while liposomes and emulsions benefit from high translational efficiency.[36] Though emulsions and liposomes share

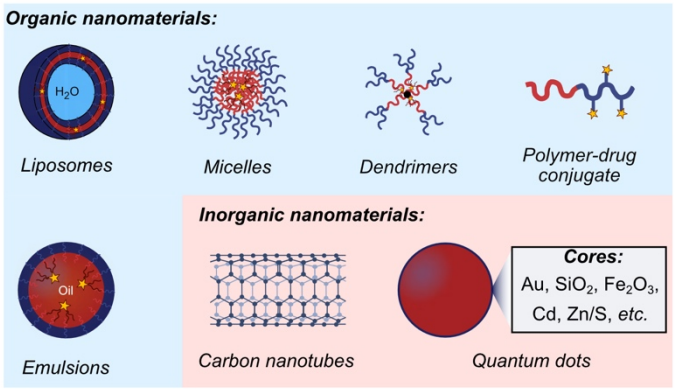

Figure 1.2. Classes of organic and inorganic nanomaterials with applications in biomedicine.

the similarity of a liquid interior core, when dispersed in water an oil-in-water emulsion will have a hydrophobic liquid core stabilized via a surfactant, while liposomes have an aqueous core stabilized by a lipid bilayer. This presents a large advantage for emulsion delivery systems, as the vast majority of FDA-approved drugs are hydrophobic.[37] As such, emulsions can encapsulate significant amounts of cargo.

Emulsions are liquid-in-liquid droplets with size distributions ranging from several nanometers to hundreds of micrometers (Figure 1.3). The formation of this liquid-liquid interface results in significant interfacial tension; as such, these systems are kinetically unstable and will phase separate over time.[38] Thus, amphiphilic molecules capable of reducing the interfacial tension between the immiscible emulsion core (dispersed phase) and surrounding aqueous environment (continuous phase) are necessary. These classes of molecules, called surfactants, play a critical role in the formation and stabilization of emulsions (Figure 1.3). Surfactant concentration plays a large role in emulsion size, where larger concentrations of surfactant generally give way to smaller droplets. Surfactant concentration is one characteristic that distinguishes nanoemulsions (<500 nm or so[39]) from macroemulsions (>500 nm), where typically nanoemulsions need high concentrations of surfactant.[40] Additionally, nanoemulsions are typically made through intensive, high energy processes (*e.g.,* ultrasonication, homogenization, or microfluidization[41]), while macroemulsions can be made comparatively low energy processes, like vortexing or hand-mixing. It is important

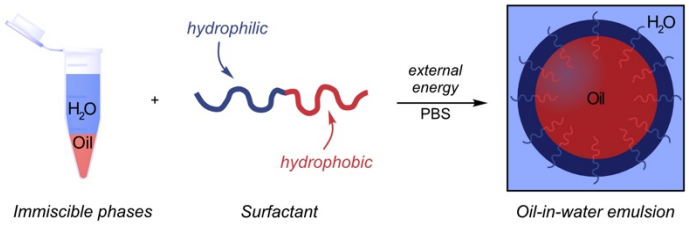

Figure 1.3. Emulsions are formed through a simple, one-step approach involving two immiscible phases (*e.g.,* oil and water), an amphiphilic surfactant, and input of external energy. The surfactant assembles at the oil-water interface to reduce interfacial tension, stabilizing the vehicles.

to note that not all classes of emulsions are inherently thermodynamically unstable, microemulsions allow for the spontaneous formation of sub-500 nm emulsions that are thermodynamically stable, however these materials are comparatively rare and have been extensively reviewed elsewhere.[42]

Surfactants can be composed of small molecules or polymers, and their structures can vary in overall complexity. Being located directly at the interface, surfactants affect surface properties like the overall charge of the droplets. For instance, rather simple phospholipids and poloxamers are routinely used for industrial applications, while more recently engineered custom peptide[43–45], polymer,[46] and nanoparticle[47] surfactants have been employed for responsive materials[48,49] and sophisticated emulsion architectures (*e.g.*, double emulsions and Janus droplets). Slight changes in surfactant structure can drastically affect the physiochemical properties of the emulsions.[50] As previously mentioned, surfactants also modify the charge of the overall droplets. We have studied the influence of charge in emulsions uptaken *in cellulo* and *in vivo*, where cationic emulsions are more readily uptaken than their anionic or neutral counterparts in both macrophage and non-macrophage cell lines.[51] Surface charge has also been employed as a surface functionalization technique, where electrostatic interactions are leveraged for the deposition of oppositely charged moieties, like polysaccharides[52,53] and biopolymers[54]. These surfactants can likewise be modified in order to affect the overall biodistribution of the employed emulsions. A common polymeric shielding agent, poly(ethylene glycol) (PEG) is extensively used in (bio)pharmaceuticals to reduce the blood clearance of PEGylated materials.[55] PEG-containing surfactants have likewise been employed within emulsion formulations in order to reduce reticuloendothelial system (RES) uptake and extend the circulation time of emulsions.[56] In addition to enhancing serum half-lives, surfactants can be modified to include tissue-targeting moieties. Previously employed targeting

agents include folic acid[57,58], RGD peptides[59], antibodies and their fragments, and oligonucleotides.[60] Ultimately, surfactants represent the primary ingredient through which emulsion surface chemistry can be controlled. The ideal surfactant for employing emulsions within biomedical applications is one which is (i) capable of stabilizing small, nano-sized droplets (<300 nm) to avoid rapid clearance, (ii) endows the surface of the material with stealth properties, (iii) is easily functionalizable, and (iv) can be made stimuli-responsive, such that emulsions can respond to environmental changes. In the design of a functionalizable, bioorthogonal drug delivery system, a surfactant that addresses these concerns is the first layer of the control. The second will be the interior core of the emulsion.

Traditional oil-in-water emulsions are composed of hydrocarbon oils. Of the five currently FDA-approved emulsion injections, the oil core is either made up of (or encapsulates) soybean oil, Clevipidine, triglycerides, amino acids, fish oil and Aprepitant.[36] In three of these five systems, the oily core is the biotherapeutic itself, typically essential fatty acids for parenteral nutrition. However, these hydrocarbons have an inherent limitation—they are generally miscible with lipid environments found within the body. To demonstrate this, we have previously rocked an aqueous suspension of olive oil-in-water nanoemulsions alongside 1-octanol as a cell-membrane mimic and observed that the interior hydrocarbon payload is rapidly pulled into the 1-octanol phase.[61] This presents a significant challenge *in cellulo* and *in vivo*, where emulsions will almost certainly encounter these types of environments. An alternative concept is the use of an interior oil which is miscible with neither aqueous nor organic environments. Towards this, we looked to perfluorocarbon oils as the core of our bioorthogonal vehicles.

Perfluorocarbons (PFCs) are fluorine-substituted hydrocarbons. The C–F bond has unique properties in and of itself; for example, its high bond strength renders these materials unusually

stable to oxidation, high temperatures and chemical treatments.[62] However, it is the *universal* substitution with fluorine that gives rise to many more interesting properties for PFC materials. Due to the strong electronegativity and low polarizability of the fluorine atom and its disinclination to participate in van der Waals interactions, PFCs will phase separate when mixed with aqueous or organic solvents. The weak intermolecular cohesiveness of PFCs also gives rise to exceptionally high gas solubilities within these liquids, with oxygen being solubilized at 12–20x higher levels in PFCs than within water.[63,64] This high oxygen solubility has made PFCs of interest as artificial blood substitutes since the findings of Clark and coworkers in 1962.[65] In these seminal reports, mice submerged in oxygenated PFC continued to breath due to the high O_2 solubility of bioinert PFCs. The immediate use of PFCs as blood substitutes was, of course, limited in that blood functions to deliver important polar compounds (*e.g.*, glucose, salts, metabolites) that are insoluble in PFCs. Clinical translation of these perfluorinated liquids thus required that they could be co-delivered in an aqueous continuous phase, thus launching the interest in PFC emulsions (Figure 1.4).[66] The first generation of PFC nanoemulsions, known as Fluosol-DA, were composed of perfluorodecalin (PFD, **1.1**, Figure 1.4) and perfluorotripropylamine (PFTPA) and stabilized by Pluronic F-68 copolymer.[67] These formulations were developed and clinically tested throughout Japan and US, achieving FDA- approval in 1989. However, Fluosol was discontinued a mere 6 years later due to a number of challenges, including droplet polydispersity, side-effects including complement activation[68], stability issues during storage, and the need to be thawed and re-oxygenated prior to administration.[67] Nearly all of these challenges were linked back to the use of Pluronic F-68 as a surfactant, with researchers at the time noting "We suspect that the toxic response noted above is due, in large measure, to the specific emulsifier used, Pluronic F-68, as appears to be the case for complement activation in man."[69,70] Pluronic F-68 belongs to a class of

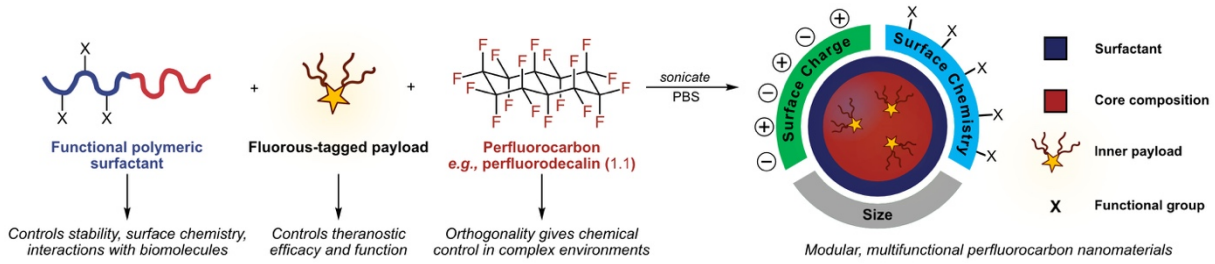

Figure 1.4. Perfluorocarbon (PFC) nanoemulsions are formed via a functional polymeric amphiphile, a fluorous-soluble payload, and an interior PFC phase (*e.g.,* perfluorodecalin, **1.1**). After ultrasonication, homogenous PFC-in-water emulsions are formed with physicochemical parameters controlled by the surfactant, including size, surface charge and surface chemistry.

polymeric surfactants known as poloxamers—triblock copolymers composed of an interior hydrophobic poly(propylene oxide) (PEO) flanked by hydrophilic PEG blocks. These were the early days of PEGylation[71], however, and it is understood that repeated administrations of PEGylated products can sometimes generate anti-PEG antibodies, resulting in a loss of therapeutic efficacy, rapid clearance[72–74], and adverse side-effects.[73,75,76] Thus, in addition to the earlier criteria established for surfactants, one should consider PEG alternatives as the hydrophilic block.[77] Of these, one such alternative is that of poly(2-oxazoline)s (POx).

POx are a class of peptidomimetic polyamides, synthesized via a controlled ring-opening polymerization (Figure 1.5).[78,79] Polymer side chains are controlled via the 2-substituted-2-oxazoline (ROx), for which various substitutions are known.[80] These range from commercially available, strongly hydrophilic simple aliphatic side-chains[79], like 2-methyl-2-oxazoline (MeOx, **1.2**) and 2-ethyl-2-oxazoline (EtOx, **1.3**), to hydrophobic side chains like 2-nonyl-2-oxazoline (NonOx, **1.4**) and 2-(perfluorohexyl)ethyl-2-oxazoline (FOx, **1.5**) to functionalizable variants synthesized through multiple steps, *e.g.*, , an alkene[81] (EneOx, **1.6**), alkyne[82] (PyneOx, **1.7**), or methyl ester[83].[84] The controlled, living nature of the polymerization results in controllable block

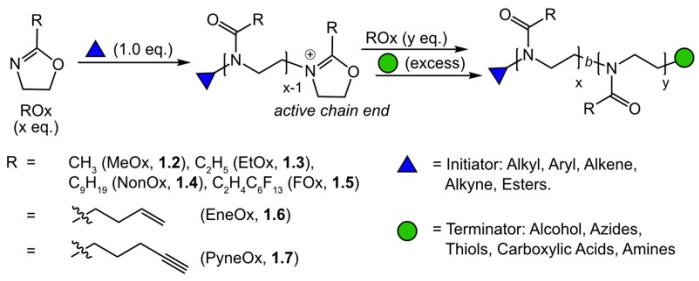

Figure 1.5. Poly(2-oxazoline)s (POx) are synthesized via a controlled ring-opening polymerization. Side-chains of 2-substituted-2-oxazolines (ROx) can be modified with aliphatic (**1.2**–**1.4**), fluorous (**1.5**), alkene (**1.6**) or alkyne (**1.7**) containing side chains. Electrophilic initiators and nucleophilic terminators provide other routes of functionalization at the head and tail of the polymer, respectively.

lengths, molecular weights, dispersities and polymer architectures, allowing access to block copolymers, star polymers, graft copolymers and polymeric conjugates. Additionally, POx can undergo microwave-assisted polymerizations, allowing access to block copolymer libraries within minutes to hours. Electrophilic initiators allow for rapid rates of initiation, and include several classes like triflates, tosylates, nosylates, and alkylhalides.[80] Conversely, nucleophilic terminating agents cap the α-terminus, and range from using water (or hydroxide) to introduce an alcohol, to functional handles like azides[85], thiols[86], carboxylic acids[87], and primary[88], secondary[89] and even tertiary amines[90]. These are only a handful of selected examples within a vast array of initiators and terminating agents, which have been extensively reviewed elsewhere.[80,91] Ultimately, POx represents a multifunctional polymer scaffold, and one which continues to grow due to its interest as a PEG alternative. In particular, P(MeOx) and P(EtOx) have been shown to be more hydrophilic than their PEG counterparts and can likewise be used to endow stealth properties to POx-conjugates.[92–95] These materials have even been explored clinically, with Serina Therapeutics forming a pipeline of P(EtOx)-based clickable conjugates via esterase-responsive cleavable linkers to pendent drug molecules, namely rotigotine and irinotecan, for neurological and oncological therapies, respectively.[96] The former of these is currently in Phase II clinical trials, while the latter

is being explored for folate-targeted chemotherapy.[97,98] These works, among others, have demonstrated that POx is non-immunogenic and largely excreted via the kidneys.[94,97] Collectively, the many promising benefits of this class of polymers led us to establish our surfactant platform based on POx.

This thesis is dedicated to studying how custom POx surfactants can be employed to control the complexity of PFC-in-water emulsions as bioorthogonal delivery vehicles. The second chapter focuses on the early development of POx within the lab, investigating how relatively simple di- and triblock copolymer structures can elucidate structure-property relationships *in vitro* and *in cellulo* for the emulsions they stabilize. This work serves as a launching point for the third chapter, in which we take promising amphiphiles and add functional handles into them, allowing for emulsion surface functionalization and controllable cellular uptake. The fourth chapter focuses on stimuli-responsive POx surfactants, and how a simple two-atom linker between blocks can dictate macro- and nanoscale droplet behavior. Additionally, this chapter describes the first fluorous tagging strategy that enables the encapsulation of hydrophilic polynucleotides, namely plasmid DNA, into the fluorous phase. The fifth chapter demonstrates how simple P(EtOx)-based amphiphiles enable a novel methodology for intracellular payload release by establishing macromolecular protein crowding as a stimulus for responsive delivery vehicles. Finally, the sixth chapter highlights collaborative work with our PFC and POx platforms, as well as preliminary findings that serve as proof of principle for future projects within the group.

1.2 References

(1) Wong, C. H.; Siah, K. W.; Lo, A. W. Estimation of Clinical Trial Success Rates and Related Parameters. *Biostatistics* **2019**, *20*, 273–286.

(2) Mullard, A. 2020 FDA Drug Approvals. *Nat. Rev. Drug Discov.* **2021**, *20*, 85–90.

(3) Roberts, T. C.; Langer, R.; Wood, M. J. A. Advances in Oligonucleotide Drug Delivery. *Nat. Rev. Drug Discov.* **2020**, *19*, 673–694.

(4) Dhuri, K.; Bechtold, C.; Quijano, E.; Pham, H.; Gupta, A.; Vikram, A.; Bahal, R. Antisense Oligonucleotides: An Emerging Area in Drug Discovery and Development. *J. Clin. Med.* **2020**, *9*, 2004.

(5) Edvard Smith, C. I.; Zain, R. Therapeutic Oligonucleotides: State of the Art. *Annu. Rev. Pharmacol. Toxicol.* **2019**, *59*, 605–630.

(6) Lu, R. M.; Hwang, Y. C.; Liu, I. J.; Lee, C. C.; Tsai, H. Z.; Li, H. J.; Wu, H. C. Development of Therapeutic Antibodies for the Treatment of Diseases. *J. Biomed. Sci.* **2020**, *27*.

(7) Tiwari, G.; Tiwari, R.; Bannerjee, S.; Bhati, L.; Pandey, S.; Pandey, P.; Sriwastawa, B. Drug Delivery Systems: An Updated Review. *Int. J. Pharm. Investig.* **2012**, *2*, 2.

(8) Zhang, L.; Gu, F. X.; Chan, J. M.; Wang, A. Z.; Langer, R. S.; Farokhzad, O. C. Nanoparticles in Medicine: Therapeutic Applications and Developments. *Clin. Pharmacol. Ther.* **2008**, *83*, 761–769.

(9) Soares, S.; Sousa, J.; Pais, A.; Vitorino, C. Nanomedicine: Principles, Properties, and Regulatory Issues. *Front. Chem.* **2018**, *6*.

(10) Farokhzad, O. C.; Langer, R. Impact of Nanotechnology on Drug Delivery. *ACS Nano* **2009**, *3*, 16–20.

(11) Mitchell, M. J.; Billingsley, M. M.; Haley, R. M.; Wechsler, M. E.; Peppas, N. A.; Langer, R. Engineering Precision Nanoparticles for Drug Delivery. *Nat. Rev. Drug Discov.* **2021**, *20*, 101–124.

(12) Whitesides, G. M. The "right" Size in Nanobiotechnology. *Nat. Biotechnol.* **2003**, *21*, 1161–1165.

(13) Gratton, S. E. A.; Ropp, P. A.; Pohlhaus, P. D.; Luft, J. C.; Madden, V. J.; Napier, M. E.; DeSimone, J. M. The Effect of Particle Design on Cellular Internalization Pathways. *Proc. Natl. Acad. Sci. U. S. A.* **2008**, *105*, 11613–11618.

(14) Liu, Y.; Tan, J.; Thomas, A.; Ou-Yang, D.; Muzykantov, V. R. The Shape of Things to Come: Importance of Design in Nanotechnology for Drug Delivery. *Ther. Deliv.* **2012**, *3*, 181–194.

(15) Nejati, S.; Mohseni Vadeghani, E.; Khorshidi, S.; Karkhaneh, A. Role of Particle Shape on Efficient and Organ-Based Drug Delivery. *Eur. Polym. J.* **2020**, *122*.

(16) Alkekhia, D.; Hammond, P. T.; Shukla, A. Layer-by-Layer Biomaterials for Drug Delivery. *Annu. Rev. Biomed. Eng.* **2020**, *22*, 1–24.

(17) Cutler, J. I.; Auyeung, E.; Mirkin, C. A. Spherical Nucleic Acids. *J. Am. Chem. Soc.* **2012**, *134*, 1376–1391.

(18) Scioli Montoto, S.; Muraca, G.; Ruiz, M. E. Solid Lipid Nanoparticles for Drug Delivery: Pharmacological and Biopharmaceutical Aspects. *Front. Mol. Biosci.* **2020**, *7*.

(19) Yi, G.; Son, J.; Yoo, J.; Park, C.; Koo, H. Application of Click Chemistry in Nanoparticle Modification and Its Targeted Delivery. *Biomater. Res.* **2018**, *22*.

(20) Li, N.; Binder, W. H. Click-Chemistry for Nanoparticle-Modification. *J. Mater. Chem.* **2011**, *21*, 16717–16734.

(21) Nair, D. P.; Podgórski, M.; Chatani, S.; Gong, T.; Xi, W.; Fenoli, C. R.; Bowman, C. N. The Thiol-Michael Addition Click Reaction: A Powerful and Widely Used Tool in Materials Chemistry. *Chem. Mater.* **2014**, *26*, 724–744.

(22) Thorek, D. L. J.; Elias, D. R.; Tsourkas, A. Comparative Analysis of Nanoparticle-Antibody Conjugations: Carbodiimide versus Click Chemistry. *Mol. Imaging* **2009**, *8*, 221–229.

(23) Liu, Y.; Hou, W.; Sun, H.; Cui, C.; Zhang, L.; Jiang, Y.; Wu, Y.; Wang, Y.; Li, J.; Sumerlin, B. S.; et al. Thiol-Ene Click Chemistry: A Biocompatible Way for Orthogonal Bioconjugation of Colloidal Nanoparticles. *Chem. Sci.* **2017**, *8*, 6182–6187.

(24) Martínez-Jothar, L.; Doulkeridou, S.; Schiffelers, R. M.; Sastre Torano, J.; Oliveira, S.; van Nostrum, C. F.; Hennink, W. E. Insights into Maleimide-Thiol Conjugation Chemistry: Conditions for Efficient Surface Functionalization of Nanoparticles for Receptor Targeting. *J. Control. Release* **2018**, *282*, 101–109.

(25) Guerrini, L.; Alvarez-Puebla, R. A.; Pazos-Perez, N. Surface Modifications of Nanoparticles for Stability in Biological Fluids. *Materials (Basel).* **2018**, *11*.

(26) Bazak, R.; Houri, M.; El Achy, S.; Kamel, S.; Refaat, T. Cancer Active Targeting by Nanoparticles: A Comprehensive Review of Literature. *J. Cancer Res. Clin. Oncol.* **2015**, *141*, 769–784.

(27) Brannon-Peppas, L.; Blanchette, J. O. Nanoparticle and Targeted Systems for Cancer Therapy. *Adv. Drug Deliv. Rev.* **2012**, *64*, 206–212.

(28) Steichen, S. D.; Caldorera-Moore, M.; Peppas, N. A. A Review of Current Nanoparticle and Targeting Moieties for the Delivery of Cancer Therapeutics. *Eur. J. Pharm. Sci.* **2013**, *48*, 416–427.

(29) Jokerst, J. V.; Lobovkina, T.; Zare, R. N.; Gambhir, S. S. Nanoparticle PEGylation for Imaging and Therapy. *Nanomedicine* **2011**, *6*, 715–728.

(30) Elias, D. R.; Poloukhtine, A.; Popik, V.; Tsourkas, A. Effect of Ligand Density, Receptor Density, and Nanoparticle Size on Cell Targeting. *Nanomedicine Nanotechnology, Biol. Med.* **2013**, *9*, 194–201.

(31) Euliss, L. E.; DuPont, J. A.; Gratton, S.; DeSimone, J. Imparting Size, Shape, and Composition Control of Materials for Nanomedicine. *Chem. Soc. Rev.* **2006**, *35*, 1095–1104.

(32) Patra, J. K.; Das, G.; Fraceto, L. F.; Campos, E. V. R.; Rodriguez-Torres, M. D. P.; Acosta-Torres, L. S.; Diaz-Torres, L. A.; Grillo, R.; Swamy, M. K.; Sharma, S.; et al. Nano Based Drug Delivery Systems: Recent Developments and Future Prospects 10 Technology. *J. Nanobiotechnology* **2018**, *16*.

(33) Ramos, A. P.; Cruz, M. A. E.; Tovani, C. B.; Ciancaglini, P. Biomedical Applications of Nanotechnology. *Biophys. Rev.* **2017**, *9*, 79–89.

(34) Srinivasan, M.; Rajabi, M.; Mousa, S. A. Multifunctional Nanomaterials and Their Applications in Drug Delivery and Cancer Therapy. *Nanomaterials* **2015**, *5*, 1690–1703.

(35) Jiang, W.; Kim, B. Y. S.; Rutka, J. T.; Chan, W. C. W. Advances and Challenges of Nanotechnology-Based Drug Delivery Systems. *Expert Opin. Drug Deliv.* **2007**, *4*, 621–633.

(36) Zhong, H.; Chan, G.; Hu, Y.; Hu, H.; Ouyang, D. A Comprehensive Map of FDA-Approved Pharmaceutical Products. *Pharmaceutics* **2018**, *10*, 1.

(37) Shultz, M. D. Two Decades under the Influence of the Rule of Five and the Changing Properties of Approved Oral Drugs. *J. Med. Chem.* **2019**, *62*, 1701–1714.

(38) Ostróżka-Cieślik, A.; Sarecka-Hujar, B. The Use of Nanotechnology in Modern Pharmacotherapy. *Multifunct. Syst. Comb. Deliv. Biosensing Diagnostics* **2017**, 139–158.

(39) Aboofazeli, R. Nanometric-Scaled Emulsions (Nanoemulsions). *Iran. J. Pharm. Res.* **2010**, *9*, 325–326.

(40) Azeem, A.; Rizwan, M.; Ahmad, F. J.; Iqbal, Z.; Khar, R. K.; Aqil, M.; Talegaonkar, S. Nanoemulsion Components Screening and Selection: A Technical Note. *AAPS PharmSciTech* **2009**, *10*, 69–76.

(41) Teng, F.; He, M.; Xu, J.; Chen, F.; Wu, C.; Wang, Z.; Li, Y. Effect of Ultrasonication on the Stability and Storage of a Soy Protein Isolate-Phosphatidylcholine Nanoemulsions. *Sci. Rep.* **2020**, *10*.

(42) McClements, D. J. Nanoemulsions versus Microemulsions: Terminology, Differences, and Similarities. *Soft Matter* **2012**, *8*, 1719–1729.

(43) Dexter, A. F.; Malcolm, A. S.; Middelberg, A. P. J. Reversible Active Switching of the Mechanical Properties of a Peptide Film at a Fluid-Fluid Interface. *Nat. Mater.* **2006**, *5*, 502–506.

(44) Hanson, J. A.; Chang, C. B.; Graves, S. M.; Li, Z.; Mason, T. G.; Deming, T. J. Nanoscale Double Emulsions Stabilized by Single-Component Block Copolypeptides. *Nature* **2008**, *455*, 85–88.

(45) Medina, S. H.; Michie, M. S.; Miller, S. E.; Schnermann, M. J.; Schneider, J. P. Fluorous Phase-Directed Peptide Assembly Affords Nano-Peptisomes Capable of Ultrasound-Triggered Cellular Delivery. *Angew. Chem. Int. Ed.* **2017**, *56*, 11404–11408.

(46) Huang, Y.; Vezeridis, A. M.; Wang, J.; Wang, Z.; Thompson, M.; Mattrey, R. F.; Gianneschi, N. C. Polymer-Stabilized Perfluorobutane Nanodroplets for Ultrasound

Imaging Agents. *J. Am. Chem. Soc.* **2017**, *139*, 15–18.

(47) Yang, Z.; Wei, J.; Sobolev, Y. I.; Grzybowski, B. A. Systems of Mechanized and Reactive Droplets Powered by Multi-Responsive Surfactants. *Nature* **2018**, *553*, 313–318.

(48) Zarzar, L. D.; Sresht, V.; Sletten, E. M.; Kalow, J. A.; Blankschtein, D.; Swager, T. M. Dynamically Reconfigurable Complex Emulsions via Tunable Interfacial Tensions. *Nature* **2015**, *518*, 520–524.

(49) Brown, P.; Butts, C. P.; Eastoe, J. Stimuli-Responsive Surfactants. *Soft Matter* **2013**, *9*, 2365–2374.

(50) McClements, D. J. Advances in Fabrication of Emulsions with Enhanced Functionality Using Structural Design Principles. *Curr. Opin. Colloid Interface Sci.* **2012**, *17*, 235–245.

(51) Estabrook, D. A.; Ennis, A. F.; Day, R. A.; Sletten, E. M. Controlling Nanoemulsion Surface Chemistry with Poly(2-Oxazoline) Amphiphiles. *Chem. Sci.* **2019**, *10*, 3994–4003.

(52) Tokle, T.; Lesmes, U.; McClements, D. J. Impact of Electrostatic Deposition of Anionic Polysaccharides on the Stability of Oil Droplets Coated by Lactoferrin. *J. Agric. Food Chem.* **2010**, *58*, 9825–9832.

(53) Mundo, J. L. M.; Zhou, H.; Tan, Y.; Liu, J.; McClements, D. J. Enhancing Emulsion Functionality Using Multilayer Technology: Coating Lipid Droplets with Saponin-Polypeptide-Polysaccharide Layers by Electrostatic Deposition. *Food Res. Int.* **2021**, *140*.

(54) Jo, Y. J.; Chun, J. Y.; Kwon, Y. J.; Min, S. G.; Choi, M. J. Formulation Development of Multilayered Fish Oil Emulsion by Using Electrostatic Deposition of Charged Biopolymers. *Int. J. Food Eng.* **2015**, *11*, 31–39.

(55) Turecek, P. L.; Bossard, M. J.; Schoetens, F.; Ivens, I. A. PEGylation of

Biopharmaceuticals: A Review of Chemistry and Nonclinical Safety Information of Approved Drugs. *J. Pharm. Sci.* **2016**, *105*, 460–475.

(56) Liu, F.; Liu, D. Long-Circulating Emulsions (Oil-in-Water) as Carriers for Lipophilic Drugs. *Pharm. Res. An Off. J. Am. Assoc. Pharm. Sci.* **1995**, *12*, 1060–1064.

(57) Kim, S. H.; Kim, J. K.; Lim, S. J.; Park, J. S.; Lee, M. K.; Kim, C. K. Folate-Tethered Emulsion for the Target Delivery of Retinoids to Cancer Cells. *Eur. J. Pharm. Biopharm.* **2008**, *68*, 618–625.

(58) Ganta, S.; Singh, A.; Rawal, Y.; Cacaccio, J.; Patel, N. R.; Kulkarni, P.; Ferris, C. F.; Amiji, M. M.; Coleman, T. P. Formulation Development of a Novel Targeted Theranostic Nanoemulsion of Docetaxel to Overcome Multidrug Resistance in Ovarian Cancer. *Drug Deliv.* **2016**, *23*, 968–980.

(59) Gianella, A.; Jarzyna, P. A.; Mani, V.; Ramachandran, S.; Calcagno, C.; Tang, J.; Kann, B.; Dijk, W. J. R.; Thijssen, V. L.; Griffioen, A. W.; et al. Multifunctional Nanoemulsion Platform for Imaging Guided Therapy Evaluated in Experimental Cancer. *ACS Nano* **2011**, *5*, 4422–4433.

(60) Sánchez-López, E.; Guerra, M.; Dias-Ferreira, J.; Lopez-Machado, A.; Ettcheto, M.; Cano, A.; Espina, M.; Camins, A.; Garcia, M. L.; Souto, E. B. Current Applications of Nanoemulsions in Cancer Therapeutics. *Nanomaterials* **2019**, *9*.

(61) Day, R. A.; Estabrook, D. A.; Logan, J. K.; Sletten, E. M. Fluorous Photosensitizers Enhance Photodynamic Therapy with Perfluorocarbon Nanoemulsions. *Chem. Commun.* **2017**, *53*, 13043–13046.

(62) Gladysz, J. A.; Curran, D. P.; Horváth, I. T. Handbook of Fluorous Chemistry. *Handb. Fluorous Chem.* **2005**, 1–595.

(63) Fraker, C. A.; Mendez, A. J.; Stabler, C. L. Complementary Methods for the Determination of Dissolved Oxygen Content in Perfluorocarbon Emulsions and Other Solutions. *J. Phys. Chem. B* **2011**, *115*, 10547–10552.

(64) Riess, J. G.; Riess, J. G. Oxygen Carriers ("blood Substitutes") - Raison d'etre, Chemistry, and Some Physiology. *Chem. Rev.* **2001**, *101*, 2797–2919.

(65) Clark, L. C.; Gollan, F. Survival of Mammals Breathing Organic Liquids Equilibrated with Oxygen at Atmospheric Pressure. *Science (80-.).* **1966**, *152*, 1755–1756.

(66) Sloviter, H. A.; Kamimoto, T. Erythrocyte Substitute for Perfusion of Brain. *Nature* **1967**, *216*, 458–460.

(67) Vorob'ev, S. I. First- and Second-Generation Perfluorocarbon Emulsions. *Pharm. Chem. J.* **2009**, *43*, 209–218.

(68) Riess, J. G.; Krafft, M. P. Fluorocarbon Emulsions as in Vivo Oxygen Delivery Systems. Background and Chemistry. *Blood Substitutes* **2006**, 259–275.

(69) Goodman, R. L.; Moore, R. E.; Davis, M. E.; Stokes, D.; Yuhas, J. M. Perfluorocarbon Emulsions in Cancer Therapy: Preliminary Observations on Presently Available Formulations. *Int. J. Radiat. Oncol. Biol. Phys.* **1984**, *10*, 1421–1424.

(70) Vercellotti, G. M.; Hammerschmidt, D. E.; Craddock, P. R.; Jacob, H. S. Activation of Plasma Complement by Perfluorocarbon Artificial Blood: Probable Mechanism of Adverse Pulmonary Reactions in Treated Patients and Rationale for Corticosteroid Prophylaxis. *Blood* **1982**, *59*, 1299–1304.

(71) Hoffman, A. S. The Early Days of PEG and PEGylation (1970s–1990s). *Acta Biomater.* **2016**, *40*, 1–5.

(72) Su, Y.; Wang, L.; Liang, K.; Liu, M.; Liu, X.; Song, Y.; Deng, Y. The Accelerated Blood

Clearance Phenomenon of PEGylated Nanoemulsion upon Cross Administration with Nanoemulsions Modified with Polyglycerin. *Asian J. Pharm. Sci.* **2018**, *13*, 44–53.

(73) Ishida, T.; Kiwada, H. Accelerated Blood Clearance (ABC) Phenomenon upon Repeated Injection of PEGylated Liposomes. *Int. J. Pharm.* **2008**, *354*, 56–62.

(74) Jiao, J.; Jiao, X.; Wang, C.; Wei, L.; Wang, G.; Deng, Y.; Song, Y. The Contribution of PEG Molecular Weights in PEGylated Emulsions to the Various Phases in the Accelerated Blood Clearance (ABC) Phenomenon in Rats. *AAPS PharmSciTech* **2020**, *21*.

(75) Zhang, P.; Sun, F.; Liu, S.; Jiang, S. Anti-PEG Antibodies in the Clinic: Current Issues and beyond PEGylation. *J. Control. Release* **2016**, *244*, 184–193.

(76) Garay, R. P.; El-Gewely, R.; Armstrong, J. K.; Garratty, G.; Richette, P. Antibodies against Polyethylene Glycol in Healthy Subjects and in Patients Treated with PEG-Conjugated Agents. *Expert Opin. Drug Deliv.* **2012**, *9*, 1319–1323.

(77) Thi, T. T. H.; Pilkington, E. H.; Nguyen, D. H.; Lee, J. S.; Park, K. D.; Truong, N. P. The Importance of Poly(Ethylene Glycol) Alternatives for Overcoming PEG Immunogenicity in Drug Delivery and Bioconjugation. *Polymers* **2020**, *12*.

(78) Hoogenboom, R. Poly(2-Oxazoline)s: A Polymer Class with Numerous Potential Applications. *Angew. Chem. Int. Ed.* **2009**, *48*, 7978–7994.

(79) Luxenhofer, R.; Han, Y.; Schulz, A.; Tong, J.; He, Z.; Kabanov, A. V.; Jordan, R. Poly(2-Oxazoline)s as Polymer Therapeutics. *Macromol. Rapid Commun.* **2012**, *33*, 1613–1631.

(80) Glassner, M.; Vergaelen, M.; Hoogenboom, R. Poly(2-Oxazoline)s: A Comprehensive Overview of Polymer Structures and Their Physical Properties. *Polym. Int.* **2018**, *67*, 32–45.

(81) Gress, A.; Völkel, A.; Schlaad, H. Thio-Click Modification of Poly[2-(3-Butenyl)-2-

Oxazoline]. *Macromolecules* **2007**, *40*, 7928–7933.

(82) Luxenhofer, R.; Jordan, R. Click Chemistry with Poly(2-Oxazoline)S. *Macromolecules* **2006**, *39*, 3509–3516.

(83) Bouten, P. J. M.; Hertsen, D.; Vergaelen, M.; Monnery, B. D.; Boerman, M. A.; Goossens, H.; Catak, S.; Van Hest, J. C. M.; Van Speybroeck, V.; Hoogenboom, R. Accelerated Living Cationic Ring-Opening Polymerization of a Methyl Ester Functionalized 2-Oxazoline Monomer. *Polym. Chem.* **2015**, *6*, 514–518.

(84) Fijten, M. W. M.; Haensch, C.; Lankvelt, B. M. V.; Hoogenboom, R.; Schubert, U. S. Clickable Poly(2-Oxazoline)s as Versatile Building Blocks. *Macromol. Chem. Phys.* **2008**, *209*, 1887–1895.

(85) Volet, G.; Lav, T. X.; Babinot, J.; Amiel, C. Click-Chemistry: An Alternative Way to Functionalize Poly(2-Methyl-2- Oxazoline). *Macromol. Chem. Phys.* **2011**, *212*, 118–124.

(86) Hsiue, G. H.; Chiang, H. Z.; Wang, C. H.; Juang, T. M. Nonviral Gene Carriers Based on Diblock Copolymers of Poly(2-Ethyl-2- Oxazoline) and Linear Polyethylenimine. *Bioconjug. Chem.* **2006**, *17*, 781–786.

(87) Miyamoto, M.; Naka, K.; Tokumizu, M.; Saegusa, T. End Capping of Growing Species of Poly(2-Oxazoline) with Carboxylic Acid: A Novel and Convenient Route To Prepare Vinyl- and Carboxy-Terminated Macromonomers. *Macromolecules* **1989**, *22*, 1604–1607.

(88) Volet, G.; Lasne Deschamps, A. C.; Catherine, A. Association of Hydrophobically α,ω-End-Capped Poly(2-Methyl-2-Oxazoline) in Water. *J. Polym. Sci. Part A Polym. Chem.* **2010**.

(89) Stadermann, J.; Komber, H.; Erber, M.; Däbritz, F.; Ritter, H.; Voit, B. Diblock Copolymer Formation via Self-Assembly of Cyclodextrin and Adamantyl End-

Functionalized Polymers. *Macromolecules* **2011**, *44*, 3250–3259.

(90) Waschinski, C. J.; Tiller, J. C. Poly(Oxazoline)s with Telechelic Antimicrobial Functions. *Biomacromolecules* **2005**, *6*, 235–243.

(91) Rossegger, E.; Schenk, V.; Wiesbrock, F. Design Strategies for Functionalized Poly(2-Oxazoline)s and Derived Materials. *Polymers (Basel).* **2013**, *5*, 956–1011.

(92) Bludau, H.; Czapar, A. E.; Pitek, A. S.; Shukla, S.; Jordan, R.; Steinmetz, N. F. POxylation as an Alternative Stealth Coating for Biomedical Applications. *Eur. Polym. J.* **2017**, *88*, 679–688.

(93) Mero, A.; Pasut, G.; Via, L. D.; Fijten, M. W. M.; Schubert, U. S.; Hoogenboom, R.; Veronese, F. M. Synthesis and Characterization of Poly(2-Ethyl 2-Oxazoline)-Conjugates with Proteins and Drugs: Suitable Alternatives to PEG-Conjugates? *J. Control. Release* **2008**, *125*, 87–95.

(94) Viegas, T. X.; Bentley, M. D.; Harris, J. M.; Fang, Z.; Yoon, K.; Dizman, B.; Weimer, R.; Mero, A.; Pasut, G.; Veronese, F. M. Polyoxazoline: Chemistry, Properties, and Applications in Drug Delivery. *Bioconjug. Chem.* **2011**, *22*, 976–986.

(95) Barz, M.; Luxenhofer, R.; Zentel, R.; Vicent, M. J. Overcoming the PEG-Addiction: Well-Defined Alternatives to PEG, from Structure-Property Relationships to Better Defined Therapeutics. *Polym. Chem.* **2011**, *2*, 1900–1918.

(96) Harris, J. M.; Bentley, M. D.; Moreadith, R. W.; Viegas, T. X.; Fang, Z.; Yoon, K.; Weimer, R.; Dizman, B.; Nordstierna, L. Tuning Drug Release from Polyoxazoline-Drug Conjugates. *Eur. Polym. J.* **2019**, *120*.

(97) Moreadith, R. W.; Viegas, T. X.; Bentley, M. D.; Harris, J. M.; Fang, Z.; Yoon, K.; Dizman, B.; Weimer, R.; Rae, B. P.; Li, X.; et al. Clinical Development of a Poly(2-

Oxazoline) (POZ) Polymer Therapeutic for the Treatment of Parkinson's Disease – Proof of Concept of POZ as a Versatile Polymer Platform for Drug Development in Multiple Therapeutic Indications. *Eur. Polym. J.* **2017**, *88*, 524–552.

(98) Scholz, C. Polymers for Biomedicine: Synthesis, Characterization, and Applications. *Wiley Online Libr.* **2017**.

CHAPTER TWO

Poly(2-oxazoline) Block Copolymers as Surfactants for Oil-in-water Nanoemulsions

Adapted from: Daniel A. Estabrook, Amanda F. Ennis, Rachael A. Day and Ellen M. Sletten*, Controlling nanoemulsion surface chemistry with poly(2-oxazoline) amphiphiles. *Chem. Sci.*, **2019**, *10*, 3994–4003. DOI: https://doi.org/10.1039/C8SC05735D.;

and

Rachael A. Day, Daniel A. Estabrook, Carolyn Wu, John O. Chapman, Alyssa J. Togle, and Ellen M. Sletten*, Systematic Study of Perfluorocarbon Nanoemulsions Stabilized by Polymer Amphiphiles *ACS Appl. Mater. Interfaces* **2020**, *12*, 38887– 38898. DOI: https://doi.org/10.1021/acsami.0c07206.

2.1 Abstract

Perfluorocarbon (PFC) nanoemulsions, surfactant-stabilized droplets of fluorous solvent in water, are simple yet versatile nanomaterials. The orthogonal nature of the fluorous phase promotes the formation of nanoemulsions through a simple, self-assembly process, while simultaneously encapsulating fluorous-tagged payloads for varied applications. The size, stability, and surface chemistry of PFC nanoemulsions are controlled by the surfactant. Here, we systematically study the effect of both the hydrophilic and hydrophobic block of polymer surfactants on PFC nanoemulsions. We find that block length and identity, the overall polymer hydrophilic: lipophilic balance (HLB) and the polymer architecture are all important factors. The ability to modulate these parameters enables initial size, stability, payload retention, cellular endocytosis, and protein

adsorption of PFC nanoemulsions to be controlled. With the insight obtained from the study of polymer amphiphiles stabilizing PFC nanoemulsion, design features required for the optimal material are obtained.

2.2 Motivations and Applications

Nanomaterials have been explored for the last few decades as drug delivery vehicles, where their role is to transport, protect and delivery insoluble drug payloads to the target tissue of interest.[1,2] As reviewed within Chapter 1, a number of nanomaterials ranging from organic to inorganic have been developed toward these purposes.[3] Additionally, advances within these fields have led to a better understanding regarding how physicochemical properties of each nanomaterial influences its fate *in vivo*.[4–9] These include challenges within 1) controlled delivery, 2) routes of cellular internalization (or lack thereof), and 3) protein corona formation impeding ligand-promoted active targeting.[10–12] Thus, for each nanomaterial it is critical to establish structure-property relationships regarding how the nanomaterial interacts with biomolecules or other components of biological media.[4,13–15] These relationships require thoroughly designed studies and an ability to reliably control a material's physicochemical properties.

A number of soft, organic nanomaterials included liposomes, polymer micelles and emulsions have had success in translation from the benchtop to the clinic.[16–18] While all of these materials undergo self-assembly, liposomes and micelles are thermodynamically stable and nanoemulsions are kinetically stable. This allows nanoemulsions to be more robust to environmental conditions, including changes in pH, temperature and dilution factors.[19,20,21] Additionally, emulsions are composed of a hydrophobic oil core suspended within an aqueous environment via a stabilizing amphiphile (*i.e.* surfactant), which allows for high loading capacities.

Despite this, emulsions suffer from premature leakage of encapsulated payloads into surrounding environments, for example hydrophobic membranes that surround cells.[22,23] To address this challenge, we look towards emulsions with an interior oil phase composed of bioorthogonal perfluorcarbon (PFC) solvents, rather than typical hydrocarbon oils (*e.g.* olive and canola oils). To encapsulate payloads within PFCs, we have concurrently investigated the use of both covalent and non-covalent fluorous tags (Figure 2.1A) to render fluorophores and therapeutics fluorous-soluble.

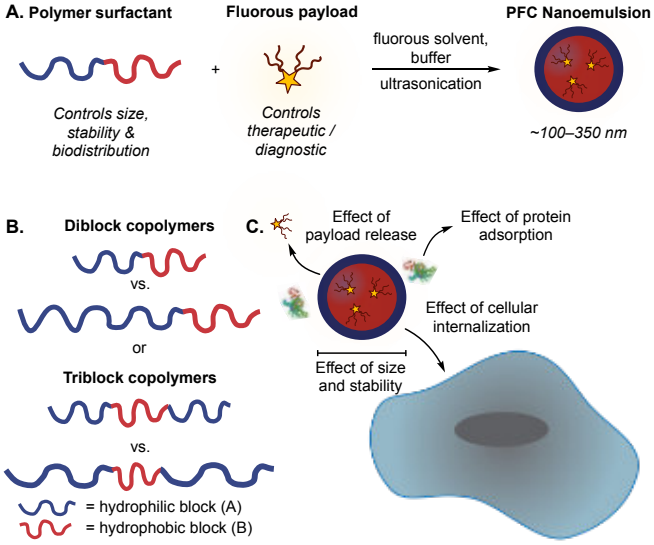

Figure 2.1 (A) One step formulation of PFC nanoemulsions stabilized by polymer surfactants containing fluorous soluble payloads. (B) Polymer amphiphile block length and architecture dictate properties. (C) Surfactants dictate the size, stability, protein adsorption and route of cellular endocytosis of PFC nanoemulsions.

Perfluorocarbons, molecules in which all C-H bonds have been replaced with C-F bonds, have unique properties. They phase separate from aqueous and organic solutions to form a dense fluorous phase.[24] Our main interest lies in perfluorocarbon-in-water nanoemulsions[25–28] stems from the orthogonality of the fluorous phase providing opportunities to selectively sequester fluorous-tagged payloads inside the droplets.[29] Historically, perfluorocarbon (PFC) nanoemulsions

have been stabilized by Pluronic F-68 for use as artificial blood substitutes;[30] however, these surfactants have been associated with formulation inconsistencies and multidose toxicity.[31–33] Contemporary applications of PFC nanoemulsions such as ^{19}F-magnetic resonance imaging,[34–36] ultrasound contrast agents,[37,38] photodynamic therapy,[27,39] and intracellular sensors[40] have spawned interest in new formulations. Previously, Sletten *et al.* looked to commercially available polymers and biomolecules for the stabilization and surface functionalization of PFC emulsions, but found these materials largely unsuitable due to large size and rapid degradation of the droplets, as well as limitations in post-emulsion functionalization.[25] Recently, volatile perfluorocarbon droplets have been effectively stabilized by Gianneschi and coworkers through triblock poly(norbornene)s,[37] and by Medina *et al.* through crosslinked peptides[41]. However, neither of these efforts explored surface modification. Taken together, these works suggest interest and need for custom polymer surfactants that facilitate stable PFC nanoemulsions with modular surface chemistries. Research has shown that PFC nanoemulsions are endocytosed by cells,[34,42,43] and the surfactant can dictate the mechanism of endocytosis.[44] However, systematic studies on how the amphiphile affects PFC nanoemulsion stability, payload retention, protein corona formation and cellular internalization have yet to be performed. This knowledge is essential to advance the utility of PFC nanoemulsions as therapeutic and diagnostic nanocarriers.

This chapter is dedicated to investigating poly(2-oxazoline) (POx) amphiphilic block copolymers as surfactants for PFC nanoemulsions, with the goal of effectively substituting the Pluronic surfactants that were originally employed for oxygen delivery.[45] Our interest in POx stems from their controlled ring opening polymerization, ease of functionalization through incorporation of functional co-monomers or end-capping, and validated alternative to poly(ethylene glycol) (PEG).[46,47] PEGylation has been widely successful at lengthening serum

half-lives and minimizing protein coronas; however, its extensive use has led to immunogenicity concerns. Thus, in the next iteration of nanomaterials, alternatives to PEG (and Pluronics) are desirable.[46] The first half of this chapter will discuss variations in the hydrophobic portion of POx amphiphiles,[48] while the latter half will focus on the role of the hydrophilic block in custom polymeric amphiphiles and readily available commercial PEG-containing surfactants for their ability to stabilize PFC nanoemulsions over time (Figure 2.1B). Subsequently, we analyze their effect on payload retention, protein corona formation, and cellular internalization (Figure 2.1C). While POx have been thoroughly investigated for micellization[49–51] and have previously been employed for chloroform-in-water macroemulsions,[52] yet their use as surfactants for nanoemulsion formation is novel.[53]

2.3 Initial Explorations: Poly(2-oxazoline)s as Surfactants for PFC Nanoemulsions

Owing to the rapid microwave-controlled assisted polymerizations of POx, we first synthesized a small library of amphiphilic diblock and triblock target POx amphiphiles and explore their ability to stabilize oil-in-water and perfluorocarbon-in-water nanoemulsions (Figure 2.2A). The polymer surfactants were designed to mimic Pluronic F-68 (**2.1**), with poly(2-methyl-2-oxazoline) (P(MeOx) replacing poly(ethylene glycol) and either poly(2-propyl-2-oxazoline) (P(PrOx)), poly(2-nonyl-2-oxazoline) (P(NonOx)), or poly(2-(perfluorohexyl)ethyl-2-oxazoline) (P(FOx))[50,51,54] replacing the hydrophobic poly(propylene oxide). The POx surfactants were synthesized through a controlled, living cationic ring-opening polymerization of corresponding 2-substituted-2-oxazoline monomers (Figure 2.2A, **2.2–2.5**). Due to the controlled nature of the polymerization mechanism, block lengths were tuned by initiator to monomer ratio. Hydrophilic blocks were kept at 30 repeat units of 2-methyl-2-oxazoline (**2.2**), while hydrophobic blocks

(composed of **2.3**, **2.4** or **2.5**) were kept at 10 repeat units. Block lengths were chosen at a ratio analogous to **2.1**, with shorter lengths to speed surfactant migration to the interface.[55] Microwave-assisted polymerization allowed for short reaction times and low dispersities (Table 2.1) compared to traditional solution phase synthesis.[56] Polymerizations were quenched with acrylic acid to aid determination of number average molecular weight (M_n) via end-group analysis. Following this

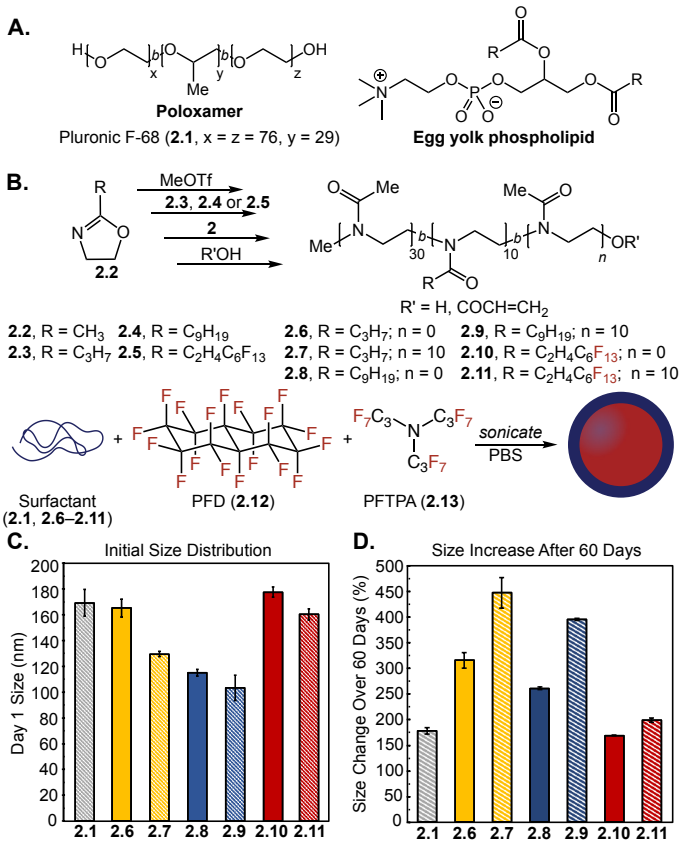

Figure 2.2 (A) Common commercial surfactants previously employed for PFC nanoemulsion formation. (B) Library of amphiphilic di- and triblock copolymers **2.6–2.11** and (C/D) their utility as surfactants for PFC nanoemulsions composed of 7:3 v/v% perfluorodecalin (PFD, **2.12**):perfluorotripropylamine (PFTPA, **2.13**). (C) Initial size distributions of POx-stabilized emulsions. Emulsions were prepared by sonicating a solution of 2.8 wt% surfactant, with 10 vol% 7:3 PFD:PFTPA in phosphate buffered saline (PBS). Emulsions were diluted 1:100 in MilliQ water prior to measurements by dynamic light scattering (DLS). Data represents the average of three independent samples; error bars represent the half-width at half-maximum averaged over the three independent samples. (D) Ostwald ripening of emulsions over 60 days monitored by DLS, see Figure 2.3 and 2.4 for raw data. Error bars represent the standard deviation of percent size changes for three independent samples.

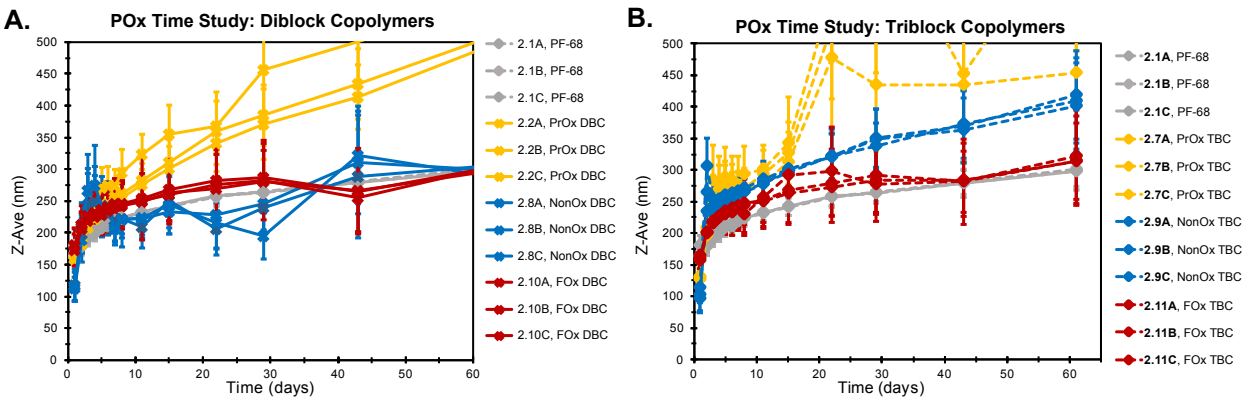

Figure 2.3. Size of PFC nanoemulsions stabilized by (A) diblock copolymers (DBC) and (B) triblock copolymers (TBC) over time. The size of nanoemulsions composed of 7:3 PFD:PFTPA v/v% stabilized (A) POx diblock copolymers **2.6** (yellow solid line, propyl-based, "PrOx DBC"), **2.8** (blue solid line, nonyl-based, "NonOx DBC"), **2.10** (red solid line, fluorous-based, "FOx DBC") and (B) POx triblock copolymers **2.7** (yellow dashed line, propyl-based, "PrOx TBC"), **2.9** (blue dashed line, nonyl-based, "NonOx TBC"), and **2.11** (red dashed line, fluorous-based, "FOx TBC") was measured by DLS over time. Nanoemulsions of identical composition but stabilized by **2.1** (grey dashed line, Pluronic F-68) were included as a control. Size measurements were performed on three independent samples (A-C), five replicates per sample. Error bars represent half-width at half-maximum.

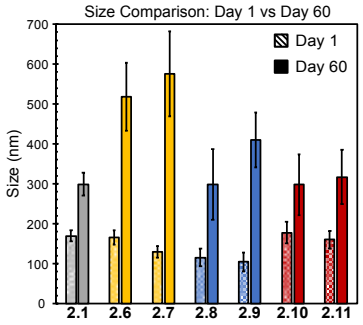

Figure 2.4. Initial (day 1) and final (day 60) size distributions of POx-stabilized emulsions. Emulsions were prepared by sonicating a solution of 2.8 wt% surfactant, with 10 vol% 7:3 PFD:PFTPA in phosphate buffered saline (PBS). Emulsions were diluted 1:100 in MilliQ water prior to measurements by dynamic light scattering (DLS). Data represents the average of three independent samples; error bars represent the half-width at half-maximum averaged over the three independent samples.

procedure, we prepared polymers **6**–**11** (Figure 2A, Table 2.1) and characterized them to have M_n from 3.5 to 8.9 kDa with narrow dispersities ($Đ \leq 1.30$).

Table 2.1. Surfactant library of amphiphilic poly(2-oxazoline)s

#	Polymer	M_n[a] (kDa)	$Đ$
2.6	P(MeOx$_{30}$-*b*-PrOx$_7$)	3.5	1.26
2.7	P(MeOx$_{30}$-*b*-PrOx$_7$-*b*-MeOx$_{30}$)	6.2	1.29
2.8	P(MeOx$_{30}$-*b*-NonOx$_{12}$)	4.8	1.24
2.9	P(MeOx$_{30}$-*b*-NonOx$_{10}$-*b*-MeOx$_{30}$)	7.4	1.29
2.10	P(MeOx$_{29}$-*b*-FOx$_9$)	6.6	1.16
2.11	P(MeOx$_{29}$-*b*-FOx$_9$-*b*-MeOx$_{29}$)	8.9	1.09

MeOx: methyl-2-oxazoline, **2.2**; PrOx: propyl-2-oxazoline, **2.3**; NonOx: nonyl-2-oxazoline, **2.4**; FOx: (perfluorohexyl)ethyl-2-oxazoline, **2.5**.
[a]Number-average molecular weight (M_n) determined by ^{1}H-NMR end-group analysis of terminal CH_3 group to polymeric backbone. Acrylic acid termination was found to be quantitative for polymers **2.6**–**2.9**, while **2.10**, **2.11** were primarily hydroxyl-terminated due to extended reaction times. The extended reaction times may also lead to chain transfer and chain coupling side reactions.[57,58]
[b]Dispersity index ($Đ$) determined by SEC analysis (eluent: DMF + 0.1M LiBr).

To test the ability for POx amphiphiles to stabilize nanoemulsions, polymers **2.6**–**2.11** were first solubilized in dimethylformamide and then diluted with phosphate buffered saline (PBS, pH 7.4) to a final surfactant loading of 2.8 wt%. This solution was combined with 10 vol% fluorous or hydrocarbon oil. Emulsions were formulated through ultrasonication for 15 minutes at 0 °C. For the fluorous solvent, we selected a 7:3 (v/v%) mixture of perfluorodecalin:perfluorotripropylamine (PFD:PFTPA, **2.12**:**2.13**) due to its use in Fluosol-DA, a previously FDA-approved PFC nanoemulsion stabilized by Pluronic F-68 (**2.1**).[30] Dynamic light scattering analysis of POx-stabilized PFC nanoemulsions showed size distributions that were comparable to or smaller than droplets stabilized by **2.1** (Figure 2.2C), with polydispersities ranging from 0.1 to 0.2. Monitoring the size over 60 days at ambient temperature indicated that propyl-2-oxazoline-containing

surfactants (**2.6**, **2.7**) were inferior, exhibiting significant destabilization (>300% change in size, Figure 2.2D, Figure 2.3, Figure 2.4) despite structural analogy to **2.1**. The main pathway for destabilization of PFC nanoemulsions is Ostwald ripening, which is represented by a gradual increase in size over time as the solvent in the smallest droplets migrates to the larger droplets.[20] Factors that affect Ostwald ripening are sample polydispersity, concentration, presence of micelles, and identity of the perfluorocarbon.[59,60] The more hydrophobic nonyl-2-oxazoline-containing surfactants (**2.8**, **2.9**) were superior to the propyl-containing surfactants with diblock **2.8** performing better than triblock **2.9**. Surfactants with fluorous components (**2.10**, **2.11**) displayed the best stability over time, on par with **2.1**. Emulsions stabilized by triblock copolymers **2.7**, **2.9**, and **2.11** resulted in smaller initial size distributions, but increased in swelling over time compared to diblock copolymers **2.6**, **2.8** and **2.10**. When employed for olive oil emulsion formation, **2.6**–**2.9** resulted in sub-250 nm droplets (Figure 2.5).

As expected, the fluorous copolymers **2.10** and **2.11** were not effective surfactants for the formation of oil-in-water nanoemulsions. After 3 weeks, oil droplets stabilized by propyl-2-oxazoline-containing surfactants (**2.6**, **2.7**) underwent phase separation. In contrast, emulsions

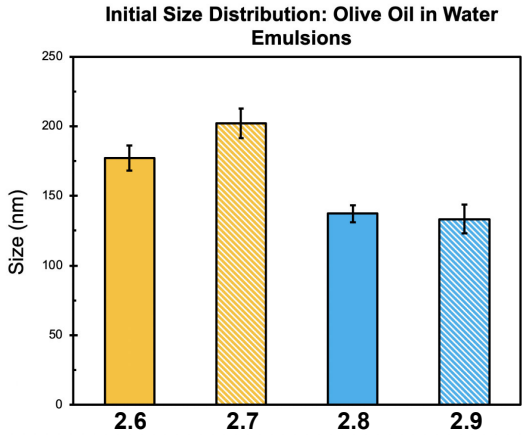

Figure 2.5. Dynamic light scattering data for the initial size distributions of POx-stabilized olive oil-in-water nanoemulsions. Error bars represent the half-width at half-maximum. Emulsions were prepared as described by the general emulsion procedure replacing 7:3 PFD (**2.12**)/PFTPA (**2.13**) with olive oil. Data are an average of three replicate measurements.

stabilized by nonyl-2-oxazoline-containing surfactants (**2.8**, **2.9**) showed no size change (Figure 2.6). These data demonstrate that the following results on PFC nanoemulsions can be extended to more conventional oil-in-water nanoemulsions. Our initial library of poly(2-oxazoline) surfactants resulted in amphiphilic copolymers that performed similarly to **2.1** yet could be prepared through a controlled and living polymerization. Diblock copolymers **2.8** and **2.10** stood out as the most promising, as **2.8** formed emulsions of small size for both oil-in-water and PFC nanoemulsions, while **2.10** formed PFC emulsions with good stability.

Ultimately, this work set the stage for our poly(2-oxazoline)-based surfactant platform. This relatively small set of amphiphilic poly(2-oxazoline)s gave us critical information on how to develop polymeric surfactants. Of particular interest was the role of the hydrophobic POx anchoring block, which here demonstrated that while low hydrophobicity (*i.e.,* propyl-containing side chains) was not adequate for long-term stabilization, one could nevertheless make PFC droplets with an initial small size (<200 nm). On the whole, we found that poly(2-nonyl-2-

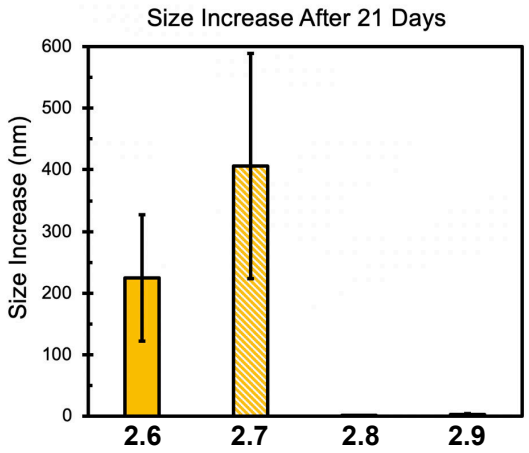

Figure 2.6. Size change of olive oil-in-water nanoemulsions over 21 days, stabilized by POx surfactants **2.6** (yellow solid bar, propyl-based diblock copolymer), **2.7** (yellow dashed bar, propyl-based triblock copolymer), **2.8** (blue solid bar, nonyl-based diblock copolymer), and **2.9** (blue dashed bar, nonyl-based triblock copolymer). Size measurements represent average of duplicate samples, three replicates per sample. Error bars represent the standard deviation of the size changes for duplicate samples.

oxazoline) surfactants, particularly diblock **2.8**, could outperform poly(2-propyl-2-oxazoline)s **2.6** and **2.7**, and even fluorous-containing oxazolines **2.10** and **2.11**. However, variants in the hydrophilic block were rather limited within this initial library, having instead focused on keeping the hydrophilic monomer identity and block length constant to directly compare di- and triblock copolymer architectures. From here, we envisioned that we could further expand this library to elucidate the role of the surfactant's hydrophilic-lipophilic balance, hydrophilic block identity, length and structure. Moreover, our interest in moving these nanoemulsion systems into living systems prompted us to consider other important biological parameters. As such, we sought to study not only size and stability, but payload retention, protein adsorption, and how these properties ultimately intertwined to influence the routes and magnitude of cellular uptake that these particles undergo.

2.4 Expanding the Surfactant Library: Influence of Hydrophilic Block on Size, Stability and Payload Retention

To expand our surfactant library, we first looked to include other commercially available surfactants previously employed for oil-in-water emulsions. These included the previous Pluronic F-68 (**2.1**) and a second poloxamer triblock copolymer with extended block lengths, Pluronic F-127 (**2.14**). Additionally, the enhanced long-term stability we had observed for fluorous-containing oxazolines inspired us to include commercial Zonyl surfactants, a set of PEG-fluoroalkyl (PFA) diblock copolymers termed FSO (**2.15**) and FSN (**2.16**). We then targeted POx polymers that varied in hydrophilic block identity—namely, poly(2-methyl-2-oxazoline) (P(MeOx)), poly(2-ethyl-oxazoline) (P(EtOx)), and PEG. Both of these poly(2-oxazoline)s were chosen due to their current

investigation as PEG substitutes. Conversely, we sought to keep the hydrophobic block consistent within these studies and chose poly(2-nonyl-2-oxazoline) block due to its promising results in our previous assays. POx amphiphiles were synthesized as described previously, with either AB (**2.8**, **2.17–2.19, 2.21–2.23**) or ABA (**2.9**, **2.20**) architectures for di- and triblock copolymer analogues, respectively. Hydrophilic block lengths were varied between 30, 60 or 90 repeat units, and hydrophobic block lengths were varied between 10 or 30 repeat units. For PEG-POx amphiphiles, the hydrophilic PEG block was varied between 1 (**2.24**), 2 (**2.25**) or 5 kDa (**2.26**) and the hydrophobic NonOx block was kept at 10 repeat units. Collectively, this surfactant library totaled 12 custom synthetic POx polymers and 4 commercial polymers.

To begin, we screened the ability of each polymeric surfactant to stabilize perfluorocarbon-in-water droplets using the previously mentioned procedure (Figure 2.7A, B). Briefly, polymer surfactant (28 mg/mL, 2.8 wt%) was dissolved in PBS and added to fluorous solvent (7:3 vol% perfluorodecalin (PFD) : perfluorotripropylamine (PFTPA)) (20 μL, 10 vol%) and ultrasonicated (90s, 35% amplitude) to form nanoemulsions. Size and PDI were analyzed by dynamic light scattering (DLS) analysis. To minimize micelle formation, all P(MeOx) and P(EtOx) containing polymers (**2.8–2.9, 2.17**–**2.23**) were first dissolved in dimethylformamide (DMF) before dilution with water and addition of fluorous solvent. The PEG_n-b-NonOx10 (**2.24**–**2.26**) were first dissolved in DMF, tetrahydrofuran (THF) and methanol (MeOH) respectively to fully solubilize the polymer. Both initial size (Figure 2.7C) and stability over 30 days (Figure 2.7D) was measured. For ease of visualization, data are grouped by Surfactant type: commercial (blue), P(MeOx) (red), P(EtOx) (green) and PEG_n-*b*-$NonOx_{10}$ (orange), with diblock copolymers (solid) differentiated from the triblock copolymers (diagonal stripes). Notably, we found that the fluorous core contributed to stability, with the PFD:PFTPA mixture displaying the largest differences between

each surfactant in both the size and stability. For select surfactants, we also explored perfluorooctyl bromide (PFOB) and perfluoro-15-crown-5-ether (PFCE), where we obtained results consistent with those recently published by Mecozzi and coworkers[60] demonstrating that the use of PFOB and PFCE as the inner phase results in more stable emulsions than those formed from PFD. While we are not certain as to whether these results are inherent to the identity of the fluorous solvent or more of a product of surfactant solubility *within* the block, it is worth noting that Ostwald ripening, being reliant on

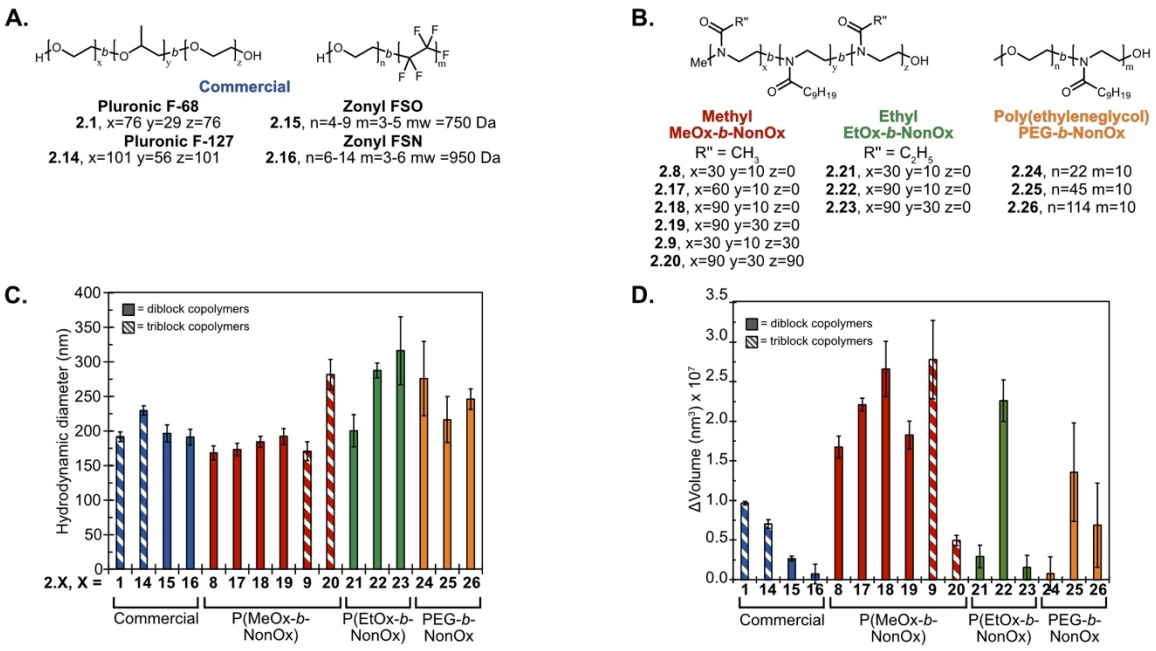

Figure 2.7. (A, B) Library of amphiphilic DBCs and TBCs. Commercial (blue), P(MeOx) (red), P(EtOx) (green), and PEG-b-NonOx (orange) (**2.1**, **2.8**, **2.9**, **2.14**–**2.26**). (C) Initial size distributions of amphiphile stabilized PFC nanoemulsions. Nanoemulsions were prepared by sonication of a solution of 2.8 wt% surfactant with 10 vol% 7:3 Perfluorodecalin (PFD): Perfluorotripropylamine (PFTPA) in phosphate buffered saline (PBS). Emulsions were diluted 1:1000 in deionized water prior to measurements by dynamic light scattering (DLS). Data represents the average of three independent samples, error bars represent the product of the dispersity and the z-average. (D) Change in volume over 30 days of emulsions shown in C. Data represents the average of three independent samples, error bars represent the standard deviation of three independent samples.

diffusion of oil molecules from the inner phase through the aqueous environment, is (typically) inversely proportional to the water solubility of the oil phase.[61] Indeed, the vast amount of research that has gone into the development of perfluorocarbon-in-water emulsions within the last few decades has pointed to the identity of the inner fluorous core as playing just as significant a role, perhaps even more so, than that of the stabilizers employed.[62,63] Of course, a primary difficulty here is that while the water solubility of fluorocarbons decreases exponentially with fluorous chain length and molecular weight, *in vivo* half-lives *increase* exponentially, limiting clinical utility.[64] One must both be cognizant of and carefully weigh the varying properties of perfluorocarbons prior to their use as the liquid core of nanoemulsions.

Initial nanoemulsion size for all polymers tested was between ~150 and 350 nm. Regardless of polymer identity, longer hydrophilic blocks resulted in larger initial sizes, which may be due to a larger molecular weight causing a slower migration to the interface. Interestingly, Pluronics **2.1** and **2.2** (Figure 2.7A) stabilized droplets with a similar size as Zonyls **2.3** and **2.4** (Figure 2.7A, C). As previously observed, the poly(2-methyl-2-oxazoline) diblock copolymers outperformed the triblock copolymers, with the long, bulky **2.20** being the worst stabilizer in the series. The comparatively less hydrophilic poly(2-ethyl-2-oxazoline) series gave rise to larger droplets than those of the methyl series, with droplet sizes increasing considerably with longer hydrophilic block lengths—for example, **2.21** was ~100 nm smaller than **2.22**. Finally, the PEG-POx hybrids displayed no clear trend between initial size and PEG block length, all falling between 200 and 300 nm.

While initial size had relatively minor changes from stabilizer to stabilizer, significant changes were observed when assaying stability of the PFC nanoemulsions over time. Here, commercial surfactants performed quite well (<1.0 nm^3), though interestingly the FDA approved Pluronic F-

68 (**2.1)** was worse than the other Pluronic explored, **2.14**, and the two Zonyl surfactants (**2.15–2.16**). The latter finding corroborates our previous conclusions that while fluorous-containing surfactants are not necessary for the initial formation of sub-200 nm PFC nanoemulsions, they do tend to display the best stabilization behavior over time. This suggests that the solubility of the hydrophobic block within the dispersed phase is critical for long-term stability of droplets.

When looking towards the expanded set of poly(2-methyl-2-oxazoline)-based surfactants, each failed to outcompete the commercial Pluronic **2.1** previously employed as FDA-approved PFC emulsifiers. Stability over time was inversely proportional to hydrophilic-lipophilic balance (HLB), with diblock copolymers containing shorter hydrophilic blocks being more stable than those with longer blocks. In fact, a nearly stepwise decrease in stability was observed when examining the diblock copolymers based on a P(MeOx)$_n$-*b*-P(NonOx)$_{10}$ scaffold when extending the P(MeOx)$_n$ block from DPs of 30 (**2.8**), to 60 (**2.17**), to 90 (**2.18**). The poor stability imparted by surfactants with longer hydrophilic blocks (*i.e.,* higher HLBs) could be recovered by compensating with longer hydrophobic blocks, as demonstrated by P(MeOx)$_{90}$-*b*-P(NonOx)$_{30}$ = **2.19**. Moreover, droplets stabilized by this surfactant had similar stability to those stabilized by **2.8**, an altogether shorter surfactant with a similar HLB, suggesting HLB dominates stabilization behavior. Interestingly, the triblock copolymer containing the longest block lengths, **2.20**, was the best P(MeOx)-based stabilizer examined within the series; however, the fact that this same stabilizer gave rise to the largest droplets of the series largely counteracts this benefit.

Though representing a smaller panel, the less hydrophilic P(EtOx)-based surfactants tended to have similar trends to those observed for the P(MeOx)-based surfactants. Notably, **2.21** and **2.23** performed well with regards to stability over time, with **2.21** standing out amongst the panel of POx amphiphiles studied with regards to both initial size and stability over time. By comparison,

results of the PEG-POx hybrids **2.24–2.26** were underwhelming. Either initial size of PFC emulsions were too large (*e.g.,* >275 nm, **2.24**), or they were unstable over time (**2.25**, **2.26**). These hybrids were also surprisingly difficult to work with regards to aforementioned changes in favorable cosolvents as PEG MW was increased and batch-to-batch variations demonstrated via the error associated with stability over time. Gratifyingly, the diblock copolymer with the shortest PEG unit (MW = 1 kDa, **2.24**) outcompeted the two commercial PEG-based Pluronic triblock copolymers, though again the fact that Pluronic stabilizers gave rise to comparatively smaller droplets should be noted.

Taken together, these data suggest that HLB of block copolymer surfactants is a critical metric with respect to stability of droplets over time; however, these same values do not always reliably correlate when moving from diblock to triblock copolymers. This indicates that polymer structure must be considered alongside overall HLB. Short diblock copolymer surfactants with a 3:1 ratio between the hydrophilic and hydrophobic blocks seem to be most promising on the whole, achieving both small initial size (<200 nm for **2.8** and **2.21**) and adequate stability over time. This ratio may be due to an adequate compromise between surfactants that are water soluble while not being *too* long as to hinder fast transfer of the polymer from the aqueous phase to the oil-water interface, though this would need to be quantitatively verified. These findings also raise the question as to whether surfactants that contain analogous HLBs but contain shorter degrees of polymerization would outcompete the surfactants that were studied within the mentioned panel. Such polymeric amphiphiles are currently under investigation within the Sletten lab.

While size and stability were parameters through which we could easily screen and select promising amphiphiles for PFC nanoemulsions, these surfactants must be able to efficiently encapsulate and retain payloads of interest within the PFC core. Sletten *et al.*'s early development

of fluorous-soluble fluorophores—termed "fluorofluorophores"—linked high degrees of fluorination (wt% F) with extended residence time within PFC nanoemulsions.[26] The lab has since expanded the set of fluorous-soluble payloads to include photosensitizers[27], cyanine fluorophores[65], fluorogenic coumarin dyes,[66] chemotherapeutic prodrugs (unpublished), and even plasmid DNA (in revision). With this development has come a need to understand and systematically alter how PFC nanoemulsion formulations can better protect encapsulated payloads from their exterior environment. Additionally, a long-term goal in the controlled delivery and release of these payloads is avoiding premature release until reaching the site of interest. An obstacle towards this goal is the leaching of interior payload from the PFC core into hydrophobic lipid environments found in biological environments, *e.g.,* the lipid bilayers of cell membranes. Towards this, we systematically study the partition of encapsulated payloads from the emulsion-containing aqueous phase into 1-octanol, employed as a cell membrane mimic.[67] The polymer library described herein were employed as surfactants for PFD:PFTPA (7:3 vol%) nanoemulsions containing the previously synthesized fluorous coumarin **2.27** (Figure 2.8). Diluted aqueous solutions of these droplets were then rocked against 1-octanol, the fluorescence of which corresponded to coumarin leached from the nanoemulsions, was monitored to determine the percent release of the dye. It is immediately apparent looking at the payload release data in Figure 2.8 that the surfactant plays a significant role in payload retention. When comparing the three hydrophilic blocks (P(MeOx), P(EtOx), and PEG), the P(MeOx) block (polymers **2.8**, **2.9**, **2.17–2.20,** red) display superior payload retention. We hypothesize this is due to the increased hydrophilicity of P(MeOx), over PEG and P(EtOx)[46] which minimizes the interaction of the nanoemulsions with the 1-octanol layer, retarding the leakage of the coumarin. The largest variability in release is observed with the PEG polymers where a clear trend with molecular weight

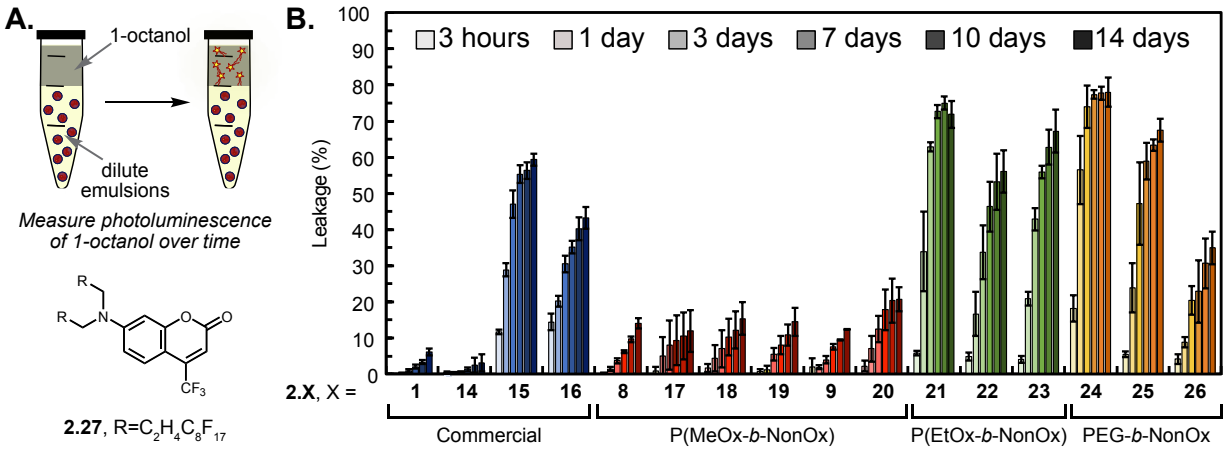

Figure 2.8. (A) Schematic of the partition experiment to determine the degree of coumarin **2.27** leaching in the presence of 1-octanol, a cell-membrane mimic. (B) Normalized fluorescence at 500 nm of 1-octanol layer representing the percentage of leached coumarin **2.27**. Fluorescence was normalized to a free control of **2.27** dissolved in 1-octanol. Bars represent the average of three independent samples and error bars represent the standard deviation of three independent samples.

is observed. The Pluronics (**2.1**, **2.14**, blue) have the largest PEG content and retain over 90% of their cargo over 14 days while the Zonyls (**2.15**, **2.16**, blue) which have short PEG blocks of 4–12 repeat units, release 30% of their cargo within 3 days. Looking at the hybrid PEG-*b*-NonOx amphiphiles (**2.24**–**2.26**), it is clear that the larger PEG chain is advantageous for cargo retention as PEG_{1K}-*b*-$NonOx_{10}$ (**2.24**) displays the worst retention of all polymers tested (74% coumarin loss after 3 days), while the PEG_{5K}-*b*-$NonOx_{10}$ (**2.26**) only loses 20% of the payload after 3 days. We attribute this molecular weight trend to the increased hydrophilicity and steric protection of the longer hydrophilic blocks at the interface, minimizing interactions of the droplets with the 1-octanol layer.[68,69]

These data suggest that the most important factor in reducing leaching of a payload from PFC nanoemulsions is the hydrophilicity of the amphiphiles. The increased hydrophilicity, either by tuning innate hydrophilicity (PEG and P(EtOx) vs. P(MeOx)) or by increasing block length (PEG1K vs. PEG5K) decreases the overall leakage of fluorous payloads. If a nanomaterial is

desired that will not release its payload, the P(MeOx) series is far superior. If slow release of payload over time is necessary, the Zonyl, P(EtOx) or PEG5K-b-NonOx would be appropriate choices. In the future, it would be beneficial to avoid direct contact between the nanoparticles and the 1-octanol layer, as previously reviewed.[70]

2.5 Conclusions

In this chapter we utilized two different polymer libraries to investigate the effect of polymer amphiphiles on stabilizing PFC nanoemulsions. The first library focused on systematically varying the hydrophobic block of the surfactant, while the second library varied the hydrophilic block. Regarding the hydrophobic block, there was no trend observed between hydrophobicity and initial size of nanoemulsions; indeed, even POx with propyl-containing side chains yielded nanoemulsions below 200 nm. This helps to explain why Pluronic F-68, despite having no block soluble within the PFC core, is nonetheless an adequate surfactant of PFC nanoemulsions. Conversely, we did observe that incorporation of fluorous-containing side chains endowed the respective di- and triblock copolymers with exceptional stabilization properties, indicating that the ability of a surfactant to "anchor" into the emulsion is likely an optimal property when formulating surfactants for PFC nanoemulsions, though not entirely necessary. Additionally, it is worth noting that many of the amphiphiles discussed herein are capable of stabilizing traditional oil-in-water nanoemulsions, oftentimes with even greater stability than observed for the PFC variants, giving credence to the importance of surfactant anchoring. On the basis of both size and stability concerns, diblock copolymers with a hydrophobic nonyl chain stuck out as a promising surfactant to move forward with.

The second half of this chapter focused on systematically varying the hydrophilic block of the surfactant and comparing libraries of resulting POx polymers to an expanded set of commercial

polymeric surfactants. Here, we chose to keep the promising hydrophobic nonyl-containing POx block consistent, and systematically vary the hydrophilic block between either methyl- or ethyl-containing POx, or even PEG. Surfactants were further varied in terms of block length, architecture, and overall hydrophilic-lipophilic balance (HLB). We observed that each of these properties plays a significant role in not only the size and stability of the droplets, but other important biological criteria like payload retention, cellular endocytosis and protein adsorption. The size of nanoemulsions was influenced by both the size and sterics of the hydrophilic block, and generally longer blocks produced larger nanoemulsions. With regards to stability, we concluded that the overall HLB of the polymer played an important role, and that a 3:1 molar ratio between the hydrophilic and hydrophobic blocks is optimal. Finally, payload retention was largely influenced by the molecular identity (and hydrophilicity) of the hydrophilic block, with this property being inversely proportional to payload leakage. This is likely due to reduced interactions between hydrophilic blocks (*e.g.,* PMeOx and PEG) with the 1-octanol layer employed in the model system.

Other important biological considerations for these nanoemulsions vehicles were studied in the manuscript from which this chapter was adapted[71], namely, cellular endocytosis and protein adsorption. However, these studies were primarily performed by colleagues and are thus largely outside the scope of this chapter. Briefly, we concluded that the cellular endocytosis and the protein adsorption are controlled by the molecular identity and the polymer architecture. The more hydrophilic polymers, the commercial and P(MeOx) polymers, undergo clathrin-mediated endocytosis while the more hydrophobic polymers, P(EtOx) and PEG_n-*b*-$NonOx_{10}$, are internalized by several mechanisms. Overall, the triblock copolymers behave similarly to the diblock copolymers, with slight differences in the identity of the proteins that are adsorbed. This

study provides necessary background on the structure—property relationship of polymer amphiphiles for the stabilization of PFC nanoemulsions. Through the identification of four criteria: hydrophilic block size, hydrophilic: lipophilic balance (HLB), molecular identity and polymer architecture, the ideal nanomaterial can be more easily realized. Future work involves combining the amphiphile design rules established here with fluorous tagged therapeutics and targeting ligands to enable efficient, personalized, and target-specific drug delivery with nanoemulsions.

2.6 Experimental Procedures

2.6.1 General experimental procedures

Reagents and Instrumentation Chemical reagents were purchased from Sigma-Aldrich, Alfa Aesar, Fisher Scientific, or Acros Organics and used without purification unless noted otherwise. Anhydrous dimethyl sulfoxide (DMSO) was obtained from a Sure-SealTM bottle (Aldrich). Anhydrous and deoxygenated solvents dichloromethane (DCM), acetonitrile (MeCN), methanol (MeOH), and tetrahydrofuran (THF) were dispensed from a Grubb's-type Phoenix Solvent Drying System. Anhydrous but oxygenated 1-butanol and chlorobenzene was prepared by drying over 4 Å molecular sieves for at least 3 days. Thin layer chromatography was performed using Silica Gel 60 F254 (EMD Millipore) plates. Flash chromatography was executed with technical grade silica gel with 60 Å pores and 40–63 μm mesh particle size (Sorbtech Technologies). Bath sonication was performed using a Branson 3800 ultrasonic cleaner. Solvent was removed under reduced pressure with a Büchi Rotovapor with a Welch self-cleaning dry vacuum pump and further dried with a Welch DuoSeal pump. Bath sonication was performed using a Branson 3800 ultrasonic cleaner. Nuclear magnetic resonance (^{1}H NMR, ^{13}C NMR, and ^{19}F NMR) spectra were taken on Bruker Avance 500 (^{1}H NMR and ^{13}C NMR) or AV-300 (^{19}F NMR) instruments and processed

with MestReNova software. All ^{1}H NMR peaks are reported in reference to $CDCl_3$ at 7.26 ppm. Size Exclusion Chromatography (SEC)/Gel Permeation Chromatography (GPC), unless otherwise noted, was conducted on a Shimadzu high performance liquid chromatography (HPLC) system with a refractive index detector RID-10A, one Polymer Laboratories PLgel guard column, and two Polymer Laboratories PLgel 5 μm mixed D columns. Eluent was DMF with LiBr (0.1 M) at 50 °C (flow rate: 0.80 mL/ min). Calibration was performed using near-monodisperse poly(methyl-methacrylate) PMMA standards from Polymer Laboratories. Masses for analytical measurements were taken on a Sartorius MSE6.6S-000-DM Cubis Micro Balance. Microwave reactions were performed using a CEM Discover SP microwave synthesis reactor. All reactions were performed in glass 10 mL microwave reactor vials purchased from CEM with silicone/PTFE caps. Flea micro PTFE-coated stir bars were used in the vials with magnetic stirring set to high and 15 seconds of premixing prior to the temperature ramping. All microwave reactions were carried out at 140 °C with the pressure release limit set to 250 psi (no reactions exceeded this limit to trigger venting) and the maximum wattage set to 250W (the power applied was dynamically controlled by the microwave instrument and did not exceed this limit for any reactions). Irradiation with light was performed with BI365 nm Inspection UV LED lamp, purchased from Risk reactor (Output power density >5000μW/cm² at 15" (38cm), voltage range 90-265V ac, output power: 3*325mW at 365nm peak).

Abbreviations

DBC = diblock copolymer; DCM = dichloromethane; DLS = dynamic light scattering; DMF = dimethyl formamide; DMSO = dimethylsulfoxide; EtOH = ethanol; HLB = Hydrophilic lipophilic balance; MeCN = acetonitrile; MeCN = acetonitrile; MeOH = methanol; MeOTf = methyl triflate;

MeOx = 2-methyl-2-oxazoline; NMR = nuclear magnetic resonance; NonOx = 2-nonyl-2-oxazoline; THF = tetrahydrofuran; PBS = Phosphate buffered saline; PFC = perfluorocarbon; PEG = poly(ethylene glycol); PFCE = perfluoro-15-crown-5-ether; PDI = polydispersity index; PFD = perfluorodecalin; PFTPA = perfluorotripropylamine; PFOB = perfluorooctylbromide; POx = poly(2-oxazoline); P(MeOx) = poly(2-methyloxazoline); P(EtOx) = poly(2-ethyloxazoline); P(NonOx) = poly(2-nonyloxazoline); SDS-PAGE = sodium dodecyl sulfate polyacrylamide gel electrophoresis; SEC = size exclusion chromatography; TBC = triblock copolymer.

General photophysics procedure

Photoluminescence spectra were obtained on a Horiba Instruments PTI QuantaMaster Series fluorometer. Quartz cuvette (0.33 cm) was used for photoluminescence measurements. Absorbance spectra were collected on a JASCO V-770 UV-Visible/NIR spectrophotometer with a 4000 nm/min or 2000 nm/min scan rate after blanking with the appropriate solvent. Quartz cuvettes (1 cm or 0.33 cm) were used for absorbance and photoluminescence measurements.

General nanoemulsion formation procedure

Polymer surfactant (5.6 mg, 2.8 wt%) was dissolved in cosolvent (20 μL, DMF, MeOH or THF) and sonicated in a bath sonicator (~15 minutes) until fully dissolved, at which point 7:3 perfluorodecalin : perfluorotripropylamine (10 vol%, 20 μL) was added, followed by PBS buffer pH 7.4 (200 μL). Pluronic F-68 (**2.1**), Pluronic F-127 (**2.14**), Zonyl FSO (**2.15**), Zonyl FSN (**2.16**) required no cosolvent. P($MeOx_x$-*b*-$NonOx_y$-*b*-$MeOx_z$) (**2.8–2.9, 2.17–2.20**), P($EtOx_x$-*b*-$NonOx_y$) (**2.21**–**2.23**) and PEG_{1K}-*b*-$NonOx_{10}$ (**2.24**) were dissolved in DMF. PEG_{2K}-*b*-$NonOx_{10}$ (**2.25**) and PEG_{5K}-*b*-$NonOx_{10}$ (**2.26**) were dissolved in THF and MeOH respectively. The mixture was

sonicated at 35% amplitude for 90 seconds at 0 °C on a QSonica (Q125) sonicator. For P($EtOx_x$-*b*-$NonOx_y$) (**2.21**–**2.23**) and PEG_n-*b*-$NonOx_m$ (**2.24** –**2.26**) polymers the mixture was sonicated at 35% amplitude for 90 seconds pulsed on for 2 seconds, off for 10 seconds at 0 °C. Sonication was performed by lowering the probe directly at the liquid-liquid interface of the two immiscible

General nanoemulsion analysis procedure

Size analysis: The bulk emulsion solution was diluted in MilliQ H_2O (20 μL emulsions in 2 mL MilliQ H_2O) in a plastic 1 cm cuvette. Size was analyzed with a Malvern Zetasizer Nano dynamic light scattering. SOP parameters: 10 runs, 10 seconds/run, three measurements, no delay between measurements, 25 °C with 120 second equilibration time. Collection parameters: Lower limit = 0.6, Upper limit = 1000, Resolution = High, Number of size classes = 70, Lower size limit = 0.4, Upper size limit = 1000, Lower threshold = 0.05, Upper threshold = 0.01. Data are representative of three replicate measurements. Size error bars represent the half-width at half-maximum of the measurements.

For assessment of the statistical significance of differences, a one-tailed Student's t-test assuming unequal sample variance was employed. Results were considered significant/not significant different per the following definitions: ns = $p > 0.05$, significant = $p < 0.05$, * = $p \leq 0.05$, ** = $p \leq 0.01$, *** = $p \leq 0.001$.

Payload release experiment

Perfluorocarbon nanoemulsions (**2.1, 2.14–2.26**) containing fluorous coumarin **2.27** were prepared by dissolving coumarin in acetone to make a stock solution (2.3 mg/mL). Coumarin **2.27** (0.05 mg, 0.04 μmol, 20 μL) was then aliquoted in to eppendorf tubes and the acetone was dried.

Once dried, perfluorocarbons (7:3 PFD: PFTPA, 20 μL) were added to dissolve the coumarin, and deionized water (200 μL) was added. Separately, the polymers were dissolved with required cosolvent. The PFC / water mixture was placed on the sonication probe, and immediately before starting the probe, the polymer solution (see general nanoemulsion formation procedure) was added. The mixture was sonicated for 90 s either continuously or pulsed as described in the general nanoemulsion formation procedure. Immediately after formation, emulsion solution (40 μL) was diluted with PBS (960 μL) and 1-octanol (500 μL) was layered on top of the water and placed on an orbital rocker at 40 rpm.

The 1-octanol (200 μL) was removed with a syringe (250 μL Hamilton) at 3 h, 1 day, 3 days, 7 days, 10 days, and 14 days and the fluorescence were measured in a 0.3 cm quartz cuvette. After measurement, the 1-octanol was carefully replaced to minimize loss during transfer and placed back on the rocker until the next measurement.

The control was fluorous coumarin **2.27** (3.2 μL, 0.007 mg, 6.09 nmol) dissolved in 1-octanol (500 μL) directly, and bath sonicated for 10 min to dissolve. This is the amount of fluorous coumarin that is expected to come into contact with the 1-octanol after the emulsions were diluted with PBS.

Photoluminescence spectra were obtained on a Horiba Instruments PTI QuantaMaster Series fluorometer.

General synthetic procedures

2.6.2 Experimental procedures

P(MeOx$_{32}$-*b*-NonOx$_9$) (**2.8**)

To a flame dried microwave vial, MeCN (1.2 mL, anhydrous) and MeOx (200 μL, 0.200 g, 2.40

mmol, 30 equiv.) were added. After brief mixing, MeOTf (8.9 μL, 13 mg, 0.078 mmol, 1.0 equiv.) was added and the mixture was heated at 140 °C in the microwave. After 7 minutes, NonOx (155 μL, 155 mg, 0.783 mmol, 10 equiv.) was added under N_2 and heated to 140 °C for 3 minutes, at which point the polymerization was quenched with MilliQ water (excess). After stirring overnight, the reaction mixture was evaporated to dryness to yield crude polymer (**2.8**) as a white solid. Polymer **2.8** was purified by dialysis against 1:1 DCM:MeOH (vol%) overnight, collected and evaporated to dryness (102 mg, 0.022 mmol, 29% yield). ^{1}H NMR (500 MHz, $CDCl_3$): δ 3.44 (m, 162H), 3.02 (m, 3H), 2.32 (m, 25H), 2.13 (m, 98H), 1.56 (m, 18H), 1.24 (m, 106H) 0.85 (t, J = 6.6 Hz, 26H). SEC: M_w = 5.0 kDa, M_n = 4.1 kDa, $Đ$ = 1.24.

P($MeOx_{62}$-*b*-$NonOx_8$) (**2.17**)

To a flame dried microwave vial, MeCN (2.1 mL, anhydrous) and MeOx (360 μL, 0.360 g, 4.32 mmol, 60 equiv.) were added. After brief mixing, MeOTf (8.0 μL, 12 mg, 0.072 mmol, 1.0 equiv.) was added and the mixture was heated at 140 °C in the microwave. After 16 minutes, NonOx (139 μL, 139 mg, 0.702 mmol, 10 equiv.) was added under N_2 and heated to 140 °C for 15 minutes, at which point the polymerization was quenched with MilliQ water (excess). After stirring overnight, the reaction mixture was evaporated to dryness to yield crude polymer (**2.17**) as a white solid. Polymer **2.17** was purified by dialysis against 1:1 DCM:MeOH (vol%) overnight, collected and evaporated to dryness (400 mg, 0.057 mmol, 80% yield). ^{1}H NMR (500 MHz, $CDCl_3$): δ 3.44 (m, 284H), 3.03 (m, 3H), 2.13 (m, 18H), 1.97 (m, 187H), 1.58 (m, 17H), 1.25 (m, 99H) 0.86 (t, J = 6.6 Hz, 25H). SEC: M_w = 8.5 kDa, M_n = 7.4 kDa, $Đ$ = 1.16.

P(MeOx$_{87}$-*b*-NonOx$_{7}$) (**2.18**)

To a flame dried microwave vial, MeCN (2.4 mL, anhydrous) and MeOx (400 μL, 0.400 g, 4.80 mmol, 90 equiv.) were added. After brief mixing, MeOTf (5.9 μL, 9 mg, 0.053 mmol, 1.0 equiv.) was added and the mixture was heated at 140 °C in the microwave. After 24 minutes, NonOx (103 μL, 103 mg, 0.519 mmol, 10 equiv.) was added under N_2 and heated to 140 °C for 21 minutes, at which point the polymerization was quenched with MilliQ water (excess). After stirring overnight, the reaction mixture was evaporated to dryness to yield crude polymer (**2.18**) as a white solid. Polymer **2.18** was purified by precipitation by dissolving in a minimal amount of DCM and dropwise addition to cold Et_2O (20:1 v/v%), collected and evaporated to dryness (462 mg, 0.053 mmol, 92% yield). ^{1}H NMR (500 MHz, $CDCl_3$): δ 3.43 (m, 376H), 3.03 (m, 3H), 2.13 (m, 307H), 1.58 (m, 15H), 1.24 (m, 70H) 0.86 (t, J = 6.6 Hz, 20H). SEC: M_w = 12.5 kDa, M_n = 11.1 kDa, $Đ$ = 1.13.

P(MeOx$_{96}$-*b*-NonOx$_{26}$) (**2.19**)

To a flame dried microwave vial, MeCN (0.75 mL, anhydrous) and MeOx (250 μL, 0.25 g, 3.00 mmol, 90 equiv.) were added. After brief mixing, MeOTf (3.7 μL, 5.6 mg, 0.033 mmol, 1.0 equiv.) was added and the mixture was heated at 140 °C in the microwave. After 14 minutes, NonOx (193 μL, 193 mg, 0.972 mmol, 30 equiv.) was added under N_2 and heated to 140 °C for 15 minutes, at which point the polymerization was quenched with MilliQ water (excess). After stirring overnight, the reaction mixture was evaporated to dryness to yield crude polymer (**2.19**) as a white solid. Polymer **2.19** was purified by dialysis against 1:1 DCM:MeOH (vol%) overnight, collected and evaporated to dryness (422 mg, 0.032 mmol, 95% yield). ^{1}H NMR (500 MHz, $CDCl_3$): δ 3.45 (m, 488H), 3.04 (m, 3H), 2.12 (m, 360H), 1.57 (m, 51H), 1.24 (m, 287H) 0.85 (t, J = 6.6 Hz, 77H).

SEC: M_w = 11.4 kDa, M_n = 10.1 kDa, $Đ$ = 1.14.

P(MeOx$_{31}$-*b*-Non$_{10}$-*b*-MeOx$_{31}$) (**2.9**)

To a flame dried microwave vial, MeCN (0.88 mL, anhydrous) and MeOx (150 μL, 0.150 g, 1.8 mmol, 30.0 equiv.) were added. After brief mixing, MeOTf (6.7 μL, 9.7 mg, 0.060 mmol, 1.0 equiv.) was added and the mixture was heated at 140 °C in the microwave. After 8 minutes, NonOx (116 μL, 116 mg, 0.586 mmol, 10 equiv.) was added under N_2 and heated to 140 °C. After 8 minutes, MeOx (150 μL, 0.15 g, 1.8 mmol, 30.0 equiv.) was added under N_2 and heated to 140 °C for 9 minutes, at which point the polymerization was quenched with MilliQ water (excess). The reaction mixture was evaporated to dryness to yield crude polymer (**2.9**) as a white solid. Polymer **2.9** was purified by dialysis against 1:1 DCM:MeOH (vol%) overnight, collected and evaporated to dryness (355 mg, 0.050 mmol, 86% yield). ^{1}H NMR (500 MHz, $CDCl_3$): δ 3.44 (m, 285H), 3.03 (m, 3H), 2.12 (m, 227H), 1.57 (m, 20H), 1.23 (m, 105H), 0.85 (t, J = 6.6 Hz, 29H). SEC: M_w = 6.5 kDa, M_n = 5.5 kDa, $Đ$ = 1.14.

P(MeOx$_{91}$-*b*-NonOx$_{28}$-*b*-MeOx$_{91}$) (**2.20**)

To a flame dried microwave vial, MeCN (0.74 mL, anhydrous) and MeOx (250 μL, 0.250 g, 3.0 mmol, 90.0 equiv.) were added. After brief mixing, MeOTf (3.7 μL, 5.4 mg, 0.033 mmol, 1.0 equiv.) was added and the mixture was heated at 140 °C in the microwave. After 14 minutes, NonOx (193 μL, 193 mg, 0.975 mmol, 30 equiv.) was added under N_2 and heated to 140 °C. After 14 minutes, MeOx (250 μL, 0.250 g, 3.0 mmol, 90.0 equiv.) was added under N_2 and heated to 140 °C for 20 minutes, at which point the polymerization was quenched with MilliQ water (excess). The reaction mixture was evaporated to dryness to yield crude polymer (**2.20**) as a white

solid. Polymer **2.20** was purified by dialysis against 1:1 DCM:MeOH (vol%) overnight, collected and evaporated to dryness (355 mg, 0.017 mmol, 86% yield). ^{1}H NMR (500 MHz, $CDCl_3$): δ 3.40 (m, 838H), 3.03 (m, 3H), 2.90-1.80 (m, 609H), 1.53 (m, 53H), 1.19 (m, 313H), 0.80 (m, 85H). SEC: M_w = 13.8 kDa, M_n = 11.0 kDa, $Đ$ = 1.22.

P(EtOx$_{33}$-*b*-NonOx$_{11}$) (**2.21**)

To a flame dried microwave vial, MeCN (1.2 mL, anhydrous) and EtOx (300 μL, 0.300 g, 3.03 mmol, 30 equiv.) were added. After brief mixing, MeOTf (11.4 μL, 16.5 mg, 0.101 mmol, 1.0 equiv.) was added and the mixture was heated at 140 °C in the microwave. After 10 minutes, NonOx (200 μL, 200 mg, 1.01 mmol, 10 equiv.) was added under N_2 and heated to 140 °C for 7 minutes, at which point the polymerization was quenched with MilliQ water (excess). After stirring overnight, the reaction mixture was evaporated to dryness to yield crude polymer (**2.21**) as a white solid. Polymer **2.21** was purified by dialysis against 1:1 DCM:MeOH (vol%) overnight, collected and evaporated to dryness (300 mg, 0.054 mmol, 60% yield). ^{1}H NMR (500 MHz, $CDCl_3$): δ 3.44 (m, 176H), 3.02 (m, 3H), 2.50-2.05 (m, 93H), 1.58 (m, 21H), 1.24 (m, 124H), 1.11 (m, 107H), 0.86 (t, J = 6.6 Hz, 30H). SEC: M_w = 3.6 kDa, M_n = 2.9 kDa, $Đ$ = 1.23.

P(EtOx$_{93}$-*b*-NonOx$_{10}$) (**2.22**)

To a flame dried microwave vial, MeCN (1.3 mL, anhydrous) and EtOx (250 μL, 0.250 g, 2.52 mmol, 90 equiv.) were added. After brief mixing, MeOTf (3.2 μL, 4.6 mg, 0.028 mmol, 1.0 equiv.) was added and the mixture was heated at 140 °C in the microwave. After 34 minutes, NonOx (55 μL, 55 mg, 0.28 mmol, 10 equiv.) was added under N_2 and heated to 140 °C for 22 minutes, at which point the polymerization was quenched with MilliQ water (excess). After stirring overnight,

the reaction mixture was evaporated to dryness to yield crude polymer (**2.22**) as a white solid. Polymer **2.22** was purified by dialysis against 1:1 DCM:MeOH (vol%) overnight, collected and evaporated to dryness (300 mg, 0.020 mmol, 55% yield). ^{1}H NMR (500 MHz, $CDCl_3$): δ 3.44 (m, 414H), 3.02 (m, 3H), 2.50-2.05 (m, 217H), 1.58 (m, 21H), 1.25 (m, 124H), 1.11 (m, 287H), 0.86 (t, J = 6.6 Hz, 31H). SEC: M_w = 8.0 kDa, M_n = 5.3 kDa, $Đ$ = 1.35.

P(EtOx$_{93}$-*b*-NonOx$_{29}$) (**2.23**)

To a flame dried microwave vial, MeCN (0.3 mL, anhydrous) and EtOx (200 μL, 0.200 g, 2.02 mmol, 90 equiv.) were added. After brief mixing, MeOTf (2.5 μL, 3.6 mg, 0.022 mmol, 1.0 equiv.) was added and the mixture was heated at 140 °C in the microwave. After 15 minutes, NonOx (133 μL, 133 mg, 0.68 mmol, 30 equiv.) was added under N_2 and heated to 140 °C for 12 minutes, at which point the polymerization was quenched with MilliQ water (excess). After stirring overnight, the reaction mixture was evaporated to dryness to yield crude polymer (**2.23**) as a white solid. Polymer **2.23** was purified by dialysis against 1:1 DCM:MeOH (vol%) overnight, collected and evaporated to dryness (274 mg, 0.018 mmol, 82% yield). ^{1}H NMR (500 MHz, $CDCl_3$): δ 3.44 (m, 478H), 3.02 (m, 3H), 2.50-2.05 (m, 251H), 1.58 (m, 58H), 1.25 (m, 333H), 1.11 (m, 287H), 0.87 (t, J = 6.6 Hz, 88H). SEC: M_w = 7.8 kDa, M_n = 6.2 kDa, $Đ$ = 1.21.

PEG$_{1K}$-*b*-NonOx$_{12}$ (**2.24**)

To a flame dried microwave vial, MeCN (0.5 mL, anhydrous) and NonOx (180 μL, 0.180 g, 0.91 mmol, 10.0 equiv.) were added. After brief mixing, PEG$_{1K}$-tosylate (100 mg, 0.09 mmol, 1.0 equiv.) was added and the mixture was heated at 140 °C in the microwave. After 26 minutes, the polymerization was quenched with MilliQ water (excess). After stirring overnight, the reaction

mixture was evaporated to dryness to yield crude polymer (**2.24**) as a white solid. Polymer **2.24** was purified by dissolving in DCM and washing against water, then further dialyzed against MeOH overnight, collected and evaporated to dryness (244 mg, 0.072 mmol, 87% yield). ^{1}H NMR (500 MHz, $CDCl_3$): δ 3.80-3.20 (m, 122H), 3.37 (m, 3H), 2.36 (m, 26H), 1.59 (m, 25H), 1.25 (m, 151H), 0.86 (t, J = 6.6 Hz, 37H). SEC: M_w = 2.6 kDa, M_n = 2.4 kDa, $Đ$ = 1.07.

PEG_{2K}-*b*-$NonOx_8$ (**2.25**)

To a flame dried microwave vial, MeCN (0.3 mL, anhydrous) and NonOx (209 μL, 0.209 g, 1.06 mmol, 10.0 equiv.) were added. After brief mixing, PEG_{2K}-tosylate (212 mg, 0.10 mmol, 1.0 equiv.) was added and the mixture was heated at 140 °C in the microwave. After 20 minutes, the polymerization was quenched with MilliQ water (excess). After stirring overnight, the reaction mixture was evaporated to dryness to yield crude polymer (**2.25**) as a white solid. Polymer **2.25** was purified by dialysis against 1:1 DCM:MeOH (vol%) overnight, collected and evaporated to dryness (278 mg, 0.078 mmol, 66% yield). ^{1}H NMR (500 MHz, $CDCl_3$): δ 3.80-3.20 (m, 222H), 3.37 (m, 3H), 2.30 (m, 16H), 1.57 (m, 16H), 1.24 (m, 95H), 0.86 (t, J = 6.6 Hz, 24H). SEC: M_w = 4.2 kDa, M_n = 3.9 kDa, $Đ$ = 1.05.

PEG_{5K}-*b*-$NonOx_8$ (**2.26**)

To a flame dried microwave vial, MeCN (0.3 mL, anhydrous) and NonOx (102 μL, 0.102 g, 0.52 mmol, 10.0 equiv.) were added. After brief mixing, PEG_{5K}-tosylate (258 mg, 0.05 mmol, 1.0 equiv.) was added and the mixture was heated at 140 °C in the microwave. After 50 minutes, the polymerization was quenched with MilliQ water (excess). After stirring overnight, the reaction mixture was evaporated to dryness to yield crude polymer (**2.26**) as a white solid. Polymer **2.26**

was purified by dialysis against 1:1 DCM:MeOH (vol%) overnight, collected and evaporated to dryness (280 mg, 0.043 mmol, 78% yield). ^{1}H NMR (500 MHz, $CDCl_3$): δ 3.80-3.20 (m, 445H), 3.35 (m, 3H), 2.31 (m, 20H), 1.54 (m, 16H), 1.22 (m, 97H), 0.84 (m, 24H). SEC: M_w = 8.5 kDa, M_n = 8.3 kDa, $Đ$ = 1.05.

2.6.3 Figure experimental procedures

Figure 2.2C. Synthesis of amphiphilic poly(2-oxazoline)s

Poly(2-oxazoline)s were synthesized via microwave protocol using kinetics previously reported in the literature.[54,57,72] See supporting synthetic chemistry experimental procedures for synthetic details.

Figure 2.2C/D. Perfluorocarbon nanoemulsion formation and stability

Emulsions were prepared as described by the general nanoemulsion formation procedure, using surfactants **2.6-11**. Three independent solutions of each emulsion were made (400 μL scale). At each time point, solutions were vortexed (~45 seconds) to resuspend the emulsions. Size was analyzed per the general nanoemulsion analysis procedure. Note: Data are representative of five replicate measurements.

Figure 2.3. Perfluorocarbon nanoemulsions stabilized by (A) diblock and (B) triblock copolymers over time.

See Figure 2.2C.

Figure 2.4. Initial and final size distributions of POx-stabilized emulsions

See Figure 2.2C.

Figure 2.5–2.6. Size distributions of POx-stabilized olive oil-in-water nanoemulsions.

Olive oil emulsions were prepared according to the general nanoemulsions formation procedure and analyzed as described by the general nanoemulsion analysis procedure.

Figure 2.7C/D. Size distributions and stability over time of POx-stabilized PFOB-in-water nanoemulsions.

Perfluorocarbon nanoemulsions stabilized by each surfactant were prepared as described in the **general nanoemulsion formation procedure**. Emulsion size was then monitored on day 1, 2, 3, 7, 14, and 30 following the **general nanoemulsions analysis procedure**. Bars represent the average of three samples and error bars represent the standard deviation of three samples.

Volume is a more accurate description of Ostwald ripening over time. Thus, diameter on day 0 and day 30 were converted to volume of a sphere

$$V = \frac{4}{3}\pi r^3$$

where r is radius. Bars represent the difference of volume on day 30 and day 0 of three samples. Error bars represent the propagation of error of three separate samples.

Figure 2.8. Payload retention of coumarin 2.27 **in the presence of 1-octanol, a cell-membrane mimic.**

Perfluorocarbon nanoemulsions (**2.1—2.16**) containing fluorous coumarin **2.27** were prepared by dissolving coumarin in acetone to make a stock solution (2.3 mg/mL). Coumarin **2.27 (**0.05 mg, 0.04 μmol, 20 μL) was then partioned to eppendorf tubes and the acetone was dried. Once dried, perfluorocarbons (7:3 PFD : PFTPA, 20 ul) were added to dissolve the coumarin, and deionized water (200 μl) was added. Separately, the polymers were dissolved with required cosolvent. The PFC / water mixture was placed on the sonication probe, and immediately before starting the probe, the polymer solution (see **general nanoemulsion formation procedure**) was added. The mixture was sonicated for 90s either continuously or pulsed as described in the **general nanoemulsion**

formation procedure. Immediately after formation, emulsions solution (40 μL) was diluted with PBS (960 μL). 1-octanol (500 μL) was layered on top of the water and placed on an orbital rocker at 40 rpm.

The 1-octanol (200 μL) was removed with a syringe (250 μL Hamilton) at 3 h, 1 day, 3 days, 7 days, 10 days, and 14 days and the fluorescence was measured in a 0.3 cm cuvette as described in the **general photophysics procedures**. After measurement, the octanol was then carefully replaced to minimize loss during transfer and placed back on the rocker until next measurement.

The control was fluorous coumarin **2.27** (3.2 μL, 0.007 mg, 6.09 nmol) dissolved in 1-octanol (500 μL) directly, and bath sonicated for 10 min to dissolve. This is the amount of fluorous coumarin that is expected to come into contact with the 1-octanol after the emulsions were diluted with PBS. Fluorimeter settings: Path length: 0.3 cm, Exc: 375 nm, collect: 400-700 nm, all slits: 2nm, Integration: 0.1 sec.

2.7 1H-NMR Spectra Relevant to Chapter Two

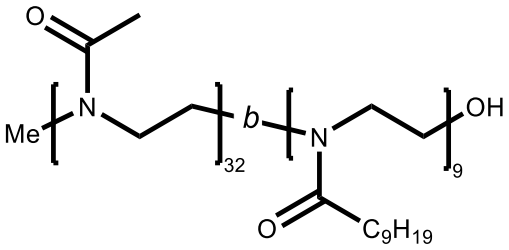

P(MeOx$_{32}$-*b*-NonOx$_9$)

2.8

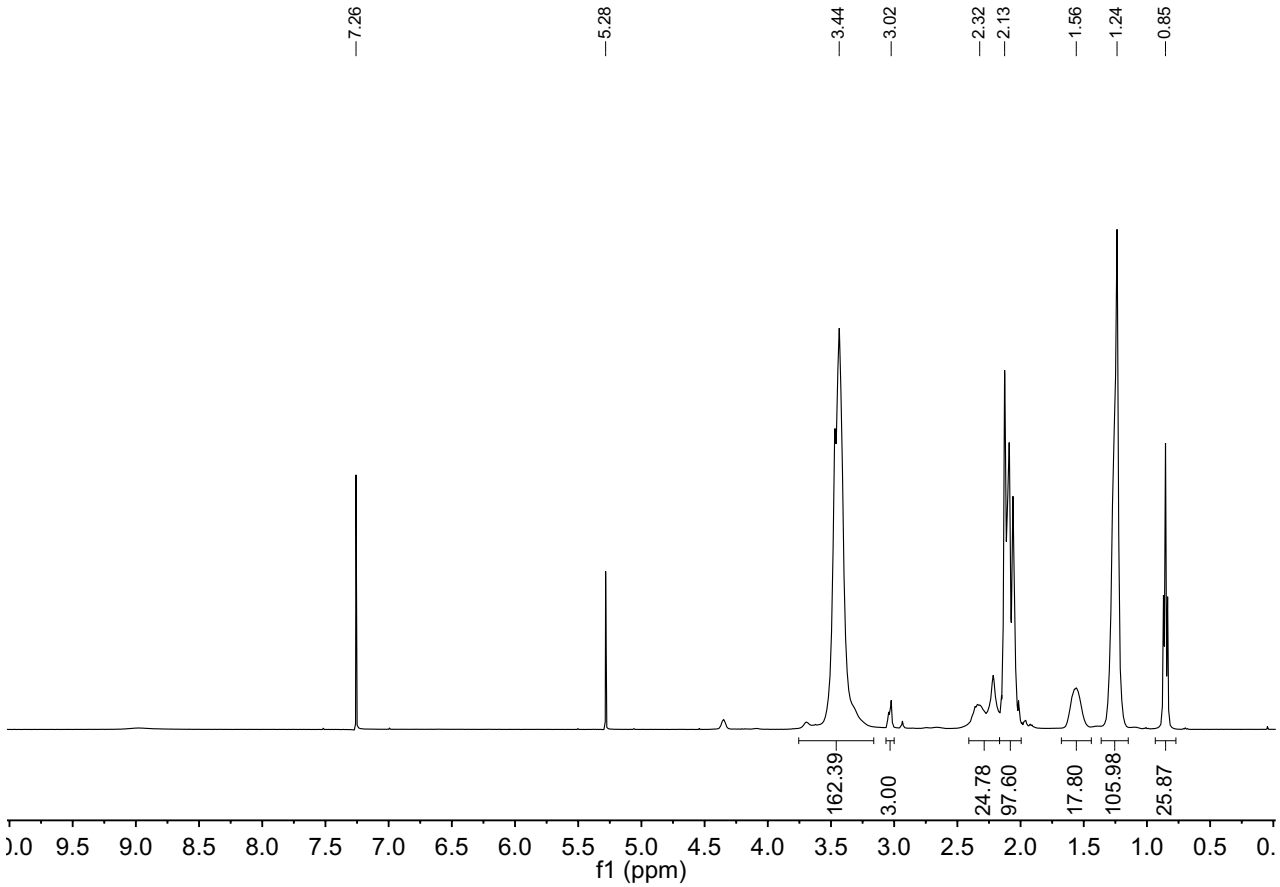

^{1}H NMR (500 MHz, $CDCl_3$) of copolymer **2.8** (MeOx$_{30}$-*b*-NonOx$_{10}$).

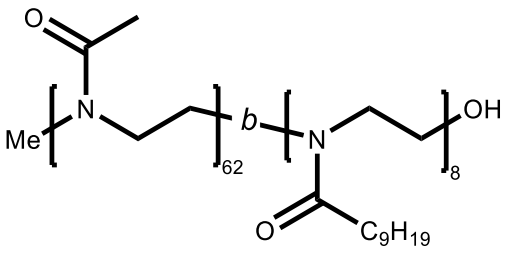

P(MeOx$_{62}$-*b*-NonOx$_8$)

2.17

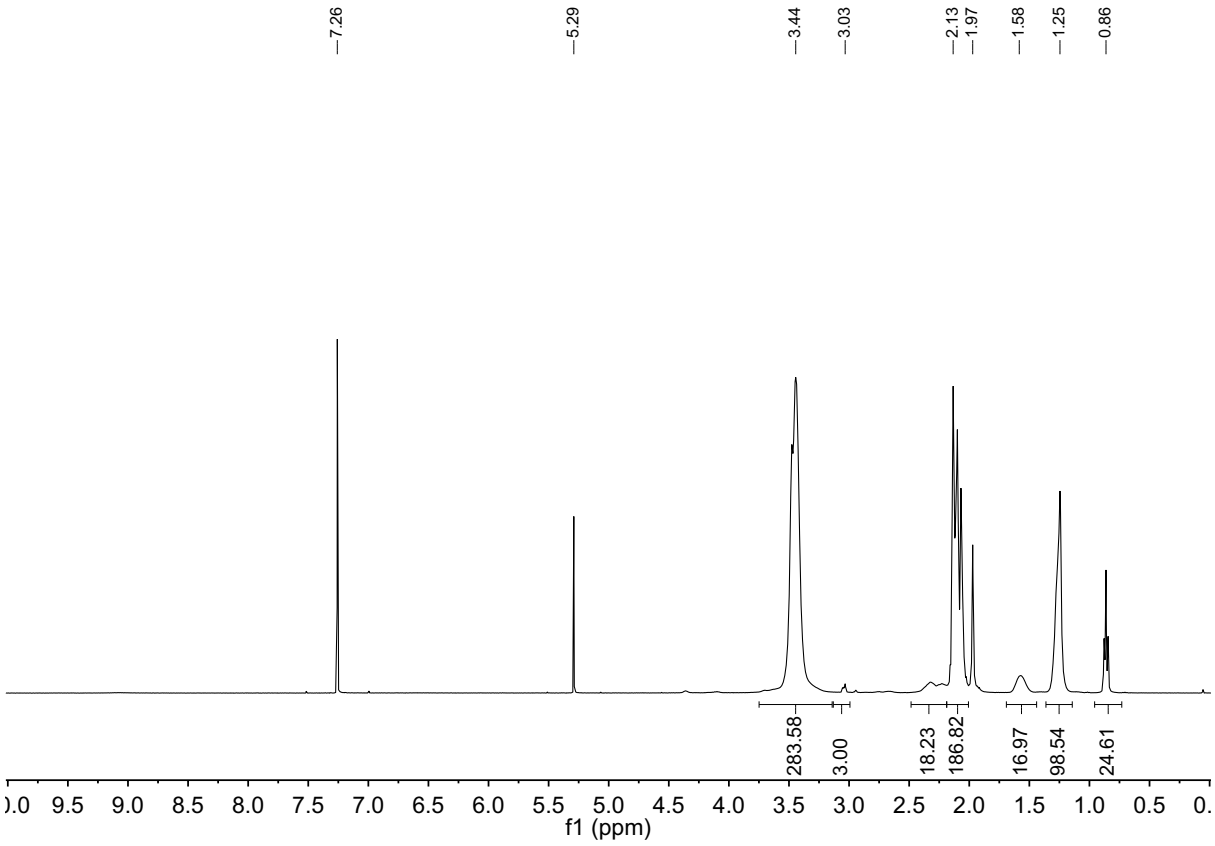

^{1}H NMR (500 MHz, $CDCl_3$) of copolymer **2.17** (MeOx$_{60}$-*b*-NonOx$_{10}$).

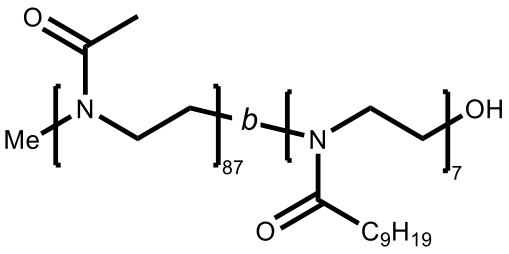

P(MeOx$_{87}$-*b*-NonOx$_7$)

2.18

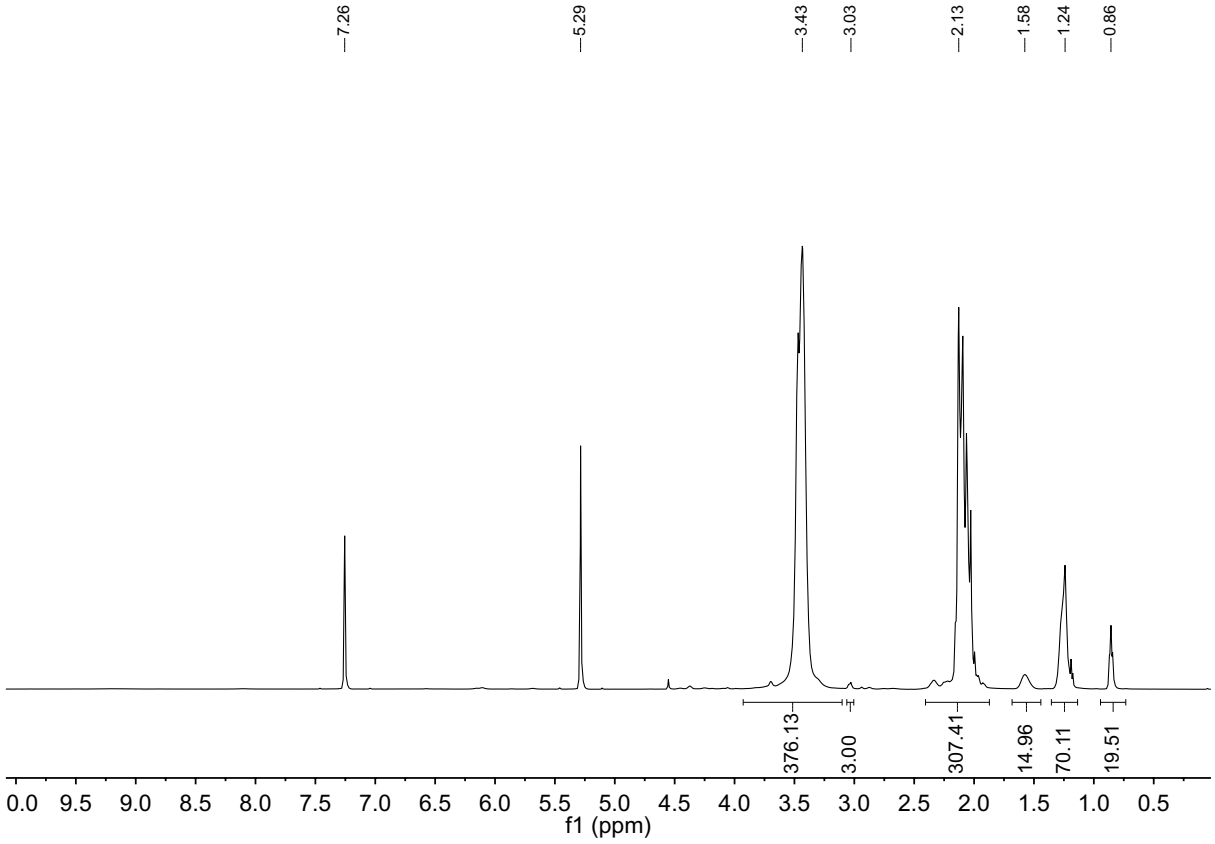

^{1}H NMR (500 MHz, $CDCl_3$) of copolymer **2.18** (MeOx$_{90}$-*b*-NonOx$_{10}$).

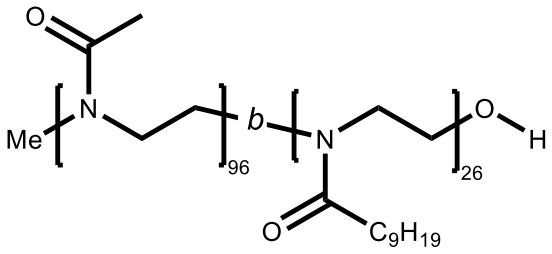

P(MeOx$_{96}$-*b*-NonOx$_{26}$)

2.19

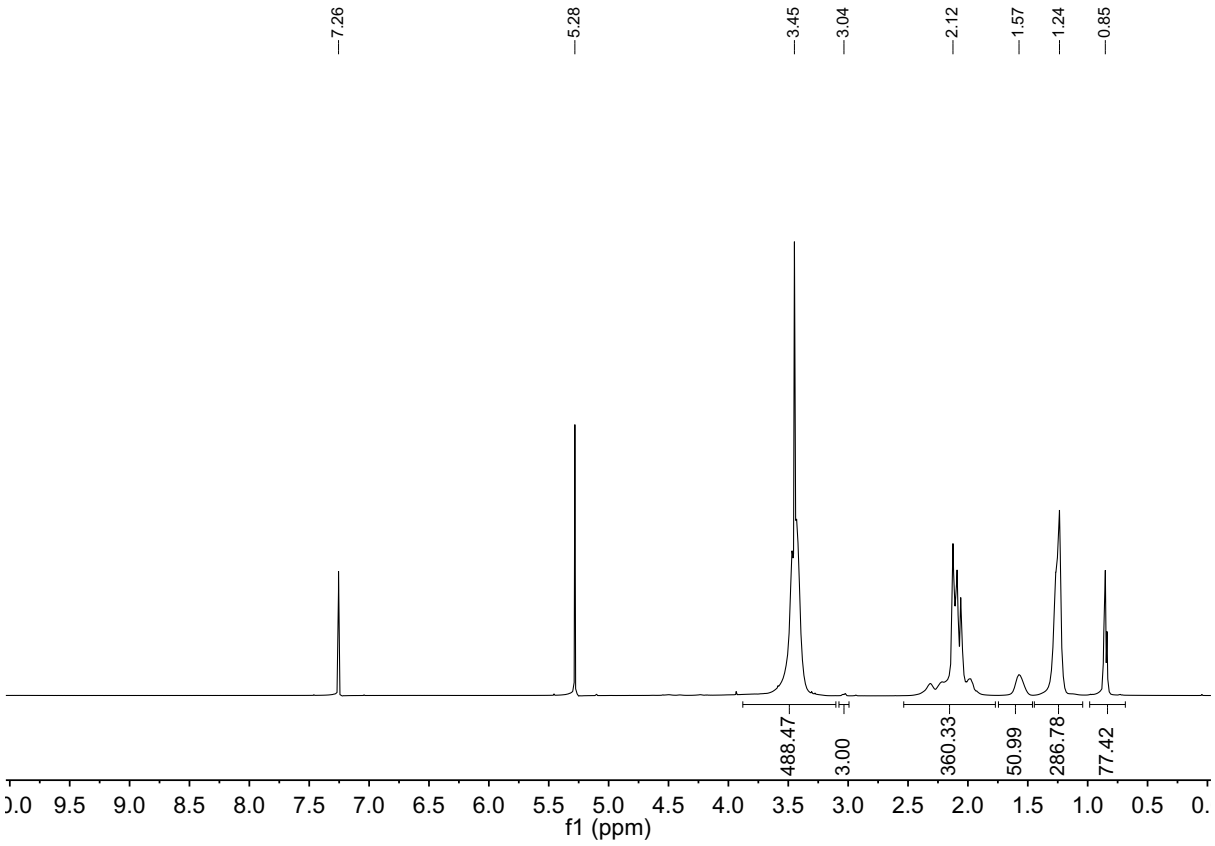

^{1}H NMR (500 MHz, $CDCl_3$) of copolymer **2.19** (MeOx$_{90}$-*b*-NonOx$_{30}$).

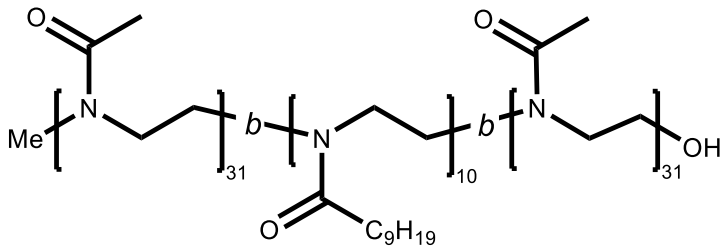

($MeOx_{31}$-*b*-$NonOx_{10}$-*b*-$MeOx_{31}$)

2.9

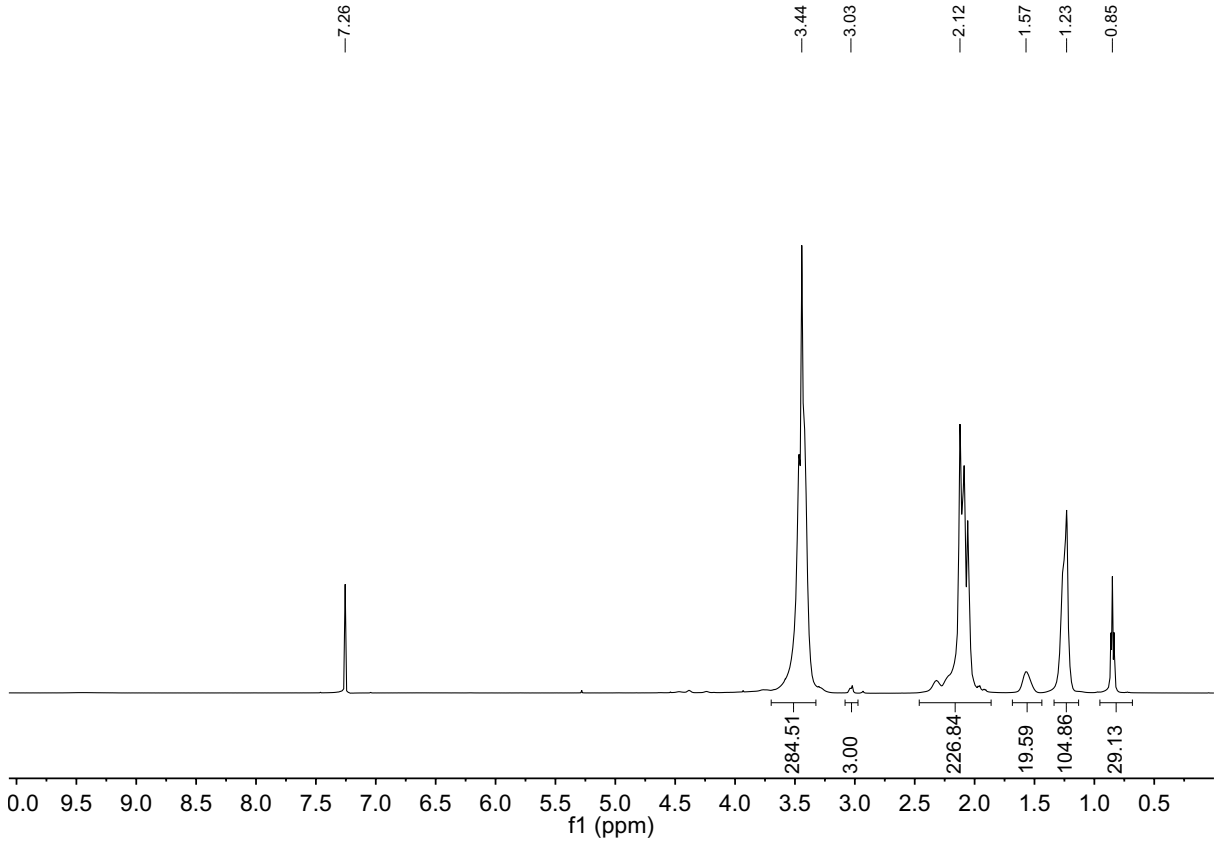

^{1}H NMR (500 MHz, $CDCl_3$) of copolymer **2.9** ($MeOx_{30}$-*b*-$NonOx_{10}$-*b*-$MeOx_{30}$).

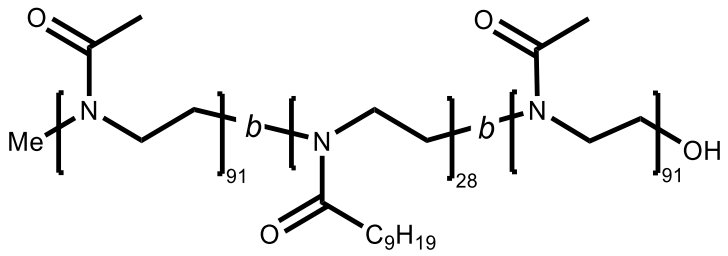

(MeOx$_{91}$-*b*-NonOx$_{28}$-*b*-MeOx$_{91}$)

2.20

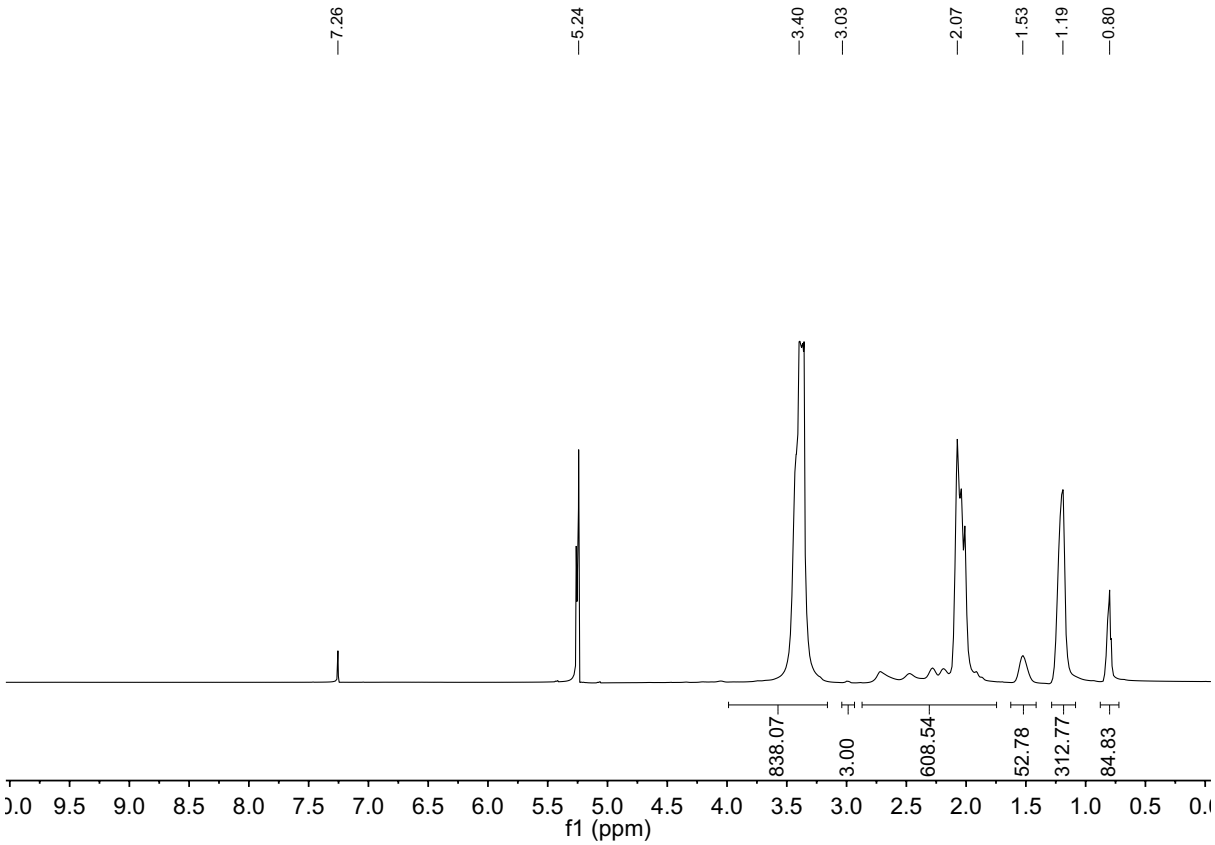

^{1}H NMR (500 MHz, $CDCl_3$) of copolymer **2.20** (MeOx$_{90}$-*b*-NonOx$_{10}$-*b*-MeOx$_{90}$).

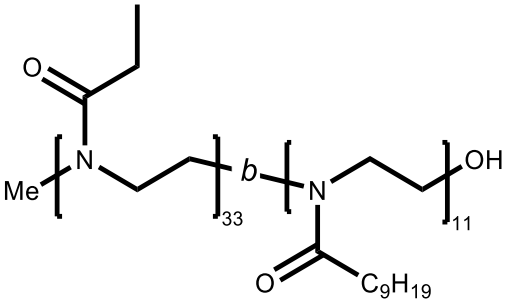

P(EtOx$_{30}$-*b*-NonOx$_{10}$)

2.21

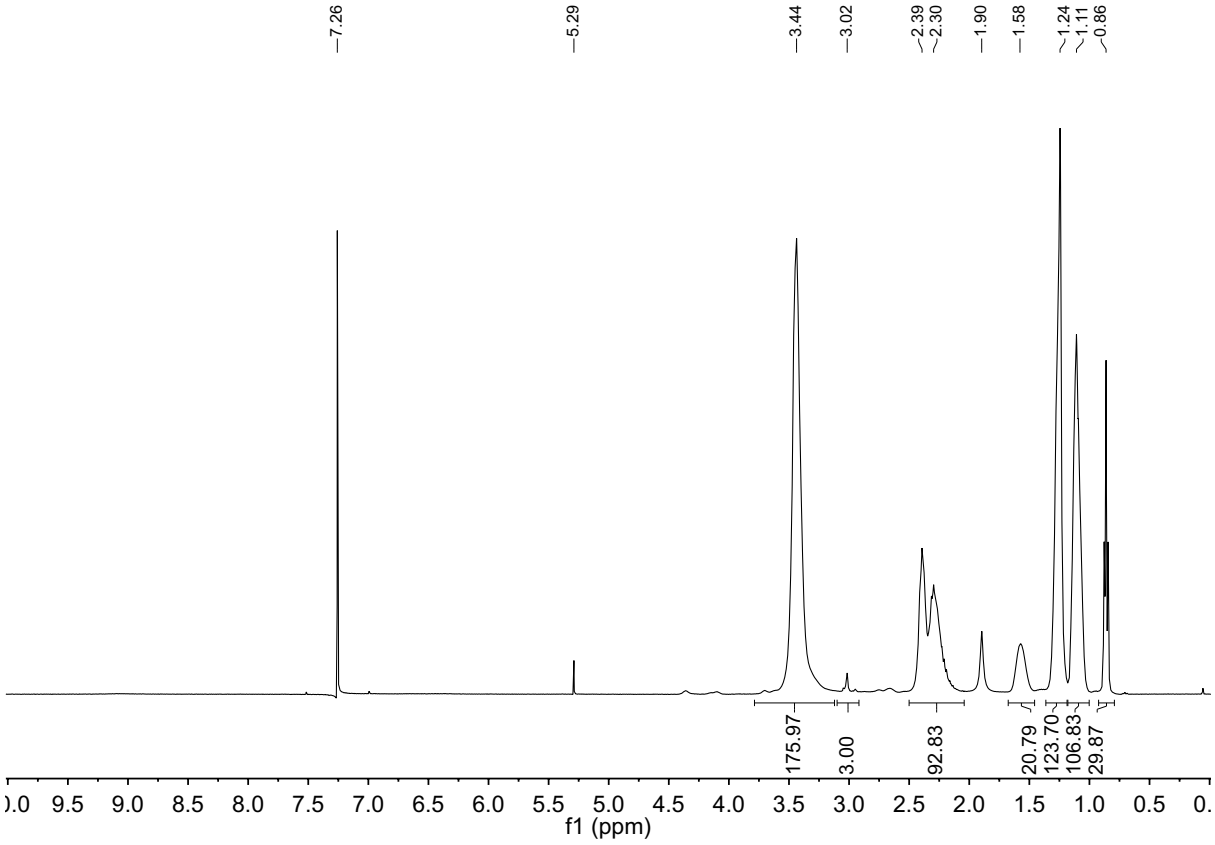

^{1}H NMR (500 MHz, $CDCl_3$) of copolymer **2.21** (EtOx$_{30}$-*b*-NonOx$_{10}$).

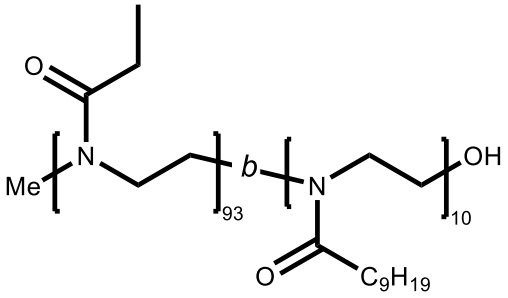

P(EtOx$_{93}$-*b*-NonOx$_{10}$)

2.22

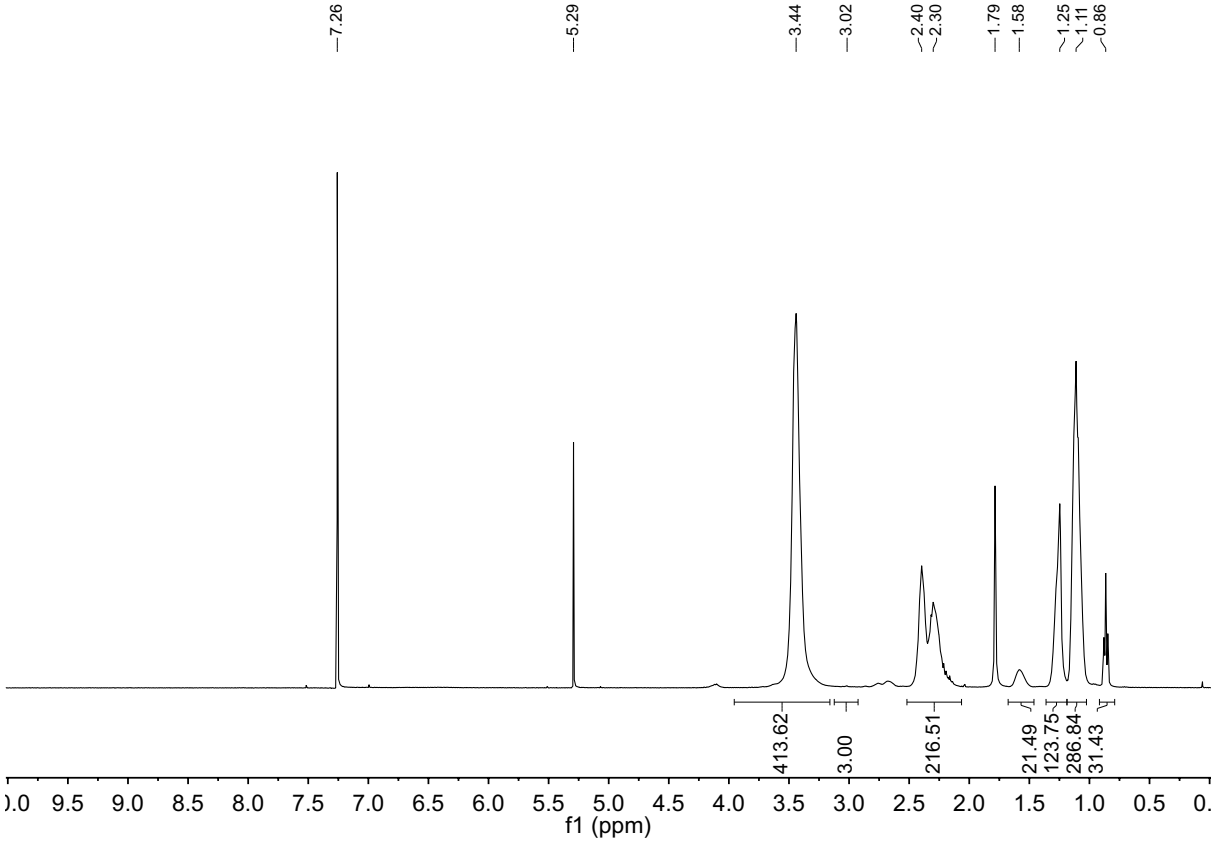

^{1}H NMR (500 MHz, $CDCl_3$) of copolymer **2.22** (EtOx$_{90}$-*b*-NonOx$_{10}$).

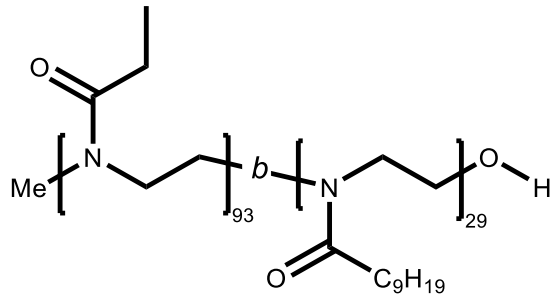

P(EtOx$_{93}$-*b*-NonOx$_{29}$)

2.23

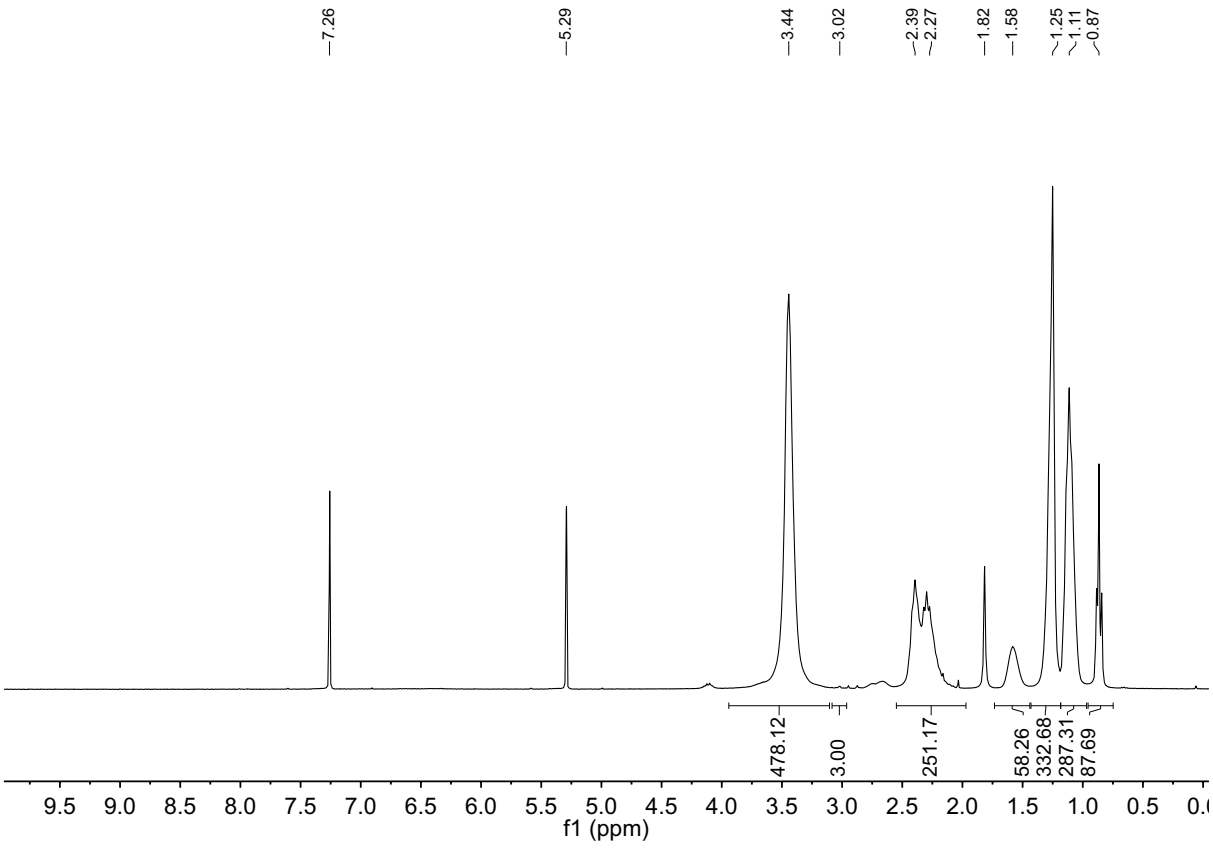

^{1}H NMR (500 MHz, $CDCl_3$) of copolymer **2.23** (EtOx$_{90}$-*b*-NonOx$_{30}$).w

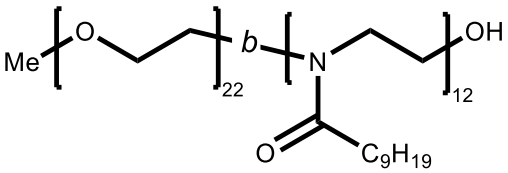

PEG_{1K}-*b*-$NonOx_{12}$

2.24

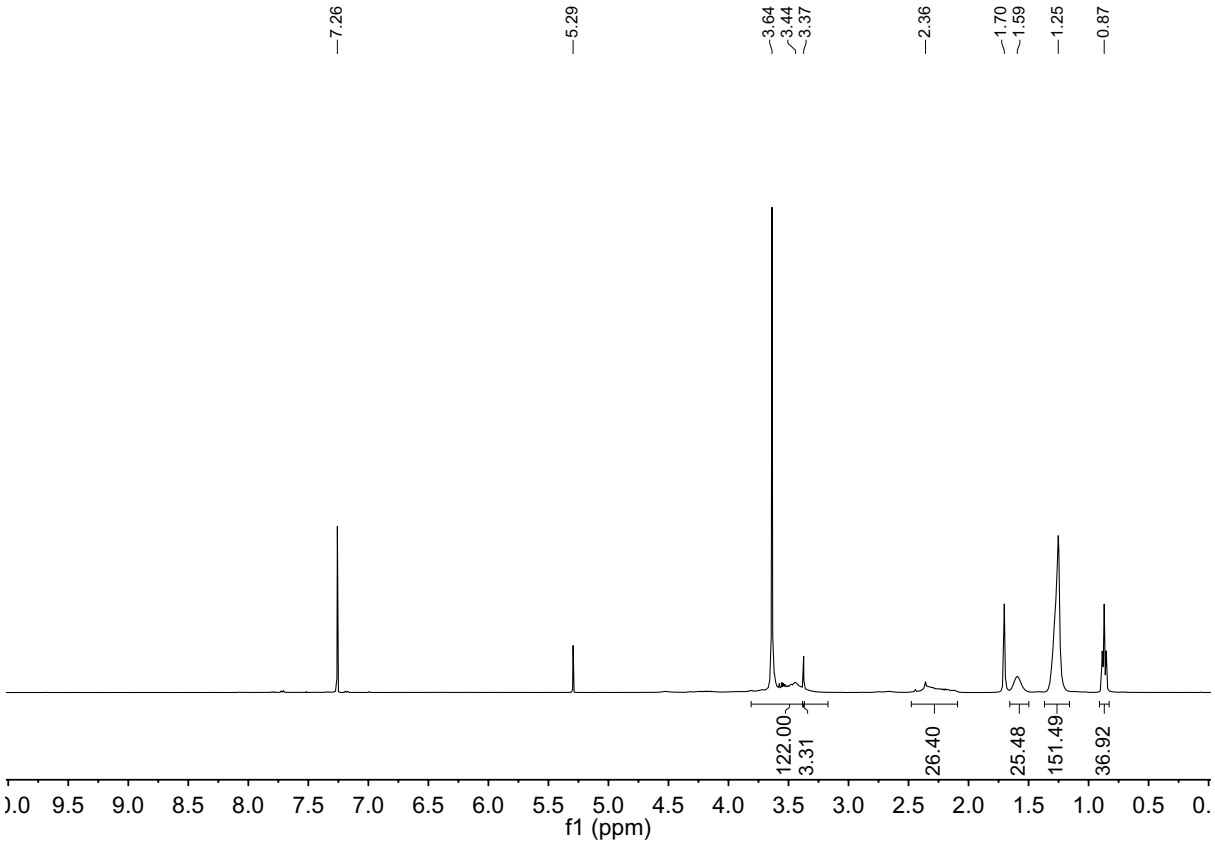

^{1}H NMR (500 MHz, $CDCl_3$) of copolymer **2.24** (PEG_{1K}-*b*-$NonOx_{10}$).

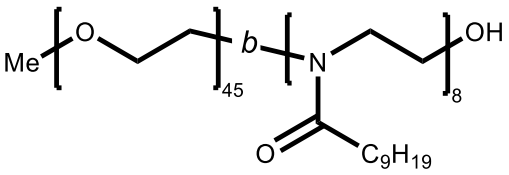

PEG_{2K}-*b*-$NonOx_8$

2.25

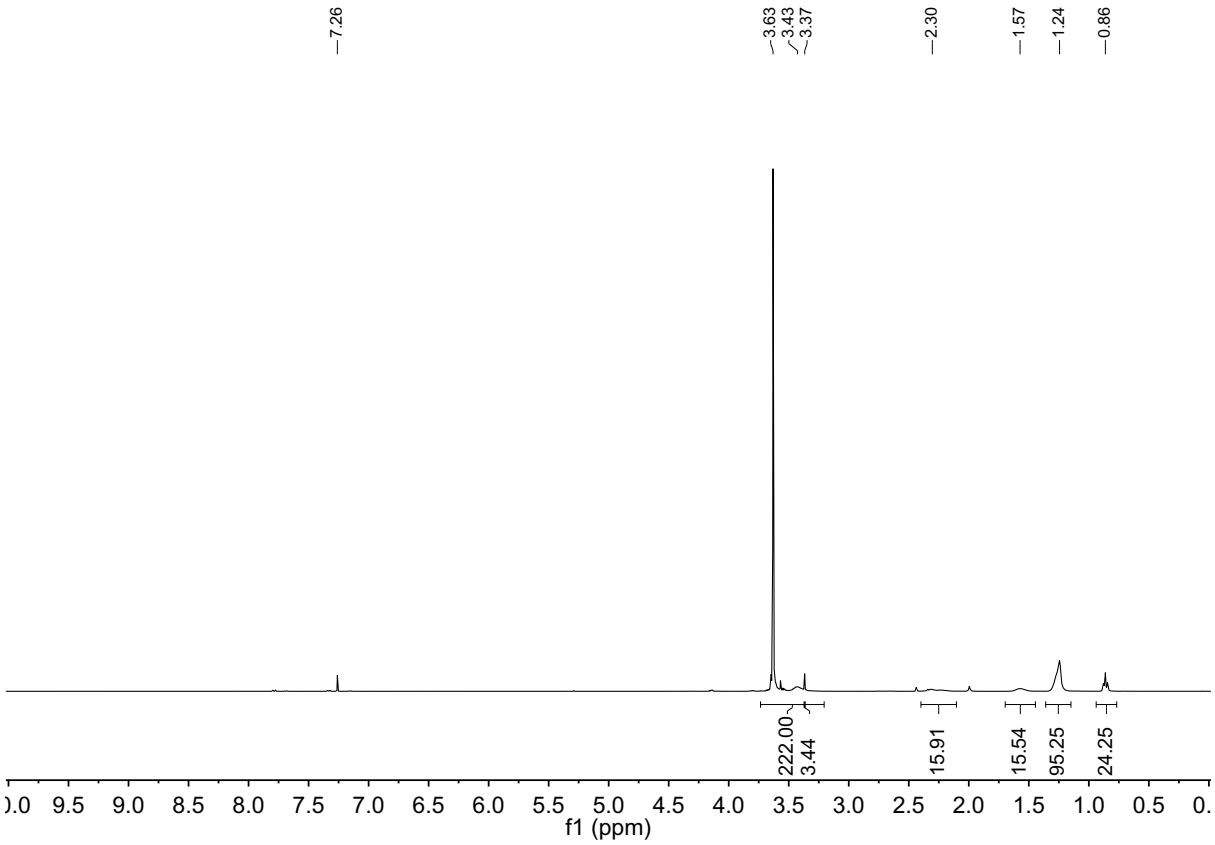

^{1}H NMR (500 MHz, $CDCl_3$) of copolymer **2.25** (PEG_{2K}-*b*-$NonOx_{10}$).

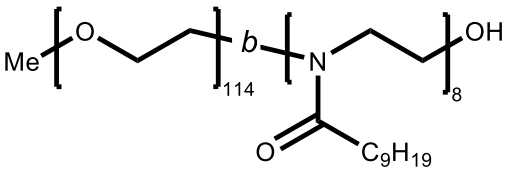

PEG_{5K}-*b*-$NonOx_8$

2.26

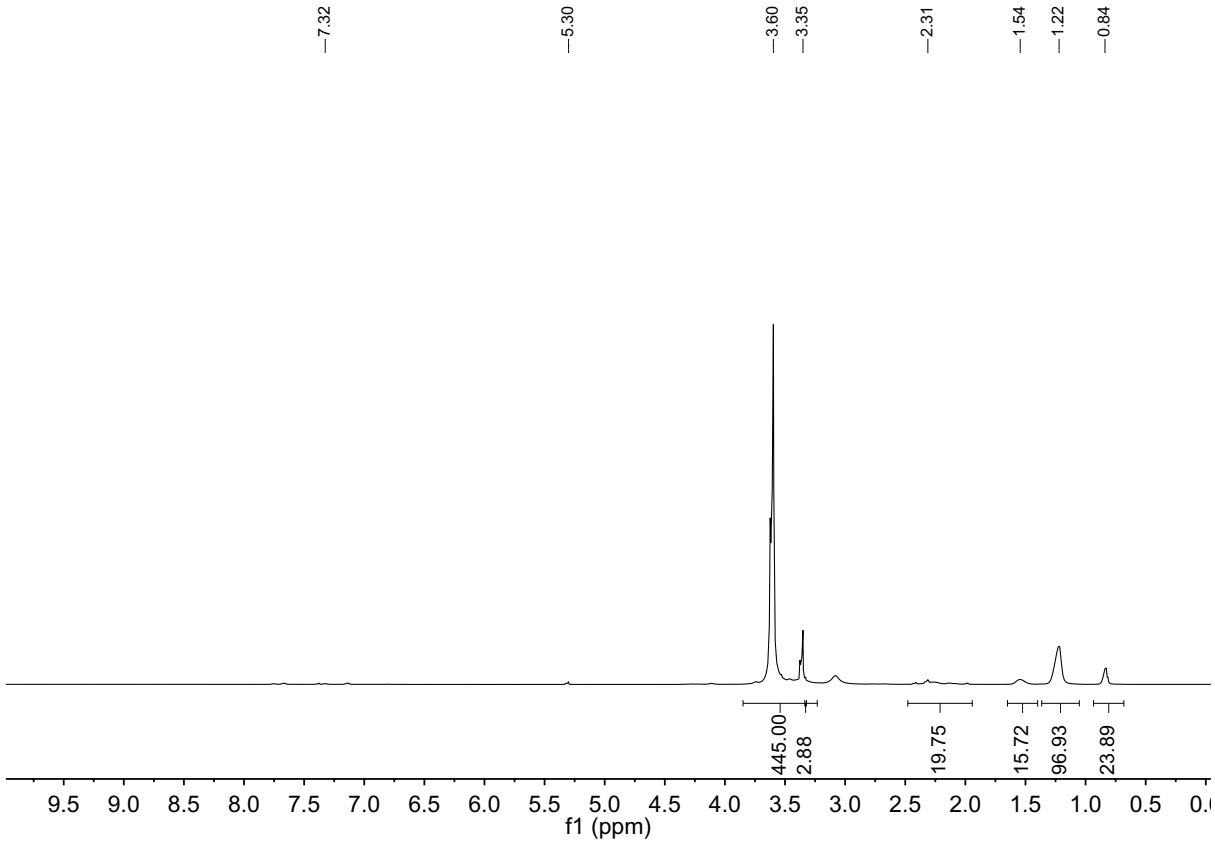

^{1}H NMR (500 MHz, $CDCl_3$) of copolymer **2.26** (PEG_{5K}-*b*-$NonOx_{10}$).

2.8 SEC-GPC Spectra Relevant to Chapter Two

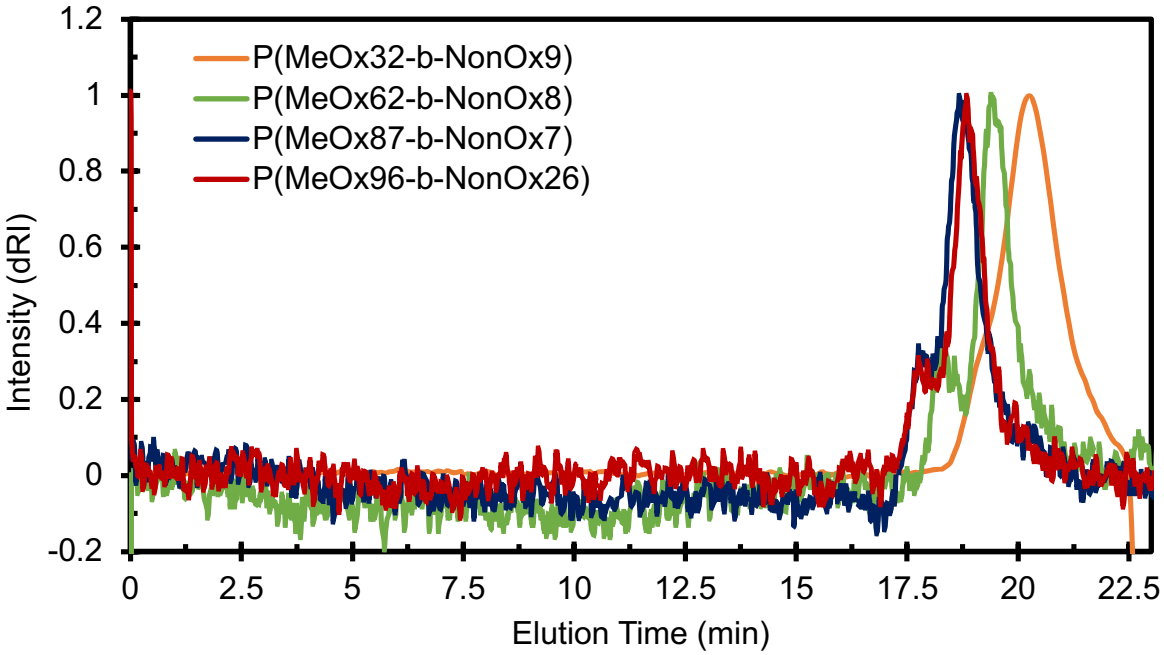

Size exclusion chromatogram of **2.8** (P(MeOx$_{30}$-*b*-NonOx$_{10}$)), **2.17** (P(MeOx$_{60}$-*b*-NonOx$_{10}$)), **2.18** (P(MeOx$_{90}$-*b*-NonOx$_{10}$)), **2.19** (P(MeOx$_{90}$-*b*-NonOx$_{10}$)). Eluent was DMF with LiBr (0.1 M) at 50 °C (flow rate: 0.80 mL/min).

Note: Shoulders have previously been observed in poly(2-oxazoline)s and may be attributed to aggregation, sample-column interactions,[4,5] or either extrinsic or intrinsic chain transfer/coupling side reactions that may occur at high monomer conversion and high reaction temperatures.[6,7]

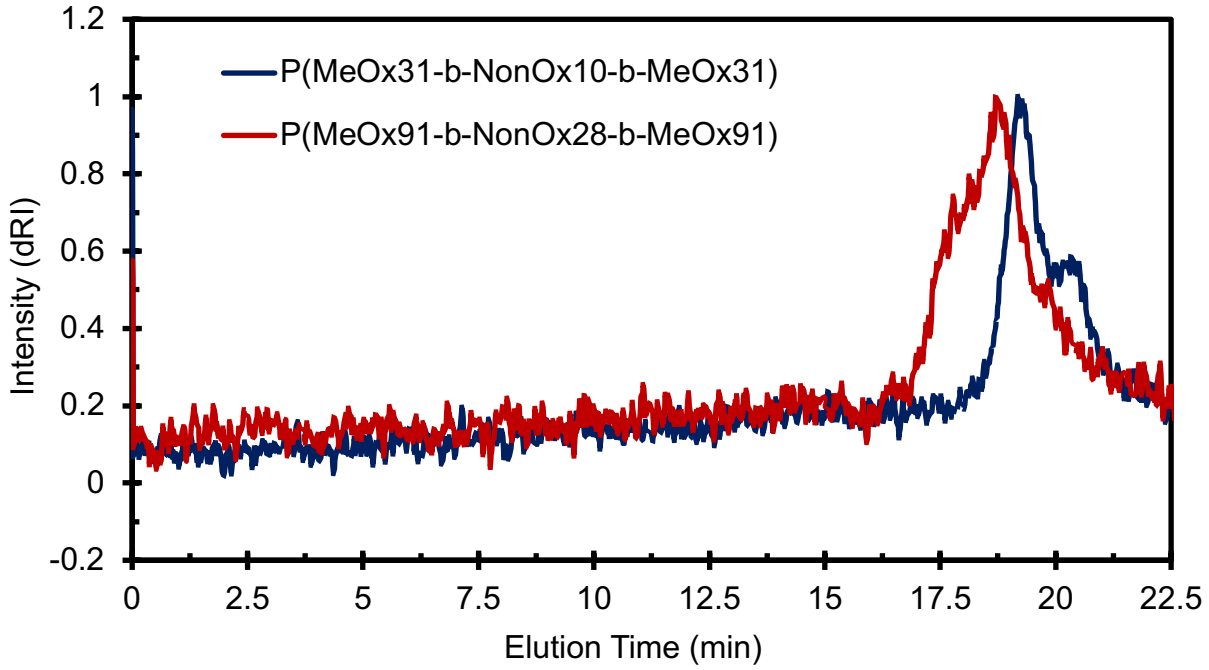

Size exclusion chromatogram of **2.9** (P(MeOx$_{30}$-*b*-Non$_{10}$-*b*-NonOx$_{30}$)), **2.20** (P(MeOx$_{90}$-*b*-Non$_{30}$-*b*-MeOx$_{90}$)). Eluent was DMF with LiBr (0.1 M) at 50 °C (flow rate: 0.80 mL/min). Note: Shoulders have previously been observed in poly(2-oxazoline)s and may be attributed to aggregation, sample-column interactions,[4,5] or either extrinsic or intrinsic chain transfer/coupling side reactions that may occur at high monomer conversion and high reaction temperatures.[6,7]

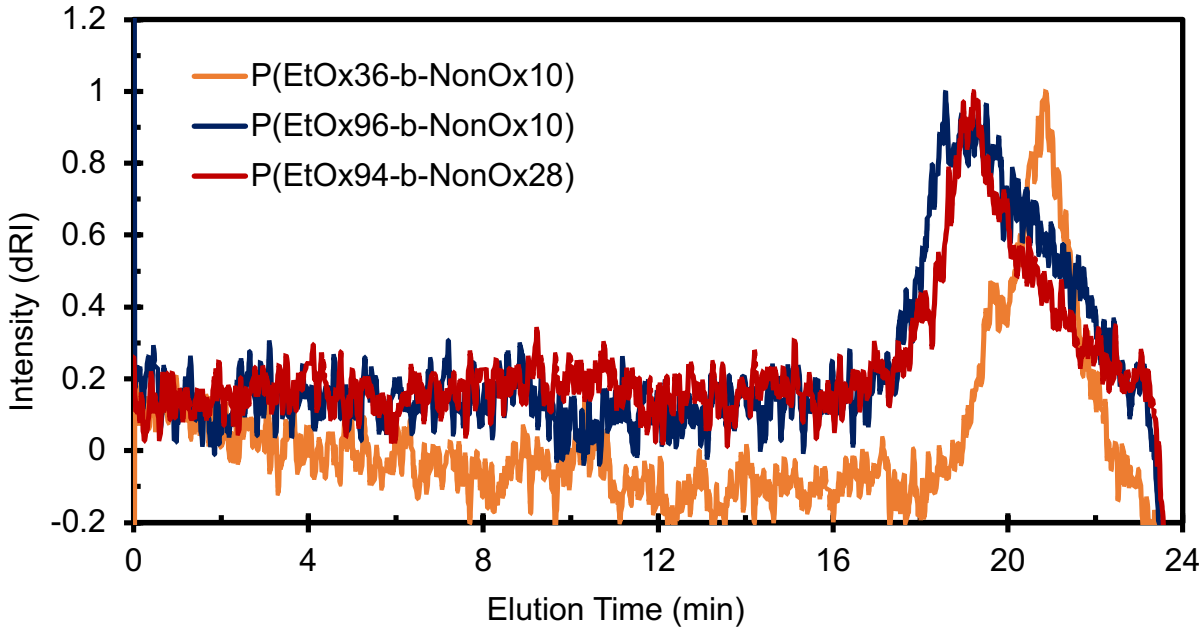

Size exclusion chromatogram of **2.21** (P(EtOx$_{30}$-*b*-NonOx$_{10}$)), **2.22** (P(EtOx$_{90}$-*b*-NonOx$_{10}$)), **2.23** (P(EtOx$_{90}$-*b*-NonOx$_{30}$)). Eluent was DMF with LiBr (0.1 M) at 50 °C (flow rate: 0.80 mL/min). Note: Shoulders have previously been observed in poly(2-oxazoline)s and may be attributed to aggregation, sample-column interactions,[4,5] or either extrinsic or intrinsic chain transfer/coupling side reactions that may occur at high monomer conversion and high reaction temperatures.[6,7]

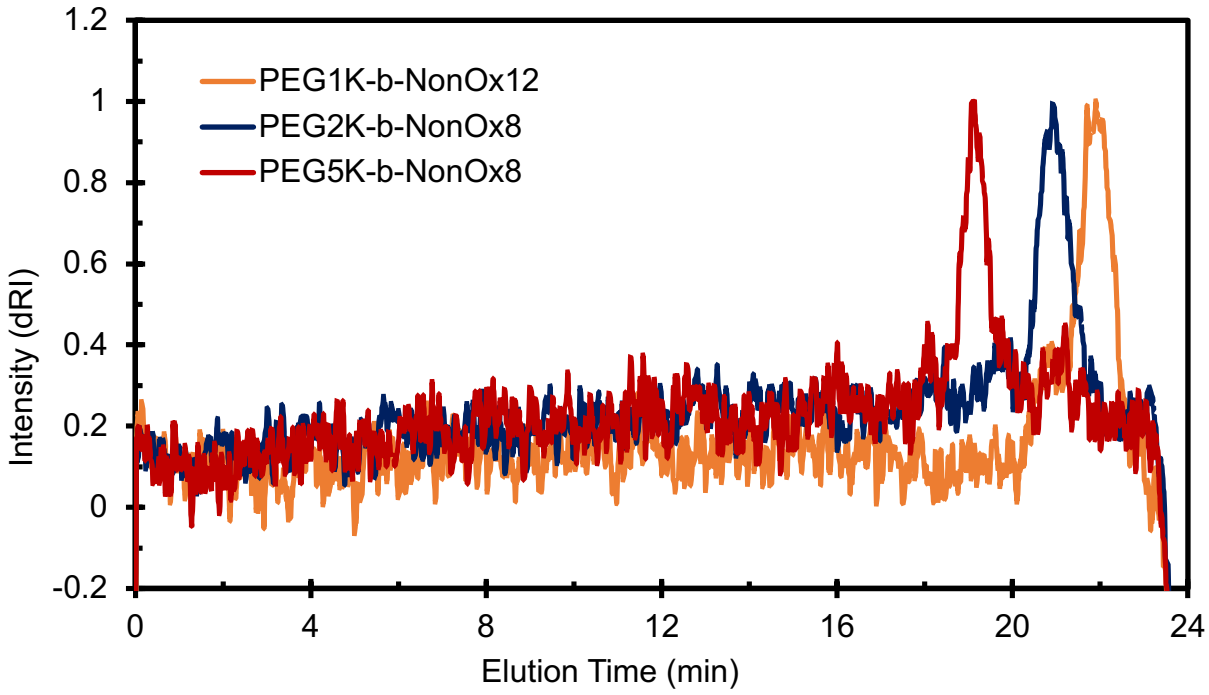

Size exclusion chromatogram of **2.24** (PEG_{1K}-*b*-$NonOx_{10}$), **2.25** (PEG_{2K}-*b*-$NonOx_{10}$), **2.26** (PEG_{5K}-*b*-$NonOx_{30}$). Eluent was DMF with LiBr (0.1 M) at 50 °C (flow rate: 0.80 mL/min).

2.9 References

(1) Shi, J.; Kantoff, P. W.; Wooster, R.; Farokhzad, O. C. Cancer Nanomedicine: Progress, Challenges and Opportunities. *Nat. Rev. Cancer* **2017**, *17*, 20–37.

(2) Bobo, D.; Robinson, K. J.; Islam, J.; Thurecht, K. J.; Corrie, S. R. Nanoparticle-Based Medicines: A Review of FDA-Approved Materials and Clinical Trials to Date. *Pharm. Res.* **2016**, *33*, 2373–2387.

(3) De Jong, W. H.; Borm, P. J. A. Drug Delivery and Nanoparticles: Applications and Hazards. *Int. J. Nanomedicine* **2008**, *3*, 133–149.

(4) Chithrani, B. D.; Ghazani, A. A.; Chan, W. C. W. Determining the Size and Shape Dependence of Gold Nanoparticle Uptake into Mammalian Cells. *Nano Lett.* **2006**, *6*, 662–668.

(5) Su, G.; Zhou, H.; Mu, Q.; Zhang, Y.; Li, L.; Jiao, P.; Jiang, G.; Yan, B. Effective Surface Charge Density Determines the Electrostatic Attraction between Nanoparticles and Cells. *J. Phys. Chem. C* **2012**, *116*, 4993–4998.

(6) Beduneau, A.; Ma, Z.; Grotepas, C. B.; Kabanov, A.; Rabinow, B. E.; Gong, N.; Mosley, R. L.; Dou, H.; Boska, M. D.; Gendelman, H. E. Facilitated Monocyte-Macrophage Uptake and Tissue Distribution of Superparmagnetic Iron-Oxide Nanoparticles. *PLoS One* **2009**, *4*, 1–12.

(7) Albanese, A.; Tang, P. S.; Chan, W. C. W. The Effect of Nanoparticle Size, Shape, and Surface Chemistry on Biological Systems. *Annu. Rev. Biomed. Eng.* **2012**, *14*, 1–16.

(8) Bai, X.; Liu, F.; Liu, Y.; Li, C.; Wang, S.; Zhou, H.; Wang, W.; Zhu, H.; Winkler, D. A.; Yan, B. Toward a Systematic Exploration of Nano-Bio Interactions. *Toxicol. Appl. Pharmacol.* **2017**, *323*, 66–73.

(9) Hauck, T. S.; Ghazani, A. A.; Chan, W. C. W. Assessing the Effect of Surface Chemistry on Gold Nanorod Uptake, Toxicity, and Gene Expression in Mammalian Cells. *Small* **2008**, *4*, 153–159.

(10) Van Haute, D.; Liu, A. T.; Berlin, J. M. Coating Metal Nanoparticle Surfaces with Small Organic Molecules Can Reduce Nonspecific Cell Uptake. *ACS Nano* **2018**, *12*, 117–127.

(11) Linares, J.; Matesanz, M. C.; Vila, M.; Feito, M. J.; Gonçalves, G.; Vallet-Regí, M.; Marques, P. A. A. P.; Portolés, M. T. Endocytic Mechanisms of Graphene Oxide Nanosheets in Osteoblasts, Hepatocytes and Macrophages. *ACS Appl. Mater. Interfaces* **2014**, *6*, 13697–13706.

(12) Francia, V.; Yang, K.; Deville, S.; Reker-Smit, C.; Nelissen, I.; Salvati, A. Corona Composition Can Affect the Mechanisms Cells Use to Internalize Nanoparticles. *ACS Nano* **2019**, *13*, 11107–11121.

(13) Vertegel, A. A.; Siegel, R. W.; Dordick, J. S. Silica Nanoparticle Size Influences the Structure and Enzymatic Activity of Adsorbed Lysozyme. *Langmuir* **2004**, *20*, 6800–6807.

(14) Durán, N.; Silveira, C. P.; Durán, M.; Martinez, D. S. T. Silver Nanoparticle Protein Corona and Toxicity: A Mini-Review. *J. Nanobiotechnology* **2015**, *13*, 1–17.

(15) Lu, F.; Wu, S. H.; Hung, Y.; Mou, C. Y. Size Effect on Cell Uptake in Well-Suspended, Uniform Mesoporous Silica Nanoparticles. *Small* **2009**, *5*, 1408–1413.

(16) Barenholz, Y. Doxil® - The First FDA-Approved Nano-Drug: Lessons Learned. *J. Control. Release* **2012**, *160*, 117–134.

(17) Peer, D.; Karp, J. M.; Hong, S.; Farokhzad, O. C.; Margalit, R.; Langer, R. Nanocarriers as an Emerging Platform for Cancer Therapy. *Nat. Nanotechnol.* **2007**, *2*, 751–760.

(18) Caruso, F.; Hyeon, T.; Rotello, V. M. Nanomedicine. *Chem. Soc. Rev.* **2012**, *41*, 2537–

2538.

(19) Aswathanarayan, J. B.; Vittal, R. R. Nanoemulsions and Their Potential Applications in Food Industry. *Front. Sustain. Food Syst.* **2019**, *3*, 1.

(20) Tadros, T.; Izquierdo, P.; Esquena, J.; Solans, C. Formation and Stability of Nano-Emulsions. *Adv. Colloid Interface Sci.* **2004**, *108–109*, 303–318.

(21) Gupta, A.; Eral, H. B.; Hatton, T. A.; Doyle, P. S. Nanoemulsions: Formation, Properties and Applications. *Soft Matter* **2016**, *12*, 2826–2841.

(22) Hörmann, K.; Zimmer, A. Drug Delivery and Drug Targeting with Parenteral Lipid Nanoemulsions - A Review. *J. Control. Release* **2016**, *223*, 85–98.

(23) Takino, T.; Konishi, K.; Takakura, Y.; Hashida, M. Long Circulating Emulsion Carrier Systems for Highly Lipophilic Drugs. *Biol. Pharm. Bull.* **1994**, *17*, 121–125.

(24) Gladysz, J. A.; Jurisch, M. Structural, Physical, and Chemical Properties of Fluorous Compounds. *Top. Curr. Chem.* **2012**, *308*, 1–24.

(25) Sletten, E. M.; Swager, T. M. Readily Accessible Multifunctional Fluorous Emulsions. *Chem. Sci.* **2016**, *7*, 5091–5097.

(26) Sletten, E. M.; Swager, T. M. Fluorofluorophores: Fluorescent Fluorous Chemical Tools Spanning the Visible Spectrum. *J. Am. Chem. Soc.* **2014**, *136*, 13574–13577.

(27) Day, R. A.; Estabrook, D. A.; Logan, J. K.; Sletten, E. M. Fluorous Photosensitizers Enhance Photodynamic Therapy with Perfluorocarbon Nanoemulsions. *Chem. Commun.* **2017**, *53*, 13043–13046.

(28) Miller, M. A.; Sletten, E. M. A General Approach to Biocompatible Branched Fluorous Tags for Increased Solubility in Perfluorocarbon Solvents. *Org. Lett.* **2018**, *20*, 6850–6854.

(29) Gladysz, J. A.; Curran, D. P.; Horváth, I. T. Handbook of Fluorous Chemistry. *Handb.*

Fluorous Chem. **2005**, 1–595.

(30) Spence, R. K.; Norcross, E. D.; Costabile, J.; McCoy, S.; Cernaianu, A. C.; Alexander, J. B.; Pello, M. J.; Atabek, U.; Camishion, R. C. Perfluorocarbons as Blood Substitutes: The Early Years. Experience with Fluosol Da-20% in the 1980S. *Artif. Cells, Blood Substitutes, Biotechnol.* **1994**, *22*, 955–963.

(31) Mitsuno, T.; Ohyanagi, H.; Naito, R. Clinical Studies of a Perfluorochemical Whole Blood Substitute (Fluosol-DA). Summary of 186 Cases. *Ann. Surg.* **1982**, *195*, 60–69.

(32) Goodman, R. L.; Moore, R. E.; Davis, M. E.; Stokes, D.; Yuhas, J. M. Perfluorocarbon Emulsions in Cancer Therapy: Preliminary Observations on Presently Available Formulations. *Int. J. Radiat. Oncol. Biol. Phys.* **1984**, *10*, 1421–1424.

(33) Riess, J. G. The Design and Development of Improved Fluorocarbon-Based Products for Use in Medicine and Biology. *Artif. Cells, Blood Substitutes, Biotechnol.* **1994**, *22*, 215–234.

(34) Janjic, J. M.; Srinivas, M.; Kadayakkara, D. K. K.; Ahrens, E. T. Self-Delivering Nanoemulsions for Dual Fluorine-19 MRI and Fluorescence Detection. *J. Am. Chem. Soc.* **2008**, *130*, 2832–2841.

(35) Kaneda, M. M.; Caruthers, S.; Lanza, G. M.; Wickline, S. A. Perfluorocarbon Nanoemulsions for Quantitative Molecular Imaging and Targeted Therapeutics. *Ann. Biomed. Eng.* **2009**, *37*, 1922–1933.

(36) Akazawa, K.; Sugihara, F.; Nakamura, T.; Matsushita, H.; Mukai, H.; Akimoto, R.; Minoshima, M.; Mizukami, S.; Kikuchi, K. Perfluorocarbon-Based 19F MRI Nanoprobes for In Vivo Multicolor Imaging. *Angew. Chem. Int. Ed.* **2018**, *57*, 16742–16747.

(37) Huang, Y.; Vezeridis, A. M.; Wang, J.; Wang, Z.; Thompson, M.; Mattrey, R. F.;

Gianneschi, N. C. Polymer-Stabilized Perfluorobutane Nanodroplets for Ultrasound Imaging Agents. *J. Am. Chem. Soc.* **2017**, *139*, 15–18.

(38) Díaz-López, R.; Tsapis, N.; Fattal, E. Liquid Perfluorocarbons as Contrast Agents for Ultrasonography and 19F-MRI. *Pharm. Res.* **2010**, *27*, 1–16.

(39) Cheng, Y.; Cheng, H.; Jiang, C.; Qiu, X.; Wang, K.; Huan, W.; Yuan, A.; Wu, J.; Hu, Y. Perfluorocarbon Nanoparticles Enhance Reactive Oxygen Levels and Tumour Growth Inhibition in Photodynamic Therapy. *Nat. Commun.* **2015**, *6*, 1–8.

(40) Patrick, M. J.; Janjic, J. M.; Teng, H.; O'Hear, M. R.; Brown, C. W.; Stokum, J. A.; Schmidt, B. F.; Ahrens, E. T.; Waggoner, A. S. Intracellular PH Measurements Using Perfluorocarbon Nanoemulsions. *J. Am. Chem. Soc.* **2013**, *135*, 18445–18457.

(41) Medina, S. H.; Michie, M. S.; Miller, S. E.; Schnermann, M. J.; Schneider, J. P. Fluorous Phase-Directed Peptide Assembly Affords Nano-Peptisomes Capable of Ultrasound-Triggered Cellular Delivery. *Angew. Chem. Int. Ed.* **2017**, *56*, 11404–11408.

(42) Kaneda, M. M.; Sasaki, Y.; Lanza, G. M.; Milbrandt, J.; Wickline, S. A. Mechanisms of Nucleotide Trafficking during SiRNA Delivery to Endothelial Cells Using Perfluorocarbon Nanoemulsions. *Biomaterials* **2010**, *31*, 3079–3086.

(43) Patrick, M. J.; Janjic, J. M.; Teng, H.; O'Hear, M. R.; Brown, C. W.; Stokum, J. A.; Schmidt, B. F.; Ahrens, E. T.; Waggoner, A. S. Intracellular PH Measurements Using Perfluorocarbon Nanoemulsions. *J. Am. Chem. Soc.* **2013**, *135*, 18445–18457.

(44) Partlow, K. C.; Lanza, G. M.; Wickline, S. A. Exploiting Lipid Raft Transport with Membrane Targeted Nanoparticles: A Strategy for Cytosolic Drug Delivery. *Biomaterials* **2008**, *29*, 3367–3375.

(45) Gould, S. A.; Rosen, A. L.; Sehgal, L. R.; Sehgal, H. L.; Langdale, L. A.; Krause, L. M.;

Rice, C. L.; Chamberlin, W. H.; Moss, G. S. Fluosol-DA as a Red-Cell Substitute in Acute Anemia. *N. Engl. J. Med.* **1986**, *314*, 1653–1656.

(46) Viegas, T. X.; Bentley, M. D.; Harris, J. M.; Fang, Z.; Yoon, K.; Dizman, B.; Weimer, R.; Mero, A.; Pasut, G.; Veronese, F. M. Polyoxazoline: Chemistry, Properties, and Applications in Drug Delivery. *Bioconjug. Chem.* **2011**, *22*, 976–986.

(47) Hoogenboom, R. Poly(2-Oxazoline)s: A Polymer Class with Numerous Potential Applications. *Angew. Chem. Int. Ed.* **2009**, *48*, 7978–7994.

(48) Estabrook, D. A.; Ennis, A. F.; Day, R. A.; Sletten, E. M. Controlling Nanoemulsion Surface Chemistry with Poly(2-Oxazoline) Amphiphiles. *Chem. Sci.* **2019**, *10*, 3994–4003.

(49) Bonné, T. B.; Lüdtke, K.; Jordan, R.; Papadakis, C. M. Effect of Polymer Architecture of Amphiphilic Poly(2-Oxazoline) Copolymers on the Aggregation and Aggregate Structure. *Macromol. Chem. Phys.* **2007**, *208*, 1402–1408.

(50) Ivanova, R.; Komenda, T.; Bonné, T. B.; Lüdtke, K.; Mortensen, K.; Pranzas, P. K.; Jordan, R.; Papadakis, C. M. Micellar Structures of Hydrophilic/Lipophilic and Hydrophilic/Fluorophilic Poly(2-Oxazoline) Diblock Copolymers in Water. *Macromol. Chem. Phys.* **2008**, *209*, 2248–2258.

(51) Kaberov, L. I.; Verbraeken, B.; Riabtseva, A.; Brus, J.; Radulescu, A.; Talmon, Y.; Stepanek, P.; Hoogenboom, R.; Filippov, S. K. Fluorophilic-Lipophilic-Hydrophilic Poly(2-Oxazoline) Block Copolymers as MRI Contrast Agents: From Synthesis to Self-Assembly. *Macromolecules* **2018**, *51*, 6047–6056.

(52) Jin, R. H. Water Soluble Star Block Poly(Oxazoline) with Porphyrin Label: A Unique Emulsion and Its Shape Direction. *J. Mater. Chem.* **2004**, *14*, 320–327.

(53) Mason, T. G.; Wilking, J. N.; Meleson, K.; Chang, C. B.; Graves, S. M. Nanoemulsions:

Formation, Structure, and Physical Properties. *J. Phys. Condens. Matter* **2006**, *18*.

(54) Kaberov, L. I.; Verbraeken, B.; Riabtseva, A.; Brus, J.; Talmon, Y.; Stepanek, P.; Hoogenboom, R.; Filippov, S. K. Fluorinated 2-Alkyl-2-Oxazolines of High Reactivity: Spacer-Length-Induced Acceleration for Cationic Ring-Opening Polymerization As a Basis for Triphilic Block Copolymer Synthesis. *ACS Macro Lett.* **2018**, *7*, 7–10.

(55) Tadros, T. Principles of Emulsion Stabilization with Special Reference to Polymeric Surfactants. *J. Cosmet. Sci.* **2006**, *57*, 153–169.

(56) Hoogenboom, R.; Wiesbrock, F.; Huang, H.; Leenen, M. A. M.; Thijs, H. M. L.; Van Nispen, S. F. G. M.; Van Der Loop, M.; Fustin, C. A.; Jonas, A. M.; Gohy, J. F.; et al. Microwave-Assisted Cationic Ring-Opening Polymerization of 2-Oxazolines: A Powerful Method for the Synthesis of Amphiphilic Triblock Copolymers. *Macromolecules* **2006**, *39*, 4719–4725.

(57) Wiesbrock, F.; Hoogenboom, R.; Leenen, M.; Van Nispen, S. F. G. M.; Van Der Loop, M.; Abeln, C. H.; Van Den Berg, A. M. J.; Schubert, U. S. Microwave-Assisted Synthesis of a 42-Membered Library of Diblock Copoly(2-Oxazoline)s and Chain-Extended Homo Poly(2-Oxazoline)s and Their Thermal Characterization. *Macromolecules* **2005**, *38*, 7957–7966.

(58) Monnery, B. D.; Jerca, V. V.; Sedlacek, O.; Verbraeken, B.; Cavill, R.; Hoogenboom, R. Defined High Molar Mass Poly(2-Oxazoline)S. *Angew. Chem. Int. Ed.* **2018**, *57*, 15400–15404.

(59) Levin, A.; Mason, T. O.; Adler-Abramovich, L.; Buell, A. K.; Meisl, G.; Galvagnion, C.; Bram, Y.; Stratford, S. A.; Dobson, C. M.; Knowles, T. P. J.; et al. Ostwalds Rule of Stages Governs Structural Transitions and Morphology of Dipeptide Supramolecular Polymers.

Nat. Commun. **2014**, *5*, 5219–5238.

(60) Barres, A. R.; Molugu, S. K.; Stewart, P. L.; Mecozzi, S. Droplet Core Intermolecular Interactions and Block Copolymer Composition Heavily Influence Oil-In-Water Nanoemulsion Stability. *Langmuir* **2019**, *35*, 12765–12772.

(61) Taylor, P. Ostwald Ripening in Emulsions. *Adv. Colloid Interface Sci.* **1998**, *75*, 107–163.

(62) Kabalnov, A. S.; Shchukin, E. D. Ostwald Ripening Theory: Applications to Fluorocarbon Emulsion Stability. *Adv. Colloid Interface Sci.* **1992**, *38*, 69–97.

(63) Riess, J. G. Reassessment of Criteria for the Selection of Perfluorochemicals for Second-Generation Blood Substitutes: Analysis of Structure/Property Relationships. *Artif. Organs* **1984**, *8*, 44–56.

(64) Krafft, M. P.; Riess, J. G. Selected Physicochemical Aspects of Poly- and Perfluoroalkylated Substances Relevant to Performance, Environment and Sustainability-Part One. *Chemosphere* **2015**, *129*, 4–19.

(65) Lim, I.; Vian, A.; Van De Wouw, H. L.; Day, R. A.; Gomez, C.; Liu, Y.; Rheingold, A. L.; Campàs, O.; Sletten, E. M. Fluorous Soluble Cyanine Dyes for Visualizing Perfluorocarbons in Living Systems. *J. Am. Chem. Soc.* **2020**, *142*, 16072–16081.

(66) Miller, M. A.; Day, R. A.; Estabrook, D. A.; Sletten, E. M. A Reduction-Sensitive Fluorous Fluorogenic Coumarin. *Synlett* **2020**, *31*, 450–454.

(67) Boija, E.; Johansson, G. Interactions between Model Membranes and Lignin-Related Compounds Studied by Immobilized Liposome Chromatography. *Biochim. Biophys. Acta - Biomembr.* **2006**, *1758*, 620–626.

(68) Delmas, T.; Piraux, H.; Couffin, A. C.; Texier, I.; Vinet, F.; Poulin, P.; Cates, M. E.; Bibette, J. How to Prepare and Stabilize Very Small Nanoemulsions. *Langmuir* **2011**, *27*, 1683–

1692.

(69) Allen, C.; Dos Santos, N.; Gallagher, R.; Chiu, G. N. C.; Shu, Y.; Li, W. M.; Johnstone, S. A.; Janoff, A. S.; Mayer, L. D.; Webb, M. S.; et al. Controlling the Physical Behavior and Biological Performance of Liposome Formulations through Use of Surface Grafted Poly(Ethylene Glycol). *Biosci. Rep.* **2002**, *22*, 225–250.

(70) Donnelly, J. E.; Ed, D.; Co-chair, F.; Hillman, C. H.; Co-chair, P. D.; Ph, D.; Etnier, J. L.; Ph, D.; Lee, S.; Ph, D.; et al. Physical Activity, Fitness, Cognitive Function, and Academic Achievement in Children: A Systematic Review. *Med. Sci. Sports Exerc.* **2017**, *48*, 1197–1222.

(71) Day, R. A.; Estabrook, D. A.; Wu, C.; Chapman, J. O.; Togle, A. J.; Sletten, E. M. Systematic Study of Perfluorocarbon Nanoemulsions Stabilized by Polymer Amphiphiles. *ACS Appl. Mater. Interfaces* **2020**, *12*, 38887–38898.

(72) Hoogenboom, R.; Fijten, M. W. M.; Thijs, H. M. L.; Van Lankvelt, B. M.; Schubert, U. S. Microwave-Assisted Synthesis and Properties of a Series of Poly(2-Alkyl-2-Oxazoline)S. *Des. Monomers Polym.* **2005**, *8*, 659–671.

CHAPTER THREE

Controlling Nanoemulsion Surface Chemistry with Poly(2-oxazoline) Amphiphiles

Adapted from: Daniel A. Estabrook, Amanda F. Ennis, Rachael A. Day and Ellen M. Sletten*
Controlling nanoemulsion surface chemistry with poly(2-oxazoline) amphiphiles. *Chem. Sci.*, **2019**, *10*, 3994–4003. DOI: https://doi.org/10.1039/C8SC05735D.

3.1 Abstract

Emulsions are dynamic materials that have been extensively employed within pharmaceutical, food and cosmetics industries. However, their use beyond conventional applications has been hindered by difficulties in surface functionalization, and an inability to selectively control physicochemical properties. Here, we employ custom poly(2-oxazoline) block copolymers to overcome these limitations. We demonstrate that poly(2-oxazoline) copolymers can effectively stabilize nanoscale droplets of perfluorocarbon in water. The controlled and living polymerization of poly(2-oxazoline)s allows for the incorporation of chemical handles into the surfactants such that covalent modification of the emulsion surface can be performed. Through post-emulsion modification of these new surfactants, we are able to access nanoemulsions with modified surface chemistries, yet consistent sizes. By decoupling size and surface charge, we explore structure-activity relationships involving the cellular uptake of nanoemulsions in both macrophage and non-macrophage cell lines. We conclude that the cellular uptake and cytotoxicity of poly(2-oxazoline)-stabilized droplets can be systematically tuned via chemical modification of emulsion surfaces.

3.2 Motivations and Applications

Facile methods to reliably prepare complex materials facilitate new technologies and medicines. Towards the development of optoelectronic materials and sensors, predictable assemblies of hard nanomaterials have enabled emergent optical, electronic, and magnetic properties.[1–4] For biomedical applications, the advantageous safety and clearance properties of soft organic materials have propelled liposomes, polymer micelles, hydrogels, and dendrimers into the research spotlight.[5–10] Surprisingly, far less attention has been placed on incorporating chemical complexity into emulsions[11–13] despite their simple formation and ability to encapsulate significant amounts of cargo.[14–16]

Emulsions are liquid-in-liquid droplets stabilized by surfactant, with size distributions ranging from several nanometers to hundreds of micrometers.[17] These materials have traditionally been employed as delivery systems[18,19] in cosmetic[20], food[21,22], and pharmaceutical industries,[23–25] with more advanced applications including templates for material synthesis[26–30] and nanoscale reactors[31–34]. While these emerging applications showcase the potential versatility of emulsions, liquid droplets remain underdeveloped compared to other soft materials.[11,12,35] Currently, a challenge in the preparation of emulsions is decoupling the size and surface charge of the materials.[36,37] Furthermore, chemically robust approaches to append functionality to the surface of emulsions are limited in comparison to conventional nanoparticles.[12,13,35,38,39]

Surfactants play a critical role in the formation and stabilization of emulsions, directly affecting the size, surface charge, and stability of the droplets (Figure 3.1A).[40,41]. This class of amphiphilic molecules can be composed of small molecules or polymers. They orient at the liquid-liquid interface to reduce interfacial tension between the immiscible emulsion core and bulk phases.

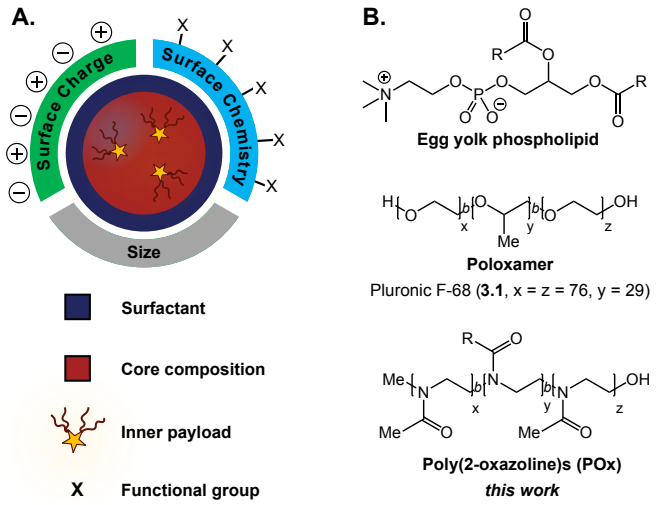

Figure 3.1 Surfactants dictate the size, charge, and surface chemistry of emulsions. Emulsion cores can be composed of several liquid phases (e.g. oil, perfluorocarbons). Payloads can be solubilized in the emulsion core and functional groups can be appended on the surface. (B) Selected surfactants for emulsion formation, including poly(2-oxazoline) surfactants presented herein.

Simple surfactants such as phospholipids and poloxamers (Figure 3.1B) are routinely used for industrial applications, while recently engineered peptide[42–44], polymer,[45] and nanoparticle[46] surfactants have produced responsive materials[47,48] and sophisticated architectures. Slight changes in surfactant structure can drastically affect the physiochemical properties of the emulsions.[39] These subtleties make the systematic alteration of a single characteristic difficult, precluding structure-property relationships. A method that will facilitate the decoupling of size and surface charge is the ability to control surface chemistry after the droplet has been formed.

3.3 Traditional Methods to Control Physicochemical Properties of Nanoemulsions

The role of the surfactant in stabilizing droplets has largely precluded the ability to engineer emulsion surfaces, particularly for nanoemulsions, whose interface composition is dictated by the need to impart kinetic stability. Conventional emulsion surface functionalization techniques involve modification of the surfactant prior to emulsification.[13,49–51] The functionalized surfactant can be employed solely or in combination with other surfactants. Limitations to this approach are

the reliance on cosurfactants[52] and the inability to decouple size and surface charge. An alternative approach is the introduction of a functionalized amphiphile after emulsification that can absorb to the surface.[49] This competitive absorption mechanism allows for surface chemistry alteration,[53] but risks desorption of the modified surfactant.[35] Other post-emulsification strategies rely on reversible chemical interactions with the surfactant at the liquid-liquid interface. Reported approaches involve electrostatic deposition,[54–56] designer peptide amphiphiles,[42,57,58] or reactive copolymer surfactants for disulfide exchange.[59] These techniques are all environment-dependent, limiting their generalizability. Irreversible covalent modification of macroemulsion surfaces have previously been enabled by end-group functionalization of commercially available surfactants.[60,61] Notably, these approaches suffer from low occupancy of functional groups on the droplet surface and did not allow access to droplet sizes relevant for biomedical applications (<200 nm).[62] Comparatively, nanoemulsion interfaces have much higher surface areas and provide a more challenging interface to both stabilize and functionalize, as exemplified by previous low-yield attempts reliant on cosurfactants.[59] To enable robust, covalent modification of nanoemulsions, we devised a versatile, top-down approach involving custom surfactants with chemical handles that undergo covalent modification at the liquid-liquid interface.

When considering the design of surfactants that will enable post-emulsion modification, we looked to amphiphilic copolymers. Polymer surfactants benefit from steric stabilization and tunable properties via alterations in block structure.[63,64] We hypothesized that chemical handles could be incorporated into the hydrophilic block without destabilizing the droplets. A popular class of polymer surfactants are poloxamers: block copolymers of poly(ethylene oxide) and poly(propylene oxide) (Figure 3.1B). While poloxamers (*e.g.* Pluronic F-68, **3.1**) have been extensively validated as surfactants for emulsions, it is synthetically challenging to incorporate

chemical functionality into them. Additionally, poly(ethylene oxide)-containing amphiphiles, like many surfactants employed for pharmaceutical emulsion formulations,[65–67] are associated with immunogenicity, making them a poor choice for materials with biomedical applications.[68,69] Recent work has suggested that poly(2-methyl-2-oxazoline) has similar protein repellent features to poly(ethylene oxide).[70–72] Poly(2-oxazoline)s (POx) are synthesized through a controlled, living polymerization, facilitating tunable block structure, length, and selective comonomer addition.[73,74] Based on these collective attributes, we focused on amphiphilic poly(2-oxazoline) surfactants to decouple the physiochemical properties of nanoemulsions and facilely control their surface chemistry.

Herein, we report a panel of POx surfactants for the stabilization and functionalization of nanoemulsions, kinetically stabilized emulsions less than 500 nm in size.[75] We showcase the controlled and living polymerization of POx to incorporate comonomers into the hydrophilic block of the surfactants to facilitate post-emulsion functionalization. We find that thiol-ene and copper-catalyzed azide-alkyne cycloaddition (CuAAC) chemistries are successful at the liquid-liquid interface, overcoming a key obstacle in emulsion functionalization.[11,12] We demonstrate that these chemistries can decouple emulsion properties by altering the charge of similarly-sized droplets.

A scenario where both the size and charge of particles directly influence function is cellular uptake. Controlling cell-nanoparticle interactions is essential for advancements in nanomedicine. Previous work has explored the relationship between size, charge, and cellular uptake by modulating the surface chemistry of gold nanoparticles,[76–78] micelles,[79] and peptide-brush polymers.[80] These studies indicate that not only is the surface chemistry important but also the nanomaterial composition. The custom surfactants reported herein allowed us to extend the scope of cellular uptake studies to include nanoemulsions. Through decoupling of size and surface

charge, we find that macrophage and non-macrophage cells display charge-dependent cellular uptake.

3.4 Employing Functional Handles Within Poly(2-oxazoline) Amphiphiles

Surfactants that could be further functionalized were synthesized by incorporating alkene and alkyne functionality into the hydrophilic poly(2-methyl-2-oxazoline) block of POx amphiphiles. Alkene and alkyne functionalities were chosen due to their ability to undergo thiol-ene and CuAAC "click" chemistries, respectively. These classes of reactions benefit from their high efficiency, modularity, and water compatibility—all desirable characteristics for the proposed post-emulsion modification route.[81,82] To prepare functionalizable POx surfactants, we initiated the polymerization of 5:30 2-(3-butenyl)-2-oxazoline (**3.4**) or 2-(4-pentynyl)-2-oxazoline (**3.5**) to methyl-2-oxazoline (**3.2**, 15 mol% alkene/alkyne) with methyl triflate. Once all monomer was consumed, nonyl-2-oxazoline (**3.3**) was introduced to the reaction mixture to form the hydrophobic block (Figure 3.2A). Previous work has demonstrated that **3.4** or **3.5** may be statistically incorporated into the poly(2-methyl-2-oxazoline) chain.[83,84] The resulting alkene- or alkyne-containing surfactants, **3.6** and **3.7** respectively, were characterized by NMR and SEC to contain the desired chemical handles and have M_n and dispersities comparable to surfactant **2.8** (Table 3.1).

Table 3.1. Characterization of functionalized amphiphilic poly(2-oxazoline)s

#	Polymer	M_n[a] (kDa)	$Đ$[b]
3.6	P((MeOx$_{30}$-*stat*-EneOx$_5$)-*b*-NonOx$_{11}$)	5.2	1.25
3.7	P((MeOx$_{29}$-*stat*-PyneOx$_5$)-*b*-NonOx$_{11}$)	5.2	1.25

PyneOx = 2-(4-pentynyl)-2-oxazoline; EneOx = 2-(3-butenyl)-2-oxazoline
[a]Number-average molecular weight (M_n) determined by ^{1}H-NMR end-group analysis of terminal CH_3 group to polymeric backbone
[b]Dispersity index ($Đ$) determined by SEC analysis (eluent: $CHCl_3$, DMF + 0.1M LiBr)

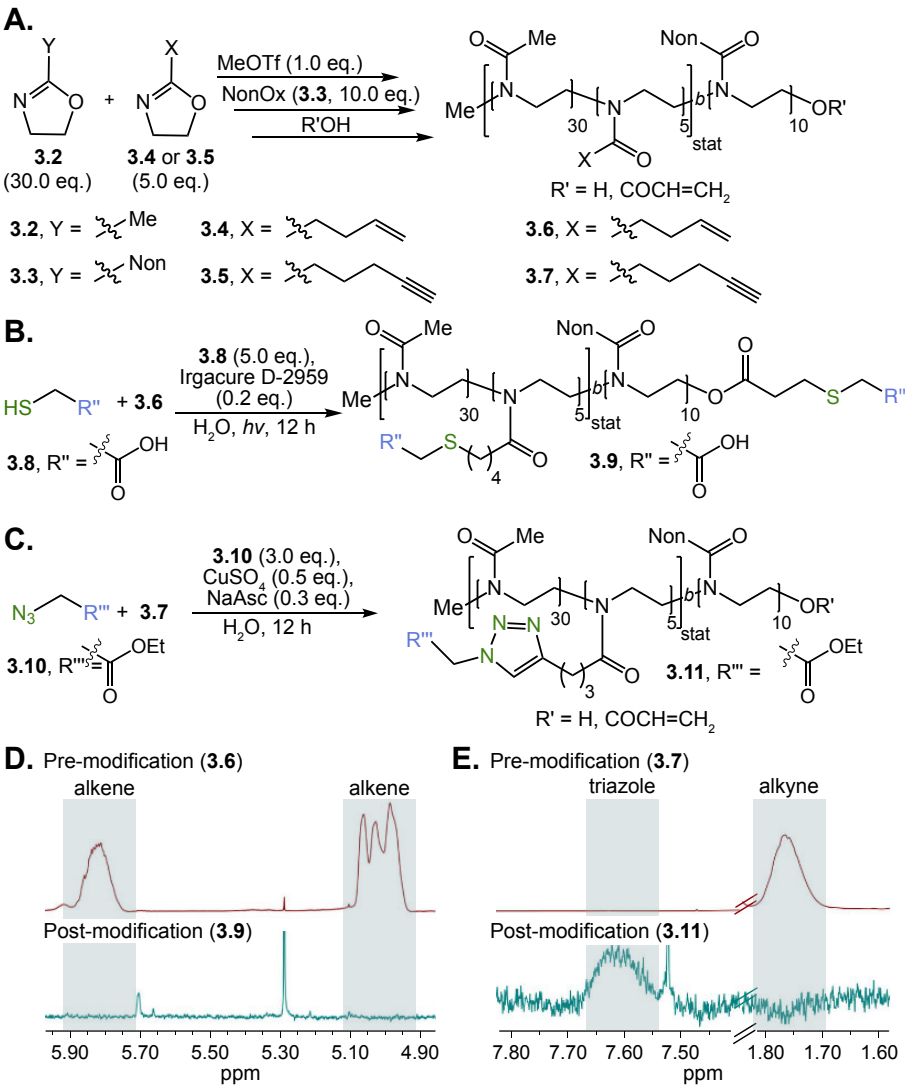

Figure 3.2 (A) Synthesis of a functionalized POx surfactant. A functional comonomer is randomly incorporated within the hydrophilic block to yield alkene (**3.6**) or alkyne (**3.7**) functionalized surfactants. (B/C) Couplings with thiol- (B) or azide-modified (C) payloads allow for modification of copolymers. (D/E) ^{1}H-NMR analysis indicates quantitative modification.

3.5 Covalent Surface Modification of Emulsions

With these polymers in hand, we first optimized conditions for thiol-ene and click chemistry based on literature precedent.[83–85] Alkene-containing POx **3.6** underwent quantitative thiol-ene chemistry by treatment with mercaptoacetic acid (**3.8**, 5.0 equiv.), Irgacure D-2959 photoinitiator (0.2 equiv.), and irradiation with 365 nm light (output power: 3 x 325mW at 365 nm) overnight

to result in modified polymer **3.9** (Figure 3.2B,D). Similarly, polymer **3.7** underwent complete conversion upon treatment with ethylazidoacetate (**3.10**, 3.0 equiv.), cupric sulfate (0.5 equiv.) and sodium ascorbate (0.3 equiv.), stirring at room temperature overnight to yield modified polymer **3.11** (Figure 3.2C,E).

Optimized thiol-ene and click chemistries were then extended from a post-polymerization to a post-emulsification modification strategy. PFC nanoemulsions stabilized by **3.6** and **3.7** were prepared following the conditions employed for nonfunctional **2.8** (Figure 3.3A). The resulting emulsions were found to be similar in size, polydispersity and long-term stability to **2.8** (Figure 3.3A,B, Figure 3.4)., indicating the presence of 15 mol% comonomer did not significantly disrupt the hydrophilic-hydrophobic balance of the surfactant. At 15 mol% incorporation of functional handles, these ~120 nm emulsions contain an estimated 3600 functional groups displayed on the droplet surface—however, this value can be easily modulated through the comonomer feed ratio, as calculated below:

Determining surface area and volume of emulsions stabilized with **3.6**:

Knowns:

- Diameter of nanoemulsions: 120 nm

$$Surface\ area\ of\ nanoemulsion = 4\pi * (120\ nm)^2 = 3600\ nm^2$$
$$Volume\ of\ nanoemulsion = \frac{4}{3}\pi * (120\ nm)^3 = 9.1 * 10^5\ nm^3$$

Determining number of emulsions stabilized with **3.6**:

Knowns:

- Volume of inner phase (fluorocarbon or hydrocarbon oil): 20 μL

$$\#\ of\ emulsions = \frac{volume\ of\ solvent}{volume\ of\ avg\ emulsion} = \frac{2.00 * 10^{19}\ nm^3}{9.1 * 10^5\ nm^3} = 2.2 * 10^{13}\ emulsions$$

Determining number of alkene molecules used in surfactant:

Variables:

- EneOx (**3.6**) polymer weight (M_n): 5152 Da

- Alkene = 12.2 mol% of total polymer

$$mols\ alkene\ monomer = \frac{5.60\ mg\ polymer}{5152\ Da} = 1.09 * 10^{-6}\ mols\ polymer$$

$$(1.09\ mols\ polymer)(12.2\ mol\%\ alkene) = 1.32 * 10^{-7}\ mols\ alkene$$

$$(1.32 * 10^{-7}\ mols\ alkene)(6.02 * 10^{23}\ molecules * mol^{-1}) = 7.95 * 10^{3.6}\ alkene\ molecules$$

Determining number of alkene molecules per emulsion:

Assumptions:

- All surfactant in solution is assembled at the liquid-liquid interface

$$\frac{\#\ of\ alkenes\ in\ surfactant}{\#\ of\ emulsions} = \frac{7.95 * 10^{3.6}\ alkenes}{2.2 * 10^{13}\ emulsions} = 3600\ alkenes\ per\ emulsion$$

Nanoemulsions prepared from **3.7** that contained alkynes on the surface were fluorescently modified by treatment with azidorhodamine **3.12** (3.0 equiv.), cupric sulfate (0.5 equiv.) and sodium ascorbate (0.3 equiv.) (Figure 3.3C). As a control, an emulsion stabilized by the corresponding non-functionalized surfactant (**2.8**) was exposed to identical conditions. Emulsion sizes were monitored before and after the reaction to confirm that the reagents did not disrupt nanoemulsion stability (Figure 3.5, 3.6). The rhodamine absorption of the emulsion solutions exposed to CuAAC conditions was measured by UV-Vis spectroscopy before and after dialysis of the samples to confirm removal of non-conjugated dye. An increased shoulder on the emulsions with conjugated alkyne suggested aggregation of the fluorophores due to high local concentration on the surface of the droplets (Figure 3.3D, red lines). Covalent modification of the surface of the droplets was confirmed after dialysis purification as the alkyne-containing emulsions retain absorption from the rhodamine while the control emulsions were no longer colored (Figure 3.3D, dashed lines). Emission spectra as well as ^{1}H-NMR of surfactant isolated post-reaction further

confirmed quantitative consumption of the alkyne chemical handles (see 1H-NMR analysis section).

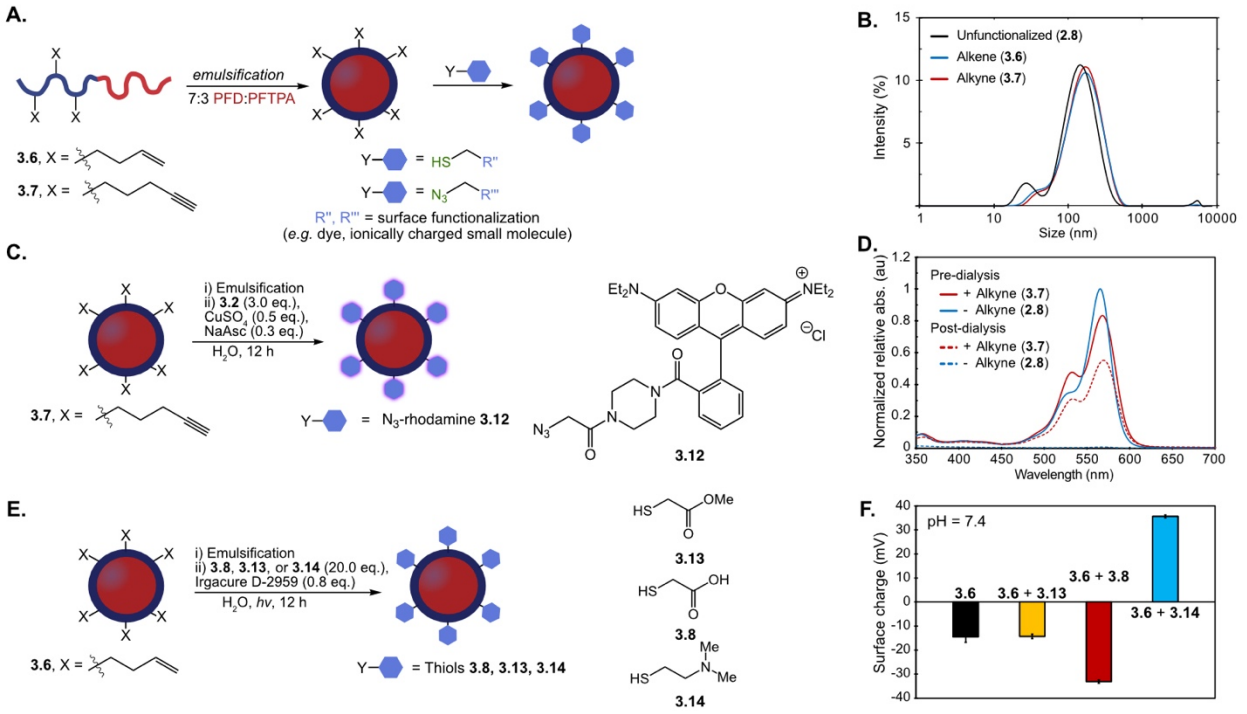

Figure 3.3 (A) Schematic of post-emulsion modification strategy with surfactants **3.6** and **3.7**. (B) Dynamic light scattering data of emulsions formed from **3.8**, **3.13**, **3.14**. Emulsions were prepared with 10 vol% 7:3 PFD/PFTPA and 2.8 wt% surfactant in PBS, diluted 1:100 in MilliQ water and analyzed via DLS. (C) CuAAC chemistry is employed for emulsion surface functionalization with azidorhodamine dye **3.12**. (D) Emulsions formed from **2.8** and **3.7** were subjected to the CuAAC chemistry conditions in (C). After 12 h, the reaction mixtures were diluted 1:100 in MilliQ water and their absorbance was measured (pre-dialysis, solid lines; red = **3.7**, blue = **2.8**). The remaining solution was dialyzed in water for 24h with 3 water changes, at which point the emulsion solution was removed and analyzed by UV/Vis at the approximate concentration as the previous measurements (post-dialysis, dotted lines; red = **3.7**, blue = **2.8**). All the data were normalized to emulsion **2.8** pre-dialysis. See Figure 3.5 for size analysis before and after reaction and dialysis. (E) Thiol-ene chemistry allows for modulation of zeta potential with thiols methyl mercaptoacetate (**3.13**), mercaptoacetic acid (**3.8**), and 2-dimethylaminoethanethiol (**3.14**). (F) Zeta potential of the emulsions at pH 7.4 before (**3.6**) and after thiol-ene modification following the conditions in (E). Black = emulsions stabilized by **3.6**; Yellow = emulsions stabilized by **3.6** and modified by **3.13**; Red = emulsions stabilized by **3.6** and modified by **3.8**; Blue = emulsions stabilized by **3.6** and modified by **3.14**. The surface charge was analyzed by diluting the reaction mixtures 1:100 in MilliQ H_2O and measuring the zeta potential. Data is representative of five replicate measurements. Error bars represent the standard deviation of five measurements. See Figure 3.7 for raw zeta potential traces.

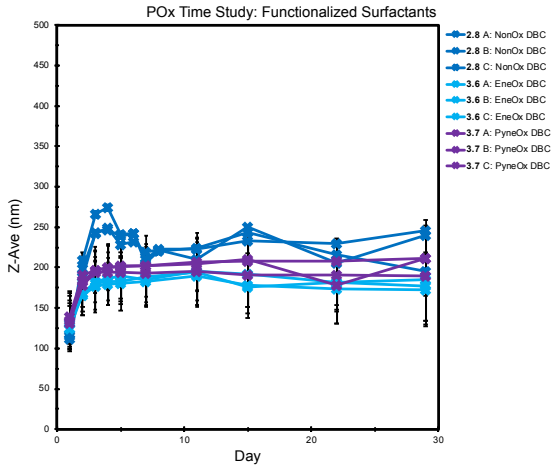

Figure 3.4. Size of PFC nanoemulsions prepared with functionalized surfactants over time. The size of nanoemulsions composed of 7:3 PFD:PFTPA v/v% stabilized by functionalized POx diblock copolymers **3.6** (light blue solid line, alkene-containing comonomer, "EneOx DBC") and **3.7** (purple dashed line, alkyne-containing comonomer, "PyneOx DBC") or unfunctionalized POx diblock **2.8** (dark blue solid line, nonyl-based, "NonOx DBC"), was measured by DLS over time. Size measurements were performed on three independent samples (A-C), five replicates per sample. Error bars represent half-width at half-maximum.

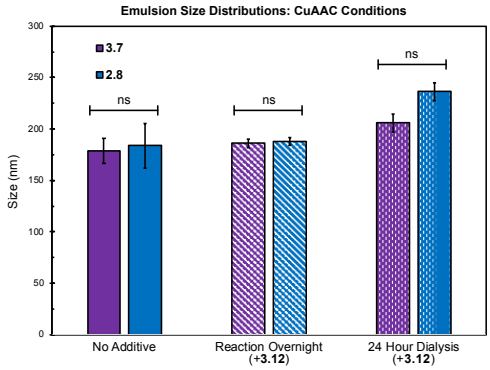

Figure 3.5. Dynamic light scattering data for alkyne-containing surfactant **3.7** (purple) and unfunctionalized surfactant **2.8** (blue) before (solid) and after (diagonal stripes) overnight CuAAC reaction with azidorhodamine **3.12**, followed by 24-hour dialysis (vertical stripes). Size measurements represent average of duplicate samples, three replicates per sample. Error bars represent the standard deviation of the size changes for duplicate samples. For assessment of the statistical significance of differences, a one-tailed Student's t-test assuming unequal sample variance was employed. Results were considered significant/not significant per the following definitions: ns = $p > 0.05$, significant = $p < 0.05$, * = $p \leq 0.05$, ** = $p \leq 0.01$, *** = $p \leq 0.001$. Statistical significance was done by comparing the two sets of emulsions at identical conditions.

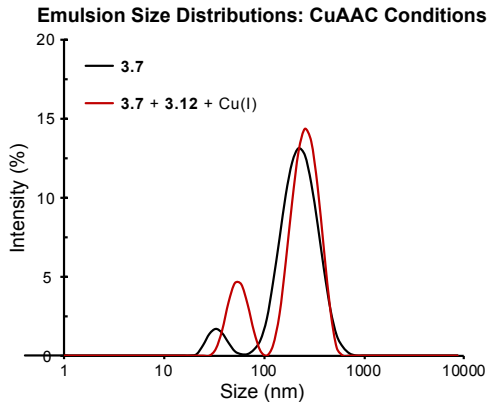

Figure 3.6. Dynamic light scattering data for the PFC nanoemulsions stabilized by alkyne-containing surfactant **3.7** before (black) and after (red) overnight CuAAC reaction with azidorhodamine **3.12**. Small population at ~50-70 nm corresponds to micelles; the observed increase in micelle size after conjugation with rhodamine **3.12** could be due to a change in hydrophilic-hydrophobic balance of the dye-micelle conjugate. Data are an average of three replicate measurements.

Alongside verification that Cu-catalyzed click chemistry was successful at the nanoemulsion surface using a rhodamine dye, we validated that the thiol-ene reaction was a viable approach for post-emulsion modification by modulating the surface charge of the droplets. Changes in surface charge could be quantified by zeta potential analysis, which did not require a purification step. PFC nanoemulsions stabilized by **3.6** were subjected to photoinitiator (0.8 equiv, Irgacure D-2959) in the presence of thiols (20.0 equiv) methyl mercaptoacetate (**3.13**), mercaptoacetic acid (**3.8**), or 2-dimethylaminoethanethiol (**3.14**), which will have different protonation states at physiological pH. These solutions were irradiated with 365 nm light overnight and the zeta potential and 1H-NMR of the samples were analyzed (Figure 3.3E/F).

As compared to control emulsions stabilized by unmodified **3.6** (black, Figure 3.3F), treatment with thiols **3.13**, **3.8** and **3.14** exhibit the expected changes in zeta potential: neutral **3.13** displays no significant change, acid **3.8** results in more negatively charged droplets, and amine **3.14** gives positively charged emulsions. The raw zeta potential traces are shown below (Figure 3.7).

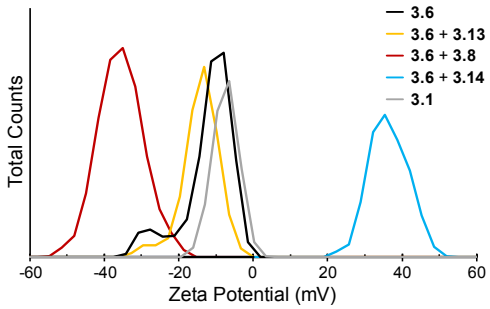

Figure 3.7. Zeta potential distributions for **3.6**-stabilized PFC emulsions modified with thiols (**3.8**, **3.13**, or **3.14**) before and after thiol-ene couplings, as shown in Figure 3.3E,F. Zeta potential traces for emulsions stabilized with functionalized surfactant **3.6** before (black) or after thiol-ene coupling with the following thiols: **3.13** (methylmercaptoacetate, yellow), **3.8** (mercaptoacetic acid, red) or **3.14** (2-dimethylaminoethanethiol, blue). Emulsions stabilized with Pluronic F-68 (**3.1**, PF-68, grey) were used as controls. Plotted is the zeta potential of the resulting emulsions at pH 7.4.

Control reactions lacking reagents (thiol, light or photoinitiator) display little change in zeta potential (Figure 3.8).

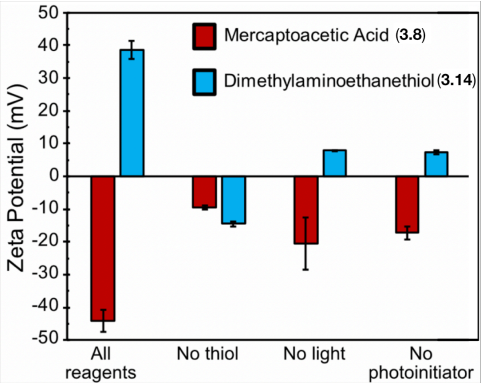

Figure 3.8. Zeta potentials for thiol-ene coupling controls. Emulsions were prepared with surfactant **3.6** and modified according to general nanoemulsion modification procedure using thiols **3.8** and **3.14**, with noted exceptions for lack of reagent. Plotted is the zeta potential of the resulting emulsions at pH 6. Data is representative of five replicate measurements. Error bars represent the standard deviation of five measurements.

Note that at physiological pH (Figure 3.9), the zeta potential of emulsions stabilized by unmodified polymer **3.6** is negative, which is consistent with results found for poly(2-methyl-2-oxazoline)s in solution.[86] The thiol-ene chemistry was further confirmed by NMR analysis of isolated surfactant after the modified emulsions have been disassembled.

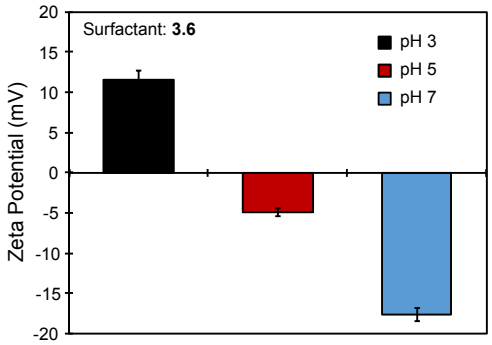

Figure 3.9. Dependence of zeta potential on pH for PFC emulsions stabilized by unmodified **3.6**. Data is representative of five replicate measurements. Error bars represent the standard deviation of five measurements.

Using the thiol-ene post-emulsification strategy, we can modulate the zeta potential of the droplets from +35 to -35 mV at pH 7.4 while keeping the size constant (Figure 3.10). Notably, it is difficult to obtain emulsions with identical sizes but varied surface charges, as ionic surfactants stabilize interfacial tensions differently compared to non-ionic surfactants.[37] We demonstrated that the pre-emulsion functionalization of the surfactants yielded distinct nanoemulsions when compared to post-emulsion modification. Polymers were prepared by reacting **3.6** with thiols **3.8**, **3.13**, or **3.14.** After isolation, these surfactants were subjected to standard PFC nanoemulsion formation conditions (Figure 3.11A). We then compared the size and surface charge of emulsions resulting from the pre- or post-emulsification approach to emulsions stabilized by unmodified surfactant **3.6** (Figure 3.11B). As expected, there was no statistically significant difference in size for emulsions modified with neutral thiol **3.13** (Figure 3.11B, yellow). In contrast, differences were observed in the size of anionic and cationic emulsions (Figure 3.11B, red and blue, respectively). Overall, emulsions formed through a pre-emulsification method varied in size by up to 35 nm, while post-emulsion modification resulted in nanoemulsions with only a 5 nm variance. These results showcase that post-emulsion surface functionalization is a viable approach to decouple the zeta potential of nanoemulsions from their size.

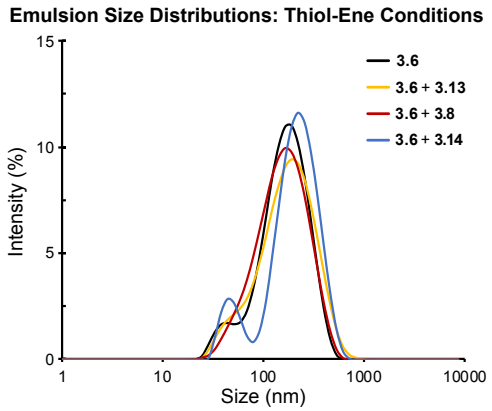

Figure 3.10. Dynamic light scattering data for the PFC nanoemulsions stabilized by alkene-containing surfactant **3.6** before (black) and after thiol-ene coupling with the following thiols: **3.13** (methylmercaptoacetate, yellow), **3.8** (mercaptoacetic acid, red) or **3.14** (2-dimethylaminoethanethiol, blue). Small population at ~50 nm corresponds to micelles. Data are an average of three replicate measurements.

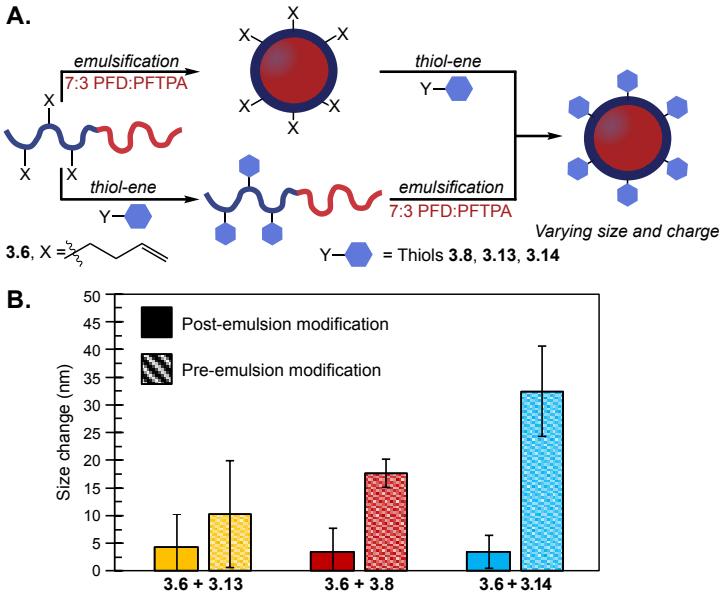

Figure 3.11. (A) Schematic of emulsions modified through pre- (top) or post- (bottom) emulsion modification methods. (B) Thiol-ene chemistries were performed on surfactant **3.6** with thiols **3.8**, **3.13** or **3.14** either before (conditions in Figure 3.2B) or after emulsification (conditions in Figure 3.3E). The emulsion were diluted 1:100 in MilliQ water and analyzed by DLS. Plotted are the size changes as determined by the absolute difference between size distributions of the resulting emulsions and control emulsions formulated with unmodified **3.6**. Size data is representative of the average of three independent samples, with three replicate measurements; error bars represent the standard deviation of three independent samples. See Figure 3.12 for emulsion size distributions and statistical significance.

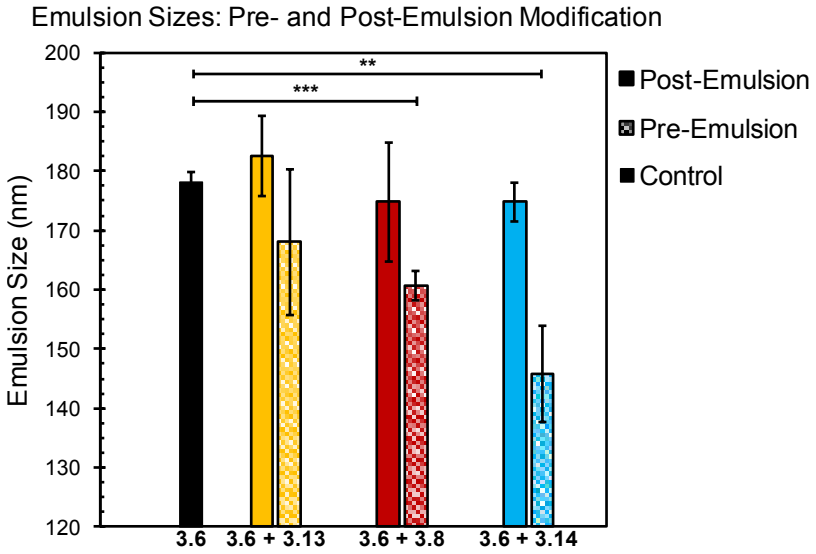

Figure 3.12. Emulsions modified through either a pre- or post-emulsion modification method as presented in Figure 3.11A, B. Thiol-ene chemistries were performed on surfactant **3.6** with thiols **3.8**, **3.13** or **3.14** either before (conditions in Figure 3.2B) or after emulsification (conditions in Figure 3.3E). The emulsions were diluted 1:100 in MilliQ water and analyzed by DLS. Plotted are nanoemulsion sizes. Size data are representative of the average of three independent samples, with three replicate measurements; error bars represent the standard deviation of the three independent samples. For assessment of the statistical significance of differences, a one-tailed Student's t-test assuming unequal sample variance was employed. Results were considered significant/not significant per the following definitions: ns = $p > 0.05$, significant = $p < 0.05$, * = $p \leq 0.05$, ** = $p \leq 0.01$, *** = $p \leq 0.001$. Statistical significance was done for each emulsion with reference to control emulsion stabilized by unmodified **3.6**.

3.6 Physicochemical Properties Control Cellular Uptake

With the ability to access this unique set of nanoemulsions, we performed a systematic study to identify how emulsion surface charge affects cellular uptake (Figure 3.13A). It is known that the size, zeta potential, and surface chemistry of nanoparticles dictate cell uptake *in vitro*,[78,87] but these experiments have primarily been performed on hard nanomaterials (*e.g.* gold nanoparticles[78,88,89]), micelles[90–92] or liposomes.[10,93,94] Results have shown that nanoparticle composition and cell type are also important factors in cell uptake, making studies on nanoemulsions an important addition to this field of study.

We assayed the cellular uptake of PFC nanoemulsions in both macrophage and non-macrophage cell lines by loading a fluorous-soluble rhodamine dye (**3.15**, Figure 3.13B)[95] into the emulsion core. The resulting fluorescent nanoemulsions were incubated with A375 (human melanoma, non-macrophage) or RAW (macrophage) cell lines for 3 hours and, after washing, their degree of fluorescence was quantified by flow cytometry (Figure 3.13C,D). We performed these studies on

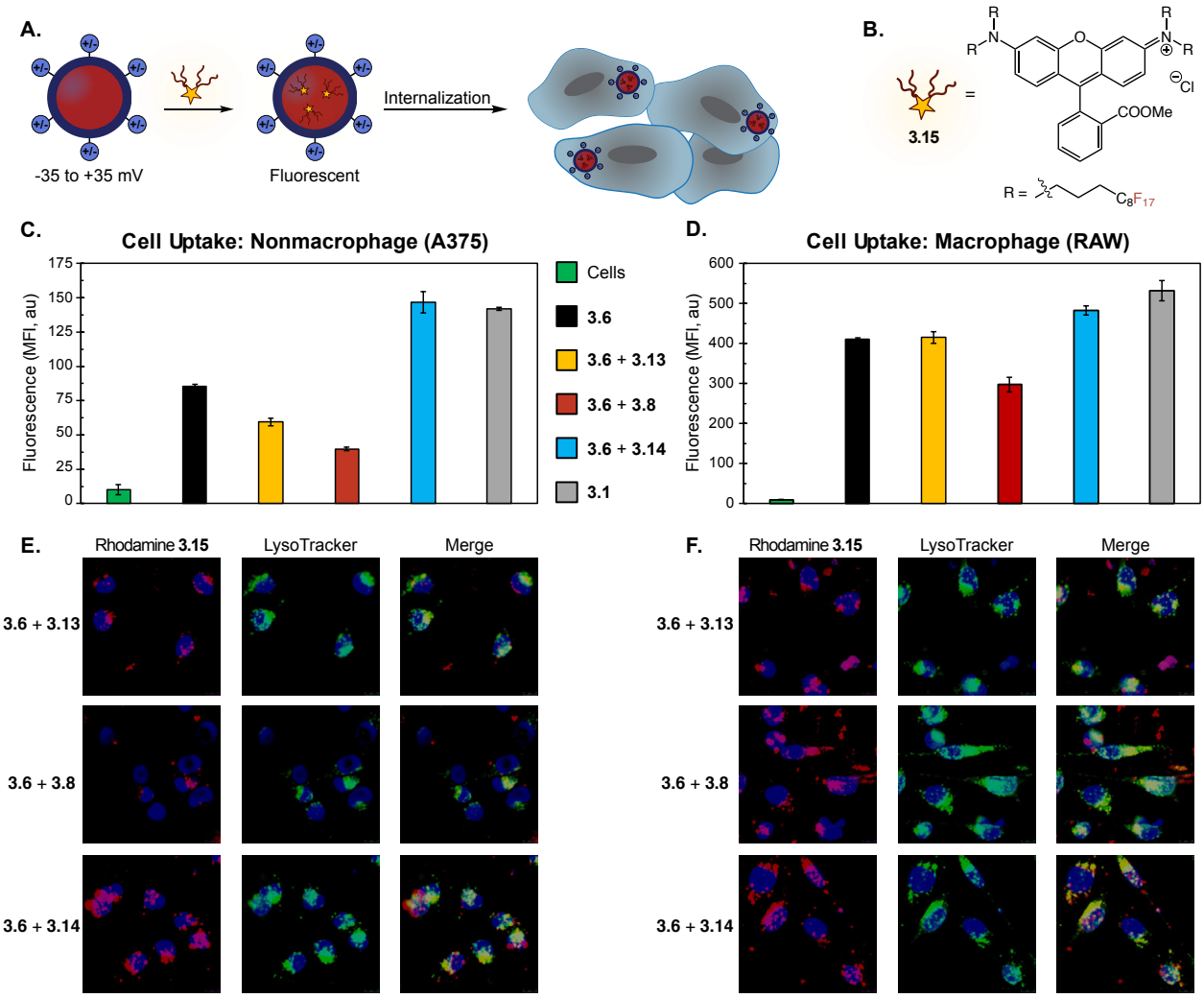

Figure 3.13 (A) Schematic of cellular uptake study of differentially charged nanoemulsions. Nanoemulsions were fluorescently labeled via the addition of a fluorous-tagged rhodamine. (B) Fluorous rhodamine **3.15**. (C/D) Flow cytometry of (C) non-macrophage (A375) and (D) macrophage (RAW) cell lines incubated with PFC nanoemulsions. PFC nanoemulsions with modified surface charges were prepared via the thiol-ene modification of emulsions formed from **3.6** as described in Figure 3.3F. Excess reagents were removed via thrice centrifugation and resuspension in MilliQ H_2O. After the final wash, the emulsions were resuspended in PBS and

3.15 in acetone was added. The emulsions were rocked for 1 min then introduced to A375 or RAW cells for 3 hours. The cells were thrice washed with excess FACS buffer (PBS plus 1% FBS) to remove non-uptaken emulsions, lifted with trypsin and transferred to a V-bottom plate. The cells were further washed *via* centrifugation (x3, FACS buffer) and analyzed by flow cytometry. Cells were gated (see Figure S3.1, S3.2) and FL2 mean fluorescence intensity (MFI) was plotted. Error bars represent the standard deviation of three replicate samples. Green = control cells; Black = emulsions stabilized by **3.6**; Yellow = emulsions stabilized by **3.6** and modified by **3.13**; Red = emulsions stabilized by **3.6** and modified by **3.8**; Blue = emulsions stabilized by **3.6** and modified by **3.14**; Grey = emulsions stabilized by **3.1**. (E/F) Confocal microscopy of (E) A375 cells and (F) RAW cells. The procedure was identical to (C/D) except for a one-hour incubation followed by five initial washes (3x media, 2x FACS buffer). After the final wash, the cells were transferred to an FBS-treated microscope slide, incubated for 1 h in media, stained with Hoescht dye and LysoTracker Green imaged via confocal microscopy. These cells were analyzed for rhodamine (Ex 532 nm, false color red) and Lysotracker Green (Ex 488 nm, false color green), and Hoescht dye (Ex 405 nm, false color blue). Scale bar indicates 10 μm. Images are representative of two independent experiments. See Figure S3.3, S3.4 for single channel images and DIC.

emulsions formed from **3.6** either unmodified or functionalized with **3.8**, **3.13**, or **3.14**. We also employed emulsions stabilized with **3.1** as a control. These experiments showed that cationic nanoemulsions were uptaken in the A375 non-macrophage cell line 250% more than the neutral emulsions and 370% more than the anionic emulsions (Figure 3.13C). This preference for cationic particles is consistent with other nanomaterial uptake studies.[96–99] Notably, conjugation with neutral thiol **3.13** resulted in cellular uptake levels similar to that of unmodified **3.6**, indicating that discrepancies in cellular uptake are due to differences in the physicochemical properties of the nanoemulsions, and not a result of the chemical modification process.

When the series of differentially charged nanoemulsions were incubated with the RAW macrophage cell line, the preference for cationic particles fell to 20% over the neutral emulsions and 60% over the anionic emulsions (Figure 3.13D). In addition, the overall uptake of nanoemulsions in RAW cells was about four-fold greater than A375 cells. Macrophage uptake appears to be particularly nanomaterial dependent as contrasting trends are apparent in the literature.[80,92,96,100,101] Our results, which demonstrate a slight preference for cationic emulsions, have also been observed for other soft materials.[80,91,102] Also of interest is the comparison of

unmodified POx emulsions to Pluronic F-68 nanoemulsions (Figure 3.13C,D, gray vs. black). The zeta potential and size of these samples are similar, yet POx-stabilized emulsions display lower uptake than Pluronic F68-stabilized emulsions in both cell lines. These results suggest that the poly(2-methyl-2-oxazoline) surface coverage reduces the non-specific uptake of the emulsions as compared to poly(ethylene oxide). Low levels of non-specific uptake are essential for the active-targeting of nanoparticles.[103–105] Thus, POx-stabilized emulsions are poised to be versatile materials for targeted delivery.

Finally, we corroborated our quantitative flow cytometry data with microscopy and analyzed the cellular localization of the modified droplets. Previous works have shown that cationic and neutral PFC nanoemulsions undergo endocytosis in both macrophage and non-macrophage cells,[106,107] while other work has found emulsions to fuse with the cell membrane[108]. To explore the cellular fate of the POx-stabilized emulsions, we performed colocalization studies with LysoTracker on A375 and RAW cells (Figure 3.13E,F). Colocalization between rhodamine and LysoTracker fluorescence suggests that the nanoemulsions are internalized via endocytosis. Notably, we also observed an interaction with the cell-surface for the cationic particles, likely due to electrostatic interactions with the anionic membrane.[96] Endocytosis was further supported by analyzing cellular uptake of nanoemulsions at 4 °C, a method of non-specifically inhibiting energy-dependent pathways.[109] We found that uptake in A375 cells was significantly reduced for all POx-stabilized emulsions (>45%, Figure 3.14). These results highlight that surface chemistry affects levels of cellular uptake, but does not change the route of internalization.[96,110]

We then assayed the cytotoxicity of A375 and RAW cells treated with the different POx emulsions as well as a Pluronic F-68 control over a 12 hour incubation period at a surfactant

concentration of 7.0 mg/mL (Figure 3.15). The anionic POx emulsions did not display any statistically significant toxicity in either cell line. Conversely, cationic emulsions displayed. significant macrophage toxicity (58% ± 1% viability) and less pronounced, though significant, loss of viability in A375 cells (87% ± 2% viability). Interestingly, the unfunctionalized POx stabilized PFC nanoemulsions resulted in substantially larger viability loss in RAW cells than the emulsions that underwent surface modification with neutral thiol **3.13** (61% ± 0.6% and 79% ± 4% viability, respectively). Collectively, our results demonstrate that a post-emulsion functionalization approach is essential for tuning the cellular uptake and viability of these diverse, yet underdeveloped, soft nanomaterials.

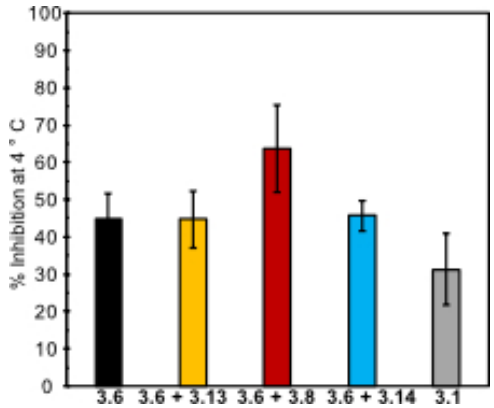

Figure 3.14. Inhibition of cellular (A375) uptake at 4 °C versus 37 °C. Black = emulsions stabilized by **3.6**; Yellow = emulsions stabilized by **3.6** and modified by **3.13**; Red = emulsions stabilized by **3.6** and modified by **3.8**; Blue = emulsions stabilized by **3.6** and modified by **3.14**; Grey = emulsions stabilized by **3.1**. Percent inhibition was determined as a ratio of cellular uptake (FL-2 fluorescence) at 4 °C versus uptake at 37 °C for one hour. Error bars represent the absolute uncertainty in uptake measurements, with three replicate samples at each temperature.

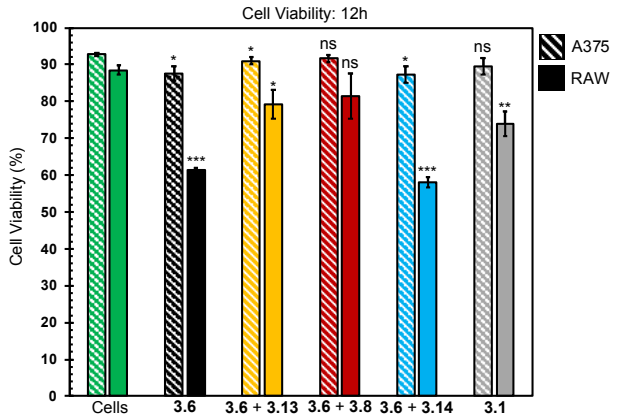

Figure 3.15. Cellular viability studies for RAW and A375 cells incubated with PFC nanoemulsions with modified surface charges over 12 hours. Surfactant concentration is ~7.0 mg/mL. Green = control cells; Black = emulsions stabilized by **3.6**; Yellow = emulsions stabilized by **3.6** and modified by **3.13**; Red = emulsions stabilized by **3.6** and modified by **3.8**; Blue = emulsions stabilized by **3.6** and modified by **3.14**; Grey = emulsions stabilized by **3.1**. Error bars represent the standard deviation of three replicate samples. For assessment of the statistical significance of differences, a one-tailed Student's t-test assuming unequal sample variance was employed Results were considered significant/not significant per the following definitions: ns = $p > 0.05$, significant = $p < 0.05$, * = $p \leq 0.05$, ** = $p \leq 0.01$, *** = $p \leq 0.001$. Statistical significance was done for each emulsion with reference to control cell (cell with no emulsion). See Figure S3.5 and Figure S3.6 for gated histograms.

3.7 Conclusions

We demonstrate the use of amphiphilic poly(2-oxazoline)s to stabilize perfluorocarbon-in-water and oil-in-water nanoemulsions. The living nature of the polymerization allows for the controlled addition of functionalizable comonomers into the hydrophilic block of the polymers to facilitate covalent emulsion functionalization. Through incorporation of these functional handles, the ability to attach azide-modified dyes and neutral or charged thiols to the surface of the droplets was achieved. We prepared a set of equal-size yet differentially charged nanoemulsions, which were employed to explore the dependence of cellular uptake on zeta potential in both macrophage and non-macrophage cell lines. We found that cationic emulsions were preferentially uptaken in both cell types. Overall levels of uptake were lower with poly(2-oxazoline) amphiphiles than poloxamers, making the surfactants and emulsions reported herein promising scaffolds for

biomedical applications. The use of this surfactant platform to enable controlled delivery in response to biologically relevant stimuli is ongoing. Additionally, the ability to modify the surface of nanoemulsions should extend these materials to areas of nanotechnology where control over chemical and physical properties is a prerequisite.

3.8 Experimental Procedures

3.8.1 General experimental procedures

Reagents and Instrumentation Chemical reagents were purchased from Sigma-Aldrich, Alfa Aesar, Fisher Scientific, or Acros Organics and used without purification unless noted otherwise. Anhydrous dimethyl sulfoxide (DMSO) was obtained from a Sure-SealTM bottle (Aldrich). Anhydrous and deoxygenated solvents dichloromethane (DCM), acetonitrile (MeCN), methanol (MeOH), and tetrahydrofuran (THF) were dispensed from a Grubb's-type Phoenix Solvent Drying System. Anhydrous but oxygenated 1-butanol and chlorobenzene was prepared by drying over 4 Å molecular sieves for at least 3 days. Thin layer chromatography was performed using Silica Gel 60 F254 (EMD Millipore) plates. Flash chromatography was executed with technical grade silica gel with 60 Å pores and 40–63 μm mesh particle size (Sorbtech Technologies). Solvent was removed under reduced pressure with a Büchi Rotovapor with a Welch self-cleaning dry vacuum pump and further dried with a Welch DuoSeal pump. Bath sonication was performed using a Branson 3800 ultrasonic cleaner. Nuclear magnetic resonance (^{1}H NMR, ^{13}C NMR, and ^{19}F NMR) spectra were taken on Bruker Avance 500 (^{1}H NMR and ^{13}C NMR) or AV-300 (^{19}F NMR) instruments and processed with MestReNova software. All ^{1}H NMR peaks are reported in reference to $CDCl_3$ at 7.26 ppm. Size Exclusion Chromatography (SEC)/Gel Permeation Chromatography (GPC), unless otherwise noted, was conducted on a Shimadzu high performance

liquid chromatography (HPLC) system with a refractive index detector RID-10A, one Polymer Laboratories PLgel guard column, and two Polymer Laboratories PLgel 5 μm mixed D columns. Eluent was DMF with LiBr (0.1 M) at 50 °C (flow rate: 0.80 mL/ min). Calibration was performed using near-monodisperse poly(methyl-methacrylate) PMMA standards from Polymer Laboratories. Masses for analytical measurements were taken on a Sartorius MSE6.6S-000-DM Cubis Micro Balance. Microwave reactions were performed using a CEM Discover SP microwave synthesis reactor. All reactions were performed in glass 10 mL microwave reactor vials purchased from CEM with silicone/PTFE caps. Flea micro PTFE-coated stir bars were used in the vials with magnetic stirring set to high and 15 seconds of premixing prior to the temperature ramping. All microwave reactions were carried out at 140 °C with the pressure release limit set to 250 psi (no reactions exceeded this limit to trigger venting) and the maximum wattage set to 250W (the power applied was dynamically controlled by the microwave instrument and did not exceed this limit for any reactions). Irradiation with light was performed with BI365 nm Inspection UV LED lamp, purchased from Risk reactor (Output power density >5000μW/cm² at 15" (38cm), voltage range 90-265V ac, output power: 3*325mW at 365nm peak).

Abbreviations

DCM = dichloromethane; DMSO = dimethylsulfoxide; EtOH = ethanol; MeCN = acetonitrile; MeOH = methanol; THF = tetrahydrofuran; PFD = perfluorodecalin; PFTPA = perfluorotripropylamine; POx = poly(2-oxazoline); DBC = diblock copolymer; TBC = triblock copolymer; MeOx = 2-methyl-2-oxazoline; NonOx = 2-nonyl-2-oxazoline, FOx = 2-(perfluorohexyl)ethyl-2-oxazoline; PyneOx = 2-(4-pentynyl)-2-oxazoline; EneOx = 2-(3-

butenyl)-2-oxazoline; MMA = methylmercaptoacetate; MAA = mercaptoacetic acid; DMAET = 2-dimethylaminoethanethiol.

General photophysics procedure

Absorbance spectra were collected on a JASCO V-770 UV-Visible/NIR spectrophotometer with a 4000 nm/min or 2000 nm/min scan rate after blanking with the appropriate solvent. Quartz cuvettes (1 cm or 0.33 cm) were used for absorbance and photoluminescence measurements.

General nanoemulsion formation procedure

Polymer surfactant (5.6 mg) was dissolved in DMF (20 μL) and sonicated in a bath sonicator (~15 minutes) until fully dissolved, at which point 7:3 perfluorodecalin:perfluorotripropylamine (10 vol%, 20 μL) or olive oil (10 vol%, 20 μL) was added, followed by PBS buffer pH 7.4 (200 μL). The mixture was sonicated at 35% amplitude for 15 minutes at 0 °C on a QSonica (Q125) sonicator. Sonication was performed by lowering the probe directly at the liquid-liquid interface of the two immiscible solvents.

General nanoemulsion analysis procedure

Size analysis: The bulk emulsion solution was diluted in MilliQ H_2O (20 μL emulsions in 2 mL MilliQ H_2O) in a plastic 1 cm cuvette. Size was analyzed with a Malvern Zetasizer Nano dynamic light scattering. SOP parameters: 10 runs, 10 seconds/run, three measurements, no delay between measurements, 25 °C with 120 second equilibration time. Collection parameters: Lower limit = 0.6, Upper limit = 1000, Resolution = High, Number of size classes = 70, Lower size limit = 0.4, Upper size limit = 1000, Lower threshold = 0.05, Upper threshold = 0.01. Data are representative

of three replicate measurements. Size error bars represent the half-width at half-maximum of the measurements.

Zeta potential analysis: The bulk emulsion solution was diluted in MilliQ H_2O (20 μL emulsions in 2 mL MilliQ H_2O) in a plastic 1 cm cuvette. Solution was then transferred to a disposable folded capillary cell for zeta potential measurements. Zeta potential was analyzed with a Malvern Zetasizer Nano. SOP parameters: Minimum: 10 runs, Maximum: 100 runs, 5 measurements, no delay between measurements, Model: Smoluchowski, 25 °C, 120 second equilibration time. Collection parameters: Auto mode. Data are representative of five replicate measurements. Zeta potential error bars represent the standard deviation of the measurements.

For assessment of the statistical significance of differences, a one-tailed Student's t-test assuming unequal sample variance was employed. Results were considered significant/not significant different per the following definitions: ns = $p > 0.05$, significant = $p < 0.05$, * = $p \leq 0.05$, ** = $p \leq 0.01$, *** = $p \leq 0.001$.

General nanoemulsion modification procedure via thiol-ene

Functionalized surfactant **3.6** containing ~8 wt% alkene (11.2 mg, 2.20 mmol) was dissolved in DMF (40 μL) and samples were sonicated in a bath sonicator (~15 minutes) until dissolved. A 7:3 mixture of perfluorodecalin:perfluorotripropylamine (10 vol%, 40 μL) was added, followed by PBS buffer pH 7.4 (400 μL). The biphasic mixture was sonicated at 35% amplitude for 90 seconds according to the general nanoemulsion formation procedure. The size was analyzed with Malvern

Zetasizer Nano dynamic light scattering according to the general nanoemulsion analysis procedure.

The emulsion solution was aliquoted (4x115 µL), giving solutions **A**-**D** (2.8 mg 3.6 per solution at ~8 wt% ≈ 0.3 mg EneOx, 2.1 µmol, 1.0 equiv.). To solution **A**, methyl mercaptoacetate was added (23, 4.0 µL, 41 µmol, 20 equiv.). To solution **B**, mercaptoacetic acid (**18**, 3.5 µL, 41 µmol, 20 equiv.) was added. To solution **C**, dimethylaminoethanethiol was added (**24**, 3.3 mg, 41µmol, 20 equiv.). A photoinitiator stock solution was made by dissolving Irgacure D-2959 (3.374 mg, 15 µmols) in MilliQ water (1 mL). Photoinitiator stock solution (115 µL, 1.6 µmol, 0.8 equiv.) was added to solutions **A**-**C**. All solutions were illuminated with 365 nm light overnight. The following morning, the emulsion size and charge was determined according to the general nanoemulsion analysis procedure.

General nanoemulsion modification procedure via CuAAC

Emulsions stabilized by surfactant **3.7** were prepared according to the general nanoemulsion procedure. A stock solution of azidorhodamine **3.12** (38.2 mg/mL) was prepared by dissolving azidorhodamine **3.12** (21 mg/mL) in MilliQ water (300 µL) and MeOH (250 µL).

A portion of the bulk emulsion solution (130 µL) was diluted with MilliQ water (290 µL) and $CuSO_4$ (0.08 mg, 0.5 µmol, 0.3 equiv.), sodium ascorbate (0.3.68 mg, 0.815 µmol, 0.50 equiv.) were added followed by azidorhodamine **3.12** (80 µL of stock solution, 3.0 mg, 3.9 µmol, 3.0 equiv.). The reaction was stirred overnight. The following morning, the emulsion size was analyzed as described in the general nanoemulsion analysis procedure.

Cell culture experimental procedures

RAW cells were donated by the lab of Professor Alexander Hoffman. A375 cells were purchased from ATCC.

RAW cells and A375 cells were cultured in Dulbecco's Modified Eagle Media (DMEM, Life Technologies, cat# 11995073) supplemented with 10% fetal bovine serum (Corning, lot# 3503.6109) and 1% penicillin-streptomycin (Life Technologies, cat# 15070063). Cells were washed with PBS, or PBS supplemented with 1% fetal bovine serum (FACS buffer). Cells were detached with trypsin digest solution (*i.e.* 0.25% trypsin, 2.21 mM EDTA (1X), (-) sodium bicarbonate (Corning, lot# 1233.7008). Cells were incubated at 37 °C, 5% CO_2, during treatments and throughout culturing, in HERACell 150i CO_2 incubators. Cells were pelleted through use of Sorvall ST 40R centrifuge (3x, 526xg, 3 min). All cell work was performed in 1300 Series A2 biosafety cabinets. Confocal microscopy was performed on a TCS SPE Leica confocal microscope containing 405 nm, 488 nm, 532 nm and 635 nm lasers.

General cell labeling procedure

Fluorous rhodamine **3.15** was synthesized as previously reported[95]. A stock solution of 9.37 mg/mL in acetone (3.29 mM) was prepared.

PF-68-stabilized emulsions were prepared as described by the general nanoemulsion formation and modification procedures. POx-stabilized emulsions were prepared and functionalized as described by the general nanoemulsion formation and modification procedures. After size and zeta

potential measurements had been taken, emulsions were washed by centrifugation and suspension (3x 900*g* followed by resusupension in 100 μL PBS). On the last wash, emulsions were resuspended in PBS buffer (100 μL). Fluorous rhodamine **3.15** stock (10 μL) was then added to each emulsion solution. Solutions were then rocked and lightly vortexed for ~1 minute to encapsulate **3.15**.

RAW or A375 cells were placed in a 96-well plate (50,000 cells per 200 μL/well) and incubated in DMEM media (37 °C, 5% CO_2, overnight) (Note: incubation of cells and thiol-ene reaction were performed over the same night). The next day, cells were washed 3x in FACS buffer (PBS + 1% FBS) by continually adding and removing 125 μL FACS buffer to the adherent cells. On the last removal of FACS buffer, the cells were suspended in 75 μL FACS buffer and then treated with 25μL **25**-loaded emulsions (total volume = 100 μL per well). The cells were incubated in the presence of emulsions (37 °C, 5% CO_2,) for 3 h. Following incubation, the cells were washed three times by PBS to remove residual emulsions (add + remove 150 μL PBS 3x) followed by addition of trypsin digest solution (100 μL, total well volume = 200 μL). The cells were incubated for 5-10 minutes at 37 °C, pipetted vigorously until cells were detached (for RAW cells, process was more difficult). Wells were then quenched by addition of DMEM media (100 μL) and the lifted cells were transferred to a 96-well V-bottom plate. Cells were then pelleted down by centrifugation (526 x *g*, 3 min, 4 °C) and resuspended in FACS buffer (200 μL), and the process was repeated three times.

Flow cytometry

On the last resuspension, cells were transferred to 1.2mL microtiter tubes with a final volume of 400 μL FACS buffer. Flow cytometry was performed on a BDBiosciences FACSCalibur equipped with 488 nm and 635 nm lasers. Fluorous rhodamine **3.15** fluorescence was measured on FL2 channel to measure cellular uptake. Fluorescence across cell lines was normalized to background control cell FL-2 fluorescence. For assessment of the statistical significance of differences, a one-tailed Student's t-test assuming unequal sample variance was employed. Results were considered significant/not significant per the following definitions: ns = $p > 0.05$, significant = $p < 0.05$, * = $p \leq 0.05$, ** = $p \leq 0.01$, *** = $p \leq 0.001$.

Microscopy

The general cell labeling procedure was followed with the following modifications:

Cells were plated at 30,000 cells/200 μL well, a 1 hour incubation was performed instead of 3 hours. Following incubation in FACS buffer (100 μL), cells were washed (3x DMEM media, 2x PBS) before lifting with trypsin. Washes in the v-bottom 96-well plate were performed with DMEM media (3 x 200 μL).

On last resuspension, the two identical wells were combined, and cells were transferred to a single-well glass microscope slide (VWR 10118-600) that had been treated with FBS (~2 mL, 30 min) and allowed to dry at rt in a biosafety cabinet to maintain sterility. The cells were allowed to adhere to slide (37 °C, 5% CO_2, 1 hour). Cells were stained with Hoechst (1 drop/1mL media, 15 min) and LysoTracker Green (100μL stock, stock: 0.2 μL probe in 4 mL FACS) before confocal images were taken.

Confocal settings were as follows: Rhodamine (532 laser-55%, 1150 gain, offset -0.6, collection 540-700nm), Hoechst (405 laser-55%, 1150 gain, offset -0.6, collection 420-500nm), LysoTracker Green (488 laser-55%, 1150 gain, offset -0.6, collection 500-540 nm), DIC (scan-BF, 575 gain, offset -0.4). Scale bar represents 10 μm. Images were processed in ImageJ.

Cell viability

The general cell labeling procedure was followed with the following modifications:

The emulsions were not loaded with rhodamine **3.15** and the incubation time was 12 hours instead of 3 hours. On the last resuspension, cells were transferred to 1.2mL microtiter tubes with a final volume of 400 μL FACS buffer (PBS + 1% FBS). Propidium iodide solution (0.5 μL, 1 mg/mL in PBS) was added to each well. Cells were incubated on ice for 15 minutes prior to flow cytometry measurements.

Live and dead controls (heat killed at 70 ^{o}C for 1 min) were used to set the range of the FL2 channel. Data were analyzed by splitting the population at ~10^2 as a live/dead line. Flow cytometry was performed as described above.

General synthetic procedures

3.8.2 Experimental procedures

Synthetic chemistry experimental procedures

<u>Witte-Seeliger and Wenker routes to aliphatic, fluorous and functionalized 2-substituted-2-oxazolines:</u>

Witte-Seeliger:

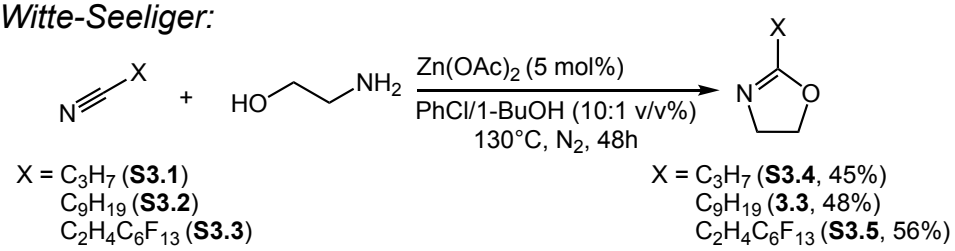

Wenker:

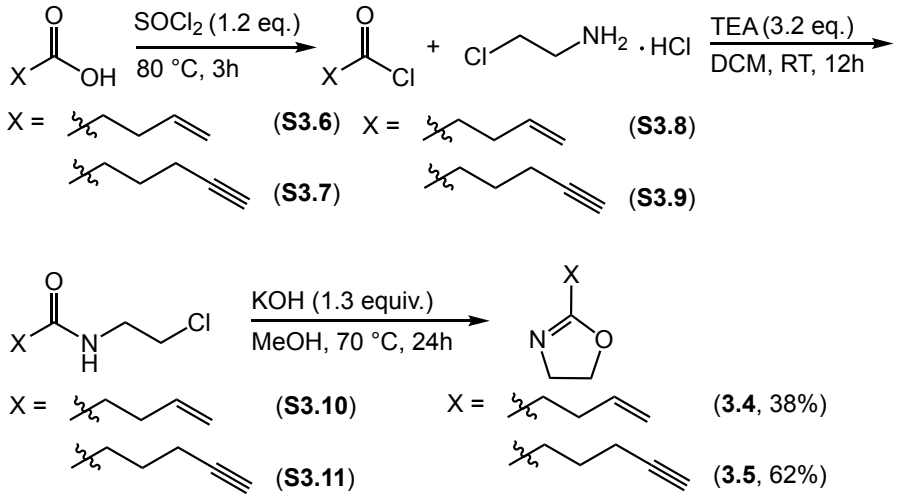

NonOx (**3.3**) was synthesized according to literature procedure.[111]

2-(3-butenyl)-2-oxazoline (EneOx, **3.4**) was synthesized according to literature procedure.[84] ^{1}H NMR (300 MHz, $CDCl_3$): δ 5.88 (m, 1H), 5.06 (m, 2H), 3.26 (t, J = 9.4 Hz, 2H), 3.86 (t, J = 9.4 Hz, 2H), 2.41 (m, 4H).

2-(4-pentynyl)-2-oxazoline (PyneOx, **3.5**) was synthesized according to literature procedure.[83] ^{1}H NMR (300 MHz, $CDCl_3$): δ 3.22 (t, J = 9.3 Hz, 2H), 3.82 (t, J = 9.3 Hz, 2H), 2.41 (t, J = 7.5 Hz, 2H), 2.28 (td, J = 7.0, 2.6 Hz, 2H), 1.97 (t, J = 2.6 Hz, 1H), 1.87 (quin, J = 7.2 Hz, 2H).

Synthesis of functionalized poly(oxazoline) block copolymers **3.6** and **3.7**:

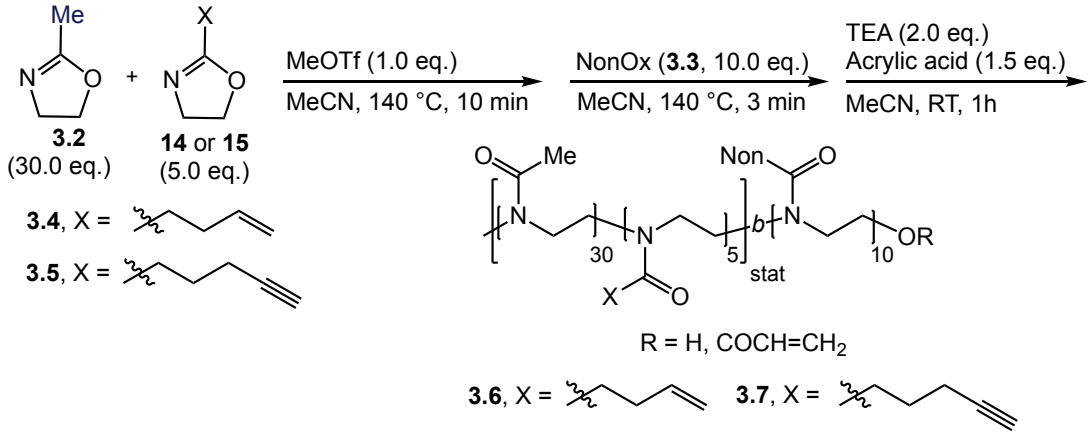

P(MeOx$_{30}$-*r*-EneOx$_5$-*b*-NonOx$_{11}$) (3.6**)**

To a flame dried microwave vial, MeCN (1.2 mL, anhydrous), MeOx (200 μL, 0.20 g, 2.4 mmol, 30 equiv.), and EneOx (30 μL, 29 mg, 0.24 mmol, 3 equiv.) were added and deoxygenated via freeze-pump-thaw (x2). Following deoxygenation, MeOTf (8.9 μL, 13 mg, 0.080 mmol, 1.0 equiv.) was added and the mixture was heated at 140 °C in the microwave. After 10 minutes, NonOx (155 μL, 155 mg, 0.783 mmol, 10 equiv.) was added under N_2 and heated to 140 °C for 3 minutes, at which point the polymerization was quenched with acrylic acid (8.0 mg, 0.12 mmol, 1.5 equiv.), followed by triethylamine (3.6 mg, 0.3.6 mmol, 2.0 equiv.) 30 minutes later. The reaction mixture was evaporated to dryness to yield crude polymer (**3.6**) as a white solid. Polymer **3.6** was purified by precipitation by dissolving in a minimal amount of DCM and dropwise addition to cold Et_2O (20:1 v/v%), collected and evaporated to dryness (204 mg, 0.040 mmol, 53% yield). ^{1}H NMR (500 MHz, $CDCl_3$): δ 6.35 (dd, J = 15.7, 1.6 Hz, 1H), 6.13 (dd, J = 6.8, 10.4 Hz, 1H), 5.84 (dd, J = 8.7, 1.6 Hz, 1H), 5.81 (m, 5H), 5.06 (m, 9H), 3.44 (m, 3.79H), 3.06 (m, 3H), 2.46 (m, 5H), 2.34 (m, 32H), 2.13 (m, 90H), 1.58 (m, 22H), 1.25 (m, 127H) 0.86

(t, J = 6.6 Hz, 33H). SEC: M_w = 5.2 kDa, M_n = 6.5 kDa, $Đ$ = 1.25. FT-IR: 2930 (C-H str) (w), 3.620 (C=O str, amide I) (vs), 1420 (CH_x-CO) (s), 93.7 cm^{-1} (=C-H bend).

P(MeOx$_{29}$-*r*-PyneOx$_5$-*b*-NonOx$_{11}$) (3.7**)**

To a flame dried microwave vial, MeCN (1.2 mL, anhydrous), MeOx (200 µL, 0.20 g, 2.4 mmol, 30 equiv.), and PyneOx (30 µL, 0.032 g, 0.235 mmol, 3 equiv.) were added and deoxygenated via freeze-pump-thaw (x2). Following deoxygenation, MeOTf (8.9 µL, 13 mg, 0.078 mmol, 1.0 equiv.) was added and the mixture was heated at 140 °C in the microwave. After 10 minutes, NonOx (155 µL, 155 mg, 0.783 mmol, 10 equiv.) was added under N_2 and heated to 140 °C for 3 minutes, at which point the polymerization was quenched with acrylic acid (8.0 mg, 0.12 mmol, 1.5 equiv.), followed by triethylamine (3.6 mg, 0.3.6 mmol, 2.0 equiv.) 30 minutes later. The reaction mixture was evaporated to dryness to yield crude polymer (**3.7**) as a white solid. Polymer **3.7** was purified by precipitation by dissolving in a minimal amount of DCM and dropwise addition to cold Et_2O (20:1 v/v%), collected and evaporated to dryness (380 mg, 0.070 mmol, 98% yield). ^{1}H NMR (500 MHz, $CDCl_3$): δ 6.33 (dd, 0.5H), 6.04 (dd, 0.5H), 5.80 (dd, 0.5H), 3.44 (m, 180H), 2.97 (m, 3H), 2.63 (m, 10H), 2.43 (m, 26H), 2.20 (m, 92H), 1.77 (m, 6H), 1.58 (m, 22H), 1.18 (m, 129H) 0.80 (t, J = 6.6 Hz, 32H). SEC: M_w = 6.4 kDa, M_n = 5.1 kDa, $Đ$ = 1.25. FT-IR: 2930 (C-H str) (w), 3.620 (C=O str, amide I) (vs), 1420 (CH_x-CO) (s), 639 cm^{-1} (≡C-H bend).

Functionalization of poly(2-oxazoline) block copolymer **3.6** with thiol **3.8**:

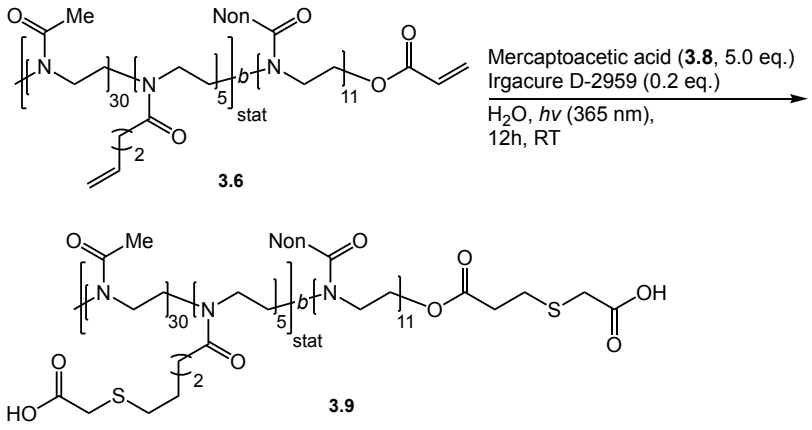

Surfactant **3.6** was modified based on thiol-ene conditions previously reported.[84,85] All reagent equivalents were calculated with respect to alkene. Briefly, functionalized surfactant **3.6** (10.6 mg ~8 wt% alkene, 1.0 equiv.) was dissolved in acetone + MeOH (1:1, 400 µL total). To this solution mercaptoacetic acid (**3.8**, 3.1 mg, 34 µmol, 5 equiv.) and Irgacure D-2959 (0.30 mg, 1.4 µmol, 0.20 equiv.) were added and briefly purged with nitrogen. The resulting mixture was irradiated with 365 nm light (power density: >5000µW/cm² at 15") at RT overnight. After the reaction had been run overnight, polymer was concentrated down, dissolved in DCM, and washed with water (x3). After drying on high vacuum, polymer **3.9** was analyzed by ^{1}H NMR and compared to polymer **3.6** (Figure 3.2D).

Functionalization of poly(2-oxazoline) block copolymer **3.7** with azide **3.10**:

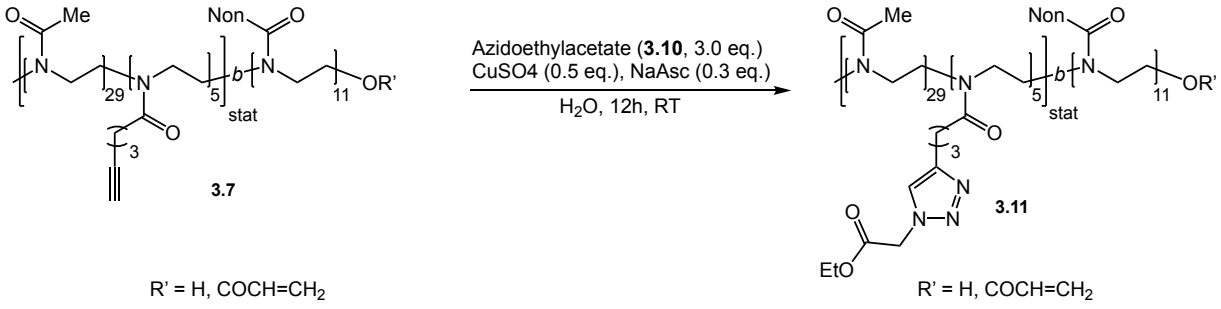

Surfactant **3.7** was modified based on CuAAC conditions previously reported.[83] All reagent

equivalents were calculated with respect to alkyne. Briefly, functionalized surfactant **3.7** (10.6 mg, ~8 wt% alkyne, 1.0 equiv.) was dissolved in tBuOH + H_2O (1:1, 400 µL total). To this solution sodium ascorbate (0.6 mg, 3 µmol, 0.5 equiv.), copper sulfate (0.3 mg, 2 µmol, 0.3 equiv.) and azidoethylacetate (**3.10**, 4.0 mg, 31 µmol, 5.0 equiv.) were added and stirred at RT overnight. After the reaction had been run overnight, polymer was concentrated down, dissolved in DCM, and washed with water (x3). After drying on high vacuum, polymer **3.11** was analyzed by ^{1}H NMR and compared to polymer **3.7** (Figure 3.2E).

Synthesis of Azidorhodamine **3.12** (*N*-(9-(2-(4-(2-azidoacetyl)piperazine-1-carbonyl)phenyl)-6-(diethylamino)-3*H*-xanthen-3-ylidene)-*N*-ethylethanaminium):

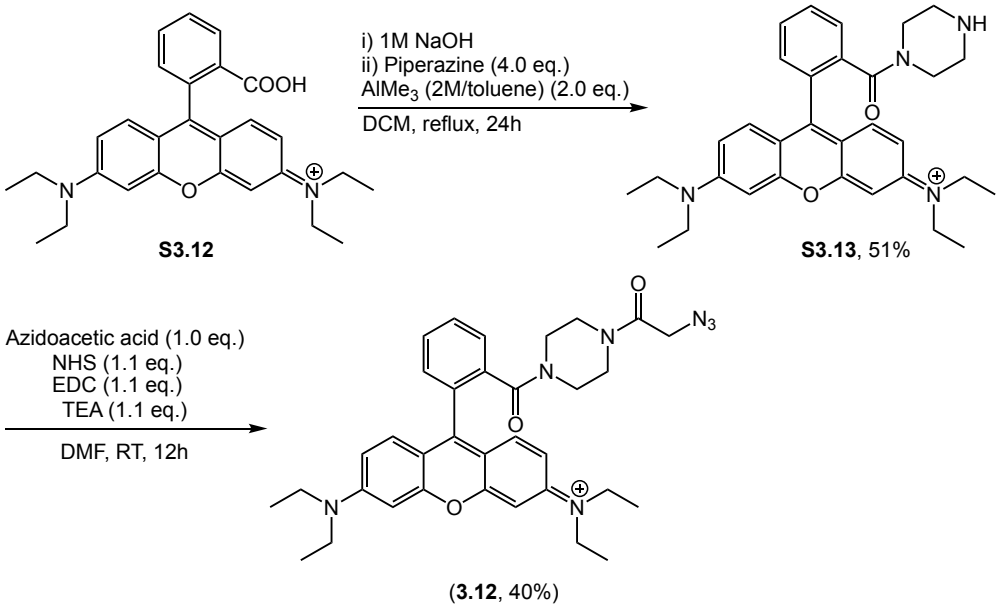

Azidorhodamine **3.12** was synthesized according to a modified literature procedure from rhodamine B piperazine amide (**S3.13**)[112], and ^{1}H-NMR was compared to literature[113].

To flame-dried dram vial, azidoacetic acid (9.0 mg, 97 µmol, 1.0 equiv.), *N*-hydroxysuccinimide (NHS, 11.3 mg, 98.2 µmol, 1.10 equiv.) and *N*-(3-dimethylaminopropyl)-N′-ethylcarbodiimide

hydrochloride (EDC, 20.4 mg, 106 μmol, 1.10 equiv.) were added followed by DMF (1.5 mL, anhydrous). The reaction was stirred at rt under N_2 for 2 hours. After 1 hour, to a separate flame-dried dram vial, rhodamine B piperazine amide S**3.13** (49.5 mg, 90.7 μmol, 1.00 equiv.) dissolved in DMF (0.5 mL, anhydrous) was added, followed by addition of triethylamine (14 μL, 100 μmol, 1.1 equiv.). The reaction was stirred at rt for 1 hour. The **S3.13**/triethylamine reaction mixture was then transferred to the azidoacetic acid vial, and rinsed with the remaining 0.5 mL DMF. The reaction was stirred under N_2 at rt overnight and purified by flash chromatography on silica gel, eluting with 40:1 DCM:MeOH to yield **3.12**. ^{1}H NMR agreed with literature values.[113] ^{1}H NMR (500 MHz, $CDCl_3$): δ 7.62-7.78 (m, 3H), 7.53-7.60 (m, 1H), 7.30-7.41 (m, 4H), 6.67 (s, 2H), 3.3.7 (m, 2H), 3.40 – 3.70 (m, 12H), 2.60 (br m, 4H), 1.22-1.29 (s, 12H).

3.8.3 Figure experimental procedures

Figure 3.2A. Synthesis and reactivity of functionalized POx surfactants 3.6 **and** 3.7

Functionalized polymers were synthesized via microwave protocol using kinetics previously reported in the literature [83,84,114,115]. See supporting experimental procedures for synthetic details.

Figure 3.2B-E. Modification of surfactant 3.6 **through thiol-ene coupling**

See supporting synthetic chemistry experimental procedures for synthetic details.

Figure 3.3B. PFC nanoemulsion with surfactants 2.8**,** 3.6**, and** 3.7

Emulsions stabilized by surfactants **2.8**, **3.6**, and **3.7** were formed as described by the general nanoemulsion formation procedure. Size was analyzed per the general nanoemulsion analysis procedure to confirm similar emulsion size distributions.

Figure 3.3C. Emulsion surface modification: CuAAC of 3.12 **with surfactant** 3.7

Emulsions stabilized by surfactants **2.8** and **3.7** were formed as described by the general nanoemulsion formation procedure. Size was analyzed per the general nanoemulsion analysis procedure to confirm similar emulsion size distributions. Both **2.8** and **3.7** were subjected to the general CuAAC modification procedures.

Figure 3.3D. Analysis of absorbance of emulsions following CuAAC with 3.12

Pre-dialysis (solids lines): After reaction with **3.12**, the emulsion solutions were diluted 1:100 and transferred to a quartz cuvette for fluorimeter measurements. Emission settings: Ex: 560 nm; Em. range: 565-700 nm; Ex. slit: 3 nm; Em. slit: 3 nm; Step size: 1; Integration: 0.01. Absorbance measurements were then taken after transferring solution to plastic cuvette.

Post dialysis (dotted lines): Emulsion solutions were then subjected to 24-hour dialysis against DI H_2O using a 3 kDa membrane cutoff dialysis tubing. Sample volumes were recorded before and after dialysis to account for possible dilution. The DI H_2O was exchanged three times. After accounting for diluting, appropriate amount of emulsion solution was transferred to a quartz cuvette and diluted to 2 mL MilliQ H_2O. For instance, prior to dialysis, solution of emulsions stabilized by surfactant **2.8** was 478 μL—after dialysis, the total volume was 550 μL (15% dilution); to account for this, 23 μL of solution (rather than 20 μL) was diluted to 2 mL.

Fluorescence and absorbance measurements were taken as previously described. Absorbance measurements were then taken after transferring solution to plastic cuvette.

Figure 3.3E/F. Emulsion surface modification: Thiols with surfactant 3.6

Emulsions stabilized by surfactant **3.6** were formed, functionalized, and analyzed as described by the general nanoemulsion formation, modification and analysis procedures.

Figure 3.4. **Size of PFC nanoemulsions over time stabilized by functionalized surfactants** 16 **and** 17

Emulsions prepared in Figure 3.3B were analyzed over time by DLS. Error bars represent the standard deviation for three independent samples.

Figure 3.5 Size data for emulsions before and after modification by CuAAC

"No Additive" (solid): Emulsions composed of **8** and **17** were prepared according to the general nanoemulsion procedure and their size was analyzed according to the general analysis procedure (raw data, Figure 3.6).

"Reaction Overnight" (diagonal stripes): Emulsions from above were subjected to conditions according to the general modification procedure with CuAAC, as described in Figure 4C. Following this procedure, their size was analyzed according to the general analysis procedure (raw data, Figure 3.6).

"24 Hour Dialysis" (vertical stripes): Emulsions from above underwent 24 hours of dialysis as described in Figure 4D. After dialysis, the size of the emulsions was analyzed according to the general analysis procedure.

Figure 3.6. Raw DLS data for emulsions before and after modification by CuAAC.

PFC nanoemulsions stabilized by alkyne- containing surfactant **3.7** before (black) and after (red) overnight CuAAC reaction with azidorhodamine **3.12**. Small population at ~50-70 nm

corresponds to micelles; the observed increase in micelle size after conjugation with rhodamine **3.12** could be due to a change in hydrophilic-hydrophobic balance of the dye-micelle conjugate. Data are an average of three replicate measurements.

Figure 3.7. Zeta potential data for emulsions modified with different thiols.

Emulsions were prepared according to the general emulsion formation, modified according to the general thiol-ene modification procedure, and analyzed according to the general nanoemulsion analysis procedure.

Figure 3.8. Controls for thiol-ene modification of nanoemulsions.

Emulsions were prepared with surfactant **16** according to the general nanoemulsion formation procedure. Emulsions were modified according to general nanoemulsion modification by thiol-ene chemistry procedure using thiols **18** and **24**, with noted exceptions for lack of reagent. Emulsions were analyzed as described by the general nanoemulsion analysis procedure.

Figure 3.9. Size analysis of emulsions modified through pre- or post-emulsion alkene modification.

Same experiment as 5B except full emulsion size plotted instead of size change. For assessment of the statistical significance of differences, a one-tailed Student's t-test assuming unequal sample variance was employed. Results were considered significant/not significant per the following definitions: ns = $p > 0.05$, significant = $p < 0.05$, * = $p \leq 0.05$, ** = $p \leq 0.01$, *** = $p \leq 0.001$. Statistical significance was done for each emulsion with reference to control emulsion stabilized by unmodified **16**.

Figure 3.10. **Size analysis of emulsions modified through pre- or post-emulsion alkene modification.**

Dynamic light scattering data for the PFC nanoemulsions stabilized by alkene-containing surfactant **16** before (black) and after thiol-ene coupling with the following thiols: **23** (methylmercaptoacetate, yellow), **18** (mercaptoacetic acid, red) or **24** (2-dimethylaminoethanethiol, blue). Small population at ~50 nm corresponds to micelles. Data are an average of three replicate measurements.

Figure 3.11. Size changes of emulsions functionalized through pre- and post-emulsion modification.

Emulsions were functionalized through either pre- or post-emulsion modification routes using the following procedures:

In the pre-emulsion route, surfactants were modified through thiol-ene couplings as described in the synthetic chemistry experimental procedures (Figure 3.2B, D.). After isolating modified surfactant, surfactant was employed for nanoemulsion formation as described by the general nanoemulsion formation procedure. The resulting emulsions were analyzed as described by the general nanoemulsion analysis procedure.

In the post-emulsion modification route, emulsions were formed, functionalized and analyzed as described by the general nanoemulsion formation, modification and analysis procedures.

Plotted are the size changes as determined by the absolute difference between size distributions of the resulting emulsions and control emulsions formulated with unmodified **3.6**. Size data are representative of the average of three independent samples, with three replicate measurements; error bars represent the standard deviation of the three independent samples. Statistical significance was done with regards to control emulsions. For assessment of the statistical significance of differences, a one-tailed Student's t-test assuming unequal sample variance was employed. Results were considered significant/not significant per the following definitions: ns = $p > 0.05$, significant = $p < 0.05$, * = $p \leq 0.05$, ** = $p \leq 0.01$, *** = $p \leq 0.001$.

Figure 3.12. Raw size distributions of emulsions functionalized through pre- and post-emulsion modification.

Emulsions modified through either a pre- or post-emulsion modification method as presented in Figure 3.11A,B. Thiol-ene chemistries were performed on surfactant **16** with thiols **18**, **23** or **24** either before (conditions in Figure 3.2B) or after emulsification (conditions in Figure 3.3E). The emulsions were diluted 1:100 in MilliQ water and analyzed by DLS. Plotted are nanoemulsion sizes. Size data are representative of the average of three independent samples, with three replicate measurements; error bars represent the standard deviation of the three independent samples. For assessment of the statistical significance of differences, a one-tailed Student's t-test assuming unequal sample variance was employed. Results were considered significant/not significant per the following definitions: ns = $p > 0.05$, significant = $p < 0.05$, * = $p \leq 0.05$, ** = $p \leq 0.01$, *** = $p \leq 0.001$. Statistical significance was done for each emulsion with reference to control emulsion stabilized by unmodified **16**.

Figure 3.13C/D. Emulsion surface modification and cellular uptake studies:

Emulsions were prepared, functionalized and analyzed as described by the general nanoemulsion formation, modification with thiol-ene and analysis procedures. Emulsions were then incubated with RAW and A375 cells and analyzed by flow cytometry according to the procedures found in general cell culture experimental procedure section.

Figure 3.14 Inhibition of cellular (A375) uptake at 4 °C versus 37 °C.

Emulsions were prepared, functionalized and analyzed as described by the general nanoemulsion formation, modification with thiol-ene and analysis procedures. Emulsions were then incubated with A375 cells and analyzed by flow cytometry according to the procedures found in the general cell culture experimental procedure section. Followed general cell labeling procedure for measurements at 4 °C with the following alterations: A375 cells were pre-incubated in cold (4 °C) media for 30 minutes prior to treatment with emulsions. Emulsion incubation was carried out for one hour in a refrigerator set at 4 °C. Emulsions were then washed according to protocol, with media and FACS buffer pre-chilled at 4 °C.

Figure 3.15. Cellular viability studies for RAW and A375 cells incubated with PFC nanoemulsions with modified surface charges.

Cell viability experiments were performed as described in the cell culture procedures. See Figure S3.5, S3.6 for gated histograms.

3.9 1H-NMR Spectra Relevant to Chapter Three

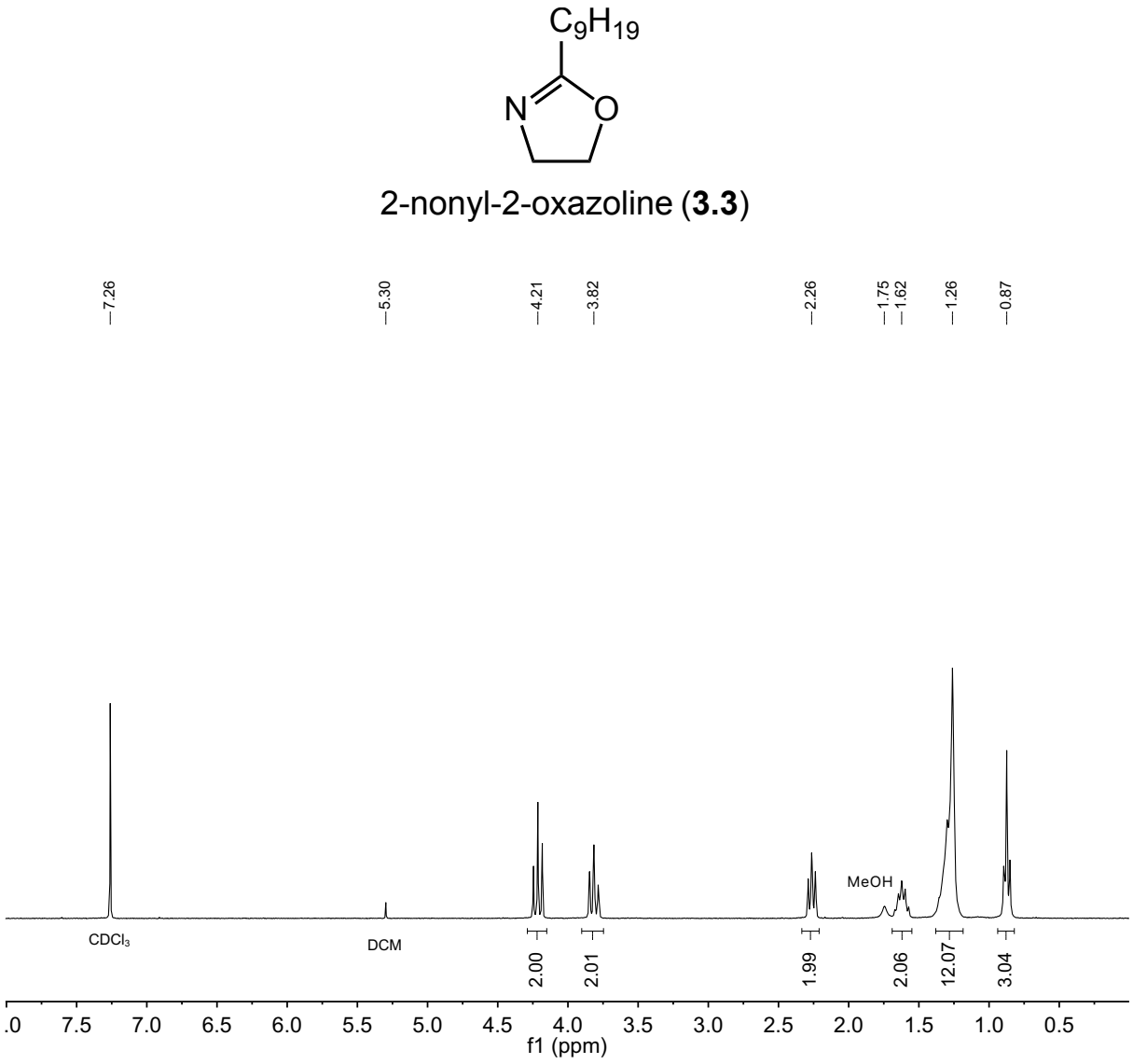

^{1}H NMR (300 MHz, $CDCl_3$) of monomer **3.3** 2-nonyl-2-oxazoline.

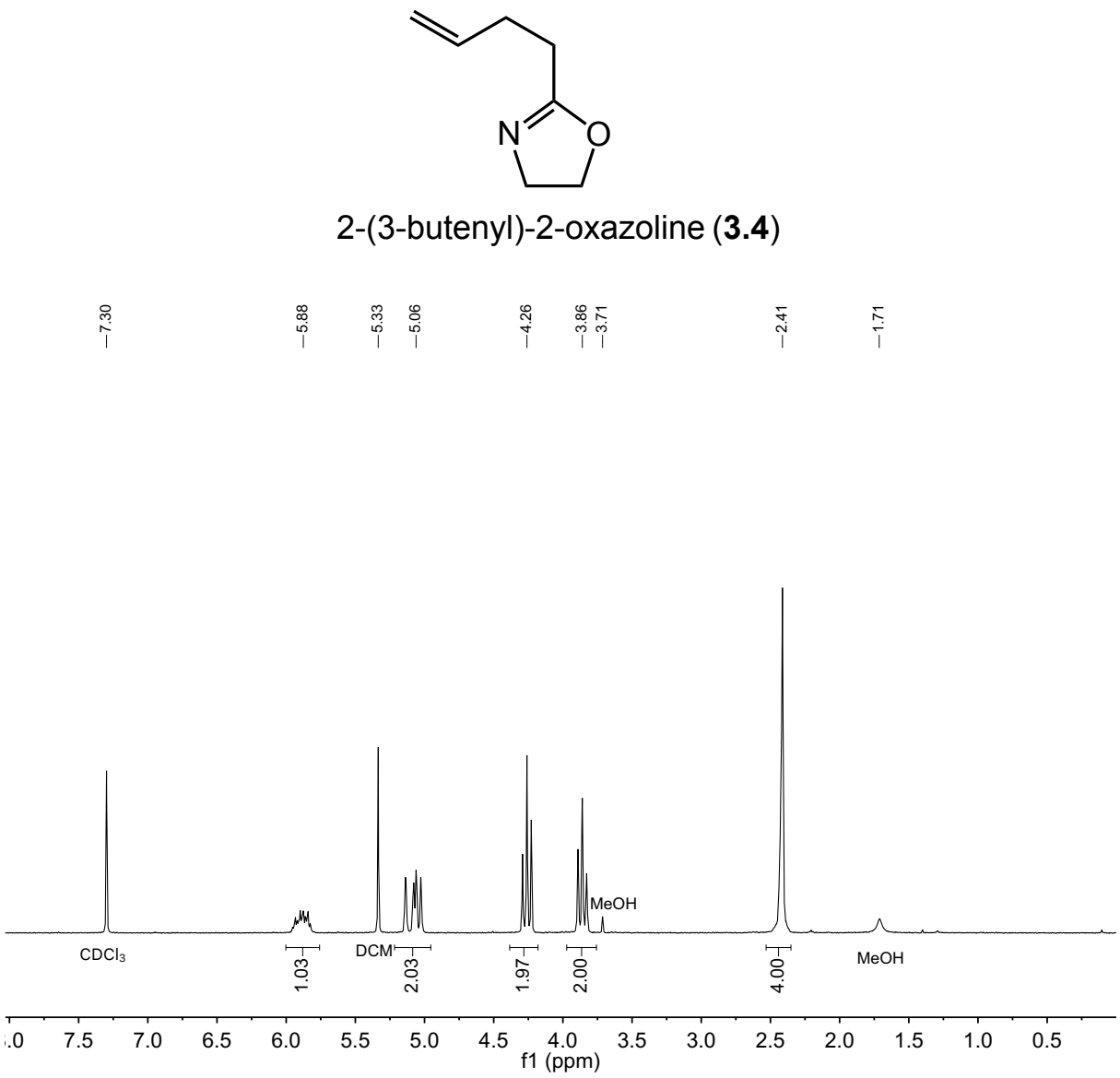

^{1}H NMR (300 MHz, $CDCl_3$) of functional comonomer **3.4** (2-(3-butenyl)-2-oxazoline (EneOx)).

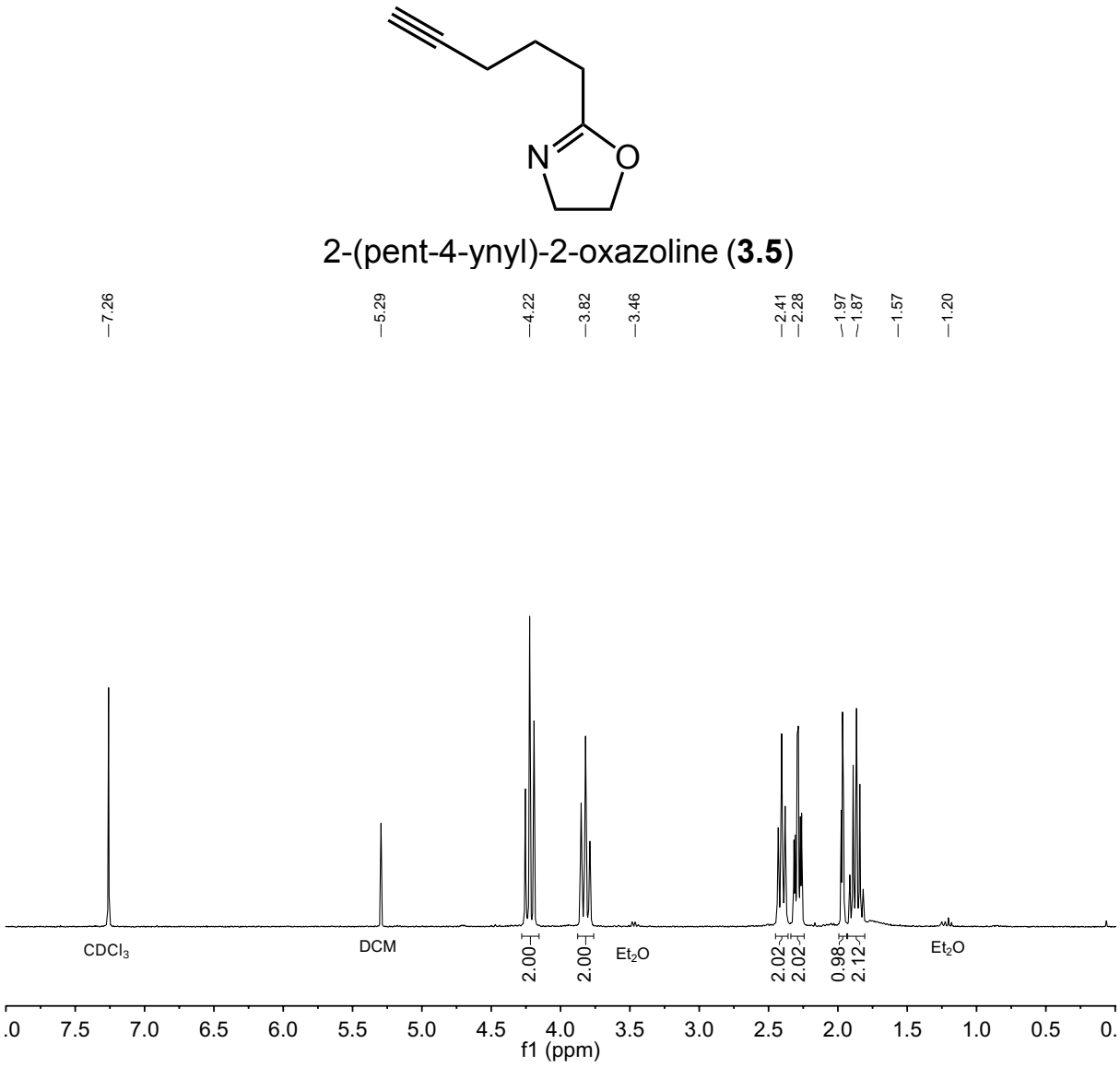

^{1}H NMR (300 MHz, $CDCl_3$) of functional comonomer **3.5** (2-(4-pentynyl)-2-oxazoline (PyneOx)).

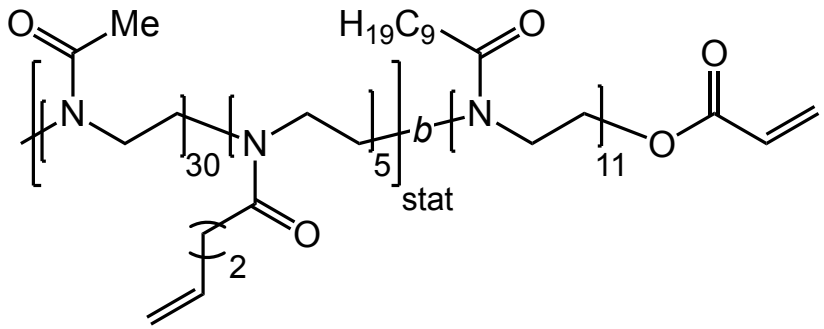

[P(MeOx)$_{30}$-*r*-P(EneOx)$_5$]-*b*-P(NonOx)$_{11}$ (**3.6**)

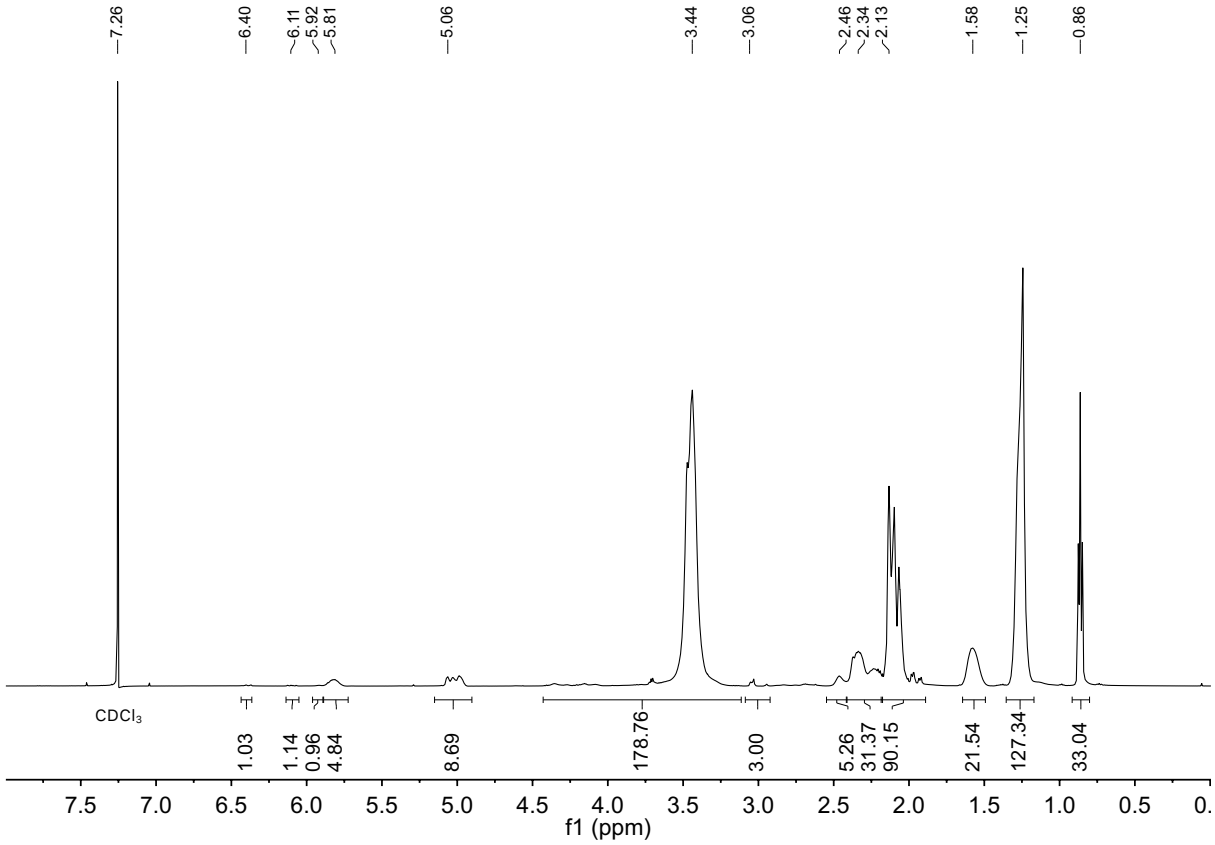

^{1}H NMR (500 MHz, $CDCl_3$) of copolymer **3.6** P(MeOx$_{30}$-*r*-EneOx$_5$-*b*-NonOx$_{11}$)

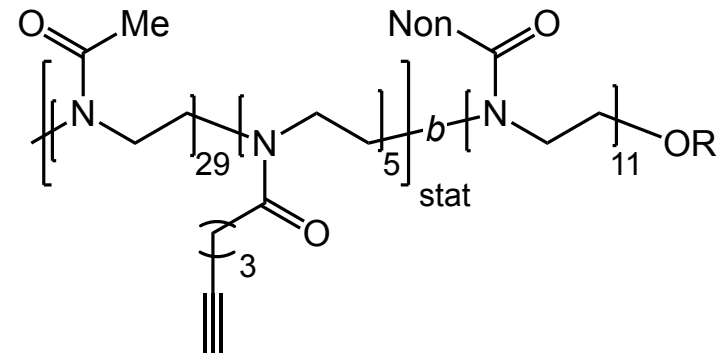

R = H, $COCH=CH_2$

$[P(MeOx)_{29}$-*r*-$P(PyneOx)_5]$-*b*-$P(NonOx)_{11}$ (**3.7**)

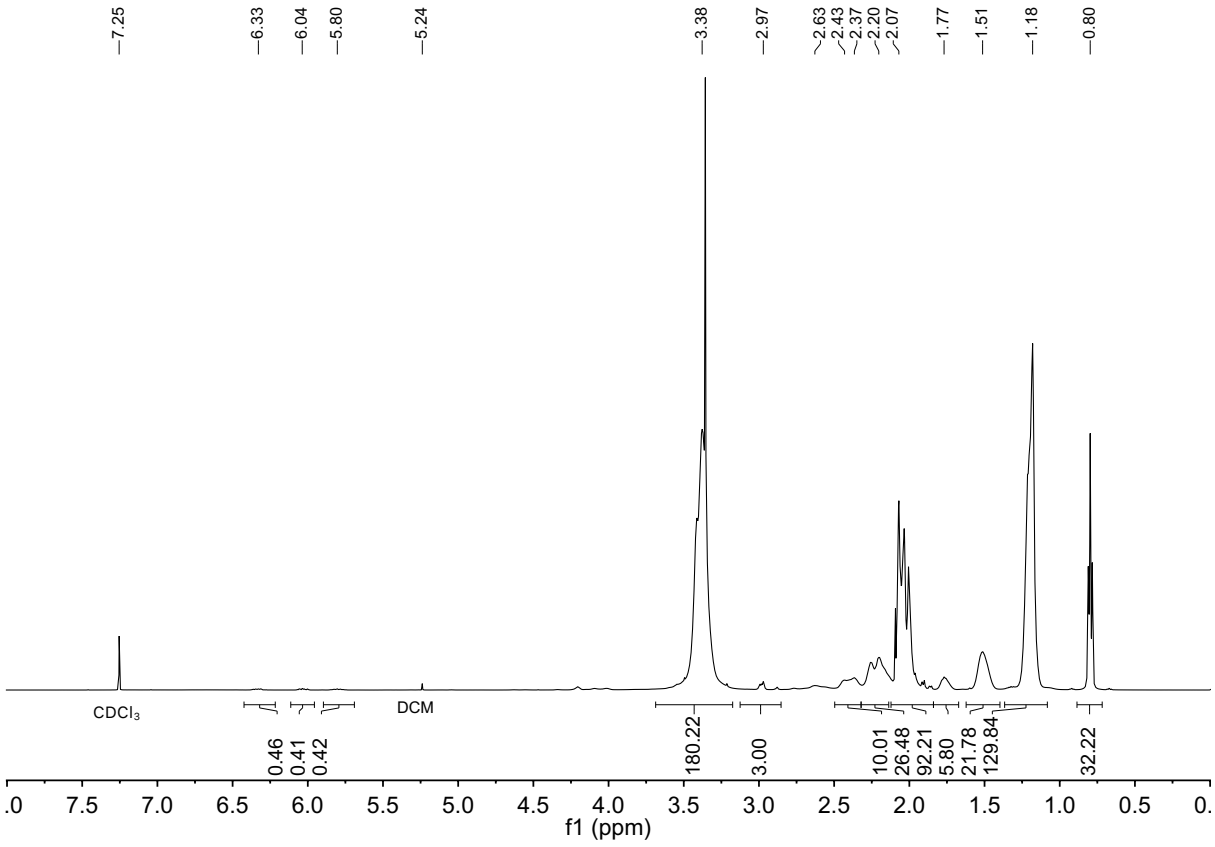

^{1}H NMR (500 MHz, $CDCl_3$) of copolymer **3.7** P($MeOx_{29}$-*r*-$PyneOx_5$-*b*-$NonOx_{11}$).

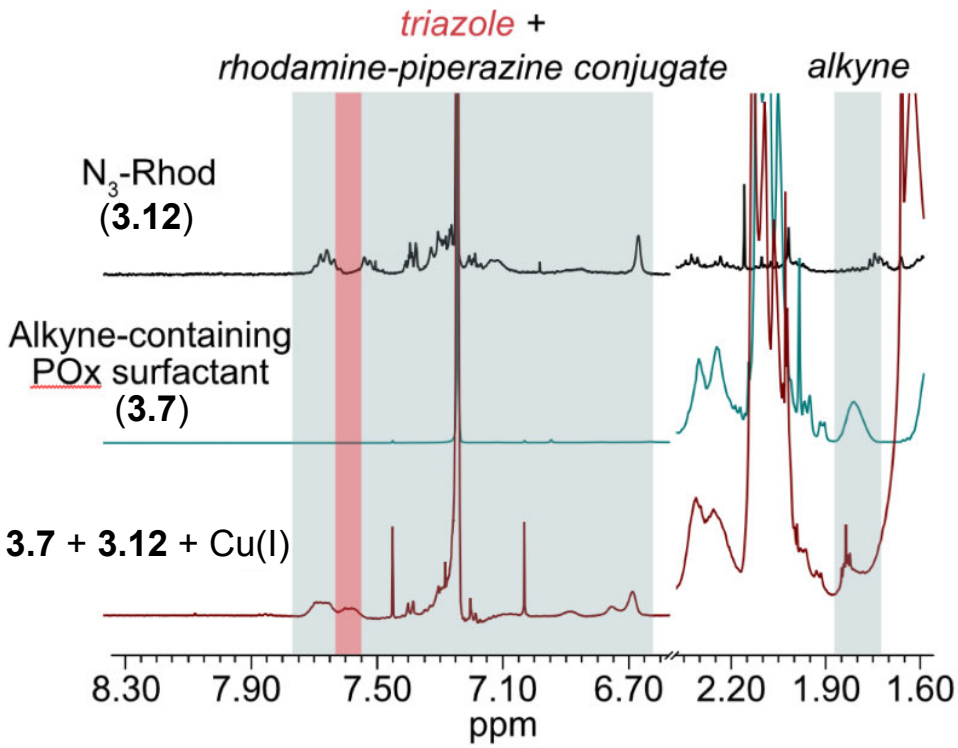

^{1}H NMR ($CDCl_3$) of isolated surfactant from post-emulsion modification of **3.7** with azidorhodamine **3.12**, overlaid in relevant regions with starting materials **3.7** and **3.12**, as demonstrated in Figure 3.3C. Evolution of triazole peak in **3.7** + **3.12** can be seen at 7.60 ppm (highlighted red region), agreeing with the triazole peak that appears in reaction of **3.7** with model azide ethylazidoacetate **3.10** (Figure 3.2C,E). Full ^{1}H NMR of purified, modified surfactant is provided below.

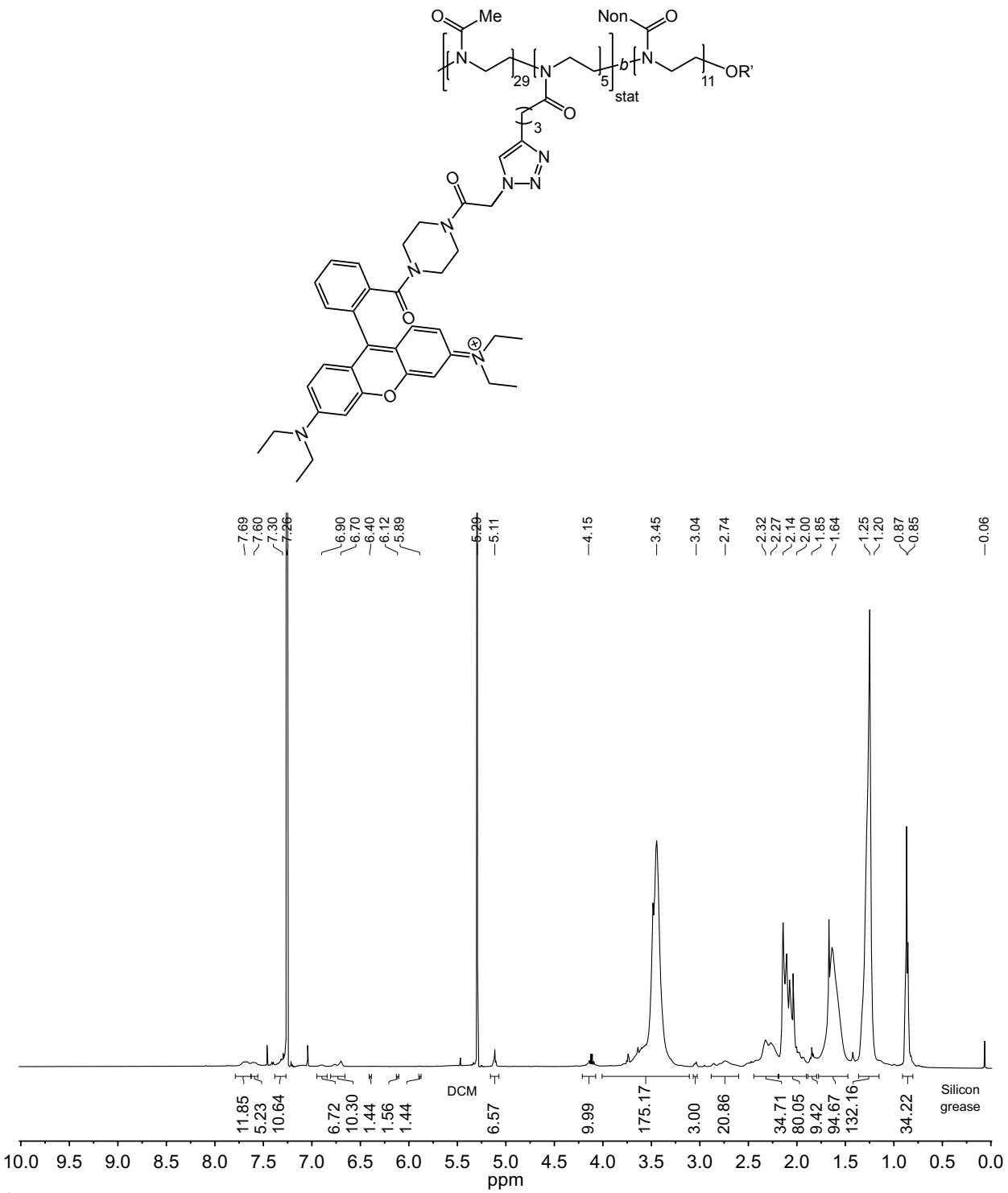

^{1}H NMR of isolated and dialyzed surfactant from post-emulsion modification of **3.7** with azidorhodamine **3.12**, as demonstrated in Figure 3.3C.

3.10 SEC-GPC Analysis Relevant to Chapter Three

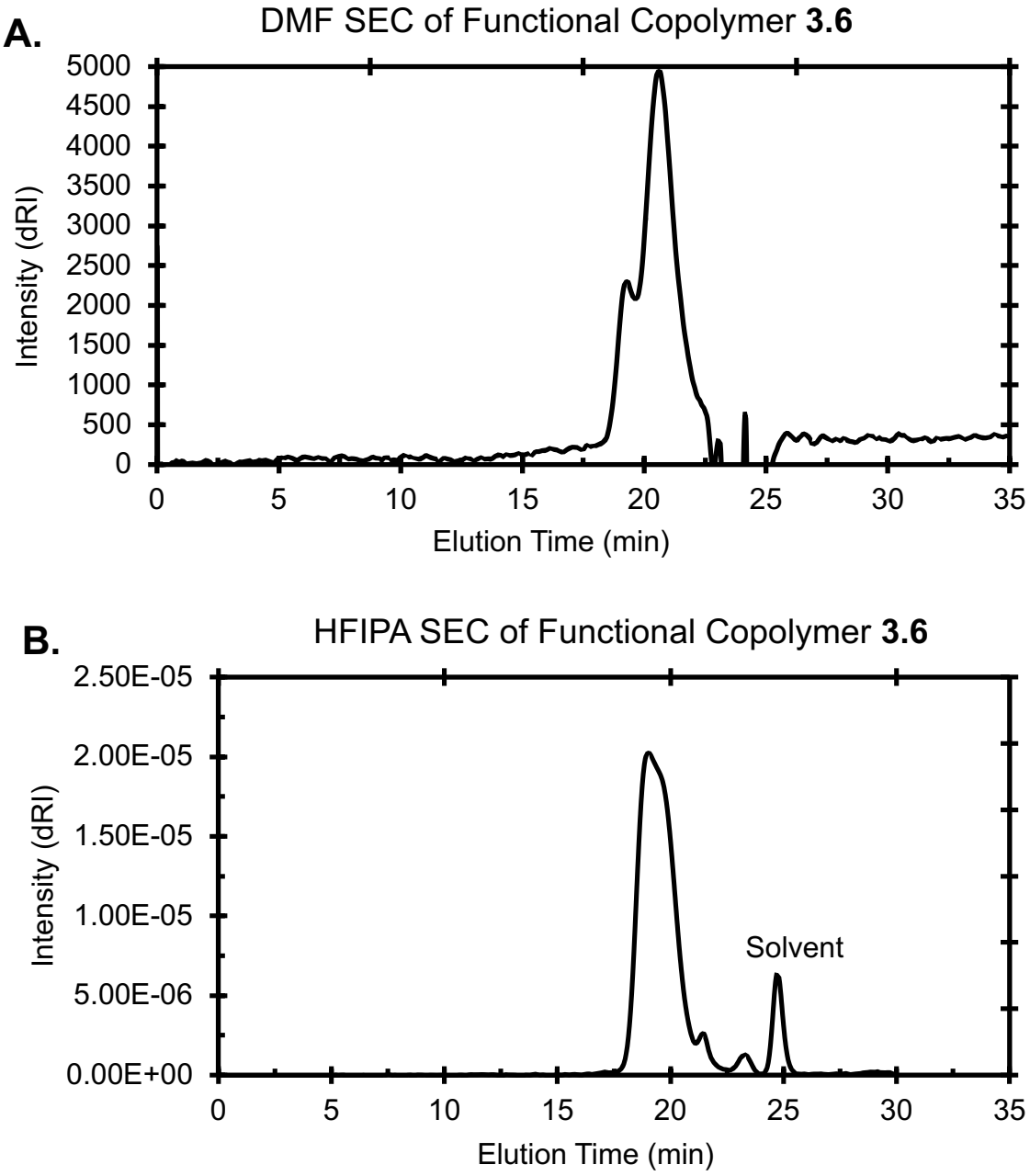

Size exclusion chromatogram of **3.6**. Eluent was either (A) DMF with LiBr (0.1 M) at 50 °C (flow rate: 0.80 mL/ min), negative peak at ~23 minutes is solvent, or (B) HFIPA at 25 °C (flow rate: 0.75 mL/min), peaks at ~23.3, 23.8 minutes are solvent. Shoulders have previously been observed in poly(2-oxazoline)s and may be attributed to aggregation, sample-column interactions,[83,116] or either extrinsic or intrinsic chain transfer/coupling side reactions that may occur at high monomer conversion and high reaction temperatures.[114,117]

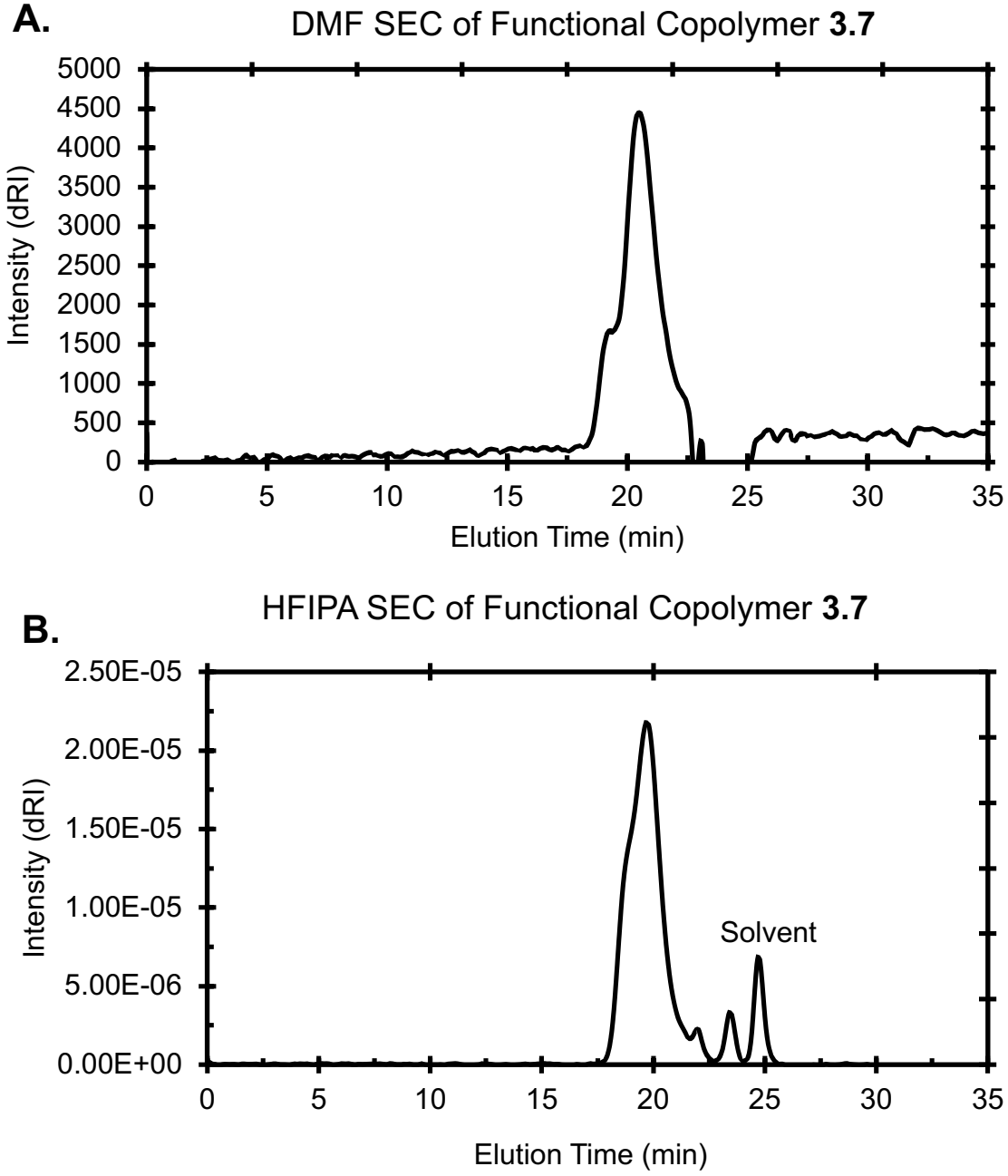

Size exclusion chromatogram of **3.7**. Eluent was either (A) DMF with LiBr (0.1 M) at 50 °C (flow rate: 0.80 mL/ min), negative peak at ~23 minutes is solvent, or (B) HFIPA at 25 °C (flow rate: 0.75 mL/min), peak at ~23.3, 23.8 minutes are solvent. Shoulders have previously been observed in poly(2-oxazoline)s and may be attributed to aggregation, sample-column interactions,[83,116] or either extrinsic or intrinsic chain transfer/coupling side reactions that may occur at high monomer conversion and high reaction temperatures.[114,117]

3.11 Supplementary Cell Analysis

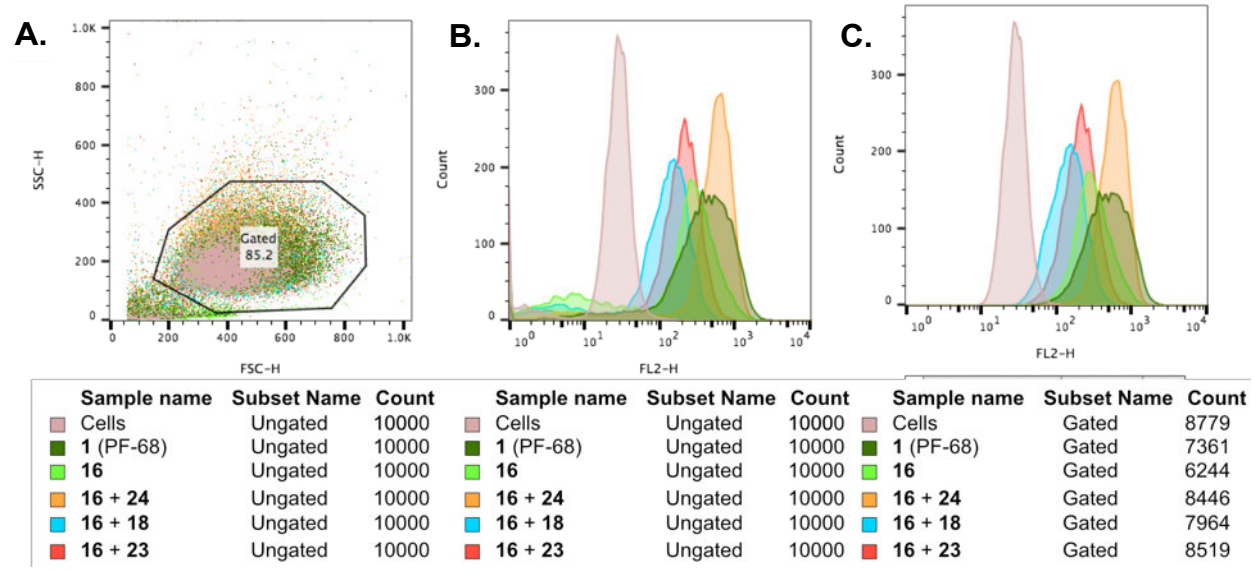

Sample name	Subset Name	Count
Cells	Ungated	10000
1 (PF-68)	Ungated	10000
16	Ungated	10000
16 + 24	Ungated	10000
16 + 18	Ungated	10000
16 + 23	Ungated	10000

Sample name	Subset Name	Count
Cells	Ungated	10000
1 (PF-68)	Ungated	10000
16	Ungated	10000
16 + 24	Ungated	10000
16 + 18	Ungated	10000
16 + 23	Ungated	10000

Sample name	Subset Name	Count
Cells	Gated	8779
1 (PF-68)	Gated	7361
16	Gated	6244
16 + 24	Gated	8446
16 + 18	Gated	7964
16 + 23	Gated	8519

Figure S3.1. Histograms for A375 cell uptake flow cytometry data in Figure 3.13C.
(A) Side scatter (SSC) vs forward scatter (FSC) overlay of A375 cells incubated for 3 hours with emulsions and washed. The gate employed for Figure 3.13C is shown. (B) Representative FL-2 histograms of each sample, ungated. (C) Representative FL-2 histograms of each sample, gated.

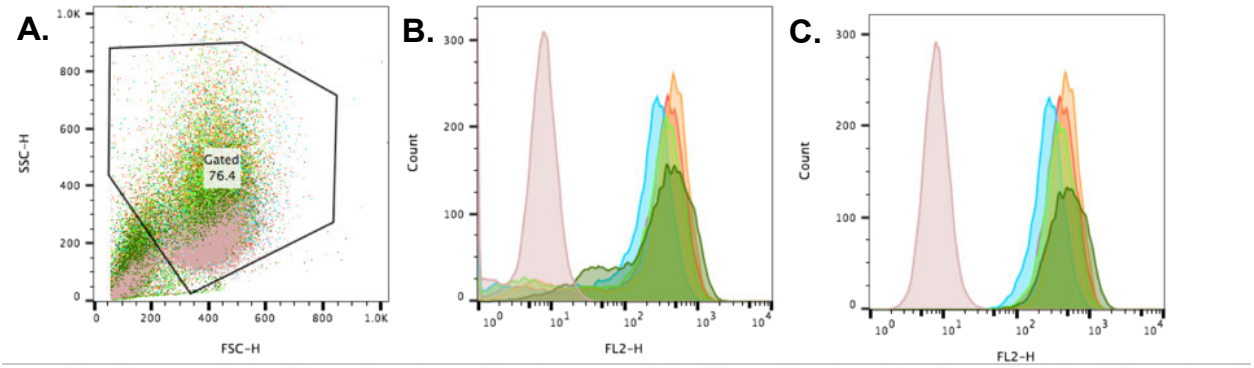

Sample name	Subset Name	Count
Cells	Ungated	10000
1 (PF-68)	Ungated	10000
16	Ungated	10000
16 + 24	Ungated	10000
16 + 18	Ungated	10000
16 + 23	Ungated	10000

Sample name	Subset Name	Count
Cells	Ungated	10000
1 (PF-68)	Ungated	10000
16	Ungated	10000
16 + 24	Ungated	10000
16 + 18	Ungated	10000
16 + 23	Ungated	10000

Sample name	Subset Name	Count
Cells	Gated	7913
1 (PF-68)	Gated	5885
16	Gated	6738
16 + 24	Gated	7332
16 + 18	Gated	7245
16 + 23	Gated	7641

Figure S3.2. Histograms for RAW cell uptake flow cytometry data in Figure 3.13D.
(A) Side scatter (SSC) vs forward scatter (FSC) of RAW cells incubated for 3 hours with emulsions and washed. The gate employed for Figure 3.13D is shown. (B) Representative FL-2 histograms of each sample, ungated. (C) Representative FL-2 histograms of each sample, gated.

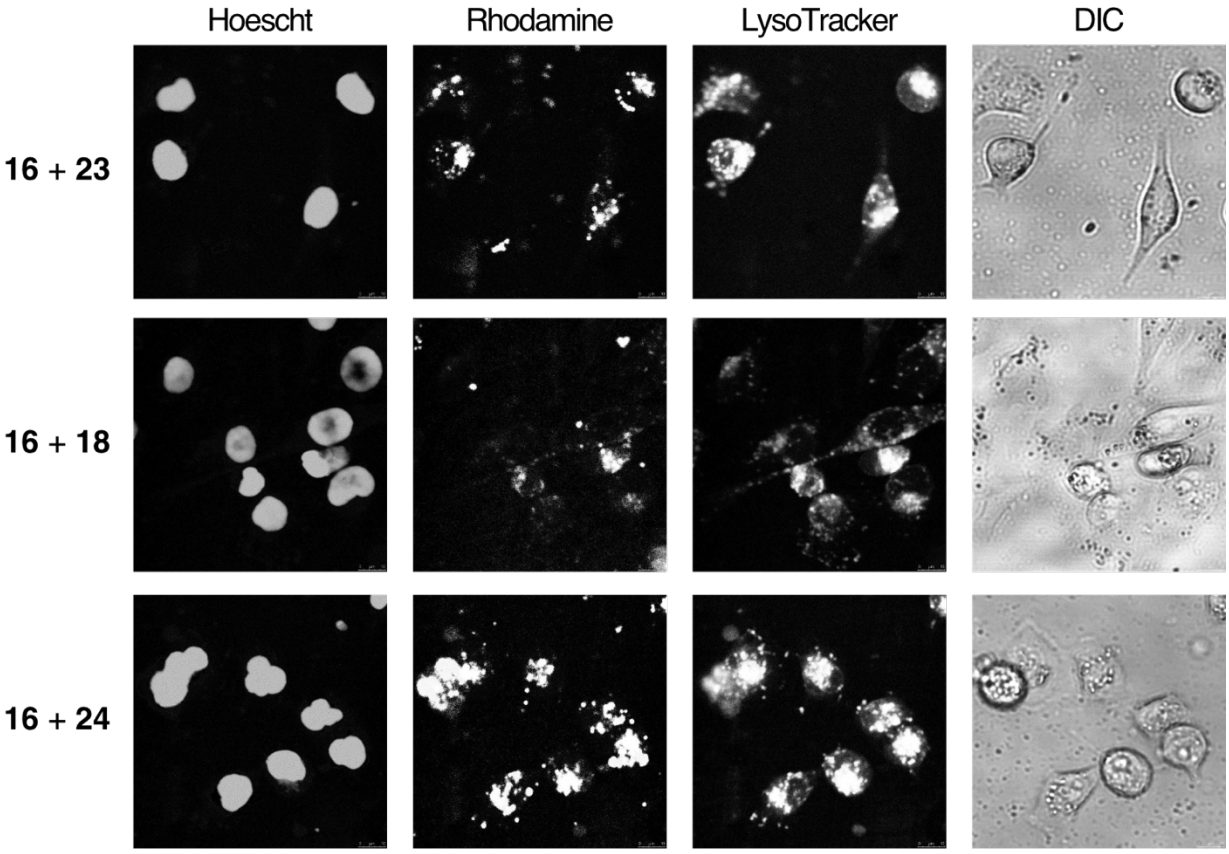

Figure S3.3. Single channel images for Figure 3.13E (confocal microscopy of A375 cells). PFC nanoemulsions with modified surface charges were prepared via the thiol-ene modification of emulsions formed from **3.6** as described in Figure 3.3E,F. Excess reagents were removed via thrice centrifugation and resuspension in MilliQ H_2O. After the final wash, the emulsions were resuspended in PBS and **25** in acetone was added. The emulsions were rocked for 1 min then introduced to A375 cells for 1 hour. The cells were washed 5x (3x media, 2x FACS buffer) to remove excess emulsions, lifted with trypsin and transferred to an FBS-treated microscope slide, incubated for 1 h in media, stained with Hoescht dye and LysoTracker Green and imaged via confocal microscopy. The cells were analyzed for rhodamine (Ex 532 nm) and Lysotracker Green (Ex 488 nm). Scale bar indicates 10 μm. Images are representative of two independent experiments.

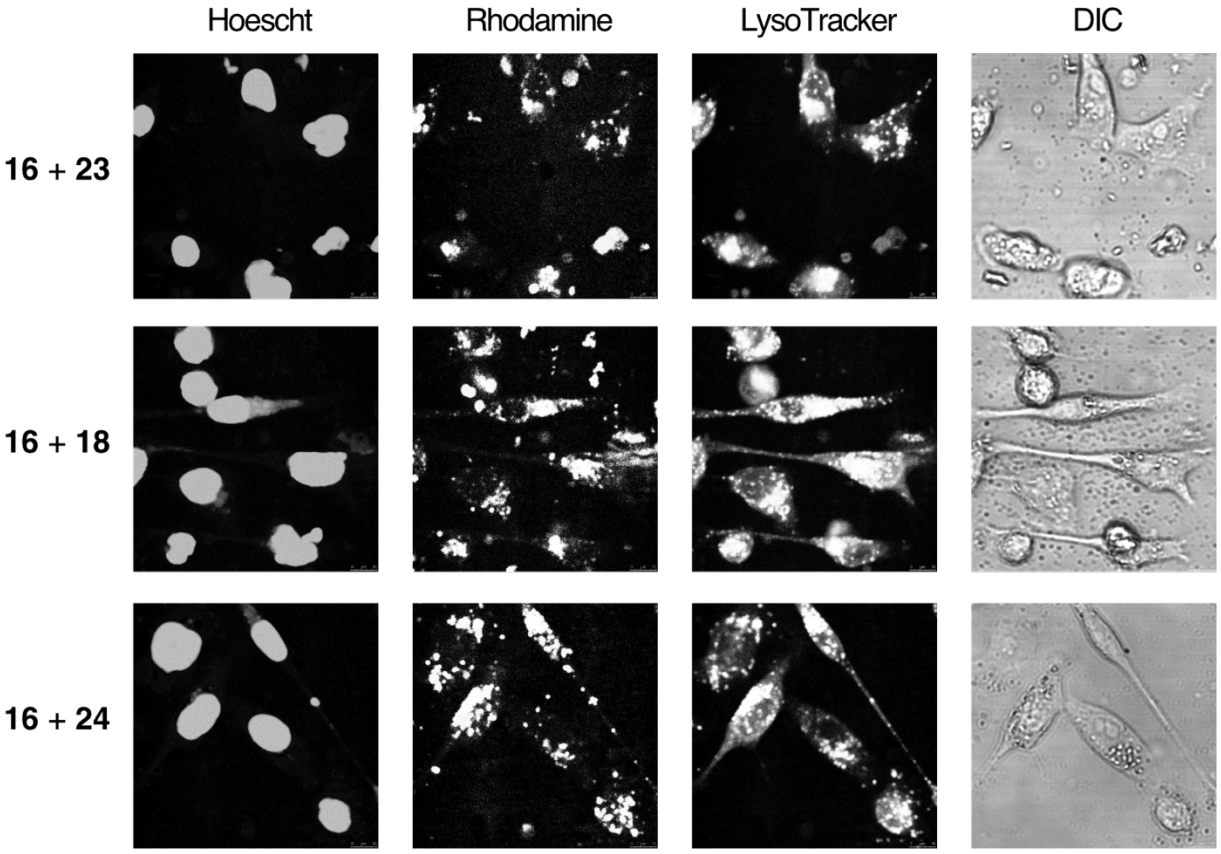

Figure S3.4. Single channel images for Figure 3.13F (confocal microscopy of RAW cells). PFC nanoemulsions with modified surface charges were prepared via the thiol-ene modification of emulsions formed from **3.6** as described in Figure 3.3E,F. Excess reagents were removed via thrice centrifugation and resuspension in MilliQ H_2O. After the final wash, the emulsions were resuspended in PBS and **3.15** in acetone was added. The emulsions were rocked for 1 min then introduced to RAW cells for 1 hour. The cells were washed 5x (3x media, 2x FACS buffer) to remove excess emulsions, lifted with trypsin and transferred to an FBS-treated microscope slide, incubated for 1 h in media, stained with Hoescht dye and LysoTracker Green and imaged via confocal microscopy. The cells were analyzed for rhodamine (Ex 532 nm) and Lysotracker Green (Ex 488 nm). Scale bar indicates 10 μm. Images are representative of two independent experiments.

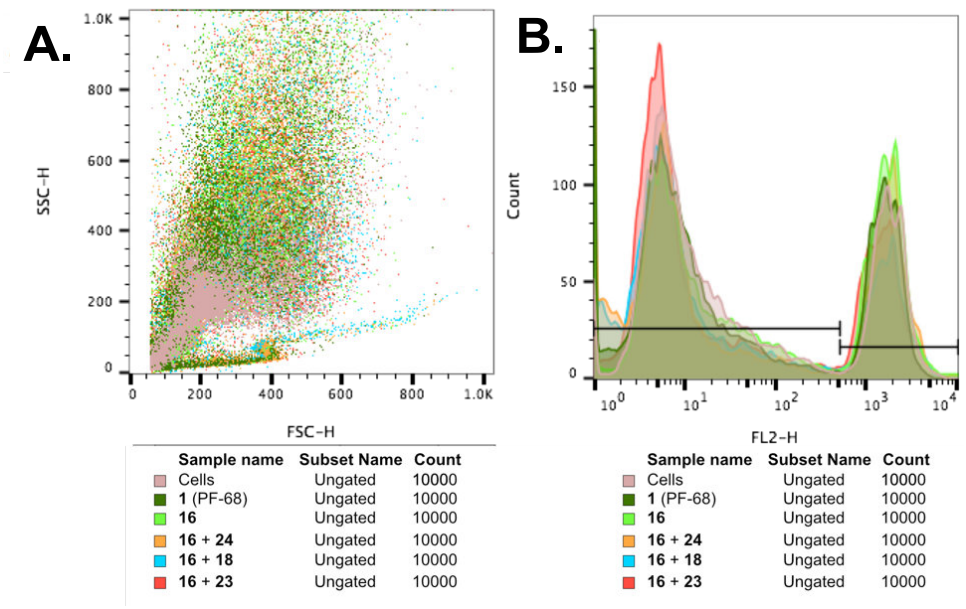

Figure S3.5. Histograms for RAW cellular viability flow cytometry data in Figure 3.15. (A) side scatter (SSC) vs forward scatter (FSC) overlay of RAW cells incubated for 12 hours with emulsions. (B) Representative FL-2 of each sample.

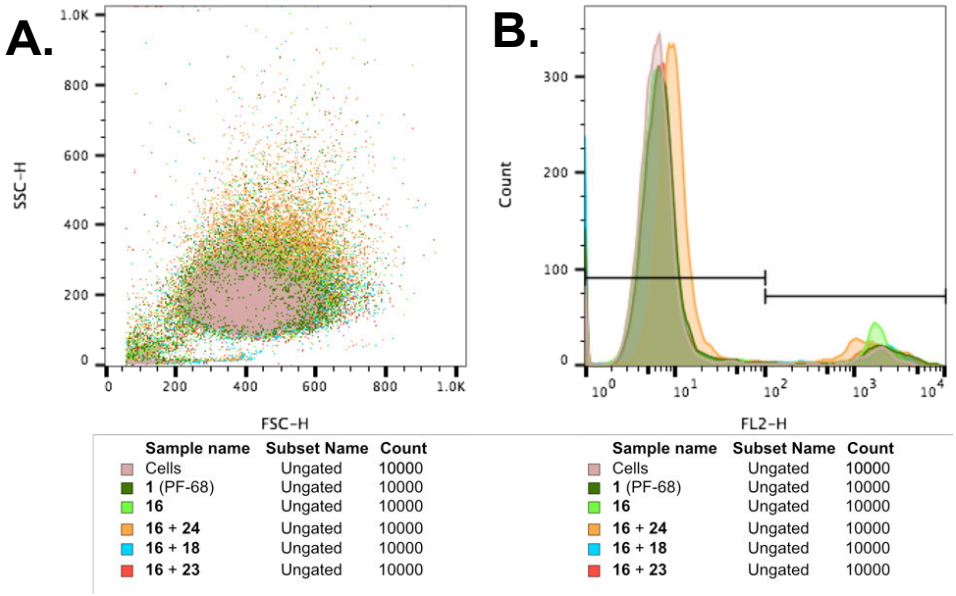

Figure S3.6. Histograms for A375 cellular viability flow cytometry data in Figure 3.15. (A) side scatter (SSC) vs forward scatter (FSC) overlay of A375 cells incubated for 12 hours with emulsions. (B) Representative FL-2 of each sample.

3.12 References

(1) Nie, Z.; Petukhova, A.; Kumacheva, E. Properties and Emerging Applications of Self-Assembled Structures Made from Inorganic Nanoparticles. *Nat. Nanotechnol.* **2010**, *5*, 15–25.

(2) Park, S.; Lim, J.-H.; Chung, S.-W.; Mirkin, C. A. Self-Assembly of Mesoscopic Metal-Polymer Amphiphiles. *Science* **2004**, *303*, 348–351.

(3) Liu, K.; Nie, Z.; Zhao, N.; Li, W.; Rubinstein, M.; Kumacheva, E. Step-Growth Polymerization of Inorganic Nanoparticles. *Science* **2010**, *329*, 197–200.

(4) Cargnello, M.; Johnston-Peck, A. C.; Diroll, B. T.; Wong, E.; Datta, B.; Damodhar, D.; Doan-Nguyen, V. V. T.; Herzing, A. A.; Kagan, C. R.; Murray, C. B. Substitutional Doping in Nanocrystal Superlattices. *Nature* **2015**, *524*, 450–453.

(5) Peer, D.; Karp, J. M.; Hong, S.; Farokhzad, O. C.; Margalit, R.; Langer, R. Nanocarriers as an Emerging Platform for Cancer Therapy. *Nat. Nanotechnol.* **2007**, *2*, 751–760.

(6) Caló, E.; Khutoryanskiy, V. V. Biomedical Applications of Hydrogels: A Review of Patents and Commercial Products. *Eur. Polym. J.* **2015**, *65*, 252–267.

(7) De las Heras Alarcón, C.; Pennadam, S.; Alexander, C. Stimuli Responsive Polymers for Biomedical Applications. *Chem. Soc. Rev.* **2005**, *34*, 276–285.

(8) Caruso, F.; Hyeon, T.; Rotello, V. M. Nanomedicine. *Chem. Soc. Rev.* **2012**, *41*, 2537–2538.

(9) Ahn, Y.; Jun, Y. Measurement of Pain-like Response to Various NICU Stimulants for High-Risk Infants. *Early Hum. Dev.* **2007**, *83*, 255–262.

(10) Ishida, T.; Harashima, H.; Kiwada, H. Liposome Clearance. *Biosci. Rep.* **2002**, *22*, 197–224.

(11) Fryd, M. M.; Mason, T. G. Advanced Nanoemulsions. *Annu. Rev. Phys. Chem.* **2012**, *63*, 493–518.

(12) Sainsbury, F.; Zeng, B.; Middelberg, A. P. Towards Designer Nanoemulsions for Precision Delivery of Therapeutics. *Curr. Opin. Chem. Eng.* **2014**, *4*, 11–17.

(13) Tayeb, H. H.; Piantavigna, S.; Howard, C. B.; Nouwens, A.; Mahler, S. M.; Middelberg, A. P. J.; He, L.; Holt, S. A.; Sainsbury, F. Insights into the Interfacial Structure-Function of Poly(Ethylene Glycol)-Decorated Peptide-Stabilised Nanoscale Emulsions. *Soft Matter* **2017**, *13*, 7953–7961.

(14) Patravale, V.; Dandekar, P.; Jain, R. Nanoparticulate Systems as Drug Carriers: The Need. *Nanoparticulate Drug Deliv.* **2012**, 1–28.

(15) Aboalnaja, K. O.; Yaghmoor, S.; Kumosani, T. A.; McClements, D. J. Utilization of Nanoemulsions to Enhance Bioactivity of Pharmaceuticals, Supplements, and Nutraceuticals: Nanoemulsion Delivery Systems and Nanoemulsion Excipient Systems. *Expert Opin. Drug Deliv.* **2016**, *13*, 1327–1336.

(16) McClements, D. J.; Jafari, S. M. General Aspects of Nanoemulsions and Their Formulation. *Nanoemulsions Formul. Appl. Charact.* **2018**, 3–20.

(17) Bibette, J.; Leal Calderon, F.; Poulin, P. Emulsions: Basic Principles. *Reports Prog. Phys.* **1999**, *62*, 969–1033.

(18) Shah, P.; Bhalodia, D.; Shelat, P. Nanoemulsion: A Pharmaceutical Review. *Syst. Rev. Pharm.* **2010**, *1*, 24–32.

(19) Tadros, T. F. Applied Surfactants: Principles and Applications. *Appl. Surfactants Princ. Appl.* **2005**, 1–634.

(20) Sonneville-Aubrun, O.; Simonnet, J. T.; L'Alloret, F. Nanoemulsions: A New Vehicle for

Skincare Products. *Adv. Colloid Interface Sci.* **2004**, *108–109*, 145–149.

(21) Velikov, K. P.; Pelan, E. Colloidal Delivery Systems for Micronutrients and Nutraceuticals. *Soft Matter* **2008**, *4*, 1964–1980.

(22) McClements, D. J. Edible Nanoemulsions: Fabrication, Properties, and Functional Performance. *Soft Matter* **2011**, *7*, 2297–2316.

(23) Fahr, A.; Liu, X. Drug Delivery Strategies for Poorly Water-Soluble Drugs. *Expert Opin. Drug Deliv.* **2007**, *4*, 403–416.

(24) Lawrence, M. J.; Rees, G. D. Microemulsion-Based Media as Novel Drug Delivery Systems. *Adv. Drug Deliv. Rev.* **2000**, *45*, 89–121.

(25) Spernath, A.; Aserin, A. Microemulsions as Carriers for Drugs and Nutraceuticals. *Adv. Colloid Interface Sci.* **2006**, *128–130*, 47–64.

(26) Chern, C. S. Emulsion Polymerization Mechanisms and Kinetics. *Prog. Polym. Sci.* **2006**, *31*, 443–486.

(27) Imhof, A.; Pine, D. J. Ordered Macroporous Materials by Emulsion Templating. *Nature* **1997**, *389*, 948–951.

(28) Anton, N.; Benoit, J. P.; Saulnier, P. Design and Production of Nanoparticles Formulated from Nano-Emulsion Templates-A Review. *J. Control. Release* **2008**, *128*, 185–199.

(29) Min, K.; Gao, H.; Matyjaszewski, K. Development of an Ab Initio Emulsion Atom Transfer Radical Polymerization: From Microemulsion to Emulsion. *J. Am. Chem. Soc.* **2006**, *128*, 10521–10526.

(30) Guan, B. Y.; Yu, L.; Lou, X. W. Formation of Asymmetric Bowl-Like Mesoporous Particles via Emulsion-Induced Interface Anisotropic Assembly. *J. Am. Chem. Soc.* **2016**, *138*, 11306–11311.

(31) Musyanovych, A.; Mailänder, V.; Landfester, K. Miniemulsion Droplets as Single Molecule Nanoreactors for Polymerase Chain Reaction. *Biomacromolecules* **2005**, *6*, 1824–1828.

(32) Zhang, W.; Zhong, Q. Microemulsions as Nanoreactors to Produce Whey Protein Nanoparticles with Enhanced Heat Stability by Sequential Enzymatic Cross-Linking and Thermal Pretreatments. *J. Agric. Food Chem.* **2009**, *57*, 9181–9189.

(33) Yang, H.; Fu, L.; Wei, L.; Liang, J.; Binks, B. P. Compartmentalization of Incompatible Reagents within Pickering Emulsion Droplets for One-Pot Cascade Reactions. *J. Am. Chem. Soc.* **2015**, *137*, 1362–1371.

(34) Manabe, K.; Sun, X. M.; Kobayashi, S. Dehydration Reactions in Water. Surfactant-Type Brønsted Acid-Catalyzed Direct Esterification of Carboxylic Acids with Alcohols in an Emulsion System. *J. Am. Chem. Soc.* **2001**, *123*, 10101–10102.

(35) Attia, M. F.; Dieng, S. M.; Collot, M.; Klymchenko, A. S.; Bouillot, C.; Serra, C. A.; Schmutz, M.; Er-Rafik, M.; Vandamme, T. F.; Anton, N. Functionalizing Nanoemulsions with Carboxylates: Impact on the Biodistribution and Pharmacokinetics in Mice. *Macromol. Biosci.* **2017**, *17*, 1–13.

(36) Tadros, T. F. Emulsion Formation, Stability, and Rheology. *Emuls. Form. Stab.* **2013**, 1–75.

(37) Fernandez, A. M.; Jebbanema, L. The Effect of Surfactant Selection on Emulsion Polymer Properties. *Paint Coatings Ind.* **2007**, *23*, 62–68.

(38) Bai, L.; McClements, D. J. Extending Emulsion Functionality: Post-Homogenization Modification of Droplet Properties. *Processes* **2016**, *4*, 1–18.

(39) McClements, D. J. Advances in Fabrication of Emulsions with Enhanced Functionality

Using Structural Design Principles. *Curr. Opin. Colloid Interface Sci.* **2012**, *17*, 235–245.

(40) Mason, T. G.; Wilking, J. N.; Meleson, K.; Chang, C. B.; Graves, S. M. Nanoemulsions: Formation, Structure, and Physical Properties. *J. Phys. Condens. Matter* **2006**, *18*, R635–R666.

(41) Hensel, J. K.; Carpenter, A. P.; Ciszewski, R. K.; Schabes, B. K.; Kittredge, C. T.; Moore, F. G.; Richmond, G. L. Molecular Characterization of Water and Surfactant AOT at Nanoemulsion Surfaces. *Proc. Natl. Acad. Sci. U. S. A.* **2017**, *114*, 13351–13356.

(42) Dexter, A. F.; Malcolm, A. S.; Middelberg, A. P. J. Reversible Active Switching of the Mechanical Properties of a Peptide Film at a Fluid-Fluid Interface. *Nat. Mater.* **2006**, *5*, 502–506.

(43) Hanson, J. A.; Chang, C. B.; Graves, S. M.; Li, Z.; Mason, T. G.; Deming, T. J. Nanoscale Double Emulsions Stabilized by Single-Component Block Copolypeptides. *Nature* **2008**, *455*, 85–88.

(44) Medina, S. H.; Michie, M. S.; Miller, S. E.; Schnermann, M. J.; Schneider, J. P. Fluorous Phase-Directed Peptide Assembly Affords Nano-Peptisomes Capable of Ultrasound-Triggered Cellular Delivery. *Angew. Chem. Int. Ed.* **2017**, *56*, 11404–11408.

(45) Huang, Y.; Vezeridis, A. M.; Wang, J.; Wang, Z.; Thompson, M.; Mattrey, R. F.; Gianneschi, N. C. Polymer-Stabilized Perfluorobutane Nanodroplets for Ultrasound Imaging Agents. *J. Am. Chem. Soc.* **2017**, *139*, 15–18.

(46) Yang, Z.; Wei, J.; Sobolev, Y. I.; Grzybowski, B. A. Systems of Mechanized and Reactive Droplets Powered by Multi-Responsive Surfactants. *Nature* **2018**, *553*, 313–318.

(47) Zarzar, L. D.; Sresht, V.; Sletten, E. M.; Kalow, J. A.; Blankschtein, D.; Swager, T. M. Dynamically Reconfigurable Complex Emulsions via Tunable Interfacial Tensions.

Nature **2015**, *518*, 520–524.

(48) Brown, P.; Butts, C. P.; Eastoe, J. Stimuli-Responsive Surfactants. *Soft Matter* **2013**, *9*, 2365–2374.

(49) Gianella, A.; Mieszawska, A. J.; Hoeben, F. J. M.; Janssen, H. M.; Jarzyna, P. A.; Cormode, D. P.; Costa, K. D.; Rao, S.; Farokhzad, O. C.; Mulder, W. J. M.; et al. Synthesis and in Vitro Evaluation of a Multifunctional and Surface-Switchable Nanoemulsion Platform. *Chem. Commun.* **2013**, *49*, 9392–9394.

(50) Praveen Kumar, G. Nanoemulsion Based Targeting in Cancer Therapeutics. *Med. Chem.* **2015**, *5*, 272–284.

(51) Akazawa, K.; Sugihara, F.; Nakamura, T.; Matsushita, H.; Mukai, H.; Akimoto, R.; Minoshima, M.; Mizukami, S.; Kikuchi, K. Perfluorocarbon-Based 19F MRI Nanoprobes for In Vivo Multicolor Imaging. *Angew. Chem. Int. Ed.* **2018**, *57*, 16742–16747.

(52) McClements, D. J.; Jafari, S. M. Improving Emulsion Formation, Stability and Performance Using Mixed Emulsifiers: A Review. *Adv. Colloid Interface Sci.* **2018**, *251*, 55–79.

(53) Ziani, K.; Chang, Y.; McLandsborough, L.; McClements, D. J. Influence of Surfactant Charge on Antimicrobial Efficacy of Surfactant-Stabilized Thyme Oil Nanoemulsions. *J. Agric. Food Chem.* **2011**, *59*, 6247–6255.

(54) Guzey, D.; McClements, D. J. Formation, Stability and Properties of Multilayer Emulsions for Application in the Food Industry. *Adv. Colloid Interface Sci.* **2006**, *128–130*, 227–248.

(55) Saberi, A. H.; Zeeb, B.; Weiss, J.; McClements, D. J. Tuneable Stability of Nanoemulsions Fabricated Using Spontaneous Emulsification by Biopolymer

Electrostatic Deposition. *J. Colloid Interface Sci.* **2015**, *455*, 172–178.

(56) Tokle, T.; Lesmes, U.; McClements, D. J. Impact of Electrostatic Deposition of Anionic Polysaccharides on the Stability of Oil Droplets Coated by Lactoferrin. *J. Agric. Food Chem.* **2010**, *58*, 9825–9832.

(57) Wang, H. F.; Wibowo, D.; Shao, Z.; Middelberg, A. P. J.; Zhao, C. X. Design of Modular Peptide Surfactants and Their Surface Activity. *Langmuir* **2017**, *33*, 7957–7967.

(58) Zeng, B. J.; Chuan, Y. P.; O'Sullivan, B.; Caminschi, I.; Lahoud, M. H.; Thomas, R.; Middelberg, A. P. J. Receptor-Specific Delivery of Protein Antigen to Dendritic Cells by a Nanoemulsion Formed Using Top-down Non-Covalent Click Self-Assembly. *Small* **2013**, *9*, 3736–3742.

(59) Chaix, C.; Pacard, E.; Elaïssari, A.; Hilaire, J. F.; Pichot, C. Surface Functionalization of Oil-in-Water Nanoemulsion with a Reactive Copolymer: Colloidal Characterization and Peptide Immobilization. *Colloids Surfaces B Biointerfaces* **2003**, *29*, 39–52.

(60) Li, M.; Jiang, W.; Chen, Z.; Suryaprakash, S.; Lv, S.; Tang, Z.; Chen, X.; Leong, K. W. A Versatile Platform for Surface Modification of Microfluidic Droplets. *Lab Chip* **2017**, *17*, 635–639.

(61) Ursuegui, S.; Mosser, M.; Wagner, A. Copper-Free Click Chemistry for Microdroplet's W/O Interface Engineering. *RSC Adv.* **2016**, *6*, 94942–94948.

(62) Tang, L.; Yang, X.; Yin, Q.; Cai, K.; Wang, H.; Chaudhury, I.; Yao, C.; Zhou, Q.; Kwon, M.; Hartman, J. A.; et al. Investigating the Optimal Size of Anticancer Nanomedicine. *Proc. Natl. Acad. Sci. U. S. A.* **2014**, *111*, 15344–15349.

(63) Dickinson, E. Interfacial Interactions and the Stability of Oil-in-Water Emulsions. *Pure Appl. Chem.* **1992**, *64*, 1721–1724.

(64) Tadros, T. Principles of Emulsion Stabilization with Special Reference to Polymeric Surfactants. *J. Cosmet. Sci.* **2006**, *57*, 153–169.

(65) Lunn, M.; Fausnight, T. Hypersensitivity to Total Parenteral Nutrition Fat-Emulsion Component in an Egg-Allergic Child. *Pediatrics* **2011**, *128*, 1025–1028.

(66) You, B. C.; Jang, A. S.; Han, J. S.; Cheon, H. W.; Park, J. S.; Lee, J. H.; Park, S. W.; Kim, D. J.; Park, C. S. A Case of Propofol-Induced Oropharyngeal Angioedema and Bronchospasm. *Allergy, Asthma Immunol. Res.* **2012**, *4*, 46–48.

(67) Peng, C. A.; Hsu, Y. C. Fluoroalkylated Polyethylene Glycol as Potential Surfactant for Perfluorocarbon Emulsion. *Artif. Cells. Blood Substit. Immobil. Biotechnol.* **2001**, *29*, 483–492.

(68) Farace, C.; Sánchez-Moreno, P.; Orecchioni, M.; Manetti, R.; Sgarrella, F.; Asara, Y.; Peula-García, J. M.; Marchal, J. A.; Madeddu, R.; Delogu, L. G. Immune Cell Impact of Three Differently Coated Lipid Nanocapsules: Pluronic, Chitosan and Polyethylene Glycol. *Sci. Rep.* **2016**, *6*, 1–14.

(69) Garay, R. P.; El-Gewely, R.; Armstrong, J. K.; Garratty, G.; Richette, P. Antibodies against Polyethylene Glycol in Healthy Subjects and in Patients Treated with PEG-Conjugated Agents. *Expert Opin. Drug Deliv.* **2012**, *9*, 1319–1323.

(70) Viegas, T. X.; Bentley, M. D.; Harris, J. M.; Fang, Z.; Yoon, K.; Dizman, B.; Weimer, R.; Mero, A.; Pasut, G.; Veronese, F. M. Polyoxazoline: Chemistry, Properties, and Applications in Drug Delivery. *Bioconjug. Chem.* **2011**, *22*, 976–986.

(71) Pidhatika, B.; Rodenstein, M.; Chen, Y.; Rakhmatullina, E.; Mühlebach, A.; Acikgöz, C.; Textor, M.; Konradi, R. Comparative Stability Studies of Poly(2-Methyl-2-Oxazoline) and Poly(Ethylene Glycol) Brush Coatings. *Biointerphases* **2012**, *7*, 1–15.

(72) Koshkina, O.; Westmeier, D.; Lang, T.; Bantz, C.; Hahlbrock, A.; Würth, C.; Resch-Genger, U.; Braun, U.; Thiermann, R.; Weise, C.; et al. Tuning the Surface of Nanoparticles: Impact of Poly(2-Ethyl-2-Oxazoline) on Protein Adsorption in Serum and Cellular Uptake. *Macromol. Biosci.* **2016**, *16*, 1287–1300.

(73) Knop, K.; Hoogenboom, R.; Fischer, D.; Schubert, U. S. Poly(Ethylene Glycol) in Drug Delivery: Pros and Cons as Well as Potential Alternatives. *Angew. Chem. Int. Ed.* **2010**, *49*, 6288–6308.

(74) Lava, K.; Verbraeken, B.; Hoogenboom, R. Poly(2-Oxazoline)s and Click Chemistry: A Versatile Toolbox toward Multi-Functional Polymers. *Eur. Polym. J.* **2015**, *65*, 98–111.

(75) Gupta, A.; Eral, H. B.; Hatton, T. A.; Doyle, P. S. Nanoemulsions: Formation, Properties and Applications. *Soft Matter* **2016**, *12*, 2826–2841.

(76) Mosquera, J.; Henriksen-Lacey, M.; García, I.; Martínez-Calvo, M.; Rodríguez, J.; Mascareñas, J. L.; Liz-Marzán, L. M. Cellular Uptake of Gold Nanoparticles Triggered by Host-Guest Interactions. *J. Am. Chem. Soc.* **2018**, *140*, 4469–4472.

(77) Pillai, P. P.; Huda, S.; Kowalczyk, B.; Grzybowski, B. A. Controlled pH Stability and Adjustable Cellular Uptake of Mixed-Charge Nanoparticles. *J. Am. Chem. Soc.* **2013**, *135*, 6392–6395.

(78) Elci, S. G.; Jiang, Y.; Yan, B.; Kim, S. T.; Saha, K.; Moyano, D. F.; Yesilbag Tonga, G.; Jackson, L. C.; Rotello, V. M.; Vachet, R. W. Surface Charge Controls the Suborgan Biodistributions of Gold Nanoparticles. *ACS Nano* **2016**, *10*, 5536–5542.

(79) Bai, Y.; Xing, H.; Wu, P.; Feng, X.; Hwang, K.; Lee, J. M.; Phang, X. Y.; Lu, Y.; Zimmerman, S. C. Chemical Control over Cellular Uptake of Organic Nanoparticles by Fine Tuning Surface Functional Groups. *ACS Nano* **2015**, *9*, 10227–10236.

(80) Adamiak, L.; Touve, M. A.; Leguyader, C. L. M.; Gianneschi, N. C. Peptide Brush Polymers and Nanoparticles with Enzyme-Regulated Structure and Charge for Inducing or Evading Macrophage Cell Uptake. *ACS Nano* **2017**, *11*, 9877–9888.

(81) Kolb, H. C.; Finn, M. G.; Sharpless, K. B. Click Chemistry: Diverse Chemical Function from a Few Good Reactions. *Angew. Chem. Int. Ed.* **2001**, *40*, 2004–2021.

(82) Hoyle, C. E.; Bowman, C. N. Thiol-Ene Click Chemistry. *Angew. Chem. Int. Ed.* **2010**, *49*, 1540–1573.

(83) Luxenhofer, R.; Jordan, R. Click Chemistry with Poly(2-Oxazoline)s. *Macromolecules* **2006**, *39*, 3509–3516.

(84) Gress, A.; Völkel, A.; Schlaad, H. Thio-Click Modification of Poly[2-(3-Butenyl)-2-Oxazoline]. *Macromolecules* **2007**, *40*, 7928–7933.

(85) Kempe, K.; Hoogenboom, R.; Jaeger, M.; Schubert, U. S. Three-Fold Metal-Free Efficient ("Click") Reactions onto a Multifunctional Poly(2-Oxazoline) Designer Scaffold. *Macromolecules* **2011**, *44*, 6424–6432.

(86) He, T.; Jańczewski, D.; Jana, S.; Parthiban, A.; Guo, S.; Zhu, X.; Lee, S. S. C.; Parra-Velandia, F. J.; Teo, S. L. M.; Vancso, G. J. Efficient and Robust Coatings Using Poly(2-Methyl-2-Oxazoline) and Its Copolymers for Marine and Bacterial Fouling Prevention. *J. Polym. Sci. Part A Polym. Chem.* **2016**, *54*, 275–283.

(87) Pelaz, B.; Del Pino, P.; Maffre, P.; Hartmann, R.; Gallego, M.; Rivera-Fernández, S.; De La Fuente, J. M.; Nienhaus, G. U.; Parak, W. J. Surface Functionalization of Nanoparticles with Polyethylene Glycol: Effects on Protein Adsorption and Cellular Uptake. *ACS Nano* **2015**, *9*, 6996–7008.

(88) Jiang, Y.; Huo, S.; Mizuhara, T.; Das, R.; Lee, Y. W.; Hou, S.; Moyano, D. F.; Duncan,

B.; Liang, X. J.; Rotello, V. M. The Interplay of Size and Surface Functionality on the Cellular Uptake of Sub-10 Nm Gold Nanoparticles. *ACS Nano* **2015**, *9*, 9986–9993.

(89) Ho, L. W. C.; Yung, W. Y.; Sy, K. H. S.; Li, H. Y.; Choi, C. K. K.; Leung, K. C. F.; Lee, T. W. Y.; Choi, C. H. J. Effect of Alkylation on the Cellular Uptake of Polyethylene Glycol-Coated Gold Nanoparticles. *ACS Nano* **2017**, *11*, 6085–6101.

(90) Wang, J.; Mao, W.; Lock, L. L.; Tang, J.; Sui, M.; Sun, W.; Cui, H.; Xu, D.; Shen, Y. The Role of Micelle Size in Tumor Accumulation, Penetration, and Treatment. *ACS Nano* **2015**, *9*, 7195–7206.

(91) Xiao, K.; Li, Y.; Luo, J.; Lee, J. S.; Xiao, W.; Gonik, A. M.; Agarwal, R. G.; Lam, K. S. The Effect of Surface Charge on in Vivo Biodistribution of PEG-Oligocholic Acid Based Micellar Nanoparticles. *Biomaterials* **2011**, *32*, 3435–3446.

(92) Yu, S. S.; Lau, C. M.; Thomas, S. N.; Gray Jerome, W.; Maron, D. J.; Dickerson, J. H.; Hubbell, J. A.; Giorgio, T. D. Size- and Charge-Dependent Non-Specific Uptake of PEGylated Nanoparticles by Macrophages. *Int. J. Nanomedicine* **2012**, *7*, 799–813.

(93) Krasnici, S.; Werner, A.; Eichhorn, M. E.; Schmitt-Sody, M.; Pahernik, S. A.; Sauer, B.; Schulze, B.; Teifel, M.; Michaelis, U.; Naujoks, K.; *et al.* Effect of the Surface Charge of Liposomes on Their Uptake by Angiogenic Tumor Vessels. *Int. J. Cancer* **2003**, *105*, 561–567.

(94) Kelly, C.; Jefferies, C.; Cryan, S.-A. Targeted Liposomal Drug Delivery to Monocytes and Macrophages. *J. Drug Deliv.* **2011**, *2011*, 1–11.

(95) Sletten, E. M.; Swager, T. M. Fluorofluorophores: Fluorescent Fluorous Chemical Tools Spanning the Visible Spectrum. *J. Am. Chem. Soc.* **2014**, *136*, 13574–13577.

(96) Fröhlich, E. The Role of Surface Charge in Cellular Uptake and Cytotoxicity of Medical

Nanoparticles. *Int. J. Nanomedicine* **2012**, *7*, 5577–5591.

(97) Verma, A.; Stellacci, F. Effect of Surface Properties on Nanoparticle-Cell Interactions. *Small* **2010**, *6*, 12–21.

(98) Zhao, F.; Zhao, Y.; Liu, Y.; Chang, X.; Chen, C.; Zhao, Y. Cellular Uptake, Intracellular Trafficking, and Cytotoxicity of Nanomaterials. *Small* **2011**, *7*, 1322–1337.

(99) Alexis, F.; Pridgen, E.; Molnar, L. K.; Farokhzad, O. C. Factors Affecting the Clearance and Biodistribution of Polymeric Nanoparticles. *Mol. Pharm.* **2008**, *5*, 505–515.

(100) Walkey, C. D.; Olsen, J. B.; Guo, H.; Emili, A.; Chan, W. C. W. Nanoparticle Size and Surface Chemistry Determine Serum Protein Adsorption and Macrophage Uptake. *J. Am. Chem. Soc.* **2012**, *134*, 2139–2147.

(101) Gustafson, H. H.; Holt-Casper, D.; Grainger, D. W.; Ghandehari, H. Nanoparticle Uptake: The Phagocyte Problem. *Nano Today* **2015**, *10*, 487–510.

(102) Miller, C. R.; Bondurant, B.; McLean, S. D.; McGovern, K. A.; O'Brien, D. F. Liposome-Cell Interactions in Vitro: Effect of Liposome Surface Charge on the Binding and Endocytosis of Conventional and Sterically Stabilized Liposomes. *Biochemistry* **1998**, *37*, 12875–12883.

(103) Blanco, E.; Shen, H.; Ferrari, M. Principles of Nanoparticle Design for Overcoming Biological Barriers to Drug Delivery. *Nat. Biotechnol.* **2015**, *33*, 941–951.

(104) Wang, B.; Galliford, C. V.; Low, P. S. Guiding Principles in the Design of Ligand-Targeted Nanomedicines. *Nanomedicine* **2014**, *9*, 313–330.

(105) Bae, Y. H.; Park, K. Targeted Drug Delivery to Tumors: Myths, Reality and Possibility. *J. Control. Release* **2011**, *153*, 198–205.

(106) Janjic, J. M.; Srinivas, M.; Kadayakkara, D. K. K.; Ahrens, E. T. Self-Delivering

Nanoemulsions for Dual Fluorine-19 MRI and Fluorescence Detection. *J. Am. Chem. Soc.* **2008**, *130*, 2832–2841.

(107) Linge, H. M.; Andersson, C.; Nordin, S. L.; Olin, A. I.; Petersson, A. C.; Mörgelin, M.; Welin, A.; Bylund, J.; Bjermer, L.; Erjefält, J.; *et al.* Midkine Is Expressed and Differentially Processed during Chronic Obstructive Pulmonary Disease Exacerbations and Ventilator-Associated Pneumonia Associated with Staphylococcus Aureus Infection. *Mol. Med.* **2013**, *19*, 314–323.

(108) Kaneda, M. M.; Sasaki, Y.; Lanza, G. M.; Milbrandt, J.; Wickline, S. A. Mechanisms of Nucleotide Trafficking during siRNA Delivery to Endothelial Cells Using Perfluorocarbon Nanoemulsions. *Biomaterials* **2010**, *31*, 3079–3086.

(109) Vranic, S.; Boggetto, N.; Contremoulins, V.; Mornet, S.; Reinhardt, N.; Marano, F.; Baeza-Squiban, A.; Boland, S. Deciphering the Mechanisms of Cellular Uptake of Engineered Nanoparticles by Accurate Evaluation of Internalization Using Imaging Flow Cytometry. *Part. Fibre Toxicol.* **2013**, *10*, 1–16.

(110) Day, R. A.; Estabrook, D. A.; Logan, J. K.; Sletten, E. M. Fluorous Photosensitizers Enhance Photodynamic Therapy with Perfluorocarbon Nanoemulsions. *Chem. Commun.* **2017**, *53*, 13043–13046.

(111) Bouten, P. J. M.; Hertsen, D.; Vergaelen, M.; Monnery, B. D.; Catak, S.; Van Hest, J. C. M.; Van Speybroeck, V.; Hoogenboom, R. Synthesis of Poly(2-Oxazoline)s with Side Chain Methyl Ester Functionalities: Detailed Understanding of Living Copolymerization Behavior of Methyl Ester Containing Monomers with 2-Alkyl-2-Oxazolines. *J. Polym. Sci. Part A Polym. Chem.* **2015**, *53*, 2649–2661.

(112) Nguyen, T.; Francis, M. B. Practical Synthetic Route to Functionalized Rhodamine Dyes.

Org. Lett. **2003**, *5*, 3245–3248.

(113) Tishinov, K.; Schmidt, K.; Häussinger, D.; Gillingham, D. G. Structure-Selective Catalytic Alkylation of DNA and RNA. *Angew. Chem. Int. Ed.* **2012**, *51*, 12000–12004.

(114) Wiesbrock, F.; Hoogenboom, R.; Leenen, M.; Van Nispen, S. F. G. M.; Van Der Loop, M.; Abeln, C. H.; Van Den Berg, A. M. J.; Schubert, U. S. Microwave-Assisted Synthesis of a 42-Membered Library of Diblock Copoly(2-Oxazoline)s and Chain-Extended Homo Poly(2-Oxazoline)s and Their Thermal Characterization. *Macromolecules* **2005**, *38*, 7957–7966.

(115) Hoogenboom, R.; Fijten, M. W. M.; Thijs, H. M. L.; Van Lankvelt, B. M.; Schubert, U. S. Microwave-Assisted Synthesis and Properties of a Series of Poly(2-Alkyl-2-Oxazoline)s. *Des. Monomers Polym.* **2005**, *8*, 659–671.

(116) Luxenhofer, R. Novel Functional Poly (2-Oxazoline) s as Potential Carriers for Biomedical Applications. **2007**, 311.

(117) Monnery, B. D.; Jerca, V. V.; Sedlacek, O.; Verbraeken, B.; Cavill, R.; Hoogenboom, R. Defined High Molar Mass Poly(2-Oxazoline)S. *Angew. Chem. Int. Ed.* **2018**, *57*, 15400–15404.

CHAPTER FOUR

Redox-responsive gene delivery from perfluorocarbon nanoemulsions through cleavable poly(2-oxazoline) surfactants

Adapted from: Daniel A. Estabrook, Rachael A. Day and Ellen M. Sletten*, Redox-responsive gene delivery from perfluorocarbon nanoemulsions through cleavable poly(2-oxazoline) surfactants. *Angew. Chem. Int. Ed.,* **2020**, *Accepted.* DOI: https://doi.org/10.1002/ange.202102413.

4.1 Abstract

The clinical utility of emulsions as delivery vehicles is hindered by a dependence on passive release. Stimuli-responsive emulsions overcome this limitation but rely on external triggers or are composed of nanoparticle-stabilized droplets that preclude sizes necessary for biomedical applications. Here, we employ cleavable poly(2-oxazoline) diblock copolymer surfactants to form perfluorocarbon (PFC) nanoemulsions that release cargo upon exposure to glutathione. These surfactants allow for the first example of redox-responsive nanoemulsions *in cellulo.* A noncovalent fluorous tagging strategy is leveraged to solubilize a GFP plasmid inside the PFC nanoemulsions, whereupon protein expression is achieved selectively when employing a stimuli-responsive surfactant. This work contributes a methodology for non-viral gene delivery and represents a general approach to nanoemulsions that respond to endogenous stimuli.

4.2 Motivations and Applications

Emulsions are among the oldest drug carriers, having been explored since World War II for parenteral delivery.[1] This long-standing interest has yet to wane as 2018 saw over 250 global clinical trials using emulsion systems.[2] In a biomedical context, these liquid-in-liquid droplets benefit from high loading capacity, enhanced bioavailability, and protection of encapsulated cargo from physical and enzymatic degradation.[3,4] Nanoemulsions—droplets less than ~200 nm—are well-suited to biomedical applications due to their small size and long-term kinetic stability.[5] While the former results in extended half-lives *in vivo* and tumor accumulation,[6] the latter allows for stability and tolerance to environmental changes (*e.g.,* pH, temperature).[7] The *in vivo* fate of nanoemulsions is affected by both the interior lipophilic core and surface properties.[8] Despite their clinical utility, currently all five FDA-approved emulsion formulations involve passive release of small molecule payloads (Figure 1).[2,7] To establish these nanomaterials as site-specific delivery vehicles, payload retention must be controlled by a biological stimulus. Here, we report perfluorocarbon (PFC)-in-water nanoemulsions where passive release is minimized due to the bioorthogonal fluorous phase and stimuli-responsive release is achieved by use of reduction-sensitive amphiphiles.

To date, efforts to deliver payloads from emulsions *in vivo* have centered on the use of ultrasound as a non-invasive exogenous trigger. In these applications, PFC nanoemulsions are chosen due to the ability of PFCs to undergo ultrasound-mediated cavitation, releasing encapsulated cargo (Figure 4.1).[9,10] Unfortunately, this behavior is accompanied by off-target effects including tissue and blood vessel damage, as well as the transient perforation of cell membranes.[11] Alternatively, Lanza and Wickline have utilized lipid-coated PFC nanoemulsions

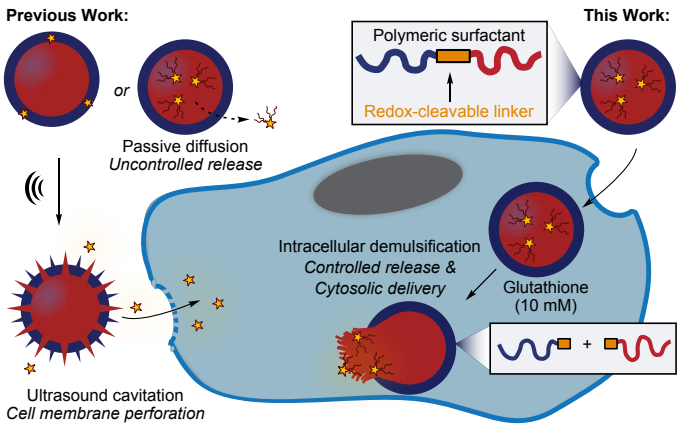

Figure 4.1. Traditional methods to control payload release from nanoemulsions are dominated by passive diffusion or ultrasound-induced cavitation (left). In this work, we employ a disulfide-containing block copolymer surfactant to stabilize oil-in-water nanoemulsions. Reduction of the cleavable surfactant triggers demulsification and release of encapsulated cargo (right).

for "contact-facilitated drug delivery."[12] However, this approach is limited to small molecule payloads loaded in the surfactant layer.

Our interest in PFC nanoemulsions stems from the bioorthogonal, nontoxic fluorous core and the ability to sequester fluorous-soluble payloads. This shields cargo from the surrounding environment and minimizes passive release in the presence of cell membrane mimics.[13,14] Certain PFCs have well-documented safety profiles, with FDA-approved applications employing the PFC as a contrast agent and/or oxygen carrier.[15] The main challenge with PFC nanoemulsions as delivery vehicles is solubilizing payloads in the fluorous phase. We have successfully encapsulated small molecule fluorophores and therapeutics within PFC nanoemulsions through covalent attachment of fluorous tags.[14,16–19] Recently, Medina and coworkers extended the payloads capable of being delivered with PFC nanoemulsions to include proteins by creating a "fluorous mask" around GFP with non-covalent fluorinated anionic tags.[20] GFP was then delivered in cells using ultrasound-induced cavitation. In this manuscript, we further extend the scope of payloads for these vehicles to include DNA using non-covalently associated cationic fluorous tags. Instead of

ultrasound-triggered delivery, we control release of the oligonucleotide through a designer surfactant that responds to intracellular concentrations of glutathione.

4.3 Synthesis of Disulfide-responsive Diblock Copolymers

To obtain a stimuli-responsive surfactant, we envisioned that a cleavable bond could link the hydrophilic and hydrophobic blocks of a diblock copolymer such that, upon stimulus, the surfactant would be irreversibly cleaved. The separated hydrophilic and hydrophobic homopolymers, having no surface activity, would no longer stabilize droplets, leading to demulsification. Previous work on responsive emulsions has involved a variety of stimuli, including pH[21–23], ions[24], gases[25,26], temperature[27,28], and redox agents[29,30]. Among these, redox agents are appealing for intracellular delivery vehicles due to the high concentration of reducing agents within the cell. Redox-responsive surfactants have been reported that contain functionalities such as ferrocenes[31,32], selenium atoms[29,33], and disulfide bonds[30,34,35]. However, these surfactants were not explored as emulsifiers for nanoemulsions.

We have previously developed poly(2-oxazoline) (POx) block copolymer surfactants capable of stabilizing oil-in-water nanoemulsions.[18,19] These amphiphiles form sub-200 nm droplets through emulsification involving either PFCs or olive oil as the emulsion core. We found that a poly(2-methyl-2-oxazoline)-*b*-poly(2-nonyl-2-oxazoline) ($P(MeOx)_{30}$-*b*-$P(NonOx)_{12}$, **4.6**, Figure 2A) diblock copolymer was optimal for emulsions of <200 nm size with stability over 60 days. Building from this, we designed a reduction-sensitive surfactant with a disulfide bond linking the $P(MeOx)_{30}$ and $P(NonOx)_{10}$ blocks (**4.5**, Figure 2A). Hydrophilic and hydrophobic homopolymers of $P(MeOx)_{30}$ and $P(NonOx)_{10}$ were synthesized through polymerization of their monomers (**4.1** and **4.3**) and terminated with potassium thioacetate.[36,37] To bias disulfide exchange, $P(MeOx)_{24}$-*t*-

SAc was reacted with Aldrithiol to yield P(MeOx)$_{27}$-*t*-SS-Pyr, **4.4**.[36,38] End-group fidelity was confirmed by ^{1}H-NMR and MALDI-TOF analysis (see Table 1 and ESI). Polymer-polymer coupling was performed via *in situ* deprotection and disulfide exchange between P(NonOx)$_{10}$-*t*-SAc, **4.2** (1.0 equiv.), and **4.4** (1.2 equiv.) to yield disulfide-linked P(MeOx)$_{27}$-SS-P(NonOx)$_{8}$, **5** (Figure 4.2A).

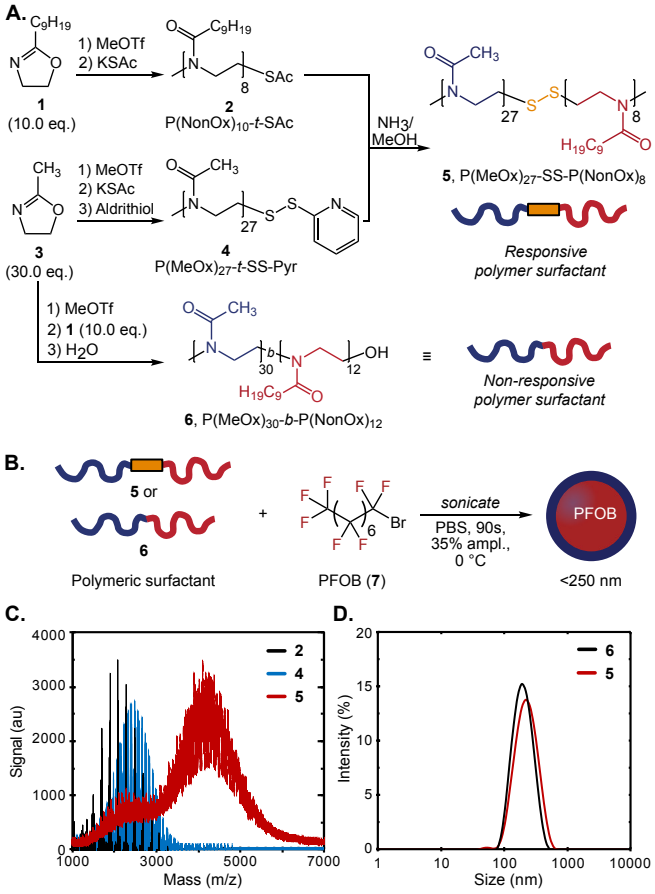

Figure 4.2. Synthesis and characterization of diblock copolymers and their use as surfactants for PFC-in-water nanoemulsions. (A) Synthesis of responsive copolymer **4.5** and control polymer **4.6**.[18] (B) Surfactants **4.5** or **4.6** stabilize perfluorooctylbromide (**4.7**, PFOB) nanoemulsions. (C) MALDI-TOF of **4.2**, **4.4** and **4.5**. (D) Dynamic light scattering of PFC nanoemulsions stabilized by **5** or **6**. Data are an average of three replicate measurements. See Figure 4.5, 4.6 for Intensity and Number % traces.

Table 4.1. Characterization of polymers **2**, **4**–**6**.

#	Polymer	M_w (kDa)	M_n (kDa)	$Đ$
4.2[a]	P(NonOx)$_{10}$-*t*-SAc	2.4	2.1	1.11
4.4[a]	P(MeOx)$_{27}$-*t*-SS-Pyr	2.4	2.3	1.06
4.5[a]	P(MeOx)$_{27}$-SS-P(NonOx)$_8$	4.2	3.8	1.09
4.6[b]	P(MeOx)$_{30}$-*b*-P(NonOx)$_{12}$	5.1	4.8	1.24

[a] Characterized by MALDI. [b] Characterized as previously reported.[18]

While homopolymer coupling was a concern, MALI-TOF demonstrated that these byproducts were minimal and mass patterns in responsive surfactant **4.5** resembled control surfactant **4.6** (Figure 2C, Figure 4.3–4.4).

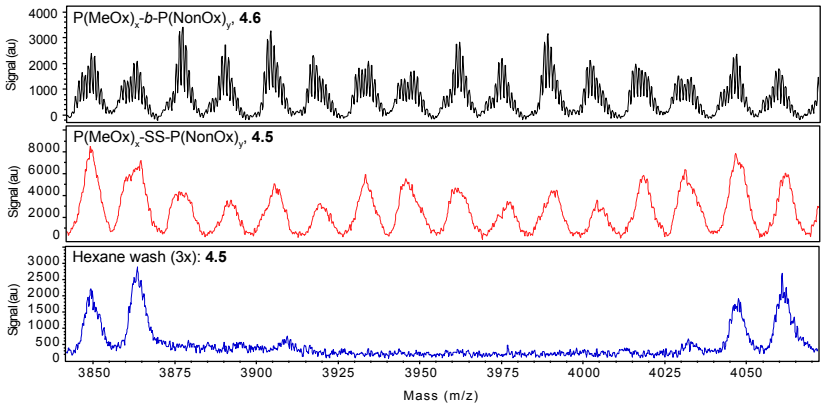

Figure 4.3. MALDI-TOF analysis of (top) control surfactant P(MeOx)$_x$-*b*-P(NonOx)$_y$ (**6**), (middle) responsive surfactant P(MeOx)$_x$-SS-P(NonOx)$_y$ (**5**), and (bottom) byproducts isolated via washing **5** with hexanes. Washing with hexanes was shown to remove primarily P(NonOx)-based byproducts, *e.g.* P(NonOx)$_x$-SS-P(NonOx)$_y$: Calculated for P(NonOx)$_9$-SS-P(NonOx)$_{10}$ $[M+Na]^+$: 3863.40; found: 3863.81.

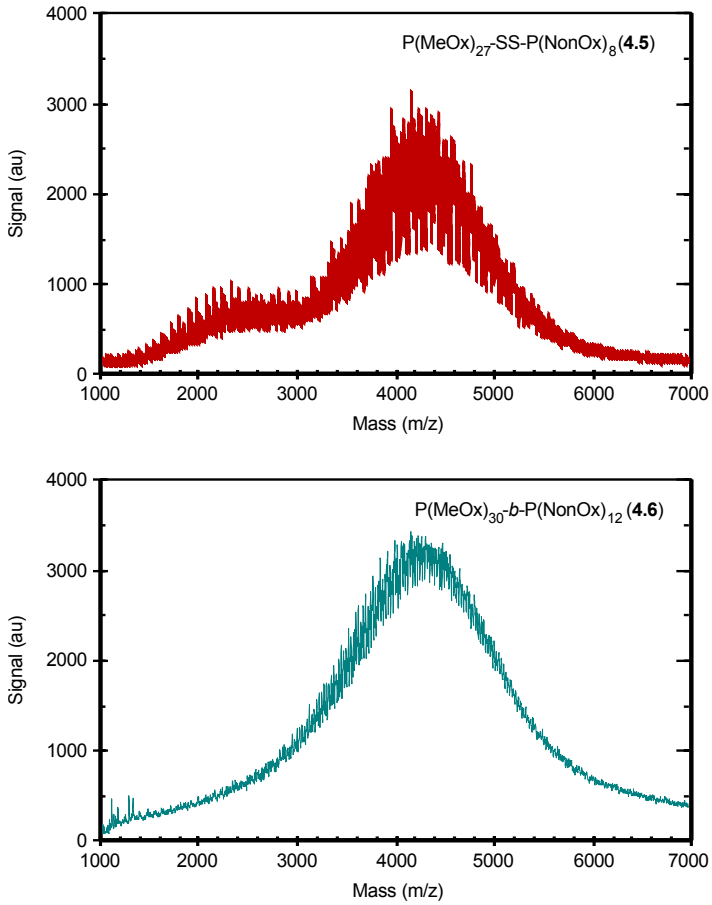

Figure 4.4. MALDI-TOF mass spectra obtained of (top) $P(MeOx)_{27}$-SS-$P(NonOx)_8$ (**5**) and (bottom) $P(MeOx)_{30}$-*b*-$P(NonOx)_{12}$ (**6**). Mass values corroborate Na+ ionization. Calculated for $P(MeOx)_{27}$-SS-$P(NonOx)_8$ $[M+Na]^+$: 4077.2; found: 4077.2. For $P(MeOx)_{27}$-SS-$P(NonOx)_8$, calculated polymer properties from 1000 to 7000 Da, M_n = 3802 Da, M_w = 4155 Da, $Đ$ = 1.09. Purity of $P(MeOx)_{27}$-SS-$P(NonOx)_8$ was determined to be 79% by comparing area under the curve (AUC) values from the 3-7 kDa mass range (polymer-polymer coupling products) to AUC values of total polymer (products + contaminants) in 1-7 kDa mass range.

4.4 Controllable Demulsification via "Smart" Surfactants

With a responsive surfactant in hand, we confirmed that **4.5** stabilized PFC-in-water nanoemulsions with a size distribution similar to our previously reported non-responsive **4.6**.[18] To form PFC nanoemulsions, polymers **4.5** or **4.6** were solubilized in dimethylformamide and diluted with phosphate buffered saline (PBS, pH 7.4) to a surfactant loading of 15 wt%. This solution was then ultrasonicated alongside 10 vol% PFC (Figure 4.2B). Dynamic light scattering analysis of the

resulting PFC nanoemulsions showed similar size distributions, with **4.5** and **4.6** stabilizing droplets of 200 nm and 180 nm, respectively (Figure 4.2D, Figure 4.5–4.6).[39]

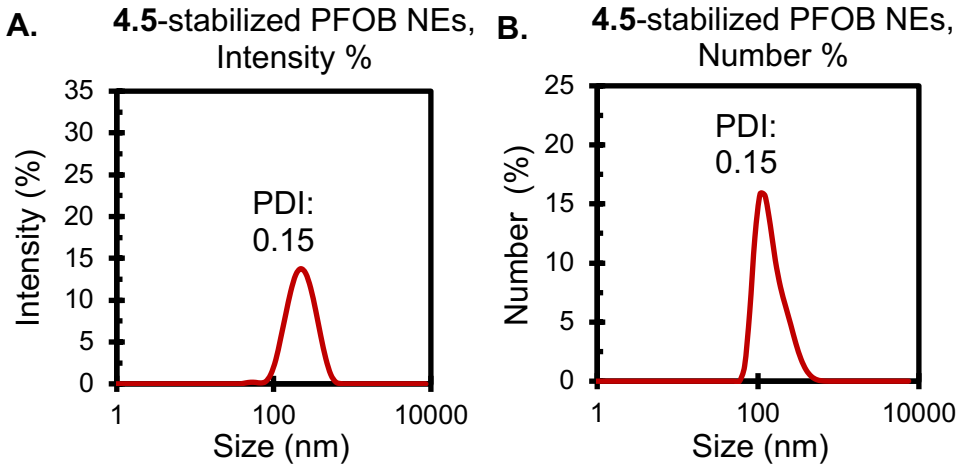

Figure 4.5. Dynamic light scattering data for PFOB nanoemulsions stabilized by responsive surfactant **4.5**. Data are an average of three replicate measurements.

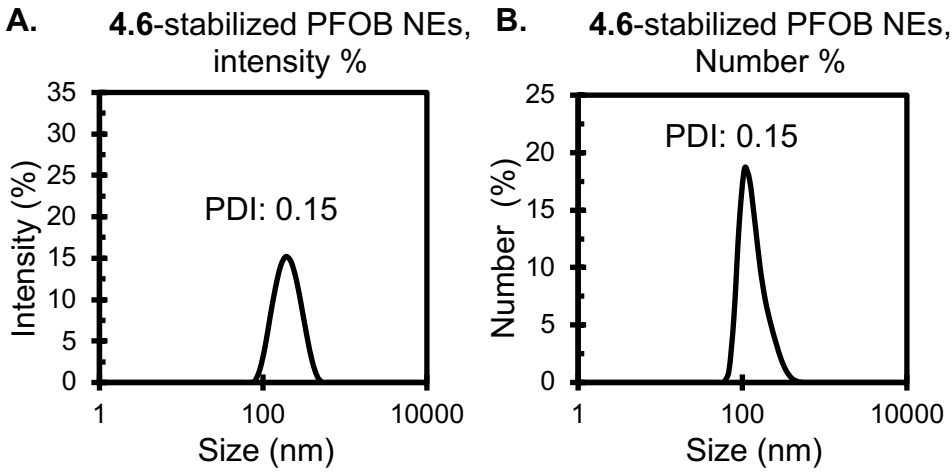

Figure 4.6. Dynamic light scattering data for PFOB nanoemulsions stabilized by non-responsive surfactant **4.6**. Data are an average of three replicate measurements.

When employed for olive oil nanoemulsions, **4.5** and **4.6** resulted in droplets of 170 nm and 140 nm, respectively (Figure 4.7–4.8).

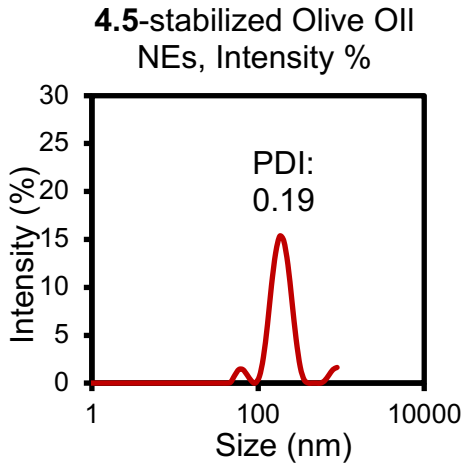

Figure 4.7. Dynamic light scattering data for olive oil nanoemulsions stabilized by responsive surfactant **4.5**. Data are an average of three replicate measurements. Note: Small population at ~70 nm corresponds to micelles. Minor aggregation at ~1000 nm. As intensity is proportional to diameter to the sixth power, the observed aggregation is minimal.

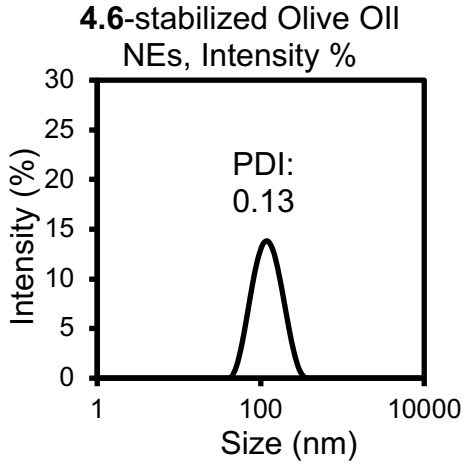

Figure 4.8. Dynamic light scattering data for olive oil nanoemulsions stabilized by non-responsive surfactant **4.6**. Data are an average of three replicate measurements.

Next, we characterized the responsive nature of the droplets. We envisioned that the disulfide would be located at the liquid-liquid interface due to positioning between the hydrophilic and hydrophobic blocks and could be accessed with reducing agent. Thus, disulfide reduction would lead to destruction of the surfactant, destabilization of the droplet, and release of encapsulated cargo (Figure 4.9A). Glutathione (GSH) was chosen as the stimulus as it is present at

concentrations 100 to 1000 times higher in the cytosol (~10 mM) than within extracellular fluids (~0.1 mM).[40]

First, we compared release behavior of **4.5**- or **4.6**-stabilized PFC droplets to GSH on the macroscale using fluorescein to track the aqueous phase and a fluorous-soluble rhodamine dye (**4.8**, Figure 4.9B)[34] to track the fluorous phase (Figure 4.9C, i). Surfactants **4.5** and **4.6** were added to each layer (2.8 wt%), and emulsified (Figure 4.9C, ii). GSH was then added at cytosolic concentrations (10 mM). After three hours, demulsification and phase separation were observed with surfactant **4.5**, while non-responsive **4.6** showed no change (Figure 4.9C, iii, Figure 4.10).

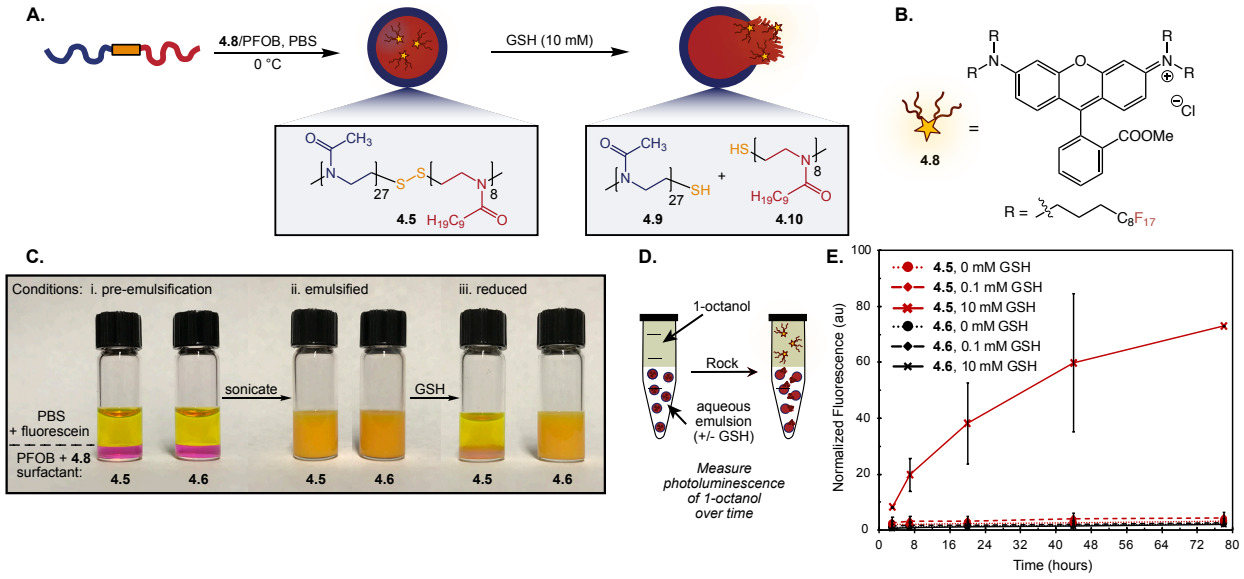

Figure 4.9. Responsive surfactants allow for demulsification and payload release in the presence of reducing agent. (A) Responsive PFC nanoemulsions from amphiphile **4.5**. When exposed to GSH (10 mM), the disulfide is reduced resulting in homopolymers **4.9** and **4.10**, facilitating payload release. (B) Model payload, rhodamine **4.8**. (C) (i) Solutions of fluorescein (3.0 mM), **4.5** or **4.6** (1.7 wt%) solubilized in PBS (pH 7.4) and combined with **4.8** solubilized in PFOB (0.13 mM). (ii) Solutions in (i) after sonication. (iii) Emulsions in (ii) treated with GSH (10 mM) and rocked (25 °C, 3 h). (D) Schematic of partition experiment to determine payload leaching, modeled by **4.8**. (D) Nanoemulsions stabilized by **4.5** or **4.6** were prepared contaning **4.8**, diluted 15-fold in PBS with varying concentrations of GSH, combined with 1-octanol, and agitated. The fluorescence of 1-octanol (Ex. 500) was measured over time. Fluorescence was normalized to **4.6**-stabilized nanoemulsions at 3 h without GSH. Error bars represent the standard deviation of two independent experiments. See Figure 4.14 for insert between 0-10 au.

Full Time Study of Figure 4.9C

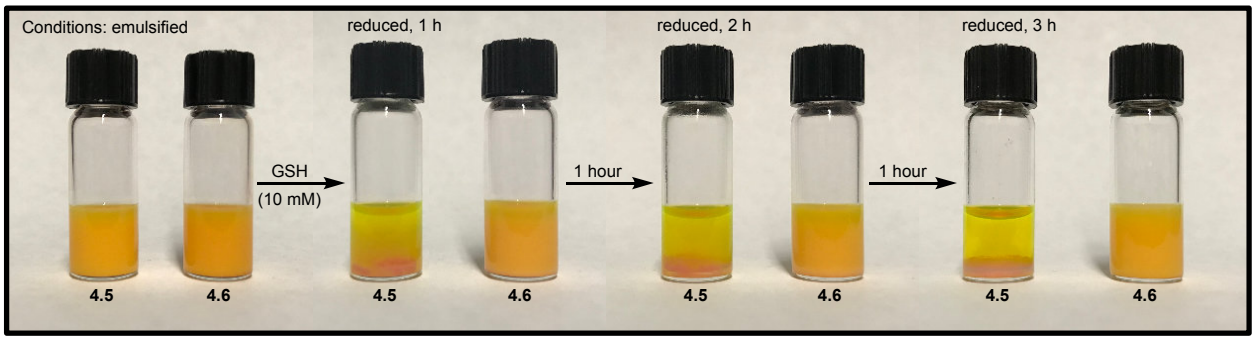

Figure 4.10. (i) Vials containing a solution of PBS (pH 7.4) and fluorescein (3.0 mM) were combined with perfluorooctylbromide containing **4.8** (0.13 mM). Polymers **4.5** or **4.6** were solubilized in the aqueous layer at 1.7 wt%. Solutions were then sonicated. Emulsions were treated with reduced GSH (10 mM, pH 7.4) and rocked at room temperature for up to three hours. After one hour, degradation of **4.5**-stabilized droplets was clear. After two hours, phase separation was observed. After three hours, solution looked similar to that at two hours, and experiment was stopped.

Turbidity of emulsion solutions in the presence of 0, 0.1, 1 and 10 mM GSH was characterized, confirming that vehicles were stable from 0–1 mM GSH (Figure 4.11).

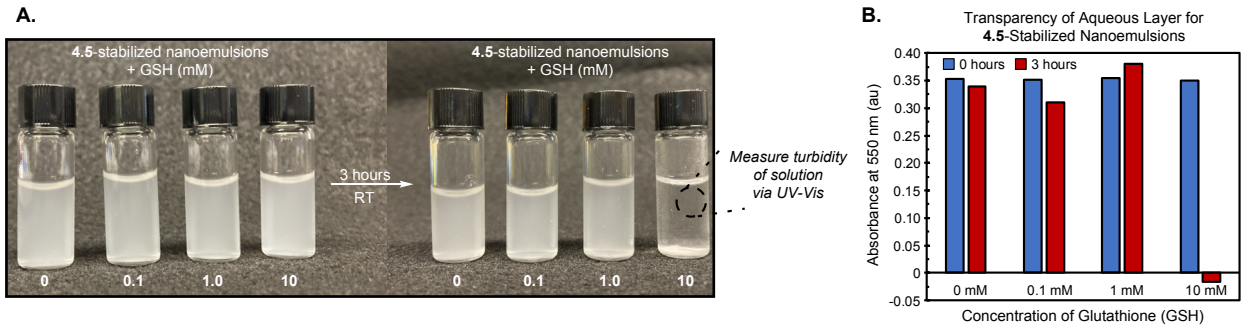

Figure 4.11. (A) Emulsion solutions stabilized by redox-responsive **4.5** were formed via the general nanoemulsion formation procedure. Emulsions were then treated with reduced GSH (0.1, 1.0 or 10 mM, pH 7.4) and rocked at 37 °C for up to three hours. After three hours, nearly quantitative phase separation was observed selectively for **4.5**-stabilized droplets within 10 mM GSH. (B) The turbidity of each emulsion solution at 0 and 3 hours was measured via UV-Vis analysis and quantified by absorbance at 550 nm. Loss of turbidity is indicative of emulsion destabilization.

We confirmed that demulsification was a result of amphiphile cleavage through MALDI-TOF analysis of responsive surfactant **4.5** after exposure to GSH (Figure 4.12, 4.13). Only trace amounts of $P(MeOx)_x$-SS-$P(NonOx)_y$ products were observed after treatment with 10 mM GSH, with the major products being thiol-capped homopolymers (**4.9**, **4.10,** Figure 4.9A), or residual disulfide-linked $P(NonOx)_x$-SS-$P(NonOx)_y$ (Fig 4.12, 4.13). We hypothesized that the hydrophobic environment hindered reduction by hydrophilic GSH.[41] Collectively, these data indicate that the disulfide is critical to demulsifying redox-responsive nanoemulsions in response to a biological trigger.

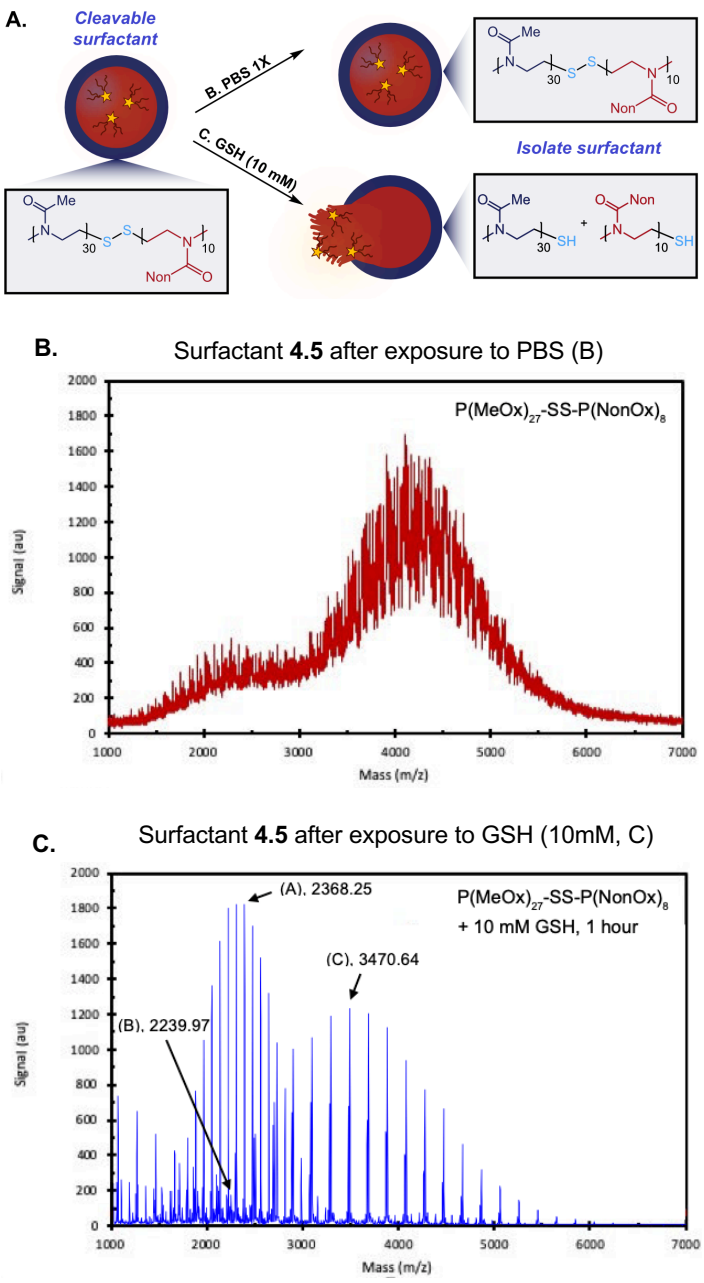

Figure 4.12. (A) Surfactant was isolated from PFOB-in-water nanoemulsions stabilized by **4.5**. Nanoemulsions were either treated with (B) PBS 1X or (C) reduced glutathione (GSH) for one hour prior to surfactant isolation, then analyzed by MALDI-TOF. Primary byproducts of reduction (bottom) are either low-molecular weight species on par with that of starting homopolymers (1-3 kDa), or scrambled disulfide-linked P(NonOx) polymers, as shown in Figure 4.13. For example, calculated for (B) $P(MeOx)_{27}$-*t*-SH $[M+Na]^+$: 2368.69; found: 2368.25. Calculated for (C) $P(NonOx)_{11}$-*t*-SH $[M+Na]^+$: 2239.97; found: 2239.79. Calculated for (C) $P(NonOx)_8$-SS-$P(NonOx)_9$ $[M+Na]^+$: 3469.04; found: 3470.64.

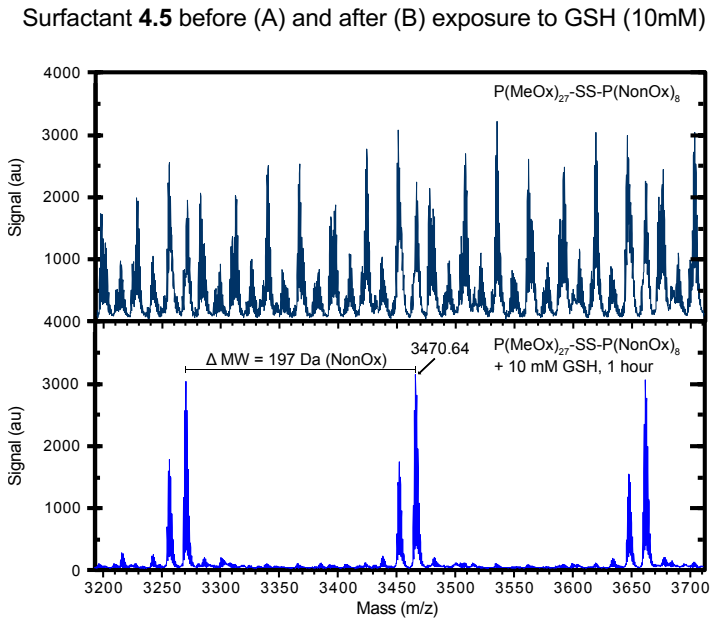

Figure 4.13. Zoomed-in MALDI-TOF analysis (see Figure 4.12 for full spectra) within 3200 to 3700 Da mass range of surfactant isolated from PFOB-in-water nanoemulsions stabilized by **4.5** with (bottom) and without (top) exposure to reduced glutathione (GSH) for one hour. Primary byproducts of reduction are scrambled disulfide-linked P(NonOx) polymers. Calculated for $P(NonOx)_8$-SS-$P(NonOx)_9$ $[M+Na]^+$: 3469.04; found: 3470.64. Observed side products (bottom) likely associated with H+ initiation from tosylic acid impurities[42]: H-$P(NonOx)_8$-SS-$P(NonOx)_9$-CH_3: 3455.02; found: 3456.63. H-$P(NonOx)_8$-SS-$P(NonOx)_9$-H: 3441.00; found: 3442.61.

4.5 Payload Release in the Presence of Biological Reducing Agents

Having confirmed that responsive amphiphiles can induce demulsification, we examined payload release kinetics. We again employed **4.8** as a payload and assayed release from nanoemulsions stabilized by **4.5** or **4.6** at no (0 mM), low (extracellular, 0.1 mM) or high (intracellular, 10 mM) levels of GSH. Emulsions were partitioned against 1-octanol, a lipid bilayer mimic (Figure 4.9D). Photoluminescence of the 1-octanol was monitored over 72 hours to determine payload leaching (Figure 4.9E). As expected, control surfactant **4.6** showed payload stability over varying concentrations of GSH (Figure 4.14 for inset between 0–10 au). Conversely, stimuli-responsive surfactant **5** demonstrated dose-response to GSH. No and low (0.1 mM)

concentrations of GSH resulted in little leaching while exposure to high (10 mM) GSH resulted in a sustained release profile.

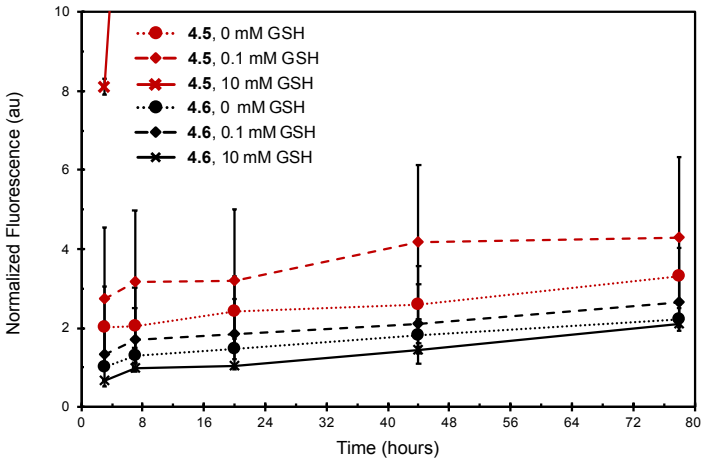

Figure 4.14. Inset of Figure 4.9E. Nanoemulsions containing **4.8** were prepared with responsive surfactant **4.5** (red) or control surfactant **4.6** (black), diluted 25-fold in PBS (pH 7.4) with varying concentrations of reduced glutathione (GSH), combined with 1-octanol, and continually agitated. The fluorescence of the 1-octanol (Ex 500) was measured over time. All fluorescence was normalized to the fluorescence of **6**-stabilized nanoemulsions at 3 hours without GSH. Error bars represent the standard deviation between two independent experiments.

Other experiments investigating release of **4.8** under multi-fold concentrations of GSH (0, 1, 0.1 and 10 mM) at physiological temperature (37 °C) demonstrated dose-dependent release of **4.8** in response to reducing concentrations (Figure 4.15).

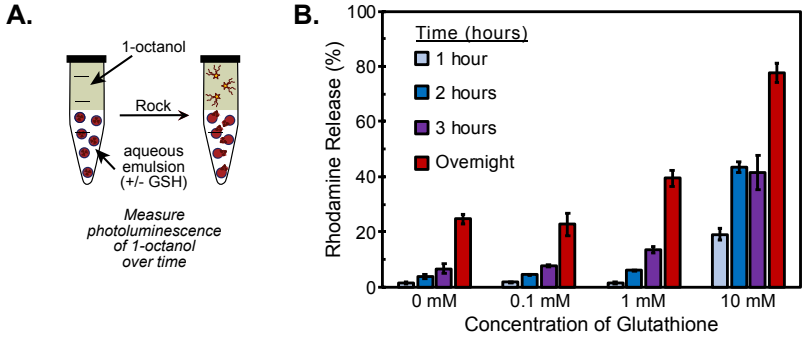

Figure 4.15. Release of rhodamine **4.8** from **4.5**-stabilized PFOB nanoemulsions in PBS containing 0, 0.1, 1.0 or 10 mM GSH at 37 °C. Nanoemulsions stabilized by **4.5** or **4.6** were prepared containing **4.8**, diluted 15-fold in PBS with varying concentrations of GSH, combined with 1-octanol, and agitated at 37 °C, 50 rpm. The fluorescence of 1-octanol (Ex. 500) was measured over time. Fluorescence was normalized to an equal volume **4.5**-stabilized emulsion aliquot directly added and sonicated within 1-octanol. Error bars represent the standard deviation of two independent experiments.

Stability of **4.5**-stabilized droplets encapsulating a panel of fluorous-soluble fluorophores[13,14,43] was corroborated within media at physiological conditions (Figure 4.16–4.18).

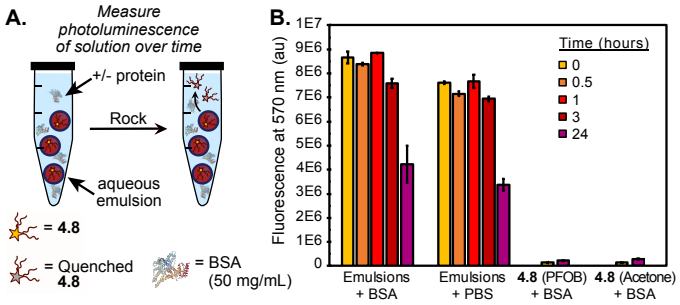

Figure 4.16. Payload release of **4.8** from **4.6**-stabilized PFOB droplets was examined in PBS with and without bovine serum albumin (BSA, 50 mg/mL). This solution was rocked at 37 °C at 50 rpm and fluorescence of the solution (Ex. 500 nm) was measured over a period of 0.5, 1, 3 and 24 hours. For comparison, free, non-encapsulated equimolar **4.8** in either PFOB or acetone was added to the same volume of PBS or BSA and measured at 0 and 24 hours. Error bars represent the standard deviation between at least two independent experiments.

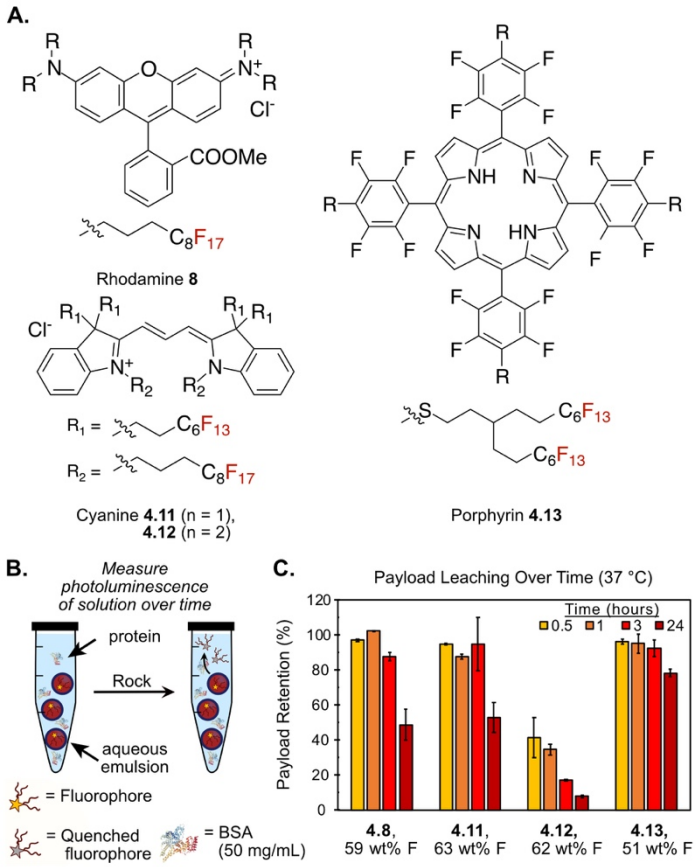

Figure 4.17. Payload release of a panel of dyes including rhodamine **4.8,** cyanine **4.11**, cyanine **4.12**, and porphyrin **4.13** from **4.6**-stabilized PFOB droplets was examined in PBS with bovine serum albumin (BSA, 50 mg/mL). This solution was rocked at 37 °C at 50 rpm and fluorescence of the solution (Ex. 500 nm) was measured over a period of 0, 0.5, 1, 3 and 24 hours. Release was calculated by comparison of fluorescence of the solution at 0 hours. Error bars represent the standard deviation between at least two independent experiments.

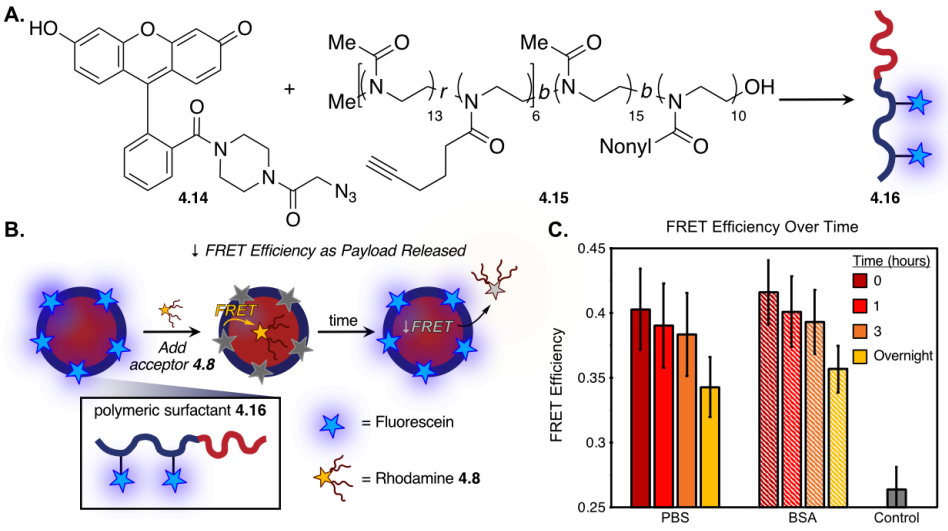

Figure 4.18 Tracking emulsion stability in PBS with and without BSA via FRET between fluorescein-labeled surfactant (FRET donor) and interior rhodamine **4.8** payload (FRET acceptor). (A) Synthesis of fluorescein-labeled surfactant **4.16** via CuAAC between azidofluorescein **4.14** and alkyne-containing POx surfactant **4.15**, adapted from previous chemistries.[18,44] (B) FRET efficiency between surfactant and **4.8** will be reduced when payload is released and no longer in close proximity to the surfactant. FRET efficiency is defined as $F_a/(F_a + F_d)$, where F_a is the acceptor emission and F_d is the donor emission. Control emulsions, referring to emulsions with only the acceptor (rhodamine **4.8**) defined the baseline. (C) FRET efficiency was measured over time in PBS with and without BSA (75 mg/mL), rocking emulsion solutions at 37 °C over 24 hours.

Additionally, release was analyzed under 5000-fold dilution by dialyzing **4.5**- and **4.6**-stabilized PFC nanoemulsions containing **4.8** in either PBS or GSH (10 mM) overnight (Figure 4.19). While control **4.6** showed payload stability with and without GSH, cleavable surfactant **5** achieved quantitative release only in GSH. We suspected that degradation of the cleavable surfactant **4.5** would likely influence release of the encapsulated payload, as (i) it is known that steric shielding and density of the surfactant influences emulsion release kinetics[45–48], (ii) we have studied the influence of polymeric surfactant identity on payload release using the same emulsion vehicles and rhodamine **4.8** payload used here,[19] and (iii) it is known that the "large specific surface area of nanoemulsions makes it prone to chemical degradation" [49], resulting in "chemical

degradation reactions at the oil-water interface [occurring] more quickly in nanoemulsions than in conventional emulsions... When O/W nanoemulsions are used as nanocarriers in delivery systems, the interfacial membrane formed by the emulsifier is an important factor in controlling the ability of the emulsion to protect the encapsulated functional compounds and to inhibit their diffusion from the oil droplets into the aqueous phase."[48] To corroborate this, we carried out several

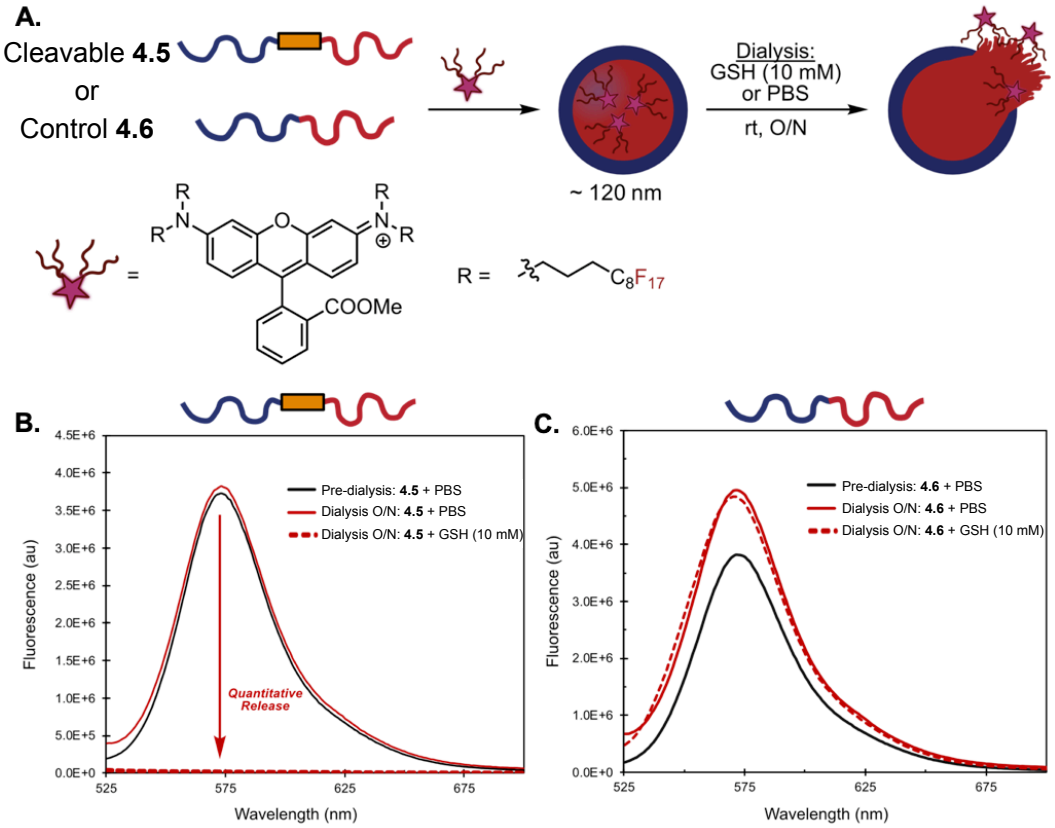

Figure 4.19. Release was analyzed under 5000-fold dilution conditions by dialyzing **4.5**- and **4.6**-stabilized PFOB emulsions containing **4.8** in either PBS or GSH (10 mM) overnight. (A) Nanoemulsions containing **4.8** were prepared with (B) responsive surfactant **4.5** or (C) control surfactant **4.6**. Emulsion solutions were dialyzed (1 kDa MWCO) against a 5000-fold dilution of PBS (pH 7.4) with or without reduced glutathione (GSH, 10 mM). The solution was then stirred overnight at room temperature. Fluorescence of dialyzed solutions were taken and directly compared to the fluorescence of solutions prior to dialysis (Ex: 500 nm, Em: 525–700 nm). While control surfactant **4.6** again showed payload stability with and without GSH, cleavable surfactant **4.5** achieved nearly quantitative release only in the presence of GSH.

experiments to probe the mechanism of emulsion destabilization and payload release, which suggest that at dilute conditions relevant to cellular delivery, destruction of the block copolymer reduces the kinetic barrier to releasing the encapsulated payload, thus delivering it to the surrounding environment.

Moreover, the kinetics of payload release of rhodamine **4.8** were examined from **4.5**-stabilized droplets at varying dilutions corresponding to fluorous solvent within GSH-supplanted buffer: 1, 10 and 20 vol%. Across these dilutions, negligible differences were observed (Figure 4.20) between time points from 20 to 90 minutes. After 90 minutes, subsequent dynamic light

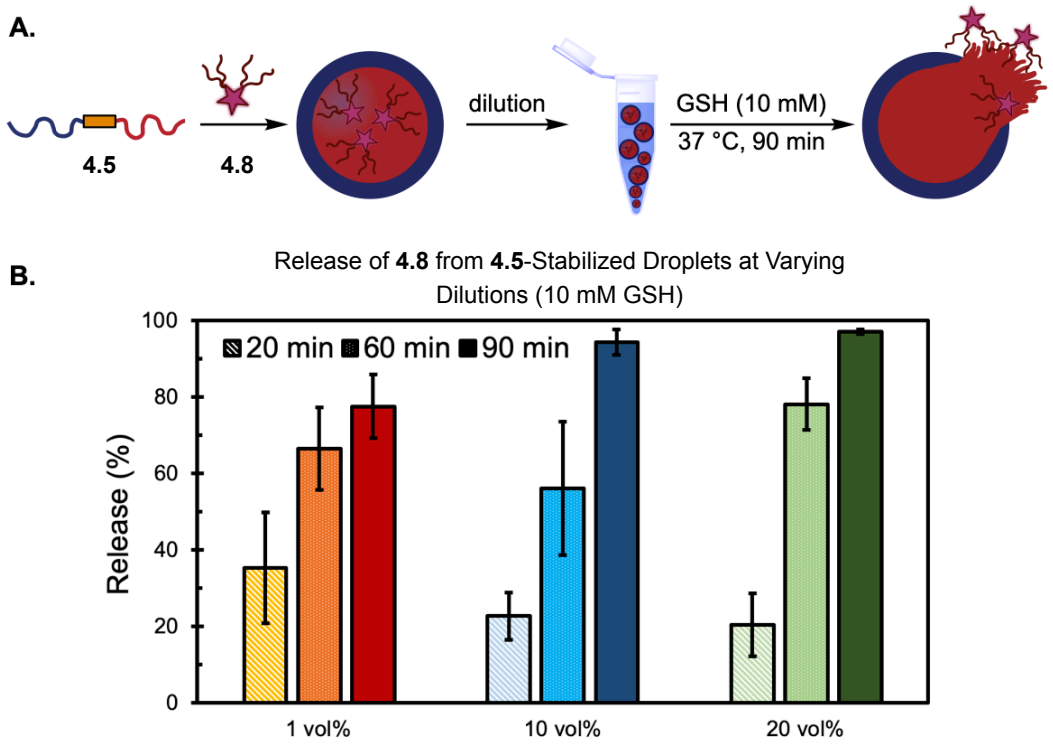

Figure 4.20. Payload release of **4.8** from **4.5**-stabilized PFOB droplets was examined at varying dilutions. No correlation was observed, suggesting coalescence was not the mechanism of degradation. (A) Nanoemulsions containing **4.8** were prepared with responsive surfactant **4.5**. Emulsion solutions were diluted with PBS (pH 7.4) containing reduced glutathione (GSH, 10 mM). The solution was then agitated at 37 °C for 90 minutes. (B) Fluorescence of solutions were taken at 20, 60, and 90 minutes (Ex: 500 nm, Em: 525–700 nm). Release percentages were calculated by comparing fluorescence values at each time point to the initial fluorescence (0 minutes) for that dilution. Error bars represent the standard deviation between at least two independent experiments.

scattering analysis of the droplets (Figure 4.21) demonstrated both a poor correlation function and shift in size distributions to smaller particulate, evidence against a coalescence degradation mechanism that would presumably result in larger droplets over the course of release.

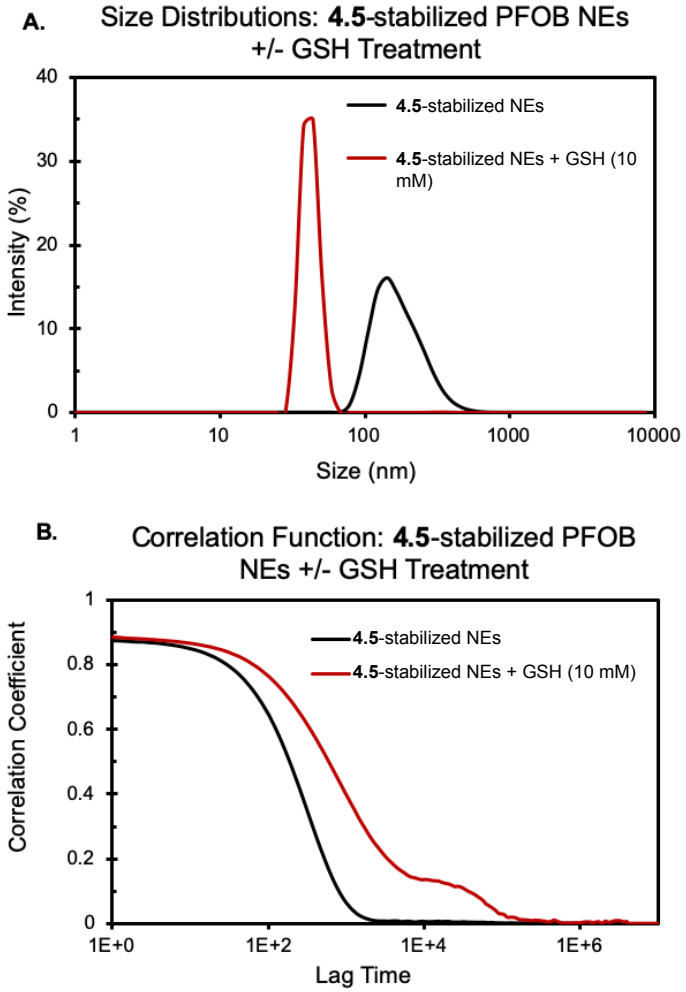

Figure 4.21. (A) Dynamic light scattering data and (B) correlation functions for PFOB nanoemulsions stabilized by responsive surfactant **4.5** and exposed to glutathione (10 mM) over 90 minutes, as described in Figure S17. Briefly, emulsion solutions were diluted with PBS (pH 7.4) containing reduced glutathione (GSH, 10 mM) at 20 vol% droplet solution. The solution was then agitated at 37 °C for 90 minutes and diluted prior to dynamic light scattering analysis according to the general nanoemulsion analysis procedure.

To explore the release mechanisms of the water-insoluble payload, we then explored the partition of free rhodamine dye **4.8** when dissolved in perfluorooctylbromide (PFOB, the solvent

composing the interior of the droplet) into water at varying dilutions of fluorous solvent (Figure 4.22). We found that, at all dilutions, less than 25% of the dye was present within PFOB, suggesting that at highly dilute conditions analogous to those within emulsion release experiments, **4.8** either partitions from fluorous liquid into PBS or aggregates when it hits an aqueous environment.

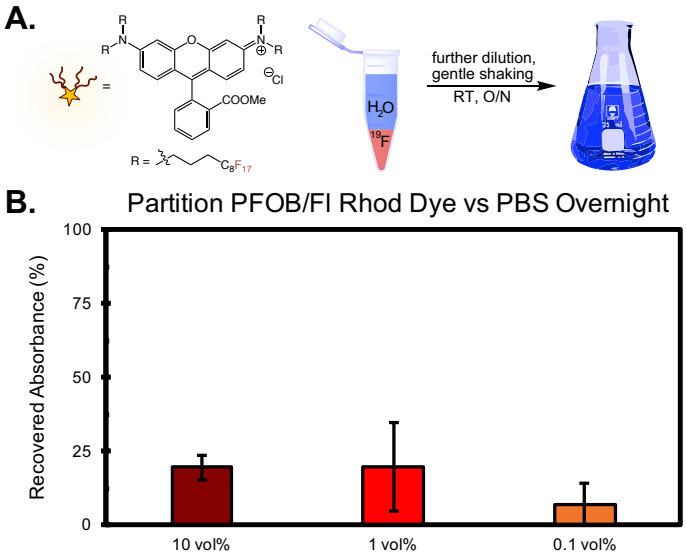

Figure 4.22. (A) Free rhodamine **4.8** (106 μM) was dissolved in PFOB and partitioned against PBS 1X at varying dilutions (0.1, 1.0, and 10 vol% of PFOB) overnight to quantify **4.8**'s partition out of the fluorous phase. (B) Volume percent is with respect to PFOB. Mixture was gently rocked at room temperature overnight. PFOB layer was recovered by light centrifugation to ensure phase separation and absorption was measured via UV-Vis analysis. Recovery was calculated via the Beer-Lambert law. Error bars represent the standard deviation between two independent experiments. At all dilutions <25% of the dye was recovered, indicating that highly dilute conditions analogous to those within emulsion release experiments cause **4.8** to partition from fluorous liquid into PBS.

To corroborate these results, we then encapsulated a nile red dye within olive oil nanoemulsions as a hydrophobic probe (Figure 4.23). In hydrophobic environments (*e.g.* olive oil) its fluorescence intensity is strong. Upon release to a polar environment (*e.g.* water) its fluorescence is rapidly quenched. When reducing agent (*i.e.,* tris(2-carboxyethyl)phosphine) was

added to the emulsion solution, fluorescence was quenched within 15 minutes. Conversely, PBS itself resulted in no change. These results suggest that soon after reduction of the redox-responsive surfactant, the interior payload quickly encounters an aqueous environment, suggesting release. Moreover, varying dilutions corresponding to 5, 1, and 0.1 vol% of olive oil did not influence this behavior—again, if coalescence was occurring, we would expect a concentration-dependent release profile.

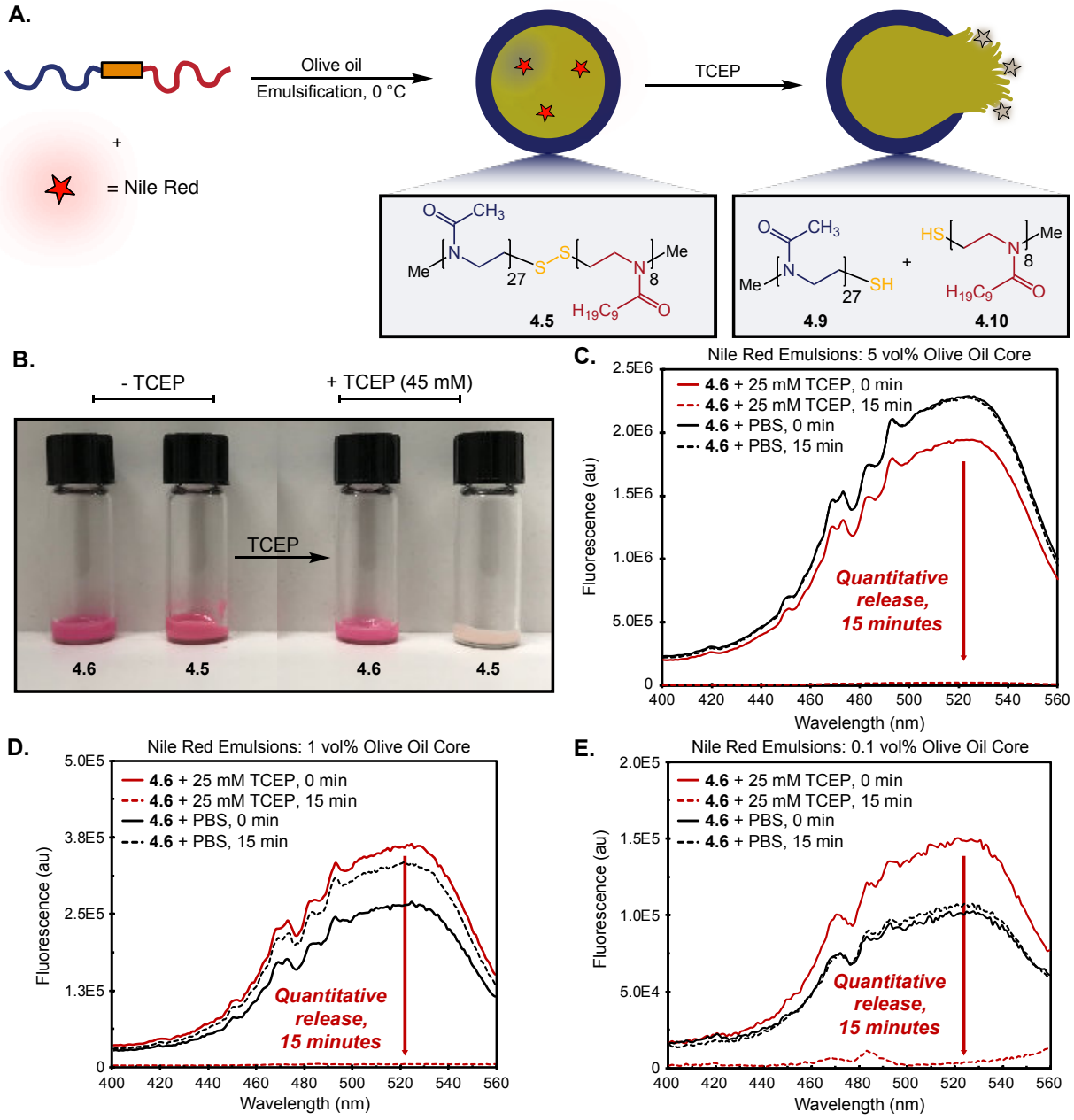

Figure 4.23. (A) Schematic of responsive olive oil-in-water nanoemulsions prepared from responsive amphiphile **4.5**. When exposed to tris(2-carboxyethyl)phosphine (TCEP), the disulfide-linked amphiphile is cleaved into thiol-capped homopolymers **4.9** and **4.10**, facilitating payload release. The encapsulated model payload—Nile Red—is used as a hydrophobic probe. In hydrophobic environments (*e.g.* olive oil) its fluorescence intensity is strong. Upon release to a polar environment (*e.g.* water) its fluorescence is rapidly quenched.[50] (B) Olive oil-in-water nanoemulsions containing Nile Red (327 μM) and stabilized by either **4.5** or **4.6** were imaged before and after treatment with TCEP hydrochloride (45 mM) at room temperature for 10 minutes. (C/D/E) Aliquots of nanoemulsion solutions described in (B) were diluted (C) 2-, (D) 10-, or (E) 100-fold in PBS (pH 7.4) After 15 minutes of treatment with TCEP (25 mM) at room temperature, excitation spectra were acquired (Em. 582 nm). Scan settings are described in general photophysics

procedure. The fluorescence of nile red is known to be strongly quenched in polar environments. Fluorescence was quenched nearly quantitatively within 15 minutes of treating 6-stabilized droplets with TCEP, indicating that the hydrophobic payload hits the aqueous phase soon after the amphiphile is cleaved. Again, this behavior does not change even under highly dilute conditions. We attribute the comparatively fast release kinetics to the ability of TCEP to approach the oil-water interface more rapidly than GSH. Collectively, these data corroborate that release of both fluorous and hydrophobic payloads can be achieved upon reduction of cleavable amphiphile **4.6**. These results illustrate the emulsion platform's capability for modified, controllable release in an intracellular environment.

Collectively, these results indicate that surfactant degradation and the loss of both surface activity and steric shielding reduces the kinetic barrier to release the encapsulated payload and thus influences the diffusion of the encapsulated fluorous dye. Additionally, gravitational separation of the interior core is likely due to the density mismatches between the aqueous and fluorous (or organic) interior core, as exhibited within Figure 4.9C. Ultimately our findings collectively point to these mechanisms of degradation, as compared to coalescence, but perhaps more importantly suggest that at dilute conditions relevant to cellular delivery, the encapsulated payload is delivered to the surrounding environment.

4.6 Redox-Responsive Gene Delivery via Encapsulation and Release of Fluorous-Tagged Plasmid DNA

After demonstrating responsive PFC nanoemulsions *in vitro*, we extended use to *in cellulo* DNA delivery. Efforts within gene delivery using polymeric materials, *e.g.,* polyethyleneimine (PEI) are often limited by inefficient gene release.[51] Nucleic acid delivery with oil nanoemulsions has been explored since the mid-90s, with the major loading strategy being electrostatic adsorption of cationic surfactants with the phosphodiester backbone.[52] More recently, plasmid encapsulation in a hydrocarbon oil core was reported and compared to surface adsorption loading methods.[53] While adsorption suffered from burst release behavior, encapsulation suffered the inverse—

plasmid was not released even after 48 h of media incubation. Herein, we demonstrate the ability to selectively release pDNA from a bioorthogonal fluorinated liquid core and drive protein expression *in cellulo*, representing an avenue for nonviral gene delivery. This first required a strategy to solubilize hydrophilic DNA into the non-polarizable fluorous phase. Fundamental studies by Bühlmann and coworkers have quantified ion pairs to be ~10^5 times stronger in fluorous solvents than organic solvents,[54] suggesting electrostatic interactions between the anionic backbone of DNA and a cationic fluorous tag would be a fruitful approach to loading PFC nanoemulsions with DNA.

We employed ammonium **4.17** with two C_6F_{13} chains[43] as a fluorous tag to solubilize plasmid (pDNA) in the fluorous phase (Figure 4.24A). Importantly, this tag is designed to maximize fluorous solubility while retaining biocompatible perfluorocarbon tags.[55] For the pDNA, we chose an eGFP plasmid such that a fluorescence readout could measure payload delivery. Notably, cytosolic delivery and nuclear entry of the pDNA are essential for gene expression (Figure 4.24B). We combined **4.17** (7.7 mg) with eGFP pDNA (5, 15 or 30 μg) and freeze-dried overnight. The pDNA/**4.17** polyplex was then dissolved in a PFC mixture and sonicated (Figure 4.24A). Model poly(2-oxazoline) amphiphile poly(2-ethyl-2-oxazoline)$_{90}$-*b*-poly(2-nonyl-2-oxazoline)$_{10}$ [19] was solubilized in dimethylformamide and diluted with PBS (pH 7.4) to a loading of 2.8 wt%. This solution was combined with 10 vol% of the PFC/pDNA/**4.17** mixture and ultrasonicated. To verify encapsulation, supernatant was separated and solution corresponding to eGFP loaded within PFC nanoemulsions was analyzed on an agarose gel (Figure 4.24C). DNA bands were assigned following literature precedent.[56] These data showed that eGFP pDNA could be loaded into PFC droplets in a dose-dependent manner from 5–30 μg. By comparison, electrophoresis of the supernatant solution showed reduced pDNA (Figure 4.25).

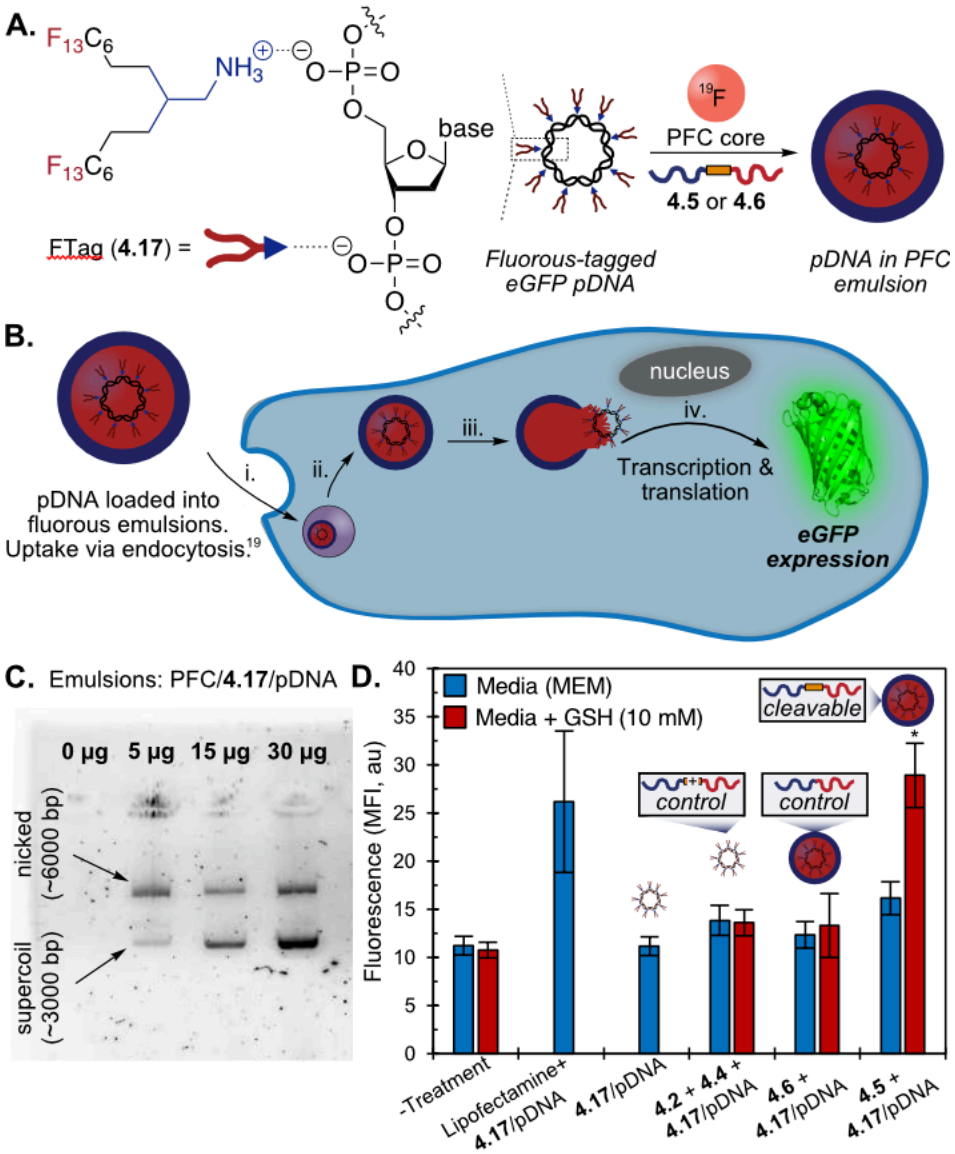

Figure 4.24. Delivery of eGFP pDNA with GSH-responsive nanoemulsions. (A) Fluorous amine tag (**4.17**) complexes with pDNA, solubilizing it within a PFC core that is sonicated in the presence of **4.5** or **4.6** to form **4.16**/eGFP PFC nanoemulsions. (B) Schematic of delivery and eGFP expression. (C) Gel electrophoresis of destroyed PFC emulsions loaded with different amounts of pDNA complexed with **4.17**. (D) Flow cytometry of HEK-293 cells incubated with PFC/**4.17**/pDNA nanoemulsions for 3 hours in MEM media (+ 10% FBS). Cells were washed and incubated with MEM media with or without GSH (10 mM) overnight. Cells were trypsonized, washed, resuspended in FACS buffer and analyzed for eGFP fluorescence by flow cytometry. Data is representative of three independent experiments. See Figure 4.S1–4.S3 for histograms of independent experiments. Statistical significance is defined by ANOVA test followed by Tukey HSD test for significance. α is defined as 0.05. See Figure 4.28 for analysis.

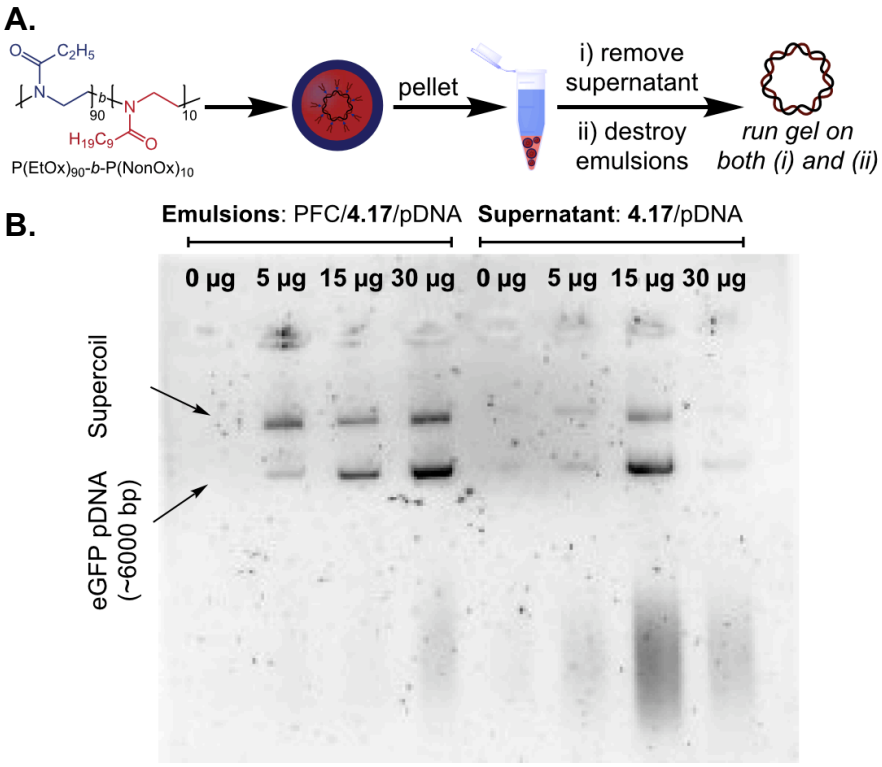

Figure 4.25. Agarose gel electrophoresis (1.2%) of **4.17**/eGFP pDNA solubilized within P(EtOx)$_{90}$-*b*-P(NonOx)$_{10}$-stabilized PFD:PFTPA nanoemulsions at varying concentrations of pDNA (5 µg, 15 µg, 30 µg). (A) As schematized, emulsions were pelleted, (i) supernatant was isolated and (ii) remaining emulsions were destroyed. (B) Solutions isolated from both phases were run on agarose gel at 120V for 45 min and stained with ethidium bromide. Data is representative of three independent experiments. For detailed information, see supplemental figure experimental protocols. P(EtOx$_{90}$-*b*-NonOx$_{10}$) was synthesized as previously reported.[19]

These data were verified by fluorescence experiments using Thiazole Orange, a DNA-binding dye suggesting that 40 ± 4% of the pDNA was encapsulated in the 30 µg sample (Figure 4.26).

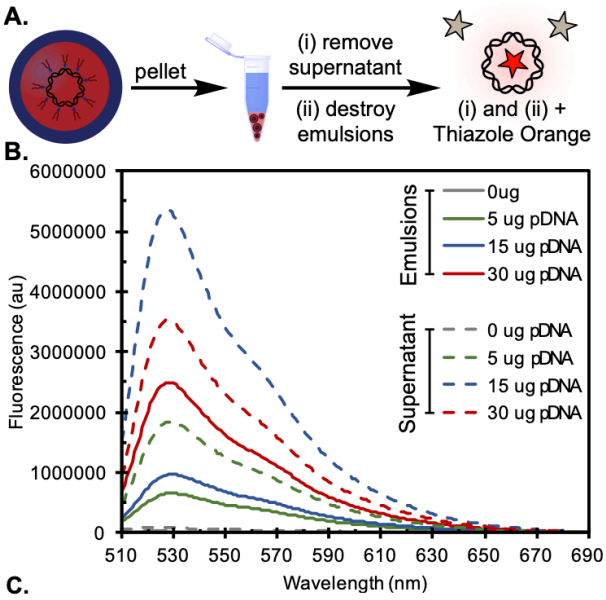

C.

	Emulsions (AUC, au)	Supernatant (AUC, au)	Encapsulation (%)
Expt 1	138952147	197374020	41.3
Expt 2	6143	8175	42.9
Expt 3	5024	9239	35.2

Figure 4.26. Fluorescence measurements of thiazole orange dye incubated with solutions isolated from **4.17** (4.5 mM)/eGFP pDNA solubilized within P(EtOx)$_{90}$-*b*-P(NonOx)$_{10}$-stabilized PFD:PFTPA nanoemulsions at varying concentrations of pDNA (5 µg, 15 µg, 30 µg). As schematized, emulsions were pelleted, (i) supernatant was isolated and (ii) remaining emulsions were destroyed. Solutions isolated from both phases were incubated with thiazole orange (1.9 mM). Fluorescence was then measured (Ex: 500 nm, Em: 510-700 nm). Data are representative of three independent experiments. For detailed information, see supplemental figure experimental protocols. (C) DNA encapsulation efficiencies, as referenced in the main text, were calculated by comparing area under the curve (AUC) values of PFC/**4.17** emulsions + 30 µg pDNA to the AUC sum of both emulsions and supernatant for that experiment. The average and standard deviation were calculated from three independent experiments to be 39.8 ± 4.1%. P(EtOx$_{90}$-*b*-NonOx$_{10}$) was synthesized as previously reported.[19]

With the **4.17**/pDNA complex loaded into PFC nanoemulsions, we investigated the ability of responsive surfactant **4.5** to promote eGFP expression (Figure 4.24B). Emulsion formation was accomplished with responsive surfactant **4.5** or control surfactant **4.6**. We also combined homopolymers **4.2** and **4.4** with perfluorocarbon containing **4.17**/pDNA complex, yielding heterogenous aggregates (Figure 4.27), to control for the role of the homopolymers.

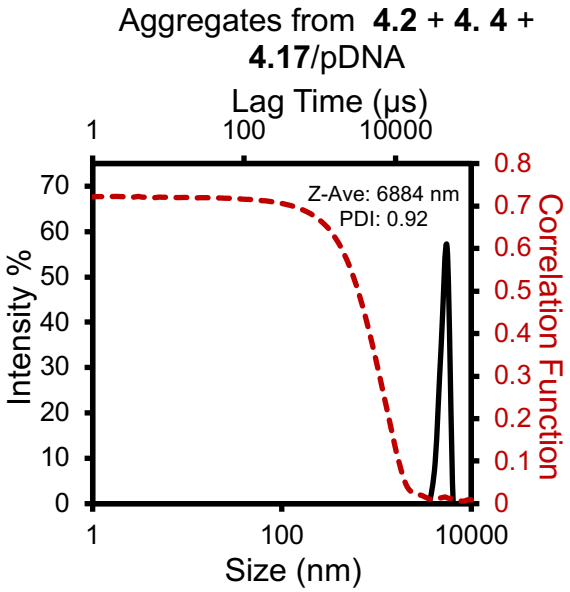

Figure 4.27. Dynamic light scattering data for **4.2** + **4.4** + **4.17**/pDNA aggregates. Data are an average of three replicate measurements.

To monitor transfection efficiency, eGFP pDNA complexed with lipofectamine was added as a positive control. Human embryonic kidney cells (HEK-293) were treated with pDNA-loaded nanomaterials for 3 hours in media (+10% FBS). Non-uptaken emulsions were then washed away and cells were incubated in the presence or absence of GSH (10 mM) overnight.[57,58] The following day, cells were washed and analyzed by flow cytometry (Figure 4.24D). Incubation with control **6**-stabilized droplets or a combination of homopolymers **4.2** and **4.4** resulted in statistically insignificant expression regardless of GSH treatment. By contrast, responsive **4.5**-stabilized emulsions showed effective eGFP expression only in cells treated with GSH buffer, while untreated cells had fluorescence similar to that of control **4.6**. These statistics are included within Figure 4.28. These data suggest that the cleavable disulfide within **4.5**-stabilized droplets enables release of encapsulated eGFP pDNA. Treating cells with endosomal escape agent chloroquine had no benefit over treatments with GSH buffer alone (see supplemental flow cytometry section).

A. **Analysis of Variance** $\alpha = 0.05$

Source	DF	Sum of Squares	Mean Square	F Ratio	Prob > F
Condition	5	1214.2935	242.859	27.9239	<.0001*
Error	63	547.9212	8.697		
C. Total	63	1762.2147			

B.

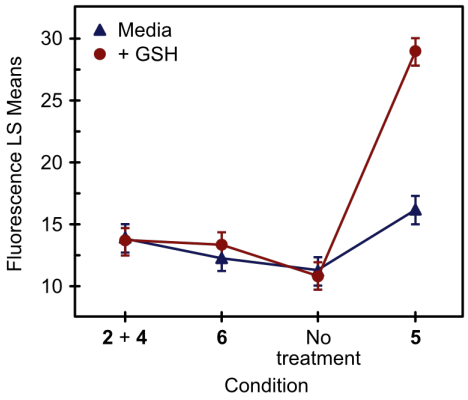

C.

LSMeans Differences Tukey HSD

Level					Least Sq. Mean
5, GSH	A				28.916667
5, Media		B			16.158333
2 + **4**,GSH		B	C		13.85000
2 + **4**,Media		B	C	D	13.60000
6, GSH			C	D E	13.308333
6, Media			C	D E	12.333333
No treat, GSH				D E	11.229167
No treat, Media				E	10.82000

Figure 4.28. Statistical tests of significance for Figure 4.24D. (A) ANOVA test of significance showing there is statistical significance with an alpha value of 0.05 across all samples. (B/C) Tukey HSD post hoc analysis showing **4.5** + GSH (10 mM) are statistically significant from all other conditions.

4.7 Conclusions

In summary, we have demonstrated the use of disulfide-linked poly(2-oxazoline) amphiphiles as stimuli-responsive surfactants for nanoemulsions. Reduction of the disulfide linkage results in destabilization of the PFC-in-water nanoemulsions and release of an encapsulated payload. While we did find that buffering cells with GSH was required to achieve adequate transfection, we envision further tuning of the reactivity-stability balance of the nanoemulsions will enable more rapid response without the need for additional GSH. Furthermore, the concept of cleavable

amphiphile surfactants presented herein can readily be extended to other endogenous stimuli such as changes in pH or reactive oxygen species. The former is potentially advantageous as endosomal escape of the nanoemulsions will not be required for delivery[59], while the latter is particularly conducive to use with PFC nanoemulsions that have high oxygen content[60]. Alongside the new approach to stimuli-responsive nanoemulsions, we present a fluorous tag strategy to solubilize a nucleic acid—plasmid DNA—within a fluorinated liquid core. Combining these advances, we demonstrated that eGFP expression is controlled by use of the responsive delivery vehicle. Overall, these cleavable polymeric amphiphiles demonstrate that macroscale behavior of droplets can be dictated by block copolymer design and are poised to expand applications of emulsions in drug delivery.

4.8 Experimental Procedures

4.8.1 General experimental procedures

Reagents and Instrumentation

Chemical reagents were purchased from Sigma-Aldrich, Alfa Aesar, Fisher Scientific, SynQuest Laboratories, Chem-Impex International or Acros Organics and used without purification unless noted otherwise. Anhydrous dimethyl sulfoxide (DMSO) was obtained from a Sure-Seal™ bottle (Aldrich). Anhydrous and deoxygenated solvents dichloromethane (DCM) and acetonitrile (MeCN) were dispensed from a Grubb's-type Phoenix Solvent Drying System built by JC Meyer.[61] Solvent was removed under reduced pressure with a Büchi Rotovapor with a Welch self-cleaning dry vacuum pump and further dried with a Welch DuoSeal pump. Lyophilization was performed with Labconco FreeZone Benchtop Freeze Dryer, 4.5 L -84 °C, operating with an Edwards RV5 Rotary Vane pump 10:03 Vacuum, set point 0.000 mbar. Dialysis was performed with pre-wetted

Spectra/Por regenerated cellulose dialysis membranes with a 1 kDa molecular weight cutoff purchased from Spectrum Laboratories. Bath sonication was performed using a Branson 3800 ultrasonic cleaner. Nuclear magnetic resonance (^{1}H NMR, ^{13}C NMR, and ^{19}F NMR) spectra were taken on Bruker Avance 500 (^{1}H NMR) instrument and processed with MestReNova 11.0.1 software. All ^{1}H NMR peaks are reported in reference to $CDCl_3$ at 7.26 ppm.

Masses for analytical measurements were taken on a Sartorius MSE6.6S-000-DM Cubis Micro Balance. Microwave reactions were performed using a CEM Discover SP microwave synthesis reactor. All reactions were performed in glass 10 mL microwave reactor vials purchased from CEM with silicone/PTFE caps. Flea micro PTFE-coated stir bars were used in the vials with magnetic stirring set to high and 15 seconds of premixing prior to the temperature ramping. All microwave reactions were carried out at 140 °C with the pressure release limit set to 250 psi (no reactions exceeded this limit to trigger venting) and the maximum wattage set to 250W (the power applied was dynamically controlled by the microwave instrument and did not exceed this limit for any reactions). Mass spectral data was obtained on a Bruker Ultraflex MALDI TOF-TOF MS. Sample preparation, mass calibration, assignment, analysis, *etc.* is described in the general MALDI-TOF analysis procedure.

Abbreviations

DCM = dichloromethane; DMSO = dimethylsulfoxide; EtOH = ethanol; MeCN = acetonitrile; MeOH = methanol; THF = tetrahydrofuran; DMF = dimethylformamide; PFOB = perfluorooctylbromide; POx = poly(2-oxazoline); DBC = diblock copolymer; MeOx = 2-methyl-2-oxazoline; NonOx = 2-nonyl-2-oxazoline; EtOx = 2-ethyl-2-oxazoline; SAc = thioacetate; SS-Pyr = dithiopyridine. DLS = dynamic light scattering; MALDI = matrix-assisted laser

desorption/ionization; NMR = nuclear magnetic resonance; PMMA = poly(methyl methacrylate); PTFE = poly(tetrafluoroethylene); DTH = 1,8,9-trihydroxyanthracene; LC/MS = Liquid chromatography-mass spectrometry; eGFP = enhanced green fluorescent protein; pDNA = plasmid DNA.

General photophysics procedure

Values were obtained in a 0.3 mL quartz cuvette on a Horiba Instruments PTI QuantaMaster Series fluorometer with the following settings:

(i) Rhodamine **4.8**, Figures 4.9, 4.14–4.20: Emission Scan. Slits 3 nm, step size 1 nm unless otherwise noted, integration time 0.1 s (Ex 500 nm, collection: 525–700nm). Where relevant, 1-octanol was returned to the sample after the measurement.

(ii) Nile Red, Figure 4.23 Excitation Scan. Slits 3 nm, step size 1 nm, integration time 0.1 s (Ex 582 nm, collection: 400–575 nm).

(iii) Thiazole Orange, Figure 4.26: Emission Scan. Slits 3 nm, step size 1 nm, integration time 0.1 s (Ex 500 nm, collection: 510–700 nm).

General nanoemulsion formation procedure

Polymer surfactant (3.0 mg) was pre-solubilized in DMF (20 μL) and vortexed gently until fully dissolved. In a separate 2 mL eppendorf tube, oil (10 vol%, 20 μL of either perfluorooctylbromide or olive oil) was added, followed by PBS buffer pH 7.4 (200 μL), 15 wt% total surfactant. Where relevant, (i) rhodamine **4.8** was encapsulated by pre-dissolving 21.6 nmol of **4.8** (5.00 μg) in PFOB, or (ii) Nile Red was encapsulated by pre-dissolving 78.5 nmol of nile red (25.0 mg) in olive oil. Finally, the polymer/DMF solution was added, and the mixture was quickly sonicated at 35%

amplitude for at least 90 seconds at 0 °C on a QSonica (Q125) sonicator. Sonication was performed by lowering the probe directly to the liquid-liquid interface of the two immiscible solvents.

General nanoemulsion analysis procedure

Size analysis: The bulk emulsion solution was diluted in MilliQ H_2O (20 μL emulsions in 2 mL MilliQ H_2O) in a plastic 1 cm cuvette. Size was analyzed with a Malvern Zetasizer Nano dynamic light scattering. SOP parameters: 10 runs, 10 seconds/run, three measurements, no delay between measurements, 25 °C with 120 second equilibration time. Collection parameters: Lower limit = 0.6, Upper limit = 1000, Resolution = High, Number of size classes = 70, Lower size limit = 0.4, Upper size limit = 1000, Lower threshold = 0.05, Upper threshold = 0.01. Data are representative of three replicate measurements.

Fluorous tagging and encapsulation of eGFP pDNA in nanoemulsions procedure

A fluorous ammonium **4.17** stock (10 mM) was prepared by dissolving **4.17** (7.7 mg, 0.010 mmol) in MeOH (1 mL). This was diluted to a 1 mM stock in water. DNA (30 μg, eGFP, addgene: 13031) (as measured by nanodrop) was placed in Eppendorf tubes, 1 mL 1 mM stock **4.17** was added and freeze dried overnight. Emulsions were prepared by dissolving the pDNA/**4.17** in 20 μL 7:3 PFD:PFTPA (vol%) and bath sonicating for 5 min. Phosphate buffered saline (PBS, 200 μL) was added, and polymer **4.5** or **4.6** (5.6 mg dissolved in 20 μL DMF) was added immediately before sonication. Emulsions were sonicated for 3 min, pulsed on for 2 s, off for 5 s. Emulsions were centrifuged (5.6 x g, 3 min) to separate un-encapsulated eGFP pDNA and resuspended in PBS.

General MALDI-TOF analysis procedure

Mass spectral data was obtained on a Bruker Ultraflex MALDI TOF-TOF MS. Samples were acquired using the linear mode.

For calibration standards: Calibration was performed using low mass calibration standards (for calibration with MW < 5730 Da). Aliquots of low mass standards were made with 10 μL of 10 μM of low mass standards in H_2O. All low mass standards were purchased from Sigma-Aldrich and aliquoted at the following concentrations: (i)-(v) at 10 pmol/μL, (vi) at 50 pmol/μL: (i) Met-Arg-Phe-Ala (MW: 524.2650 Da), (ii) Angiotensin II (MW: 1046.5418 Da), (iii) Angiotensin I (MW: 1296.6853 Da), (iv) Substance P (MW: 1347.7354 Da), (v) Neurotensin (MW: 1672.9170 Da), (vi) ACTH (18-39, MW: 2465.1989 Da) and (vi) bovine insulin (MW: 5730.6081 Da, average MW: 5734.51 Da). Matrix solution of alpha-cyano-4-hydroxycinnamic acid (Sigma-Aldrich) was prepared in 50/50 MeCN/H_2O + 0.1% TFA (vol%) at 10 mg/mL. Added 10 μL of this matrix solution directly to an aliquot of low mass standards and mixed thoroughly on vortex.

For polymer analytes: Matrix solution of 1,8,9-trihydroxyanthracene (DTH, Fluka Analytical, >99.0%) was prepared in $CHCl_3$ at 20 mg/mL. Counterion solution of sodium trifluoroacetate (NaTFA, Sigma-Aldrich, 98%) was prepared in MilliQ water at 2 mg/mL. Polymer analyte solutions were prepared in $CHCl_3$ at 10 mg/mL. Solutions were combined at a 3:3:1 matrix:analyte:counter-ion ratio and mixed thoroughly on a vortex. Samples (1 μL x 3) were then spotted in triplicate on the MALDI target plate via the dried-droplet method. Mass calibration, assignment, and analysis was performed on Bruker Daltonik's FlexAnalysis 3.4 software.

General synthetic procedures

4.8.2 Experimental procedures

Synthetic chemistry experimental procedures

Synthesis of poly(2-oxazoline) block copolymer **4.6**:

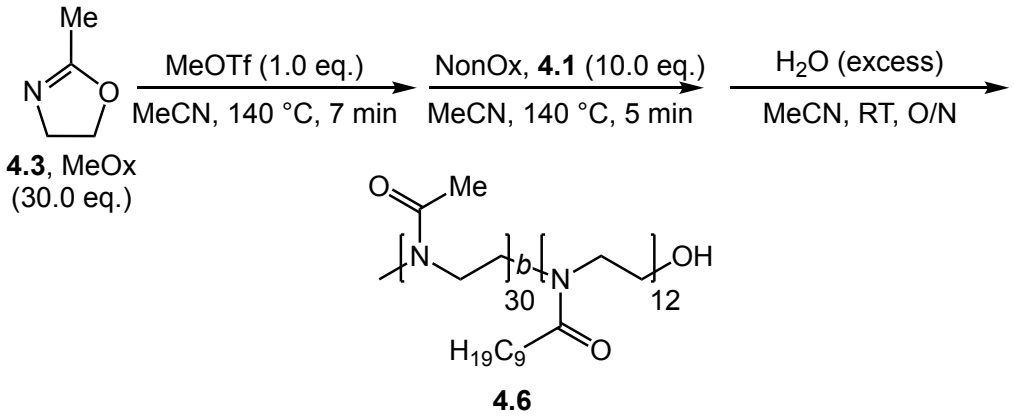

P($MeOx_{30}$-*b*-$NonOx_{12}$) (**4.6**) was synthesized as previously reported.[18]

Synthesis of end-functionalized poly(oxazoline) polymers **4.S1**, **4.2**, and **4.4**:

P$(MeOx)_{24}$-*t*-SAc (4.S1)

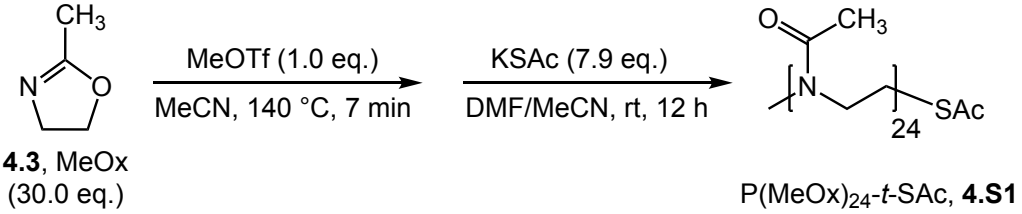

To a flame dried microwave vial, MeCN (3.0 mL, anhydrous) and MeOx (**4.3**, 500 μL, 0.500 g, 5.88 mmol, 30 equiv.) were added. After purging with nitrogen, MeOTf (22 μL, 32 mg, 0.19 mmol, 1.0 equiv.) was added and the mixture was heated at 140 °C in the microwave. After 9 minutes, the polymerization was quenched with dry potassium thioacetate (0.167 g, 1.50 mmol, 7.9 equiv.) and anhydrous DMF (3.0 mL) was added to solubilize the potassium thioacetate. The reaction

mixture was stirred overnight at room temperature. The following day, the reaction mixture was evaporated to dryness to yield crude polymer (**S1**) as an off-white solid. Polymer **4.S1** was purified by precipitation by dissolving in a minimal amount of DCM and dropwise addition to cold Et_2O (20:1 v/v%) three times, collected and evaporated to dryness, yielding the pure product **4.S1** as an off-white solid (462 mg, 0.175 mmol, 93% yield). ^{1}H NMR (500 MHz, $CDCl_3$): δ 3.41 (m, 113H), 3.00 (m, 3H), 2.33 (m, 3H), 2.10 (m, 87H). MALDI: Calculated for P(MeOx)$_{24}$-*t*-SAc $[M+Na]^+$: 2155.4; found: 2154.9. Calculated polymer properties (1000–3500 Da), M_n = 2241 Da, M_w = 2111 Da, $Đ$ = 1.06.

P(NonOx)$_{10}$-*t*-SAc (4.2**)**

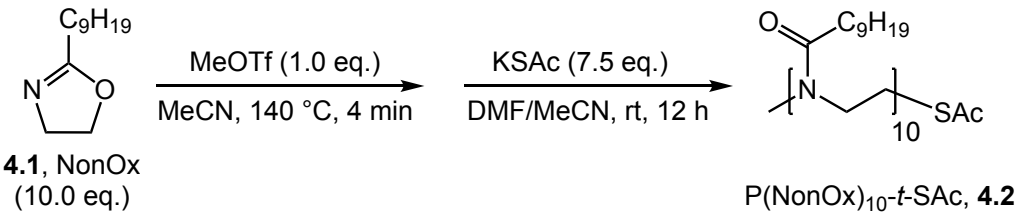

4.1, NonOx (10.0 eq.)

P(NonOx)$_{10}$-*t*-SAc, **4.2**

To a flame dried microwave vial, MeCN (1.3 mL, anhydrous) and NonOx (**4.1**, 500 μL, 0.500 g, 2.53 mmol, 10 equiv.) were added. After purging with nitrogen, MeOTf (29 μL, 42 mg, 0.25 mmol, 1.0 equiv.) was added and the mixture was heated at 140 °C in the microwave. After 4 minutes, the polymerization was quenched with dry potassium thioacetate (0.217 g, 1.90 mmol, 7.5 equiv.) and anhydrous DMF (1.3 mL) was added to solubilize the potassium thioacetate. The reaction mixture was stirred overnight at room temperature. The following day, the reaction mixture was evaporated to dryness to yield crude polymer (**4.2**) as an off-white solid. Polymer **4.2** was purified by 24-hour dialysis against DCM/MeOH (50:50 vol%) using a 1 kDa membrane cutoff dialysis

tubing. The solution was collected and evaporated to dryness, yielding the pure product **2** as an off-white solid (462 mg, 0.224 mmol, 93% yield). ^{1}H NMR (500 MHz, $CDCl_3$): δ 3.45 (m, 33H), 3.02 (m, 3H), 2.34 (m, 22H), 1.59 (m, 20H), 1.27 (m, 113H) 0.88 (t, J = 6.6 Hz, 28H). MALDI: Calculated for P(NonOx)$_{10}$-*t*-SAc $[M+Na]^+$: 2084.8; found: 2084.3. Calculated polymer properties (1000–3500 Da), M_n = 2142 Da, M_w = 2372 Da, $Đ$ = 1.11.

P(MeOx)$_{27}$-*t*-SS-Pyr (4.4**)**

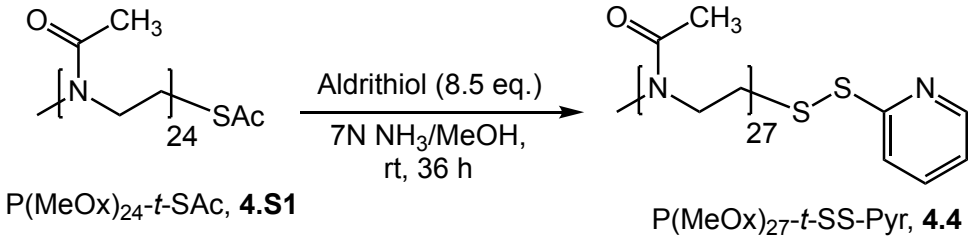

P(MeOx)$_{24}$-*t*-SAc, **4.S1**

P(MeOx)$_{27}$-*t*-SS-Pyr, **4.4**

To a flame dried scintillation vial, **4.S1** (MeOx-*t*-SAc) (0.21 g, 0.079 mmol, 1.0 equiv.) and aldrithiol (0.149 g, 0.676 mmol, 8.5 equiv.) were added. After purging with nitrogen, 7N NH_3/MeOH (5 mL) was added and vial's septa was exchanged with a sealed cap under nitrogen flow. The reaction mixture was stirred for 36 hours at room temperature, after which it was evaporated to dryness to yield crude polymer (**4.4**) as a yellow solid. Polymer **4.4** was purified by precipitation by dissolving in a minimal amount of DCM and dropwise addition to cold Et_2O (20:1 v/v%) three times, collected and evaporated to dryness, yielding the pure product **4.4** as an off-white solid (0.20 g, 0.074 mmol, 94% yield). ^{1}H NMR (500 MHz, $CDCl_3$): δ 8.51 (d, J = 4.9 Hz, 1H), 7.68 (m, 2H), 7.18 (s, 1H), 3.68 (m, 4H), 3.48 (m, 96H), 3.07 (m, 3H), 2.98 (m, 2H), 2.17 (m, 84H). MALDI: Calculated for P(NonOx)$_{10}$-*t*-SAc $[M+Na]^+$: 2084.8; found: 2084.3. Calculated polymer properties (1000 –3500 Da), M_n = 2142 Da, M_w = 2372 Da, $Đ$ = 1.11.

Synthesis of disulfide-linked polymer **4.5**:

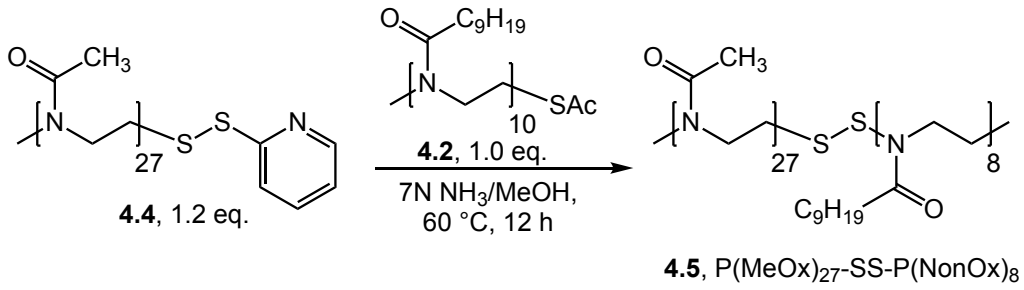

To a flame dried scintillation vial, **4.4** ($P(MeOx)_{27}$-*t*-SS-Pyr, 0.13 g, 0.045 mmol, 1.0 equiv.) and **4.2** ($P(NonOx)_{10}$-*t*-SAc, 0.10 g, 0.049 mmol, 1.0 equiv.) were added. Anhydrous DCM (1.6 mL) and 7N NH_3/MeOH (1.6 mL) were added under N_2, and vial's septa was exchanged with a sealed cap under nitrogen flow. The reaction mixture was stirred overnight at 60 °C. The reaction mixture was then evaporated to dryness to yield crude polymer (**4.5**) as a yellow solid. The polymer was washed with diethyl ether (3x) and hexanes (3x) to yield product **4.5** as a white solid (0.134 g, 0.033 mmol, 66% yield). ^{1}H NMR (500 MHz, $CDCl_3$): δ 3.50 (m, 162H), 3.10 (m, 6H), 2.19 (m, 112H), 1.63 (m, 15H), 1.30 (m, 74H), 0.91 (t, J = 6.6 Hz, 20H). MALDI: Calculated for $P(MeOx)_{27}$-SS-$P(NonOx)_8$ $[M+Na]^+$: 4077.2; found: 4077.2. Calculated polymer properties from 1000 to 7000 Da, M_n = 3802 Da, M_w = 4155 Da, $Đ$ = 1.09. Purity of $P(MeOx)_{27}$-SS-$P(NonOx)_8$ was determined to be 79% by comparing area under the curve (AUC) values from the 3-7 kDa mass range (polymer-polymer coupling products) to AUC values of total polymer (products + contaminants) in 1–7 kDa mass range.

4.8.3 Figure experimental procedures

Figure 4.2A. Synthesis of block copolymers 4.5 **and** 4.6**.**

See supporting synthetic chemistry experimental procedures.

Figure 4.2B,D. Perfluorocarbon nanoemulsion formation and stability

Perfluorooctylbromide-in-water nanoemulsions were prepared as described by the general nanoemulsion formation procedure, using responsive surfactant **4.5** or control surfactant **4.6**. Size was analyzed per the general nanoemulsion analysis procedure. Note: Data are representative of three replicate measurements.

Figure 4.2C. MALDI analysis of end-group functionalized POx polymers 4.2**,** 4.4 **and disulfide-linked amphiphile** 4.5**.**

End-group functionalized polymers were synthesized via microwave protocol using kinetics previously reported in the literature, terminated and further modified using established procedures [36,38,62–64]. See supporting experimental procedures for synthetic details.

Figure 4.3. MALDI-TOF analysis of control surfactant P(MeOx)$_x$-*b*-P(NonOx)$_y$ (4.6**), responsive surfactant P(MeOx)$_x$-SS-P(NonOx)$_y$ (**5**), and byproducts.**

See synthetic chemistry experimental procedures for synthesis of **4.5** and **4.6**. See general MALDI-TOF analysis procedure for characterization details.

Figure 4.4. MALDI-TOF analysis of responsive surfactant P(MeOx)$_x$-SS-P(NonOx)$_y$ (top, 4.5**) and control surfactant P(MeOx)$_x$-*b*-P(NonOx)$_y$ (bottom,** 4.6**).**

See synthetic chemistry experimental procedures for synthesis of **4.5** and **4.6**. See general MALDI-TOF analysis procedure for characterization details.

Figure 4.5–4.8. Size of PFOB and Olive Oil nanoemulsions stabilized by POx surfactants 4.5 **or** 4.6**.**

Emulsions were prepared as described by the general nanoemulsion formation procedures and analyzed as described by the general nanoemulsion analysis procedure. Data are an average of three replicate measurements.

Figure 4.9A. Use of disulfide-linked surfactant 4.5 **for PFOB nanoemulsion formation**

Perfluorooctylbromide-in-water nanoemulsions with model payload **4.8** encapsulated were prepared as described by the general nanoemulsion formation procedure, using responsive surfactant **4.5** or control surfactant **4.6**.

Figure 4.9C. Demulsification of 5**-stabilized PFOB nanoemulsions in response to glutathione (GSH).**

(i) Dram vials containing a solution of fluorescein in PBS (2.0 mL, 3 mM fluorescein, pH 7.4) was placed on top of a solution of **4.8** in perfluorooctylbromide (200 μL, 0.13 mM **4.8**). Polymers **4.5** or **4.6** were then added to the aqueous layer with a final concentration of 1.7 wt%. (ii) Emulsification was performed by transferring solutions to eppendorf tubes and ultrasonicating for three minutes at 35% amplitude, 0 °C. (iii) Reduced GSH was then added as a solid to the solution

for a final concentration of 10 mM, and dram vials were rocked at room temperature for up to three hours and monitored. After three hours, the experiment was stopped by lightly centrifuging (rapid pulse up to 900 *g*) to remove solution from sides of dram vial before images were taken.

Figure 4.9D,E. Leaching of rhodamine payload 4.8 **when stabilized by** 4.5 **or** 4.6 **in the presence of varying concentrations of reduced glutathione.**

Emulsions containing **4.8** were prepared by pre-dissolving **4.8** (0.05 mg, 20 nmol) in PFOB, (20 μL, 10 vol%). Emulsions were formed and analyzed according to the general nanoemulsion formation and analysis procedures. Emulsions were then diluted (50 μL emulsions in 1.25 mL PBS +/- glutathione (GSH)). Solutions containing 0.1 and 10 mM GSH in PBS were made from a diluted 20 mM GSH stock (pH'd to 7.4 after addition of reduced GSH via 0.5M NaOH). These 1.25 mL solutions were placed in the presence of 1-octanol (0.5 mL) in an Eppendorf tube. The biphasic samples were then rocked for over three days. The Eppendorf tubes containing the samples were allowed to roll freely on a KJ-201BD Orbital shaker at 20 rpm. The fluorescence of the 1-octanol layer was monitored to determine the amount of **4.8** that was released from the emulsions (Figure 4.9D). Emission values were obtained by taking an aliquot (~200 μL) of the 1-octanol in a 0.3 mL quartz cuvette and measuring the fluorescence on a Horiba Instruments PTI QuantaMaster Series fluorometer with the following settings: slits 3 nm, step size 1 nm, integration time 0.1 s (Ex 500 nm, collection 525–700nm). The 1-octanol was returned to the sample after the measurement.

Figure 4.10. Demulsification of 4.5-stabilized PFOB nanoemulsions in response to glutathione (GSH, 10 mM).

Dram vials containing a solution fluorescein dissolved in PBS (pH 7.4, 2.0 mL, 3 mM fluorescein) and a solution of **4.8** dissolved in perfluorooctylbromide (200 μL, 0.13 mM **4.8**). Polymers **4.5** or **4.6** were then solubilized in the aqueous layer at 1.7 wt%. Emulsification was performed by transferring solutions to eppendorf tubes and ultrasonicating for three minutes at 35% amplitude, 0 °C and resulted in visibly similar emulsion solutions. Solutions were then transferred back to dram vials. Reduced GSH was added as a solid to final concentration of 10 mM, and dram vials were rocked at room temperature for up to three hours and monitored. After one hour, degradation was clear. After two hours, phase separation was observed. After three hours, solution looked similar to that at two hours, and the experiment was stopped by lightly centrifuging (rapid pulse up to 3k rpm) to remove the solution from the sides of the dram vial before imaging.

Figure 4.11. Visual demulsification and quantified turbidity of 4.5-stabilized PFOB nanoemulsions in response to glutathione (GSH, 0.1, 1 and 10 mM).

Emulsion solutions stabilized by redox-responsive **4.5** were formed via the general nanoemulsion formation procedure. An aliquot of emulsion solution was taken (50 μL) and diluted within PBS with and without reduced GSH (1250 μL, 0.1, 1.0 or 10 mM, pH 7.4) and rocked at 37 °C for three hours. After three hours, (A) nearly quantitative phase separation was observed selectively for **4.5**-stabilized droplets within 10 mM GSH. (B) The turbidity of each emulsion solution at 0 and 3 hours was measured via UV-Vis analysis and quantified by absorbance at 550 nm. Absorbance was blanked against PBS.

Figure 4.12, 4.13. MALDI-TOF analysis of surfactant isolated from PFOB-in-water nanoemulsions stabilized by 4.5 **with and without exposure to reduced glutathione (GSH) for one hour.**

Emulsions were prepared as described by the general nanoemulsion formation procedures using responsive surfactant **4.5**. The emulsion solution was then diluted (20 μL emulsions in 780 μL PBS + glutathione (10 mM GSH)). Solutions containing 10 mM GSH in PBS were made from a diluted 20 mM GSH stock (pH'd to 7.4 after addition of reduced GSH via 0.5M NaOH). The solution was then rocked for one hour and emulsions were spun down at 900 *g* for 3 minutes. The supernatant was removed, and pelleted emulsions were resuspended in DCM, vortexed to demulsify, and evaporated to dryness. The resulting off-white surfactant was analyzed per general MALDI-TOF analysis procedure.

Figure 4.14. Leaching of rhodamine payload 4.8 **when stabilized by** 4.5 **or** 4.6 **in the presence of varying concentrations of reduced glutathione.**

Inset of Figure 4.9E. See Figure 4.9D,E experimental procedure.

Figure 4.15. Release of rhodamine 4.8 **from** 4.5**-stabilized droplets in 0, 0.1, 1.0 and 10 mM GSH under physiological conditions.**

Emulsions containing **4.8** were prepared by pre-dissolving **4.8** (0.05 mg, 20 nmol) in PFOB (20 μL, 10 vol%). Emulsions were formed and analyzed according to the general nanoemulsion formation and analysis procedures. Emulsions were then diluted (50 μL emulsions in 1.25 mL PBS +/- glutathione (GSH)). Solutions containing 0.1, 1.0, and 10 mM GSH in PBS were made from a diluted 20 mM GSH stock (pH'd to 7.4 after addition of reduced GSH via 0.5M NaOH). These

1.25 mL solutions were placed in the presence of 1-octanol (0.5 mL) in an Eppendorf tube. The biphasic samples were then rocked at 37 °C at 50 rpm. The fluorescence of the 1-octanol layer was monitored to determine the amount of **4.8** that was released from the emulsions. Emission values were obtained by taking an aliquot (~200 μL) of the 1-octanol in a 0.3 mL quartz cuvette and measuring the fluorescence on a Horiba Instruments PTI QuantaMaster Series fluorometer with the following settings: slits 3 nm, step size 2 nm, integration time 0.1 s (Ex 500 nm, collection 525–700nm). The 1-octanol was returned to the sample after the measurement. Fluorescence was normalized to an equal volume **4.5**-stabilized emulsion aliquot (50 μL) directly added and sonicated within 1-octanol (500 μL). Error bars represent the standard deviation of two independent experiments.

Figure 4.16. Release of 4.8 **from** 4.6**-stabilized PFOB droplets in PBS with and without BSA.** Payload release of **4.8** from **4.6**-stabilized PFOB droplets was examined in PBS with and without bovine serum albumin (BSA, 50 mg/mL). This solution was rocked at 37 °C at 50 rpm and fluorescence of the solution (Ex: 500 nm, Em: 525–700 nm). was measured over a period of 0.5, 1, 3 and 24 hours. For comparison, free, non-encapsulated equimolar **4.8** in either PFOB or acetone was added to the same volume of PBS or BSA and measured at 0 and 24 hours. Error bars represent the standard deviation between at least two independent experiments.

Figure 4.17. Release of a panel of fluorophores from 4.6**-stabilized PFOB nanoemulsions in PBS with and without BSA.**

4.6-stabilized PFOB nanoemulsions encapsulating cyanines **4.11** or **4.12** (0.03 mg)[14], rhodamine **4.8** (0.03 mg), and porphyrin **4.13** (0.06 mg)[43] were formed by pre-dissolving each dye in PFOB

(20 μL) and following the general nanoemulsion formation procedure. From here, aliquots of emulsion solutions (25 μL) were then diluted in PBS (175 μL) with and without BSA (50 mg/mL total). This solution was rocked at 37 °C at 50 rpm and fluorescence of the solution (Ex. 500 nm) was measured over a period of 0, 0.5, 1, 3 and 24 hours. Release was calculated by comparison of fluorescence of the solution at 0 hours. Error bars represent the standard deviation between at least two independent experiments.

Figure 4.18. Monitoring stability of 4.6**-stabilized PFOB nanoemulsions via FRET assay.** (A) Synthesis of fluorescein-labeled surfactant **4.16** via CuAAC between azidofluorescein **4.14** and alkyne-containing POx surfactant **4.15**, adapted from previous chemistries.[18,44] (B) Labeled surfactant **4.16** was employed as cosurfactants alongside surfactant **4.6** (1:100 wt%, 28 mg/mL total) for rhodamine **4.8**-containing perfluorooctylbromide (PFOB) nanoemulsions. Emulsions were formed via the general nanoemulsion formation procedure and diluted (1.1 vol% PFOB) within PBS with and without BSA (75 mg/mL). (C) FRET efficiency was measured by directly taking an aliquot of solution (~200 μL) and taking fluorescence of solutions. Fluorometer settings: Ex. 450 nm; Em: 470–700 nm. Acceptor emission was taken at 526 nm, donor emission was taken at 570 nm. FRET efficiency is defined as $F_a/(F_a + F_d)$, where F_a is the acceptor emission and F_d is the donor emission.

Figure 4.19. Release of rhodamine payload 4.8 **from** 4.5**-stabilized droplets under dialysis conditions.**

Nanoemulsions containing **4.8** were prepared with either responsive surfactant **4.5** or control surfactant **4.6** using the general emulsion formation protocol. Emulsion solutions (40 μL) were

combined with PBS (940 μL, 25-fold dilution) and dialyzed using regenerated cellulose membrane with a 1 kDa MWCO against a 200 mL solution (200-fold dilution) of PBS (pH 7.4) with or without reduced glutathione (GSH, 10 mM) to a total dilution of 5000-fold. The solution was then stirred overnight at room temperature. Fluorescence of the dialyzed solutions were taken and directly compared to the fluorescence of solutions prior to dialysis. Fluorescence solutions: 10 μL + 490 μL MilliQ H_2O. Fluorometer settings: Ex: 500 nm; Em: 525–700 nm; 5 nm slits; Int: 0.1s; Step Size: 1 nm.

Figure 4.20. Release of rhodamine 4.8 **from** 4.5**-stabilized droplets at varying dilutions in the presence of reduced glutathione.**

Nanoemulsions containing **4.8** were prepared with responsive surfactant **4.5**, per general emulsion formation protocol. Emulsion solutions (20 μL) were diluted with PBS (pH 7.4) containing reduced glutathione (GSH, 10 mM) to a total volume of 200 μL. The solution was then agitated at 37 °C for 90 minutes. Fluorescence of solutions were directly taken at 20, 60, and 90 minutes. Release percentages were calculated by comparing fluorescence values at each time point to the initial fluorescence (0 minutes) for that dilution. Error bars represent the standard deviation between at least two independent experiments. Fluorometer settings: Ex: 500 nm; Em: 525–700 nm; 3 nm slits; Int: 0.1s; Step Size: 1 nm.

Figure 4.21. Dynamic light scattering analysis of 4.5**-stabilized droplets in the presence of reduced glutathione.**

Droplets were taken from samples prepared as described in Figure 4.20, corresponding to a dilution of 20 vol%. Emulsions were formed and analyzed according to the general nanoemulsion formation and analysis procedures.

Figure 4.22. Partition of free rhodamine 4.8 **in PFOB against PBS 1X.**

Rhodamine **4.8** was dissolved in PFOB (1050 μL, 106 μM). Absorption of this solution was measured via UV-Vis analysis. 3x300 μL aliquots of this **4.8**/PFOB solution were removed and diluted with PBS 1X accordingly: (i) 10 vol%, 3 mL PBS, (ii) 1 vol%, 30 mL PBS, (iii) 0.1 vol%, 300 mL PBS. Mixture was gently rocked at 150 rpm at room temperature overnight. PFOB layer was recovered and absorption was measured via UV-Vis analysis. Recovery was calculated via the Beer-Lambert law. Error bars represent the standard deviation between two independent experiments.

Figure 4.23. Nile Red release from olive oil-in-water nanoemulsions when stabilized by 4.5 **in the presence of tris(2-carboxyethyl)phosphine (TCEP).**

Olive oil-in-water nanoemulsions containing Nile Red (327 μM) and stabilized by either **4.5** or **4.6** were prepared per general nanoemulsion formation and analysis procedures. For encapsulation of Nile Red, addition of dye in an acetone stock was added to an Eppendorf tube and dried under air. Olive oil (20 μL) was added to solubilize dye. Emulsion solutions were directly transferred to dram vials and imaged. Where relevant, TCEP hydrochloride (45 mM) was then added as a solid to emulsion solutions and rocked at ~45 rpm at room temperature for 10 minutes. (C/D/E) To

determine how quickly release occurred, aliquots of nanoemulsion solutions described in (B) were diluted in PBS (pH 7.4). Afterwards, TCEP hydrochloride (45 mM) was then added as a solid to emulsion solutions and rocked at ~45 rpm at room temperature for 15 minutes. Intensity values were obtained by taking an aliquot (~200 μL) of the diluted solution in a 0.3 mL quartz cuvette and performing an excitation scan on a Horiba Instruments PTI QuantaMaster Series fluorometer with the following settings: slits 3 nm, step size 1 nm, integration time 0.1 s (Em 582 nm, collection 400–575 nm). Scan settings are described in the general photophysics procedure.

Figure 4.24A. Fluorous tagging and encapsulation of eGFP pDNA in PFD:PFTPA nanoemulsions.

Fluorous ammonium **4.17** stock (10 mM) was made by dissolving **4.17** in MeOH. This was diluted to a stock in water (1 mM). pDNA (eGFP, addgene: 13031, 30 μg) (as measured by nanodrop) was placed in Eppendorf tubes, 1 mL 0.1 mM stock **4.17** was added, freeze dried overnight. Emulsions were prepared by dissolving the pDNA/**4.17** in 20 μL 7:3 PFD:PFTPA (vol%) and bath sonicating for 5 min. Phosphate buffered saline (PBS, 200 μL) was added, and polymer **4.5** or **4.6** (5.6 mg dissolved in 20 μL DMF) was added immediately before sonication. Emulsions were sonicated for 3 min, pulsed on for 2 s, off for 5 s. Emulsions were centrifuged (5.6 x g, 3 min) and supernatant was discarded.

Figure 4.24C. Gel electrophoresis of PFD/PFTPA/4.17**/pDNA nanoemulsions.**

Emulsions were formed as described in Figure 4.24A. Polymer P(EtOx)$_{90}$-*b*-P(NonOx)$_{10}$ was used as a model polymeric surfactant. The emulsions were then centrifuged (5.6 x *g*, 3 min) and the supernatant was collected. The emulsions were resuspended with 200 μL PEG-8k (100 mg/mL).

Phenol and chloroform (~200 µL each) were added to the resuspended emulsions and the supernatant, and vortexed followed by immediate centrifugation (18 x *g*, 5 min). The aqueous (top) layer was removed and placed in new vials, chloroform (~200 µL) was added, vortexed, and centrifuged (18 x *g*, 5 min). The aqueous (top) layer was removed again and placed in new vials with 20 µL acetate buffer (5 mM, pH 5.5) and 500 µL ethanol. This was placed in -80 °C freezer overnight. The next day, the eppendorf tubes were centrifuged to pellet any DNA present (18 x *g*, 5 min) and the supernatant was decanted. The pellet was washed with 70% ethanol, centrifuged (18 x *g*, 5 min), supernatant decanted, and dried at room temperature (~10 min). DNA pellets were dissolved in 50 µL MilliQ water. 2 µL of loading buffer was added to each sample, then loaded onto a 1.2% agarose gel. The gel was run for 45 min, 120 V and visualized with ethidium bromide.

Figure 4.24D. Flow cytometry of HEK-293 cells incubated with PFD/PFTPA/4.17**/pDNA nanoemulsions.**

Emulsions were formed as described in Figure 4.24A. Polymers **5** or **6** were used for responsive and control emulsions, respectively. Emulsions were then centrifuged (5.6 x *g*, 3 min), supernatant was discarded and emulsions were resuspended in PBS (200 µL). 200,000 HEK293 cells (ATCC: CRL-1573) were plated in 12 well plate (Fisher, cat# FB012928), and allowed to adhere overnight. Media (MEM, Gibco cat# 11095080) was removed and replaced with two treatments (media + emulsions, or media + emulsions + glutathione (GSH, 10 mM)) with a total volume of 1 mL. Positive control (lipofectamine) followed Invitrogen's Lipofectamine® 2000 DNA Transfection Reagent Protocol. The cells were incubated with treatment for 3 hours at 37 °C and then washed gently to remove treatment. Media or GSH (10 mM) was added back and cells were incubated overnight at 37 ˚C. The next day, cells were lifted via trypsonization, washed via centrifugation

(526 x *g*, 3 min) and resuspended in 200 µL FACS buffer (PBS, 1% FBS). The cells were analyzed for GFP (FL-1) fluorescence via flow cytometry.

Figure 4.25. Gel electrophoresis of 4.17**/pDNA PFOB nanoemulsions: encapsulation vs. supernatant.**

Emulsions were formed as described in Figure 4.24A and the fluorous tagging and encapsulation of eGFP pDNA in the nanoemulsions procedure. Polymer $P(EtOx)_{90}$-*b*-$P(NonOx)_{10}$ was used as a model polymeric surfactant. The emulsions were then centrifuged (5.6 x *g*, 3 min) and the supernatant was collected. The emulsions were resuspended with 200 µL PEG-8k (100 mg/mL). Phenol and chloroform (~200 µL each) were added to the resuspended emulsions and the supernatant, and vortexed followed by immediate centrifugation (18 x *g*, 5 min). The aqueous (top) layer was removed and placed in new vials, chloroform (~200 µL) was added, vortexed, and centrifuged (18 x *g*, 5 min). The aqueous (top) layer was removed again and placed in new vials with 20 µL acetate buffer (5 mM, pH 5.5) and 500 µL ethanol. This was placed in -80 °C freezer overnight. The next day, the eppendorf tubes were centrifuged to pellet any DNA present (18 x *g*, 5 min) and the supernatant was decanted. The pellet was washed with 70% ethanol, centrifuged (18 x *g*, 5 min), supernatant decanted, and dried at room temperature (~10 min). DNA pellets were dissolved in 50 µL MilliQ water. 2 µL of loading buffer was added to each sample, then loaded onto a 1.2% agarose gel. The gel was run for 45 min, 120 V and visualized with ethidium bromide.

Figure 4.26. Thiazole orange assay to quantify encapsulation efficiency of pDNA.

Emulsions were formed as described in Figure 4.24A and the fluorous tagging and encapsulation of eGFP pDNA in the nanoemulsions procedure. Polymer $P(EtOx)_{90}$-*b*-$P(NonOx)_{10}$ was used as a model polymeric surfactant. The emulsions were then centrifuged (5.6 x *g*, 3 min) and the supernatant was collected. The emulsions were resuspended with 200 µL PEG-8k (100 mg/mL). Phenol and chloroform (~200 µL each) were added to the resuspended emulsions and the supernatant, and vortexed followed by immediate centrifugation (18 x *g*, 5 min). The aqueous (top) layer was removed and placed in new vials, chloroform (~200 µL) was added, vortexed, and centrifuged (18 x *g*, 5 min). The aqueous (top) layer was removed again and placed in new vials with 20 µL acetate buffer (5 mM, pH 5.5) and 500 µL ethanol. This was placed in -80 °C freezer overnight. The next day, the eppendorf tubes were centrifuged to pellet any DNA present (18 x *g*, 5 min) and the supernatant was decanted. The pellet was washed with 70% ethanol, centrifuged (18 x *g*, 5 min), supernatant decanted, and dried at room temperature (~10 min). DNA pellets were dissolved in 50 µL MilliQ water. Thiazole orange (0.5 µL, 1.9 mM, Fisher cat# 50-176-3367) was added, fluorescence was measured. Fluorometer settings: Ex: 500 nm; Em: 510-700 nm; Slits: 3 nm; Int: 0.1 s; Step Size: 1 nm. DNA encapsulation efficiencies, as referenced in the main text, were approximated by comparing area under the curve (AUC) values of PFC/**11** emulsions + 30 µg pDNA to the AUC sum of both emulsions and supernatant for that experiment. The average and standard deviation were calculated from three independent experiments.

Figure 4.27. Dynamic light scattering data for **4.2** + **4.4** + **4.17**/pDNA aggregates. Aggregates were prepared following the general nanoemulsion formation procedures using **4.2** and **4.4** (14 mg/mL each) and analyzed as described by the general nanoemulsion analysis procedure.

Aggregation is observed due to lack of amphiphilicity for the two cleaved homopolymers (**4.2** and **4.4**). Data are an average of three replicate measurements.

Figure 4.28. Statistical tests of significance for Figure 4.24D.

ANOVA test of significance showing there is statistical significance with an alpha value of 0.05 across all samples. Tukey HSD post hoc analysis showing **4.5** + GSH are statistically significant from all other conditions.

4.9 1H-NMR Spectra Relevant to Chapter Four

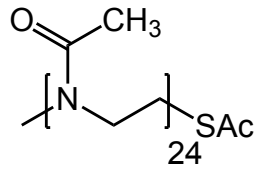

P(MeOx)$_{24}$-*t*-SAc (**4.S1**)

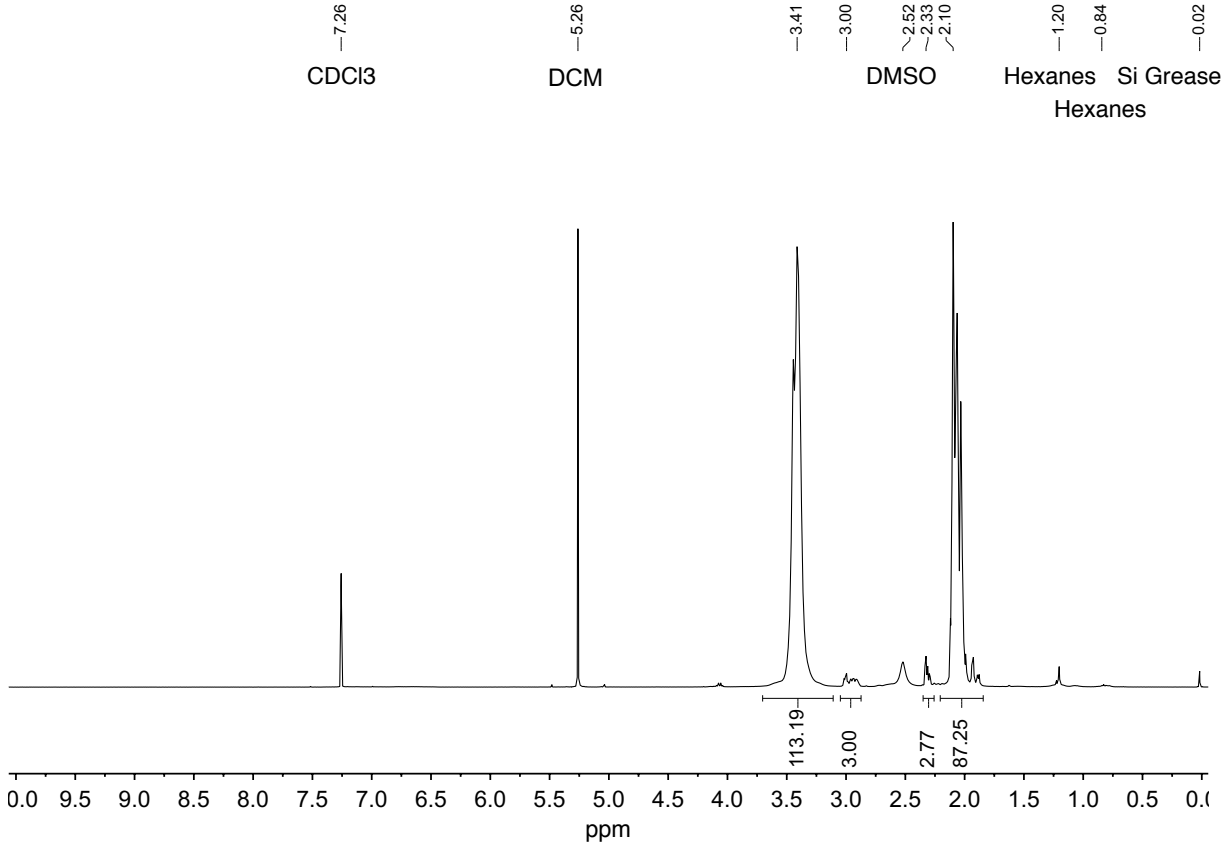

^{1}H NMR (500 MHz, $CDCl_3$) of copolymer **4.S1** P(MeOx)$_{24}$-*t*-SAc. Note: block lengths determined per MALDI-TOF analysis.

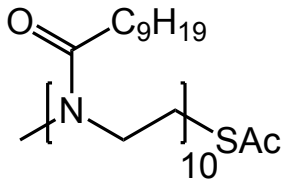

P(NonOx)$_{10}$-*t*-SAc (**4.2**)

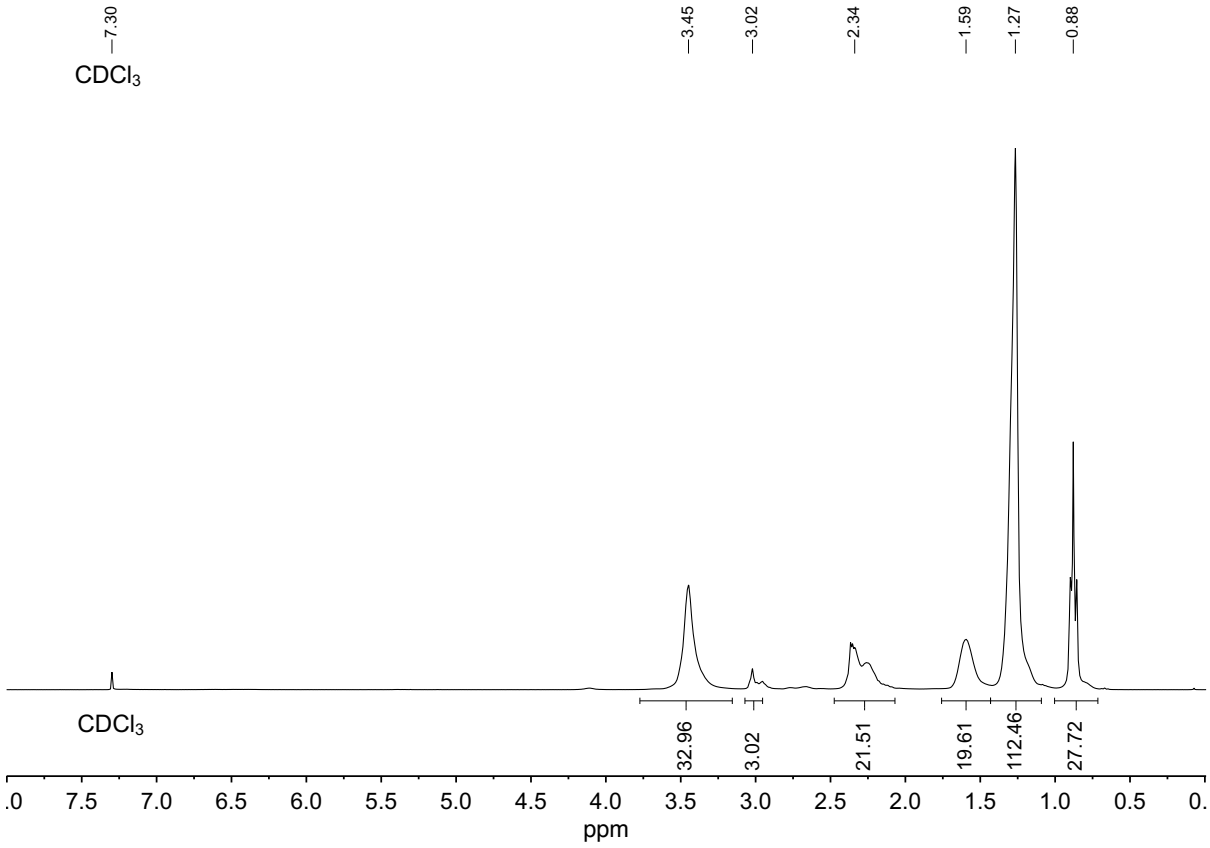

^{1}H NMR (500 MHz, $CDCl_3$) of homopolymer **4.2** P(NonOx)$_{10}$-*t*-SAc. Note: block lengths determined per MALDI-TOF analysis.

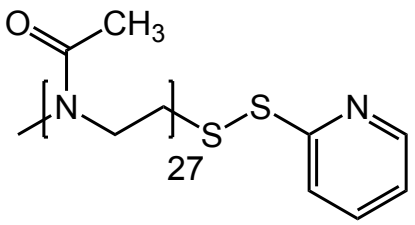

P(MeOx)$_{27}$-*t*-SS-Pyr (**4.4**)

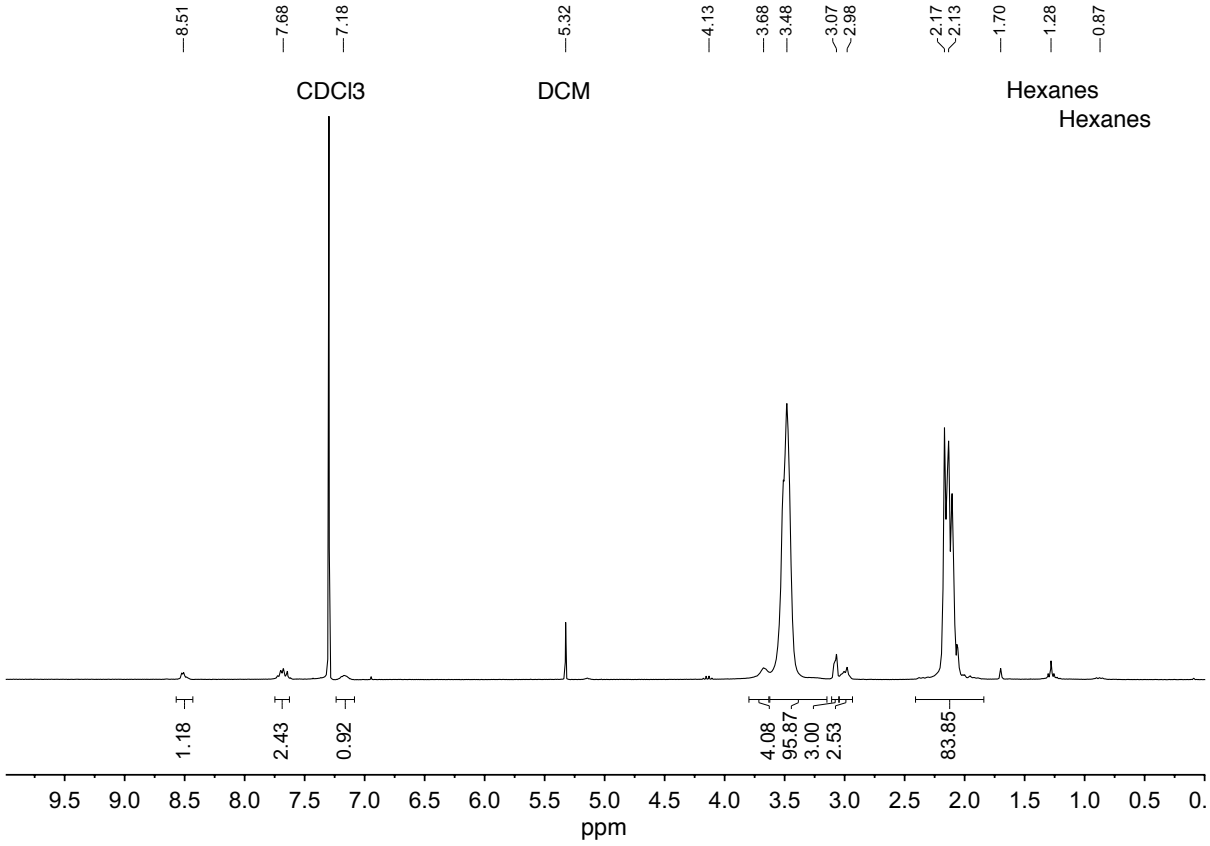

^{1}H NMR (500 MHz, $CDCl_3$) of copolymer **4.4** P(MeOx)$_{27}$-*t*-SS-Pyr. Note: block lengths determined per MALDI-TOF analysis.

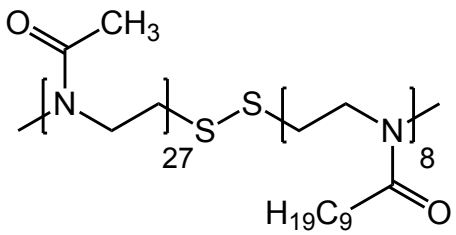

P(MeOx)$_{27}$-SS-P(NonOx)$_8$ (**4.5**)

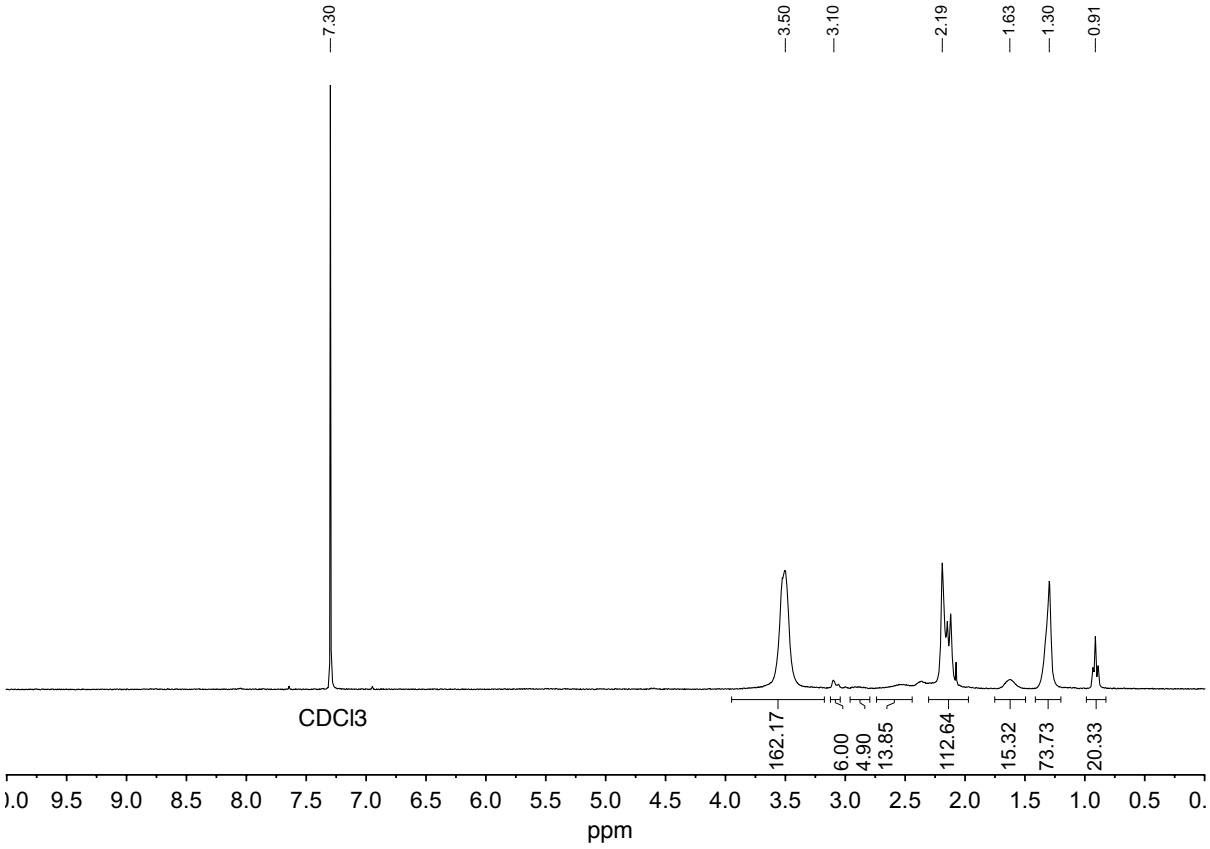

^{1}H NMR (500 MHz, $CDCl_3$) of copolymer **4.5** P(MeOx)$_{27}$-SS-P(NonOx)$_8$. Note: block lengths determined per MALDI-TOF analysis.

4.10 MALDI-TOF Analysis Relevant to Chapter Four

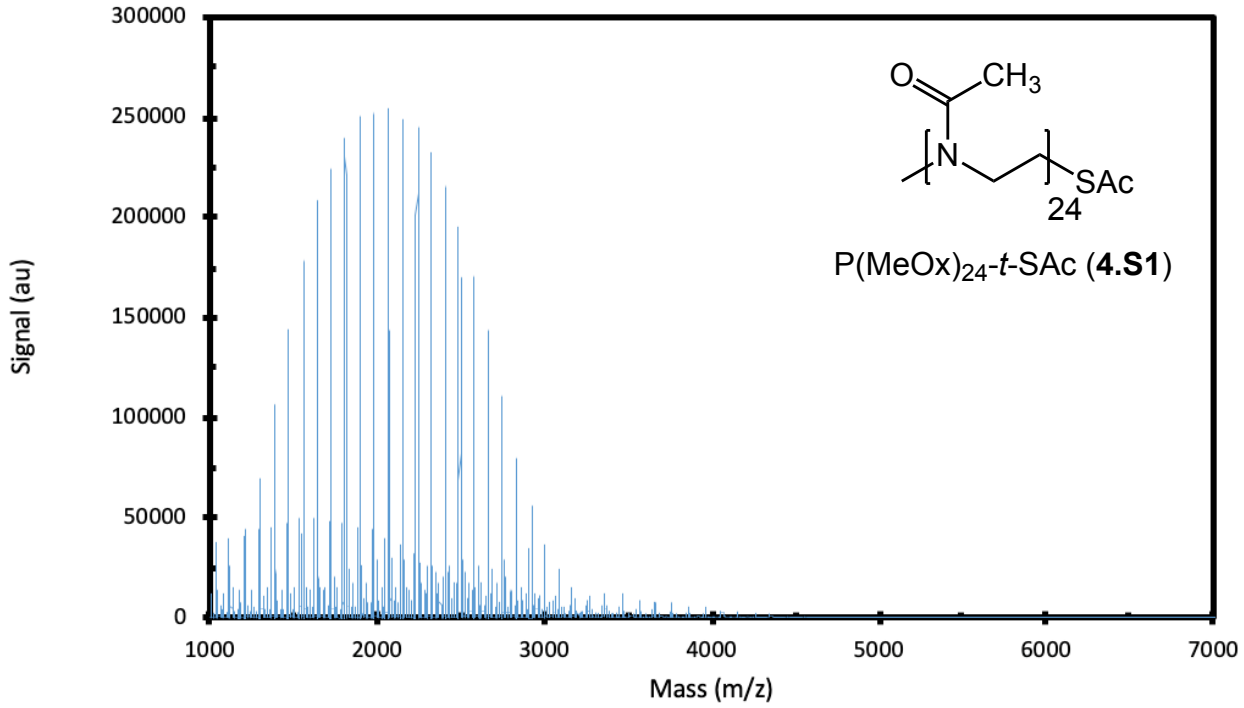

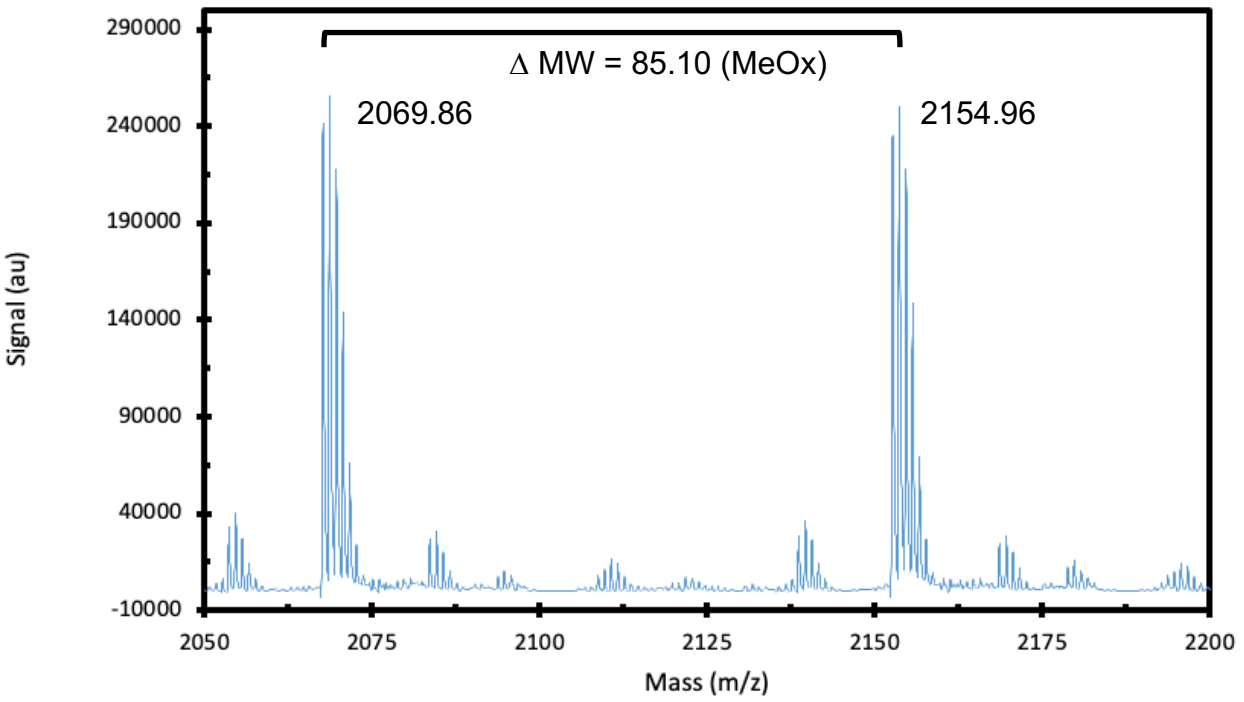

MALDI-TOF mass spectra obtained of P(MeOx)$_{24}$-*t*-SAc (**4.S1**). Mass values corroborate Na+ ionization and end-group termination with thioacetate. Calculated for P(MeOx)$_{24}$-*t*-SAc $[M+Na]^+$: 2155.4; found: 2155.0. Calculated polymer properties from 1000 to 3500 Da, M_n = 2241 Da, M_w = 2111 Da, $Đ$ = 1.06.

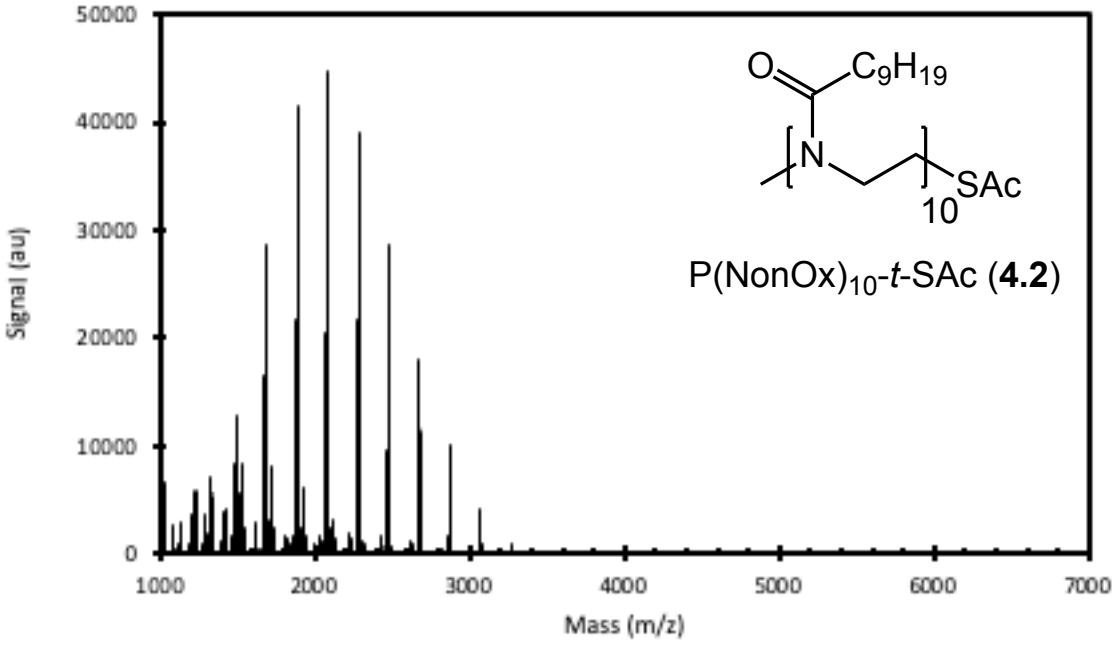

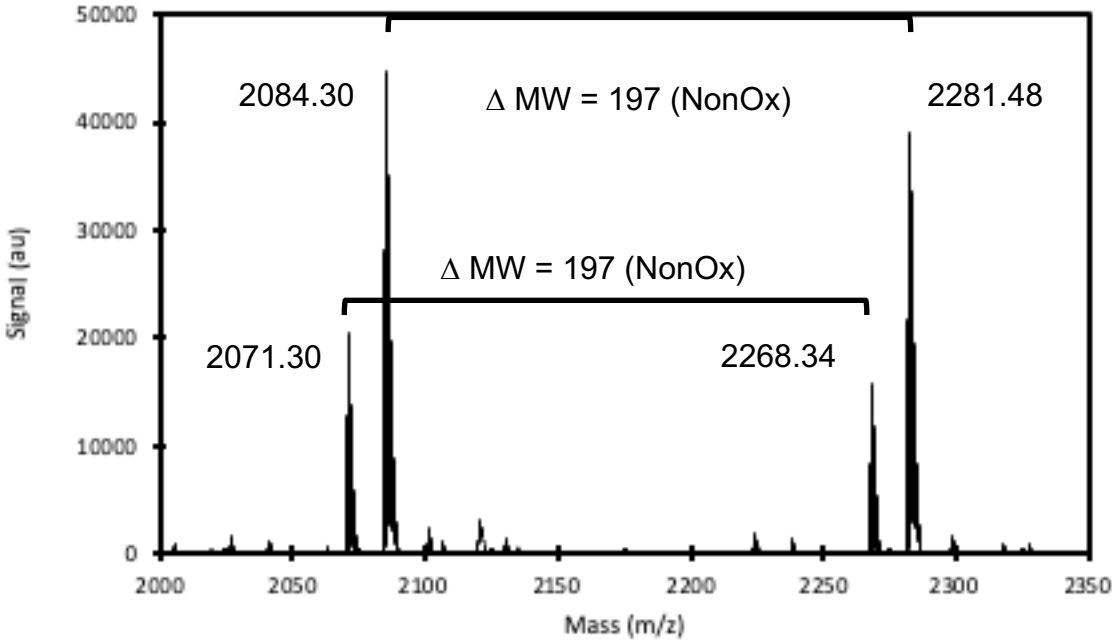

MALDI-TOF mass spectra obtained of P(NonOx)$_{10}$-*t*-SAc (**4.2**). Mass values corroborate Na+ ionization. Calculated for P(NonOx)$_{10}$-*t*-SAc $[M+Na]^+$: 2084.80; found: 2084.30. Observed side products likely associated with H+ initiation from tosylic acid impurities[42]: H-P(NonOx)$_{10}$-*t*-SAc $[M+Na]^+$: 2070.78; found: 2071.30. Calculated polymer properties from 1000 to 3500 Da, M_n = 2142 Da, M_w = 2372 Da, $Đ$ = 1.11.

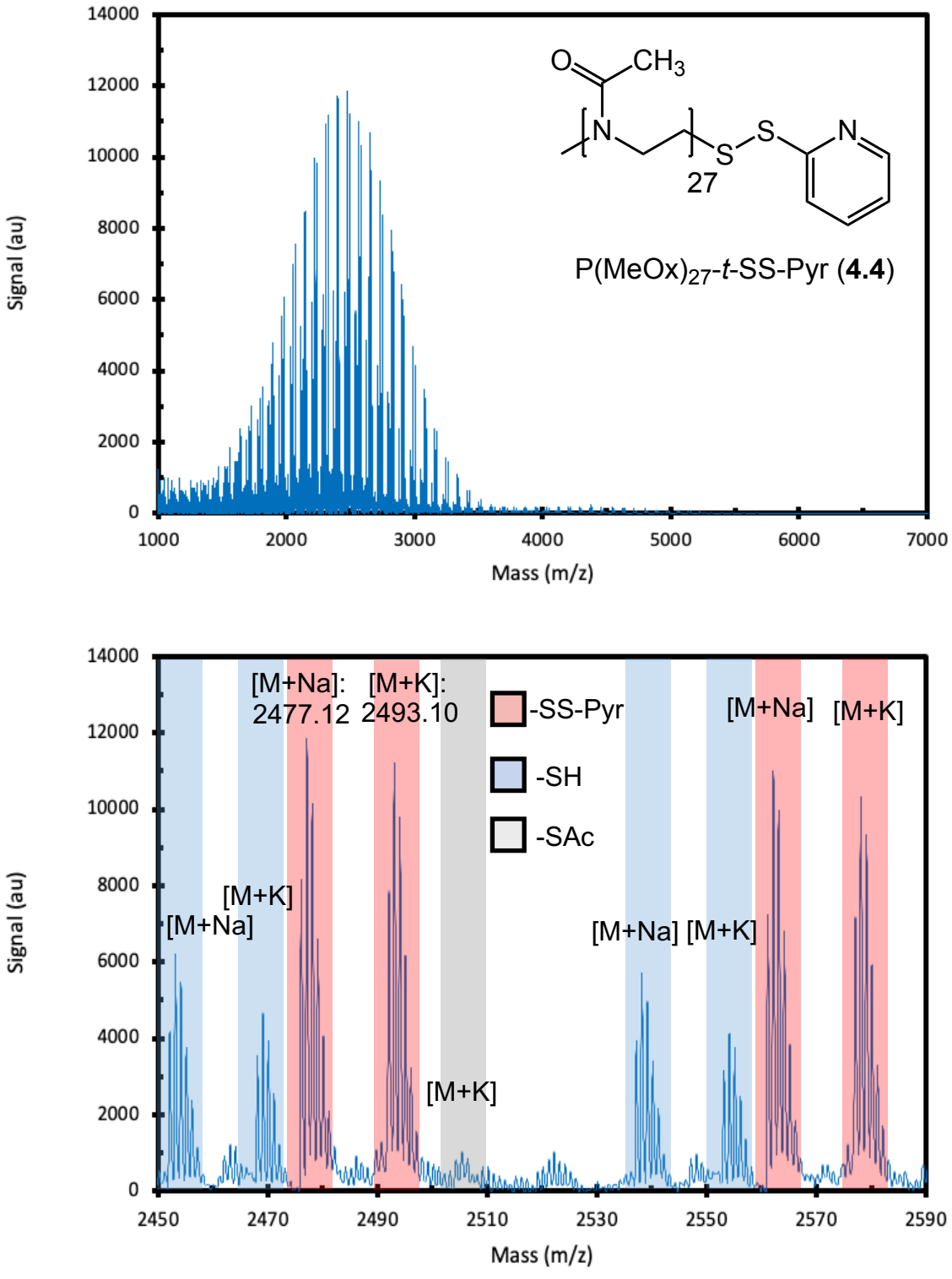

MALDI-TOF mass spectra obtained of P(MeOx)$_{27}$-*t*-SS-Pyr (**4.4**). Mass values corroborate Na+/K+ ionization and post-polymerization functionalization with pyridyl disulfide. Aminolysis

deprotection is quantitative, though residual P(MeOx)$_n$-*t*-SH is observed. Ionization for both Na+ and K+ and adducts are observed for each species. Calculated for MeOx$_{27}$-*t*-SS-Pyr $[M+Na]^+$: 2477.69; found: 2477.12. Calculated polymer properties from 1000 to 4000 Da, M_n = 2411 Da, M_w = 2284 Da, $Đ$ = 1.06.

4.11 Flow Cytometry Relevant to Chapter Four

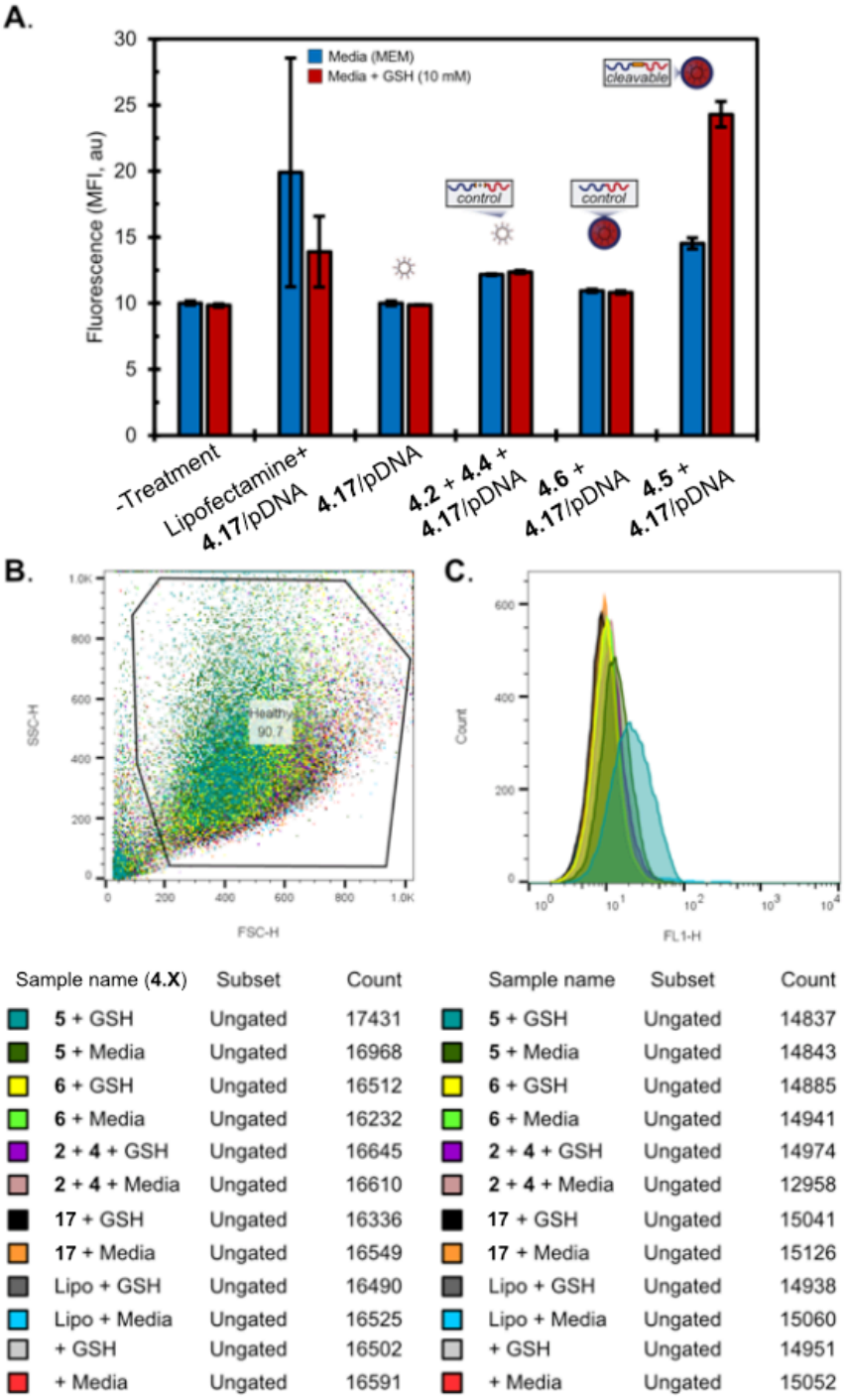

Sample name (**4.X**)	Subset	Count
5 + GSH	Ungated	17431
5 + Media	Ungated	16968
6 + GSH	Ungated	16512
6 + Media	Ungated	16232
2 + **4** + GSH	Ungated	16645
2 + **4** + Media	Ungated	16610
17 + GSH	Ungated	16336
17 + Media	Ungated	16549
Lipo + GSH	Ungated	16490
Lipo + Media	Ungated	16525
+ GSH	Ungated	16502
+ Media	Ungated	16591

Sample name	Subset	Count
5 + GSH	Ungated	14837
5 + Media	Ungated	14843
6 + GSH	Ungated	14885
6 + Media	Ungated	14941
2 + **4** + GSH	Ungated	14974
2 + **4** + Media	Ungated	12958
17 + GSH	Ungated	15041
17 + Media	Ungated	15126
Lipo + GSH	Ungated	14938
Lipo + Media	Ungated	15060
+ GSH	Ungated	14951
+ Media	Ungated	15052

First replicate of HEK-293 cells incubated with PFD/PFTPA/4.17**/pDNA nanoemulsions in presence of multiple cellular treatments.**

Emulsions were formed as described in Figure 4.24A. Polymers **4.5** or **4.6** were used for responsive and control emulsions, respectively. Polymers **4.2** and **4.4** were used together as controls along with free DNA delivered in media. Emulsions were then centrifuged (5.6 x *g*, 3 min), supernatant was discarded and emulsions were resuspended in PBS (200 μL). 100,000 HEK293 cells (ATCC: CRL-1573) were plated in 96 well plate (Fisher, cat# FB012928), and allowed to adhere overnight. Complete media (MEM +10% FBS +1% PS, Gibco cat# 11095080) was removed and replaced with media + emulsions. Positive control (lipofectamine) followed Invitrogen's Lipofectamine® 2000 DNA Transfection Reagent Protocol. The cells were incubated with treatment for 3 hours at 37 °C and then washed gently to remove treatment. Media or GSH (10 mM) was added back and cells were incubated overnight at 37 ˚C. The next day, cells were lifted via trypsonization, washed via centrifugation (526 x *g*, 3 min) and resuspended in 200 μL FACS buffer (PBS, 1% FBS). The cells were analyzed for GFP (FL-1) fluorescence via flow cytometry.

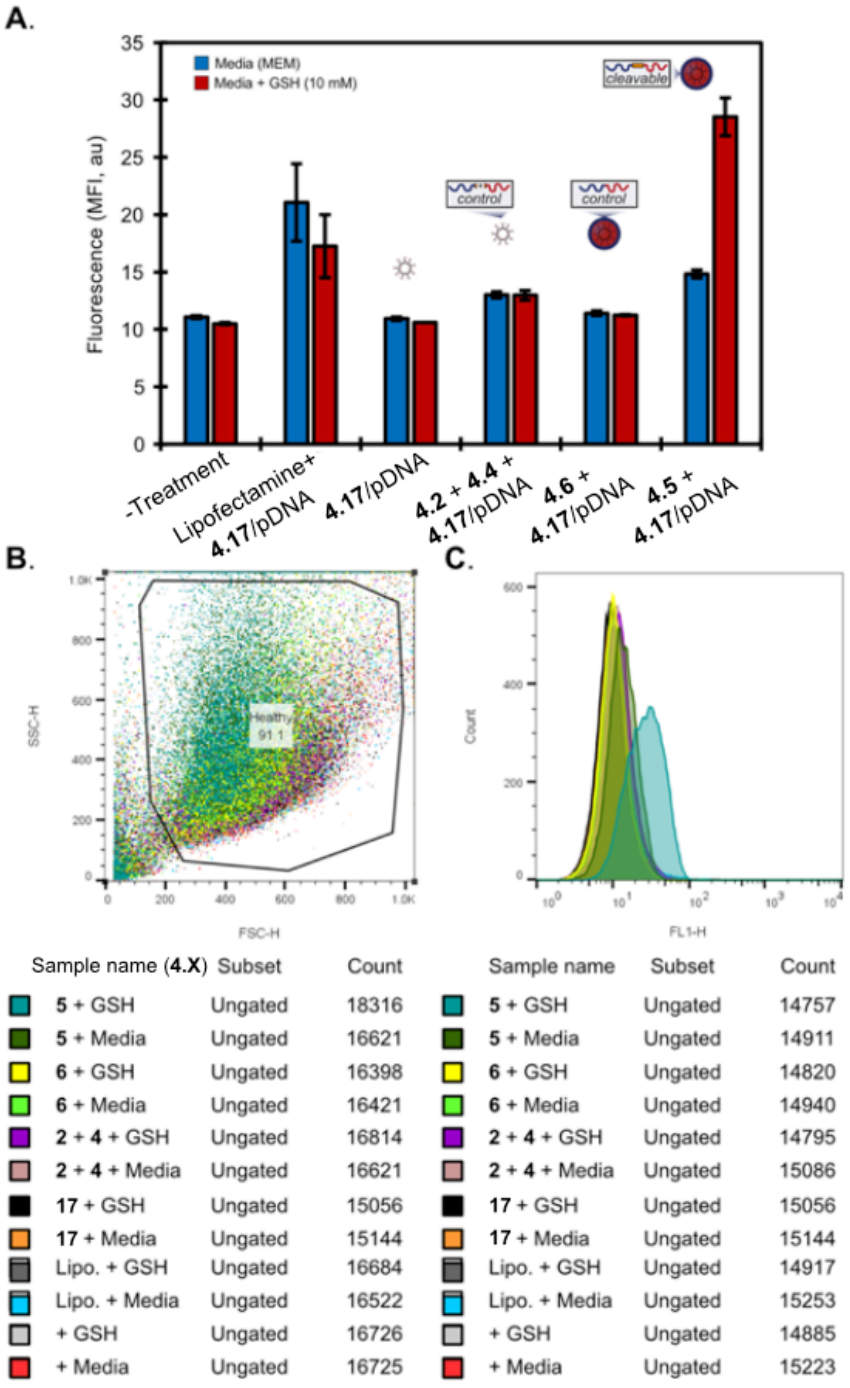

Sample name (4.X)	Subset	Count
5 + GSH	Ungated	18316
5 + Media	Ungated	16621
6 + GSH	Ungated	16398
6 + Media	Ungated	16421
2 + **4** + GSH	Ungated	16814
2 + **4** + Media	Ungated	16621
17 + GSH	Ungated	15056
17 + Media	Ungated	15144
Lipo. + GSH	Ungated	16684
Lipo. + Media	Ungated	16522
+ GSH	Ungated	16726
+ Media	Ungated	16725

Sample name	Subset	Count
5 + GSH	Ungated	14757
5 + Media	Ungated	14911
6 + GSH	Ungated	14820
6 + Media	Ungated	14940
2 + **4** + GSH	Ungated	14795
2 + **4** + Media	Ungated	15086
17 + GSH	Ungated	15056
17 + Media	Ungated	15144
Lipo. + GSH	Ungated	14917
Lipo. + Media	Ungated	15253
+ GSH	Ungated	14885
+ Media	Ungated	15223

Second replicate of HEK-293 cells incubated with PFD/PFTPA/4.17**/pDNA nanoemulsions in presence of multiple cellular treatments.**

Emulsions were formed as described in Figure 4.24A. Polymers **4.5** or **4.6** were used for responsive and control emulsions, respectively. Polymers **4.2** and **4.4** were used together as controls along

with free DNA delivered in media. Emulsions were then centrifuged (5.6 x *g*, 3 min), supernatant was discarded and emulsions were resuspended in PBS (200 μL). 100,000 HEK293 cells (ATCC: CRL-1573) were plated in 96 well plate (Fisher, cat# FB012928), and allowed to adhere overnight. Complete media (MEM +10% FBS +1% PS, Gibco cat# 11095080) was removed and replaced with media + emulsions. Positive control (lipofectamine) followed Invitrogen's Lipofectamine® 2000 DNA Transfection Reagent Protocol. The cells were incubated with treatment for 3 hours at 37 °C and then washed gently to remove treatment. Media or GSH (10 mM) was added back and cells were incubated overnight at 37 ˚C. The next day, cells were lifted via trypsonization, washed via centrifugation (526 x *g*, 3 min) and resuspended in 200 μL FACS buffer (PBS, 1% FBS). The cells were analyzed for GFP (FL-1) fluorescence via flow cytometry.

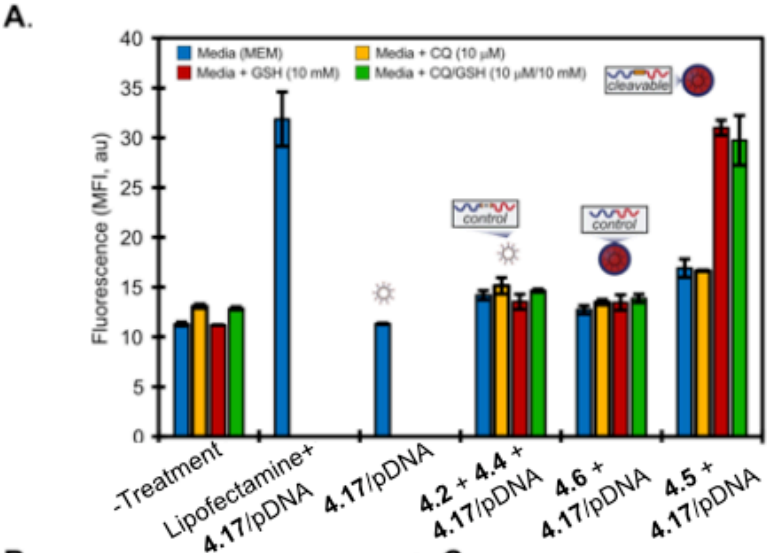

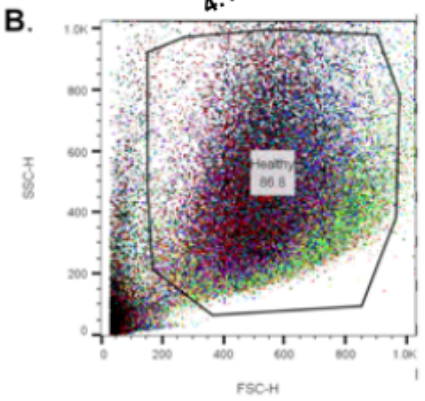

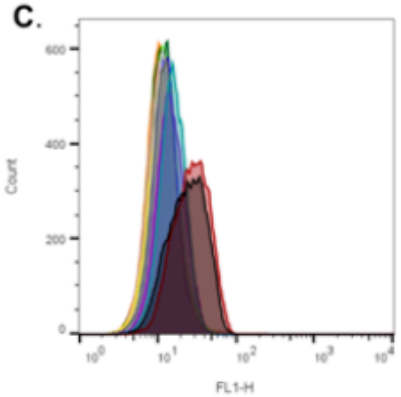

Sample name (**4.X**)	Subset	Count
6 + CQ/GSH	Ungated	21927
6 + GSH	Ungated	20278
6 + CQ	Ungated	18359
6 + Media	Ungated	17329
5 + CQ/GSH	Ungated	17137
5 + GSH	Ungated	16829
5 + CQ	Ungated	17586
5 + Media	Ungated	17020
2 + **4** + CQ/GSH	Ungated	17089
2 + **4** + GSH	Ungated	17287
2 + **4** + CQ	Ungated	17808
2 + **4** + Media	Ungated	17021
17 /pDNA	Ungated	17198
Lipo	Ungated	16944
+ CQ / GSH	Ungated	17059
+ GSH	Ungated	16900
+ CQ	Ungated	17736
+ Media	Ungated	16995

Sample name (**4.X**)	Subset	Count
6 + CQ/GSH	Ungated	14240
6 + GSH	Ungated	14571
6 + CQ	Ungated	14790
6 + Media	Ungated	14645
5 + CQ/GSH	Ungated	14642
5 + GSH	Ungated	14746
5 + CQ	Ungated	14784
5 + Me(**17**	Ungated	14723
2 + **4** + **17**l/GSH	Ungated	14729
2 + **4** + GSH	Ungated	14658
2 + **4** + CQ	Ungated	14776
2 + **4** + Media	Ungated	14730
17 /pDNA	Ungated	14767
Lipo	Ungated	14815
+ CQ / GSH	Ungated	14753
+ GSH	Ungated	14780
+ CQ	Ungated	14746
+ Media	Ungated	14752

Third replicate of HEK-293 cells incubated with PFD/PFTPA/4.17**/pDNA nanoemulsions and use of multiple cellular treatments, including chloroquine.**

Emulsions were formed as described in Figure 4.24A. Polymers **4.5** or **4.6** were used for responsive and control emulsions, respectively. Polymers **4.2** and **4.4** were used together as controls along with free DNA delivered in media. Emulsions were then centrifuged (5.6 x *g*, 3 min), supernatant was discarded and emulsions were resuspended in PBS (200 μL). 200,000 HEK293 cells (ATCC: CRL-1573) were plated in 96 well plate (Fisher, cat# FB012928), and allowed to adhere overnight. Complete media (MEM +10% FBS +1% PS, Gibco cat# 11095080) was removed and replaced with two treatments at a total volume of 200 μL: (i) media + emulsions, (ii) media + emulsions + chloroquine (CQ, 50 μM. Positive control (lipofectamine) followed Invitrogen's Lipofectamine® 2000 DNA Transfection Reagent Protocol. The cells were incubated with treatment for 3 hours at 37 °C and then washed gently to remove treatment. Media or GSH (10 mM) was added to GSH wells and cells were incubated overnight at 37 ˚C. The next day, cells were lifted via trypsonization, washed via centrifugation (526 x *g*, 3 min) and resuspended in 200 μL FACS buffer (PBS, 1% FBS). The cells were analyzed for GFP (FL-1) fluorescence via flow cytometry.

4.12 References

(1) Collins-Gold, L. C.; Lyons, R. T.; Bartholow, L. C. Parenteral Emulsions for Drug Delivery. *Adv. Drug Deliv. Rev.* **1990**, *5*, 189–208.

(2) Zhong, H.; Chan, G.; Hu, Y.; Hu, H.; Ouyang, D. A Comprehensive Map of FDA-Approved Pharmaceutical Products. *Pharmaceutics* **2018**, *10*, 1.

(3) Chime, S. A.; Kenechukwu, F. C.; Attama, A. A. Nanoemulsions — Advances in Formulation, Characterization and Applications in Drug Delivery. *Appl. Nanotechnol. Drug Deliv.* **2014**.

(4) Pathak, K.; Pattnaik, S.; Swain, K. Application of Nanoemulsions in Drug Delivery. *Nanoemulsions Formul. Appl. Charact.* **2018**, 415–433.

(5) Mason, T. G.; Wilking, J. N.; Meleson, K.; Chang, C. B.; Graves, S. M. Nanoemulsions: Formation, Structure, and Physical Properties. *J. Phys. Condens. Matter* **2006**, *18*, R635–R666.

(6) Nel, A.; Ruoslahti, E.; Meng, H. New Insights into "Permeability" as in the Enhanced Permeability and Retention Effect of Cancer Nanotherapeutics. *ACS Nano* **2017**, *11*, 9567–9569.

(7) Singh, Y.; Meher, J. G.; Raval, K.; Khan, F. A.; Chaurasia, M.; Jain, N. K.; Chourasia, M. K. Nanoemulsion: Concepts, Development and Applications in Drug Delivery. *J. Control. Release* **2017**, *252*, 28–49.

(8) Ganta, S.; Talekar, M.; Singh, A.; Coleman, T. P.; Amiji, M. M. Nanoemulsions in Translational Research - Opportunities and Challenges in Targeted Cancer Therapy. *AAPS PharmSciTech* **2014**, *15*, 694–708.

(9) Rapoport, N. Phase-Shift, Stimuli-Responsive Perfluorocarbon Nanodroplets for Drug

Delivery to Cancer. *Wiley Interdiscip. Rev. Nanomedicine Nanobiotechnology* **2012**, *4*, 492–510.

(10) Kripfgans, O. D.; Fowlkes, J. B.; Miller, D. L.; Eldevik, O. P.; Carson, P. L. Acoustic Droplet Vaporization for Therapeutic and Diagnostic Applications. *Ultrasound Med. Biol.* **2000**, *26*, 1177–1189.

(11) Rapoport, N.; Gao, Z.; Kennedy, A. Multifunctional Nanoparticles for Combining Ultrasonic Tumor Imaging and Targeted Chemotherapy. *J. Natl. Cancer Inst.* **2007**, *99*, 1095–1106.

(12) Winter, P. M.; Cai, K.; Caruthers, S. D.; Wickline, S. A.; Lanza, G. M. Emerging Nanomedicine Opportunities with Perfluorocarbon Nanoparticles. *Expert Rev. Med. Devices* **2007**, *4*, 137–145.

(13) Sletten, E. M.; Swager, T. M. Fluorofluorophores: Fluorescent Fluorous Chemical Tools Spanning the Visible Spectrum. *J. Am. Chem. Soc.* **2014**, *136*, 13574–13577.

(14) Lim, I.; Vian, A.; Van De Wouw, H. L.; Day, R. A.; Gomez, C.; Liu, Y.; Rheingold, A. L.; Campàs, O.; Sletten, E. M. Fluorous Soluble Cyanine Dyes for Visualizing Perfluorocarbons in Living Systems. *J. Am. Chem. Soc.* **2020**, *142*, 16072–16081.

(15) Riess, J. G. Understanding the Fundamentals of Perfluorocarbons and Perfluorocarbon Emulsions Relevant to in Vivo Oxygen Delivery. *Artif. Cells. Blood Substit. Immobil. Biotechnol.* **2005**, *33*, 47–63.

(16) Miller, M. A.; Day, R. A.; Estabrook, D. A.; Sletten, E. M. A Reduction-Sensitive Fluorous Fluorogenic Coumarin. *Synlett* **2020**, *31*, 450–454.

(17) Day, R. A.; Estabrook, D. A.; Logan, J. K.; Sletten, E. M. Fluorous Photosensitizers Enhance Photodynamic Therapy with Perfluorocarbon Nanoemulsions. *Chem. Commun.*

2017, *53*, 13043–13046.

(18) Estabrook, D. A.; Ennis, A. F.; Day, R. A.; Sletten, E. M. Controlling Nanoemulsion Surface Chemistry with Poly(2-Oxazoline) Amphiphiles. *Chem. Sci.* **2019**, *10*, 3994–4003.

(19) Day, R. A.; Estabrook, D. A.; Wu, C.; Chapman, J. O.; Togle, A. J.; Sletten, E. M. Systematic Study of Perfluorocarbon Nanoemulsions Stabilized by Polymer Amphiphiles. *ACS Appl. Mater. Interfaces* **2020**, *12*, 38887–38898.

(20) Sloand, J. N.; Nguyen, T. T.; Zinck, S. A.; Cook, E. C.; Zimudzi, T. J.; Showalter, S. A.; Glick, A. B.; Simon, J. C.; Medina, S. H. Ultrasound-Guided Cytosolic Protein Delivery via Transient Fluorous Masks. *ACS Nano* **2020**, *14*, 4061–4073.

(21) Fujii, S.; Cai, Y.; Weaver, J. V. M.; Armes, S. P. Syntheses of Shell Cross-Linked Micelles Using Acidic ABC Triblock Copolymers and Their Application as PH-Responsive Particulate Emulsifiers. *J. Am. Chem. Soc.* **2005**, *127*, 7304–7305.

(22) Tu, F.; Lee, D. Shape-Changing and Amphiphilicity-Reversing Janus Particles with PH-Responsive Surfactant Properties. *J. Am. Chem. Soc.* **2014**, *136*, 9999–10006.

(23) Liu, K.; Jiang, J.; Cui, Z.; Binks, B. P. PH-Responsive Pickering Emulsions Stabilized by Silica Nanoparticles in Combination with a Conventional Zwitterionic Surfactant. *Langmuir* **2017**, *33*, 2296–2305.

(24) Binks, B. P.; Rodrigues, J. A. Inversion of Emulsions Stabilized Solely by Ionizable Nanoparticles. *Angew. Chem. Int. Ed.* **2005**, *44*, 441–444.

(25) Liu, Y.; Jessop, P. G.; Cunningham, M.; Eckert, C. A.; Liotta, C. L. Switchable Surfactants. *Science* **2006**, *313*, 958–960.

(26) Jiang, J.; Zhu, Y.; Cui, Z.; Binks, B. P. Switchable Pickering Emulsions Stabilized by

Silica Nanoparticles Hydrophobized in Situ with a Switchable Surfactant. *Angew. Chem. Int. Ed.* **2013**, *52*, 12373–12376.

(27) Binks, B. P.; Murakami, R.; Armes, S. P.; Fujii, S. Temperature-Induced Inversion of Nanoparticle-Stabilized Emulsions. *Angew. Chem. Int. Ed.* **2005**, *44*, 4795–4798.

(28) Wiese, S.; Spiess, A. C.; Richtering, W. Microgel-Stabilized Smart Emulsions for Biocatalysis. *Angew. Chem. Int. Ed.* **2013**, *52*, 576–579.

(29) Kong, W.; Guo, S.; Wu, S.; Liu, X.; Zhang, Y. Redox-Controllable Interfacial Properties of Zwitterionic Surfactant Featuring Selenium Atoms. *Langmuir* **2016**, *32*, 9846–9853.

(30) Sivakumar, S.; Bansal, V.; Cortez, C.; Chong, S. F.; Zelikin, A. N.; Caruso, F. Degradable, Surfactant-Free, Monodisperse Polymer-Encapsulated Emulsions as Anticancer Drug Carriers. *Adv. Mater.* **2009**, *21*, 1820–1824.

(31) Aydogan, N.; Abbott, N. L. Comparison of the Surface Activity and Bulk Aggregation of Ferrocenyl Surfactants with Cationic and Anionic Headgroups. *Langmuir* **2001**, *17*, 5703–5706.

(32) Tsuchiya, K.; Orihara, Y.; Kondo, Y.; Yoshino, N.; Ohkubo, T.; Sakai, H.; Abet, M. Control of Viscoelasticity Using Redox Reaction. *J. Am. Chem. Soc.* **2004**, *126*, 12282–12283.

(33) Zhang, Y.; Chen, H.; Liu, X.; Zhang, Y.; Fang, Y.; Qin, Z. Effective and Reversible Switching of Emulsions by an Acid/Base-Mediated Redox Reaction. *Langmuir* **2016**, *32*, 13728–13735.

(34) Jong, L. I.; Abbott, N. L. Chemodegradable Surfactant System Based on Oxidation of Disulfide Bonds Using Hypochlorite. *Langmuir* **2000**, *16*, 5553–5561.

(35) Deng, Z.; Yuan, S.; Xu, R. X.; Liang, H.; Liu, S. Reduction-Triggered Transformation of

Disulfide-Containing Micelles at Chemically Tunable Rates. *Angew. Chem. Int. Ed.* **2018**, *57*, 8896–8900.

(36) Hsiue, G. H.; Chiang, H. Z.; Wang, C. H.; Juang, T. M. Nonviral Gene Carriers Based on Diblock Copolymers of Poly(2-Ethyl-2- Oxazoline) and Linear Polyethylenimine. *Bioconjug. Chem.* **2006**, *17*, 781–786.

(37) Hoogenboom, R.; Wiesbrock, F.; Huang, H.; Leenen, M. A. M.; Thijs, H. M. L.; Van Nispen, S. F. G. M.; Van Der Loop, M.; Fustin, C. A.; Jonas, A. M.; Gohy, J. F.; et al. Microwave-Assisted Cationic Ring-Opening Polymerization of 2-Oxazolines: A Powerful Method for the Synthesis of Amphiphilic Triblock Copolymers. *Macromolecules* **2006**, *39*, 4719–4725.

(38) Velluto, D.; Thomas, S. N.; Simeoni, E.; Swartz, M. A.; Hubbell, J. A. PEG-b-PPS-b-PEI Micelles and PEG-b-PPS/PEG-b-PPS-b-PEI Mixed Micelles as Non-Viral Vectors for Plasmid DNA: Tumor Immunotoxicity in B16F10 Melanoma. *Biomaterials* **2011**, *32*, 9839–9847.

(39) We attributed slight changes in size to be a result of minor $P(MeOx)_n$ impurities within **4.5** that reduced surfactant loading.

(40) Cheng, R.; Feng, F.; Meng, F.; Deng, C.; Feijen, J.; Zhong, Z. Glutathione-Responsive Nano-Vehicles as a Promising Platform for Targeted Intracellular Drug and Gene Delivery. *J. Control. Release* **2011**, *152*, 2–12.

(41) A similar observation was previously noted in the redox reaction of Selenium-containing surfactants with H_2O_2, described as "generally time-consuming… [partially due to the] hydrophobic environment where Selenium atoms are located, which is unfavorable for coming into contact with hydrophilic H_2O_2."[29]

(42) Moreadith, R. W.; Viegas, T. X.; Bentley, M. D.; Harris, J. M.; Fang, Z.; Yoon, K.; Dizman, B.; Weimer, R.; Rae, B. P.; Li, X.; *et al.* Clinical Development of a Poly(2-Oxazoline) (POZ) Polymer Therapeutic for the Treatment of Parkinson's Disease – Proof of Concept of POZ as a Versatile Polymer Platform for Drug Development in Multiple Therapeutic Indications. *Eur. Polym. J.* **2017**, *88*, 524–552.

(43) Miller, M. A.; Sletten, E. M. A General Approach to Biocompatible Branched Fluorous Tags for Increased Solubility in Perfluorocarbon Solvents. *Org. Lett.* **2018**, *20*, 6850–6854.

(44) Chen, Y.; Chen, Z. Fluorescein-Core Piperazine as a Fluorescent Labeling Reagent for Highly Sensitive Determination of Jasmonic Acid by High-Performance Liquid Chromatography. *Anal. Methods* **2013**, *5*, 1733–1738.

(45) Kamaly, N.; Yameen, B.; Wu, J.; Farokhzad, O. C. Degradable Controlled-Release Polymers and Polymeric Nanoparticles: Mechanisms of Controlling Drug Release. *Chem. Rev.* **2016**, *116*, 2602–2663.

(46) Parlato, M. C.; Jee, J. P.; Teshite, M.; Mecozzi, S. Synthesis, Characterization, and Applications of Hemifluorinated Dibranched Amphiphiles. *J. Org. Chem.* **2011**, *76*, 6584–6591.

(47) Tadros, T. Principles of Emulsion Stabilization with Special Reference to Polymeric Surfactants. *J. Cosmet. Sci.* **2006**, *57*, 153–169.

(48) McClements, D. J.; Rao, J. Food-Grade Nanoemulsions: Formulation, Fabrication, Properties, Performance, Biological Fate, and Potential Toxicity. *Crit. Rev. Food Sci. Nutr.* **2011**, *51*, 285–330.

(49) Aswathanarayan, J. B.; Vittal, R. R. Nanoemulsions and Their Potential Applications in

Food Industry. *Front. Sustain. Food Syst.* **2019**, *3*, 1.

(50) Fowler, S. D.; Greenspan, P. Application of Nile Red, a Fluorescent Hydrophobic Probe, for the Detection of Neutral Lipid Deposits in Tissue Sections: Comparison with Oil Red O. *J. Histochem. Cytochem.* **1985**, *33*, 833–836.

(51) Grigsby, C. L.; Leong, K. W. Balancing Protection and Release of DNA: Tools to Address a Bottleneck of Non-Viral Gene Delivery. *J. R. Soc. Interface* **2010**, *7*.

(52) Teixeira, H. F.; Bruxel, F.; Fraga, M.; Schuh, R. S.; Zorzi, G. K.; Matte, U.; Fattal, E. Cationic Nanoemulsions as Nucleic Acids Delivery Systems. *Int. J. Pharm.* **2017**, *534*, 356–367.

(53) Fraga, M.; Bruxel, F.; Diel, D.; De Carvalho, T. G.; Perez, C. A.; Magalhães-Paniago, R.; Malachias, Â.; Oliveira, M. C.; Matte, U.; Teixeira, H. F. PEGylated Cationic Nanoemulsions Can Efficiently Bind and Transfect PIDUA in a Mucopolysaccharidosis Type i Murine Model. *J. Control. Release* **2015**, *209*, 37–46.

(54) Boswell, P. G.; Bühlmann, P. Fluorous Bulk Membranes for Potentiometric Sensors with Wide Selectivity Ranges: Observation of Exceptionally Strong Ion Pair Formation. *J. Am. Chem. Soc.* **2005**, *127*, 8958–8959.

(55) Krafft, M. P.; Riess, J. G. Per- and Polyfluorinated Substances (PFASs): Environmental Challenges. *Curr. Opin. Colloid Interface Sci.* **2015**, *20*, 192–212.

(56) Ando, S.; Putnam, D.; Pack, D. W.; Langer, R. PLGA Microspheres Containing Plasmid DNA: Preservation of Supercoiled DNA via Cryopreparation and Carbohydrate Stabilization. *J. Pharm. Sci.* **1999**, *88*, 126–130.

(57) Koo, A. N.; Lee, H. J.; Kim, S. E.; Chang, J. H.; Park, C.; Kim, C.; Park, J. H.; Lee, S. C. Disulfide-Cross-Linked PEG-Poly(Amino Acid)s Copolymer Micelles for Glutathione-

Mediated Intracellular Drug Delivery. *Chem. Commun.* **2008**, *48*, 6570–6572.

(58) Tang, L. Y.; Wang, Y. C.; Li, Y.; Du, J. Z.; Wang, J. Shell-Detachable Micelles Based on Disulfide-Linked Block Copolymer as Potential Carrier for Intracellular Drug Delivery. *Bioconjug. Chem.* **2009**, *20*, 1095–1099.

(59) Gao, W.; Chan, J. M.; Farokhzad, O. C. PH-Responsive Nanoparticles for Drug Delivery. *Sci. Exch.* **2009**, *2*, 249–249.

(60) Cheng, Y.; Cheng, H.; Jiang, C.; Qiu, X.; Wang, K.; Huan, W.; Yuan, A.; Wu, J.; Hu, Y. Perfluorocarbon Nanoparticles Enhance Reactive Oxygen Levels and Tumour Growth Inhibition in Photodynamic Therapy. *Nat. Commun.* **2015**, *6*, 1–8.

(61) Pangborn, A. B.; Giardello, M. A.; Grubbs, R. H.; Rosen, R. K.; Timmers, F. J. Safe and Convenient Procedure for Solvent Purification. *Organometallics* **1996**, *15*, 1518–1520.

(62) Wiesbrock, F.; Hoogenboom, R.; Leenen, M.; Van Nispen, S. F. G. M.; Van Der Loop, M.; Abeln, C. H.; Van Den Berg, A. M. J.; Schubert, U. S. Microwave-Assisted Synthesis of a 42-Membered Library of Diblock Copoly(2-Oxazoline)s and Chain-Extended Homo Poly(2-Oxazoline)s and Their Thermal Characterization. *Macromolecules* **2005**, *38*, 7957–7966.

(63) Hoogenboom, R.; Fijten, M. W. M.; Thijs, H. M. L.; Van Lankvelt, B. M.; Schubert, U. S. Microwave-Assisted Synthesis and Properties of a Series of Poly(2-Alkyl-2-Oxazoline)s. *Des. Monomers Polym.* **2005**, *8*, 659–671.

(64) Bauhuber, S.; Liebl, R.; Tomasetti, L.; Rachel, R.; Goepferich, A.; Breunig, M. A Library of Strictly Linear Poly(Ethylene Glycol)-Poly(Ethylene Imine) Diblock Copolymers to Perform Structure-Function Relationship of Non-Viral Gene Carriers. *J. Control. Release* **2012**, *162*, 446–455.

CHAPTER FIVE

Macromolecular crowding as an intracellular stimulus for responsive nanomaterials

Adapted from: "Macromolecular crowding as an intracellular stimulus for responsive nanomaterials", Estabrook, D. A.; Chapman, J. O.; Yen, S.; Campàs, O.; Sletten, E. M.*, *submitted.*

5.1 Abstract

Stimuli-responsive materials are routinely exploited in biological, materials and sensing applications with the goal of triggering a change in structure or morphology at the site of interest. Here, we introduce a new endogenous stimulus—biomacromolecule crowding—which we achieve by leveraging changes in the thermoresponsive properties of polymers upon high concentrations of crowding agents. We prepare poly(2-oxazoline) amphiphiles that exhibit lower critical solution temperatures (LCST) in serum above physiological temperature. We demonstrate that these amphiphiles can either self-assemble into micelles or stabilize oil-in-water nanoemulsions, with both nanostructures demonstrating instability at temperatures above the LCST. We then showcase that the transformations traditionally observed upon heating nanoemulsions can instead be induced at physiological temperatures through the addition of synthetic crowders and albumins, demonstrating that "thermoresponsive" materials can be made "crowding responsive." Importantly, the LCST dependence on crowding can be tuned such that the system is stable to low extracellular concentrations of protein but destabilizes at high intracellular concentrations. Ultimately, we demonstrate that the cytosol is an effective stimulus for nanoemulsions, with

droplet fusion occurring upon injection into cells of zebrafish embryos. With this report, we set the stage for the wide-ranging class of thermoresponsive materials to respond to macromolecule concentration rather than conventional temperature changes.

5.2 Challenges of stimuli-responsive nanomaterials

The interface of materials chemistry and biomedicine has birthed next-generation "smart" materials that incorporate chemical functionalities to selectively respond to environmental changes.[1] A subset of these materials are nanostructures that respond to biological (endogenous) or externally applied (exogenous) stimuli.[2] Common exogenous stimuli include light, heat, ultrasound, magnetic or electric fields and must be applied in a clinical setting. Conversely, endogenous stimuli rely on inherent biological differences at the target tissue (Figure 5.1A). Typical endogenous stimuli are chemical changes (*e.g.,* pH, ionic strength, redox, oxygen concentration or reactive oxygen species) or biomolecular changes (*e.g.,* enzymes). Many materials have been designed to undergo physical changes when encountering specific chemical environments or biomolecules causing swelling, fusion, disassembly/dissociation, sol-gel transitions, uncapping or degradation.[3] The challenge in designing these materials is a balance between sensitivity to stimuli and stability to benchtop and extracellular conditions. For instance, premature cleavage of pH-responsive linkers[4] is a well-documented limitation. Here we take a fundamentally distinct approach to endogenous stimuli and leverage the physical environment of the cell itself as a trigger for responsive vehicles. We accomplish this by creating nanomaterials which respond to the cell's highly crowded environment (Figure 5.1B, D), rather than any particular chemical or enzymatic stimulus.

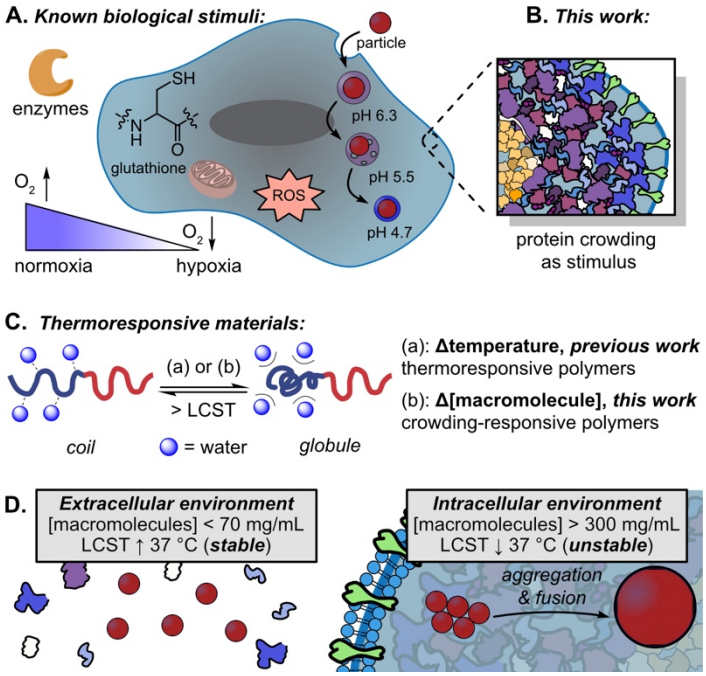

Figure 5.1. Macromolecular crowding as an endogenous stimulus for nanomaterials by leveraging changes in lower critical solution temperature of thermoresponsive polymers. (A) Common chemical and biomolecular intracellular stimuli. (B) Presented herein: intracellular protein concentrations (*e.g.* >300 mg/mL) as a stimulus for "smart" vehicles. (C) Illustration of LCST-containing thermoresponsive materials and response to (a) previous work using conventional heating and (b) this work employing macromolecular crowders. (D) Schematic of the highly crowded environment of the cell inducing nanomaterial fusion.

5.3 Macromolecular crowding as an intracellular stimulus

It has been known for over half a century that the interior of a cell is highly crowded, with the total macromolecular concentration being upwards of 400 mg/mL in eukaryotic cells; by comparison, blood plasma includes approximately 70-80 mg/mL of solutes.[5] This phenomenon is referred to as "macromolecular crowding", since the sum of these macromolecules occupies 20-30% of available volume.[6] Imaging techniques have visualized the spatial heterogeneity of this crowding[7–10] and it has been estimated that the average distance between adjacent proteins is similar to the size of a protein itself (< 10 nm).[11] Studies over the past few decades have increasingly focused on the consequences crowding has on macromolecular interactions, as has

been extensively reviewed by Minton[12], Zimmerman[13], Ellis[6], and Elcock[14]. Macromolecular crowding is primarily an entropically-driven phenomenon which favors transformations such as protein-protein association and compaction that free up space for surrounding crowders. When considering the design of a system that could make use of macromolecular crowding, we looked towards materials with a phase transition governed by entropy–namely, thermoresponsive polymers.[15]

Thermoresponsive polymers exhibit temperature-dependent solubility. The majority of thermoresponsive materials leverage polymers that have a lower critical solution temperature (LCST). The LCST is the point at which a polymer transitions from a hydrated soluble state (coil) to an aggregated insoluble state (globule, Figure 5.1C). The coil-to-globule transition is entropically driven due to the release of hydrogen-bound water. LCST-transitions have been employed to create nanomaterials that respond to exogenous stimuli, most obviously heat but other additional stimuli that can lead to a temperature change such as light, oscillating magnetic field, or high frequency ultrasound.[16] With this report, we demonstrate that the transition from a coil-to-globule state can also be induced by a change in macromolecule concentration and introduce "crowding-responsive materials." (Figure 5.1C). The presence of crowder lowers the LCST of a thermoresponsive polymer allowing for nanomaterials to be generated that have an LCST above physiological temperature outside the cell but below physiological temperature in the highly crowded environment of the cytosol (Figure 5.1D).

5.4 Developing thermoresponsive poly(2-oxazoline)s

The most popular thermoresponsive polymer in the literature is poly(*N*-isopropylacrylamide) (PNIPAM). PNIPAM, with a well-characterized LCST at ~32 °C. PNIPAM has been employed as

the active component of responsive micelles, films, nanoparticles, hydrogels, polymersomes and Pickering emulsions.[15,17] Two fundamental studies using PNIPAM as a protein mimic to analyze protein folding in the cytosol suggested that PNIPAM is crowding responsive, with the LCST decreasing by ~15 degrees in the presence of poly(ethylene glycol).[18,19] However, PNIPAM was not suited for the creation of materials that are triggered by intracellular protein concentrations because its starting LCST was below physiological temperature (37 °C). Additional challenges with PNIPAM include the hysteresis of the coil-to-globule transition[20] and biocompatibility concerns of the polymer and monomer,[21] which have sparked interest in PNIPAM alternatives.[22]

A promising thermoresponsive polymer scaffold distinct from PNIPAM is poly(2-oxazoline)s (POx). POxs are peptidomimetic polymers synthesized via a controlled ring-opening polymerization.[20] Owing to this controlled polymerization, side-chains, copolymer compositions and architectures can be easily modified to influence the resulting polymer properties, including the LCST.[23] Variations in the hydrophilicity of the side-chain can significantly modulate or even eliminate the LCST. For example, homopolymers derived from the extremely hydrophilic 2-methyl-2-oxazoline (MeOx) display no observable LCST (Figure 5.2A), while poly(2-butyl-2-oxazoline)s are insoluble in water at ambient conditions.[23] Between these extremes, derivatives of 2-ethyl-2-oxazoline (EtOx) exhibit LCSTs from 60 to 100 °C depending on molar mass, concentration, and composition of (co)polymers (Figure 5.2A).[20] Due to this modularity, we chose to pursue EtOx-containing polymers such that the LCST in either dilute or crowded environments could be tailored by polymer structure and architecture. We appended the responsive EtOx block to a non-responsive hydrophobic poly(2-nonyl-2-oxazoline) (NonOx) block to create polymer amphiphiles that can self-assemble into micelles[24] or act as surfactants for nanoemulsions[25] allowing access to two common nanomaterial scaffolds.

We synthesized amphiphilic copolymers with the hydrophilic block being derived from nonresponsive MeOx (*i.e.*, $P(MeOx)_{90}$-*b*-$P(NonOx)_{10}$, **5.1**) or thermoresponsive EtOx (*i.e.*, $P(MeOx)_{90}$-*b*-$P(NonOx)_{10}$, **5.2**, Figure 5.2A). Block lengths were designed such that they were consistent between thermoresponsive and control polymers, and were chosen due to a combination of surfactant efficiency[25] and increased hydrophilic block length to ensure water solubility. Next, we established that amphiphiles **5.1** and **5.2** form similar micelle or emulsion nanostructures but undergo distinct transitions upon heating due to the different LCSTs of **5.1** and **5.2** (Figure 5.2B, Figure 5.2C).

5.5 Formulation of temperature-responsive nanomaterials

Micelles of **5.1** or **5.2** (deemed **5.1@micelles** or **5.2@micelles**, respectively) were prepared by directly solubilizing **5.1** or **5.2** in PBS buffer at a concentration of 5 mg/mL and vortexing. Dynamic light scattering indicated **5.1@micelles** and **5.2@micelles** were 24 and 32 nm, respectively (Figure 2D). To analyze the thermoresponsive properties of **5.1@micelles** and **5.2@micelles,** we performed turbidity measurements using UV/Vis analysis. This classic method of characterizing thermoresponsive polymers identifies the LCST by the onset of increasing absorbance during temperature dependent UV/Vis spectroscopy.[26] The absorbance increases as a result of large micelle aggregates forming which scatter UV/Vis light as the polymer becomes insoluble (Figure 2B,F). Here, we defined the LCST as the temperature at which the absorbance at 550 nm begins to increase (≥0.05 au ≈ ≤90% transmittance). In Figure 2F, the **5.2@micelles** show a clear increase in absorbance at 550 nm beginning at 60 °C (blue, dashed line), consistent with previously reported P(EtOx)-based micelles.[27] In contrast, **5.1@micelles** do not display a change

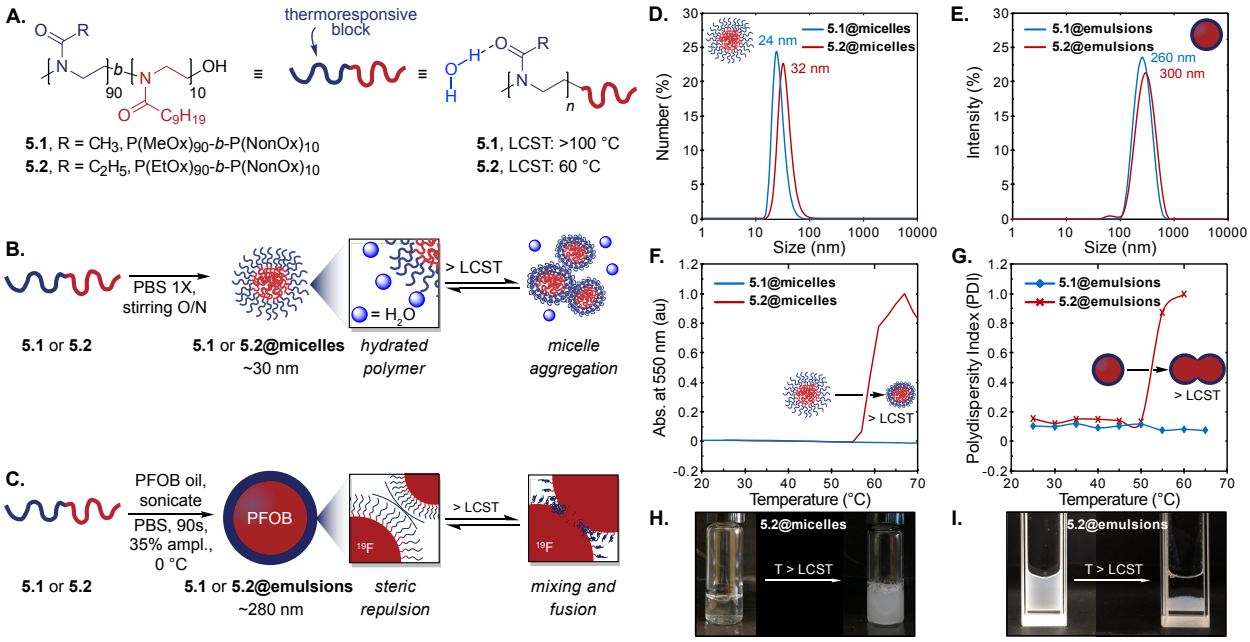

Figure 5.2. Thermoresponsive micelles and emulsions composed of poly(2-oxazoline) amphiphiles. (A) Synthesis of amphiphilic diblock copolymers with nonyl-containing hydrophobic block and either methyl- (**1**) or ethyl-containing (**2**) hydrophilic block. (B/C) The use of polymeric surfactants **5.1** or **5.2** as either (B) micelles or (C) stabilizers for perfluorooctylbromide (PFOB) nanoemulsions and their respective transformations when heated above the LCST. (D/E) Dynamic light scattering analysis of **5.1** (blue) and **5.2** (red)-stabilized (D) micelles and (E) nanoemulsions. Data are an average of three replicate measurements. See Figure 5.3–5.4 for supplementary DLS traces. (F/G) Characterization of LCST transition via (F) absorbance spectra at 550 nm or (G) polydispersity index traces versus temperature for **@micelles** (F) or **@emulsions** (G), respectively. Data are representative of at least three replicate experiments. (H) **5.2@micelles** or (I) **5.2@emulsions** show macroscopic changes above the LCSTs.

in absorbance across 20–70 °C (red, dashed line). The thermoresponsive behavior of **5.2@micelles** is also visually apparent upon heating (Figure 2H). These results indicate that **5.2@micelles** are responsive above physiological temperatures and **5.1@micelles** are a non-responsive control.

Amphiphiles **5.1** and **5.2** are also effective surfactants to stabilize perfluorocarbon (PFC) nanoemulsions. Our interest in PFC nanoemulsions stems from the bioorthogonal, nontoxic fluorous core and the ability to sequester fluorous-soluble payloads within the core of the emulsions, shielding them from the exterior environment and minimizing passive release.[25,28–31] Specifically, we employed the PFC perfluorooctyl bromide (PFOB) due to its previous clinical use

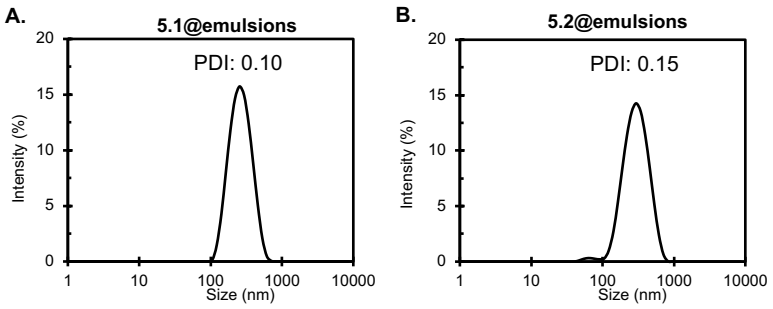

Figure 5.3. Dynamic light scattering analysis of nanoemulsions stabilized by (A) **5.1@emulsions** and (B) **5.2@emulsions**. Data are an average of three replicate measurements.

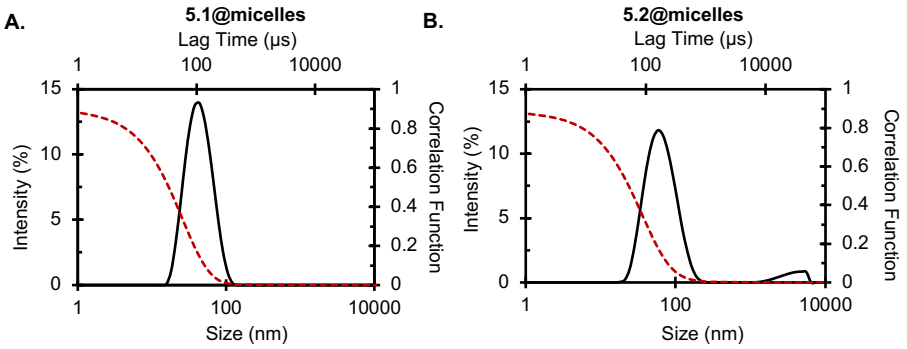

Figure 5.4. Dynamic light scattering analysis of micelles stabilized by (A) **5.1@micelles** and (B) **5.2@micelles**. Data are an average of three replicate measurements.

as a contrast agent and oxygen carrier.[32] We prepared PFOB-in-water nanoemulsions by dissolving **5.1** or **5.2** in PBS to a final surfactant loading of 28 wt%. This solution was then combined with 10 vol% perfluorooctyl bromide (PFOB), and ultrasonication was performed directly at the liquid-liquid interface of the two immiscible solvents to yield **5.1@emulsions** or **5.2@emulsions** (see SI p. S39 for details). DLS analysis indicated **5.1@emulsions** and **5.2@emulsions** were similar in size at 260 and 300 nm, respectively, with polydispersities of 0.10 and 0.15 (Figure 5.2E).

The thermoresponsive properties of nanoemulsions are far less explored compared to micelles. Drawing from previous reports on thermoresponsive macroemulsions,[17,33] we expect nanoemulsion fusion to occur as the LCST is passed. Mechanistically, hydrated P(EtOx)$_{90}$-*b*-

$P(Non)_{10}$ behaves as an amphiphile able to stabilize the liquid-liquid interface and provide steric repulsion between emulsions. When heated above the LCST, the hydrophilicity of the P(EtOx) block decreases significantly, yielding a poor amphiphile and loss of steric shielding. The nanoemulsions then undergo mixing and large-scale fusion due to polymer aggregation (Figure 5.2C).

To analyze the thermoresponsive properties of nanoemulsions, a traditional UV/Vis turbidity assay was not applicable due to the significant light scattering of 300 nm particles. As we expected large changes in the size of the nanoemulsions due to fusion when surpassing the LCST, we envisioned DLS analysis would be effective for determining the LCST transition of nanoemulsions. Similar assays have literature precedent for other thermoresponsive materials.[34] We examined **5.1@emulsion** and **5.2@emulsion** via DLS with temperature control, tracking polydispersity indexes as a measure of particle homogeneity in 5 °C temperature increments (Figure 5.2G). As expected, no temperature-dependent changes were observed for **5.1@emulsions** (blue, solid line). **5.2@emulsions** exhibited significant changes in polydispersity between 51 and 55 °C, suggesting an LCST. Interesting the LCST of **5.2@emulsions** was lower than that of **5.2@micelles** and we attributed this modest decrease to the higher local concentration and restricted mobility of polymer at the oil-water interface compared to solubilized in solution as micelles.[27,35,36] The thermoresponsive behavior of **5.2@emulsions** was also visually evident in a cuvette with phase separation occurring at temperatures above 55 °C after significant nanoemulsion fusion (Figure 5.2I). To further validate emulsion fusion above the LCST, we formulated larger macroemulsions from **5.1** and **5.2** (deemed **5.1@macroemulsions** and **5.2@macroemulsions**, respectively) such that individual droplets could be visualized by light

microscopy. Using an epifluorescence microscope equipped with a heat stage, clear coalescence was observed for **5.2@macroemulsions** when heating from 50 to 65 °C (Figure 5.5).

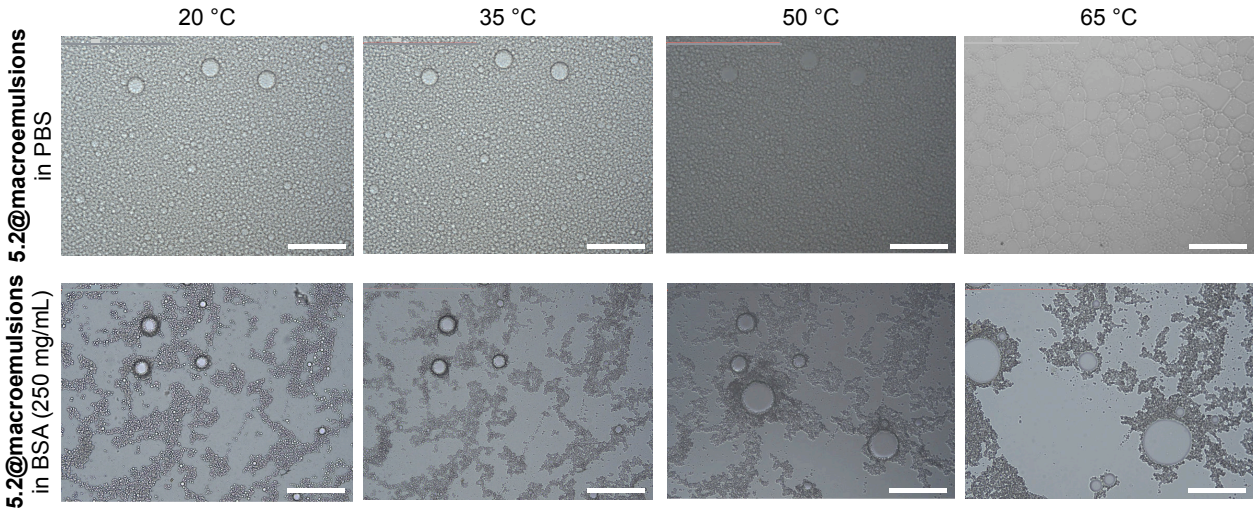

Figure 5.5. Heat-stage microscopy of **5.2@macroemulsions** in either PBS or BSA (250 mg/mL) from 20 to 65 °C. Samples were heated at a ramp of 5 °C/min from 20–65 °C and visualized under a 50X objective. See general macroemulsion formation procedure for further details. Scale bar = 50 μm.

At this point, we had established micelle and nanoemulsion materials which underwent robust aggregation or fusion when surpassing an LCST 15 to 25 °C above physiological temperature. To further deconvolute the contribution of each block and gain insight on how to tune the overall LCST, we synthesized a small library of block copolymers (**5.3**–**5.5**, Figure 5.6). As shown in Figure S6, we found that both reducing the length of the EtOx block from 90 to 30, as well as exchanging the NonOx block with considerably less hydrophobic monomers had little influence on the LCST, either as micelles in solution or when employed as a surfactant for PFOB nanoemulsions. These results indicate that the nature of the hydrophilic block dominates LCST behavior within these vehicles. As such, the LCST of the system can be tuned through the employed hydrophilic monomers.[20,23]

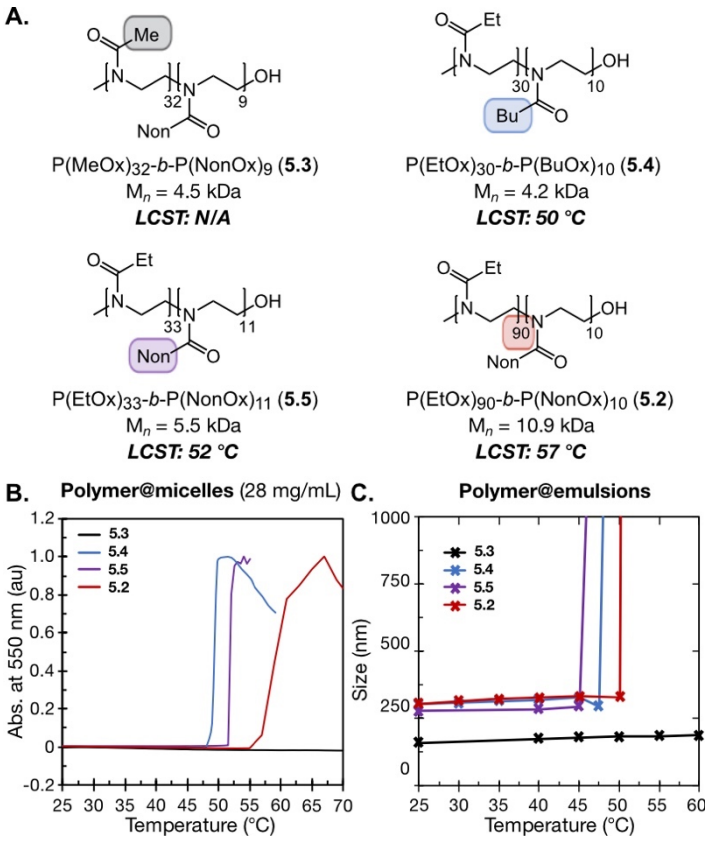

Figure 5.6 (A) Library of supplementary block copolymers (**5.3**-**5.5**), with corresponding block lengths and M_n, as determined by ^{1}H-NMR analysis. Polymer **5.2** is given as reference. (B) LCSTs of each **polymer@micelles** (5 mg/mL **5.3**–**5.5** in PBS) as determined by UV-Vis analysis. LCST is defined as the temperature at which relative absorbance at 550 nm ≥ 0.05 au. (C) LCSTs of **polymer@emulsions** (**5.3**–**5.5** employed as polymeric surfactants for perfluorooctylbromide-in-water nanoemulsions) as determined by DLS. LCST is defined as the temperature at which the nanoemulsions suddenly aggregate, leading to a dramatic increase in the size (>1000 nm).

5.6 Synthetic crowders alter LCST transitions of polymers and nanomaterials

Next, we analyzed the effect of crowding agents on the LCST of **5.2@micelles and 5.2@emulsions**—the critical result necessary for generating nanomaterials that respond to macromolecule concentration (Figure 5.7A, i–iii). Using a panel of synthetic crowding agents commonly employed to mimic an intracellular environment (**3–5,** Figure 5.7A, iv.),[14] we found that crowding agents strongly influenced the LCST. Polymers **3–5** were chosen for initial studies as they facilitate the exploration of crowding effects without the need for concentrated cell extracts

that could have unintended consequences including specific protein-protein interactions and denaturation.[6] Interactions between crowders and the material of interest should be avoided and thus studies with more than one crowding agent with varying monomeric structures, molecular weights, and conformations in aqueous solution are imperative to determine that the observed response is due to crowding.

Crowders PEG-10k (**5.6**), Ficoll-400 (**5.7**), and Dextran-70 (**5.8**) (Figure 5.7A, iv.) were dissolved in PBS (pH 7.4, 1X) at varying concentrations, then **5.2@micelles** were added at a constant concentration (5 mg/mL). The solutions were then analyzed by temperature-controlled UV-Vis. Strikingly, each crowder demonstrated dose-dependent reduction of the LCST of **5.2@micelles** (Figure 5.7B). At 50 mg/mL, we found the sensitivity of **5.2@micelles**' LCST, from highest to lowest, to fall in the following order: Dextran-70 (40.2 ± 0.9 °C), PEG-10k (43.8 ± 0.8 °C), and Ficoll-400 (51.3 ± 0.1 °C). At 200 mg/mL, all synthetic crowders caused **2** to precipitate out at room temperature (~25 °C). By comparison, **5.1@micelles** showed no LCST behavior even when incubated at the highest concentrations of synthetic crowders (250 mg/mL, Figure 5.9), demonstrating that the thermoresponsive block is critical to inducing this phase transition.

Similarly, PFOB nanoemulsions stabilized by thermoresponsive **2** were formed as previously mentioned. These **5.2@emulsions** were then diluted with PBS containing crowding agents (**5.6–5.8**) at varying concentrations (0–250 mg/mL, Figure 5.7C). We observed that the LCST of **5.2** was significantly more responsive to crowding agents when at the PFOB-water interface than when assembled as micelles. Synthetic crowders induced demulsification at physiological temperatures when ≥50 mg/mL crowder was present. We hypothesize that this is due to differences in occupied volume between the micelles and emulsions–namely, that the 300 nm emulsions are larger and

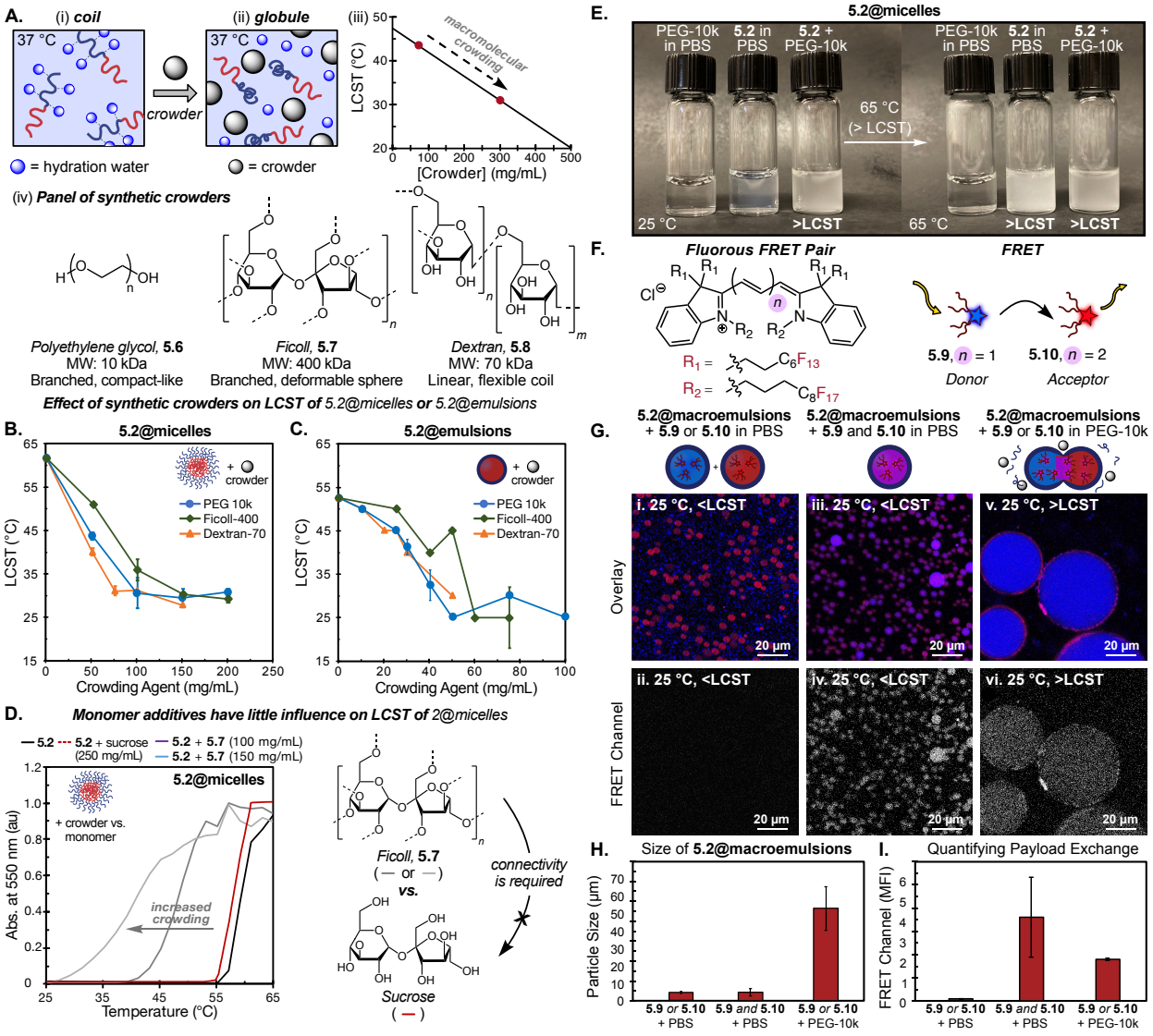

Figure 5.7. Macromolecular crowding is capable of reducing the LCST of thermoresponsive **5.2** in a dose-dependent manner, inducing coil-to-globule transitions at room temperature. (A) Crowding effects were studied through a panel of three synthetic crowders: polyethylene glycol (PEG)-10k (**5.6**), Ficoll-400 (**5.7**) and Dextran-70 (**5.8**). (B) LCST of **5.2@micelles** as a function of PEG 10k (blue), Ficoll-400 (green), and Dextran-70 (orange) concentration. LCST values determined via UV/Vis analysis (see Figure 5.8). Error bars represent the standard deviation between two independent measurements. (C) LCST of **5.2@emulsions** as a function of PEG 10k (blue), Ficoll-400 (green), and Dextran-70 (orange) concentration. LCST values determined via DLS analysis (see Figure 5.10). Error bars represent the standard deviation between two independent measurements. (D) Control experiment for temperature-dependent absorbance traces of **5.2@micelles** in PBS with either (i) no additive (black line), (ii) Ficoll-400 macromolecular crowding agent (100–150 mg/mL, purple and blue lines) or (iii) monomeric sucrose (250 mg/mL, dashed red line). (E) (i) Solutions of PEG-10k (250 mg/mL), **5.2@micelles** (5 mg/mL), or both **5.2@micelles** and PEG-10k (5 and 250 mg/mL, respectively) solubilized in PBS (pH 7.4) and photographed at room temperature and 65 °C. (F) Illustration of FRET transfer between fluorous

cyanine dyes **5.9** and **5.10**. (G) Confocal microscopy of **5.2@macroemulsions** containing **5.9**, **5.10**, or both **5.9** and **5.10**. Solutions were solubilized in either PBS (i–iv) or PEG-10k (v–vi, 250 mg/mL). For i, iii, and v, dyes were independently excited, and channels were overlaid (Blue, **5.9**: Ex. 488 nm, collected 520–620 nm. Red, **5.10**: Ex. 635 nm, collected 700–800 nm). For ii, iv, and vi, FRET was performed (Ex. 488, collected 700–800 nm). (H) Average particle size for each solution as determined by Fiji analysis of (G). Values and error bars are representative of at least twenty droplets for each control sample (i–iv), and all four droplets for the crowded solution (v–vi). (I) Mean fluorescence intensities (MFI) within FRET channel for each solution calculated via Fiji. Values and error bars are representative of at least five droplets.

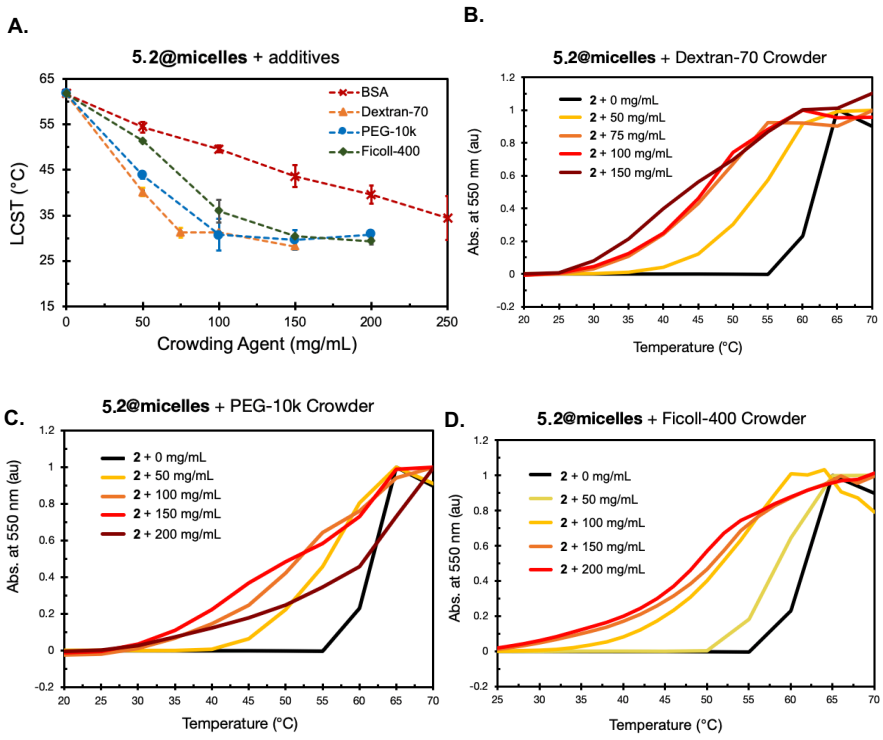

Figure 5.8. Response of **5.2@micelles** to various crowders. A. Compiled data showing the influence of macromolecular crowders on LCST of **5.2@micelles**. Polymer **5.2** (5 mg/mL) was dissolved in PBS (1X, pH 7.4) containing synthetic or biological macromolecular crowding agents (50–250 mg/mL). LCST was defined as the onset of turbidity, *i.e.,* the temperature at which absorbance at 550 nm was ≥0.05 AU. Error bars represent the standard deviation of at least two independent experiments. See B-D for raw UV-Vis traces. (B/C/D) Temperature-dependent absorbance traces at 550 nm of solutions with **5.2@micelles** (5 mg/mL) in PBS (1X, pH 7.4) containing (B) Dextran-70 (**5.8,** 0–150 mg/mL), (C) PEG-10k (**5.6**, 50–200 mg/mL) or (D) Ficoll-400 (**5.7**, 50–200 mg/mL). Data obtained via UV-Vis analysis, analyzed at 550 nm from 25 to 65 °C with 0.1 °C increments, 15 second equilibration between measurements, blanked versus polymer solution at room temperature (~25 °C).

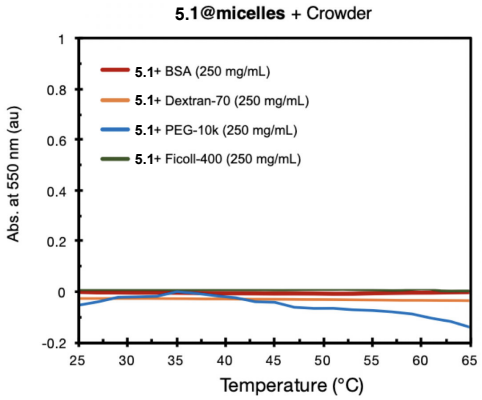

Figure 5.9 Temperature-dependent absorbance traces at 550 nm of solutions with **5.1@micelles** (5 mg/mL) in PBS (1X, pH 7.4) containing macromolecular crowding agents (250 mg/mL). Analyzed at 550 nm from 25 to 65 °C with 0.1 °C increments, 15 second equilibration between measurements, blanked versus polymer solution at room temperature (~25 °C).

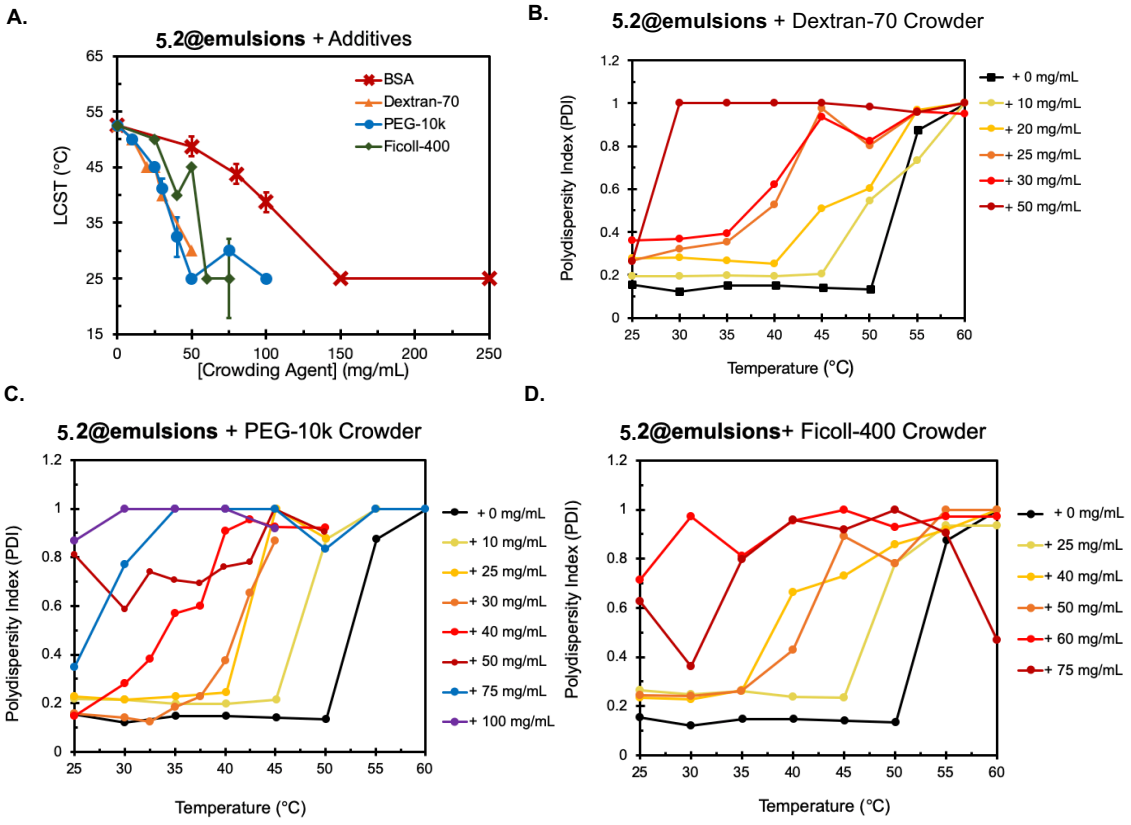

Figure 5.10. Response of **5.2@emulsions** to various crowders. (A) Compiled data showing the influence of macromolecular crowders on LCST of **5.2@emulsions**. Polymer **5.2** (28 mg/mL) was dissolved in PBS (1X, pH 7.4) and pulse sonicated against PFOB (10% vol) for 90 seconds. This solution was diluted in PBS containing synthetic or biological macromolecular crowding agents (50–250 mg/mL) at 10 vol% emulsion solution. LCST was defined as the onset of

heterogeneity/aggregation, as represented by the polydispersity index of the solution ≥0.50. Error bars represent the standard deviation of at least two independent experiments. (B/C/D) Temperature-dependent polydispersity indexes of solutions with **5.2@emulsions** (10 vol%) in PBS (1X, pH 7.4) containing (B) Dextran-70 (0–50 mg/mL), (C) PEG-10k (10–100 mg/mL), or (D) Ficoll-400 (25–75 mg/mL). Data obtained via DLS analysis, analyzed from 25 to 60 °C with 5 °C increments, 120 second equilibration between measurements.

thus more sensitive to crowding than the 30 nm micelles. This rationale agrees with previous work showing that for different colloid-crowder mixtures the excluded volume effects—referring to inaccessible volume occupied by these materials—are influenced by the size of both the colloids and crowder additive.[37,38]

To further corroborate that the observed reduction in LCST was induced by macromolecular crowding rather than specific interactions, control experiments were performed for both micelles and emulsions with monomer subunits (*i.e.,* sucrose, Figure 5.7D), as well as hydrogen bond acceptors (*i.e.,* 18-crown-6) and small molecule viscogens (*i.e.,* ethylene glycol), shown in Figure 5.11.

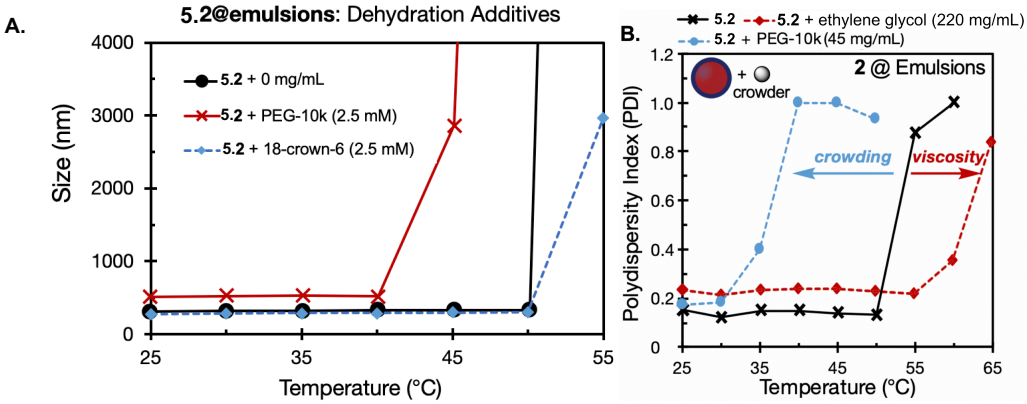

Figure 5.11. 5.2@emulsions in the presence of small molecule additives. (A) Control experiment for size analysis of **5.2@emulsions** in PBS (1X, pH 7.4) containing either (i) no additive (black line), (ii) PEG-10k macromolecular crowder (25 mg/mL, red line) or (iii) equimolar 18-crown-6 (dashed blue line). 18-crown-6 was previously shown to have the same hydration/dehydration features as poly(ethylene glycol) from 10–80 °C.[39] Size analysis was used as solution viscosity did not interfere with size measurements. (B) Control experiment for temperature-dependent fusion of **5.2@emulsions** with either (i) no additive (black line), (ii) PEG-10k macromolecular crowding agent (45 mg/mL, dashed blue line) or (iii) monomeric ethylene glycol (220 mg/mL, dashed red line). Bulk solution viscosities were matched by additive concentration per literature precedent.[40]

The samples were analyzed from 25 to 55 °C with 5 °C increments, 90 second equilibration between measurements.

Excitingly, none of these additives were successful in reducing the LCST of **5.2@micelles** or **5.2@emulsions**, suggesting that the presence of macromolecules is required (Figure 5.7D). Additional controls of increasing polymer concentration (Figure 5.12A), serially diluting emulsion solutions (Figure 5.12B), varying pH (Figure 5.12C), or increasing the salinity of the solution to physiological conditions (137 mM NaCl, 1X PBS, Figure 5.12D) led to minimal changes of the LCST of **5.2@micelles** and **5.2@emulsions.**

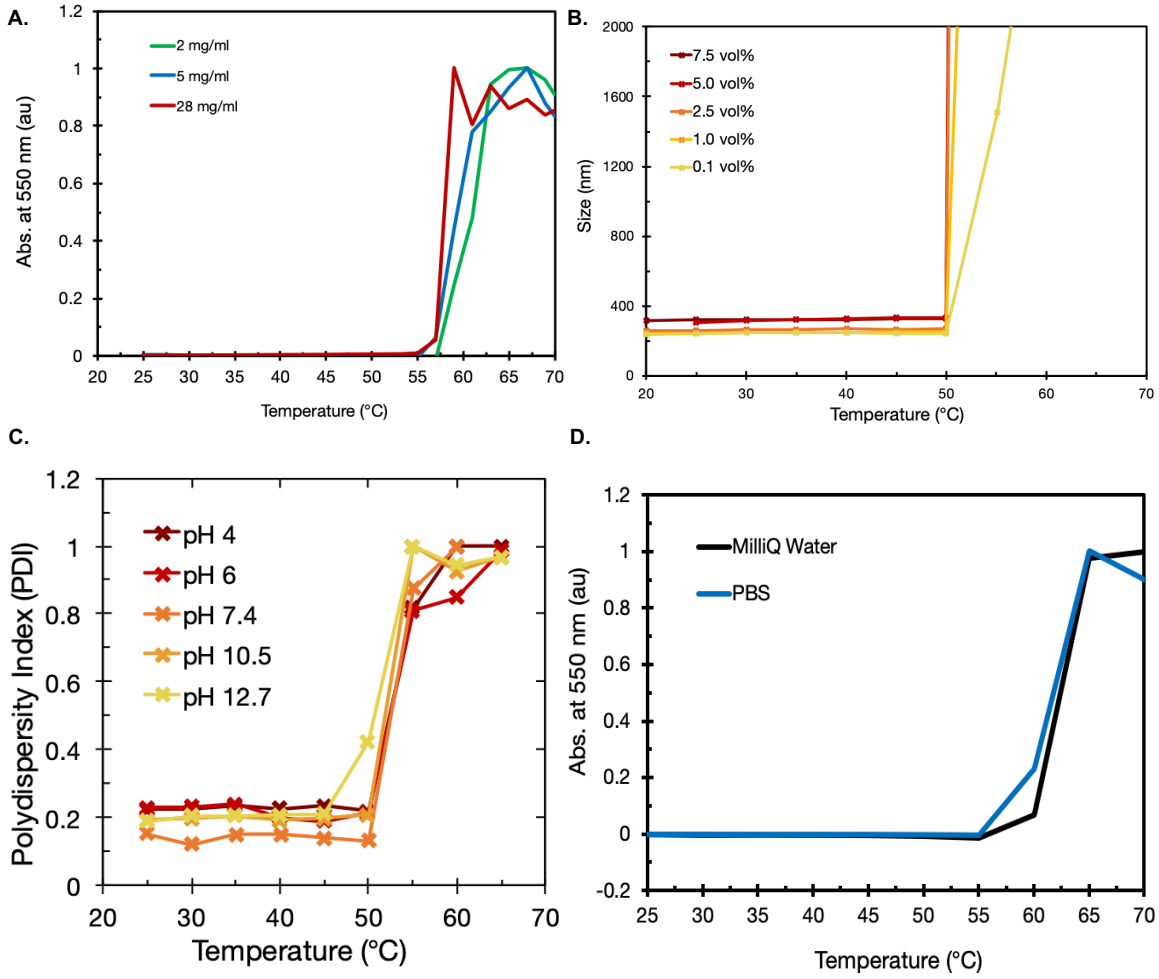

Figure 5.12. Controls for **5.2@micellles** and **5.2@emulsions**. (A) Temperature-dependent absorbance traces at 550 nm of solutions with **5.2@micelles** in PBS, from 2 to 28 mg/mL. Analyzed at 550 nm from 25 to 70 °C with 0.1 °C increments, 15 second equilibration between

measurements, blanked and normalized versus polymer solution at room temperature (~25 °C). (B) Temperature-dependent dynamic light scattering traces for serial dilutions of **5.2@emulsions**. Samples were analyzed from 20 to 70 °C with 5 °C increments, 90 second equilibration between measurements. Volume percentages in the legend correspond to volume % PFOB after serial dilution, with each solution made and analyzed independently. (C) Temperature-dependent dynamic light scattering traces of **5.2@emulsion** solutions at pH ranges from 4 to 13. Solutions were pH'd in PBS (1X) using 0.5M NaOH or HCl and analyzed from 25 to 65 °C with 5 °C increments, 90 second equilibration between measurements. (D) Temperature-dependent normalized absorbance traces at 550 nm of solutions with **5.2@micelles** in either MilliQ water (black line) or PBS (1X, pH 7.4, blue line). Analyzed at 550 nm from 25 to 70 °C with 0.1 °C increments, 15 second equilibration between measurements, blanked versus polymer solution at room temperature (~25 °C).

The influence of crowder on LCST transitions can also be macroscopically visualized. As shown in Figure 5.7E, at 25 °C separate solutions of crowder PEG-10k and **5.2@micelles** dissolved in PBS are transparent, yet a mixture of **5.2@micelles** in PEG-10k (250 mg/mL) is turbid, indicating the coil-to-globule transition has already occurred. When solutions are heated to 65 °C (>LCST), PEG-10k in PBS remains transparent while **5.2@micelles** in PBS also becomes visually cloudy, akin to **5.2@micelles** in PEG-10k at room temperature. By comparison, similar solutions of **5.1@micelles** remain visually transparent with or without PEG-10k at either room temperature or 65 °C (Figure 5.13).

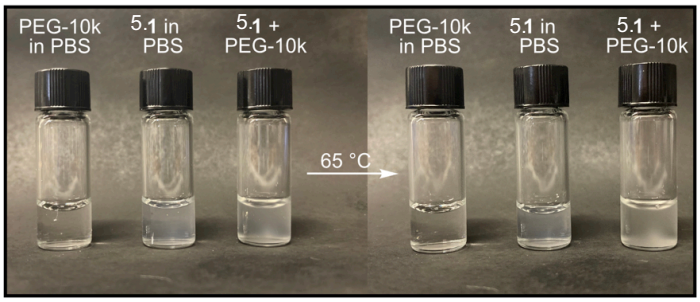

Figure 5.13. (i) Solutions of PEG-10k (250 mg/mL), **5.1@micelles** (5 mg/mL), or both **5.1@micelles** and PEG-10k (5 and 250 mg/mL, respectively) solubilized in PBS (pH 7.4) and photographed at both room temperature and 65 °C.

Additional experiments employing both **5.1@emulsions** and **5.2@emulsions** in the presence of PEG-10k crowder showed selective crowder response only for **5.2@emulsions** (Figure 5.14).

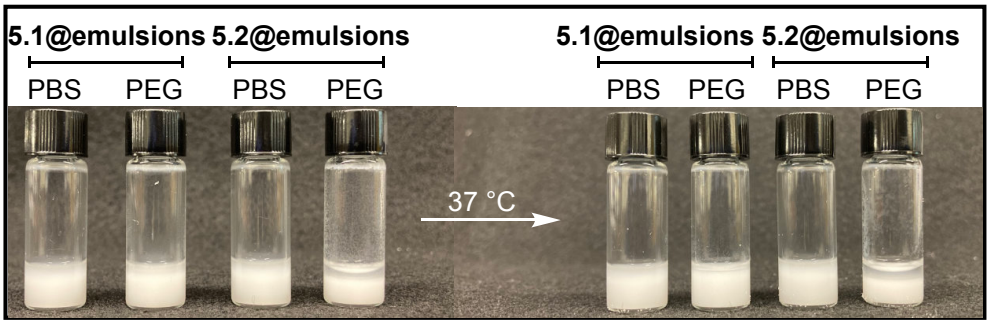

Figure 5.14. Crowder response of **5.1@** or **5.2@emulsions**. Vials containing solutions of **5.1**- or **5.2@emulsions** were formed according to the general nanoemulsion formation procedure, with slight modifications–PFOB and PBS were emulsified at a 1:2 vol% ratio (rather than 1:10 vol%) to ensure visual phase separation. Emulsions solutions were then further diluted at a 1:1 vol% ratio with PBS 1X (pH 7.4) or a 200 mg/mL PEG-10k in PBS stock (to a total PEG-10k concentration of 100 mg/mL). Solutions were briefly heated at 37 °C for 10 minutes on a hot plate, removed and directly photographed.

To directly visualize the crowding-induced fusion of emulsions, we performed microscopy on **5.2@macroemulsions.** These macroemulsions were formed through a slightly modified emulsification procedure (SI p. S39) which allowed for encapsulation of fluorophores **5.9** and/or **5.10** and yielded stable macroemulsions with a diameter of ~3-5 μm. We designed a Förster resonance energy transfer (FRET)-based assay employing fluorous-soluble FRET pairs **5.9** and **5.10** (Figure 5.7F) to clearly visualize the fusion of **5.2@macroemulsions**. **5.2@macroemulsions** containing **5.9** and/or **5.10** were visualized with confocal microscopy under various crowding conditions (Figure 5.7G). A negative control (Figure 5.7G, i,ii) involved two populations of 4.1±0.5 μm emulsions each containing **5.9** or **5.10**, while a positive control (Figure 5.7G, iii,iv) employed one population of 4±1 μm emulsions with pre-mixed **5.9** and **5.10** in the PFOB core. Overlaying blue (Ex. 488 nm, Em. 520–620 nm) and red (Ex. Ex. 635 nm, Em. 700–800 nm) channels of the negative control showed distinct populations of emulsions (i), while FRET channel

(Ex. 488, Em. 700–800 nm) showed no appreciable signal (ii). By comparison, the positive control showed overlay of dyes (iii) and apparent FRET (iv). Finally, mixing independent emulsions in the presence of PEG-10k as a crowder (250 mg/mL) resulted not only in large-scale fused emulsion aggregates of 50±10 μm, but colocalization (v) and FRET (vi). These data corroborate that the presence of crowder results in emulsion fusion (Figure 5.7H) and facilitates payload exchange (Figure 5.7I). Also apparent in the overlaid image with crowder present (Figure 5.7G, (v)) is dye **5.10** localized to the interface of emulsions, which is distinct from the localization of **5.10** in the positive and negative controls (Figure 5.15).

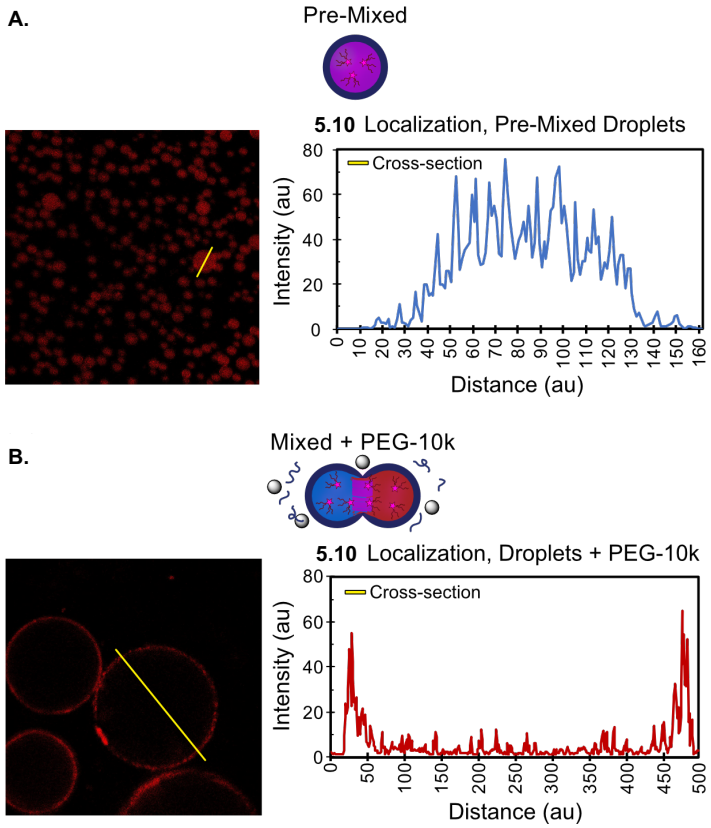

Figure 5.15. Localization of **5.10** within **5.2@emulsions** in (i) PBS or (ii) PEG-10k solution in PBS (250 mg/mL), as shown in Figure 5.7H. PFOB droplets were diluted at 10 vol% in either solution.

Interestingly, these results are analogous to our previous studies that demonstrated the movement of **5.10** from the core of the emulsion to the interface in the absence of surfactant.[41] We believe that, upon crowding, the coil-to-globule transition decreases the ability for **5.2** to stabilize the perfluorocarbon-water interface leading to interior payload **5.10** to transfer to the interface and decrease the interfacial tension of the droplets. Collectively, the observed, fusion, FRET and localization of **5.10** at the interface only in the presence of crowder support the macromolecule-concentration induced fusion of **5.2@emulsions**.

5.7 Tuning polymeric LCSTs through changes in protein concentration

For macromolecule concentration to be employed as an endogenous stimulus for smart nanomaterials, the observed decrease in LCST upon synthetic crowder addition must be emulated with biomacromolecules (Figure 5.16A, i, ii). We employed bovine serum albumin (BSA) as a model protein and looked to establish that **5.2@micelles** and **5.2@emulsions** would have an LCST above physiological temperature at extracellular concentrations of serum proteins (~70-80 mg/mL)[5] and below physiological temperature at intracellular protein levels (~150–300 mg/mL). We have defined these regions as a stable window (red, Figure 5.16A, iii) and response window (blue, Figure 5.16A, iii), respectively. We reasoned that BSA was an appropriate protein for initial experiments as albumins compose roughly half of total protein mass in serum[42], and BSA's molecular weight is nearly identical to the average weight of crowding proteins in the cytoplasm (67 kDa)[43].

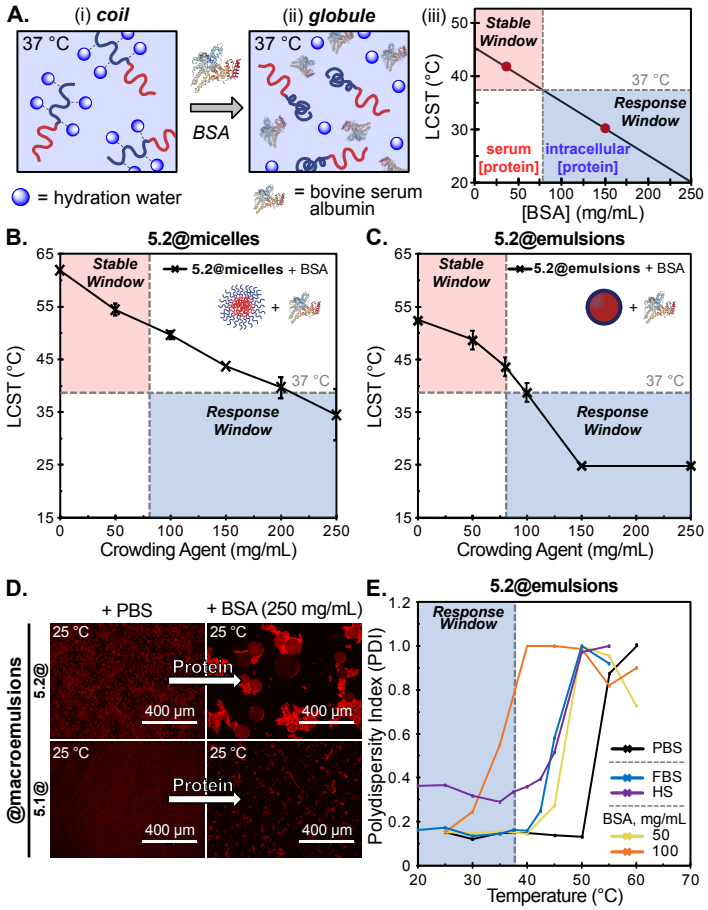

Figure 5.16. Response of **5.2@micelles** and **5.2@emulsions** to protein concentration. (A) (i,ii) Schematic of model protein bovine serum albumin (BSA) inducing a coil-to-globule LCST transitions of thermoresponsive **5.2** at physiological temperature. (iii) Schematized plot of LCST vs. protein temperature defining two regions of interest: the stable window (red) representing extracellular protein concentrations at physiological temperature and the response window (blue) representing intracellular biomacromolecule concentrations at physiological temperature. (B) LCST of **5.2@micelles** as a function of BSA concentration. LCST values determined via UV/Vis analysis (see Figure S28). Error bars represent the standard deviation between two independent measurements. (C) LCST of **5.2@emulsions** as a function of BSA concentration. LCST values determined via DLS analysis (see Figure S29) Error bars represent the standard deviation between two independent measurements. (D) Fluorescence microscopy of **5.2@emulsions** or **5.1@emulsions** containing rhodamine **5.11** in the presence of PBS (pH 7.4) or PBS/BSA solutions (250 mg/mL) at room temperature. Scale bars: 400 µm. (E) Temperature-dependent polydisperity measurements of **5.2@emulsions** in the presence of BSA (50 mg, yellow; 100 mg, orange), FBS: fetal bovine serum (36 mg/mL total protein, blue), HS: human serum (52 mg/mL total protein, purple) or no additive (black).

We again performed UV-Vis to assay **5.2@micelles** and DLS to analyze **5.2@emulsions** when incubated in concentrations of BSA. We found that the LCST of either vehicle could be reduced

below 37 °C by high concentrations of BSA (>200 mg/mL, Figure 5.16B,C, Figure 5.17, Figure 5.18).

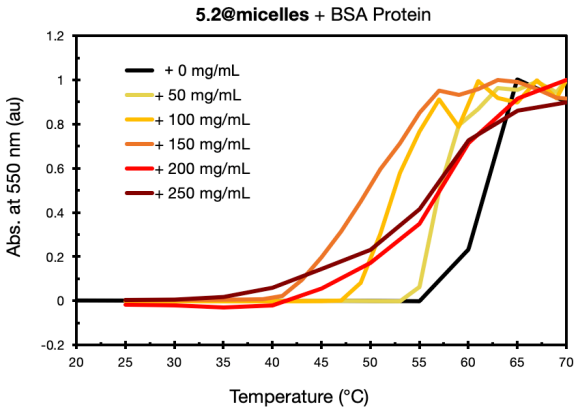

Figure 5.17. Temperature-dependent absorbance traces at 550 nm of solutions with **5.2@micelles** (5 mg/mL) in PBS (1X, pH 7.4) containing BSA (0–200 mg/mL). Samples were analyzed at 550 nm from 25 to 70 °C with 0.1 °C increments, 15 second equilibration between measurements, blanked versus polymer solution at room temperature (~25 °C). Data are representative of at least two independent experiments.

As was the case with the synthetic crowding agents, we observed different responses for **5.2@micelles** and **5.2@emulsions**, with **5.2@emulsions** showing a greater decrease in LCST upon addition of BSA.

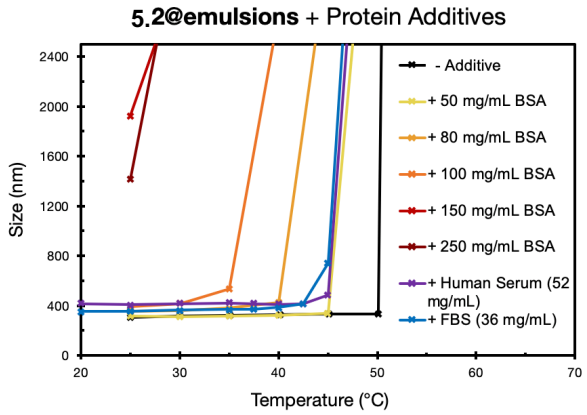

Figure 5.18. Temperature-dependent size analysis of **5.2@emulsions** diluted at 10 vol% (i) PBS containing BSA (50–200 mg/mL), (ii) human serum media (contains ~52 mg/mL human serum albumin), (iii) fetal bovine serum (contains ~36 mg/mL fetal bovine serum albumin) or no additive. Size analysis was used as solution viscosity did not interfere with size measurements. Samples were analyzed via DLS from 25 to 70 °C with 5 °C increments, 120 second equilibration between measurements. Data are representative of at least three independent experiments.

Excitingly, both nanomaterials reach the response window at high concentrations of protein. We verified this response was specific to thermoresponsive **5.2** and not observed when using control **5.1**, both for micelles (Figure 5.9) and emulsions (Figure 5.19, 5.20).

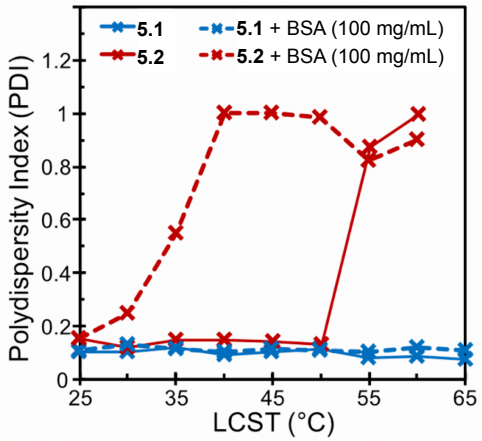

Figure 5.19. Temperature-dependent polydispersity indexes of **5.1@** and **5.2@emulsion** solutions with and without BSA additive (100 mg/mL), as analyzed by DLS.

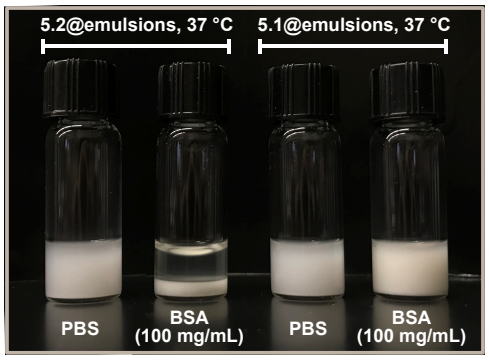

Figure 5.20. Vials containing solutions of **5.1-** or **5.2@emulsions** in the presence of PBS 1X (pH 7.4) or PBS/BSA solutions (100 mg/mL). Solutions were briefly heated at 37 °C for 10 minutes.

These data suggest that the response to crowder is not dependent on protein-polymer interactions, but rather the thermoresponsive behavior of the employed polymer. As such, we envision the critical point at which each nanostructure passes into the response window can be tuned through modification of the LCST of the hydrophilic block, following established literature on POx LCST transitions.[20] With **5.2@emulsions** giving a more robust transition into the response window and the opportunity to analyze both **5.2@emulsions** and **5.2@macroemulsions**, we moved forward further characterizing the emulsions response to albumin concentrations before moving into cellular environments.

To visualize the fusion process induced by BSA, we formulated **5.1@macroemulsions** and **5.2@macroemulsions** containing a fluorous soluble rhodamine payload (**5.11**, Figure 5.21).[29]

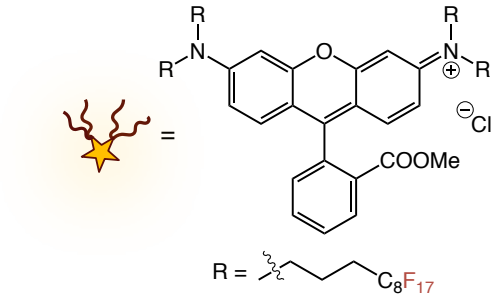

Figure 5.21. Structure of fluorous-soluble rhodamine **5.11** synthesized as previously reported.[29]

Epifluorescence microscopy analysis demonstrated that upon injection of BSA at concentrations similar to intracellular protein levels (250 mg/mL), aggregation and fusion of **5.2@macroemulsions** occurred within two minutes at room temperature (Figure 5.16D, Figure 5.5). Importantly, the morphology of control **5.1@macroemulsions** was unchanged. Notably, BSA exposure causes rhodamine **5.11** to localize at the oil-water interface similar to **5.10**, again corroborating that crowding induces a reduction in surface activity of **5.2**.

Next, we analyzed the LCST of **5.2@emulsions** in the presence of the more biologically relevant fetal bovine serum (FBS) and human serum (HS) to support that **5.2@emulsions** would remain stable when outside the cell. Temperature-dependent DLS of **5.2@emulsions** solutions were analyzed in PBS, BSA (50, 100 mg/mL), FBS (36 mg/mL total protein), and HS (52 mg/mL total protein) (Figure 5.16E). Interestingly, the FBS and HS solutions had a similar influence on the LCST of **5.2@emulsions** that 50 mg/mL of BSA in PBS did. As desired, all three solutions showed demulsification onset above physiological temperature (~40 °C), suggesting that **5.2@emulsions** would be stable outside the cell. These results also suggest that macromolecular crowding effects dominated over the influence of other serum additives (*e.g.,* ions, triglyceride, glucose, cholesterol, *etc.*), which is in agreement with our previous controls that salt, pH, and small molecule additives did not affect the LCST (Figure 5.7D, Figure 5.11). To confirm that these changes were not due to protein-polymer interactions, we performed control experiments comparing the response of **5.1@emulsions** and **5.2@emulsions** to BSA. Size analysis showed that **5.1@emulsions** were stable in the presence of 100 mg/mL BSA even at upwards of 65 °C (Figure 5.19), in stark contrast to **5.2@emulsions** in the same conditions. Additionally, macroscopic demulsification was visualized only for **5.2@emulsions** in 100 mg/mL of BSA at 37 °C (Figure 5.20).

5.8 Mechanism for LCST sensitivity by crowding agents

Our data showed a significant difference in the lowering of the LCST in the presence of synthetic crowders and protein. For **5.2@emulsions**, 100 mg/mL of synthetic crowders **5.6**-**5.8** lowered the LCST below even room temperature (25 °C), while the same concentration of BSA only lowered the LCST to that of physiological temperature (37 °C). Looking into this discrepancy further, we hypothesized that the influence of the crowder on the LCST correlated with the crowder's conformation in solution. For example, the highly globular BSA has less of an influence on the LCST than branched, extended, crowders such as Ficoll-400.[44] We analyzed the role of crowder size by plotting the concentration at which crowder induces fusion of **5.2@emulsions** at room temperature against the crowder's overlap concentration (Figure 5.22). The overlap concentration is a known metric derived from the molecular weight and radius of gyration of the polymer in aqueous solution, and thus describes the conformation of these polymers at different concentration regimes in water.

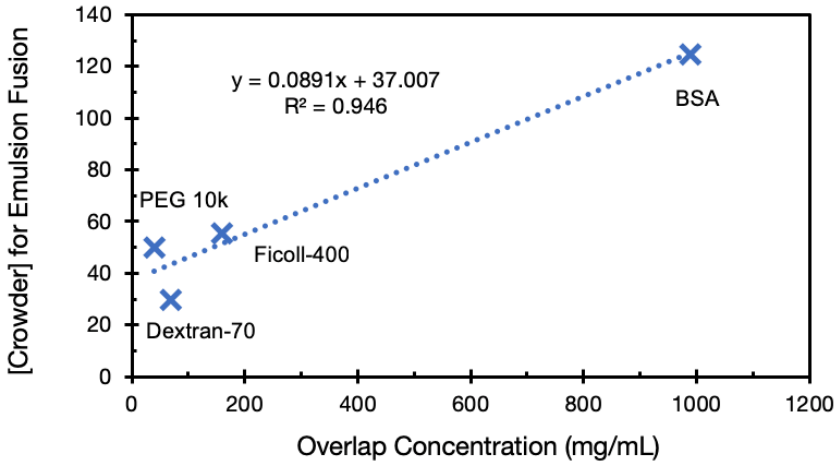

Figure 5.22. Minimum concentration of crowder needed to induce fusion of **5.2@emulsions** (mg/mL) versus overlap concentration of crowder (mg/mL) for panel of studied crowders. Critical aggregation concentration is defined as the minimum concentration of crowder needed to trigger fusion of PFOB NEs at room temperature, as determined by dynamic light scattering analysis.

Generally, we observed that crowders with low overlap concentrations have a larger influence on the LCST than highly globular biomacromolecules. This relationship was further corroborated by studying how a single crowder, PEG, at five different molecular weights influenced the LCST of **5.2@emulsions**. As observed for a series of PEG at 1, 2, 4, 8 and 10 kDa, the overlap concentration and critical aggregation concentration shared a linear correlation across the series (Figure 5.23). These data support that the effects we have observed with model polymers and proteins should extend to the crowded, complex intracellular environment.

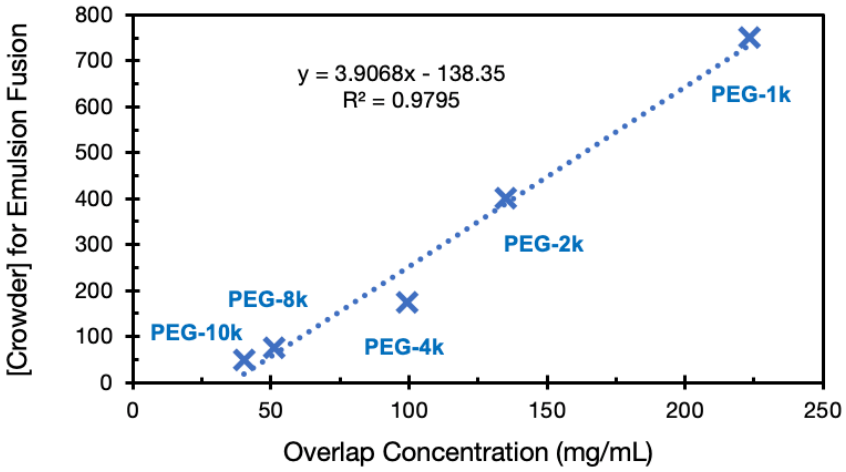

Figure 5.23. Overlap concentration (mg/mL) versus critical aggregation concentration (mg/mL) of **5.2@emulsions** for PEG crowder at varying molecular weights: 1, 2, 4, 8 and 10 kDa. Critical aggregation concentration is defined as the minimum concentration of crowder needed to trigger demulsification of PFOB NEs at room temperature, as determined by dynamic light scattering analysis. Overlap concentrations were taken from the literature.[37]

5.9 Zebrafish microinjections demonstrate *in vivo* utility

Finally, we tested the responsive nature of **5.2@emulsions** *in vivo*, when introduced to the cytosol of cells in living embryos. We microinjected **5.1@emulsions** or **5.2@emulsions** containing fluorous rhodamine **5.11** into the cell (blastomere) of zebrafish embryos at the 1-cell stage (Figure 5.24A). The embryos were then imaged ~90 minutes later by confocal microscopy at the 8-cell stage. 10X maximum intensity projection images are representative of the 3D

distribution of the emulsions (Figure 5.24B), while 40X confocal sections show a focused cross-section of the emulsions inside the

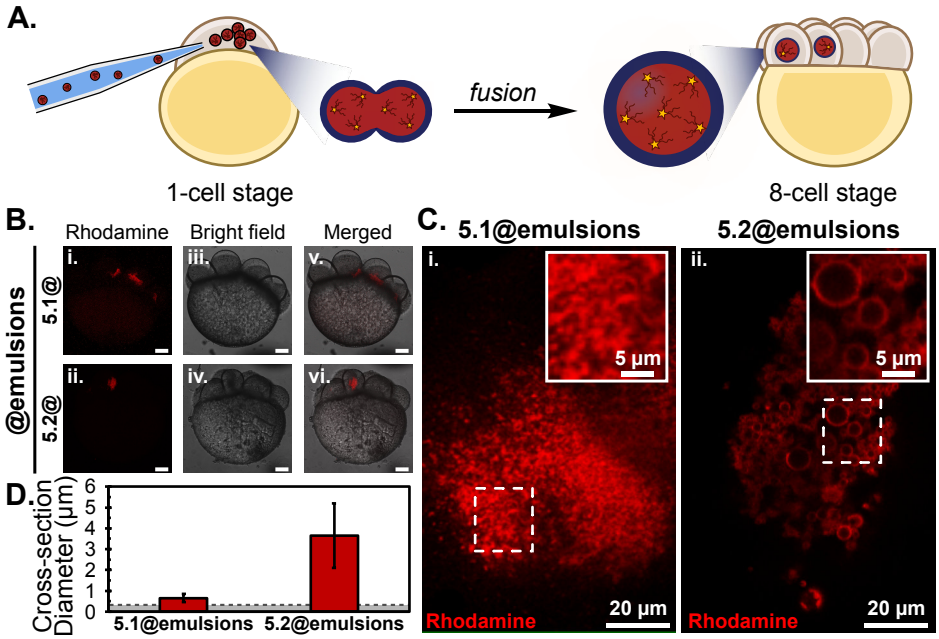

Figure 5.24. Fusion of **5.2@emulsions** in response to intracellular environment. (A) Schematic of microinjections of **5.1@emulsions** or **5.2@emulsions** containing fluorous rhodamine **5.11** into zebrafish at the 1-cell stage and imaged at the 8-cell stage. (B) Confocal micrograph of injected nanoemulsions at 8 cell stage (10X). Maximum intensity projections of **5.11**-containing droplets (red, i, ii, Ex. 543 nm, Em. 554–685 nm); Bright field images (iii, iv); Merged (v, vi). Scale bar = 100 µm. (C) Morphology of the (i) **5.1@emulsions** and (ii) **5.2@emulsions** in zebrafish blastomeres under a 40X lens (single optical section). Scale bar = 20 µm. Data are representative of five separate embryos for each emulsion. Inset (scale bar = 5 µm) more clearly shows fused emulsion droplets with **5.11** at the interface for **5.2@emulsions**, but not **5.1@emulsions.** (D) Cross-section diameters of **5.1@** and **5.2@emulsions** after microinjection. Values were obtained via analysis of optical sections (40X) in ImageJ. Error bars represent the standard deviation of droplet diameters across zebrafish embryos (n > 90). See supplementary information for zebrafish replicates (n = 5) and control images in PBS buffer.

embryo (Figure 5.24C). Strikingly, while **5.1@emulsions** were well-dispersed and near their size prior to injection, **5.2@emulsions** had diameters over ten times the initial size, indicating vehicle fusion was occurring. These results are further highlighted through image analysis of the cross-section diameters for each population of emulsions (Figure 5.24D), suggesting a similar emulsion fusion mechanism as we observed *in vitro* when injecting emulsions into simple concentrated BSA

solutions (Figure 5.16F). Control experiments imaging both **5.1@emulsions** and **5.2@emulsions** in PBS buffer at the same time period showed that both vehicles showed sizes below the achievable resolution (*i.e.,* pixel size ≤ 377 nm, replicates within supplementary information), agreeing with previous DLS data (Figure 5.2E, 5.3). These studies showcase that the heterogenous crowded environment of the cell is able to induce a significant LCST change in thermoresponsive materials leading to the first use of intracellular protein crowding as a stimulus for responsive nanomaterials.

The finding that thermoresponsive materials are also crowding-responsive materials provides opportunities to reinvent many nano- and biomaterial systems. For example, Pietrangel and coworkers have demonstrated temperature-dependent drug release from micelles with PNIPAM as the hydrophilic block due to a coil-to-globule transition[45], which can now potentially be re-engineered to respond to intracellular protein concentration rather than exogenously applied heat. While the results herein focus on POx nanostructures, we observed similar effects of protein concentration on PNIPAM (Figure 5.25), suggesting that crowding-responsive behavior can be extended to other ubiquitous LCST-containing polymers.

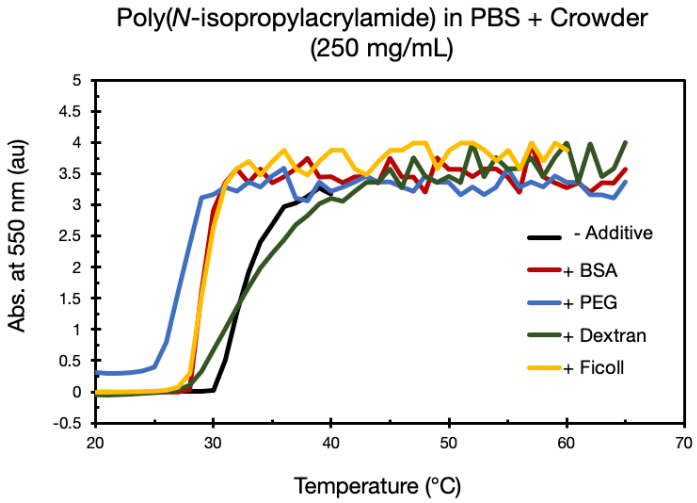

Figure 5.25. Temperature-dependent absorbance traces at 550 nm of solutions with free commercial poly(*N*-isopropylacrylamide) (PNIPAM, 5 mg/mL) in PBS (1X, pH 7.4) containing varying crowders (250 mg/mL). Samples were analyzed at 550 nm from 25 to 65 °C with 0.1 °C increments, 15 second equilibration between measurements, blanked versus polymer solution at room temperature (~25 °C). Data are representative of at least two independent experiments.

5.10 Conclusions

We have demonstrated the first use of macromolecular crowding as an endogenous stimulus for nanomaterials. Poly(2-oxazoline) amphiphiles were synthesized with readily tunable LCSTs and used either in solution as micelles or as stabilizing agents for oil-in-water nanoemulsions. Sensitivity to crowding was first evaluated using a panel of synthetic polymers to establish how crowding affected the phase transitions and stability of both nanomaterials. We then moved to BSA as a model protein and found that the dose-dependent ΔLCST of these materials could be tailored such that they were stable to extracellular concentrations of protein ("stable window") but destabilized in intracellular concentrations ("response window"). The comparison of LCST changes to either the highly globular BSA or a panel of synthetic crowders demonstrated that while all crowders indiscriminately reduced the LCST, the magnitude of this reduction correlated with the crowder's conformation in solution. Ultimately, an understanding of this

sensitivity was exploited to induce the irreversible fusion of oil-in-water emulsions within zebrafish cells.

Taken together, these data suggest that macromolecular crowding is a routine variable for materials chemists to consider when designing thermoresponsive systems. Here we establish the importance of using *in vitro* crowders to appropriately model the environment that these vehicles will eventually meet *in vivo*, a relationship that is currently unexplored in these fields. We liken these findings to early reports that served as a clarion call for biochemists to consider crowding effects on protein-protein interactions, which have become increasingly appreciated in the decades since.[6] Towards practical applications, our findings suggest that an understanding of these effects could even be leveraged to exploit varying protein concentrations in different cell types or organelles for targeted response.[46] Separately, as polymers with coil-to-globule transitions have been used as protein folding mimics, we expect that these findings could help inform topics in liquid-liquid phase separation[47], membraneless organelle assembly[48], molecular chaperones[49], macromolecular sensing[50], and protein-protein interactions within crowded environments. Ultimately, we envision that the capability of macromolecules to induce entropically-driven phase transitions is a generalizable phenomenon with significant consequences when translating molecules from a dilute test tube to the interior of a cell.

5.11 Experimental Procedures

5.11.1 General experimental procedures

Reagents and Instrumentation Chemical reagents were purchased from Sigma-Aldrich, VWR, Alfa Aesar, Fisher Scientific, SynQuest Laboratories, Chem-Impex International or Acros Organics and used without purification unless noted otherwise. Bovine serum albumin (Fraction

V, Heat-Shock Treated) was purchased from MilliporeSigma. Fetal bovine serum (FBS) was purchased from Genesee Scientific, Lot# P078430. Human serum (HS) was purchased from Sigma-Aldrich, Batch# SLBX6020. Anhydrous and deoxygenated acetonitrile (MeCN) was dispensed from a Grubb's-type Phoenix Solvent Drying System built by JC Meyer.[51] Solvent was removed under reduced pressure with a Büchi Rotovapor with a Welch self-cleaning dry vacuum pump and further dried with a Welch DuoSeal pump. Dialysis was performed with pre-wetted Spectra/Por 6 regenerated cellulose dialysis membranes with a 1 kDa molecular weight cutoff purchased from Spectrum Laboratories. Bath sonication was performed using a Branson 3800 ultrasonic cleaner. Nuclear magnetic resonance (^{1}H NMR, ^{13}C NMR) spectra were taken on Bruker Avance 500 (^{1}H NMR) instrument and processed with MestReNova 11.0.1 software. All ^{1}H NMR peaks are reported in reference to $CDCl_3$ at 7.26 ppm.

Masses for analytical measurements were taken on a Sartorius MSE6.6S-000-DM Cubis Micro Balance. Microwave reactions were performed using a CEM Discover SP microwave synthesis reactor. All reactions were performed in glass 10 mL microwave reactor vials purchased from CEM with silicone/PTFE caps. Flea micro PTFE-coated stir bars were used in the vials with magnetic stirring set to high and 15 seconds of premixing prior to the temperature ramping. All microwave reactions were carried out at 140 °C with the pressure release limit set to 250 psi (no reactions exceeded this limit to trigger venting) and the maximum wattage set to 250W (the power applied was dynamically controlled by the microwave instrument and did not exceed this limit for any reactions).

Abbreviations

DCM = dichloromethane; DMSO = dimethylsulfoxide; EtOH = ethanol; MeCN = acetonitrile; MeOH = methanol; THF = tetrahydrofuran; DMF = dimethylformamide; POx = poly(2-oxazoline); DBC = diblock copolymer; MeOx = 2-methyl-2-oxazoline; EtOx = 2-ethyl-2-oxazoline; NonOx = 2-nonyl-2-oxazoline; DLS = dynamic light scattering; NMR = nuclear magnetic resonance; PNIPAM = poly(*N*-isopropylacrylamide); LCST = lower critical solution temperature; PFC = perfluorocarbon; PFOB = perfluorooctylbromide; PEG = poly(ethylene glycol); FRET = Förster resonance energy transfer; BSA = bovine serum albumin; FBS = fetal bovine serum; HS = human serum.

General epifluorescence procedure

Epifluorescence was performed on an EVOS® FL microscope. Imaging was done using EVOS™ Light Cube, RFP 2.0 (531/40 nm Excitation; 593/40 nm Emission) or EVOS™ Light Cube, DAPI 2.0 (357/44 nm Excitation; 447/60 nm Emission). Samples were prepared via respective dilutions transferred to a flat glass microscope slide with coverslip. Imaging was performed within five minutes of transferring sample. Image analysis was performed with Fiji.[52]

General confocal procedure

Confocal microscopy was performed on a TCS SPE Leica confocal microscope containing 405 nm, 488 nm, 532 nm and 635 nm lasers. Confocal settings were as follows: Cyanine **6** (488 laser-50%, 1200 gain, offset -0.35, collection 520-620 nm), Cyanine **7** (635 laser-50%, 800 gain, offset -0.35, collection 700-800nm), FRET (488 laser-51%, 1200 gain, offset -0.35, collection 700-800nm), DIC (scan-BF, 600 gain, offset -0.50). Scale bar represents 20 μm.

General heat-stage microscopy procedure

Heat-stage microscopy was performed on a Nikon Eclipse lV100D-U microscope equipped with a Linkam LTSE420-P Temperature Controlled Probe Stage. Sample was heated at a ramp of 5 °C/min from 20–65 °C and visualized under a 50X objective.

General nanoemulsion formation procedure

Polymer surfactant (5.6 mg) was pre-solubilized in PBS buffer pH 7.4 (200 μL, 28 wt% total surfactant) and vortexed gently until fully dissolved. In a separate 2 mL eppendorf tube, oil (10 vol%, 20 μL of perfluorooctylbromide) was added. Where relevant, rhodamine **5.11** was encapsulated by pre-dissolving 4.32 nmol of **5.11** (0.001 mg) in PFOB. Finally, the polymer/PBS solution was added, and the mixture was quickly sonicated at 35% amplitude for at least 90 seconds at 0 °C on a QSonica (Q125) sonicator. For surfactant **1**, no pulse was used. For surfactant **5.2**, a pulse of 2 seconds ON, 5 seconds OFF was used to avoid solution temperature rising above the LCST of **5.2**. Sonication was performed by lowering the probe directly at the liquid-liquid interface of the two immiscible solvents.

General micelle formation procedure

Polymer surfactant (5.0 mg) was solubilized in PBS buffer pH 7.4 (1 mL) and vortexed gently until fully dissolved. In some instances, **5.4** and **5.5** required brief annealing (<15 seconds) of heating above the LCST to solubilize.

General macroemulsion formation procedure

Polymer surfactant (5.6 mg) was pre-solubilized in PBS buffer pH 7.4 (200 μL, 28 wt% total surfactant) and vortexed gently until fully dissolved. In a separate 2 mL eppendorf tube, oil (10 vol%, 40 μL of perfluorooctylbromide) was added. Where relevant, **5.9**, **5.10** or **5.11** was encapsulated by pre-dissolving 21.6 nmol of either dye in PFOB. PBS was then added on top of the dye/PFOB layer (153 μL). Finally, the polymer/PBS solution was added (7 μL to total surfactant loading of 1 mg/mL), and the mixture was quickly sonicated at 20% amplitude for 15 seconds at 0 °C on a QSonica (Q125) sonicator. Sonication was performed by lowering the probe directly at the liquid-liquid interface of the two immiscible solvents.

General nanoemulsion analysis procedure

Size analysis: The bulk emulsion solution was diluted in MilliQ H_2O (20 μL emulsions in 2 mL MilliQ H_2O) in a plastic 1 cm cuvette. Size was analyzed with a Malvern Zetasizer Nano dynamic light scattering. SOP parameters: 10 runs, 10 seconds/run, three measurements, no delay between measurements, 25 °C with 120 second equilibration time. Collection parameters: Lower limit = 0.6, Upper limit = 1000, Resolution = High, Number of size classes = 70, Lower size limit = 0.4, Upper size limit = 1000, Lower threshold = 0.05, Upper threshold = 0.01.

For temperature-dependent measurements: unless otherwise noted, the bulk emulsion solution was diluted in PBS (1X, pH 7.4) with or without crowding agent (20 μL emulsions + 180 μL PBS) in a low-volume quartz batch cuvette. Size was analyzed with a Malvern Zetasizer Nano dynamic light scattering. Temperature ranges from 15 to 70 °C and is explicitly mentioned for each

experiment. Temperature ramped in 5 °C increments, 90 second equilibration between measurements. SOP parameters are as reported above.

General emulsion LCST determination

Size and polydispersity were analyzed per the general nanoemulsion size analysis procedure. Measurements were taken from 25 to 65 °C with 5 °C increments. LCST was defined as the rapid increase in either size (≥1000 μm) or polydispersity index (≥0.50) that accompanied demulsification. In certain cases of high crowding, polydispersity index was used due to artificial inflation of measured size as the solution viscosity increases.

General micelle analysis procedure

Size analysis: Polymer was solubilized at given concentration (typically, 5 mg/mL) in a plastic 1 cm cuvette. Size was analyzed with a Malvern Zetasizer Nano dynamic light scattering. SOP parameters: 10 runs, 10 seconds/run, three measurements, no delay between measurements, 25 °C with 120 second equilibration time. Collection parameters: Lower limit = 0.6, Upper limit = 10000, Resolution = Normal, Number of size classes = 70, Lower size limit = 0.4, Upper size limit = 1000, Lower threshold = 0.05, Upper threshold = 0.01.

General micelle LCST determination

Absorbance profiles of polymeric surfactants were obtained in PBS 1X (pH 7.4) at 5 mg/mL polymer. Analyzed from 25 to 70 °C with 0.1 °C increments, 15 second equilibration between measurements, blanked versus polymer solution at room temperature (~25 °C). Spectra was taken from 300–700 nm in a 0.3 mL quartz cuvette without stirring. Temperature controlled via UV-Vis

equipped with air-cooled Peltier. Analysis was performed at 550 nm. The LCST was defined as the temperature at which the relative absorbance at 550 nm begins to increase (≥0.05 au, ≤90% transmittance).[26]

Zebrafish experimental procedures

Zebrafish *in vivo* microscopy assay

Zebrafish (*Danio rerio*) were maintained under standard conditions[53]. Animal husbandry and experiments were done according to protocols approved by the Institutional Animal Care and Use Committee (IACUC) at the University of California Santa Barbara. Transgenic zebrafish line *Tg(actb2:mem-NeoGreen)^{hm37}* were microinjected with either **5.1@emulsions or 5.2@emulsions** containing **5.11** (*vide supra*) at 1-2 cell stage. Injected embryos were dechorinated by 1 mg/mL pronase (Roche, Ref #10165921001) and then mounted on glass bottom dishes (MatTek, Part # P35G-1.5-14-C) with 1% methylcellulose (Sigma, #MS0512-100G) for imaging. Images were acquired on a Zeiss LSM780 confocal microscope with either 10X lens (Zeiss, EC Plan-Neofluar 10X/0.30 M27) or 40X (Zeiss, LD C-Apochromat 40x/1.1W korr M27) lens around 8 cell stage (1.5 hours post fertilization). Acquired images were processed by Zen 3.0 SR black (Zeiss) and Fiji.[52] 3D reconstructions (Videos S3, S4) were processed by IMARIS 9.7.0 (Bitplane).

General synthetic procedures

5.11.2 Experimental procedures

Synthetic chemistry experimental procedures

Synthesis of poly(2-oxazoline) block copolymers **5.1** and **5.2**:

$P(MeOx)_{87}$-*b*-$P(NonOx)_7$ (**5.1**) and $P(EtOx)_{93}$-*b*-$P(NonOx)_{10}$ (**5.2**) were synthesized as previously reported.[25]

Synthesis of supplementary poly(2-oxazoline) block copolymers **5.3, 5.5**:

$P(MeOx)_{32}$-*b*-$P(NonOx)_9$ (**5.3**) and $P(EtOx)_{33}$-*b*-$P(NonOx)_{11}$ (**5.5**) were synthesized as previously reported.[25,54]

Synthesis of supplementary poly(2-oxazoline) block copolymer **5.4**:

$P(EtOx)_{30}$-*b*-$P(BuOx)_{10}$ (**5.4**) was synthesized as follows: To a flame dried microwave vial, MeCN (1.0 mL, anhydrous) and EtOx (200 μL, 0.200 g, 2.02 mmol, 30 equiv.) were added. After purging with nitrogen, MeOTf (7.6 μL, 11 mg, 0.07 mmol, 1.0 equiv.) was added and the mixture was heated at 140 °C in the microwave.

After 12 minutes, BuOx (85 μL, 0.085 g, 0.67 mmol, 10 equiv) was added to the vial and the mixture was again heated at 140 °C in the microwave. After 8 minutes, the polymerization was quenched with excess MilliQ water (~200 μL). The reaction mixture was stirred overnight at room temperature. The following day, the reaction mixture was evaporated to dryness to yield crude polymer (**5.4**) as an off-white solid. Polymer **5.4** was purified by precipitation by dissolving in a minimal amount of DCM and dropwise addition to cold Et_2O (20:1 v/v%) three times, collected and evaporated to dryness, yielding the pure product **5.4** as an off-white solid (178 mg, 0.0500 mmol, 62% yield). ^{1}H NMR (500 MHz, $CDCl_3$): δ 3.37 (m, 159H), 2.95 (m, 3H), 2.30 (m, 93H), 1.50 (m, 18H), 1.26 (m, 19H), 1.04 (m, 91H), 0.84 (m, 28H).

5.11.3 Figure experimental procedures

Figure 5.2A. Synthesis of block copolymers **5.1** and **5.2**. See supporting synthetic chemistry experimental procedures and references.[25]

Figure 5.2D/E. Dynamic light scattering analysis of micelles and PFOB nanoemulsions stabilized by **5.1** or **5.2**. Perfluorooctylbromide-in-water nanoemulsions were prepared as described by the general nanoemulsion formation procedure, using responsive surfactant **5.1** or control surfactant **5.2**. Size was analyzed per the general nanoemulsion analysis procedure. Note: Data are representative of three replicate measurements.

Figure 5.2F. Temperature-dependent absorbance traces at 550 nm for **5.1-** or **5.2@micelles**. Absorbance profiles of free **5.1** or **5.2** were obtained in PBS 1X (pH 7.4) at 5 mg/mL polymer. Analyzed from 25 to 70 °C with 0.1 °C increments, 15 second equilibration between measurements, blanked versus polymer solution at room temperature (~25 °C). Note: Data are representative of the average of three independent measurements.

Figure 5.2G. Temperature-dependent polydispersity index traces for **5.1-** or **5.2@emulsions**, respectively, stabilized by either control surfactant **5.1** or thermoresponsive surfactant **5.2**. Polydispersity was analyzed via temperature-dependent DLS analysis, with 20 μL emulsion solution (10 vol% PFOB) diluted with 180 μL PBS (to a total of 1 vol% PFOB). Analyzed from 20 to 70 °C with 5 °C increments, 90 second equilibration between measurements. Note: Data are representative of the average of three independent measurements, each performed with three replicate measurements.

Figure 5.3. Size of PFOB nanoemulsions stabilized by POx surfactants **5.1** or **5.2**. Emulsions were prepared as described by the general nanoemulsion formation procedures and analyzed as described by the general nanoemulsion analysis procedure. Data are an average of three replicate measurements.

Figure 5.4. Size of micelles stabilized by POx surfactants **5.1** or **5.2**. Emulsions were prepared as described by the general micelle formation procedures and analyzed as described by the general micelle analysis procedure. Data are an average of three replicate measurements.

Figure 5.5. Heat-stage microscopy of **5.2@macroemulsions** in PBS or BSA. Macroemulsions were formed via general macroemulsion formation procedure and diluted with either PBS or BSA (250 mg/mL) from 20 to 65 °C. Sample was heated at a ramp of 5 °C/min from 20–65 °C and visualized under a 50X objective. Scale bar = 100 μm.

Figure 5.6. Library of block copolymers, corresponding LCSTs and PFOB emulsion degradation temperatures.

(A) See synthetic chemistry experimental procedures for synthesis of **5.3**–**5.5** and **5.2**. (B) Temperature-dependent absorbance traces at 550 nm for polymers **5.3**–**5.5** and **5.2**. Absorbance profiles were obtained by directly dissolving polymers in PBS (1X, pH 7.4) at 5 mg/mL. Analyzed from 25 to 60 °C with 0.1 °C increments, 15 second equilibration between measurements, blanked versus polymer solution at room temperature (~25 °C). Note: Data are representative of the average of three independent measurements. (C) Temperature-dependent size traces for PFOB emulsions

stabilized by **5.3**–**5.5** and **5.2.** Polydispersity was analyzed via temperature-dependent DLS analysis, with 20 μL emulsion solution (10 vol% PFOB) diluted with 180 μL PBS (to a total of 1 vol% PFOB). Analyzed from 20 to 70 °C with 5 °C increments, 90 second equilibration between measurements. Note: Data are representative of the average of three independent measurements, each performed with three replicate measurements.

Figure 5.7B. LCST variation for **5.2@micelles** versus macromolecular crowding agent (mg/mL). LCST was determined by temperature-controlled UV-Vis analysis, performed on **5.2** and crowder dissolved in PBS (1X, pH 7.4) with polymer **5.2** at a final concentration of 5 mg/mL and crowders are varying concentrations. LCST was defined as the onset temperature at which absorbance begins to increase. Note: Data are representative of the average of two independent measurements.

Figure 5.7C. LCST variation for **5.2@emulsions** versus macromolecular crowding agent (mg/mL). LCST was determined by temperature-controlled DLS analysis, with 20 μL emulsion solution (10 vol% PFOB) diluted with 180 μL PBS/crowder solution (to a total of 200 μL, 1 vol% PFOB). Analyzed from 20 to 70 °C with 5 °C increments, 90 second equilibration between measurements. LCST was defined as the onset temperature at which polydispersity has increased (PDI > 0.5). Note: Data are representative of the average of three independent measurements, each performed with two independent measurements.

Figure 5.7D. Temperature-dependent absorbance traces at 550 nm of **5.2@micelles** in PBS with either (i) no additive (black line), (ii) Ficoll-400 macromolecular crowding agent (100–150 mg/mL, purple and blue lines) or (iii) monomeric sucrose (250 mg/mL, dashed red line). Analyzed

from 25 to 70 °C with 0.1 °C increments, 15 second equilibration between measurements, blanked versus polymer solution at room temperature (~25 °C).

Figure 5.7E. Macroscopic LCST at room temperature for **5.2@micelles** in presence of PEG-10k crowder. Vials containing (i) solutions of PEG-10k (250 mg/mL), **5.2** (5 mg/mL), or both **5.2** and PEG-10k (5 and 250 mg/mL, respectively) solubilized in PBS (pH 7.4). Solutions were directly photographed before and after brief (<30 seconds) heating at 65 °C on a hot plate.

Figure 5.7G. Confocal microscopy of **5.2@macroemulsions** containing **5.9**, **5.10**, or both **5.9** and **5.10**. 12 nmol of **5.9** and **5.10** were each dissolved in 40 μL of PFOB in an eppendorph. For droplets containing both dyes, **5.9** and **5.10** were co-solubilized in 40 μL of PFOB in an eppendorph. PBS was added on top of the PFOB (153 μL), followed by a stock solution of **5.2** in PBS (28 mg/mL, 7 μL) to a total concentration of [**5.2**] = 1 mg/mL. Solution was vortexed and sonicated on ice for ~15 seconds. Emulsion solutions were then diluted to a total of 5 vol% in either PBS (i–iv) or PEG-10k (v–vi, 250 mg/mL). For i, iii, and v, dyes were independently excited and channels were overlaid (Blue, **5.9**: Ex. 488 nm, collected 520–620 nm. Red, **5.10**: Ex. 635 nm, collected 700–800 nm). For ii, iv, and vi, FRET was performed (Ex. 488, collected 700–800 nm).

Figure 5.7H. Average particle size for each solution (*i.e.,* within i, iii and v). Image analysis was performed in Fiji.[52] Values and error bars are representative of at least twenty droplets for each control sample, and all four droplets for the crowded solution.

Figure 5.7I. Mean fluorescence intensities (MFI) within FRET channel for each solution (*i.e.,* ii, iv and vi). Image analysis was performed in Fiji.[52] Values and error bars are representative of at least five droplets.

Figure 5.8A. Crowder-dependent LCST changes of **5.2@micelles**. Micelles were diluted in PBS (1X, pH 7.4) at 5 mg/mL containing macromolecular crowding agents (0–250 mg/mL). **5.2**-stabilized micelles were formed via the general micelle formation procedure. Analyzed from 25 to 70 °C with 0.1 °C increments, 15 second equilibration between measurements, blanked versus polymer solution at room temperature (~25 °C).

Figure 5.8B. Temperature-dependent absorbance traces at 550 nm of solutions with **5.2@micelles** (5 mg/mL) in PBS (1X, pH 7.4) containing Dextran-70 (50–150 mg/mL). **5.2@micelles** were formed via the general micelle formation procedure. Analyzed from 25 to 65 °C with 0.1 °C increments, 15 second equilibration between measurements, blanked versus polymer solution at room temperature (~25 °C). Data is representative of at least two independent experiments.

Figure 5.8C. Temperature-dependent absorbance traces at 550 nm of **5.2@micelles** (5 mg/mL) in PBS (1X, pH 7.4) containing PEG-10k (50–200 mg/mL). **5.2@micelles** were formed via the general micelle formation procedure. Analyzed from 25 to 65 °C with 0.1 °C increments, 15 second equilibration between measurements, blanked versus polymer solution at room temperature (~25 °C). Data is representative of at least two independent experiments.

Figure 5.8D. Temperature-dependent absorbance traces at 550 nm of solutions with **5.2@micelles** (5 mg/mL) in PBS (1X, pH 7.4) containing Ficoll-400 (50–200 mg/mL). **5.2@micelles** were formed via the general micelle formation procedure. Analyzed from 25 to 65 °C with 0.1 °C increments, 15 second equilibration between measurements, blanked versus polymer solution at room temperature (~25 °C). Data is representative of at least two independent experiments.

Figure 5.9. Temperature-dependent absorbance traces at 550 nm of **5.1@micelles** (5 mg/mL) in PBS (1X, pH 7.4) containing macromolecular crowding agents (250 mg/mL). **5.1@micelles** were formed via the general micelle formation procedure. Analyzed from 25 to 65 °C with 0.1 °C increments, 15 second equilibration between measurements, blanked versus polymer solution at room temperature (~25 °C).

Figure 5.10A. Crowder-dependent LCST changes of **5.2@emulsions**. Emulsions were diluted in PBS (1X, pH 7.4) at 10 vol% containing macromolecular crowding agents (0–250 mg/mL). **5.2@emulsions** were formed via the general emulsion formation procedure. Analyzed from 20 to 70 °C with 5 °C increments, 90 second equilibration between measurements.

Figure 5.10B. Temperature-dependent polydispersity indexes traces of **5.2@emulsions** (10 vol%) in PBS (1X, pH 7.4) containing Dextran-70 (10–50 mg/mL). **5.2@emulsions** were formed via the general emulsion formation procedure. Analyzed from 25 to 60 °C with 5 °C increments, 120 second equilibration between measurements. LCST was defined as the onset of heterogeneity/aggregation, *i.e.,* the polydispersity index of the solution was ≥0.50. Data is representative of at least two independent experiments.

Figure 5.10C. Temperature-dependent polydispersity indexes traces of **5.2@emulsions** (10 vol%) in PBS (1X, pH 7.4) containing PEG-10k (10–100 mg/mL). **5.2@emulsions** were formed via the general emulsion formation procedure. Analyzed from 25 to 60 °C with 5 °C increments, 120 second equilibration between measurements. LCST was defined as the onset of heterogeneity/aggregation, *i.e.,* the polydispersity index of the solution was ≥0.50. Data is representative of at least two independent experiments.

Figure 5.10D. Temperature-dependent polydispersity indexes traces of **5.2@emulsions** (10 vol%) in PBS (1X, pH 7.4) containing Ficoll-400 (25–75 mg/mL). **5.2@emulsions** were formed via the general emulsion formation procedure. Analyzed from 25 to 60 °C with 5 °C increments, 120 second equilibration between measurements. LCST was defined as the onset of heterogeneity/aggregation, *i.e.,* the polydispersity index of the solution was ≥0.50. Data is representative of at least two independent experiments.

Figure 5.11A. Temperature-dependent polydispersity indexes traces of **5.2@emulsions** in PBS (1X, pH 7.4) containing either (i) no additive (black line), (ii) PEG-10k macromolecular crowder (25 mg/mL, red line) or (iii) equimolar 18- crown-6 (dashed blue line). Analyzed from 25 to 55 °C with 5 °C increments, 90 second equilibration between measurements, with dilutions done according to the temperature-dependent nanoemulsion analysis procedure.

Figure 5.11B. Temperature-dependent dynamic light scattering traces of **5.2@emulsions** solutions in PBS (1X, pH 7.4) containing either (i) no additive (black line), (ii) PEG-10k macromolecular crowder (45 mg/mL, blue dashed line) or (iii) ethylene glycol viscogen to make up either the same viscosity (220 mg/mL, dashed red line) or double the viscosity (450 mg/mL,

dashed purple line). Bulk viscosity comparisons between PEG and ethylene glycol were taken from literature precedent.[40] Analyzed from 25 to 65 °C with 5 °C increments, 90 second equilibration between measurements.

Figure 5.12A. Temperature-dependent absorbance traces at 550 nm of solutions with **5.2@micelles** in PBS, from 2 to 28 mg/mL. Absorbance profiles were obtained by directly dissolving **2** in PBS (1X, pH 7.4) at 5 mg/mL. Analyzed from 25 to 70 °C with 0.1 °C increments, 15 second equilibration between measurements, blanked versus polymer solution at room temperature (~25 °C). Note: Data are representative of the average of three independent measurements.

Figure 5.12B. Temperature-dependent size traces for serial dilutions of **5.2@emulsions**. A stock of **2@emulsions** was formed via the general emulsion formation procedure. Dilutions were performed in PBS (1X, pH 7.4). Volume percentages in the legend correspond to volume % PFOB after serial dilution. Analyzed from 20 to 70 °C with 5 °C increments, 90 second equilibration between measurements.

Figure 5.12C. Temperature-dependent polydispersity index of **5.2@emulsions** solutions at pH ranges from 4 to 13. Solutions were pH'd in PBS (1X) using 0.5M NaOH or HCl. Analyzed from 25 to 65 °C with 5 °C increments, 90 second equilibration between measurements. **5.2@emulsions** were formed via the general emulsion formation procedure and diluted according to the temperature-dependent general nanoemulsion analysis procedure.

Figure 5.12D. Temperature-dependent absorbance traces at 550 nm of **5.2@micelles** in either MilliQ water or PBS (1X, pH 7.4). Analyzed from 25 to 70 °C with 0.1 °C increments, 15 second equilibration between measurements, blanked versus polymer solution at room temperature (~25 °C).

Figure 5.13. 5.1@micelles in presence of PEG-10k crowder. Vials containing solutions of PEG-10k (250 mg/mL), **5.1@micelles** (5 mg/mL), or both **5.1@micelles** and PEG-10k (5 and 250 mg/mL, respectively) solubilized in PBS (pH 7.4). Solutions were directly photographed before and after brief (<10 minutes) heating at 65 °C on a hot plate.

Figure 5.14. Crowder response of **5.1@** or **5.2@emulsions**. Vials containing solutions of **5.1@**- or **5.2@emulsions** were formed according to the general nanoemulsion formation procedure, with slight modifications–PFOB and PBS were emulsified at a 1:2 vol% ratio (rather than 1:10 vol%) to ensure visual phase separation. Emulsions solutions were then further diluted at a 1:1 vol% ratio with PBS 1X (pH 7.4) or a 200 mg/mL PEG-10k in PBS stock (to a total PEG-10k concentration of 100 mg/mL). Solutions were briefly heated at 37 °C for 10 minutes on a hot plate, removed and directly photographed.

Figure 5.15A/B. Localization of **5.10** within **5.2@emulsions** in (i) PBS or (ii) PEG-10k solution in PBS (250 mg/mL), as shown in Figure 3G. PFOB droplets were diluted at 10 vol% in either solution.

Figure 5.16B. LCST variation for **5.2@micelles** versus bovine serum albumin (mg/mL). LCST was determined by temperature-controlled UV-Vis analysis, performed on **5.2** and BSA dissolved in PBS (1X, pH 7.4) with polymer **5.2** at a final concentration of 5 mg/mL and BSA at varying

concentrations. LCST was defined as the onset temperature at which absorbance begins to increase. Note: Data are representative of the average of two independent measurements.

Figure 5.16C. LCST variation for **5.2@emulsions** versus bovine serum albumin (mg/mL). LCST was determined by temperature-controlled DLS analysis, with 20 μL emulsion solution (10 vol% PFOB) diluted with 180 μL PBS/BSA solution (to a total of 200μL, 1 vol% PFOB). Analyzed from 20 to 70 °C with 5 °C increments, 90 second equilibration between measurements. LCST was defined as the onset temperature at which polydispersity has increased (PDI > 0.5). Note: Data are representative of the average of three independent measurements, each performed with two independent measurements.

Figure 5.16D. Optical microscopy of **5.1@emulsions** and **5.2@emulsions** in the presence of PBS 1X (pH 7.4) or PBS/BSA solutions (250 mg/mL) at room temperature. Emulsions were formed per the general nanoemulsion formation procedure. On an epifluorescence microscope, added 100 μL of either PBS 1X or PBS/BSA stock (250 mg/mL BSA), followed by 20 μL of **5.1@emulsions** or **5.2@emulsions**. Solution was pipetted at least three times to mix. Recorded images after ~20 seconds of equilibration, scale bar: 200 μm. Note: Images are representative of three independent experiments.

Figure 5.16E. Temperature-dependent polydispersity index traces for **5.2@emulsions**, analyzed via temperature-dependent DLS analysis. Each solution contained 20 μL emulsion solution (10 vol% PFOB). Emulsions were then diluted accordingly: either with 180 μL PBS +/- BSA (to a total of 1 vol% PFOB), or directly with fetal bovine serum (FBS) or human serum (HS). Protein

contents were obtained via the specification sheets, as mentioned in the general experiment section. Analyzed from 20 to 70 °C with 5 °C increments, 90 second equilibration between measurements. Note: Data are representative of the average of three independent measurements, each performed with three replicate measurements.

Figure 5.17. Temperature-dependent absorbance traces at 550 nm of solutions with **5.2@micelles** (5 mg/mL) in PBS (1X, pH 7.4) containing BSA (50–200 mg/mL). **5.2**-stabilized micelles were formed via the general micelle formation procedure. Analyzed from 25 to 70 °C with 0.1 °C increments, 15 second equilibration between measurements, blanked versus polymer solution at room temperature (~25 °C). Data is representative of at least two independent experiments.

Figure 5.18. Temperature-dependent DLS traces of **5.2@emulsions** diluted at 10 vol% (i) PBS containing BSA (50–200 mg/mL), (ii) human serum media (contains ~52 mg/mL human serum albumin), or (iii) fetal bovine serum (contains ~36 mg/mL fetal bovine serum albumin). **5.2**-stabilized emulsions were formed via the general emulsion formation procedure. Analyzed from 25 to 70 °C with 5 °C increments, 120 second equilibration between measurements. Data is representative of at least three independent experiments.

Figure 5.19. Temperature-dependent heterogeneity of **5.1**- and **5.2@emulsions** solutions with (dashed line) and without (solid line) BSA additive (100 mg/mL), as analyzed by DLS according to the Figure 3B experimental procedure.

Figure 5.20. Crowder-induced phase separation of **5.2@emulsions**. Vials containing solutions of **5.1**- or **5.2**-stabilized PFOB droplets were formed according to the general nanoemulsion formation procedure, with slight modifications–PFOB and PBS were emulsified at a 1:2 vol% ratio (rather than 1:10 vol%) to ensure visual phase separation. Emulsions solutions were then further diluted at a 1:1 vol% ratio with PBS 1X (pH 7.4) or a 200 mg/mL BSA in PBS stock (to a total BSA concentration of 100 mg/mL). Solutions were briefly heated at 37 °C for 10 minutes on a hot plate, removed and directly photographed.

Figure 5.22. Minimum concentration of crowder needed to induce fusion of **5.2@emulsions** (mg/mL) versus overlap concentration of crowder (mg/mL). All dilutions done according to the temperature-dependent nanoemulsion analysis procedure.

Figure 5.23. Minimum concentration of crowder needed to induce fusion of **5.2@emulsions** (mg/mL) versus overlap concentration (mg/mL) of PEG crowder at varying molecular weights: 1, 2, 4, 8 and 10 kDa. Critical aggregation concentration is defined as the minimum concentration of crowder needed to trigger demulsification of PFOB NEs at room temperature, as determined by dynamic light scattering analysis. Data is a summation of temperature-dependent DLS traces of solutions with **5.2@emulsions** (10 vol%) in PBS (1X, pH 7.4) containing PEG at varying molecular weights and concentrations. **5.2@emulsions** were formed via the general emulsion formation procedure. Analyzed from 25 to 60 °C with 5 °C increments, 120 second equilibration between measurements. LCST was defined as the onset of heterogeneity/aggregation, *i.e.,* the polydispersity index of the solution was ≥0.50. Data is representative of at least two independent experiments.

Figure 5.24B/C. Transgenic zebrafish line *Tg(actb2:mem-NeoGreen)*^{hm37} were microinjected with either **5.1@emulsions** or **5.2@emulsions** containing rhodamine **5.11** at 1-cell stage. Injected embryos were dechorinated by 2 mg/mL pronase and mounted on glass bottom dishes with 1% methylcellulose for imaging. Images were acquired on a Zeiss LSM780 confocal microscope with either 10X lens or 40X lens at 8-cell stage. Acquired images were processed by Zen 3.0 SR black (Zeiss) and Fiji.[52] See Figure S35, S36 for zebrafish replicates (n = 5). See Figure S35, S36 for injections into PBS buffer.

Figure 5.24D. Cross-section diameters for **5.1@emulsions** and **5.2@emulsions** were obtained via the 40X single plane images. Image analysis was performed in Fiji.[52] Mean and standard deviation values represent the droplet diameters across zebrafish embryos (n > 90). See Figure S35, S36 for zebrafish replicates (n = 5) and control images in PBS buffer.

Figure 5.25. Temperature-dependent absorbance traces at 550 nm of solutions with free commercial poly(*N*-isopropylacrylamide) (PNIPAM, 5 mg/mL) in PBS (1X, pH 7.4) containing varying crowders (250 mg/mL). Analyzed from 25 to 65 °C with 0.1 °C increments, 15 second equilibration between measurements, blanked versus polymer solution at room temperature (~25 °C). Data is representative of at least two independent experiments.

5.12 1H-NMR Spectra Relevant to Chapter Five

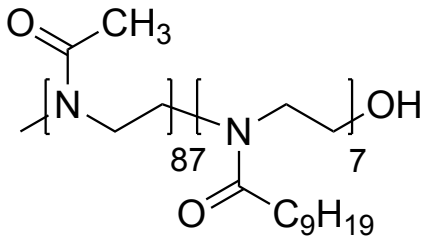

P(MeOx)$_{87}$-*b*-P(NonOx)$_7$ (**5.1**)

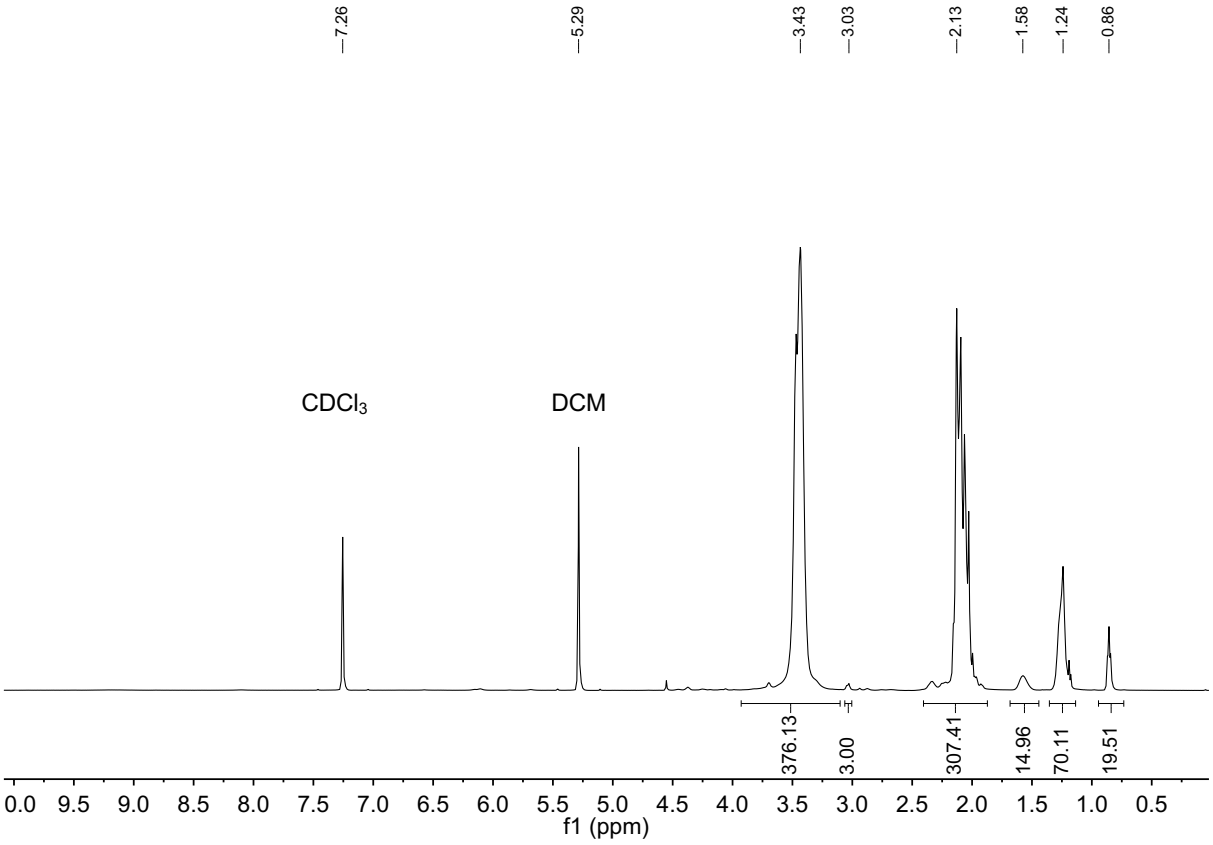

^{1}H NMR (500 MHz, $CDCl_3$) of copolymer **5.1** P(MeOx)$_{87}$-*b*-P(NonOx)$_7$.

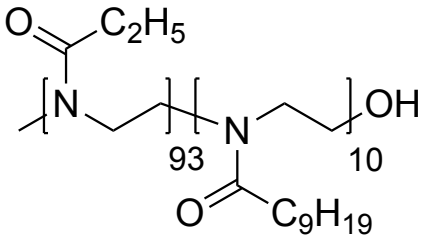

P(EtOx)$_{93}$-*b*-P(NonOx)$_{10}$ (**5.2**)

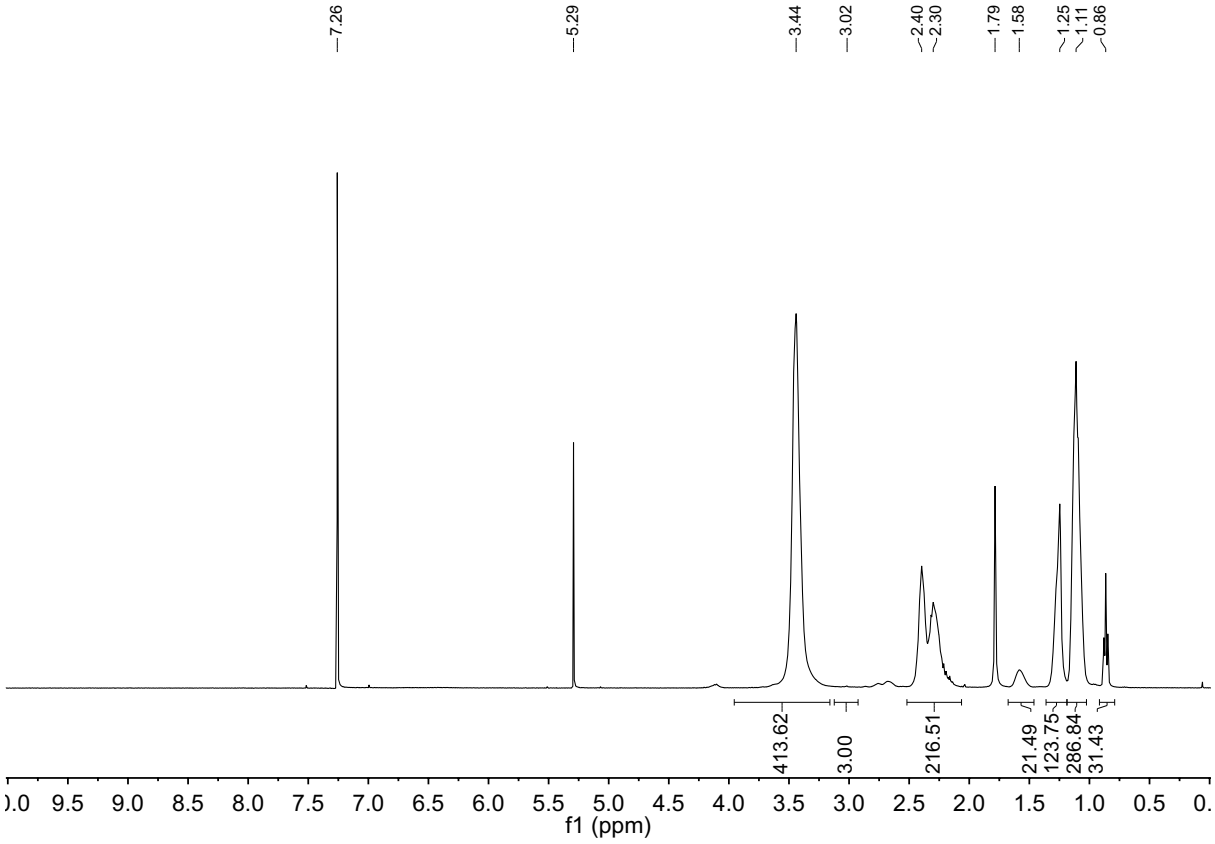

^{1}H NMR (500 MHz, $CDCl_3$) of copolymer **5.2** P(EtOx)$_{93}$-*b*-P(NonOx)$_{10}$.

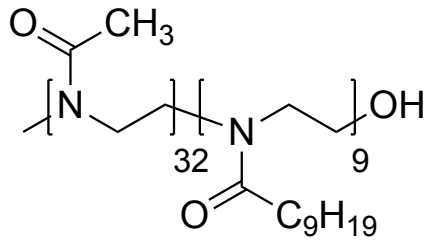

P(MeOx)$_{32}$-*b*-P(NonOx)$_9$ (**5.3**)

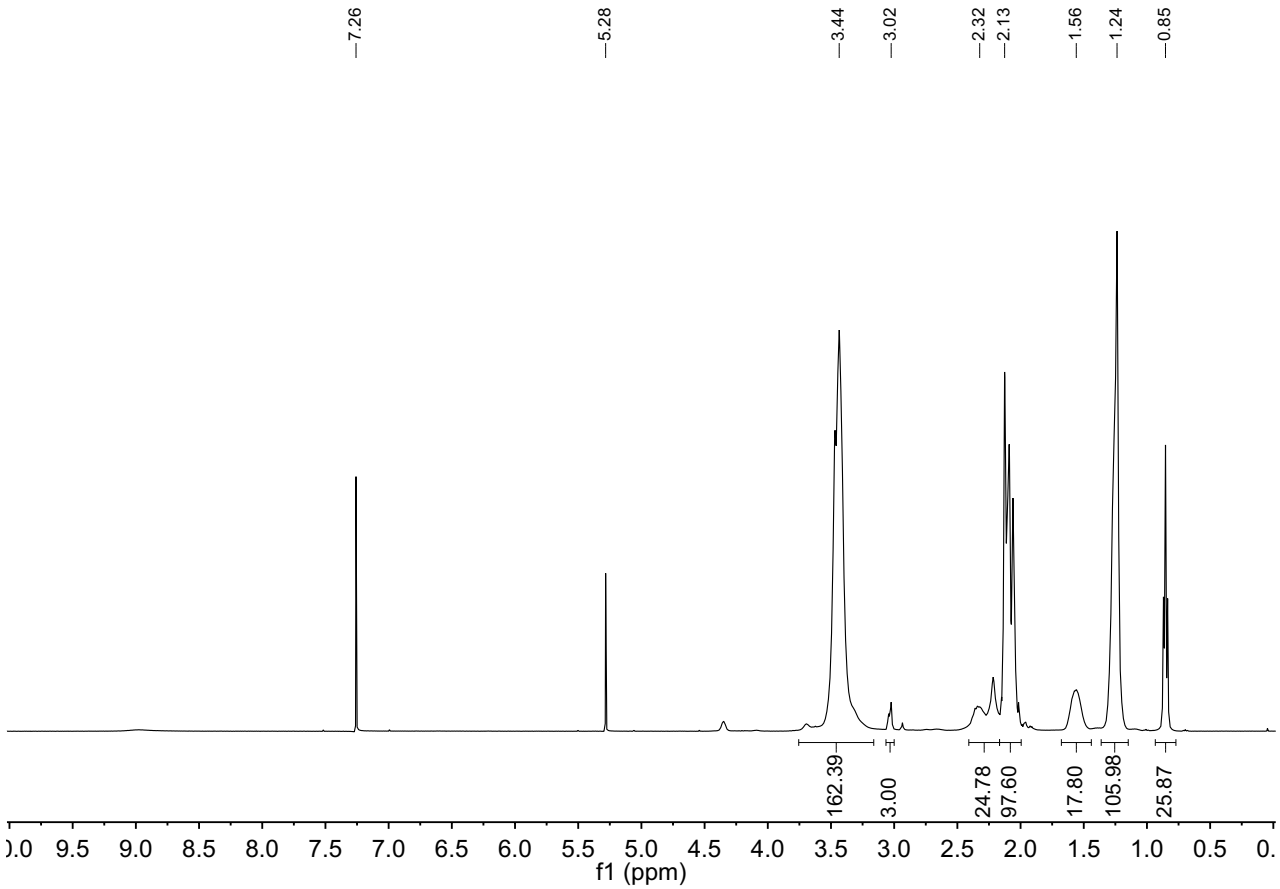

^{1}H NMR (500 MHz, $CDCl_3$) of copolymer **5.3** P(MeOx)$_{32}$-*b*-P(NonOx)$_9$.

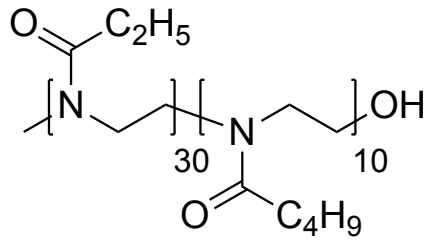

P(EtOx)$_{30}$-*b*-P(BuOx)$_{10}$ (**5.4**)

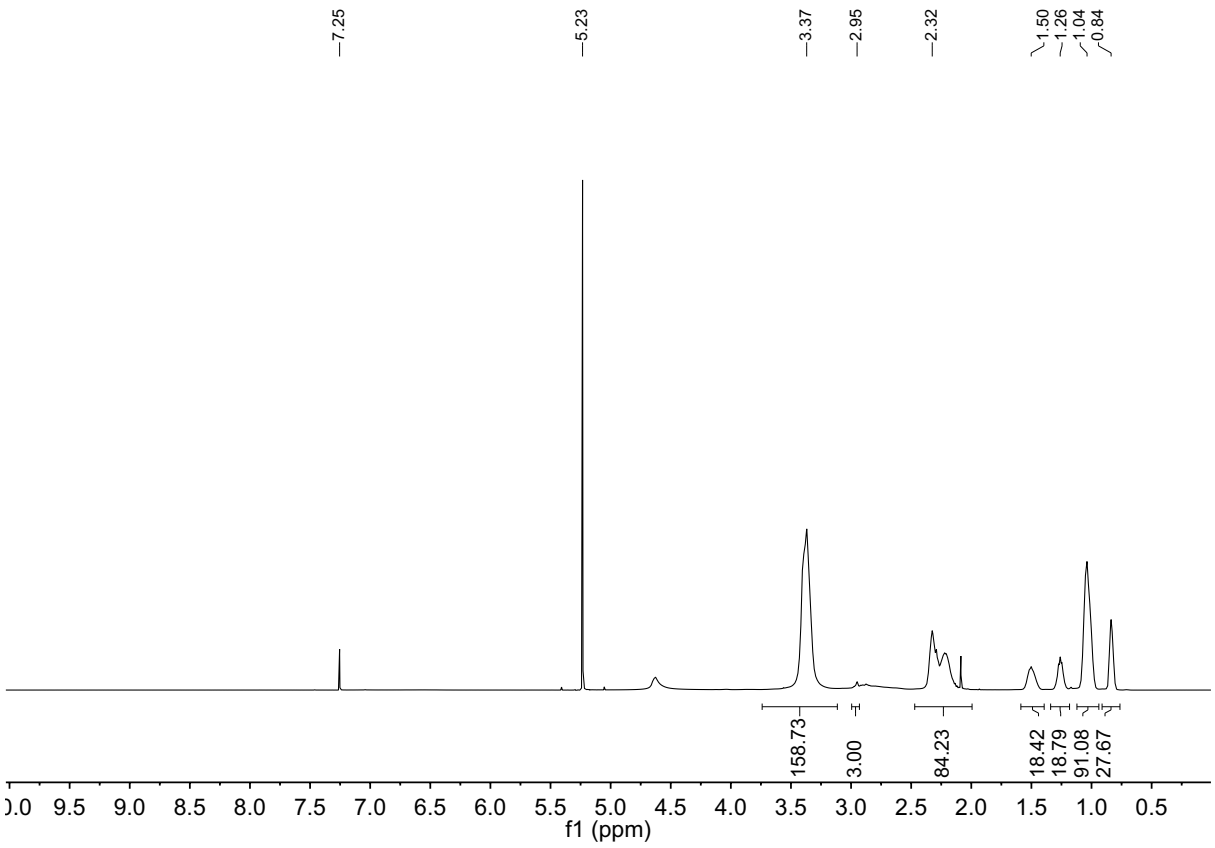

^{1}H NMR (500 MHz, $CDCl_3$) of copolymer **5.4** P(EtOx)$_{30}$-*b*-P(BuOx)$_{10}$.

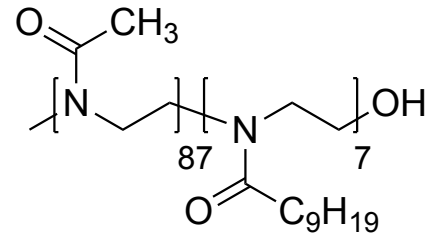

P(EtOx)$_{33}$-*b*-P(NonOx)$_{11}$ (**5.5**)

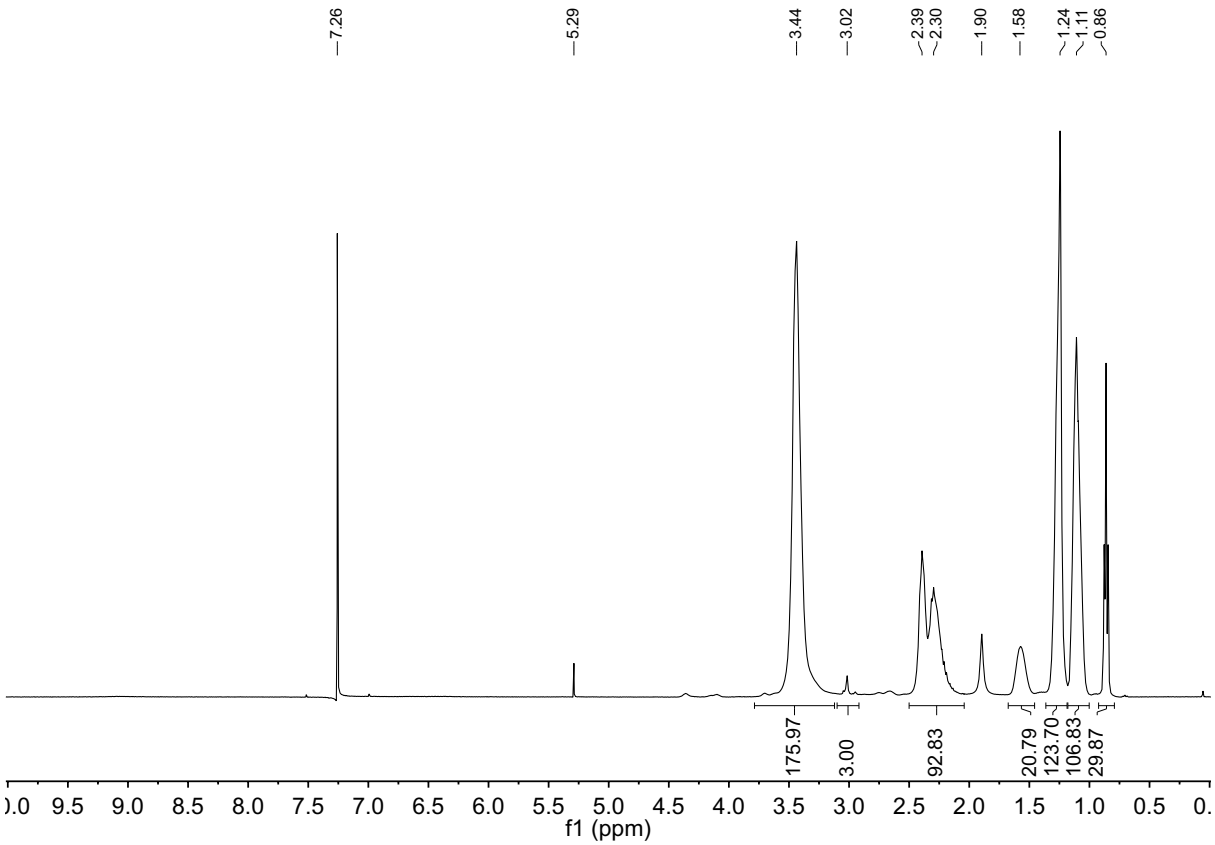

^{1}H NMR (500 MHz, $CDCl_3$) of copolymer **5.5** P(EtOx$_{33}$-*b*-NonOx$_{11}$).

5.13 References

(1) Mura, S.; Nicolas, J.; Couvreur, P. Stimuli-Responsive Nanocarriers for Drug Delivery. *Nat. Mater.* **2013**, *12*, 991–1003.

(2) Vijayakameswara Rao, N.; Ko, H.; Lee, J.; Park, J. H. Recent Progress and Advances in Stimuli-Responsive Polymers for Cancer Therapy. *Front. Bioeng. Biotechnol.* **2018**, *6*.

(3) Morey, M.; Pandit, A. Responsive Triggering Systems for Delivery in Chronic Wound Healing. *Adv. Drug Deliv. Rev.* **2018**, *129*, 169–193.

(4) Karimi, M.; Eslami, M.; Sahandi-Zangabad, P.; Mirab, F.; Farajisafiloo, N.; Shafaei, Z.; Ghosh, D.; Bozorgomid, M.; Dashkhaneh, F.; Hamblin, M. R. PH-Sensitive Stimulus-Responsive Nanocarriers for Targeted Delivery of Therapeutic Agents. *Wiley Interdiscip. Rev. Nanomedicine Nanobiotechnology* **2016**, *8*, 696–716.

(5) Jung, F. T. Blood and Other Body Fluids. *Jama* **1961**, *178*, 92.

(6) Ellis, R. J. Macromolecular Crowding: Obvious but Underappreciated. *Trends Biochem. Sci.* **2001**, *26*, 597–604.

(7) Lippincott-Schwartz, J.; Snapp, E.; Kemvorthy, A. Studying Protein Dynamics in Living Cells. *Nat. Rev. Mol. Cell Biol.* **2001**, *2*, 444–456.

(8) Medalia, O.; Weber, I.; Frangakis, A. S.; Nicastro, D.; Gerisch, G.; Baumeister, W. Macromolecular Architecture in Eukaryotic Cells Visualized by Cryoelectron Tomography. *Science* **2002**, *298*, 1209–1213.

(9) Gura Sadovsky, R.; Brielle, S.; Kaganovich, D.; England, J. L. Measurement of Rapid Protein Diffusion in the Cytoplasm by Photo-Converted Intensity Profile Expansion. *Cell Rep.* **2017**, *18*, 2795–2806.

(10) Xiang, L.; Chen, K.; Yan, R.; Li, W.; Xu, K. Single-Molecule Displacement Mapping

Unveils Nanoscale Heterogeneities in Intracellular Diffusivity. *Nat. Methods* **2020**, *17*, 524–530.

(11) Zimmerman, S. B.; Trach, S. O. Estimation of Macromolecule Concentrations and Excluded Volume Effects for the Cytoplasm of Escherichia Coli. *J. Mol. Biol.* **1991**, *222*, 599–620.

(12) Zhou, H. X.; Rivas, G.; Minton, A. P. Macromolecular Crowding and Confinement: Biochemical, Biophysical, and Potential Physiological Consequences. *Annu. Rev. Biophys.* **2008**, *37*, 375–397.

(13) Zimmerman, S. B.; Minton, A. P. Macromolecular Crowding: Biochemical, Biophysical, and Physiological Consequences. *Annu. Rev. Biophys. Biomol. Struct.* **1993**, *22*, 27–65.

(14) Elcock, A. H. Models of Macromolecular Crowding Effects and the Need for Quantitative Comparisons with Experiment. *Curr. Opin. Struct. Biol.* **2010**, *20*, 196–206.

(15) Ward, M. A.; Georgiou, T. K. Thermoresponsive Polymers for Biomedical Applications. *Polymers (Basel).* **2011**, *3*, 1215–1242.

(16) Zardad, A. Z.; Choonara, Y. E.; du Toit, L. C.; Kumar, P.; Mabrouk, M.; Demarco Kondiah, P. P.; Pillay, V. A Review of Thermo- and Ultrasound-Responsive Polymeric Systems for Delivery of Chemotherapeutic Agents. *Polymers (Basel).* **2016**, *8*, 1–22.

(17) Tsuji, S.; Kawaguchi, H. Thermosensitive Pickering Emulsion Stabilized by Poly(N-Isopropylacrylamide)-Carrying Particles. *Langmuir* **2008**, *24*, 3300–3305.

(18) Ding, Y.; Zhang, G. Collapse and Aggregation of Poly(N-Isopropylacrylamide) Chains in Aqueous Solutions Crowded by Polyethylene Glycol. *J. Phys. Chem. C* **2007**, *111*, 5309–5312.

(19) Sakota, K.; Tabata, D.; Sekiya, H. Macromolecular Crowding Modifies the Impact of

Specific Hofmeister Ions on the Coil-Globule Transition of PNIPAM. *J. Phys. Chem. B* **2015**, *119*, 10334–10340.

(20) Hoogenboom, R.; Thijs, H. M. L.; Jochems, M. J. H. C.; Van Lankvelt, B. M.; Fijten, M. W. M.; Schubert, U. S. Tuning the LCST of Poly(2-Oxazoline)s by Varying Composition and Molecular Weight: Alternatives to Poly(N-Isopropylacrylamide)? *Chem. Commun.* **2008**, No. 44, 5758–5760.

(21) Cooperstein, M. A.; Canavan, H. E. Assessment of Cytotoxicity of (N-Isopropyl Acrylamide) and Poly(N-Isopropyl Acrylamide)-Coated Surfaces. *Biointerphases* **2013**, *8*, 1–12.

(22) Lutz, J. F.; Akdemir, Ö.; Hoth, A. Point by Point Comparison of Two Thermosensitive Polymers Exhibiting a Similar LCST: Is the Age of Poly(NIPAM) Over? *J. Am. Chem. Soc.* **2006**, *128*, 13046–13047.

(23) Hoogenboom, R.; Schlaad, H. Thermoresponsive Poly(2-Oxazoline)s, Polypeptoids, and Polypeptides. *Polym. Chem.* **2017**, *8*, 24–40.

(24) Lambermont-Thijs, H. M. L.; Hoogenboom, R.; Fustin, C. A.; Bomal-D'Haese, C.; Gohy, J. F.; Schubert, U. S. Solubility Behavior of Amphophilic Block and Random Copolymers Based on 2-Ethyl-2-Oxazoline and 2-Nonyl-2-Oxazoline in Binary Water-Ethanol Mixtures. *J. Polym. Sci. Part A Polym. Chem.* **2009**, *47*, 515–522.

(25) Day, R. A.; Estabrook, D. A.; Wu, C.; Chapman, J. O.; Togle, A. J.; Sletten, E. M. Systematic Study of Perfluorocarbon Nanoemulsions Stabilized by Polymer Amphiphiles. *ACS Appl. Mater. Interfaces* **2020**, *12*, 38887–38898.

(26) Zhang, Q.; Weber, C.; Schubert, U. S.; Hoogenboom, R. Thermoresponsive Polymers with Lower Critical Solution Temperature: From Fundamental Aspects and Measuring

Techniques to Recommended Turbidimetry Conditions. *Mater. Horizons* **2017**, *4*, 109–116.

(27) Ten Brummelhuis, N.; Schlaad, H. Stimuli-Responsive Star Polymers through Thiol-Yne Core Functionalization/ Crosslinking of Block Copolymer Micelles. *Polym. Chem.* **2011**, *2*, 1180–1184.

(28) Sletten, E. M.; Swager, T. M. Readily Accessible Multifunctional Fluorous Emulsions. *Chem. Sci.* **2016**, *7*, 5091–5097.

(29) Sletten, E. M.; Swager, T. M. Fluorofluorophores: Fluorescent Fluorous Chemical Tools Spanning the Visible Spectrum. *J. Am. Chem. Soc.* **2014**, *136*, 13574–13577.

(30) Miller, M. A.; Sletten, E. M. A General Approach to Biocompatible Branched Fluorous Tags for Increased Solubility in Perfluorocarbon Solvents. *Org. Lett.* **2018**, *20*, 6850–6854.

(31) Miller, M. A.; Day, R. A.; Estabrook, D. A.; Sletten, E. M. A Reduction-Sensitive Fluorous Fluorogenic Coumarin. *Synlett* **2020**, *31*, 450–454.

(32) Riess, J. G. Understanding the Fundamentals of Perfluorocarbons and Perfluorocarbon Emulsions Relevant to in Vivo Oxygen Delivery. *Artif. Cells. Blood Substit. Immobil. Biotechnol.* **2005**, *33*, 47–63.

(33) Sun, J.; Wang, W.; He, F.; Chen, Z. H.; Xie, R.; Ju, X. J.; Liu, Z.; Chu, L. Y. On-Chip Thermo-Triggered Coalescence of Controllable Pickering Emulsion Droplet Pairs. *RSC Adv.* **2016**, *6*, 64182–64192.

(34) Dinari, A.; Abdollahi, M.; Sadeghizadeh, M. Design and Fabrication of Dual Responsive Lignin-Based Nanogel via “Grafting from” Atom Transfer Radical Polymerization for Curcumin Loading and Release. *Sci. Rep.* **2021**, *11*, 1–16.

(35) Kowalczuk, A.; Kronek, J.; Bosowska, K.; Trzebicka, B.; Dworak, A. Star Poly(2-Ethyl-2-Oxazoline)s-Synthesis and Thermosensitivity. *Polym. Int.* **2011**, *60*, 1001–1009.

(36) Chapman, R.; Bouten, P. J. M.; Hoogenboom, R.; Jolliffe, K. A.; Perrier, S. Thermoresponsive Cyclic Peptide – Poly(2-Ethyl-2-Oxazoline) Conjugate Nanotubes. *Chem. Commun.* **2013**, *49*, 6522–6524.

(37) Kozer, N.; Kuttner, Y. Y.; Haran, G.; Schreiber, G. Protein-Protein Association in Polymer Solutions: From Dilute to Semidilute to Concentrated. *Biophys. J.* **2007**, *92*, 2139–2149.

(38) McClements, D. J. Comments on Viscosity Enhancement and Depletion Flocculation by Polysaccharides. *Food Hydrocoll.* **2000**, *14*, 173–177.

(39) Shikata, T.; Okuzono, M.; Sugimoto, N. Temperature-Dependent Hydration/Dehydration Behavior of Poly(Ethylene Oxide)s in Aqueous Solution. *Macromolecules* **2013**, *46*, 1956–1961.

(40) Kozer, N.; Kuttner, Y. Y.; Haran, G.; Schreiber, G. Protein-Protein Association in Polymer Solutions: From Dilute to Semidilute to Concentrated. *Biophys. J.* **2007**, *92*, 2139–2149.

(41) Lim, I.; Vian, A.; Van De Wouw, H. L.; Day, R. A.; Gomez, C.; Liu, Y.; Rheingold, A. L.; Campàs, O.; Sletten, E. M. Fluorous Soluble Cyanine Dyes for Visualizing Perfluorocarbons in Living Systems. *J. Am. Chem. Soc.* **2020**, *142*, 16072–16081.

(42) Geyer, P. E.; Holdt, L. M.; Teupser, D.; Mann, M. Revisiting Biomarker Discovery by Plasma Proteomics. *Mol. Syst. Biol.* **2017**, *13*, 942.

(43) Bickmore, W. A.; Sutherland, H. G. E. Addressing Protein Localization within the Nucleus. *EMBO J.* **2002**, *21*, 1248–1254.

(44) Venturoli, D.; Rippe, B. Ficoll and Dextran vs. Globular Proteins as Probes for Testing Glomerular Permselectivity: Effects of Molecular Size, Shape, Charge, and Deformability. *Am. J. Physiol. - Ren. Physiol.* **2005**, *288*.

(45) Sun, X. L.; Tsai, P. C.; Bhat, R.; Bonder, E. M.; Michniak-Kohn, B.; Pietrangelo, A. Thermoresponsive Block Copolymer Micelles with Tunable Pyrrolidone-Based Polymer Cores: Structure/Property Correlations and Application as Drug Carriers. *J. Mater. Chem. B* **2015**, *3*, 814–823.

(46) Theillet, F. X.; Binolfi, A.; Frembgen-Kesner, T.; Hingorani, K.; Sarkar, M.; Kyne, C.; Li, C.; Crowley, P. B.; Gierasch, L.; Pielak, G. J.; et al. Physicochemical Properties of Cells and Their Effects on Intrinsically Disordered Proteins (IDPs). *Chem. Rev.* **2014**, *114*, 6661–6714.

(47) Hyman, A. A.; Weber, C. A.; Jülicher, F. Liquid-Liquid Phase Separation in Biology. *Annu. Rev. Cell Dev. Biol.* **2014**, *30*, 39–58.

(48) Gomes, E.; Shorter, J. The Molecular Language of Membraneless Organelles. *J. Biol. Chem.* **2019**, *294*, 7115–7127.

(49) Sataloff, R. T.; Johns, M. M.; Kost, K. M. Molecular Aspects of the Stress Response: Chaperones, Membranes and Networks. *Mol. Asp. Stress Response Chaperones, Membr. Networks* **2007**.

(50) Boersma, A. J.; Zuhorn, I. S.; Poolman, B. A Sensor for Quantification of Macromolecular Crowding in Living Cells. *Nat. Methods* **2015**, *12*, 227–229.

(51) Pangborn, A. B.; Giardello, M. A.; Grubbs, R. H.; Rosen, R. K.; Timmers, F. J. Safe and Convenient Procedure for Solvent Purification. *Organometallics* **1996**, *15*, 1518–1520.

(52) Schindelin, J.; Arganda-Carreras, I.; Frise, E.; Kaynig, V.; Longair, M.; Pietzsch, T.;

Preibisch, S.; Rueden, C.; Saalfeld, S.; Schmid, B.; et al. Fiji: An Open-Source Platform for Biological-Image Analysis. *Nat. Methods* **2012**, *9*, 676–682.

(53) Nüsslein-Volhard, C.; Dahm, R. Zebrafish: A Practical Approach. **2002**, 328.

(54) Estabrook, D. A.; Ennis, A. F.; Day, R. A.; Sletten, E. M. Controlling Nanoemulsion Surface Chemistry with Poly(2-Oxazoline) Amphiphiles. *Chem. Sci.* **2019**, *10*, 3994–4003.

CHAPTER SIX

Collaborative Highlights, Preliminary Work, and Future Directions

Adapted from: "Perfluorocarbon nanoemulsion promotes the delivery of reducing equivalents for electricity-driven microbial CO_2 reduction", Rodrigues, R.; Guan, X.; Iñiguez, J.; Estabrook, D.; Chapman, J.; Huang, S.; Sletten, E.; Liu, C.*, *Nature Catal.*, **2019**, *2*, 407−414. DOI: https://doi.org/10.1038/s41929-019-0264-0; "Perfluorocarbon Nanoemulsions Create a Beneficial O_2 Microenvironment in N_2-fixing Biological | Inorganic Hybrid", Lu, S.; Rodrigues, R. M.; Huang, S.; Estabrook, D.; Chapman, J. O.; Guan, X.; Sletten, E. M.; Liu, C.*, *submitted*.

6.1 Abstract

This chapter is dedicated to both highlighting collaborative efforts, as well as preliminary findings on projects that establish future directions for our perfluorocarbon (PFC) nanoemulsion platform. The first section will summarize an ongoing collaboration with Professor Chong Liu's lab here at UCLA that extends the PFC emulsion platform to electricity-driven microbial fixation. This section includes published and recently submitted work. The second section will discuss the development of thermoresponsive polymeric surfactants for use in silica nanoparticle-mediated non-invasive imaging, a manuscript currently in preparation by Professor Jeffrey Zink's lab. Finally, preliminary findings in host-guest mediated emulsion fusion will be discussed, laying the groundwork for future projects within the lab.

6.2 Converting Carbon Dioxide to Commodity Chemicals: Employing Perfluorocarbons as Gas Carriers in Bioelectrochemical Systems

As global temperatures continue to trend towards a tipping point, greenhouse gases such as carbon dioxide (CO_2) are currently found at atmospheric levels not seen since some four million years ago.[1] As technologies and political strategies aim to reduce our current carbon footprints, there is concurrent interest in the ability to remove, convert and store carbon dioxide as commodity chemicals.[2,3] While there are a number of strategies involving the use of electricity, light or heat, many of these techniques are hindered by limitations in their overall energy efficiency and productivity.[4,5] Of course, certain biological systems have evolved to meet these needs through photosynthetic processes, converting carbon dioxide and water into organic molecules using sunlight. Drawing inspiration from these organisms, Chong Liu *et al.* had previously developed biological | inorganic hybrids capable of chemically reducing CO_2 at higher energy efficiencies than natural photosynthetic systems.[6] These biocompatible catalytic systems are capable of removing carbon dioxide from the air at energy efficiencies roughly 10 times that of plants. Despite this success, a limitation of the system is that necessary gases within the conversion pathway–like H_2 or N_2–do not stay dissolved in the aqueous environment. To overcome this bottleneck, the Liu group aimed to exploit the high gas solubilities of our PFC nanoemulsion systems in a biological | inorganic hybrid that converts carbon dioxide to a feedstock chemical, here acetic acid (Figure 6.1).

The system developed by Liu and coworkers employs a microbial catalyst, *Sporomusa ovata* bacterium, capable of electricity-driven CO_2 fixation to acetic acid. These bacteria require H_2 to reduce CO_2 via the Wood–Ljungdahl pathway.[7,8] In this system, H_2 is generated from an

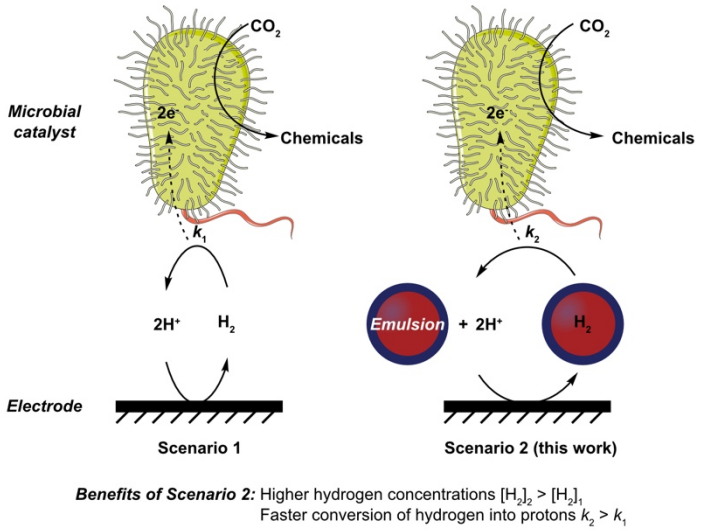

Figure 6.1. Schematic of the biological | inorganic hybrid hybrid system that integrates water-splitting catalysts with CO_2-fixing microorganisms. Scenario 1: Traditional electrochemical catalysts yield H_2, a gaseous product with limited solubility in water ($[H_2]_1$). Generated H_2 is transferred as a reducing equivalent to microbes and dispersed in the bulk solution for CO_2 reduction with a kinetic rate of k_1. The rate of CO_2 fixation and subsequently the productivity relies on the mass transport of H_2 from the electrode to the microbes in the solution. Scenario 2: Here, we apply PFC nanoemulsions as the H_2 carrier to accelerate the transfer of reducing equivalents. PFC nanoemulsions not only increase the H_2 concentration in the solution ($[H_2]_2$) but also accelerate the transfer kinetics (k_2), which increases the rate of CO_2 fixation. Here the local H_2 concentrations ($[H_2]_1$, $[H_2]_2$) and transfer kinetics (k_1, k_2) are correlated.

inorganic Co-P alloy catalyst loaded onto an electrode[6,9], whereafter it is transferred to the microbes and oxidized via hydrogenases. In a traditional system, H_2 delivery from the electrode is rate-determining (illustrated as k_1, Figure 6.1) and concentrations are limited by solubility in water[10] ($[H_2]_1$), reducing overall efficiency. Alternatively, it is known that PFC liquids have extraordinarily high gas solubilities due to weak intermolecular interactions.[11] These materials have previously been employed as the interior core of nanoemulsions, where the PFC liquid is suspended as droplets within an aqueous environment, for oxygen delivery.[12,13] For hydrogen, solubility in PFCs is up to an order of magnitude higher than in water.[14] We hypothesized that PFC emulsions could be used as a H_2 carrier within an improved system (Figure 6.1) and benefit from

high H_2 solubility ($[H_2]_2$) and accelerated gas delivery kinetics (k_2) due to small emulsion sizes (<300 nm).

In choosing our PFC emulsion core, we looked to work examining gas solubility within certain PFCs. Previously, it was demonstrated that perfluorohexanes (PFH, **6.1**) and perfluorodecalin (PFD, **6.2**) have high O_2 solubility, with PFH gas solubility being about 20% higher than that of PFD (Figure 6.2).[15] Other methods have analyzed emulsified variants of these PFCs and found that gas solubility was independent of both the particle size of emulsions as well as the employed surfactant (including Lecithin, Span 20 and Pluronic F-68).[16] In a practical sense, PFH is a comparatively inexpensive PFC, and thus amenable to scaling to volumes required by the catalytic system (~100 mL or more). This was a significant concern, as we typically make PFC nanoemulsions on ~200 µL scales. However, PFH in and of itself is difficult to formulate into stable droplets—due to its low boiling point (57 °C), 100% v/v PFH nanoemulsion solutions expanded over time at ambient conditions in preliminary experiments. By comparison, PFD has a high boiling point (142 °C) and we have previously employed it within nanoemulsion formulations with long-term benchtop stability.[17–19] With this rationale, we formulated a 1:1 v/v%

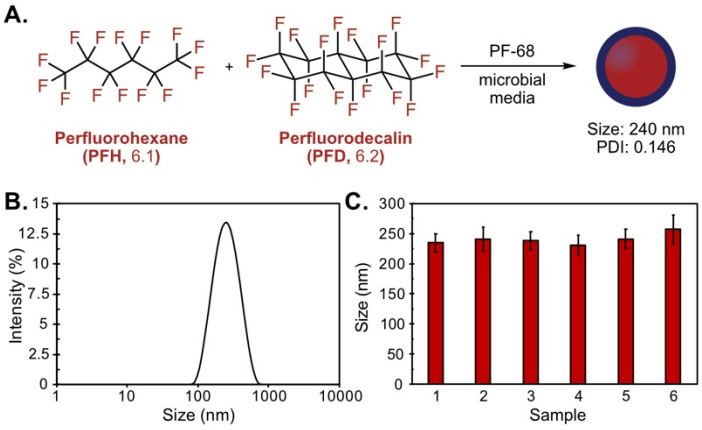

Figure 6.2. Formation and analysis of PFC nanoemulsions. A. Perfluorohexanes (PFH, **6.1**) and perfluorodecalin (PFD, **6.2**) were mixed in a 1:1 v/v% ratio and diluted with media (total PFC 9 vol%). B. DLS analysis of nanoemulsions. C. Replicability of PFC emulsion formulations, showing average size and error associated with each batch. Errors bar represent the average of three measurements.

formulation of PFH:PFD nanoemulsions stabilized by Pluronic F-68 (2.8 wt%), a commercial block copolymer solubilized within either baseline microbial culture media or phosphate buffer (Figure 6.2). On a typical scale, 10 mL batches were made by combining PFD (450 µl) and PFH (450 µl) in a 15 ml centrifuge tube. The total volume was then diluted up to 10 mL with the relevant surfactant-containing buffer. Ultrasonication at the PFC-water interface (35% amplitude) for 5 minutes on ice resulted in stable emulsions. Note that it was critical to move the probe throughout the entire solution to effectively homogenize the solution. Analysis of PFD/PFH emulsions via dynamic light scattering resulted in sizes of roughly 240 nm with low polydispersity index (PDI: 0.146) (Figure 6.2B). As previously noted, large volumes of PFC emulsion solutions were necessary for the biocatalytic system, which required many 10 mL batches formulated in rapid succession. Gratifyingly the formulation protocol was reliable, resulting in similar size distributions from batch-to-batch, as demonstrated through DLS analysis of six batches within Figure 6.2C. Stability over four days at 34 °C was also analyzed, showing that nanoemulsions underwent Ostwald ripening over the first ~48 hours, growing to about 550 nm before plateauing (Figure 6.3). Emulsions were thus either used fresh or re-sonicated immediately before use.

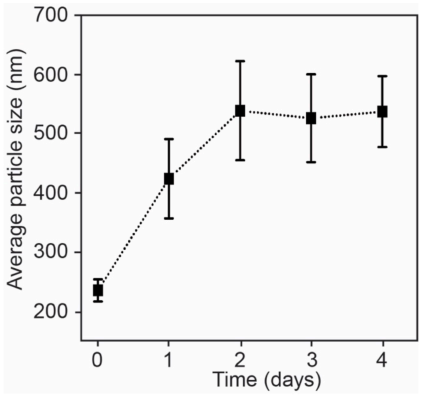

Figure 6.3. The change of average size of 2.5% PFC nanoemulsion over four days at 34°C in baseline medium. Error bars represent the average of three measurements.

When employing our PFC nanoemulsions within the biological | inorganic hybrid, Liu and coworkers observed several important phenomena that enabled these materials to enhance the overall efficiency of the system, recently published in *Nature Catalysis*.[20] Firstly, PFC nanoemulsions had non-specific interactions with the *S. ovata* microbes, resulting in large surface coverage. This created a local environment enriched with H_2 at the nanoemulsion surface, leading to accelerated gas transfer. Overall throughput of CO_2 reduction into acetic acid was increased by 190% via introducing PFC emulsions into the system, achieving nearly 100% Faradaic efficiency and productivity levels among the highest in bioelectrochemical systems. A second general takeaway is that PFCs are inert to both the inorganic catalyst and biologically compatible with the bacterium. We concluded that higher efficiencies are achievable through use of nanoscale gas carriers, and the benefits of PFCs could be applied to other systems of electricity-driven microbial fixation. As PFCs can possess high gas solubilities for other gases (*e.g.,* N_2, CH_4), we demonstrated the generalizability of this platform through a second collaboration towards nitrogen fixation.

6.3 Nitrogen and Carbon Dioxide Fixation

In addition to multi-carbon commodity chemicals, inorganic and microbial catalysts can yield pharmaceutical precursors[21] and organic nitrogen fertilizers[22]. However, this interplay can be difficult when incompatibilities within the catalytic pathway arise. For example, in the case of N_2 fixation, nitrogenase enzymes are sensitive to O_2 concentrations, yet N_2-fixing diazotrophs require O_2. This results in a stringent, Goldilocks O_2 requirement that is easily perturbed by O_2 generation, diffusion and consumption within water-splitting electrocatalysis (Figure 6.4).[23,24] Previous methods to alleviate this include constant gas streaming[25], O_2-reactive redox mediators[26,27], and O_2-reducing wire array electrodes[21]. These techniques limit the utility of the

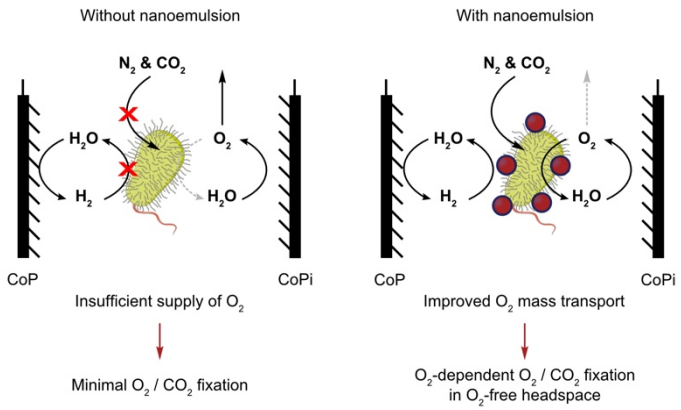

Figure 6.4. Schematic of the bacterial microenvironment created by PFC nanoemulsions and its benefits for O_2 mass transport. CoP, cobalt-phosphorous alloy for hydrogen evolution reaction; CoPi, cobalt phosphate for water oxidation reaction.

biological | inorganic hybrid by introducing additional energy costs that are impractical for their ultimate application. As an alternative, in collaboration with the Liu group we hypothesized that PFC gas carriers could be used to transport and deliver O_2 from the electrode to the bacteria[28]. Based off our previous findings, we envisioned that nonspecific interactions between PFC emulsions and N_2-fixing *X. autotrophicus* could result in a desirable bacterial extracellular microenvironment (Figure 6.4).

PFC nanoemulsions were formulated using the same solvents and volume ratios as our previous report, namely a ~240 nm emulsion core made up of 50:50 vol% ratio of PFH:PFD and stabilized by Pluronic F-68 (Figure 6.2B). These materials were added to an O_2-free reactor headspace and were thus entirely relying on the electrochemically generated O_2 (Figure 6.4). To examine microbial binding, these PFC nanoemulsions were fluorescently labeled with previously reported fluorous rhodamine **6.3** (Figure 6.5A,B).[29] Confocal images of fluorescent nanoemulsions incubated with *X. autotrophicus* labeled with green fluorescent nucleic acid stain

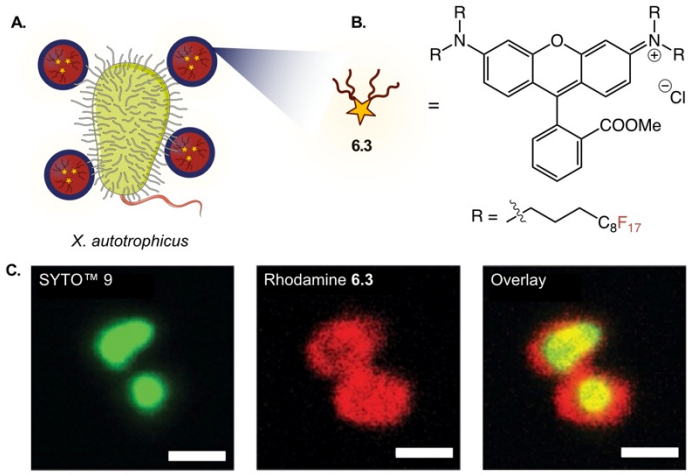

Figure 6.5. A. Schematic of colocalization experiment with fluorescent confocal microscopy. C, Fluorescent images of bacteria *X. autotrophicus* stained with SYTOTM 9 (pseudo-colored green), PFC nanoemulsions tagged with fluorous rhodamine (pseudo-colored red), and the overlay images of both fluorescent emissions. PFC nanoemulsion loading, 2.5 volume percentage (v/v). D, Zoom-in images in the highlighted area in C. Scale bars = 10 and 1 μm in C and D, respectively.

demonstrated that emulsions formed a corona around the bacteria, creating an extracellular environment that could dictate bacterial metabolism (Figure 6.5C).[28] Quantitative characterizations by Liu and coworkers indicate that this nonspecific binding between the microbes and nanoemulsions creates a microenvironment of enhanced O_2 transport and availability, analogous to previous findings with H_2.[20] Overall, the use of PFCs preserved cell viability of the microbes and led to a 250% increase in Faradic efficiency for N_2 fixation over five days. These works, currently submitted, demonstrate that the nonspecific binding between PFC nanoemulsions and bacteria creates a beneficial microenvironment within these biological | inorganic hybrids. In the future, we envision that PFC nanoemulsion parameters, *e.g.*, surface charge, could be controlled to modify these binding events.

6.4 Thermoresponsive Poly(2-oxazoline) Coatings for Magnetic Resonance Imaging Nanoparticles

Magnetic resonance imaging (MRI) is a non-invasive diagnostic technique. The first agent designed for contrast-enhanced (CE-) MRI became globally available for clinical use in 1988, called Magnevist ©.[30] Marketed by Bayer, this gadolinium (Gd)-containing contrast agent helped launch the field of CE-MRI, a valuable diagnostic imaging tool that is now used in roughly 30 million procedures each year (data per Bayer HealthCare).[31] Innovations to increase the precision and utility of MRI has increased over these years, as well as expanding the use of MRI to therapeutic practices. Of the latter, one such technique employs MRI-guided high-intensity focused ultrasound (HIFU): a minimally invasive ablation technique used to treat localized cancers.[32–34] FDA-approved uses include therapies for uterine fibroids, prostate tissue, bone metastases, essential tremor, and tremor-dominating Parkinson's disease.[35–37] With Ce-MRI monitoring, HIFU can be spatially controlled to increase tissue temperatures and trigger ablation within select regions of a few mm^3.[32,38] As such, there is ongoing interest in materials that can further enhance the contrast of these Gd-containing functionalities. Recently, the Zink group here at UCLA developed a Gd-containing mesoporous silica nanoparticle (MSN) that could be modulated with HIFU.[39] The system, illustrated within Figure 6.6, encapsulates Gd chelates within MSNs coated with a thermoresponsive coating. As HIFU heats the surroundings, the thermoresponsive coating becomes hydrophobic and shrinks, precluding water access to the Gd. This, in turn, modifies the MRI relaxivity (namely the T_1 relaxation time), which ultimately enhances contrast nearly 100-fold. Early proof-of-principle work by Tian Deng *et al.* employed a popular thermoresponsive polymer as the coating, poly(*N*-isopropylacrylamide) (PNIPAM, 6.4, Figure 6.6), attached to the MSN surface via amide couplings. However, this system was limited

in that the LCST of P(NIPAM) is 32 °C, well below physiological temperature (37 °C). The goal of this collaboration, currently in preparation, was to develop a functional poly(2-oxazoline) (POx) with an LCST slightly above 37 °C, such that local thermal heating *via* HIFU could selectively

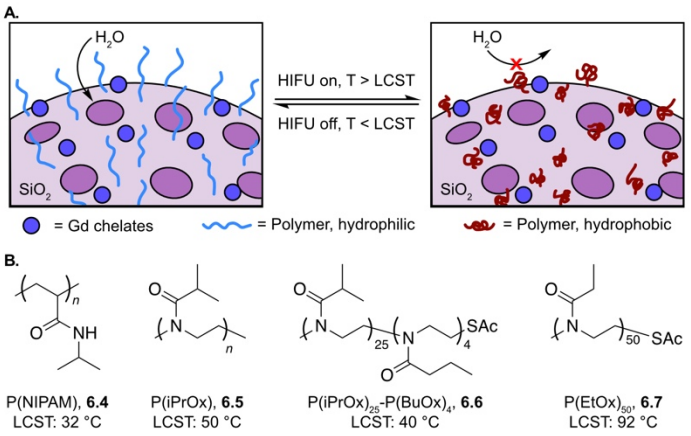

Figure 6.6. A. Schematic of polymer-coated mesoporous silica nanoparticles with gadolinium (Gd)-containing chelators for contrast-enhanced magnetic resonance imaging (Ce-MRI). Without high intensity focused ultrasound (HIFU), the polymer coating is below its lower critical solution temperature (LCST) and hydrophilic, allowing water access to the Gd chelators. Upon application of HIFU, local heating triggers the polymer's LCST, transitioning it to a hydrophobic, shrunken coiled state that repels water. This change in water access results in variation and enhanced signal within Ce-MRI. B. The LCST of polymer coatings can be varied depending on polymer structure and architecture, as shown for polymers **6.4**–**6.7**.

trigger the transition and ultimately modulate Ce-MRI contrast at physiologically relevant temperature.

As noted within Chapter 5, POx are a class of LCST-containing polymers. Unlike P(NIPAM), the side-chains of POx can be easily modified, and chain lengths of aliphatic groups can be gradually extended in order to modify the LCST. One such polymer is poly(2-isopropyl-2-oxazoline (PiPrOx, **6.5**), a structural analogue of PNIPAM, containing an LCST of ~45–50 °C.[40,41] Additionally, copolymer ratios of these monomers can be modified in order to vary the LCST. For instance, one can gradually increase the feed ratio of more hydrophobic monomers (*e.g.*, 2-butyl-2-oxazoline, BuOx) versus hydrophilic monomers (*e.g.*, iPrOx) to reduce the LCST as desired.

Rainer Jordan and coworkers previously reported the influence of these copolymerizations, demonstrating that P(iPrOx)$_{25-n}$-P(BuOx)$_n$ statistical copolymers varied in their LCSTs from 25–50 °C when n = 0, 1, 2, 3 or 5.[40] The drastic shift in LCST through incorporation of only a handful of hydrophobic BuOx monomers demonstrates the sensitivity of these structure-property relationships. As such, to develop functional copolymers with an LCST slightly above physiological temperature we chose to pursue a P(iPrOx)$_{24}$-P(BuOx)$_4$ (**6.6**) scaffold end-capped with a thioacetate functionality for eventual thiol-maleimide coupling to MSN surfaces (Figure 6.6). Additionally, homopolymer poly(2-ethyl-2-oxazoline (PEtOx, **6.7**) end-capped with thioacetate was included as a polymer coating with an LCST far above physiological temperature (92 °C).

The synthesis of P(iPrOx)$_{24}$-P(BuOx)$_4$-*t*-SAc (**6.6**) is shown in Figure 6.7A. For statistical copolymers, both monomers (iPrOx and BuOx) are added simultaneously, followed by anhydrous acetonitrile (MeCN) and methyl triflate (MeOTf) as initiator. The microwave-assisted polymerization is run at 140 °C for 12 minutes until completion. Termination is performed with potassium thioacetate (KSAc) pre-solubilized within anhydrous DMF. The solution is then stirred

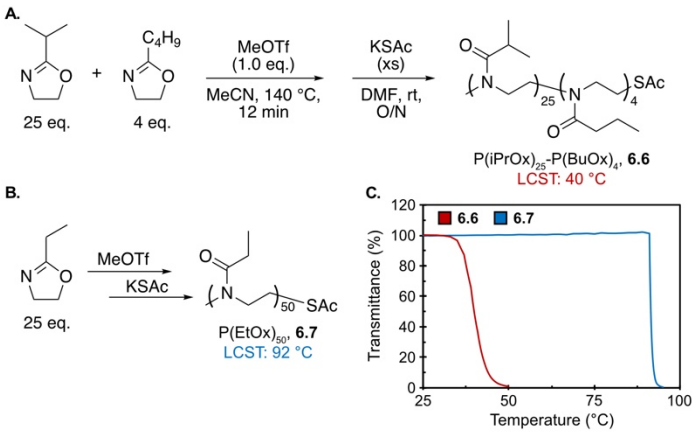

Figure 6.7. A. Synthesis of P(iPrOx)$_{25}$-P(BuOx)$_4$-*t*-SAc copolymer **6.6**. B. Abbreviated synthesis of homopolymer P(EtOx)$_{50}$-*t*-SAc **6.7**. C. Temperature-dependent UV-Vis analysis for solutions of **6.6** and **6.7** solubilized in DI water to determine lower critical solution temperature (LCST) of each polymer.

at room temperature overnight. This procedure is analogous to the thioacetate end-capping strategy discussed within Chapter 4. The following day, the polymer is concentrated, solubilized with chloroform and filtered to remove excess potassium thioacetate. The polymer is further purified via precipitation into cold hexane three times. A similar synthetic procedure is followed for simple homopolymer P(EtOx)$_{50}$-*t*-SAc, **6.7**, abbreviated within Figure 6.7B. Temperature-dependent UV-Vis analysis is then performed on polymers solubilized within MilliQ water, as described in the supporting experimental information. As shown within Figure 6.7C, the LCSTs of **6.6** and **6.7** were determined to be 40 and 92 °C, respectively.

This section describes the synthesis of a functional POx with an LCST slightly above physiological temperature, and the general utility of POx copolymers in being able to reliably tune LCST transitions. Tian Deng and coworkers are currently working to take these thermoresponsive POx materials forward via conjugation to MSNs and employment within Ce-MRI HIFU experiments. The manuscript, currently in preparation, will aim to compare MSNs modified with different polymers, and evaluating the effect of the LCST transition via investing MRI intensity changes versus temperature changes. Additionally, Zink *et al.* are interested in probing whether the mechanism of the contrast enhancement is a result of local hydrophobicity changes, or a mechano-effect influencing polymer relaxation dynamics. Collectively, these results will help establish the use of thermoresponsive polymer coatings within HIFU-assisted Ce-MRI applications in clinically relevant settings.

6.5 Preliminary Findings Towards Host-Guest Mediated Emulsion Fusion and Targeted *In Situ* Drug Synthesis

A primary goal in the development of all pharmaceuticals is the delivery of a potent drug to its desired location. As highlighted here, one way to achieve this is through the development of nanomaterials (*e.g.*, nanoemulsions) that can encapsulate, protect, and selectively deliver a payload of interest to the target site.[42–44] An alternative, well-precedented strategy is exploiting known metabolic pathways (enzymatic or chemical) in the body to convert a purposefully inactive form of the drug to its active parent drug. These derivatives, termed prodrugs in 1958[45], have become increasingly popular in modern drug design as a better understanding of adsorption, distribution, metabolism, excretion and toxicity properties allows chemists to more accurately predict *in vivo* bioconversion.[46,47] Nowadays, ~10-12% of FDA-approved small-molecule new chemical entities are classified as prodrugs.[46,48] While this prodrug strategy has seen successes, challenges include acceptable stability, optimal (and nearly quantitative) conversion rates, and a lack of site-specific enzymes that are likewise promiscuous and capable of bioconverting prodrugs.[46] We hypothesized that these two strategies could be bridged through a nanomedicine-controlled prodrug strategy. This strategy, illustrated within Figure 6.8, involves the encapsulation of two drug precursors, *e.g.,* D_1 and D_2, into the core of two separate nanoemulsions, *e.g.,* NE_1 and NE_2. These drug precursors would each include functionalities capable of reacting quickly and efficiently with one another. To promote emulsion fusion, surface-surface interactions will be dictated through noncovalent host-guest chemistry (Figure 6.8A, *vide infra*). Site-specific uptake of nanoemulsions can be controlled via either passive targeting[49] (*e.g.,* enhanced permeability and retention (EPR) effect[50]) or active routes[51,52] (*e.g.,* ligands targeting overexpressed receptors

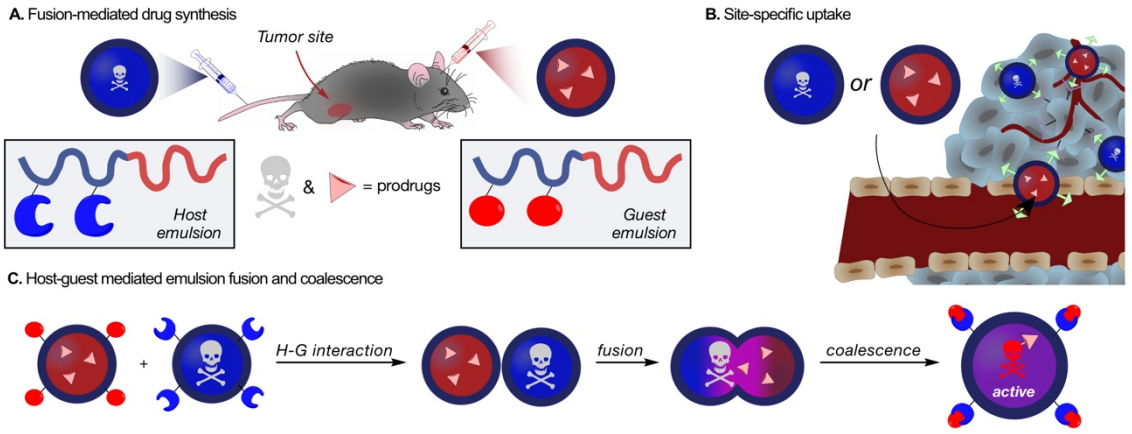

Figure 6.8. A. Illustration of fusion-mediated drug synthesis. Two separate payloads are loaded into two separate nanoemulsions, injected at different spots throughout the body. These nanoemulsions then circulate systemically with the goal of eventually being uptaken into the target tumor tissue. B. Site-specific tumor uptake of nanoemulsions leads to colocalization. C. Host-guest surfactant interactions between the two nanoemulsions leads to surface-surface binding, emulsion fusion causing the payloads to mix, and eventual emulsion coalescence.

on target cells[53]). This specificity results in the colocalization and high local concentration of nanoemulsions (Figure 6.8B). This eventually allows the two sets of emulsions to meet one another whereafter host-guest interactions cause surface-surface binding, emulsion fusion and eventual emulsion coalescence (Figure 6.8C). We hypothesize that these binding events can be controlled through the relative strength of these noncovalent interactions via modifications in host-guest chemistry.

To incorporate host and guest motifs onto the surface of nanoemulsions, we first looked to establish proof-of-principle via simple, commercially available host molecules that could be incorporated into surfactants. Cyclodextrins (CDs) are cyclic oligosaccharides composed of glucose residues linked through six, seven, or eight alpha-(1,4)-linked glycosidic bonds, termed α-, β- and γ-CD, respectively. Of these, βCD is the most accessible and low-priced, and is FDA-approved due to its low toxicity profile.[54,55] The hydrophobic cavity of βCDs can encapsulate a variety of guest molecules, including drugs, surfactants, and polymers, and the hydrophilic

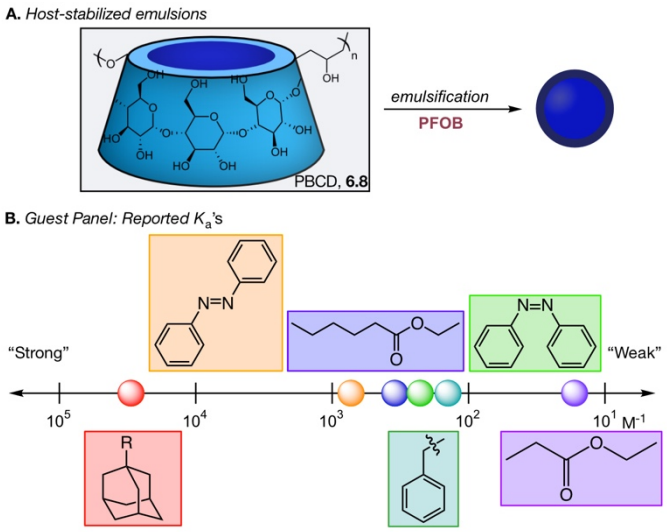

Figure 6.9. A. "Host" emulsions are stabilized by using poly(β-cyclodextrin) as a surfactant. B. Host-guest binding strength can be controlled via reported association constants of the employed guests.

external surface makes them water-soluble.[56] Previously, Sletten *et al.* demonstrated that poly(βCD) (**6.8**, Figure 6.9A) was capable of stabilizing ~200 nm PFC nanoemulsions with good bench-top stability over 2 weeks. We envisioned that **6.8** could likewise be used as a surfactant for PFOB-in-water nanoemulsions, whereafter βCD host molecules would be displayed on the surface. In designing a potential guest, there are a variety of functionalities available, including adamantanes, azophenols, aliphatic esters, and phenyls (Figure 6.9B). The binding affinity of these guests can vary, from high binding adamantanes[57] (K_a = 10^4–10^5 M^{-1}) to low binding ethyl propionate[58] (K_a = 38 M^{-1}). We envisioned that a functionalizable POx surfactant capable of readily appending modified guest molecules would allow for fine-tuning of host-guest mediated emulsion fusion.

We previously had experience synthesizing alkene-containing POx surfactant **6.9** and modifying it via light-promoted thiol-ene chemistry (Figure 6.10A). There are a number of readily available thiol-containing functionalities that potentially could be used as guests, including

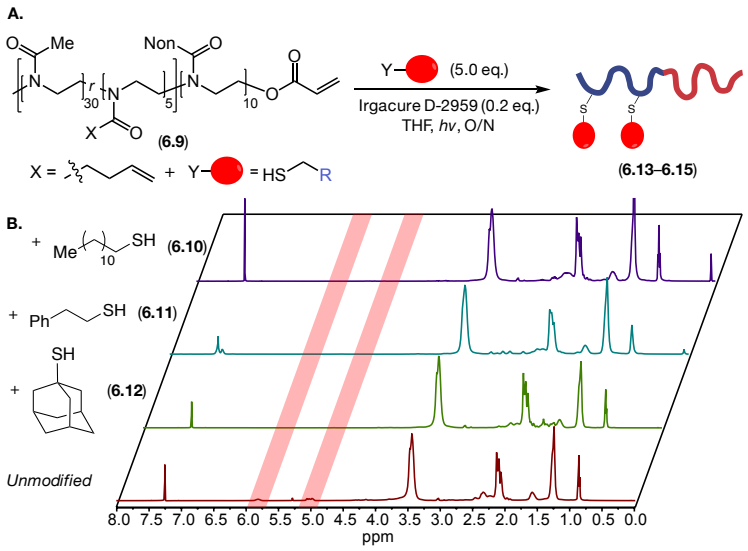

Figure 6.10. A. Functionalizable poly(2-oxazoline) surfactant **6.9** is modified via thiol-ene chemistries to "guest" surfactants **6.13**–**6.15**. B. 1H-NMR spectra suggesting quantitative conversion of **6.9** with thiols **6.10**, **6.11**, and **6.12**.

undecanethiol **6.10**, phenylethanethiol **6.11**, and adamantanethiol **6.12**. Upon exposing **6.9** to previously optimized thiol-ene conditions (Figure 6.10A, see Chapter 3), quantitative modification with **6.10**, **6.11** and **6.12** to thiol-modified polymers **6.13**–**6.15** was observed by 1H-NMR. Having access to both host and guest surfactants, we then moved to establish their capability as surfactants for PFOB-in-water emulsions.

Early preliminary data focused on examining the host-guest coalescence of PβCD **6.8** and adamantane **6.15**. To visualize the fusion process, we purposefully made macroemulsions stabilized by either **6.8** (Figure 6.11A) or **6.15** (Figure 6.11D) and stained the interior fluorous core of each with its own dye, either fluorous-soluble coumarin **6.16** (Figure 6.11B) or **6.17** (Figure 6.11E). Both sets of emulsions were then visualized with minimal background noise via epifluorescence microscopy, a technique used for several of the following experiments (Figure 6.11C, 6.11F).

To visualize fusion, host and guest emulsions were then mixed in a 1:1 vol% ratio. Compared to the homogenously dispersed emulsion solutions observed in Figure 6.11C, F, mixing the host and guest emulsions predictably resulted in large-scale aggregation and fusion, shown in

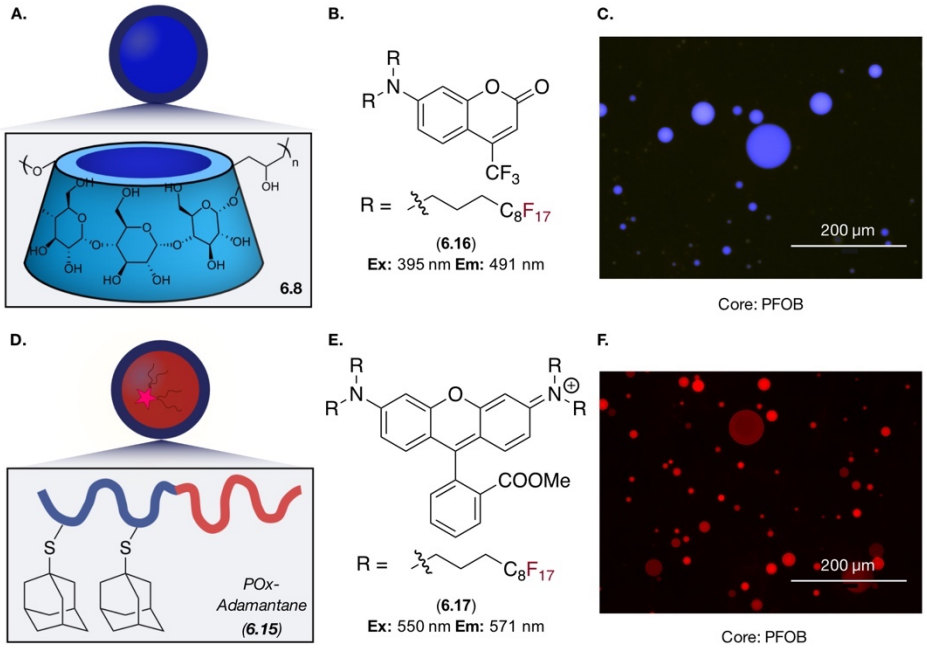

Figure 6.11. A. Host emulsions stabilized by PβCD **6.8**. B. Fluorous-soluble coumarin **6.16**, encapsulated in the core of host emulsions. C. **6.16**-containing PFOB-in-water macroemulsions, visualized via epifluorescence microscopy. D. Guest emulsions stabilized by adamantane-containing **6.15**. E. Fluorous-soluble rhodamine **6.17**, encapsulated in the core of guest emulsions. F. **6.17**-containing PFOB-in-water macroemulsions, visualized via epifluorescence microscopy.

Figure 6.12A. Host-guest interactions were apparent, with select host emulsions being surrounded by guest emulsions, indicating emulsion-emulsion attraction (Figure 6.12A, B). Notably, we also highlighted instances of guest-guest contact, which could perhaps be due to surfactant exchange between droplets, limiting the specificity of the system. In the future, fluorescent labeling of the surfactants themselves could help distinguish whether exchange was occurring, or whether guest-guest contact is due to some other phenomena. To corroborate emulsion fusion, we analyzed the colocalization of the once independently loaded dyes (**6.16** and **6.17**) within the cross-section of Figure 6.11A. Plotting pixel intensity versus distance demonstrated that both **6.16** and **6.17** were

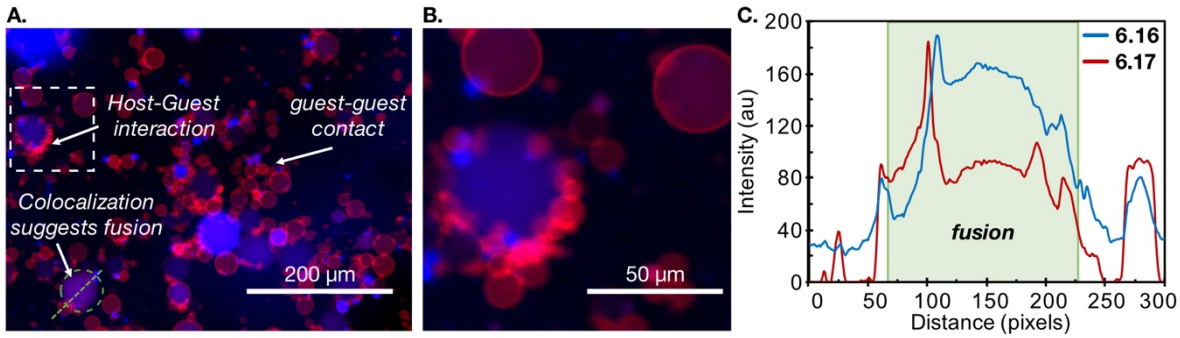

Figure 6.12. A. **6.8**- and **6.15**-stabilized droplets, termed host and guest emulsions, respectively, mixed in equal volumes and visualized via epifluorescence microscopy. B. Highlighted droplets showing host-guest interactions. C. Cross section pixel intensity versus distance for **6.16** and **6.17**, as shown in A.

colocalized within the droplet core (Figure 6.11C). While these results demonstrated that host-guest interactions could result in droplet fusion, we wanted to further quantify this behavior through an ensemble average. To do this, we looked towards flow cytometry analysis.

The size of emulsions can be easily controlled through varying the volume ratio of the interior core. Here, the PFOB is varied between 5–50 vol%, diluted with PBS containing surfactant (0.5 mg/mL), and ultrasonicated for 30 seconds at 20% amplitude. In general, the macroemulsion formulation differs from the general nanoemulsion formation procedures described in earlier chapters through three factors: (i) increased oil volume %, (ii) reduced surfactant loading, and (iii) reduced ultrasonication amplitude. Note that though vortexing and hand mixing was capable of making macroemulsions using the same formulation, resulting droplets were more polydisperse and underwent rapid droplet destabilization and phase separation compared to those formed *via* ultrasonication. Macroemulsions were visualized *via* epifluorescence microscopy and size analysis was further analyzed via flow cytometry. For emulsion formulations with 10 vol% PFOB, the median droplet size was <2 µm (Figure 6.13A). By comparison, formulations with 50 vol% PFOB resulted in much larger droplets with median diameters of >50 µm (Figure 6.13C). When run

through flow, side scatter (SSC) versus forward scatter (FSC) plots provide information about the granularity and size of the droplets, respectively (Figure 6.13B, D). These FSC and SSC values were then averaged for each emulsion formulation at varying volumes of PFOB (5, 10, 15, 25 and 50 vol%) and are shown within Figure 6.13E and F. Generally, we observed that macroemulsions do not get significantly larger than ~3 μm until over 15 vol% of PFOB is used, and the FSC values do not change significantly below this regime. This could represent a limitation in the flow analysis for smaller macroemulsions, as the fusion of two, say, 2 μm droplets would yield a parent droplet with a size indistinguishable from the two daughter droplets. However, 25 and 50 vol% of PFOB gives rise to both increased FSC and, interestingly, higher SSC values. These two properties share an exponential correlation within the SSC vs FSC scatter plots (Figure 6.13 B, D). These results were unexpected, and it is currently unclear what increased granularity suggests in the context of emulsions. In the future, nanomaterial standards (*e.g.,* polystyrene spheres) could be used to help

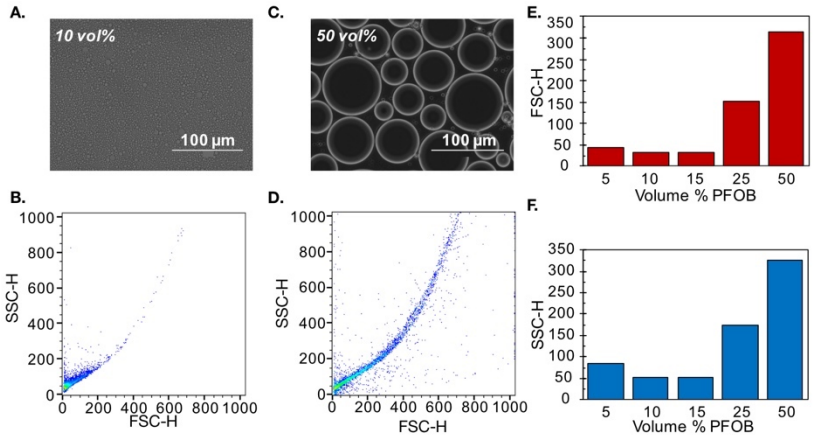

Figure 6.13. Macroemulsions with variable size were analyzed through epifluorescence microscopy and flow cytometry. Macroemulsions were formed with 10 vol% PFOB and analyzed via (A) epifluorescence microscopy and (B) flow cytometry. Larger macroemulsions were formed with 50 vol% PFOB and analyzed via (C) epifluorescence microscopy and (D) flow cytometry. The relative size of macroemulsions can be analyzed through comparing the forward scatter (FSC, E) or side scatter (SSC, F) of emulsion samples versus the amount of PFOB employed in the formulations.

with flow cytometry analysis to help orient the user, optimize instrument settings, and perhaps even allow for size quantification. However, these preliminary results suggested that flow cytometry analysis was capable of identifying emulsions, and we next moved to exploiting the multicolor capabilities of flow cytometry to further probe host-guest fusion.

The flow cytometer is equipped with multiple laser lines and optical filters, *e.g.,* FL-1 (533 ± 30 nm), FL-2 (585 ± 40 nm), and FL-3 (670 LP). Fluorophores must be used that are both well-suited to each laser line, and do not bleed into other lines. Our previously reported fluorous rhodamine **6.17**[29] (Figure 6.14A) and cyanine **6.18**[59] (Figure 6.14B) match the FL-2 and FL-3 channels, respectively. Host emulsions, again stabilized by poly(βCD) **6.8** (Figure 6.14C), were used to encapsulate **6.18**. Flow cytometry on this emulsion solution resulted in high FL-3 signal, with minimal FL-2 background after compensation, indicating encapsulation of fluorophore. Conversely, a set of control guest emulsions were formulated using Pluronic F-68 **6.19** as a surfactant and cyanine **6.18** as the payload. When these emulsions were analyzed by flow cytometry, we observed low FL-3 signal and minimal FL-2 background. As **6.19** lacks guest characteristics, we employed these materials to determine whether we could distinguish between distinct emulsion populations even upon mixing the two. We mixed these two populations of emulsions in a 1:1 vol% mixture (total [PFOB]: 3 vol%) and gently rocked for five minutes to allow emulsions to interact (Figure 6.15A). After this incubation time, the mixture was analyzed through flow cytometry. We observed that the two populations of emulsions could be visually distinguished from one another–the majority of emulsions fell into either quadrant 1 (Q1), indicating **6.18** encapsulation, or into quadrant 3 (Q3), indicating **6.17** encapsulation (Figure

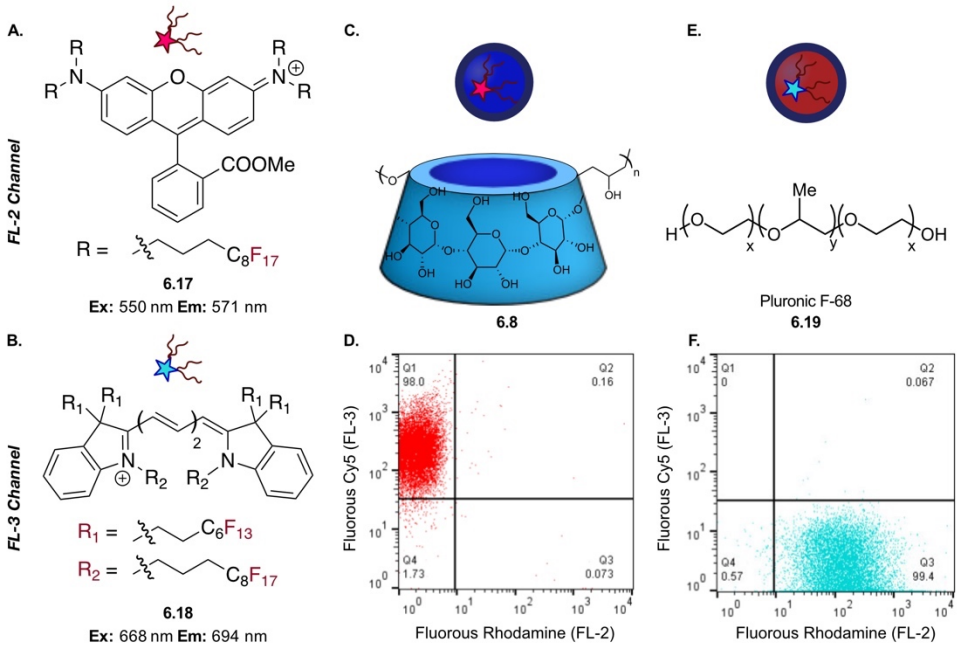

Figure 6.14. Fluorophores allow for host and guest emulsions to be independently visualized via flow cytometry with two different laser lines. A. Structure of previously reported fluorous rhodamine **6.17**. B. Structure of previously reported fluorous cyanine **6.18**. C. Host emulsions stabilized by poly(βCD) **6.8** encapsulate cyanine **6.18**. D. FL-3 versus FL-2 signal for host emulsions in C. E. Control emulsions stabilized by Pluronic F-68 **6.19** encapsulate cyanine **6.18**. F. FL-3 versus FL-2 signal for control emulsions in E.

6.15B). By comparison, ~5% of the counted emulsions displayed high levels of fluorescence for both, falling into Q2. These data suggest that both the amount of background emulsion fusion and possible fluorophore exchange between droplets (without fusion) is negligible.

Conversely, we expected that mixing emulsions stabilized by host **6.8** or adamantane-modified POx **6.15** would result in droplet fusion due to the high association constant between PβCD and adamantane moieties. Macroemulsions of each were formulated as previously described and mixed in the same volume ratios as mentioned above (Figure 6.15C). Flow analysis showed strikingly that after five minutes of mixing, ~97% of emulsions had high levels of both fluorophores, indicating that emulsion fusion had occurred (Figure 6.15D). Further flow analysis did not show obvious increases in size *via* FSC signal, however, a possible limitation of flow when

working with small macroemulsions. Epifluorescence microscopy further confirmed fluorophore colocalization, corroborating that these instrumentation techniques can be valuable in tandem.

Finally, we devised a control experiment to ensure that it was truly the adamantane functionality on POx **6.15** that caused host-guest fusion, and not the POx itself. We formed macroemulsions using unmodified POx **6.9** and mixed these solutions with host emulsions (Figure 6.15E). Unfortunately, flow cytometry demonstrated that significant levels of either background fusion or fluorophore exchange was occurring, constituting about ~70% of the population (Figure 6.15F). Based on previous experiments, there seems to be little rhodamine **6.17** exchange between labeled and unlabeled PFOB-in-water droplets, even at high droplet concentrations. Additionally,

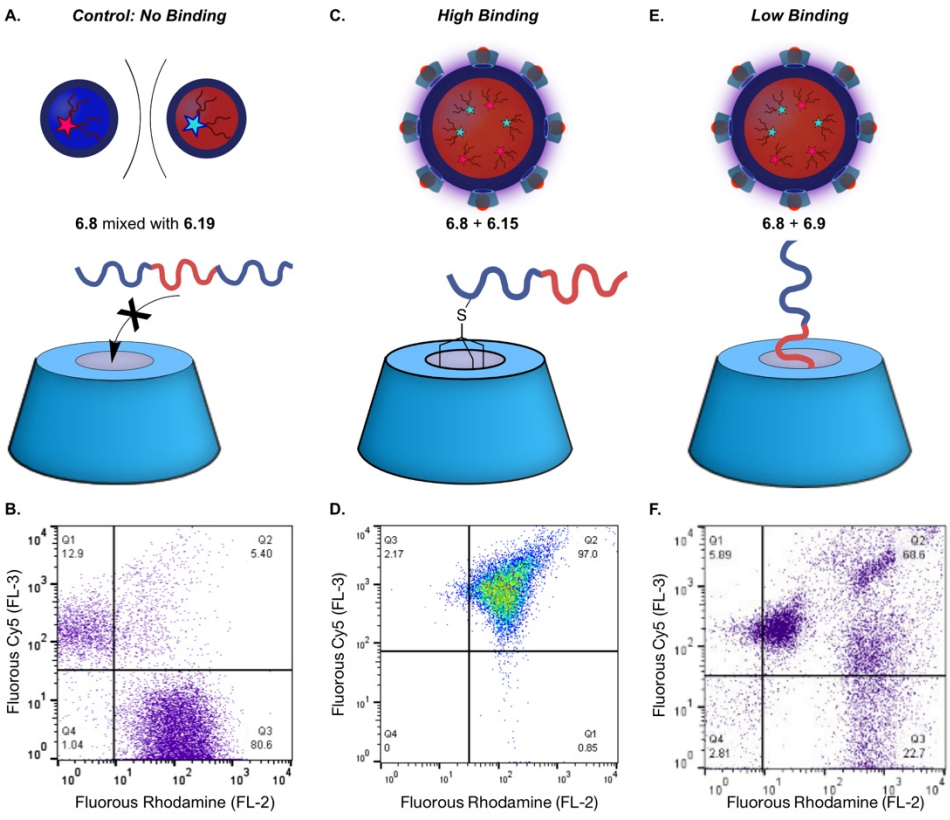

Figure 6.15. Controlled emulsion fusion by combining host PβCD emulsions with other surface-functionalized emulsions that vary in binding strength. A. Emulsion formulations with surfactant **6.8** are mixed with emulsions stabilized by (A) **6.19**, (C) **6.15**, or (E) **6.9**. Host emulsions contain **6.18** and "guest" (or control) emulsions contain **6.17**. Mixed solutions are then analyzed by (B, D, F) flow cytometry analysis.

previous reports have reported an association constant of ~10^3 M^{-1} between βCD and the hydrophobic poly(2-nonyl-2-oxazoline) (PNonOx) side chains used in **6.9**.[60] We hypothesize that background signal is a result of emulsion fusion, rather than fluorophore exchange.

The ability to control emulsion fusion should concurrently allow us to control payload exchange between droplets. As previously discussed, this could be leveraged into a prodrug strategy in which two distinct reactive molecules are encapsulated within the inert interior of the PFC droplets. Upon fusion these two molecules would then mix and react to synthesize a therapeutic drug. This strategy requires a handful of pre-requisites: (1) payloads must be soluble within the oil core, (2) payload exchange between unfused droplets must be minimal, and (3) the reaction between the two payloads must be exceptionally fast and high-yielding with innocuous byproducts. To address solubility concerns of (1), we chose to first pursue traditional hydrocarbon oil-in-water emulsions, such that we could capitalize on commercially available reagents and avoid the difficulties associated with fluorous synthesis. Additionally, we envisioned that *in situ* fluorophore synthesis could be a promising route to visually observe the mixing and subsequent reaction of payloads, including any potential background exchange (2). Finally, the reaction criteria outlined within (3) motivated us to look towards bioorthogonal click chemistry reactions.[61] One such reaction stuck out to us that seemed to meet the criteria necessary for these preliminary studies, which was a styrene-tetrazine reaction resulting in a fluorogenic substituted dihydropyridazine previously employed in protein labeling (Figure 6.16A).[62] As both the styrene (**6.20**) and dipyridyl-tetrazine (**6.21**) are commercially available, we first encapsulated each within DCE macroemulsions stabilized by crowding-responsive POx surfactant **5.2** (1 mg/mL in PBS) previously optimized. This preliminary experiment was designed such that payloads were either pre-mixed within macroemulsions (Figure 2A) or solubilized within two distinct populations of

droplets that were further diluted within either PBS (Figure 2D) or Ficoll-400 crowder (250 mg/mL) (Figure 2G). These droplets were then visualized via epifluorescence microscopy. As expected, droplets containing pre-mixed reagents gradually increased in fluorescence over time (signal was observable after ~30 minutes), and after 2 hours were highly fluorescent within the DAPI channel (Ex. 357±44 nm, Em. 447±60 nm) (Figure 6.16 B, C). This exciting finding demonstrated that the general concept of fluorophore synthesis as a means to investigate *in situ* synthesis was an effective assay. However, limitations of the system were soon observed. The negative control experiment, namely the 1:1 vol% mixing of distinct droplet populations within PBS (Figure 6.16D), gave high background noise that rivaled the fluorescence observed for the pre-mixed droplets (Figure 6.16E, F). As such, the experiment aiming to purposefully fuse the

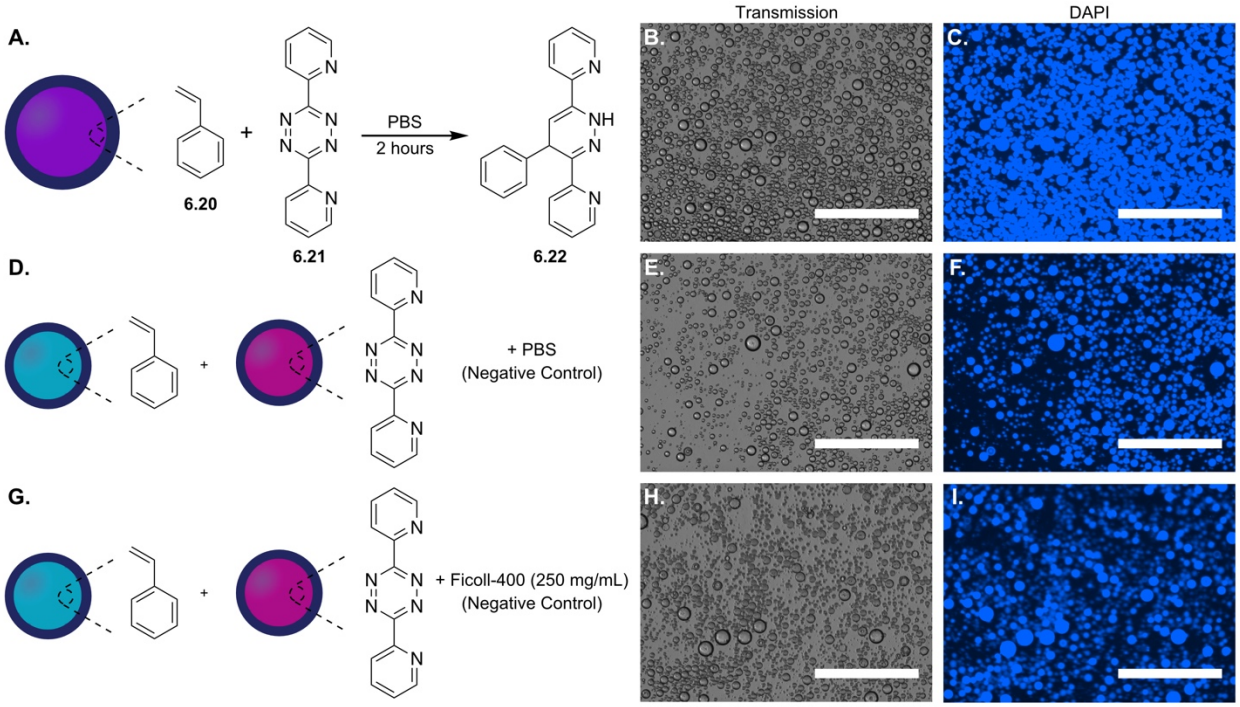

Figure 6.16. Dichloroethane macroemulsions containing styrene **6.20** and tetrazine **6.21** react to yield fluorophore **6.22**. Reagents **6.20** and **6.21** were either (A) both pre-mixed in DCE, or (B/C) solubilized in isolated emulsion populations and further diluted in either (D) PBS or (G) Ficoll-400 crowder in PBS (250 mg/mL). Emulsion populations were rocked for 2 hours at room temperature and visualized with epifluorescence microscopy (B, C, E, F, H, I). Scale bars: 400 μm.

droplets and selectively exchange payloads via a crowding stimulus (Figure 6.16G) yielded similar levels of fluorescence (Figure 6.16 H, I.). This challenge of high background signal suggests that (1) either payload **6.20** or **6.21** could be exchanging between droplets, or (2) macroemulsions are destabilizing (thereby exchanging payloads) and being reformed during the brief vortexing that was done prior to imaging. We hypothesized that tetrazine **6.21** could be partially water soluble, yet a partition experiment between DCE/PBS showed ~95% retention in DCE even after 1 hour of shaking. As such, we screened other oil emulsion compositions in an effort to both create stable droplets, and to attempt to enhance the solubility of the precursor payloads. Unfortunately, oil cores of either 100% toluene or 50/50% mesitylene and DCE both gave similarly poor results. Collectively, it does seem that this fluorogenic styrene-tetrazine reaction has great potential as an easily accessible proof-of-principle assay, though further optimization of macroemulsion formulations and compositions is needed. Additionally, one could look to extend this work to PFC emulsions through the design and synthesis of fluorous-soluble precursors.

Future directions within this host-guest mediated emulsion fusion project should first include a prioritization in the synthesis of modular POx surfactants that, when unmodified, have limited interactions with the host emulsion of interest. In the case of PβCD **6.8** emulsions, simply reducing the chain length of the hydrophobic block from NonOx to, say, 2-propyl-2-oxazoline (PrOx) could help to reduce this background fusion, based on literature precedent.[60] It would then need to be validated that the conjugation of a strongly binding guest, *e.g.,* admantane, selectively causes fusion. Based on these preliminary experiments, I would expect that the general polymeric structure, P((hydrophilic)$_x$-*r*-P(functional)$_y$)-*b*-P(hydrophobic)$_z$ employed within this chapter sufficiently display these functionalities on the emulsion surface for host-guest recognition. Surface functionalization strategies discussed within Chapter 3 corroborate this. From here, one

would ideally select 3–4 more guests that vary in their binding strengths, conjugate them to the chosen POx backbone, and attempt to correlate emulsion fusion with association constant. One could envision the use of stimuli-responsive guests that would be low-binding and thus stable upon mixing with host emulsions (OFF state), but upon introduction of a chemical or physical stimulus (*e.g.,* pH or light), the guest would convert to a high-binding variant (ON state) that selectively promotes emulsion-emulsion fusion. Consistencies for both size and volume dilutions will be necessary across these experiments, and it is here that the current macroemulsion formation strategies may prove insufficient to achieve the narrow polydispersities necessary. An alternative is the use of a microfluidics-based approach, currently under consideration within the lab. While macroscale experiments have proved invaluable in the latter half of my PhD for investigating emulsion-emulsion interactions, I would caution future students against making assumptions that the same phenomena one observes at the macroscale is identical to those that may occur on the nanoscale. Finally, the ultimate application would be intertwining this control with the encapsulation of two independent prodrugs that, only upon colocalization at a site of interest and encountering the selected stimulus *in vivo*, fuse together and react to create a therapeutic molecule that is then released from the emulsion. This project, though currently in its infancy, would allow us to control chemistries in a living system through the introduction of the fluorous phase and selectivity of interfacial interactions through our custom surfactant platform.

6.6 Conclusions

The perfluorocarbon (PFC) emulsion platform discussed throughout this thesis revolves around two components: the interior fluorous core and custom poly(2-oxazoline) (POx) stabilizing surfactants. Both elements have opened new doors for collaborations here at UCLA, with the

former yielding a fruitful and ongoing collaboration with Professor Chong Liu's lab for biological | inorganic hybrids, and the latter in developing thermoresponsive POx coatings for MRI nanocontrast agents. Both of these avenues have potential beyond the works described herein, and I expect that future students will find further uses of this platform. For example, the surfactant-PFC-oxygen/nitrogen components of the platform, all localized within some ~300 nm of one another, could be conceptualized as an unexplored solid-liquid-gas interface with catalytic potential to address challenges in heterogenous catalysis.[63] These include low reaction efficiencies due to low gas solubility within oil,[64] a limitation that PFCs seem particularly well-suited to overcome. Additionally, PFC emulsions have a number of biomedically relevant advantages that have yet to be thoroughly explored within our lab, including their capabilities as ^{19}F-MRI contrast agents. These capabilities could be leveraged alongside our fluorous-soluble fluorophores for multimodal imaging, and to track the fate of PFCs separate from the solubilized payload. While much of the optimization performed on our PFC delivery platform up to this point has focused on *in vitro* and *in cellulo* work, a natural progression will be moving *in vivo* within the near future. With this, a new set of challenges will be encountered, likely including the need to control biodistribution and avoid concerns like rapid clearance via the reticuloendothelial system. While I hope that the modularity of the POx platform will allow for some degree of tuning here (for instance, modification of size and surface charge), I fully expect that these advances will need to be merged with active targeting motifs currently being explored within the group. With that, I look forward to seeing future students not only capitalize on some of the preliminary work expanded upon within this chapter, but likewise develop new tools and techniques that will further establish PFC nanoemulsions as a bioorthogonal delivery platform.

6.7 Experimental Procedures

6.7.1 General experimental procedures

Reagents and Instrumentation Chemical reagents were purchased from Sigma-Aldrich, Alfa Aesar, Fisher Scientific, or Acros Organics and used without purification unless noted otherwise. Anhydrous and deoxygenated solvents dichloromethane (DCM), acetonitrile (MeCN), and methanol (MeOH) were dispensed from a Grubb's-type Phoenix Solvent Drying System. Thin layer chromatography was performed using Silica Gel 60 F254 (EMD Millipore) plates. Flash chromatography was executed with technical grade silica gel with 60 Å pores and 40–63 μm mesh particle size (Sorbtech Technologies). Solvent was removed under reduced pressure with a Büchi Rotovapor with a Welch self-cleaning dry vacuum pump and further dried with a Welch DuoSeal pump. Bath sonication was performed using a Branson 3800 ultrasonic cleaner. Nuclear magnetic resonance (^{1}H NMR) spectra were taken on Bruker Avance 500 (^{1}H NMR and ^{13}C NMR) or AV-300 (^{19}F NMR) instruments and processed with MestReNova software. All ^{1}H NMR peaks are reported in reference to $CDCl_3$ at 7.26 ppm. Size Exclusion Chromatography (SEC)/Gel Permeation Chromatography (GPC), unless otherwise noted, was conducted on a Shimadzu high performance liquid chromatography (HPLC) system with a refractive index detector RID-10A, one Polymer Laboratories PLgel guard column, and two Polymer Laboratories PLgel 5 μm mixed D columns. Eluent was DMF with LiBr (0.1 M) at 50 °C (flow rate: 0.80 mL/ min). Calibration was performed using near-monodisperse poly(methyl-methacrylate) PMMA standards from Polymer Laboratories. Masses for analytical measurements were taken on a Sartorius MSE6.6S-000-DM Cubis Micro Balance. Microwave reactions were performed using a CEM Discover SP microwave synthesis reactor. All reactions were performed in glass 10 mL microwave reactor vials purchased from CEM with silicone/PTFE caps. Flea micro PTFE-coated stir bars were used in the

vials with magnetic stirring set to high and 15 seconds of premixing prior to the temperature ramping. All microwave reactions were carried out at 140 °C with the pressure release limit set to 250 psi (no reactions exceeded this limit to trigger venting) and the maximum wattage set to 250W (the power applied was dynamically controlled by the microwave instrument and did not exceed this limit for any reactions). Irradiation with light was performed with BI365 nm Inspection UV LED lamp, purchased from Risk reactor (Output power density >5000μW/cm² at 15" (38cm), voltage range 90-265V ac, output power: 3*325mW at 365nm peak).

Abbreviations

DCM = dichloromethane; DMSO = dimethylsulfoxide; EtOH = ethanol; MeCN = acetonitrile; MeOH = methanol; THF = tetrahydrofuran; PFC = perfluorocarbon; PFH = perfluorohexanes; PFD = perfluorodecalin; PF-68 = Pluronic F-68; PDI = polydispersity index; MRI = magnetic resonance imaging; CE = contrast-enhanced; HIFU = high intensity focused ultrasound; MSN = mesoporous silica nanoparticles; PNIPAM = poly(N-isopropylacrylamide); POx = poly(2-oxazoline); LCST = lower critical solution temperature; iPrOx = 2-isopropyl-2-oxazoline; BuOx = 2-butyl-2-oxazoline; EtOx = 2-ethyl-2-oxazoline; MeOx = 2-methyl-2-oxazoline; NonOx = 2-nonyl-2-oxazoline; PrOx = 2-propyl-2-oxazoline; KSAc = potassium thioacetate; DMF = dimethylformamide; EPR = enhanced permeability and retention; CD = cyclodextrin; SSC = side scatter; FSC = forward scatter; FL = fluorescence.

General nanoemulsion formation procedure

Pluronic F-68, was added (2.8 wt%) to the relevant buffer and sonicated in a bath sonicator, Branson 3800 ultrasonic cleaner, to dissolve the polymer thoroughly. PFD (450 μl) and PFH

(450 µl) were combined in a 15 mL centrifuge tube. The total volume was diluted up to 10 mL with the relevant surfactant-containing buffer. Baseline medium was used as the buffer for all the experiments, except RDE experiments in which a phosphate buffer was used instead. The liquid was then sonicated at a 35% amplitude for 5 min (3 W, Qsonica). The size distributions of the resulting nanoemulsions were analyzed following the DLS procedure outlined below.

Poly(2-oxazoline) surfactant (5.6 mg) was dissolved in DMF (20 µL) and sonicated in a bath sonicator (~15 minutes) until fully dissolved, at which point perfluorooctylbromide (10 vol%, 20 µL) was added, followed by PBS buffer pH 7.4 (200 µL). The mixture was sonicated at 35% amplitude for 15 minutes at 0 °C on a QSonica (Q125) sonicator. Sonication was performed by lowering the probe directly at the liquid-liquid interface of the two immiscible solvents.

General nanoemulsion analysis procedure

Size analysis: The bulk emulsion solution was diluted in MilliQ H_2O (20 µL emulsions in 2 mL MilliQ H_2O) in a plastic 1 cm cuvette. Size was analyzed with a Malvern Zetasizer Nano dynamic light scattering. SOP parameters: 10 runs, 10 seconds/run, three measurements, no delay between measurements, 25 °C with 120 second equilibration time. Collection parameters: Lower limit = 0.6, Upper limit = 1000, Resolution = High, Number of size classes = 70, Lower size limit = 0.4, Upper size limit = 1000, Lower threshold = 0.05, Upper threshold = 0.01. Data are representative of three replicate measurements. Size error bars represent the half-width at half-maximum of the measurements.

General macroemulsion formation procedure

Polymer surfactant (28 mg) was pre-solubilized in PBS buffer pH 7.4 (1 mL, 28 wt% total surfactant) and vortexed gently until fully dissolved. In a separate 2 mL eppendorf tube, perfluorooctylbromide oil (varied from 5–50 vol%, X μL) was added. Where relevant, **6.17** or **6.18** was encapsulated by pre-dissolving either dye in PFOB. PBS was then added on top of the dye/PFOB layer (200 - X μL). Finally, the polymer/PBS solution was added to a total surfactant loading of 0.5 mg/mL, and the mixture was quickly sonicated at 20% amplitude for 30 seconds at 0 °C on a QSonica (Q125) sonicator. Sonication was performed by lowering the probe directly at the liquid-liquid interface of the two immiscible solvents.

Flow cytometry

Emulsion solutions were transferred to 1.2 mL microtiter tubes with a final volume of 400 μL FACS buffer. Flow cytometry was performed on a BDBiosciences FACSCalibur equipped with 488 nm and 635 nm lasers. Fluorous rhodamine **6.17** fluorescence was measured on FL-2 channel. Fluorous cyanine **6.18** fluorescence was measured on FL-3 channel.

General epifluorescence procedure

Epifluorescence was performed on an EVOS® FL microscope. Imaging was done using EVOS™ Light Cube, RFP 2.0 (531/40 nm Excitation; 593/40 nm Emission) or EVOS™ Light Cube, Cy5 2.0 (635/18 nm Excitation; 692/40 nm Emission). Samples were prepared via respective dilutions transferred to a flat glass microscope slide with coverslip. Imaging was performed within five minutes of transferring sample. Image analysis was performed with Fiji.[65]

General synthetic procedures

6.7.2 Experimental procedures

Synthetic chemistry experimental procedures

Synthesis of poly(2-oxazoline) block copolymer **6.6:**

To a flame dried microwave vial, MeCN (0.7 mL, anhydrous), iPrOx (200 μL, 0.200 g, 1.77 mmol, 24 equiv.), and BuOx (19 μL, 0.019 g, 0.15 mmol, 2 equiv.) were added. After purging with nitrogen, MeOTf (8.3 μL, 12 mg, 0.07 mmol, 1.0 equiv.) was added and the mixture was heated at 140 °C in the microwave. After 17 minutes, the polymerization was quenched with potassium thioacetate (64 mg, 0.55 mmol, 7.5 equiv.), and stirred at room temperature overnight. The following day, the reaction mixture was evaporated to dryness to yield crude polymer (**6.6**) as a yellow-brown solid. Polymer **6.6** was purified by precipitation by dissolving in a minimal amount of DCM and dropwise addition to cold hexanes (20:1 v/v%) three times, collected and evaporated to dryness, yielding the pure product **6.6** as an off-white solid (120 mg, 60% yield). ^{1}H NMR (500 MHz, $CDCl_3$): δ 3.46 (m, 111H), 3.07 (m, 3H), 2.91 (m, 21H), 2.66 (m, 10H), 2.36 (m, 8H), 2.27 (m, 3H), 1.35 (m, 9H), 1.11 (s, 152H), 0.92 (m, 12H).

Synthesis of poly(2-oxazoline) block copolymer **6.7:**

To a flame dried microwave vial, MeCN (750 μL, anhydrous) and EtOx (250 μL, 0.250 g, 2.52 mmol, 50.0 equiv.) were added. MeOTf (5.7 μL, 8.3 mg, 0.050 mmol, 1.0 equiv.) was added and the mixture was heated at 140 °C in the microwave. After 16 minutes, the polymerization was quenched with potassium thioacetate (43 mg, 0.38 mmol, 7.5 equiv.), and stirred at room temperature overnight. The reaction mixture was evaporated to dryness to yield crude polymer (**6.7**) as a yellow-brown solid. Polymer **6.7** was purified by precipitation by dissolving in a minimal

amount of DCM and dropwise addition to cold Et_2O (20:1 v/v%), collected and evaporated to dryness (152 mg, 61% yield). ^{1}H NMR (500 MHz, $CDCl_3$): δ 3.45 (m, 200H), 3.02 (m, 3H), 2.40–2.14 (m, 101H), 1.11 (t, 149H).

Synthesis of functionalized poly(oxazoline) block copolymer **6.9**:

See Chapter 3.

Functionalization of poly(2-oxazoline) block copolymer **6.9** with thiols **6.10, 6.11, 6.12**:

Surfactant **6.9** was modified based on thiol-ene conditions previously reported.[17,66,67] All reagent equivalents were calculated with respect to alkene. Briefly, functionalized surfactant **6.9** (50 mg ~8 wt% alkene, 1.0 equiv.) was dissolved in anhydrous THF (2 mL). To this solution, thiols (**18**, 5 equiv.) and Irgacure D-2959 (0.30 mg, 1.4 μmol, 0.20 equiv.) were added and briefly purged with nitrogen. The resulting mixture was irradiated with 365 nm light (power density: >5000μW/cm² at 15") at RT overnight. After the reaction had been run overnight, polymer was concentrated down, dissolved in DCM, and dialyzed against DCM:MeOH (1:1 vol%) overnight. After concentrating and drying on high vacuum, polymers **6.13**–**6.15** were analyzed by ^{1}H NMR and compared to polymer **6.9** to corroborate quantitative conversion (Figure 6.10).

6.7.3 Figure experimental procedures

Figure 6.2A. Perfluorocarbon nanoemulsion formation with microbial media.

Pluronic F-68, was added (2.8 wt%) to the relevant buffer and sonicated in a bath sonicator, Branson 3800 ultrasonic cleaner, to dissolve the polymer thoroughly. PFD (450 μl) and PFH

(450 µl) were combined in a 15 mL centrifuge tube. The total volume was diluted up to 10 mL with the relevant surfactant-containing buffer. Baseline medium was used as the buffer for all the experiments, except RDE experiments in which a phosphate buffer was used instead. The liquid was then sonicated at a 35% amplitude for 5 min (3 W, Qsonica).

Figure 6.2B/C. Perfluorocarbon nanoemulsion size.

The bulk emulsion solution was diluted in MilliQ H_2O (20 µL emulsions in 2 mL MilliQ H_2O) in a plastic 1 cm cuvette. Size was analyzed with a Malvern Zetasizer Nano dynamic light scattering. SOP parameters: 10 runs, 10 seconds/run, three measurements, no delay between measurements, 25 °C with 120 second equilibration time. Collection parameters: Lower limit = 0.6, Upper limit = 1000, Resolution = High, Number of size classes = 70, Lower size limit = 0.4, Upper size limit = 1000, Lower threshold = 0.05, Upper threshold = 0.01. Data are representative of three replicate measurements. Size error bars represent the half-width at half-maximum of the measurements.

Figure 6.3. Perfluorocarbon nanoemulsion size over time.

Sizes of emulsions were analyzed as described within figure experimental procedure for Figure 6.2B/C over a period of four days.

Figure 6.5B. Synthesis of fluorous rhodamine 6.3**.**

See synthesis as previously described.[29]

Figure 6.5C. Colocalization between PFC nanoemulsions and *X. autotrophicus*.

Collaborators performed this experiment, see reference.[28] Briefly, Cultures of *X. autotrophicus* (OD_{600} = 1.0) were harvested and re-suspended with 0.85% NaCl solution with OD_{600} adjusted to 0.1. Each 1 mL of the resulted bacterial suspension was incubated in hard at room temperature for 15 mins with 1.5 μL of microbial-binding SYTO™ 9 dye solution from the LIVE/DEAD™ BacLight™ Bacterial Viability and Counting Kit. The fluorescently tagged *X. autotrophicus* was separated via centrifugation (6000 rpm, 5 min) and re-suspended in 1 mL minimal medium containing 2.5% fluorescently tagged PFC nanoemulsion (*vide supra*). Suspension of *X. autotrophicus* without the addition of nanoemulsion was prepared in parallel as the control sample. The prepared samples incubated in dark for 1 hr for completion of nanoemulsion binding and loaded to a 35-mm glass bottom dish (μ-dish, ibidi), whose bottom glass was coated with a layer of poly-l-lysine (treated with 0.01% poly-*L*-lysine solution overnight and dried). The mixture was allowed to sit in the dish for 0.5 hr before all liquid was slowly removed by pipetting. The glass-surface of the dish was gently washed 5 times with filtered microbial minimal medium. Last, 1 mL of minimal medium was added to the dish to keep the sample hydrated before imaging.

Experiments of confocal microcopy (Leica Confocal SP8 MP) was conducted at Advanced Light Microscopy and Spectroscopy Laboratory at California Nanoscience Institute, UCLA. The data was acquired using Leica Application Suite X (LASX) on *x*-*y* mode at a scanning resolution of 14.6 nm per pixel, taking *x*-*y* cross-sectional images with a 100× oil objective lens (Leica 100× HC PL APO OIL CS2 NA/1.4). Fluorescence from SYTO™ 9 in the microbes was monitored at 490nm~520nm by a 470-nm laser excitation; the fluorescence from fluorous rhodamine in PFC nanoemulsions was monitored at 580nm~650nm by a 550-nm laser excitation. The intensities of

fluorescence emissions were collected by photon multiplier tube (PMT) detectors. The fluorescence images of microbes and PFC nanoemulsions were taken separately and merged.

Figure 6.7A. Synthesis of thermoresponsive polymers 6.6 **and** 6.7**.**

See synthetic chemistry procedures below.

Figure 6.9A. Formation of PFOB emulsions from poly(BCD).

See general nano- and macroemulsion formation procedures.

Figure 6.10A. Modification of alkene-containing 6.9 **to produce polymers** 6.13–6.15**.**

See synthetic chemistry procedures below.

Figure 6.11C. Formation of 6.8**-stabilized macroemulsions encapsulating payload** 6.16**.**

6.8-stabilized PFOB macroemulsions encapsulating cyanine **6.16** (0.03 mg)[59] were formed by pre-dissolving each dye in PFOB (40 μL) and following the general macroemulsion formation procedure.

Figure 6.11F. Formation of 6.15**-stabilized macroemulsions encapsulating payload** 6.17**.**

6.15-stabilized PFOB macroemulsions encapsulating rhodamine **6.17** (0.03 mg) were formed by pre-dissolving each dye in PFOB (40 μL) and following the general macroemulsion formation procedure.

Figure 6.12A/B. Host-guest emulsion fusion visualized by microscopy.

Fluorophore-labeled **6.8**- and **6.15**-stabilized droplets were formed following the general macroemulsion formation procedure. Emulsion solutions were then diluted (10 μL of each solution) in PBS 1X (180 μL) and rocked for five minutes. Solution was then re-suspended if aggregation was observed, and ~50–80 μL of solution was transferred to glass slide for epifluorescence microscopy.

Figure 6.12C. Fluorophore colocalization upon host-guest fusion.

Image analysis was performed with Fiji.[65] Cross-section is shown in Figure 6.12A.

Figure 6.13A/C. Macroemulsion formation with variable volume percent of inner fluorous core.

See general macroemulsion formation procedure.

Figure 6.13B/D. Flow cytometry analysis of macroemulsions.

Macroemulsions were formed as described in Figure 6.13A/C. These emulsion solutions were then diluted with 2 μL of emulsion solution added to 200 μL of PBS before analysis by flow cytometry.

Figure 6.14D/F. Flow cytometry analysis of (D) 6.8**-stabilized macroemulsions and (F)** 6.19**-stabilized macroemulsions.**

Macroemulsions were formulated as described in Figure 6.12A/B. These emulsion solutions were then diluted with 2 μL of emulsion solution added to 200 μL of PBS before analysis by flow cytometry.

Figure 6.15A–F. Flow cytometry analysis of host 6.8**-stabilized emulsions mixed with "guest" emulsions stabilized by** 6.19**,** 6.15 **or** 6.9**.**

Macroemulsions were formed as previously described. Emulsion solutions were diluted in a 1:1 ratio, total PFOB of 3 vol% in PBS, and mixed at room temperature for five minutes. Solutions were then analyzed by flow cytometry, mapping FL3 versus FL2.

6.8 1H-NMR Spectra Relevant to Chapter Six

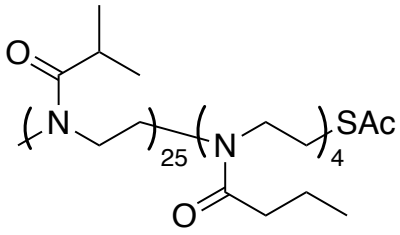

$P(iPrOx)_{25}$-$P(BuOx)_4$, **6.6**

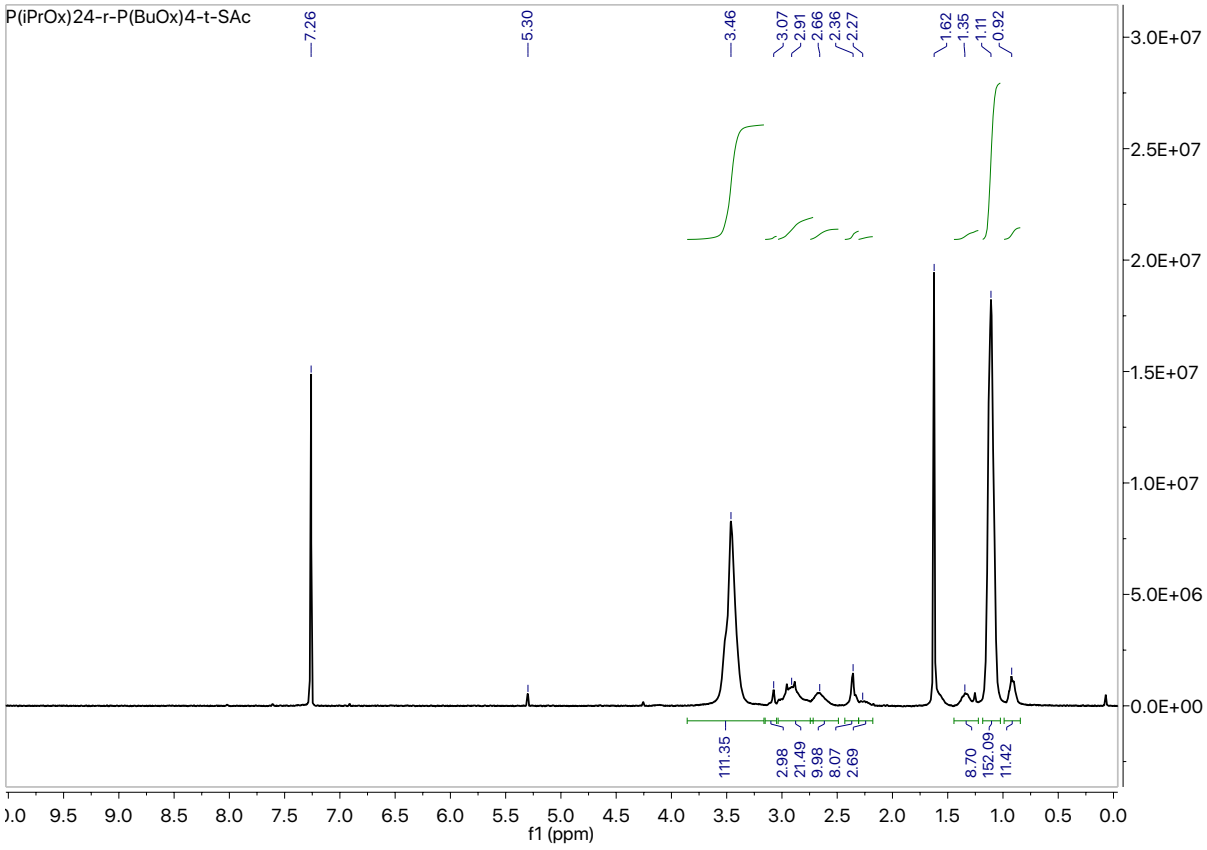

^{1}H NMR (500 MHz, $CDCl_3$) of copolymer **6.6** ($P(iPrOx)_{25}$-*r*-$P(iPrOx)_{25}$)-*t*-SAc.

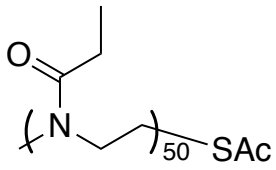

P(EtOx)$_{50}$, **6.7**

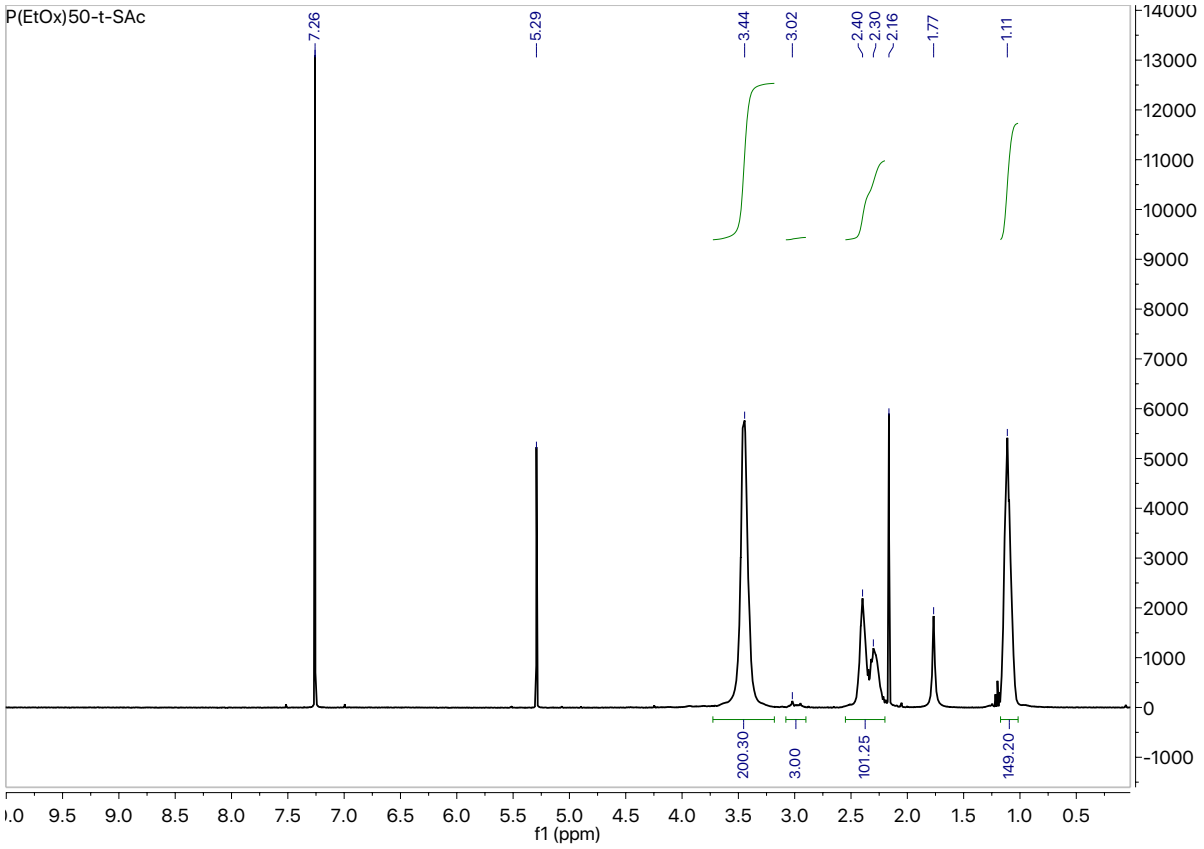

^{1}H NMR (500 MHz, $CDCl_3$) of copolymer **6.7** P(EtOx)$_{50}$-*t*-SAc.

6.9 References

(1) Lenton, T. M.; Rockström, J.; Gaffney, O.; Rahmstorf, S.; Richardson, K.; Steffen, W.; Schellnhuber, H. J. Climate Tipping Points — Too Risky to Bet Against. *Nature* **2019**, *575*, 592–595.

(2) Chu, S.; Majumdar, A. Opportunities and Challenges for a Sustainable Energy Future. *Nature* **2012**, *488*, 294–303.

(3) Nocera, D. G. Solar Fuels and Solar Chemicals Industry. *Acc. Chem. Res.* **2017**, *50*, 616–619.

(4) Bushuyev, O. S.; De Luna, P.; Dinh, C. T.; Tao, L.; Saur, G.; van de Lagemaat, J.; Kelley, S. O.; Sargent, E. H. What Should We Make with CO2 and How Can We Make It? *Joule* **2018**, *2*, 825–832.

(5) Appel, A. M.; Bercaw, J. E.; Bocarsly, A. B.; Dobbek, H.; Dubois, D. L.; Dupuis, M.; Ferry, J. G.; Fujita, E.; Hille, R.; Kenis, P. J. A.; et al. Frontiers, Opportunities, and Challenges in Biochemical and Chemical Catalysis of CO2 Fixation. *Chem. Rev.* **2013**, *113*, 6621–6658.

(6) Liu, C.; Colón, B. C.; Ziesack, M.; Silver, P. A.; Nocera, D. G. Water Splitting-Biosynthetic System with CO2 Reduction Efficiencies Exceeding Photosynthesis. *Science (80-.).* **2016**, *352*, 1210–1213.

(7) Nevin, K. P.; Woodard, T. L.; Franks, A. E.; Summers, Z. M.; Lovley, D. R. Microbial Electrosynthesis: Feeding Microbes Electricity to Convert Carbon Dioxide and Water to Multicarbon Extracellular Organic Compounds. *MBio* **2010**, *1*.

(8) Aryal, N.; Tremblay, P. L.; Lizak, D. M.; Zhang, T. Performance of Different Sporomusa Species for the Microbial Electrosynthesis of Acetate from Carbon Dioxide. *Bioresour.*

Technol. **2017**, *233*, 184–190.

(9) Jiang, N.; You, B.; Sheng, M.; Sun, Y. Electrodeposited Cobalt-Phosphorous-Derived Films as Competent Bifunctional Catalysts for Overall Water Splitting. *Angew. Chem. Int. Ed.* **2015**, *54*, 6251–6254.

(10) P, D. CRC Handbook of Chemistry and Physics. *J. Mol. Struct.* **1992**, *268*, 320.

(11) Gladysz, J. A.; Curran, D. P.; Horváth, I. T. Handbook of Fluorous Chemistry. *Handb. Fluorous Chem.* **2005**, 1–595.

(12) Riess, J. G.; Riess, J. G. Oxygen Carriers ("blood Substitutes") - Raison d'etre, Chemistry, and Some Physiology. *Chem. Rev.* **2001**, *101*, 2797–2919.

(13) Riess, J. G.; Krafft, M. P. Fluorocarbon Emulsions as in Vivo Oxygen Delivery Systems. Background and Chemistry. *Blood Substitutes* **2006**, 259–275.

(14) At, A. Dissolving Gases in FLUTEC ™ Liquids. **2005**.

(15) Dias, A. M. A.; Freire, M.; Coutinho, J. A. P.; Marrucho, I. M. Solubility of Oxygen in Liquid Perfluorocarbons. *Fluid Phase Equilib.* **2004**, *222–223*, 325–330.

(16) Freire, M. G.; Dias, A. M. A.; Coutinho, J. A. P.; Coelho, M. A. Z.; Marrucho, I. M. Enzymatic Method for Determining Oxygen Solubility in Perfluorocarbon Emulsions. *Fluid Phase Equilib.* **2005**, *231*, 109–113.

(17) Estabrook, D. A.; Ennis, A. F.; Day, R. A.; Sletten, E. M. Controlling Nanoemulsion Surface Chemistry with Poly(2-Oxazoline) Amphiphiles. *Chem. Sci.* **2019**, *10*, 3994–4003.

(18) Sletten, E. M.; Swager, T. M. Readily Accessible Multifunctional Fluorous Emulsions. *Chem. Sci.* **2016**, *7*, 5091–5097.

(19) Day, R. A.; Estabrook, D. A.; Wu, C.; Chapman, J. O.; Togle, A. J.; Sletten, E. M.

Systematic Study of Perfluorocarbon Nanoemulsions Stabilized by Polymer Amphiphiles. *ACS Appl. Mater. Interfaces* **2020**, *12*, 38887–38898.

(20) Rodrigues, R. M.; Guan, X.; Iñiguez, J. A.; Estabrook, D. A.; Chapman, J. O.; Huang, S.; Sletten, E. M.; Liu, C. Perfluorocarbon Nanoemulsion Promotes the Delivery of Reducing Equivalents for Electricity-Driven Microbial CO2 Reduction. *Nat. Catal.* **2019**, *2*, 407–414.

(21) Liu, C.; Gallagher, J. J.; Sakimoto, K. K.; Nichols, E. M.; Chang, C. J.; Chang, M. C. Y.; Yang, P. Nanowire-Bacteria Hybrids for Unassisted Solar Carbon Dioxide Fixation to Value-Added Chemicals. *Nano Lett.* **2015**, *15*, 3634–3639.

(22) Rago, L.; Zecchin, S.; Villa, F.; Goglio, A.; Corsini, A.; Cavalca, L.; Schievano, A. Bioelectrochemical Nitrogen Fixation (e-BNF): Electro-Stimulation of Enriched Biofilm Communities Drives Autotrophic Nitrogen and Carbon Fixation. *Bioelectrochemistry* **2019**, *125*, 105–115.

(23) Malik, K. A.; Schlegel, H. G. Chemolithoautotrophic Growth of Bacteria Able to Grow under N2-Fixing Conditions. *FEMS Microbiol. Lett.* **1981**, *11*, 63–20.

(24) Malik, K. A.; Schlegel, H. G. Enrichment and Isolation of New Nitrogen-Fixing Hydrogen Bacteria. *FEMS Microbiol. Lett.* **1980**, *8*, 101–104.

(25) Liu, C.; Sakimoto, K. K.; Colón, B. C.; Silver, P. A.; Nocera, D. G. Ambient Nitrogen Reduction Cycle Using a Hybrid Inorganic-Biological System. *Proc. Natl. Acad. Sci. U. S. A.* **2017**, *114*, 6450–6455.

(26) Oughli, A. A.; Conzuelo, F.; Winkler, M.; Happe, T.; Lubitz, W.; Schuhmann, W.; Rüdiger, O.; Plumeré, N. A Redox Hydrogel Protects the O2-Sensitive [FeFe]-Hydrogenase from Chlamydomonas Reinhardtii from Oxidative Damage. *Angew. Chem.*

Int. Ed. **2015**, *54*, 12329–12333.

(27) Plumeré, N.; Rüdiger, O.; Oughli, A. A.; Williams, R.; Vivekananthan, J.; Pöller, S.; Schuhmann, W.; Lubitz, W. A Redox Hydrogel Protects Hydrogenase from High-Potential Deactivation and Oxygen Damage. *Nat. Chem.* **2014**, *6*, 822–827.

(28) Lu, S.; Rodrigues, R. M.; Huang, S.; Estabrook, D. A.; Chapman, J. O.; Guan, X.; Sletten, E. M.; Liu, C. Perfluorocarbon Nanoemulsions Create a Beneficial O2 Microenvironment in N2-Fixing Biological | Inorganic Hybrid. *Submitted* **2021**.

(29) Sletten, E. M.; Swager, T. M. Fluorofluorophores: Fluorescent Fluorous Chemical Tools Spanning the Visible Spectrum. *J. Am. Chem. Soc.* **2014**, *136*, 13574–13577.

(30) Lohrke, J.; Frenzel, T.; Endrikat, J.; Alves, F. C.; Grist, T. M.; Law, M.; Lee, J. M.; Leiner, T.; Li, K. C.; Nikolaou, K.; et al. 25 Years of Contrast-Enhanced MRI: Developments, Current Challenges and Future Perspectives. *Adv. Ther.* **2016**, *33*, 1–28.

(31) Guo, B. J.; Yang, Z. L.; Zhang, L. J. Gadolinium Deposition in Brain: Current Scientific Evidence and Future Perspectives. *Front. Mol. Neurosci.* **2018**, *11*.

(32) Maloney, E.; Hwang, J. H. Emerging HIFU Applications in Cancer Therapy. *Int. J. Hyperth.* **2015**, *31*, 302–309.

(33) Leslie, T. A.; Kennedy, J. E. High-Intensity Focused Ultrasound Principles, Current Uses, and Potential for the Future. *Ultrasound Q.* **2006**, *22*, 263–272.

(34) Jang, H. J.; Lee, J. Y.; Lee, D. H.; Kim, W. H.; Hwang, J. H. Current and Future Clinical Applications of High-Intensity Focused Ultrasound (HIFU) for Pancreatic Cancer. *Gut Liver* **2010**, *4*.

(35) Cheng, C. A.; Chen, W.; Zhang, L.; Wu, H. H.; Zink, J. I. A Responsive Mesoporous Silica Nanoparticle Platform for Magnetic Resonance Imaging-Guided High-Intensity

Focused Ultrasound-Stimulated Cargo Delivery with Controllable Location, Time, and Dose. *J. Am. Chem. Soc.* **2019**, *141*, 17670–17684.

(36) Schlesinger, D.; Benedict, S.; Diederich, C.; Gedroyc, W.; Klibanov, A.; Larner, J. MR-Guided Focused Ultrasound Surgery, Present and Future. *Med. Phys.* **2013**, *40*.

(37) Duc, N. M.; Keserci, B. Emerging Clinical Applications of High-Intensity Focused Ultrasound. *Diagnostic Interv. Radiol.* **2019**, *25*, 398–409.

(38) de Senneville, B. D.; Ries, M.; Bartels, L. W.; Moonen, C. T. W. MRI-Guided High Intensity Focused Ultrasound of Liver and Kidney. *arXiv* **2020**.

(39) Deng, T.; Zhang, L.; Wu, H. H.; Zink, J. I. A Nanoparticle Enabled Focused Ultrasound-Stimulated Magnetic Resonance Imaging Spotlight. *Chem. Commun.* **2019**, *55*, 10261–10264.

(40) Huber, S.; Jordan, R. Modulation of the Lower Critical Solution Temperature of 2-Alkyl-2-Oxazoline Copolymers. *Colloid Polym. Sci.* **2008**, *286*, 395–402.

(41) Luxenhofer, R.; Schulz, A.; Roques, C.; Li, S.; Bronich, T. K.; Batrakova, E. V.; Jordan, R.; Kabanov, A. V. Doubly Amphiphilic Poly(2-Oxazoline)s as High-Capacity Delivery Systems for Hydrophobic Drugs. *Biomaterials* **2010**, *31*, 4972–4979.

(42) Soares, S.; Sousa, J.; Pais, A.; Vitorino, C. Nanomedicine: Principles, Properties, and Regulatory Issues. *Front. Chem.* **2018**, *6*.

(43) Bobo, D.; Robinson, K. J.; Islam, J.; Thurecht, K. J.; Corrie, S. R. Nanoparticle-Based Medicines: A Review of FDA-Approved Materials and Clinical Trials to Date. *Pharm. Res.* **2016**, *33*, 2373–2387.

(44) Liu, Y.; Tan, J.; Thomas, A.; Ou-Yang, D.; Muzykantov, V. R. The Shape of Things to Come: Importance of Design in Nanotechnology for Drug Delivery. *Ther. Deliv.* **2012**, *3*,

181–194.

(45) Albert, A. Chemical Aspects of Selective Toxicity. *Nature* **1958**, *182*, 421–423.

(46) Rautio, J.; Meanwell, N. A.; Di, L.; Hageman, M. J. The Expanding Role of Prodrugs in Contemporary Drug Design and Development. *Nat. Rev. Drug Discov.* **2018**, *17*, 559–587.

(47) Rautio, J.; Kumpulainen, H.; Heimbach, T.; Oliyai, R.; Oh, D.; Järvinen, T.; Savolainen, J. Prodrugs: Design and Clinical Applications. *Nat. Rev. Drug Discov.* **2008**, *7*, 255–270.

(48) Zawilska, J. B.; Wojcieszak, J.; Olejniczak, A. B. Prodrugs: A Challenge for the Drug Development. *Pharmacol. Reports* **2013**, *65*, 1–14.

(49) Patel, J. K.; Patel, A. P. Passive Targeting of Nanoparticles to Cancer. *Surf. Modif. Nanoparticles Target. Drug Deliv.* **2019**, 125–143.

(50) Shi, Y.; van der Meel, R.; Chen, X.; Lammers, T. The EPR Effect and beyond: Strategies to Improve Tumor Targeting and Cancer Nanomedicine Treatment Efficacy. *Theranostics* **2020**, *10*, 7921–7924.

(51) Byrne, J. D.; Betancourt, T.; Brannon-Peppas, L. Active Targeting Schemes for Nanoparticle Systems in Cancer Therapeutics. *Adv. Drug Deliv. Rev.* **2008**, *60*, 1615–1626.

(52) Yoo, J.; Park, C.; Yi, G.; Lee, D.; Koo, H. Active Targeting Strategies Using Biological Ligands for Nanoparticle Drug Delivery Systems. *Cancers* **2019**, *11*.

(53) Yu, X.; Trase, I.; Ren, M.; Duval, K.; Guo, X.; Chen, Z. Design of Nanoparticle-Based Carriers for Targeted Drug Delivery. *J. Nanomater.* **2016**, *2016*, 1–15.

(54) Del Valle, E. M. M. Cyclodextrins and Their Uses: A Review. *Process Biochem.* **2004**, *39*, 1033–1046.

(55) Wankar, J.; Kotla, N. G.; Gera, S.; Rasala, S.; Pandit, A.; Rochev, Y. A. Recent Advances

in Host–Guest Self-Assembled Cyclodextrin Carriers: Implications for Responsive Drug Delivery and Biomedical Engineering. *Adv. Funct. Mater.* **2020**, *30*.

(56) Valente, A. J. M.; Söderman, O. The Formation of Host-Guest Complexes between Surfactants and Cyclodextrins. *Adv. Colloid Interface Sci.* **2014**, *205*, 156–176.

(57) Schibilla, F.; Voskuhl, J.; Fokina, N. A.; Dahl, J. E. P.; Schreiner, P. R.; Ravoo, B. J. Host–Guest Complexes of Cyclodextrins and Nanodiamonds as a Strong Non-Covalent Binding Motif for Self-Assembled Nanomaterials. *Chem. - A Eur. J.* **2017**, *23*, 16059–16065.

(58) Goubet, I.; Dahout, C.; Sémon, E.; Guichard, E.; Le Quéré, J. L.; Voilley, A. Competitive Binding of Aroma Compounds by β-Cyclodextrin. *J. Agric. Food Chem.* **2001**, *49*, 5916–5922.

(59) Lim, I.; Vian, A.; Van De Wouw, H. L.; Day, R. A.; Gomez, C.; Liu, Y.; Rheingold, A. L.; Campàs, O.; Sletten, E. M. Fluorous Soluble Cyanine Dyes for Visualizing Perfluorocarbons in Living Systems. *J. Am. Chem. Soc.* **2020**, *142*, 16072–16081.

(60) De La Rosa, V. R.; Nau, W. M.; Hoogenboom, R. Tuning Temperature Responsive Poly(2-Alkyl-2-Oxazoline)s by Supramolecular Host-Guest Interactions. *Org. Biomol. Chem.* **2015**, *13*, 3048–3057.

(61) Sletten, E. M.; Bertozzi, C. R. Bioorthogonal Chemistry: Fishing for Selectivity in a Sea of Functionality. *Angew. Chem. Int. Ed.* **2009**, *48*, 6974–6998.

(62) Shang, X.; Song, X.; Faller, C.; Lai, R.; Li, H.; Cerny, R.; Niu, W.; Guo, J. Fluorogenic Protein Labeling Using a Genetically Encoded Unstrained Alkene. *Chem. Sci.* **2017**, *8*, 1141–1145.

(63) Sievers, C.; Scott, S. L.; Noda, Y.; Qi, L.; Albuquerque, E. M.; Rioux, R. M. Phenomena

Affecting Catalytic Reactions at Solid−Liquid Interfaces. *ACS Catal.* **2016**, *6*, 8286–8307.

(64) Bai, X.; Song, N.; Wen, L.; Huang, X.; Zhang, J.; Zhang, Y.; Zhao, Y. Environmentally Benign Multiphase Solid-Liquid-Gas Catalysis. *Green Chem.* **2020**, *22*, 895–902.

(65) Schindelin, J.; Arganda-Carreras, I.; Frise, E.; Kaynig, V.; Longair, M.; Pietzsch, T.; Preibisch, S.; Rueden, C.; Saalfeld, S.; Schmid, B.; et al. Fiji: An Open-Source Platform for Biological-Image Analysis. *Nat. Methods* **2012**, *9*, 676–682.

(66) Gress, A.; Völkel, A.; Schlaad, H. Thio-Click Modification of Poly[2-(3-Butenyl)-2-Oxazoline]. *Macromolecules* **2007**, *40*, 7928–7933.

(67) Kempe, K.; Hoogenboom, R.; Jaeger, M.; Schubert, U. S. Three-Fold Metal-Free Efficient ("Click") Reactions onto a Multifunctional Poly(2-Oxazoline) Designer Scaffold. *Macromolecules* **2011**, *44*, 6424–6432.